

# Exploiting tumor hypoxia for cancer treatment

Citation for published version (APA):

Niemans, R. S. T. (2018). *Exploiting tumor hypoxia for cancer treatment*. [Doctoral Thesis, Maastricht University]. Gildeprint Drukkerijen. <https://doi.org/10.26481/dis.20180626rn>

## Document status and date:

Published: 01/01/2018

## DOI:

[10.26481/dis.20180626rn](https://doi.org/10.26481/dis.20180626rn)

## Document Version:

Publisher's PDF, also known as Version of record

## Please check the document version of this publication:

- A submitted manuscript is the version of the article upon submission and before peer-review. There can be important differences between the submitted version and the official published version of record. People interested in the research are advised to contact the author for the final version of the publication, or visit the DOI to the publisher's website.
- The final author version and the galley proof are versions of the publication after peer review.
- The final published version features the final layout of the paper including the volume, issue and page numbers.

[Link to publication](#)

## General rights

Copyright and moral rights for the publications made accessible in the public portal are retained by the authors and/or other copyright owners and it is a condition of accessing publications that users recognise and abide by the legal requirements associated with these rights.

- Users may download and print one copy of any publication from the public portal for the purpose of private study or research.
- You may not further distribute the material or use it for any profit-making activity or commercial gain
- You may freely distribute the URL identifying the publication in the public portal.

If the publication is distributed under the terms of Article 25fa of the Dutch Copyright Act, indicated by the "Taverne" license above, please follow below link for the End User Agreement:

[www.umlib.nl/taverne-license](http://www.umlib.nl/taverne-license)

## Take down policy

If you believe that this document breaches copyright please contact us at:

[repository@maastrichtuniversity.nl](mailto:repository@maastrichtuniversity.nl)

providing details and we will investigate your claim.

# **Exploiting tumor hypoxia for cancer treatment**

## Copyright

PhD thesis, Maastricht University, The Netherlands

© Raymon S.T. Niemans, Eijsden, 2018

All rights reserved. No part of this thesis may be reproduced or transmitted in any form or by any means without prior written permission from the author.



Cover	Ilse Modder, <a href="http://www.ilsemodder.nl">www.ilsemodder.nl</a>
Lay-out	Ilse Modder, <a href="http://www.ilsemodder.nl">www.ilsemodder.nl</a>
Printed by	Gildeprint, <a href="http://www.gildeprint.nl">www.gildeprint.nl</a>
ISBN	9789462339781

# **Exploiting tumor hypoxia for cancer treatment**

DISSERTATION

to obtain the degree of Doctor at Maastricht University,  
on the authority of the Rector Magnificus, Prof. dr. Rianne M. Letschert  
in accordance with the decision of the Board of Deans,  
to be defended in public  
on Tuesday June 26th 2018 at 12:00 hours

by

**Raymon Servatius Theodorus Niemans**

**Supervisor:**

Prof. dr. P. Lambin

**Co-supervisors:**

Dr. L.J. Dubois

Dr. A. Yaromina

**Assessment Committee:**

Prof. dr. F.C.S. Ramaekers (chair)

Prof. dr. J. Bussink (Radboud UMC, Nijmegen, The Netherlands)

Dr. R. Godschalk

Prof. dr. G.R.M.M. Haenen

Prof. dr. K.J. Williams (University of Manchester, Manchester, UK)



# Table of contents

Chapter 1	General introduction and outline of this thesis	8
Chapter 2	New ways to image and target tumor hypoxia and its molecular responses <i>Previously published:</i> Dubois, L.J., et al., <i>New ways to image and target tumour hypoxia and its molecular responses. Radiother Oncol, 2015. 116(3): p. 352-7.</i>	36
Chapter 3	Synthesis and <i>in vivo</i> biological evaluation of <sup>68</sup> Ga-labeled carbonic anhydrase IX targeting small molecules for positron emission tomography <i>Previously published:</i> Sneddon, D., et al., <i>Synthesis and in Vivo Biological Evaluation of (68)Ga-Labeled Carbonic Anhydrase IX Targeting Small Molecules for Positron Emission Tomography. J Med Chem, 2016. 59(13): p. 6431-43.</i>	56
Chapter 4	New approach of delivering cytotoxic drugs towards CA IX expressing cells: A concept of dual-target drugs <i>Previously published:</i> van Kuijk, S.J., et al., <i>New approach of delivering cytotoxic drugs towards CAIX expressing cells: A concept of dual-target drugs. Eur J Med Chem, 2017. 127: p. 691-702.</i>	110
Chapter 5	Novel fluorinated carbonic anhydrase IX inhibitors reduce hypoxia-induced acidification and clonogenic survival of cancer cells <i>Accepted and to be published by Oncotarget.</i>	164
Chapter 6	Hypoxia-activated prodrugs and (lack of) clinical progression: the need for hypoxia-based biomarker patient selection in phase III clinical trials <i>In preparation.</i>	200

Chapter 7	Hypoxic cell killing by CP-506, a novel hypoxia-activated prodrug <i>In preparation.</i>	224
Chapter 8	Antitumor effects of the novel hypoxia-activated prodrug CP-506 combined with radiotherapy or immunotherapy <i>In preparation.</i>	256
Chapter 9	Discussion and future perspectives	278
Addenda	- Summary	300
	- Nederlandstalige samenvatting	304
	- Valorization addendum	308
	- Acknowledgements/Dankwoord	313
	- Curriculum vitae	319
	- List of publications	320



# CHAPTER 1

General introduction  
and outline of this thesis

# Cancer

## History & epidemiology

Evidence of what is now called cancer can be found throughout recorded human history, as far back as the time of ancient Egypt. The Edwin Smith Papyrus ( $\pm 3000$  B.C.) mentions 8 cases of removal of breast tumors or ulcers, adding that “there is no treatment” [1]. Growths suggestive of osteosarcomas have been found in mummies originating from the same period. The Greek “Father of Medicine” Hippocrates (460-370 B.C.) coined the terms “carcinoma” and “carcinoma” to describe non-ulcer forming and ulcer-forming tumors, respectively. With these words he was referring to a crab, most likely because the shape of the tumors he was describing reminded him of this animal. These words were later translated from Greek into the Latin word “cancer” by the Roman physician Celsus (28-50 B.C.) [2].

Nowadays, cancer is a major cause of morbidity and mortality worldwide. In 2012, approximately 14.1 million new cases were diagnosed, and 8.2 million cancer-related deaths were reported, corresponding to incidence and mortality rates of 182 and 102 per 100,000, respectively. The five most common types of cancer together contribute for almost 50% of total incidence rates, being lung (13.0%), breast (11.9%), colorectal (9.7%), prostate (7.9%) and stomach (6.8%) cancer [3]. The five types of cancer with the highest mortality rates are lung (19.4%), liver (9.1%), stomach (8.8%), colorectal (8.5%) and breast (6.4%). Unfortunately, incidence rates have been and are still increasing, with an expected number of annual new cancer cases of almost 24 million by 2035 [4, 5].

## Causes

90-95% of cancers are associated with exposure to environmental and lifestyle risks, whereas the remaining 5-10% can be attributed to genetic defects. Most cancer-related deaths are due to dietary choices (30-35%), tobacco smoking (25-30%) and infections (15-20%) [6]. Other common factors include radiation, stress, physical activity and environmental pollutants.

Cancer arises due to mutations in the DNA of a normal cell, caused by external mutagens or genetically inherited. These mutations accumulate and lead to a multistep process in which gain-of-function oncogenes and loss-of-function tumor suppressor genes slowly transform the normal cell into a malignant cell with increased proliferation and lifespan. This genomic instability, together with tumor promoting inflammation, facilitates the ac-

quisition of the so-called “Hallmarks of Cancer”: capabilities that affect the cell and its interaction with the microenvironment, and are needed for malignant growth. These hallmarks are sustained proliferative signaling, evasion of growth suppressors, evasion of immune destruction, replicative immortality, invasion and metastasis, sustained angiogenesis, evasion of cell death and deregulation of cellular energetics [7, 8]. Some of these hallmarks will be discussed in more detail later.

## **Treatments**

Conventional cancer therapies include surgery (removal of (parts of) the tumor), radiotherapy (applying ionizing radiation to the tumor cells to induce DNA damage) and different kinds of chemotherapies (generally cytotoxins that interfere with mitosis). However, research on new treatment options focuses more and more on targeted treatments including antibodies, small molecules, antiangiogenics and viral therapy [9], because these new therapies have the potential to cause less side effects, exhibit more localized treatment delivery, achieve higher concentration of anticancer therapeutics and decrease resistance of the cancer cells toward the treatment. Lately, immunotherapies, in which the patient’s own immune system is induced and/or stimulated to eradicate cancer cells, have also emerged as promising new cancer treatments [10]. Additionally, cancer treatment nowadays is mainly focused on combinations of afore mentioned treatments. By simultaneously targeting different pathways, such combination treatments can enhance efficacy in an additive or even synergistic manner compared to a monotherapy approach. This also might lead to a lower required dosage of each individual treatment, thus reducing toxicity [11].

## **Tumor hypoxia**

### **Causes**

As a tumor grows, it needs supportive vasculature for the delivery of sufficient levels of oxygen and nutrients. To proliferate, cells need to be within 70-150  $\mu\text{m}$  of a perfused blood vessel [12]. Solid tumors therefore exploit one of the hallmarks of cancer, namely sustained angiogenesis, i.e. the formation of new blood vessels from the existing ones. However, angiogenic regulators are often imbalanced in tumors, and angiogenic genes and signaling pathways lack feedback regulatory control, leading to abnormal, chaotic, fragile and hyperpermeable tumor vasculature [13, 14]. Therefore, not all tumor cells will be within the diffusion limit of oxygen from perfused blood vessels, leading to the formation of dif-

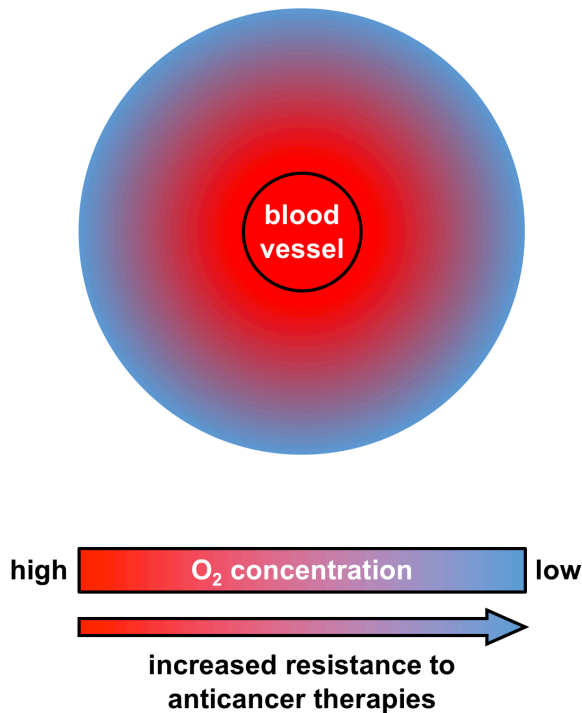
fusion-limited (chronic) hypoxia. Additionally, the disordered tumor vasculature causes transient changes in blood flow, potentially causing a temporary shutdown resulting in perfusion-limited (acute) hypoxia. Where normal physiological oxygen levels range between 1 and 11% [15], hypoxic tumor areas can potentially contain no oxygen at all (anoxia) [16].

### **Tumor hypoxia increases tumor cell malignancy and therapeutic resistance**

Up to 60% of solid tumors exhibit detectable hypoxic areas [17], and tumor hypoxia has been associated with poor prognosis [16, 18]. Tumor hypoxia aggravates the malignant tumor cell phenotype: it promotes genomic instability [19], angiogenesis [20], and resistance to apoptosis [21], it induces autophagy [22] and changes in central metabolic pathways and in the global metabolome [23, 24], it suppresses DNA repair pathways [19], it increases invasion and metastasis [25], it modulates tyrosine kinase-mediated cell signaling pathways [26], it mediates escape from the immune system [27], it alters histone methylation [28], it coordinates the metabolic response to hypoxia-induced reductive stress [29] and it provides a niche for cancer stem cells [30]. Hypoxia can thus greatly contribute to the Hallmarks of Cancer. Additionally, tumor hypoxia poses therapeutic problems (Figure 1). In well-oxygenated cells, oxygen reacts with radical species on the DNA caused directly or indirectly by ionizing radiation, which makes the damage permanent. In hypoxic cells, this so-called oxygen-enhancement effect is missing or reduced [31-33]. Also, hypoxic tumors are intrinsically more resistant to radiation, e.g. through increased levels of heat-shock proteins or increased numbers of cells with diminished apoptotic potential or increased proliferation potential [21, 34-37]. Hypoxia also induces resistance to chemotherapeutic agents, e.g. by inhibiting cell proliferation [38], causing tissue acidosis [39], or decreasing cytotoxicity of some agents [40-42]. Additionally, intrinsic resistance of tumor cells to chemotherapeutic agents can be enhanced by hypoxia, due to the expression of hypoxic stress proteins and loss of apoptotic potential [43-49]. Limited perfusion in hypoxic areas also limits drug delivery [50]. Regarding immunotherapies, tumor hypoxia can interfere with T lymphocyte effector function, regulate natural killer and natural killer T cell activity, induce resistance to cell-mediated cytotoxicity, induce immune suppression, contribute to immune tolerance, and impair T cell infiltration [51, 52].

Tumor hypoxia thus is a promising therapeutic target to exploit in cancer treatment. By combining conventional treatments, which target aerobic cells, with hypoxia-targeting strategies, a greater anticancer effect can be achieved. Over the years, several strategies to

combat tumor hypoxia have been explored, three important approaches being modulation of tumor oxygenation and using hypoxia-activated prodrugs (HAPs) either as radiosensitizers or as hypoxia-specific cytotoxins. Examples of each of these approaches will be discussed below.



**Figure 1:** Schematic representation of diffusion-limited (chronic) hypoxia. With increasing distance from a blood vessel, oxygen concentration decreases and resistance to certain anticancer therapies, including radiotherapy, chemotherapy and likely immunotherapy, increases.

### Modulation of tumor oxygenation

One way to combat tumor hypoxia is to oxygenate the tumor, reducing or completely eliminating the hypoxic areas, and thus making the cells more susceptible to existing cancer treatments. Several options to modulate tumor oxygenation have been and are still being investigated. Hyperbaric oxygen therapy (HBOT; 100% O<sub>2</sub> at elevated atmospheric pressure) enhances the amount of dissolved oxygen in the plasma (thus independent of hemoglobin), increasing oxygen tissue delivery and thus increasing normal tissue but also tumor oxygenation [53]. However, despite this reduced diffusion-limited hypoxia, hypoxic

regions are still detectable [54], possibly being perfusion-limited hypoxic regions which are not affected by HBOT. Still, in clinical trials in various tumor types, HBOT combined with radiotherapy reduced tumor growth and improved local control, resulting in increased survival. Additionally, HBOT even diminished some negative side effects of radiotherapy, such as the injury of normal tissue after radiation [55, 56]. In other trials however, this combination therapy was not effective, or was accompanied by a high prevalence of severe late complications, potentially due to excessive radiation doses per fraction [55, 56]. The combination of HBOT with chemotherapy seems promising, however its effectiveness seems to heavily depend on which cytotoxic agent is used, the experimental conditions, and the tumor type [55, 56]. Beneficial effects of HBOT are diverse and vary with tumor type, malignancy, size of the lesion, and clinical state of the patient. These effects are also dependent on the oxygenation protocol used. As such, HBOT as adjuvant cancer treatment has not made it into clinical practice as (adjuvant) cancer treatment yet. Most research on HBOT now seems to focus on its beneficial effects in reducing radiation-induced normal tissue injuries, since HBOT is capable of promoting wound healing [55, 57, 58].

Tumor oxygenation can also be increased by CON: the inhalation of carbogen, a gas mixture of  $\geq 95\%$   $O_2$  and  $\leq 5\%$   $CO_2$  which decreases diffusion-limited hypoxia, together with the administration of nicotinamide, a vasoactive agent which decreases perfusion-limited hypoxia [59-64]. A clinical trial with bladder carcinoma patients showed significant differences in overall survival, risk of death and local relapse in favor of the combination of radiotherapy with CON [65]. In a phase 2 clinical trial, combining accelerated radiotherapy with carbogen and nicotinamide (ARCON) in head and neck cancer resulted in improved local control, which could however not be repeated in a phase 3 clinical trial [66, 67]. Because of this lack of efficacy, and, possibly, the high treatment burden of AR for patients, ARCON has also not made it into clinical practice.

Myo-inositol trispyrophosphate (ITPP) is an allosteric effector of hemoglobin. ITPP accumulates in erythrocytes and, by binding to it, decreases the binding affinity of hemoglobin to oxygen [68]. Specifically, under hypoxic conditions, this leads to an enhanced release of oxygen and thus elevated oxygen levels in hypoxic tumors (16). Preclinically, ITPP treatment improves survival of animals across several tumor models, especially when combined with chemotherapy [69-77], and inhibits tumor spread [69]. A clinical trial in patients is currently underway [78]. However, in a preclinical glioblastoma model, ITPP as a monotherapy was ineffective, and in combination with radiotherapy even reduced the latter's effectiveness [79].

# Hypoxia-activated prodrugs in cancer treatment

## Hypoxia-activated prodrugs as radiosensitizers

The use of hypoxia-activated prodrugs (HAPs) to eradicate hypoxic tumor cells is a promising approach in cancer treatment. HAPs are activated specifically in hypoxic conditions, where they, in general, act as either radiosensitizers or as DNA-damaging cytotoxins. As stated before, in well-oxygenated cells, oxygen reacts with radical species on the DNA caused directly or indirectly by ionizing radiation, which makes the damage permanent. In hypoxic cells, this same effect can be obtained by using HAPs as oxygen mimetic radiosensitizers. Nitroimidazoles are the most common HAP radiosensitizers; their electron-affinic nitro-group is designed to react with the same radical species on the DNA as oxygen does in well-oxygenated cells [80]. Misonidazole exhibited considerable antitumor activity [81], but when combined with fractionated radiotherapy, delayed peripheral neuropathies were observed [82, 83]. Etanidazole seemed to be more potent, but no beneficial effects were found when combined with fractionated radiotherapy [81, 84]. In contrast, nimorazole has been more of a success: it significantly improved the effect of radiotherapy in head and neck tumors, without major side effects [85], and is now standard of care for the treatment of head and neck squamous cell carcinoma in Denmark [85, 86], with several exploratory clinical trials still ongoing or planned [87-89]. Novel oxygen mimetic radiosensitizers are being investigated but are not in clinical development yet [90-92].

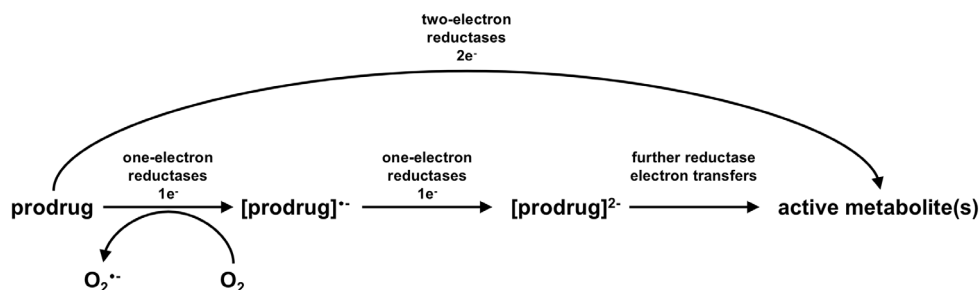
## Hypoxia-activated prodrugs as hypoxia-specific cytotoxins

The other class of HAPs releases or is metabolized to DNA-damaging cytotoxins specifically in hypoxic conditions. These HAPs are continuously being developed, tested and selected for favorable properties. They should be able to penetrate from a blood vessel to hypoxic cells deep within a tumor, without being activated too early in the surrounding less-hypoxic cells. Also, it should preferentially be activated at oxygen levels low enough to prevent activation under normal physiological conditions. Additionally, the active metabolite(s) should be able to kill non-proliferating cells, since these are typically found in hypoxic tumor areas, and should exert a bystander effect: the ability to diffuse from the hypoxic activator cells to better-oxygenated surrounding cells and kill these too [93].

In order to release or activate their effector, these HAPs have to be enzymatically reduced [94]. This can be done by both one- and two-electron oxidoreductases (Figure 2). One-electron reductases reduce the HAP to an inactive, oxygen-sensing intermediate, which is back-oxidized to the parental HAP and reactive oxygen species (ROS) when oxygen is pres-

ent. The ROS are detoxified by superoxide dismutase and thus the HAP has no effect in normal tissues. In hypoxic tissues however, the inactive intermediate is further reduced, or fragments, to generate an active, cytotoxic metabolite [95]. Two-electron reductases reduce the HAP immediately to its active metabolite, thus bypassing the oxygen-sensing inactive intermediate. Where in the case of one-electron activation HAP selectivity is determined by the ability of oxygen to back-oxidize the inactive intermediate and/or the overexpression of oxidoreductases in the tumor, in the case of two-electron activation this selectivity is largely determined by the latter only [96].

Several early HAPs yielded good results in *in vitro* tumor cell lines and *in vivo* preclinical animal models, however stranded in development during clinical trials due to disappointing results [97-103]. Several other HAPs are in different stages of clinical development [87, 104, 105]. Three of the most extensively investigated HAPs are tirapazamine, evofosfamide and PR-104.



**Figure 2:** General activation mechanism of hypoxia-activated prodrugs.

### Tirapazamine

Tirapazamine (TPZ) is an aromatic N-oxide, which is reduced by one-electron reductases to a radical species which, in hypoxic conditions, undergoes further spontaneous reactions to form DNA-damaging oxidizing hydroxyl or benzotriazinyl radicals [106]. TPZ reduced cell viability in a hypoxia selective manner in a range of cancer cell lines *in vitro*, and inhibited growth of a range of human tumor xenografts when combined with radiotherapy and cisplatin *in vivo* [107]. TPZ then entered clinical trials, in which it was investigated in phase 2 trials in combination therapies with cisplatin, etoposide and/or radiotherapy in several cancer types. Promising toxicity profiles and indicative anticancer effects were obtained in these trials [108-111], however several phase 3 clinical trials showed no beneficial effects

of adding TPZ to chemotherapy and/or radiotherapy in several cancer types [112-114]. It was found that TPZ is not able to reach deeply into severe hypoxic areas because it is too quickly metabolized in the surrounding, less hypoxic areas [115]. As such, TPZ has not made it into clinical practice.

### **Evofosfamide**

Evofosfamide (TH-302) is a 2-nitroimidazole, which is reduced by one-electron reductases to a radical anion. In hypoxic conditions, this radical anion intermediate is further reduced and/or fragmentizes to form bromo-isophosphoramidate mustard, a DNA-alkylating agent [116]. *In vivo*, evofosfamide has been shown to target hypoxic cells and enhance the therapeutic effects of doxorubicin and docetaxel in human tumor xenografts [117]. Moreover, induction of transient hypoxia sensitizes tumor xenografts to evofosfamide [118]. Several more *in vivo* human tumor xenograft studies showed that adding evofosfamide to a treatment with cytotoxic drugs, targeted therapeutics or radiotherapy increases anticancer effects and reduces repopulation of tumors by hypoxic cells after reoxygenation [119-125]. In phase 1 and 2 clinical trials, evofosfamide toxicity was manageable, and promising anti-tumor effects were observed in some patients treated with evofosfamide as a monotherapy or in combination with doxorubicin or gemcitabine [126-130]. However, two large-scale phase 3 trials combining evofosfamide with gemcitabine or doxorubicin recently showed no improved overall survival [131, 132]. Since then, clinical development of evofosfamide has slowed down.

### **PR-104**

PR-104 is a phosphate ester pre-prodrug that is converted to the prodrug PR-104A by phosphatase-mediated hydrolysis. This prodrug is then reduced by one- and/or two-electron reductases to the PR-104H (hydroxylamine) and PR-104M (amine) metabolites [133], which can kill cells by cross-linking the DNA. *In vitro* and *in vivo*, PR-104 was found to be selectively active in hypoxia in a range of cancer cell lines and human tumor xenografts [134]. A maximum tolerated dose was established in a phase 1 clinical trial, and a phase 2 trial combining PR-104 with gemcitabine or docetaxel in small cell lung cancer was initiated [135]. However, severe dose-limiting myelotoxicity was observed, and the trial was halted [135]. *In vitro* PR-104 was found to be activated in normoxia, and thus in an oxygen-insensitive manner, by the two-electron reductase aldo-keto reductase 1C3 (AKR1C3) [133, 136]. This is a likely explanation for the toxicity observed in afore-mentioned trial. In advanced hepatocellular carcinoma, the combination of PR-104 and sorafenib caused

significant thrombocytopenia and neutropenia [137]. This toxicity is explained by the fact that normally PR-104A undergoes glucuronidation leading to clearance from the blood plasma [138]. Glucuronidation is however compromised in patients with advanced hepatocellular carcinoma [137-139], thereby exacerbating PR-104 toxicity. Due to these toxic effects plasma exposure of PR-104A is insufficiently high [140-142], limiting its clinical applicability in solid tumors. Glucuronidation of PR-104A can also greatly suppress its nitroreduction and thereby limit its effectiveness [138]. Positive results were obtained in a phase 1/2 trial in acute myeloid leukemia (AML) and acute lymphoblastic leukemia (ALL), which are AKR1C3 positive, although no correlation was found between functional AKR1C3 and drug efficacy [143]. PR-104 could thus potentially be used in acute leukemias, which requires further investigation. However, the fact that PR-104 can be off-target activated in normoxia by AKR1C3 limits its use as a HAP in solid tumors. As for the other HAPs mentioned before, clinical development of PR-104 has largely halted. No HAP of the cytotoxin-releasing class has made it into clinical practice yet.

## Targeting the hypoxia molecular response

### The HIF pathway

Another way of targeting tumor hypoxia is to target its molecular response, e.g. targeting a hypoxia-inducible factor (HIF)-regulated protein which is implicated in cancer progression. The stabilization of HIF-1 $\alpha$  plays a key role in the adaptation of tumor cells to the hostile hypoxic environment [144, 145]. HIF-1 $\alpha$  is expressed in every tissue, however under normoxic conditions it is continuously hydroxylated by prolyl-hydroxylases (PHDs) using molecular oxygen as a co-factor [146, 147]. Hydroxylated HIF-1 $\alpha$  is recognized by the E3 ubiquitin ligase complex containing the von Hippel-Lindau tumor suppressor protein (pVHL), and rapidly proteasomally degraded with a half-life of <1 minute [148]. Hypoxia exposure, however, inhibits the functioning of PHDs, stabilizing HIF-1 $\alpha$  which can then dimerize with the constitutively expressed HIF-1 $\beta$ . This HIF protein complex translocates to the nucleus, where it interacts with co-factor P300 and binds to hypoxia-response element (HRE) regions, which are present in the promotor region of multiple (>100) genes [149]. As a result, these genes are transcribed and aid the cell in its survival in hypoxic conditions [144, 145]. For example, HIF regulates anaerobic energy production, induces extracellular acidity, and enhances angiogenesis via upregulation of glucose transporter 1 (GLUT1), monocarboxylate transporter 4 (MCT4) and vascular endothelial growth factor

(VEGF), respectively [149-151].

### **Carbonic anhydrase IX**

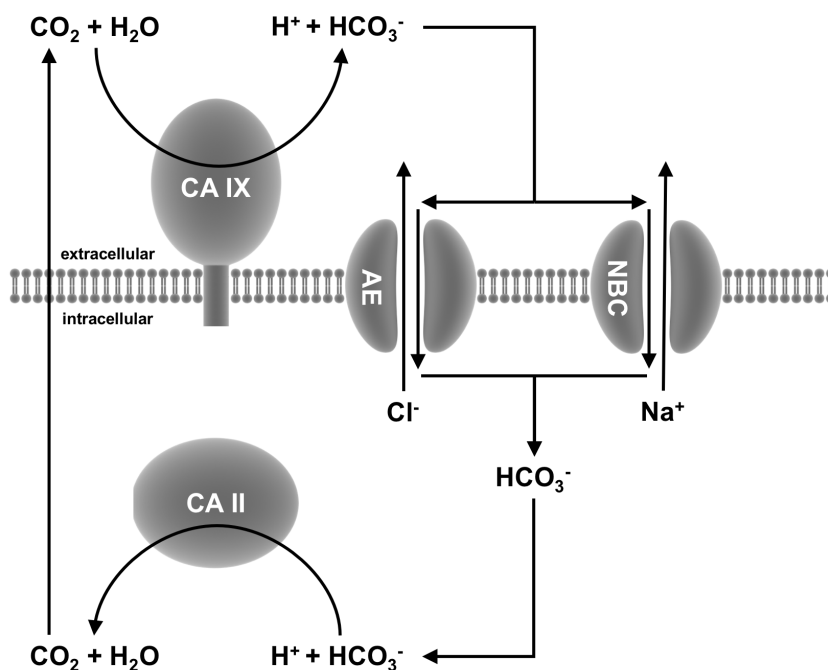
An HRE sequence is also present in the promotor region of the carbonic anhydrase 9 (*CA9*) gene, meaning that CA IX expression is mainly HIF regulated [152]. CA IX is a zinc-containing glycoprotein and belongs to the family of carbonic anhydrase enzymes [153, 154]. To date, 15 carbonic anhydrases have been discovered, all of which facilitate the hydration of carbon dioxide to bicarbonate and a proton, or vice versa. CA IX and CA XII are transmembrane proteins that are associated with cancer [155, 156]. CA IX expression is predominantly found in tumors, and only marginal CA IX expression can be found in normal tissues (in gastric, intestinal and gallbladder epithelia) [157]; therefore, CA IX expression serves as an endogenous hypoxia marker. Importantly, CA IX has been found to select for and to maintain an aggressive cancer cell phenotype and to promote metastasis formation. Hydration of carbon dioxide by CA IX leads to extracellular accumulation of protons, and thus extracellular acidification. This stimulates degradation of the extracellular matrix, thereby promoting tumor invasion [158]. The formed bicarbonate is transported back intracellular by sodium bicarbonate transporters (NBCs) or anion exchangers (AEs). CA II, forming a metabolon with CA IX, catalyzes the reaction of bicarbonate with an intracellular proton to carbon dioxide and water, creating a buffer system (Figure 3). Intracellular bicarbonate slightly alkalizes the intracellular environment, thereby promoting tumor cell proliferation and survival in the hostile extracellular acidic microenvironment [159-161]. Additionally, CA IX expression is associated with several stem cell markers [162], thus it may be involved in the maintenance of therapy resistant cancer stem cells. Moreover, CA IX was found to re-localize to the invading lamellipodia of migrating tumor cells due to its ability to maintain a proton gradient, facilitating invasion and metastasis formation [163]. Lastly, CA IX may also facilitate tumor cell migration via its glycosylated part which aids in cellular attachment [164, 165]. CA IX is thus a potential prognostic biomarker. Indeed, in a recent meta-analysis CA IX expression was found to be a negative prognostic factor in cancer patients regardless of the tumor type or site, or treatment [166]. For the very same reasons, CA IX is also an attractive target for anticancer treatment [167-171].

### **Carbonic anhydrase IX inhibitors in cancer treatment**

The CA IX-specific antibody girentuximab (G250) was the first CA IX inhibitor to go into clinical trials, however due to lack in efficacy its further clinical development was stopped [172, 173]. Another CA IX-specific antibody, VII/20, was shown to have anticancer effects

in an *in vivo* colorectal carcinoma xenograft model [174], but no further studies have been reported.

Several small molecule CA IX inhibitors have been identified, generally belonging to a variety of chemical classes, including the sulfonamides, sulfamates, sulfamides and coumarins [175-177]. Only few, however, have been investigated in *in vivo* animal models, and so far only one, SLC-0111, has made it into clinical trials [178]. *In vivo* SLC-0111 inhibited growth of CA IX- (or CA XII)-expressing tumors only [179, 180], and inhibited metastasis formation [179]. Results of a phase 1 clinical trial have not yet been published [181]. As it is the first small molecule CA IX inhibitor to be tested in a clinical trial, these results are eagerly awaited.



**Figure 3:** The CA IX-CA II metabolon, a buffer system that maintains intracellular pH. CA IX: carbonic anhydrase IX; CA II: carbonic anhydrase II; AE: anion exchanger; NBC: sodium bicarbonate transporter.

A rather new approach of targeting CA IX-expressing cells is to conjugate small molecule CA IX inhibitors to a cytotoxic agent, thereby specifically directing this agent to CA IX expressing (hypoxic, therapy resistant) cells. This is the so-called dual targeting approach. These drugs consist of different anticancer drugs, conjugated to a CA IX targeting moiety,

which should thus exert their effects specifically in CA IX expressing cells. This should increase tumor specificity of the parental drugs, increase drug concentrations in the tumor only, and potentially decrease normal tissue toxicity. Such a conjugate molecule, consisting of the cytotoxic agent mertansine (DM1, a tubulin inhibitor) conjugated to a acetazolamide derivative (general CA inhibitor), was recently shown to exhibit a potent antitumor effect *in vivo* [182].

Non-invasive detection of CA IX expression can aid in the successful development of CA IX targeting cancer treatments. A number of CA IX-specific imaging tracers has been developed and used for preclinical CA IX imaging [183]. Usually these tracers are antibodies, affibodies, or small molecule inhibitors, labeled with a fluorescent probe for fluorescent imaging, or with a radioactive probe for positron emission tomography (PET) imaging. None of these imaging tracers are currently being used in clinical practice.

Concluding, a few CA IX inhibitors and imaging agents are in different stages of clinical development, but none have been implemented into clinical practice yet.

## Outline of this thesis

Tumor hypoxia is a promising therapeutic target to exploit in cancer treatment, however, so far only one of these treatments (nimorazole) has made it into the clinical practice. Chapter 2 summarizes recent progress of several novel treatments targeting tumor hypoxia or its molecular response, including HAPs and monoclonal antibodies and small molecule inhibitors targeting CA IX. Detection of hypoxia or CA IX could aid in the decision of which patients would benefit from a hypoxia- or CA IX-targeting treatment, respectively. Chapter 2 summarizes several hypoxia imaging markers currently being evaluated in clinical trials, and outlines research performed on CA IX imaging tracers. Chapter 2 also proposes window-of-opportunity trials to implement non-invasive imaging as an important tool to prove anti-tumor efficacy of experimental drugs early during drug development. Furthermore, this thesis outlines research performed on novel CA IX-targeting imaging tracers and inhibitors. Chapter 3 describes the design, synthesis and biological evaluation of novel  $^{68}\text{Ga}$ -radiolabeled small-molecule sulfonamides targeting CA IX, intended to be used in PET imaging. Chapter 4 describes the design, synthesis and biological evaluation of novel dual targeting drugs, a new approach of delivering cytotoxic drugs to CA IX expressing cells. Chapter 5 describes the design, synthesis and biological evaluation of novel fluorinated high-affinity CA IX inhibitors.

No HAP has made it into clinical practice yet. The failure of several HAPs in clinical trials could partly be due to unsuccessful/insufficient patient selection and stratification. Chapter 6 proposes how future clinical HAP studies should be set up, to be able to correctly assess the effects of the HAP and to ensure that these promising new cancer treatments will be successfully translated to the clinic.

The fact that PR-104 can be off-target activated under normoxia by AKR1C3, and, possibly, its glucuronidation, limit its use as a HAP in solid tumors. To tackle these limitations, the PR-104 molecule was adjusted so that it cannot be activated by AKR1C3, and cannot be glucuronidated, resulting in the novel HAP CP-506. Chapter 7 describes the very first therapeutic results of this new compound as a monotherapy in *in vitro* 2D and 3D tumor cell culture, and in *in vivo* human tumor xenograft models. HAPs are mainly intended to be used in combination therapies, necessitated by the need to inactivate well-oxygenated cells as well, although interaction between CP-506 and other therapies is also expected apart from spatial cooperation. Chapter 8 describes the results of the combination of CP-

506 with radiotherapy and/or immunotherapy (L19-IL2), which was tested in *in vivo* animal models.

Lastly, Chapter 9 provides a general discussion of the work outlined in this thesis. Additionally, future directions on how to advance with these novel treatments are discussed.

**Table 1:** Schematic presentation of the outline of this thesis.

Exploiting tumor hypoxia for cancer treatment	
<u>Chapter 1:</u> General introduction	
<u>Chapter 2:</u> Recent progress in tumor hypoxia imaging and targeting	
Targeting CA IX	Using HAPs
<u>Chapter 3:</u> New CA IX PET imaging tracer	<u>Chapter 6:</u> Clinical HAP trial design
<u>Chapter 4:</u> New dual-target drugs targeting CA IX	<u>Chapter 7:</u> The new HAP CP-506 as monotherapy
<u>Chapter 5:</u> New CA IX inhibitors	<u>Chapter 8:</u> The new HAP CP-506 in combination therapies
<u>Chapter 9:</u> Discussion and future perspectives	

# References

1. Breasted, J.H., *The Edwin Smith Surgical papyrus*. special edition, 1984 ed. 1930, Chicago, Illinois: The University Chicago Press.
2. American Cancer Society. *Early History of Cancer*. 2014-12-06 Available from: <https://www.cancer.org/cancer/cancer-basics/history-of-cancer/what-is-cancer.html>.
3. *World Cancer Report 2014*. 2014, World Health Organization: Lyon.
4. Bray, F., et al., *Global cancer transitions according to the Human Development Index (2008-2030): a population-based study*. *Lancet Oncol*, 2012. **13**(8): p. 790-801.
5. Ferlay J, Soerjomataram I, Ervik M, Dikshit R, Eser S, Mathers C, Rebelo M, Parkin DM, Forman D, Bray, F. *GLOBOCAN 2012 v1.0, Cancer Incidence and Mortality Worldwide: IARC CancerBase No. 11*. [Internet] Lyon, France: International Agency for Research on Cancer; 2013 Available from: <http://globocan.iarc.fr>.
6. Anand, P., et al., *Cancer is a preventable disease that requires major lifestyle changes*. *Pharm Res*, 2008. **25**(9): p. 2097-116.
7. Hanahan, D. and R.A. Weinberg, *The hallmarks of cancer*. *Cell*, 2000. **100**(1): p. 57-70.
8. Hanahan, D. and R.A. Weinberg, *Hallmarks of cancer: the next generation*. *Cell*, 2011. **144**(5): p. 646-74.
9. Urruticoechea, A., et al., *Recent advances in cancer therapy: an overview*. *Curr Pharm Des*, 2010. **16**(1): p. 3-10.
10. Khalil, D.N., et al., *The future of cancer treatment: immunomodulation, CARs and combination immunotherapy*. *Nat Rev Clin Oncol*, 2016. **13**(5): p. 273-90.
11. Bayat Mokhtari, R., et al., *Combination therapy in combating cancer*. *Oncotarget*, 2017. **8**(23): p. 38022-38043.
12. Thomlinson, R.H. and L.H. Gray, *The histological structure of some human lung cancers and the possible implications for radiotherapy*. *Br J Cancer*, 1955. **9**(4): p. 539-49.
13. Forster, J.C., et al., *A review of the development of tumor vasculature and its effects on the tumor microenvironment*. *Hypoxia (Auckl)*, 2017. **5**: p. 21-32.
14. Ziyad, S. and M.L. Iruela-Arispe, *Molecular mechanisms of tumor angiogenesis*. *Genes Cancer*, 2011. **2**(12): p. 1085-96.
15. Carreau, A., et al., *Why is the partial oxygen pressure of human tissues a crucial parameter? Small molecules and hypoxia*. *J Cell Mol Med*, 2011. **15**(6): p. 1239-53.
16. Hockel, M. and P. Vaupel, *Tumor hypoxia: definitions and current clinical, biologic, and molecular aspects*. *J Natl Cancer Inst*, 2001. **93**(4): p. 266-76.
17. Tatum, J.L., et al., *Hypoxia: importance in tumor biology, noninvasive measurement by imaging, and value of its measurement in the management of cancer therapy*. *Int J Radiat Biol*, 2006. **82**(10): p. 699-757.
18. Nordmark, M., et al., *Prognostic value of tumor oxygenation in 397 head and neck tumors after primary radiation therapy. An international multi-center study*. *Radiother Oncol*, 2005. **77**(1): p. 18-24.
19. Luoto, K.R., R. Kumareswaran, and R.G. Bristow, *Tumor hypoxia as a driving force in genetic instability*. *Genome*

- Integr, 2013. **4**(1): p. 5.
20. Harris, A.L., *Hypoxia--a key regulatory factor in tumour growth*. Nat Rev Cancer, 2002. **2**(1): p. 38-47.
  21. Graeber, T.G., et al., *Hypoxia-mediated selection of cells with diminished apoptotic potential in solid tumours*. Nature, 1996. **379**(6560): p. 88-91.
  22. Viry, E., et al., *Autophagy: an adaptive metabolic response to stress shaping the antitumor immunity*. Biochem Pharmacol, 2014. **92**(1): p. 31-42.
  23. Sun, R.C. and N.C. Denko, *Hypoxic regulation of glutamine metabolism through HIF1 and SIAH2 supports lipid synthesis that is necessary for tumor growth*. Cell Metab, 2014. **19**(2): p. 285-92.
  24. Kucharzewska, P., H.C. Christianson, and M. Belting, *Global profiling of metabolic adaptation to hypoxic stress in human glioblastoma cells*. PLoS One, 2015. **10**(1): p. e0116740.
  25. Chang, Q., et al., *Hypoxia predicts aggressive growth and spontaneous metastasis formation from orthotopically grown primary xenografts of human pancreatic cancer*. Cancer Res, 2011. **71**(8): p. 3110-20.
  26. Gluck, A.A., et al., *Interplay between receptor tyrosine kinases and hypoxia signaling in cancer*. Int J Biochem Cell Biol, 2015. **62**: p. 101-14.
  27. Barsoum, I.B., et al., *A mechanism of hypoxia-mediated escape from adaptive immunity in cancer cells*. Cancer Res, 2014. **74**(3): p. 665-74.
  28. Intlekofer, A.M., et al., *Hypoxia Induces Production of L-2-Hydroxyglutarate*. Cell Metab, 2015. **22**(2): p. 304-11.
  29. Oldham, W.M., et al., *Hypoxia-Mediated Increases in L-2-hydroxyglutarate Coordinate the Metabolic Response to Reductive Stress*. Cell Metab, 2015. **22**(2): p. 291-303.
  30. Ye, J., et al., *The cancer stem cell niche: cross talk between cancer stem cells and their microenvironment*. Tumour Biol, 2014. **35**(5): p. 3945-51.
  31. Gray, L.H., et al., *The concentration of oxygen dissolved in tissues at the time of irradiation as a factor in radiotherapy*. Br J Radiol, 1953. **26**(312): p. 638-48.
  32. Hall, E.J. and A.J. Giaccia, *Radiobiology for the radiologist*. 6th ed. 2006, Philadelphia: Lippincott Williams & Wilkins. ix, 546 p.
  33. Tannock, I., *The basic science of oncology*. 5th ed. 2013, New York: McGraw-Hill. xi, 575 p.
  34. Hockel, M., et al., *Hypoxic cervical cancers with low apoptotic index are highly aggressive*. Cancer Res, 1999. **59**(18): p. 4525-8.
  35. Kim, C.Y., et al., *Selection of human cervical epithelial cells that possess reduced apoptotic potential to low-oxygen conditions*. Cancer Res, 1997. **57**(19): p. 4200-4.
  36. Samali, A. and T.G. Cotter, *Heat shock proteins increase resistance to apoptosis*. Exp Cell Res, 1996. **223**(1): p. 163-70.
  37. Zhivotovsky, B., B. Joseph, and S. Orrenius, *Tumor radiosensitivity and apoptosis*. Exp Cell Res, 1999. **248**(1): p. 10-7.
  38. Bedford, J.S. and J.B. Mitchell, *The effect of hypoxia on the growth and radiation response of mammalian cells in culture*. Br J Radiol, 1974. **47**(562): p. 687-96.
  39. Wike-Hooley, J.L., J. Haveman, and H.S. Reinhold, *The relevance of tumour pH to the treatment of malignant disease*.

- Radiother Oncol, 1984. **2**(4): p. 343-66.
40. Durand, R.E., *Keynote address: the influence of microenvironmental factors on the activity of radiation and drugs*. Int J Radiat Oncol Biol Phys, 1991. **20**(2): p. 253-8.
  41. Teicher, B.A., et al., *Classification of antineoplastic treatments by their differential toxicity toward putative oxygenated and hypoxic tumor subpopulations in vivo in the FSaIIc murine fibrosarcoma*. Cancer Res, 1990. **50**(11): p. 3339-44.
  42. Durand, R.E., *The influence of microenvironmental factors during cancer therapy*. In Vivo, 1994. **8**(5): p. 691-702.
  43. Anthoney, D.A., et al., *Microsatellite instability, apoptosis, and loss of p53 function in drug-resistant tumor cells*. Cancer Res, 1996. **56**(6): p. 1374-81.
  44. Sethi, T., et al., *Extracellular matrix proteins protect small cell lung cancer cells against apoptosis: a mechanism for small cell lung cancer growth and drug resistance in vivo*. Nat Med, 1999. **5**(6): p. 662-8.
  45. Hickman, J.A., et al., *Apoptosis and cancer chemotherapy*. Philos Trans R Soc Lond B Biol Sci, 1994. **345**(1313): p. 319-25.
  46. Rice, G.C., C. Hoy, and R.T. Schimke, *Transient hypoxia enhances the frequency of dihydrofolate reductase gene amplification in Chinese hamster ovary cells*. Proc Natl Acad Sci U S A, 1986. **83**(16): p. 5978-82.
  47. Mattern, J., et al., *Association of resistance-related protein expression with poor vascularization and low levels of oxygen in human rectal cancer*. Int J Cancer, 1996. **67**(1): p. 20-3.
  48. Ausserer, W.A., et al., *Regulation of c-jun expression during hypoxic and low-glucose stress*. Mol Cell Biol, 1994. **14**(8): p. 5032-42.
  49. Sakata, K., et al., *Hypoxia-induced drug resistance: comparison to P-glycoprotein-associated drug resistance*. Br J Cancer, 1991. **64**(5): p. 809-14.
  50. Wang, B., L. Hu, and T. Siahaan, *Drug delivery : principles and applications*. Second edition. ed. 2016, Hoboken, New Jersey: John Wiley & Sons Inc. xxii, 697 pages.
  51. Chaplin, D., et al., *Therapeutic significance of microenvironmental factors*. Blood Perfusion and Microenvironment of Human Tumors, 1998: p. 131-143.
  52. Chouaib, S., et al., *Hypoxic stress: obstacles and opportunities for innovative immunotherapy of cancer*. Oncogene, 2017. **36**(4): p. 439-445.
  53. Brizel, D.M., et al., *The mechanisms by which hyperbaric oxygen and carbogen improve tumour oxygenation*. Br J Cancer, 1995. **72**(5): p. 1120-4.
  54. Thews, O. and P. Vaupel, *Spatial oxygenation profiles in tumors during normo- and hyperbaric hyperoxia*. Strahlenther Onkol, 2015. **191**(11): p. 875-82.
  55. Stepien, K., R.P. Ostrowski, and E. Matyja, *Hyperbaric oxygen as an adjunctive therapy in treatment of malignancies, including brain tumours*. Med Oncol, 2016. **33**(9): p. 101.
  56. Moen, I. and L.E. Stuhr, *Hyperbaric oxygen therapy and cancer--a review*. Target Oncol, 2012. **7**(4): p. 233-42.
  57. Ravi, P., et al., *The role of hyperbaric oxygen therapy in the prevention and management of radiation-induced complications of the head and neck - a systematic review of literature*. J Stomatol Oral Maxillofac Surg, 2017. **118**(6): p.

- 359-362.
58. Borab, Z., et al., *Systematic review of hyperbaric oxygen therapy for the treatment of radiation-induced skin necrosis*. J Plast Reconstr Aesthet Surg, 2017. **70**(4): p. 529-538.
  59. Chaplin, D.J., M.R. Horsman, and M.J. Trotter, *Effect of nicotinamide on the microregional heterogeneity of oxygen delivery within a murine tumor*. J Natl Cancer Inst, 1990. **82**(8): p. 672-6.
  60. Horsman, M.R., D.J. Chaplin, and J. Overgaard, *Combination of nicotinamide and hyperthermia to eliminate radiore-sistant chronically and acutely hypoxic tumor cells*. Cancer Res, 1990. **50**(23): p. 7430-6.
  61. Martin, L., et al., *Changes in the oxygenation of head and neck tumors during carbogen breathing*. Radiother Oncol, 1993. **27**(2): p. 123-30.
  62. Bussink, J., et al., *Vascular architecture and microenvironmental parameters in human squamous cell carcinoma xenografts: effects of carbogen and nicotinamide*. Radiother Oncol, 1999. **50**(2): p. 173-84.
  63. Bussink, J., et al., *Effects of nicotinamide and carbogen on oxygenation in human tumor xenografts measured with luminescence based fiber-optic probes*. Radiother Oncol, 2000. **57**(1): p. 21-30.
  64. Rojas, A., et al., *Carbogen and nicotinamide as radiosensitizers in a murine mammary carcinoma using conventional and accelerated radiotherapy*. Int J Radiat Oncol Biol Phys, 1996. **34**(2): p. 357-65.
  65. Hoskin, P.J., et al., *Radiotherapy with concurrent carbogen and nicotinamide in bladder carcinoma*. J Clin Oncol, 2010. **28**(33): p. 4912-8.
  66. Janssens, G.O., et al., *Accelerated radiotherapy with carbogen and nicotinamide for laryngeal cancer: results of a phase III randomized trial*. J Clin Oncol, 2012. **30**(15): p. 1777-83.
  67. Kaanders, J.H., et al., *ARCON: experience in 215 patients with advanced head-and-neck cancer*. Int J Radiat Oncol Biol Phys, 2002. **52**(3): p. 769-78.
  68. Fylaktakidou, K.C., et al., *Inositol tripyrophosphate: a new membrane permeant allosteric effector of haemoglobin*. Bioorg Med Chem Lett, 2005. **15**(6): p. 1605-8.
  69. Limani, P., et al., *The Allosteric Hemoglobin Effector ITPP Inhibits Metastatic Colon Cancer in Mice*. Ann Surg, 2017. **266**(5): p. 746-753.
  70. Limani, P., et al., *Antihypoxic Potentiation of Standard Therapy for Experimental Colorectal Liver Metastasis through Myo-Inositol Trispyrophosphate*. Clin Cancer Res, 2016. **22**(23): p. 5887-5897.
  71. Aprahamian, M., et al., *Myo-InositolTrisPyroPhosphate treatment leads to HIF-1alpha suppression and eradication of early hepatoma tumors in rats*. Chembiochem, 2011. **12**(5): p. 777-83.
  72. Derbal-Wolfrom, L., et al., *Increasing the oxygen load by treatment with myo-inositol trispyrophosphate reduces growth of colon cancer and modulates the intestine homeobox gene Cdx2*. Oncogene, 2013. **32**(36): p. 4313-8.
  73. Kieda, C., et al., *Stable tumor vessel normalization with pO<sub>2</sub> increase and endothelial PTEN activation by inositol trispyrophosphate brings novel tumor treatment*. J Mol Med (Berl), 2013. **91**(7): p. 883-99.
  74. Raykov, Z., et al., *Myo-inositol trispyrophosphate-mediated hypoxia reversion controls pancreatic cancer in rodents and enhances gemcitabine efficacy*. Int J Cancer, 2014. **134**(11): p. 2572-82.

75. Sihn, G., et al., *Anti-angiogenic properties of myo-inositol trispyrophosphate in ovo and growth reduction of implanted glioma*. FEBS Lett, 2007. **581**(5): p. 962-6.
76. Fornvik, K., et al., *ITPP Treatment of RG2 Glioblastoma in a Rat Model*. Anticancer Res, 2016. **36**(11): p. 5751-5755.
77. Ignat, M., et al., *Development of a methodology for in vivo follow-up of hepatocellular carcinoma in hepatocyte specific Trim24-null mice treated with myo-inositol trispyrophosphate*. J Exp Clin Cancer Res, 2016. **35**(1): p. 155.
78. Limani, P., et al., *Development of OXY111A, a novel hypoxia-modifier as a potential antitumor agent in patients with hepato-pancreato-biliary neoplasms - Protocol of a first Ib/IIa clinical trial*. BMC Cancer, 2016. **16**(1): p. 812.
79. Iyengar, S. and D. Schwartz, *Failure of Inositol Trispyrophosphate to Enhance Highly Effective Radiotherapy of GL261 Glioblastoma in Mice*. Anticancer Res, 2017. **37**(3): p. 1121-1125.
80. Wardman, P., *Chemical radiosensitizers for use in radiotherapy*. Clin Oncol (R Coll Radiol), 2007. **19**(6): p. 397-417.
81. Overgaard, J., *Clinical evaluation of nitroimidazoles as modifiers of hypoxia in solid tumors*. Oncol Res, 1994. **6**(10-11): p. 509-18.
82. Grigsby, P.W., et al., *Irradiation with or without misonidazole for patients with stages IIIB and IVA carcinoma of the cervix: final results of RTOG 80-05*. Radiation Therapy Oncology Group. Int J Radiat Oncol Biol Phys, 1999. **44**(3): p. 513-7.
83. Saunders, M. and S. Dische, *Clinical results of hypoxic cell radiosensitisation from hyperbaric oxygen to accelerated radiotherapy, carbogen and nicotinamide*. Br J Cancer Suppl, 1996. **27**: p. S271-8.
84. Lee, D.J., et al., *Results of an RTOG phase III trial (RTOG 85-27) comparing radiotherapy plus etanidazole with radiotherapy alone for locally advanced head and neck carcinomas*. Int J Radiat Oncol Biol Phys, 1995. **32**(3): p. 567-76.
85. Overgaard, J., et al., *A randomized double-blind phase III study of nimorazole as a hypoxic radiosensitizer of primary radiotherapy in supraglottic larynx and pharynx carcinoma. Results of the Danish Head and Neck Cancer Study (DAHANCA) Protocol 5-85*. Radiother Oncol, 1998. **46**(2): p. 135-46.
86. Overgaard, J., et al., *Plasma osteopontin, hypoxia, and response to the hypoxia sensitizer nimorazole in radiotherapy of head and neck cancer: results from the DAHANCA 5 randomised double-blind placebo-controlled trial*. Lancet Oncol, 2005. **6**(10): p. 757-64.
87. Mistry, I.N., et al., *Clinical Advances of Hypoxia-Activated Prodrugs in Combination With Radiation Therapy*. Int J Radiat Oncol Biol Phys, 2017. **98**(5): p. 1183-1196.
88. Toustrup, K., et al., *Validation of a 15-gene hypoxia classifier in head and neck cancer for prospective use in clinical trials*. Acta Oncol, 2016. **55**(9-10): p. 1091-1098.
89. Eustace, A., et al., *A 26-gene hypoxia signature predicts benefit from hypoxia-modifying therapy in laryngeal cancer but not bladder cancer*. Clin Cancer Res, 2013. **19**(17): p. 4879-88.
90. Uto, Y., et al., *Design of antiangiogenic hypoxic cell radiosensitizers: 2-nitroimidazoles containing a 2-aminomethylene-4-cyclopentene-1,3-dione moiety*. Bioorg Med Chem, 2008. **16**(11): p. 6042-53.
91. Nakae, T., et al., *Design, synthesis, and radiosensitizing activities of sugar-hybrid hypoxic cell radiosensitizers*. Bioorg Med Chem, 2008. **16**(2): p. 675-82.

92. Bonnet, M., et al., *Next-Generation Hypoxic Cell Radiosensitizers: Nitroimidazole Alkylsulfonamides*. J Med Chem, 2018.
93. Phillips, R.M., *Targeting the hypoxic fraction of tumours using hypoxia-activated prodrugs*. Cancer Chemother Pharmacol, 2016. **77**(3): p. 441-57.
94. Denny, W.A., W.R. Wilson, and M.P. Hay, *Recent developments in the design of bioreductive drugs*. Br J Cancer Suppl, 1996. **27**: p. S32-8.
95. Wilson, W.R. and M.P. Hay, *Targeting hypoxia in cancer therapy*. Nat Rev Cancer, 2011. **11**(6): p. 393-410.
96. Workman, P., *Enzyme-directed bioreductive drug development revisited: a commentary on recent progress and future prospects with emphasis on quinone anticancer agents and quinone metabolizing enzymes, particularly DT-diaphorase*. Oncol Res, 1994. **6**(10-11): p. 461-75.
97. Kappen, L.S., et al., *Oxygen transfer from the nitro group of a nitroaromatic radiosensitizer to a DNA sugar damage product*. Biochemistry, 1989. **28**(11): p. 4540-2.
98. Dische, S., *Chemical sensitizers for hypoxic cells: a decade of experience in clinical radiotherapy*. Radiother Oncol, 1985. **3**(2): p. 97-115.
99. Dische, S., et al., *Clinical testing of the radiosensitizer Ro 07-0582: experience with multiple doses*. Br J Cancer, 1977. **35**(5): p. 567-79.
100. Urtasun, R., et al., *Radiation and nitroimidazoles in supratentorial high grade gliomas: a second clinical trial*. Br J Cancer, 1982. **46**(1): p. 101-8.
101. Dische, S., et al., *A trial of Ro 03-8799 (pimonidazole) in carcinoma of the uterine cervix: an interim report from the Medical Research Council Working Party on advanced carcinoma of the cervix*. Radiotherapy and Oncology. **26**(2): p. 93-103.
102. Urtasun, R.C., et al., *Intervention with the hypoxic tumor cell sensitizer etanidazole in the combined modality treatment of limited stage small-cell lung cancer. A one-institution study*. Int J Radiat Oncol Biol Phys, 1998. **40**(2): p. 337-42.
103. Eschwege, F., et al., *Results of a European randomized trial of Etanidazole combined with radiotherapy in head and neck carcinomas*. Int J Radiat Oncol Biol Phys, 1997. **39**(2): p. 275-81.
104. Hunter, F.W., B.G. Wouters, and W.R. Wilson, *Hypoxia-activated prodrugs: paths forward in the era of personalised medicine*. Br J Cancer, 2016. **114**(10): p. 1071-7.
105. Wigerup, C., S. Pahlman, and D. Bexell, *Therapeutic targeting of hypoxia and hypoxia-inducible factors in cancer*. Pharmacol Ther, 2016. **164**: p. 152-69.
106. Shinde, S.S., et al., *Spin trapping of radicals other than the \*OH radical upon reduction of the anticancer agent tirapazamine by cytochrome P450 reductase*. J Am Chem Soc, 2009. **131**(40): p. 14220-1.
107. Marcu, L. and I. Olver, *Tirapazamine: from bench to clinical trials*. Curr Clin Pharmacol, 2006. **1**(1): p. 71-9.
108. Le, Q.T., et al., *Phase II study of tirapazamine, cisplatin, and etoposide and concurrent thoracic radiotherapy for limited-stage small-cell lung cancer: SWOG 0222*. J Clin Oncol, 2009. **27**(18): p. 3014-9.

109. Miller, V.A., et al., *Phase II study of the combination of the novel bioreductive agent, tirapazamine, with cisplatin in patients with advanced non-small-cell lung cancer*. *Ann Oncol*, 1997. **8**(12): p. 1269-71.
110. Rischin, D., et al., *Tirapazamine, Cisplatin, and Radiation versus Fluorouracil, Cisplatin, and Radiation in patients with locally advanced head and neck cancer: a randomized phase II trial of the Trans-Tasman Radiation Oncology Group (TROG 98.02)*. *J Clin Oncol*, 2005. **23**(1): p. 79-87.
111. Treat, J., et al., *Tirapazamine with cisplatin in patients with advanced non-small-cell lung cancer: a phase II study*. *J Clin Oncol*, 1998. **16**(11): p. 3524-7.
112. Williamson, S.K., et al., *Phase III trial of paclitaxel plus carboplatin with or without tirapazamine in advanced non-small-cell lung cancer: Southwest Oncology Group Trial S0003*. *J Clin Oncol*, 2005. **23**(36): p. 9097-104.
113. Rischin, D., et al., *Tirapazamine, cisplatin, and radiation versus cisplatin and radiation for advanced squamous cell carcinoma of the head and neck (TROG 02.02, HeadSTART): a phase III trial of the Trans-Tasman Radiation Oncology Group*. *J Clin Oncol*, 2010. **28**(18): p. 2989-95.
114. DiSilvestro, P.A., et al., *Phase III randomized trial of weekly cisplatin and irradiation versus cisplatin and tirapazamine and irradiation in stages IB2, IIA, IIB, IIB, and IVA cervical carcinoma limited to the pelvis: a Gynecologic Oncology Group study*. *J Clin Oncol*, 2014. **32**(5): p. 458-64.
115. Hicks, K.O., et al., *Multicellular resistance to tirapazamine is due to restricted extravascular transport: a pharmacokinetic/pharmacodynamic study in HT29 multicellular layer cultures*. *Cancer Res*, 2003. **63**(18): p. 5970-7.
116. Meng, F., et al., *Molecular and cellular pharmacology of the hypoxia-activated prodrug TH-302*. *Mol Cancer Ther*, 2012. **11**(3): p. 740-51.
117. Saggar, J.K. and I.F. Tannock, *Activity of the hypoxia-activated pro-drug TH-302 in hypoxic and perivascular regions of solid tumors and its potential to enhance therapeutic effects of chemotherapy*. *Int J Cancer*, 2014. **134**(11): p. 2726-34.
118. Wojtkowiak, J.W., et al., *Pyruvate sensitizes pancreatic tumors to hypoxia-activated prodrug TH-302*. *Cancer Metab*, 2015. **3**(1): p. 2.
119. Hu, J., et al., *Synergistic induction of apoptosis in multiple myeloma cells by bortezomib and hypoxia-activated pro-drug TH-302, in vivo and in vitro*. *Mol Cancer Ther*, 2013. **12**(9): p. 1763-73.
120. Liapis, V., et al., *Hypoxia-activated pro-drug TH-302 exhibits potent tumor suppressive activity and cooperates with chemotherapy against osteosarcoma*. *Cancer Lett*, 2015. **357**(1): p. 160-9.
121. Meng, F., et al., *Enhancement of hypoxia-activated prodrug TH-302 anti-tumor activity by Chk1 inhibition*. *BMC Cancer*, 2015. **15**: p. 422.
122. Peeters, S.G., et al., *TH-302 in Combination with Radiotherapy Enhances the Therapeutic Outcome and Is Associated with Pretreatment [18F]HX4 Hypoxia PET Imaging*. *Clin Cancer Res*, 2015. **21**(13): p. 2984-92.
123. Saggar, J.K. and I.F. Tannock, *Chemotherapy Rescues Hypoxic Tumor Cells and Induces Their Reoxygenation and Repopulation-An Effect That Is Inhibited by the Hypoxia-Activated Prodrug TH-302*. *Clin Cancer Res*, 2015. **21**(9): p. 2107-14.

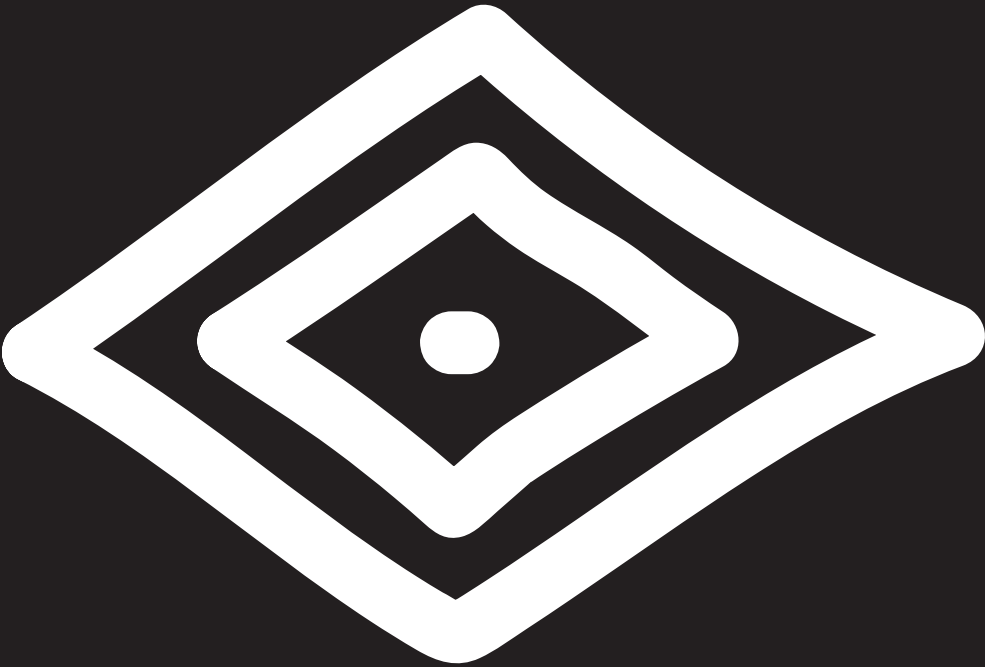
124. Sun, J.D., et al., *Efficacy and safety of the hypoxia-activated prodrug TH-302 in combination with gemcitabine and nab-paclitaxel in human tumor xenograft models of pancreatic cancer*. *Cancer Biol Ther*, 2015. **16**(3): p. 438-49.
125. Yoon, C., et al., *Hypoxia-activated chemotherapeutic TH-302 enhances the effects of VEGF-A inhibition and radiation on sarcomas*. *Br J Cancer*, 2015. **113**(1): p. 46-56.
126. Ganjoo, K.N., et al., *A phase I study of the safety and pharmacokinetics of the hypoxia-activated prodrug TH-302 in combination with doxorubicin in patients with advanced soft tissue sarcoma*. *Oncology*, 2011. **80**(1-2): p. 50-6.
127. Weiss, G.J., et al., *Phase 1 study of the safety, tolerability, and pharmacokinetics of TH-302, a hypoxia-activated prodrug, in patients with advanced solid malignancies*. *Clin Cancer Res*, 2011. **17**(9): p. 2997-3004.
128. Weiss, G.J., et al., *Resolution of Cullen's sign in patient with metastatic melanoma responding to hypoxia-activated prodrug TH-302*. *Dermatol Reports*, 2011. **3**(3): p. e56.
129. Chawla, S.P., et al., *Phase II study of the safety and antitumor activity of the hypoxia-activated prodrug TH-302 in combination with doxorubicin in patients with advanced soft tissue sarcoma*. *J Clin Oncol*, 2014. **32**(29): p. 3299-306.
130. Borad, M.J., et al., *Randomized Phase II Trial of Gemcitabine Plus TH-302 Versus Gemcitabine in Patients With Advanced Pancreatic Cancer*. *J Clin Oncol*, 2015. **33**(13): p. 1475-81.
131. Tap, W.D., et al., *Doxorubicin plus evofosfamide versus doxorubicin alone in locally advanced, unresectable or metastatic soft-tissue sarcoma (TH CR-406/SARC021): an international, multicentre, open-label, randomised phase 3 trial*. *Lancet Oncol*, 2017. **18**(8): p. 1089-1103.
132. *Clinical Trial Testing TH-302 in Combination With Gemcitabine in Previously Untreated Subjects With Metastatic or Locally Advanced Unresectable Pancreatic Adenocarcinoma*. Available from: <https://ClinicalTrials.gov/show/NCT01746979>.
133. Guise, C.P., et al., *The bioreductive prodrug PR-104A is activated under aerobic conditions by human aldo-keto reductase 1C3*. *Cancer Res*, 2010. **70**(4): p. 1573-84.
134. Patterson, A.V., et al., *Mechanism of action and preclinical antitumor activity of the novel hypoxia-activated DNA cross-linking agent PR-104*. *Clin Cancer Res*, 2007. **13**(13): p. 3922-32.
135. McKeage, M.J., et al., *PR-104 a bioreductive pre-prodrug combined with gemcitabine or docetaxel in a phase Ib study of patients with advanced solid tumours*. *BMC Cancer*, 2012. **12**: p. 496.
136. Guise, C.P., et al., *Identification of human reductases that activate the dinitrobenzamide mustard prodrug PR-104A: a role for NADPH:cytochrome P450 oxidoreductase under hypoxia*. *Biochem Pharmacol*, 2007. **74**(6): p. 810-20.
137. Abou-Alfa, G.K., et al., *PR-104 plus sorafenib in patients with advanced hepatocellular carcinoma*. *Cancer Chemother Pharmacol*, 2011. **68**(2): p. 539-45.
138. Gu, Y., M.D. Tingle, and W.R. Wilson, *Glucuronidation of anticancer prodrug PR-104A: species differences, identification of human UDP-glucuronosyltransferases, and implications for therapy*. *J Pharmacol Exp Ther*, 2011. **337**(3): p. 692-702.
139. Abbattista, M.R., et al., *Pre-clinical activity of PR-104 as monotherapy and in combination with sorafenib in hepatocellular carcinoma*. *Cancer Biol Ther*, 2015. **16**(4): p. 610-22.

140. Jameson, M.B., et al., *A phase I trial of PR-104, a nitrogen mustard prodrug activated by both hypoxia and aldo-keto reductase 1C3, in patients with solid tumors*. *Cancer Chemother Pharmacol*, 2010. **65**(4): p. 791-801.
141. McKeage, M.J., et al., *A phase I trial of PR-104, a pre-prodrug of the bioreductive prodrug PR-104A, given weekly to solid tumour patients*. *BMC Cancer*, 2011. **11**: p. 432.
142. Patel, K., et al., *A combined pharmacokinetic model for the hypoxia-targeted prodrug PR-104A in humans, dogs, rats and mice predicts species differences in clearance and toxicity*. *Cancer Chemother Pharmacol*, 2011. **67**(5): p. 1145-55.
143. Konopleva, M., et al., *Phase I/II study of the hypoxia-activated prodrug PR104 in refractory/relapsed acute myeloid leukemia and acute lymphoblastic leukemia*. *Haematologica*, 2015. **100**(7): p. 927-34.
144. Denko, N.C., *Hypoxia, HIF1 and glucose metabolism in the solid tumour*. *Nat Rev Cancer*, 2008. **8**(9): p. 705-13.
145. Wouters, B.G. and M. Koritzinsky, *Hypoxia signalling through mTOR and the unfolded protein response in cancer*. *Nat Rev Cancer*, 2008. **8**(11): p. 851-64.
146. Berra, E., et al., *HIF prolyl-hydroxylase 2 is the key oxygen sensor setting low steady-state levels of HIF-1alpha in normoxia*. *EMBO J*, 2003. **22**(16): p. 4082-90.
147. Semenza, G.L., *Hydroxylation of HIF-1: oxygen sensing at the molecular level*. *Physiology (Bethesda)*, 2004. **19**: p. 176-82.
148. Yu, A.Y., et al., *Temporal, spatial, and oxygen-regulated expression of hypoxia-inducible factor-1 in the lung*. *Am J Physiol*, 1998. **275**(4 Pt 1): p. L818-26.
149. Liu, W., et al., *Targeted genes and interacting proteins of hypoxia inducible factor-1*. *Int J Biochem Mol Biol*, 2012. **3**(2): p. 165-78.
150. Neri, D. and C.T. Supuran, *Interfering with pH regulation in tumours as a therapeutic strategy*. *Nat Rev Drug Discov*, 2011. **10**(10): p. 767-77.
151. Parks, S.K., J. Chiche, and J. Pouyssegur, *pH control mechanisms of tumor survival and growth*. *J Cell Physiol*, 2011. **226**(2): p. 299-308.
152. Wykoff, C.C., et al., *Hypoxia-inducible expression of tumor-associated carbonic anhydrases*. *Cancer Res*, 2000. **60**(24): p. 7075-83.
153. Sedlakova, O., et al., *Carbonic anhydrase IX, a hypoxia-induced catalytic component of the pH regulating machinery in tumors*. *Front Physiol*, 2014. **4**: p. 400.
154. Pastorek, J., et al., *Cloning and characterization of MN, a human tumor-associated protein with a domain homologous to carbonic anhydrase and a putative helix-loop-helix DNA binding segment*. *Oncogene*, 1994. **9**(10): p. 2877-88.
155. Alterio, V., et al., *Multiple binding modes of inhibitors to carbonic anhydrases: how to design specific drugs targeting 15 different isoforms?* *Chem Rev*, 2012. **112**(8): p. 4421-68.
156. Supuran, C.T., *Carbonic anhydrases: novel therapeutic applications for inhibitors and activators*. *Nat Rev Drug Discov*, 2008. **7**(2): p. 168-81.
157. Pastorekova, S., et al., *Carbonic anhydrase IX, MN/CA IX: analysis of stomach complementary DNA sequence and ex-*

- pression in human and rat alimentary tracts. Gastroenterology*, 1997. **112**(2): p. 398-408.
158. Stock, C. and A. Schwab, *Protons make tumor cells move like clockwork. Pflugers Arch*, 2009. **458**(5): p. 981-92.
159. Swietach, P., et al., *Tumor-associated carbonic anhydrase 9 spatially coordinates intracellular pH in three-dimensional multicellular growths. J Biol Chem*, 2008. **283**(29): p. 20473-83.
160. Swietach, P., et al., *The role of carbonic anhydrase 9 in regulating extracellular and intracellular pH in three-dimensional tumor cell growths. J Biol Chem*, 2009. **284**(30): p. 20299-310.
161. McIntyre, A., et al., *Disrupting Hypoxia-Induced Bicarbonate Transport Acidifies Tumor Cells and Suppresses Tumor Growth. Cancer Res*, 2016. **76**(13): p. 3744-55.
162. Lock, F.E., et al., *Targeting carbonic anhydrase IX depletes breast cancer stem cells within the hypoxic niche. Oncogene*, 2013. **32**(44): p. 5210-9.
163. Svastova, E., et al., *Carbonic anhydrase IX interacts with bicarbonate transporters in lamellipodia and increases cell migration via its catalytic domain. J Biol Chem*, 2012. **287**(5): p. 3392-402.
164. Zavada, J., et al., *Human tumour-associated cell adhesion protein MN/CA IX: identification of M75 epitope and of the region mediating cell adhesion. Br J Cancer*, 2000. **82**(11): p. 1808-13.
165. Csaderova, L., et al., *The effect of carbonic anhydrase IX on focal contacts during cell spreading and migration. Front Physiol*, 2013. **4**: p. 271.
166. van Kuijk, S.J., et al., *Prognostic Significance of Carbonic Anhydrase IX Expression in Cancer Patients: A Meta-Analysis. Front Oncol*, 2016. **6**: p. 69.
167. Wykoff, C.C., et al., *Expression of the hypoxia-inducible and tumor-associated carbonic anhydrases in ductal carcinoma in situ of the breast. Am J Pathol*, 2001. **158**(3): p. 1011-9.
168. Smeland, E., et al., *Prognostic impacts of hypoxic markers in soft tissue sarcoma. Sarcoma*, 2012. **2012**: p. 541650.
169. Stewart, D.J., et al., *Membrane carbonic anhydrase IX expression and relapse risk in resected stage I-II non-small-cell lung cancer. J Thorac Oncol*, 2014. **9**(5): p. 675-84.
170. Kim, S.J., et al., *Prognostic value of carbonic anhydrase IX and Ki-67 expression in squamous cell carcinoma of the tongue. Jpn J Clin Oncol*, 2007. **37**(11): p. 812-9.
171. Douglas, C.M., et al., *Lack of prognostic effect of carbonic anhydrase-9, hypoxia inducible factor-1alpha and bcl-2 in 286 patients with early squamous cell carcinoma of the glottic larynx treated with radiotherapy. Clin Oncol (R Coll Radiol)*, 2013. **25**(1): p. 59-65.
172. Siebels, M., et al., *A clinical phase I/II trial with the monoclonal antibody cG250 (RENCAREX(R)) and interferon-alpha-2a in metastatic renal cell carcinoma patients. World J Urol*, 2011. **29**(1): p. 121-6.
173. Chamie, K., et al., *Adjuvant Weekly Girentuximab Following Nephrectomy for High-Risk Renal Cell Carcinoma: The ARISER Randomized Clinical Trial. JAMA Oncol*, 2017. **3**(7): p. 913-920.
174. Zatovicova, M., et al., *Carbonic anhydrase IX as an anticancer therapy target: preclinical evaluation of internalizing monoclonal antibody directed to catalytic domain. Curr Pharm Des*, 2010. **16**(29): p. 3255-63.
175. Supuran, C.T., *How many carbonic anhydrase inhibition mechanisms exist? J Enzyme Inhib Med Chem*, 2016. **31**(3):

- p. 345-60.
176. Supuran, C.T., *Advances in structure-based drug discovery of carbonic anhydrase inhibitors*. Expert Opin Drug Discov, 2017. **12**(1): p. 61-88.
177. Supuran, C.T., *Structure-based drug discovery of carbonic anhydrase inhibitors*. J Enzyme Inhib Med Chem, 2012. **27**(6): p. 759-72.
178. Supuran, C.T., *Carbonic Anhydrase Inhibition and the Management of Hypoxic Tumors*. Metabolites, 2017. **7**(3).
179. Lou, Y., et al., *Targeting tumor hypoxia: suppression of breast tumor growth and metastasis by novel carbonic anhydrase IX inhibitors*. Cancer Res, 2011. **71**(9): p. 3364-76.
180. Pacchiano, F., et al., *Ureido-substituted benzenesulfonamides potently inhibit carbonic anhydrase IX and show anti-metastatic activity in a model of breast cancer metastasis*. J Med Chem, 2011. **54**(6): p. 1896-902.
181. *Safety Study of SLC-0111 in Subjects With Advanced Solid Tumours*. Available from: <https://ClinicalTrials.gov/show/NCT02215850>.
182. Krall, N., et al., *A small-molecule drug conjugate for the treatment of carbonic anhydrase IX expressing tumors*. Angew Chem Int Ed Engl, 2014. **53**(16): p. 4231-5.
183. Kazokaite, J., et al., *An update on anticancer drug development and delivery targeting carbonic anhydrase IX*. PeerJ, 2017. **5**: p. e4068.





# CHAPTER 2

## New ways to image and target tumor hypoxia and its molecular responses

Ludwig J. Dubois, **Raymon Niemans**, Simon J.A. van Kuijk, Kranthi M. Panth, Nanda-Kumar Parvathaneni, Sarah G.J.A. Peeters, Catharina M.L. Zegers, Nicolle H. Rekers, Marike W. van Gisbergen, Rianne Biemans, Natasja G. Lieuwes, Linda Spiegelberg, Ala Yaromina, Jean-Yves Winum, Marc Vooijs, Philippe Lambin

**Previously published:**

Dubois, L.J., *et al.*, New ways to image and target tumour hypoxia and its molecular responses. *Radiother Oncol*, 2015. 116(3): p. 352-7.

## Abstract

Tumour hypoxia and its molecular responses have been shown to be associated with poor prognosis. Detection of hypoxia, preferably in a non-invasive manner, could therefore predict treatment outcome and serve as a tool to individualize treatment. This review gives an overview of recent literature on hypoxia imaging markers currently used in clinical trials. Furthermore, recent progress made in targeting hypoxia (hypoxia-activated prodrugs) or hypoxia response (carbonic anhydrase IX inhibitors) is summarized. Last, window-of-opportunity trials implementing non-invasive imaging are proposed as an important tool to prove anti-tumour efficacy of experimental drugs early during drug development.

## Introduction

It is well established that tumours are not a collection of relatively homogeneous cancer cells, but act as organs with a complexity that might even exceed that of healthy tissues. Therefore to understand the biology of a tumour both the different individual cell types within a tumour as well as its microenvironment need to be studied [1]. Within this review, we will focus on hypoxia, a common characteristic of solid tumours, which has been associated with poor prognosis [2]. Detection of hypoxia, preferably in a non-invasive manner, could predict treatment outcome and serve as a tool to support treatment decisions. Such non-invasive imaging approaches that are routinely available in clinical practice including positron emission tomography (PET), magnetic resonance imaging (MRI) and perfusion computed tomography (CT) are able to accurately and reliably image hypoxia in tumours. Over the last decade, these diagnostic techniques are developing into versatile tools integrated in treatment monitoring, outcome prediction and treatment targeting. A meta-analysis evaluating the relationship between hypoxia imaging and outcome after radiation treatment demonstrated a uniform tendency for poor response when tumours were hypoxic. This was not only observed for widely used hypoxic PET tracers, but also when hypoxia was indirectly evaluated using perfusion-CT or DCE-MRI [3].

While the prognostic significance of tumoural hypoxia on outcome has been established more than two decades ago only recently compounds are being tested in clinical trials that enable monitoring and selective elimination of hypoxic tumours cells. Here we will provide an update on the current status of hypoxia imaging agents and strategies to combat tumour hypoxia.

## Hypoxia PET imaging tracers

Multiple PET tracers suitable for the detection of hypoxia have been developed, validated and shown to exhibit different characteristics. The ideal hypoxia tracer has complete clearance of unbound tracer at time of imaging, thus only bound in oxygen deprived tissues resulting in high signal to noise ratios [3]. We recently reviewed the PET hypoxia tracers that were validated in preclinical and clinical studies and reported accurate quantification methods and clinical applications [4]. The most investigated PET hypoxia tracer is fluoromisonidazole (FMISO). However, due to concerns regarding FMISO stability, metabolite

formation and slow clearance properties [5,6], alternative hypoxia PET tracers with different clearance and hydrophilicity characteristics have been developed trying to overcome these limitations: fluoroazomycin arabinoside (FAZA), fluoroerythronitroimidazole (FETNIM) and fluorinated etanidazole derivatives (EF1, EF3, EF5), which all have been extensively reviewed previously [3,4,7].

More recently, the hydrophilic flortanidazole (HX4), with preferred pharmacokinetics and clearance properties, has been synthesized through click-chemistry [8] showing 82% intact and 84% unmetabolized tracer at 2 h post injection (h p.i.) in plasma and urine respectively [9]. HX4 has been evaluated in a preclinical rhabdomyosarcoma rat tumour model, where binding was causally dependent on tumoural oxygenation status. Furthermore, a significant spatial relationship at tumour-microregional level between HX4 distribution and the exogenous hypoxia marker pimonidazole staining was observed [10,11]. Studies in primates and healthy volunteers [9] and in patients with histologically proven solid cancer [12] provided evidence for a good safety profile. Recently, in non-small cell lung cancer patients, image contrast was found to be superior 4 h p.i. compared with earlier time points and uptake patterns were strongly correlated between two scans [13]. Overlap studies between HX4 and the metabolism tracer FDG indicated that on average 24% of the hypoxic volume is outside the FDG volume [14]. Similar results have been obtained for head and neck cancer patients [15], suggesting that hypoxia PET imaging provides complementary information to FDG imaging.

Due to the large heterogeneity in uptake, differences in tumour and animal models, different time points of imaging and anaesthesia observed in the literature, it is difficult to compare different hypoxia markers. Although characterization of new hypoxia markers should be preferably performed in multiple cancer models, highly additive data can be expected from comparisons of different tracers within the same tumour models [3,11]. Recently, we performed a comparative study characterizing the clinically approved hypoxia markers FMISO, FAZA and HX4 on tumour to blood ratio (TBR), reproducibility and reversibility within a rat rhabdomyosarcoma model [16]. Blood clearance for FAZA and HX4 became similar 3 h p.i., while for FMISO as expected clearance from normal tissues was significantly lower. Differences in tumour uptake resulted in significantly higher TBR for HX4 compared to the other tracers. Reproducibility and spatial overlap between two PET acquisitions over a 48 h time period was high for both FMISO and HX4. Furthermore, decreasing the hypoxic fraction using carbogen resulted in loss of FMISO uptake, while

increased hypoxia achieved by breathing 7% oxygen, further enhanced FAZA and HX4 uptake. Another study performed a similar comparison in a SQ20b head and neck xenograft mouse model and found similar tumour to muscle ratios for FMISO, FAZA and HX4 [10]. However, these results were obtained at 80-90 min p.i., a time point which is probably too early for evaluation since normal tissue clearance is still ongoing. A comparative study in head and neck cancer patients found similar tumour to muscle ratios for HX4 imaging at 1.5 h p.i. and FMISO imaging at 2 h p.i. [17]. For HX4 higher uptake and increasing ratios would be expected at later time points based on our clinical results [13]. Recently a simulation study, comparing FMISO, FAZA and HX4 based on their respective physical and chemical properties, revealed that tracer clearance and diffusion are the major parameters influencing image contrast. Highest clearance and image contrast was observed for HX4, but also the largest patient-to-patient variation, which might be a concern for clinical imaging to define tumour hypoxia based on a reliable threshold value [18].

Current available tracers have proven to be reliable for evaluation of tumour hypoxia, although with inherent problems resulting in clinical limitations. Alternative tracers, such as HX4, are promising with respect to deliver higher contrast images, whereas FMISO remains a robust reproducible hypoxia marker. It is not inconceivable that more tracers will be developed; but currently existing PET tracers should rather be used in clinic with standardized protocols enabling comparisons between different institutes. Furthermore, applicability and clinical validation should be proven in multiple cancer types and tracers need be tested with respect to their prognostic and predictive value.

## Hypoxia targeting

The compelling evidence for hypoxia in tumour tissue and its therapeutic importance makes hypoxia a high priority target for cancer therapy. Bioreductive prodrugs selectively activated under hypoxia and drugs that inhibit molecular targets in hypoxic cells (vide infra) are currently extensively investigated. A recent overview described the challenges and opportunities of these strategies [19]. The clinically most advanced hypoxia-activated prodrug is tirapazamine (TPZ). Although promising results have been reported in a number of Phase 2 trials, TPZ failed in several Phase 3 clinical trials since no survival benefit was observed when incorporated into standard therapy regimens. Possible explanations are its poor tumour penetration, low in vivo potency at tolerable doses and unacceptable

toxicity levels and lack of patient selection with high levels of tumour hypoxia [20]. A more potent hypoxia-activated prodrug currently undergoing early clinical testing is TH-302. It is a 2-nitroimidazole conjugated to bromo-isophosphoramidate mustard, which is released and activated upon very low levels of oxygen [21] and diffuses to surrounding cells creating a cytotoxic bystander effect [19]. TH-302 displayed clinical activity when used as single agent, which makes it unique compared to earlier generation hypoxia-activated cytotoxins which demonstrate anti-tumour activity only when used in combination with radiation or chemotherapy [22]. Furthermore, TH-302 efficacy was correlated with the hypoxic fraction across different tumour models [23-26]. Phase 1 trials have proved TH-302 safety with nausea, vomiting and fatigue as the most frequently occurring toxicities. Other trials successfully combined TH-302 with doxorubicin in patients with advanced soft tissue sarcoma [27] or with gemcitabine in patients with advanced pancreatic cancer [28]. A phase 3 double-blind, placebo-controlled trial has been initiated in which patients with advanced pancreatic cancer were randomized to gemcitabine combined with TH-302 or placebo [29]. Recently our group has evaluated the efficacy of TH-302 in a rat rhabdomyosarcoma and a human H460 xenograft model, using growth delay as endpoint. TH-302 in both models significantly inhibited tumour growth and markedly sensitized tumours to radiation. Furthermore, the therapeutic effect of TH-302 was dependent on the tumour oxygenation status prior to local radiotherapy that was modified by either carbogen (to improve oxygenation) or low oxygen containing gas (to increase hypoxia) breathing [30]. Increasing tumour oxygenation has shown potential for improving radiotherapy efficacy in several randomized clinical trials [31,32]. In spite of positive results, these strategies using hyperbaric oxygen or carbogen combined with vasodilating agents have not gained clinical traction due to practical limitations, toxicity and relatively modest clinical benefit [33]. An alternative strategy to achieve improved tumour oxygenation is to decrease cellular oxygen consumption using for example metformin, an inhibitor of the mitochondrial NADH dehydrogenase, also known as complex 1, activity in the mitochondrial electron transport respiration chain [34]. Recently, it has been demonstrated that metformin increases tumour response to radiotherapy, through a reduction in oxygen consumption and improved tumour oxygenation [35]. For future personalized cancer medicine, evaluation of hypoxia biomarkers and patient stratification will be essential to apply hypoxia targeting treatments to change radiotherapy response.

## Hypoxia molecular response

As tumours progress from an early to later stage disease, supply of oxygen becomes limited. Cancer cells must therefore alter their metabolism to an anaerobic glycolytic phenotype, resulting in a less efficient energy production and intracellular acidosis. In order to survive cancer cells must adapt to this acidic microenvironment, which helps promote metastases [36]. One of the important molecular responses to hypoxia is the stabilization of the hypoxia inducible factor (HIF)-1 $\alpha$ , enabling interaction with HIF-1 $\beta$ . The complex translocates to the nucleus where it binds to hypoxia responsive elements (HRE) in the promoter region of target genes, such as vascular endothelial growth factor (VEGF), glucose transporters 1 (GLUT-1) and carbonic anhydrase IX (CAIX) [37]. CAIX as well as other membrane transporters, like the sodium-proton exchanger 1 (NHE-1) and the monocarboxylate transporters (MCT), are upregulated to counteract the hypoxia-induced intracellular acidosis. CAIX is a tumour specific dimeric membrane bound zinc metallo-enzyme, which catalyses the reversible hydration of carbon dioxide to bicarbonate and a proton to help maintain the cells pH homeostasis [38]. High tumoural CAIX expression has been associated with poor prognosis, tumour progression and aggressiveness [39]. Inhibition of its function would therefore be a promising anticancer approach to target the hypoxic compartment of tumours.

## CAIX imaging tracers

A molecular imaging approach based on selective ligands to accessible proteins overexpressed at sites of hypoxia is desired. Such an agent could help physicians to decide which patients would benefit from adjuvant hypoxia-targeted therapy, e.g. anti-CAIX therapy. One strategy is using antibodies or antibody fragments targeted against transmembrane CAIX expression. The highly specific antibody M75 recognizes the extracellular proteoglycan-like domain of CAIX and is used for Western blotting and immunohistochemistry [40]. Specific accumulation of iodine-125 radiolabelled derivative has been observed in HT29 tumour-bearing mice [41]. Independently, the monoclonal G250 antibody was developed as a biomarker for renal cell carcinoma [42]. A chimeric version of G250 (cG250) has been radiolabelled with iodine-124, zirconium-89 or indium-111 for diagnostic purposes [43]. However, no apparent correlation has been observed between cG250 uptake and pimonidazole labelling or CAIX staining in head and neck tumour models attributed to the

large interval between cG250 injection and immunohistochemical evaluation [44]. Pepsin degradation of intact cG250 antibodies resulted in  $F(ab')_2$  fragments with a smaller molecular weight resulting in faster clearance from blood and healthy tissues. Zirconium-89 labelled cG250- $F(ab')_2$  fragments were found to spatially correlate with CAIX expression [45]. Furthermore, fully human CAIX single-chain variable fragment (scFv) minibodies have been generated using phage-display technology. They recognize the extracellular carbonic anhydrase domain, but do not inhibit CAIX activity and do not bind to the other transmembrane enzyme CAXII [46]. Recently, near-infrared (NIR) fluorescent monoclonal antibodies against CAIX and CAXII have been successfully tested for the non-invasive detection of breast cancer metastasis [47]. A dual labelled antibody combining indium-111 or iodine-125 nuclear with NIR imaging has proven feasible for preoperative and intraoperative detection of CAIX expressing renal cell carcinomas [48,49].

A second approach is the use of small molecules specifically targeting the active site of CAIX. Several classes of small molecules with low (nM) affinity have been extensively described, but due to the high degree of homology among CA isotypes, small molecules are generally not specific for one isoform [50]. To prevent interaction with the intracellular CA isoforms charged species or bulky groups such as FITC, albumin or sugar moieties are added to the small molecule. These strategies prevent transportation across membranes, but do not guarantee selectivity between CAIX and CAXII, both transmembrane enzymes with their catalytic domains oriented extracellularly. Attempts to design specific compounds targeting each isoform separately have been recently reviewed [51].

We and others have demonstrated *in vitro* that small molecule binding requires not only CAIX expression but also its hypoxic activation [52,53]. This offers a big advantage compared with antibodies against CAIX, since these small molecules can distinguish cells that are currently hypoxic from those that were previously hypoxic, while antibodies do not since their long half-life after reoxygenation [54]. *In vivo*, we have reported significant accumulation of fluorescent sulfonamides in HT29 xenografts, which was causally related with tumour oxygenation. Furthermore, bound sulfonamide decreased rapidly upon tumour reoxygenation [55]. Similar results have been obtained using fluorescent acetazolamide derivatives showing preferential targeting of CAIX overexpressing SK-RC-52 renal cell xenografts [56]. Recently, a series of sulfonamide derivatives conjugated with NIR fluorescent dyes having up to 50-fold higher selectivity for CAIX compared to the intracellular and other transmembrane isoforms has been designed. High tumoural uptake

with little accumulation in other organs, except for the kidneys, has been observed using fluorescence molecular tomography [57]. Several synthesis strategies have been proposed to enable nuclear imaging, however most attempts were not successful in showing specific enhanced tumour uptake. We have synthesized and evaluated a technetium-99m labelled sulfonamide for visualization of CAIX expression by SPECT imaging. Despite favourable affinity values maximum tumour uptake was low (<0.5% ID/g) even after varying physicochemical properties of the molecules [58,59]. A range of sulfonamides conjugated metal complexes have recently been designed for metallic radionuclide imaging. Although high *in vitro* uptake was observed, cellular binding between CAIX positive and negative cell lines was not obviously different [60]. Besides metal chelation approaches, direct fluorine-18 radiolabelling of CAIX targeted molecules has been assessed. Several compounds have been synthesized, such as 7-(2-fluoroethoxy)coumarin (FEC) and U-104 [61], the tertiary sulfonamides 4a-c [62] and VM4-037A [63]. Although all derivatives showed good affinity for CAIX with excellent plasma stability, uptake in HT-29 xenografts was minimal which precludes their application as CAIX imaging agents.

## CAIX targeting

Inhibiting CAIX can be done either by the use of monoclonal antibodies or with small molecule inhibitors. Antibody approaches are mostly based on the concept of antibody dependent cell cytotoxicity (ADCC). A leading example is cG250, marketed as RENCAREX®, which is extensively investigated as an anticancer immunotherapy [64]. Phase 1 and 2 trials have demonstrated safety and efficacy as monotherapy or in combination with interferon (IFN)- $\alpha$  for the treatment of renal cell carcinoma (RCC) [65]. This antibody was also tested in the double-blind, placebo-controlled phase 3 aRISER trial for adjuvant therapy of clear cell RCC, but as announced by WILEX AG the antibody failed to meet the primary endpoint, since no improvement in median disease-free survival was observed compared to placebo. Several new antibodies currently tested in preclinical settings show promising results regarding anti-tumour effects [66,67].

Specific inhibition of different carbonic anhydrase isoforms using small molecules is an active field of research and has been extensively reviewed [50,68,69]. Membrane-impermeable acetazolamide derivatives [56] and aromatic sulfonamides [70] were able to reduce tumour growth and proliferation. Treatment of mammary-tumour bearing mice

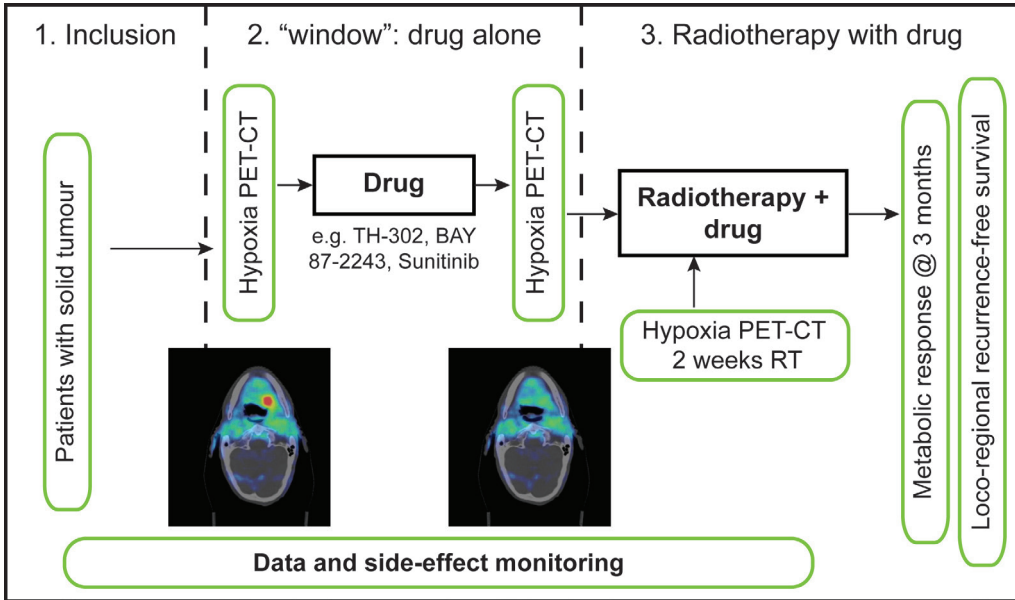
with CAIX-specific sulfonamide and glycosylcoumarin inhibitors resulted in a significant reduction in tumour growth and lung metastasis formation [71]. One of the several potent CAIX inhibitors identified from a DNA-encoded chemical library screen has shown high and specific accumulation in tumour models [72].

A new class of sulfamate inhibitors proved to be excellent candidates for low dosage anti-metastatic drugs [73], but were ineffective in reducing primary tumour growth [73,74]. Combining small molecules targeting CAIX with conventional therapies might yield even better efficacy. Recently, a CAIX dependent sensitizing effect of indanesulfonamides [75] and acetazolamide [76] on respectively radio- and chemotherapy has been demonstrated. Similarly combination of paclitaxel with orally administered U-104 significantly affected primary tumour growth and metastasis formation by reducing the breast cancer stem cell population [77]. Nitroimidazole and sulfamide based dual targeting drugs reduced hypoxic extracellular acidification *in vitro*, inhibited tumour growth at low dosage and sensitized tumours to both radiation [78] and doxorubicin [79]. This dual-targeting strategy appeared to be more effective than single targeting molecules. Recently, a family of novel small-molecule drug conjugates comprising of a linker cleavable in the extracellular space and a potent cytotoxic payload targeting CAIX has been designed and characterized. The disulfide-linked conjugate with maytansinoid DM1 as cytotoxic payload and an acetazolamide derivative as the targeting ligand has shown potent anti-tumour effects in renal cell carcinoma models with only minimal toxicity [80]. These results indicate that targeted delivery of potent cytotoxic agents using CAIX directed ligands may provide therapeutic benefits over current standard of care. The first clinical trial (NCT02215850) testing a small molecule CAIX inhibitor, named SLC-0111, is currently ongoing and is focused on testing the safety in subjects with advanced solid tumours.

## Window-of-opportunity trial

Although there is a high number of new promising anti-cancer agents under preclinical and clinical investigation, the success rate of approved drugs for clinical practice has not been significantly increased. Improved clinical trial designs, such as 'window-of-opportunity' trials will help to select effective drugs at an earlier stage and to identify patients which potentially will benefit of the drug. In this trial, the patient agrees to delay combined conventional anti-cancer therapy to first receive the experimental drug, with the aim to obtain

knowledge about anti-tumour activity in a disease state that is not disturbed by previous or simultaneous treatments [81]. The question has been raised whether these trials should be more widely applied in early phases of drug development knowing the progress in imaging and monitoring tumour progression [82] to prevent expensive long-lasting classical clinical testing of inefficacious drugs. Using this trial approach, hypoxia imaging can be used as a biomarker of response, especially suitable in the context of testing hypoxia (response) targeting drugs. Upon patient inclusion, baseline hypoxia should be acquired followed by the experimental targeting drug. A post-treatment hypoxia PET scan will assess the effect of the single treatment by comparison of the hypoxic fractions between the two scans (Fig. 1). This window-of-opportunity trial can precede a phase 1 trial testing safety of the experimental drug in combination with conventional treatment, e.g. radiotherapy, or a randomized phase 2 clinical trial. We have used this concept preclinically to proof efficacy of the hypoxia-activated cytotoxic prodrug TH-302. The hypoxic fraction assessed with HX4 PET imaging in the rhabdomyosarcoma model was significantly reduced at day 4 upon TH-302 treatment, while vehicle treatment was ineffective. Additionally, TH-302 was not only effective as monotherapy, but also sensitized tumours to a single dose of radiation [30]. Similarly, BAY 87-2243, an inhibitor of mitochondrial complex 1, resulted in reduced HIF-1 $\alpha$  activity and pimonidazole binding prior to radiotherapy improving local tumour control [83,84]. Its efficacy has also been shown by a dramatic reduction in FAZA PET signal before significant changes in tumour volume were observed [85]. Finally sunitinib treatment resulted in improved tumour oxygenation as FAZA uptake in Caki-1 renal cell xenografts [86] and in patients with soft-tissue sarcomas [87] was significantly reduced during therapy. Upon withdrawal of sunitinib therapy, FAZA uptake increased again, indicating a rebound in tumour hypoxia. These examples clearly highlight the importance of imaging the hypoxic fraction of tumours to monitor treatment response.



**Figure 1:** Window-of-opportunity trial concept implementing non-invasive hypoxia imaging before and after drug administration followed by phase 1 or 2 trial combining radiotherapy and experimental drug. Additional hypoxia imaging can be included in step 3 for early response monitoring. HX4 hypoxia PET-CT images from a patient with head and neck cancer are shown as proof of concept.

## Conclusions

Current clinically available hypoxia PET tracers, although showing different characteristics, have proven to be reliable for evaluation of tumour hypoxia. Much progress has been made in the synthesis and evaluation of high affinity small molecules targeting CAIX. Nevertheless, proper clinically-suited diagnostic tools are still lacking. The window-of-opportunity trial concept implementing non-invasive imaging to monitor treatment response is an important tool to provide evidence of anti-tumour efficacy in earlier stages of drug development.

## Acknowledgements

Authors acknowledge financial support from the QuIC-ConCePT project, which is partly funded by EFPIA companies and the Innovative Medicine Initiative Joint Undertaking (IMI JU) under Grant Agreement No. 115151. Authors also acknowledge financial support from the EU 7th framework program (METOXIA, EURECA, ARTFORCE, REQUITE), NGI Pre-Seed Grant (no. 93612005), Worldwide Cancer Research grant (n° 15-0345), La Ligue contre le Cancer (comité des Pyrénées-Orientales), Kankeronderzoekfonds Limburg from the Health Foundation Limburg and the Dutch Cancer Society (KWF UM 2011-5020, KWF UM 2012-5394, KWF UM 2015-7635, KWF MAC 2013-6089 and KWF MAC 2013-6425).

### **Conflict of interest**

None of the authors have any conflict of interest to declare.

## References

1. Hanahan D, Weinberg RA. Hallmarks of cancer: the next generation. *Cell* 2011;144:646-74.
2. Nordmark M, Bentzen SM, Rudat V, et al. Prognostic value of tumor oxygenation in 397 head and neck tumors after primary radiation therapy. An international multi-center study. *Radiother Oncol* 2005;77:18-24.
3. Horsman MR, Mortensen LS, Petersen JB, Busk M, Overgaard J. Imaging hypoxia to improve radiotherapy outcome. *Nat Rev Clin Oncol* 2012;9:674-87.
4. Peeters SG, Zegers CM, Yaromina A, Van Elmpt W, Dubois L, Lambin P. Current preclinical and clinical applications of hypoxia PET imaging using 2-nitroimidazoles. *Q J Nucl Med Mol Imaging* 2015;59:39-57.
5. Rasey JS, Koh WJ, Evans ML, et al. Quantifying regional hypoxia in human tumors with positron emission tomography of [18F]fluoromisonidazole: a pretherapy study of 37 patients. *Int J Radiat Oncol Biol Phys* 1996;36:417-28.
6. Krohn KA, Link JM, Mason RP. Molecular imaging of hypoxia. *J Nucl Med* 2008;49 Suppl 2:129S-48S.
7. Lopci E, Grassi I, Chiti A, et al. PET radiopharmaceuticals for imaging of tumor hypoxia: a review of the evidence. *Am J Nucl Med Mol Imaging* 2014;4:365-84.
8. Kolb HC, Finn MG, Sharpless KB. Click Chemistry: Diverse Chemical Function from a Few Good Reactions. *Angew Chem Int Ed Engl* 2001;40:2004-21.
9. Doss M, Zhang JJ, Belanger MJ, et al. Biodistribution and radiation dosimetry of the hypoxia marker 18F-HX4 in monkeys and humans determined by using whole-body PET/CT. *Nucl Med Commun* 2010;31:1016-24.
10. Carlin S, Zhang H, Reese M, Ramos NN, Chen Q, Ricketts SA. A comparison of the imaging characteristics and microregional distribution of 4 hypoxia PET tracers. *J Nucl Med* 2014;55:515-21.
11. Dubois LJ, Lieuwes NG, Janssen MH, et al. Preclinical evaluation and validation of [18F]HX4, a promising hypoxia marker for PET imaging. *Proc Natl Acad Sci U S A* 2011;108:14620-5.
12. van Loon J, Janssen MH, Ollers M, et al. PET imaging of hypoxia using [18F]HX4: a phase I trial. *Eur J Nucl Med Mol Imaging* 2010;37:1663-8.
13. Zegers CM, van Elmpt W, Wiertz R, et al. Hypoxia imaging with [(1)(8)F]HX4 PET in NSCLC patients: defining optimal imaging parameters. *Radiother Oncol* 2013;109:58-64.
14. Zegers CM, van Elmpt W, Reymen B, et al. In vivo quantification of hypoxic and metabolic status of NSCLC tumors using [18F]HX4 and [18F]FDG-PET/CT imaging. *Clin Cancer Res* 2014;20:6389-97.
15. Zegers CM, van Elmpt W, Hoebbers FJ, et al. Imaging of tumour hypoxia and metabolism in patients with head and neck squamous cell carcinoma. *Acta oncologica* 2015:1-7.
16. Peeters SG, Zegers CM, Lieuwes NG, et al. A comparative study of the hypoxia PET tracers [(1)(8)F]HX4, [(1)(8)F]FAZA, and [(1)(8)F]FMISO in a preclinical tumor model. *Int J Radiat Oncol Biol Phys* 2015;91:351-9.
17. Chen L, Zhang Z, Kolb HC, Walsh JC, Zhang J, Guan Y. (1)(8)F-HX4 hypoxia imaging with PET/CT in head and neck cancer: a comparison with (1)(8)F-FMISO. *Nucl Med Commun* 2012;33:1096-102.
18. Wack LJ, Monnich D, van Elmpt W, et al. Comparison of [18F]-FMISO, [18F]-FAZA and [18F]-HX4 for PET imaging

- of hypoxia - a simulation study. *Acta oncologica* 2015;1-8.
19. Wilson WR, Hay MP. Targeting hypoxia in cancer therapy. *Nat Rev Cancer* 2011;11:393-410.
  20. Reddy SB, Williamson SK. Tirapazamine: a novel agent targeting hypoxic tumor cells. *Expert Opin Investig Drugs* 2009;18:77-87.
  21. Meng F, Evans JW, Bhupathi D, et al. Molecular and cellular pharmacology of the hypoxia-activated prodrug TH-302. *Mol Cancer Ther* 2012;11:740-51.
  22. Bennewith KL, Dedhar S. Targeting hypoxic tumour cells to overcome metastasis. *BMC cancer* 2011;11:504.
  23. Cardenas-Rodriguez J, Li Y, Galons JP, et al. Imaging biomarkers to monitor response to the hypoxia-activated prodrug TH-302 in the MiaPaCa2 flank xenograft model. *Magn Reson Imaging* 2012;30:1002-9.
  24. Hu J, Van Valckenborgh E, Dehui X, et al. Synergistic induction of apoptosis in multiple myeloma cells by bortezomib and hypoxia-activated prodrug TH-302, in vivo and in vitro. *Mol Cancer Ther* 2013.
  25. Liu Q, Sun JD, Wang J, et al. TH-302, a hypoxia-activated prodrug with broad in vivo preclinical combination therapy efficacy: optimization of dosing regimens and schedules. *Cancer Chemother Pharmacol* 2012;69:1487-98.
  26. Sun JD, Liu Q, Wang J, et al. Selective tumor hypoxia targeting by hypoxia-activated prodrug TH-302 inhibits tumor growth in preclinical models of cancer. *Clin Cancer Res* 2012;18:758-70.
  27. Chawla SP, Cranmer LD, Van Tine BA, et al. Phase II study of the safety and antitumor activity of the hypoxia-activated prodrug TH-302 in combination with doxorubicin in patients with advanced soft tissue sarcoma. *J Clin Oncol* 2014;32:3299-306.
  28. Borad MJ, Reddy SG, Bahary N, et al. Randomized Phase II Trial of Gemcitabine Plus TH-302 Versus Gemcitabine in Patients With Advanced Pancreatic Cancer. *J Clin Oncol* 2015;33:1475-81.
  29. Van Cutsem E, Fram R, Schlichting M, Ryan D. P-0173 \* Phase 3 trial of gemcitabine and TH-302 compared with gemcitabine and placebo in patients with pancreatic adenocarcinoma: The MAESTRO Trial. *Ann Oncol* 2013;24:iv38-iv121.
  30. Peeters SG, Zegers CM, Biemans R, et al. TH-302 in Combination with Radiotherapy Enhances the Therapeutic Outcome and Is Associated with Pretreatment [18F]HX4 Hypoxia PET Imaging. *Clin Cancer Res* 2015.
  31. Janssens GO, Rademakers SE, Terhaard CH, et al. Accelerated radiotherapy with carbogen and nicotinamide for laryngeal cancer: results of a phase III randomized trial. *J Clin Oncol* 2012;30:1777-83.
  32. Overgaard J. Hypoxic modification of radiotherapy in squamous cell carcinoma of the head and neck--a systematic review and meta-analysis. *Radiother Oncol* 2011;100:22-32.
  33. Overgaard J. Hypoxic radiosensitization: adored and ignored. *J Clin Oncol* 2007;25:4066-74.
  34. van Gisbergen MW, Voets AM, Starmans MH, et al. How do changes in the mtDNA and mitochondrial dysfunction influence cancer and cancer therapy? Challenges, opportunities and models. *Mutat Res Rev Mutat Res* 2015;764:16-30.
  35. Zannella VE, Dal Pra A, Muaddi H, et al. Reprogramming metabolism with metformin improves tumor oxygenation and radiotherapy response. *Clin Cancer Res* 2013;19:6741-50.
  36. Gatenby RA, Gillies RJ. Why do cancers have high aerobic glycolysis? *Nat Rev Cancer* 2004;4:891-9.

37. Wouters BG, Koritzinsky M. Hypoxia signalling through mTOR and the unfolded protein response in cancer. *Nat Rev Cancer* 2008;8:851-64.
38. Alterio V, Hilvo M, Di Fiore A, et al. Crystal structure of the catalytic domain of the tumor-associated human carbonic anhydrase IX. *Proc Natl Acad Sci U S A* 2009;106:16233-8.
39. Potter CP, Harris AL. Diagnostic, prognostic and therapeutic implications of carbonic anhydrases in cancer. *Br J Cancer* 2003;89:2-7.
40. Pastorekova S, Zavadova Z, Kostal M, Babusikova O, Zavada J. A novel quasi-viral agent, MaTu, is a two-component system. *Virology* 1992;187:620-6.
41. Chrastina A, Zavada J, Parkkila S, et al. Biodistribution and pharmacokinetics of 125I-labeled monoclonal antibody M75 specific for carbonic anhydrase IX, an intrinsic marker of hypoxia, in nude mice xenografted with human colorectal carcinoma. *Int J Cancer* 2003;105:873-81.
42. Oosterwijk E, Ruiter DJ, Hoedemaeker PJ, et al. Monoclonal antibody G 250 recognizes a determinant present in renal-cell carcinoma and absent from normal kidney. *Int J Cancer* 1986;38:489-94.
43. Cheal SM, Punzalan B, Doran MG, et al. Pairwise comparison of 89Zr- and 124I-labeled cG250 based on positron emission tomography imaging and nonlinear immunokinetic modeling: in vivo carbonic anhydrase IX receptor binding and internalization in mouse xenografts of clear-cell renal cell carcinoma. *Eur J Nucl Med Mol Imaging* 2014;41:985-94.
44. Troost EG, Bussink J, Kaanders JH, et al. Comparison of different methods of CAIX quantification in relation to hypoxia in three human head and neck tumor lines. *Radiother Oncol* 2005;76:194-9.
45. Hoeben BA, Kaanders JH, Franssen GM, et al. PET of hypoxia with 89Zr-labeled cG250-F(ab')<sub>2</sub> in head and neck tumors. *J Nucl Med* 2010;51:1076-83.
46. Ahlskog JK, Schliemann C, Marling J, et al. Human monoclonal antibodies targeting carbonic anhydrase IX for the molecular imaging of hypoxic regions in solid tumours. *Br J Cancer* 2009;101:645-57.
47. Tafreshi NK, Bui MM, Bishop K, et al. Noninvasive detection of breast cancer lymph node metastasis using carbonic anhydrases IX and XII targeted imaging probes. *Clin Cancer Res* 2012;18:207-19.
48. Muselaers CH, Rijpkema M, Bos DL, et al. Radionuclide and Fluorescence Imaging of Clear Cell Renal Cell Carcinoma Using Dual Labeled Anti-Carbonic Anhydrase IX Antibody G250. *J Urol* 2015.
49. Muselaers CH, Stillebroer AB, Rijpkema M, et al. Optical Imaging of Renal Cell Carcinoma with Anti-Carbonic Anhydrase IX Monoclonal Antibody Girentuximab. *J Nucl Med* 2014;55:1035-40.
50. Supuran CT. Carbonic anhydrases: novel therapeutic applications for inhibitors and activators. *Nat Rev Drug Discov* 2008;7:168-81.
51. Alterio V, Di Fiore A, D'Ambrosio K, Supuran CT, De Simone G. Multiple binding modes of inhibitors to carbonic anhydrases: how to design specific drugs targeting 15 different isoforms? *Chem Rev* 2012;112:4421-68.
52. Dubois L, Douma K, Supuran CT, et al. Imaging the hypoxia surrogate marker CA IX requires expression and catalytic activity for binding fluorescent sulfonamide inhibitors. *Radiother Oncol* 2007;83:367-73.

53. Svastova E, Hulikova A, Rafajova M, et al. Hypoxia activates the capacity of tumor-associated carbonic anhydrase IX to acidify extracellular pH. *FEBS Lett* 2004;577:439-45.
54. Rafajova M, Zatovicova M, Kettmann R, Pastorek J, Pastorekova S. Induction by hypoxia combined with low glucose or low bicarbonate and high posttranslational stability upon reoxygenation contribute to carbonic anhydrase IX expression in cancer cells. *Int J Oncol* 2004;24:995-1004.
55. Dubois L, Lieuwes NG, Maresca A, et al. Imaging of CA IX with fluorescent labelled sulfonamides distinguishes hypoxic and (re)-oxygenated cells in a xenograft tumour model. *Radiother Oncol* 2009;92:423-8.
56. Ahlskog JK, Dumelin CE, Trussel S, Marlind J, Neri D. In vivo targeting of tumor-associated carbonic anhydrases using acetazolamide derivatives. *Bioorg Med Chem Lett* 2009;19:4851-6.
57. Groves K, Bao B, Zhang J, et al. Synthesis and evaluation of near-infrared fluorescent sulfonamide derivatives for imaging of hypoxia-induced carbonic anhydrase IX expression in tumors. *Bioorg Med Chem Lett* 2012;22:653-7.
58. Akurathi V, Dubois L, Celen S, et al. Development and biological evaluation of (9)(9)mTc-sulfonamide derivatives for in vivo visualization of CA IX as surrogate tumor hypoxia markers. *Eur J Med Chem* 2014;71:374-84.
59. Akurathi V, Dubois L, Lieuwes NG, et al. Synthesis and biological evaluation of a <sup>99m</sup>Tc-labelled sulfonamide conjugate for in vivo visualization of carbonic anhydrase IX expression in tumor hypoxia. *Nucl Med Biol* 2010;37:557-64.
60. Dilworth JR, Pascu SI, Waghorn PA, et al. Synthesis of sulfonamide conjugates of Cu(II), Ga(III), In(III), Re(V) and Zn(II) complexes: carbonic anhydrase inhibition studies and cellular imaging investigations. *Dalton Trans* 2015;44:4859-73.
61. Pan J, Lau J, Mesak F, et al. Synthesis and evaluation of <sup>18</sup>F-labeled carbonic anhydrase IX inhibitors for imaging with positron emission tomography. *J Enzyme Inhib Med Chem* 2014;29:249-55.
62. Lau J, Pan J, Zhang Z, et al. Synthesis and evaluation of (<sup>18</sup>F)-labeled tertiary benzenesulfonamides for imaging carbonic anhydrase IX expression in tumours with positron emission tomography. *Bioorg Med Chem Lett* 2014;24:3064-8.
63. Peeters SG, Dubois L, Lieuwes NG, et al. [<sup>18</sup>F]VM4-037 MicroPET Imaging and Biodistribution of Two In Vivo CAIX-Expressing Tumor Models. *Mol Imaging Biol* 2015.
64. Surfus JE, Hank JA, Oosterwijk E, et al. Anti-renal-cell carcinoma chimeric antibody G250 facilitates antibody-dependent cellular cytotoxicity with in vitro and in vivo interleukin-2-activated effectors. *J Immunother Emphasis Tumor Immunol* 1996;19:184-91.
65. Siebels M, Rohrmann K, Oberneder R, et al. A clinical phase I/II trial with the monoclonal antibody cG250 (REN-CAREX(R)) and interferon-alpha-2a in metastatic renal cell carcinoma patients. *World J Urol* 2011;29:121-6.
66. Birkhauser FD, Koya RC, Neufeld C, et al. Dendritic cell-based immunotherapy in prevention and treatment of renal cell carcinoma: efficacy, safety, and activity of Ad-GM.CAIX in immunocompetent mouse models. *J Immunother* 2013;36:102-11.
67. Chang DK, Moniz RJ, Xu Z, et al. Human anti-CAIX antibodies mediate immune cell inhibition of renal cell carcinoma in vitro and in a humanized mouse model in vivo. *Mol Cancer* 2015;14:119.

68. McDonald PC, Winum JY, Supuran CT, Dedhar S. Recent developments in targeting carbonic anhydrase IX for cancer therapeutics. *Oncotarget* 2012;3:84-97.
69. Neri D, Supuran CT. Interfering with pH regulation in tumours as a therapeutic strategy. *Nat Rev Drug Discov* 2011;10:767-77.
70. Cianchi F, Vinci MC, Supuran CT, et al. Selective inhibition of carbonic anhydrase IX decreases cell proliferation and induces ceramide-mediated apoptosis in human cancer cells. *J Pharmacol Exp Ther* 2010;334:710-9.
71. Lou Y, McDonald PC, Oloumi A, et al. Targeting tumor hypoxia: suppression of breast tumor growth and metastasis by novel carbonic anhydrase IX inhibitors. *Cancer Res* 2011;71:3364-76.
72. Buller F, Mannocci L, Zhang Y, Dumelin CE, Scheuermann J, Neri D. Design and synthesis of a novel DNA-encoded chemical library using Diels-Alder cycloadditions. *Bioorg Med Chem Lett* 2008;18:5926-31.
73. Gieling RG, Babur M, Mamnani L, et al. Antimetastatic effect of sulfamate carbonic anhydrase IX inhibitors in breast carcinoma xenografts. *J Med Chem* 2012;55:5591-600.
74. Meijer TW, Bussink J, Zatovicova M, et al. Tumor microenvironmental changes induced by the sulfamate carbonic anhydrase IX inhibitor S4 in a laryngeal tumor model. *PLoS One* 2014;9:e108068.
75. Dubois L, Peeters S, Lieuwes NG, et al. Specific inhibition of carbonic anhydrase IX activity enhances the in vivo therapeutic effect of tumor irradiation. *Radiother Oncol* 2011;99:424-31.
76. Gieling RG, Parker CA, De Costa LA, et al. Inhibition of carbonic anhydrase activity modifies the toxicity of doxorubicin and melphalan in tumour cells in vitro. *J Enzyme Inhib Med Chem* 2013;28:360-9.
77. Lock FE, McDonald PC, Lou Y, et al. Targeting carbonic anhydrase IX depletes breast cancer stem cells within the hypoxic niche. *Oncogene* 2013;32:5210-9.
78. Dubois L, Peeters SG, van Kuijk SJ, et al. Targeting carbonic anhydrase IX by nitroimidazole based sulfamides enhances the therapeutic effect of tumor irradiation: a new concept of dual targeting drugs. *Radiother Oncol* 2013;108:523-8.
79. Rami M, Dubois L, Parvathaneni NK, et al. Hypoxia-targeting carbonic anhydrase IX inhibitors by a new series of nitroimidazole-sulfonamides/sulfamides/sulfamates. *J Med Chem* 2013;56:8512-20.
80. Krall N, Pretto F, Decurtins W, Bernardes GJ, Supuran CT, Neri D. A small-molecule drug conjugate for the treatment of carbonic anhydrase IX expressing tumors. *Angew Chem Int Ed Engl* 2014;53:4231-5.
81. Orloff J, Douglas F, Pinheiro J, et al. The future of drug development: advancing clinical trial design. *Nat Rev Drug Discov* 2009;8:949-57.
82. Glimelius B, Lahn M. Window-of-opportunity trials to evaluate clinical activity of new molecular entities in oncology. *Ann Oncol* 2011;22:1717-25.
83. Helbig L, Koi L, Bruchner K, et al. BAY 87-2243, a novel inhibitor of hypoxia-induced gene activation, improves local tumor control after fractionated irradiation in a schedule-dependent manner in head and neck human xenografts. *Radiation oncology* 2014;9:207.
84. Helbig L, Koi L, Bruchner K, et al. Hypoxia-inducible factor pathway inhibition resolves tumor hypoxia and im-

proves local tumor control after single-dose irradiation. *International journal of radiation oncology, biology, physics* 2014;88:159-66.

85. Chang E, Liu H, Unterschemmann K, et al. 18F-FAZA PET imaging response tracks the reoxygenation of tumors in mice upon treatment with the mitochondrial complex I inhibitor BAY 87-2243. *Clin Cancer Res* 2015;21:335-46.
86. Chapman DW, Jans HS, Ma I, et al. Detecting functional changes with [(18)F]FAZA in a renal cell carcinoma mouse model following sunitinib therapy. *Eur J Nucl Med Mol Imaging* 2014;4:27.
87. Lewin J, Khamly KK, Young RJ, et al. A phase Ib/II translational study of sunitinib with neoadjuvant radiotherapy in soft-tissue sarcoma. *Br J Cancer* 2014;111:2254-61.



# CHAPTER 3

## Synthesis and *in vivo* biological evaluation of $^{68}\text{Ga}$ -labeled carbonic anhydrase IX targeting small molecules for positron emission tomography

Deborah Sneddon\*, **Raymon Niemans\***, Matthias Bauwens, Ala Yaromina, Simon J. A. van Kuijk, Natasja G. Lieuwes, Rianne Biemans, Ivo Pooters, Paul A. Pellegrini, Nigel A. Lengkeek, Ivan Greguric, Kathryn F. Tonissen, Claudiu T. Supuran, Philippe Lambin, Ludwig Dubois, Sally-Ann Poulsen

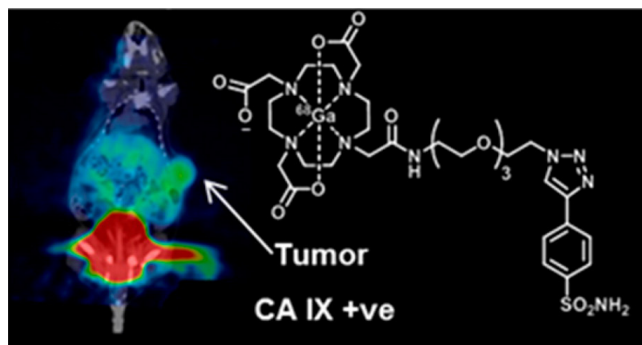
*\*These authors contributed equally.*

### **Previously published:**

Sneddon, D., *et al.*, Synthesis and *in Vivo* Biological Evaluation of  $(^{68}\text{Ga})$ -Labeled Carbonic Anhydrase IX Targeting Small Molecules for Positron Emission Tomography. *J Med Chem*, 2016. 59(13): p. 6431-43.

## Abstract

Tumor hypoxia contributes resistance to chemo- and radiotherapy, while oxygenated tumors are sensitive to these treatments. The indirect detection of hypoxic tumors is possible by targeting carbonic anhydrase IX (CA IX), an enzyme overexpressed in hypoxic tumors, with sulfonamide-based imaging agents. In this study, we present the design and synthesis of novel gallium radiolabeled small molecule sulfonamides targeting CA IX. The compounds display favorable *in vivo* pharmacokinetics and stability. We demonstrate that our lead compound, [<sup>68</sup>Ga]-**2**, discriminates CA IX-expressing tumors *in vivo* in a mouse xenograft model using positron emission tomography (PET). This compound shows specific tumor accumulation and low uptake in blood and clears intact to the urine. These findings were reproduced in a second study using PET/computed tomography. Small molecules investigated to date utilizing <sup>68</sup>Ga for preclinical CA IX imaging are scarce, and this is one of the first effective <sup>68</sup>Ga compounds reported for PET imaging of CA IX.



## Introduction

Molecular imaging with positron emission tomography (PET) has had a profound impact on primary diagnosis, management, therapy monitoring, and prognosis in cancer; it is noninvasive and provides personalized care to patients by informing treatment decisions and evaluating treatment response. Hypoxia (low oxygen concentration) is a characteristic feature of solid tumors. Hypoxic cells co-opt adaptive mechanisms to switch to a glycolytic metabolism, promote cell proliferation, evade immune attack, induce angiogenesis, invade, and metastasize [1]. Tumor hypoxia is a negative prognostic factor associated with a more aggressive phenotype, specifically with resistance to chemo- and radiotherapy. For example, up to a 3-fold higher radiation dose is needed to achieve the same level of tumor cell death in hypoxic tumors as in oxygenated tumors [2]. The implementation of a hypoxia-guided clinical management strategy, such as hypoxia radiation sensitizers (e.g. nimorazole [3]) or hypoxia-specific cytotoxic therapy (e.g., TH-302; Figure 1A) [4], to those patients most likely to benefit is currently not possible, as there is no established method in routine clinical practice that is (i) noninvasive, (ii) routine to prepare, and (iii) indicative of the hypoxic cell population [2]. Most current methods to detect hypoxia are invasive (e.g., require surgery) and are subject to technical issues that cause sampling errors.

Small-molecule molecular probes for imaging of hypoxia with PET may be split into two broad categories: “direct” and “indirect” imaging probes. Nitroimidazoles are direct imaging probes for the detection of hypoxia with PET, with one compound, <sup>18</sup>F-fluoromisonidazole (<sup>18</sup>F-FMISO) in limited clinical use [5]. Second- and third-generation nitroimidazoles, <sup>18</sup>F-FAZA and <sup>18</sup>F-HX4, respectively, have been shown by us to address the pharmacokinetic (PK) problems of <sup>18</sup>F-FMISO (slow tumor-specific accumulation and nonspecific washout), but better probes for hypoxia are still required [5-8].

A critical cellular response to hypoxia is the stabilization and activation of the transcription factor hypoxia inducible factor-1 $\alpha$  (HIF-1 $\alpha$ ). HIF-1 $\alpha$  regulates the expression of genes required for survival under hypoxia. In principle, the gene products may be used as targets for imaging of tumor hypoxia with indirect probes and bypass the drawbacks associated with nitroimidazole probes [9]. Carbonic anhydrase IX (CA IX) is one of the most highly induced HIF-1 $\alpha$  responsive genes and is proposed as the “gold standard” endogenous marker of cellular hypoxia [10-13]. CA IX expression is a negative prognostic factor in several types of cancer [14]. Additionally CA IX (over)expression is thought to predict the thera-

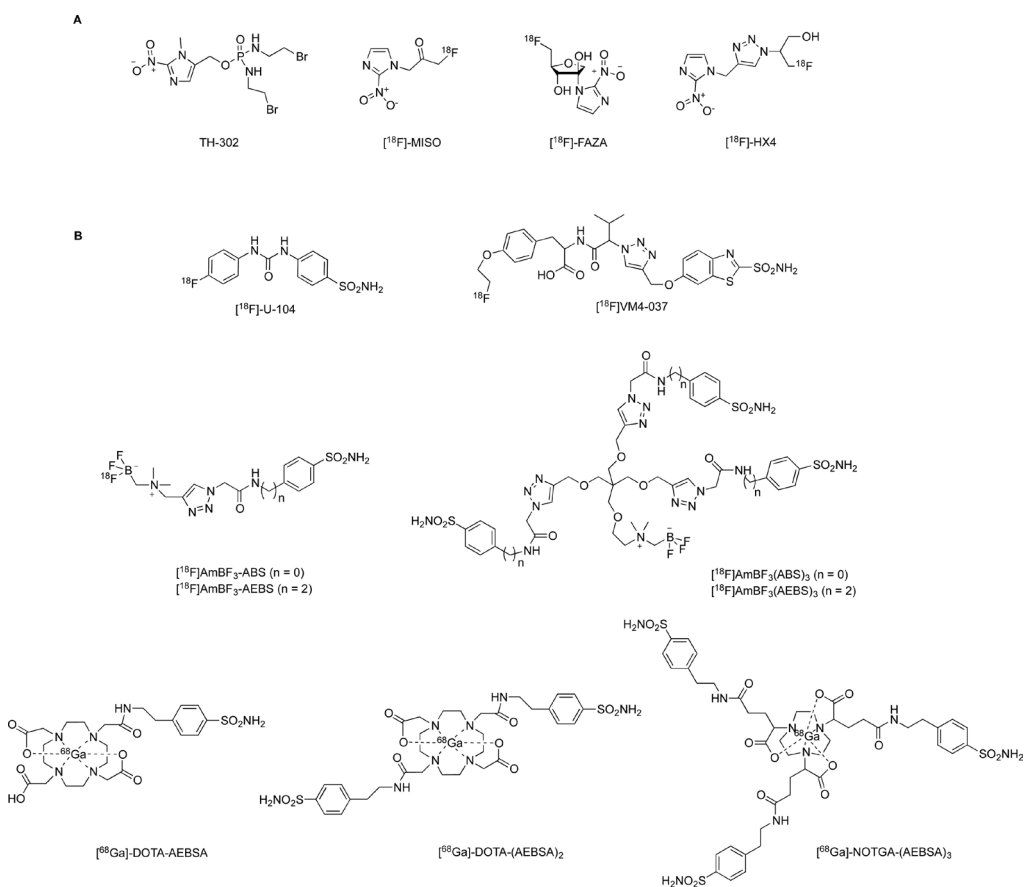
peutic effect of CA IX-targeting anticancer therapies. CA IX is overexpressed and sustained in many solid tumors, including breast, brain (glioblastoma), clear cell renal, colorectal, head and neck, bladder, and non-small cell lung carcinomas, but expression in normal tissues is restricted to the stomach and gastrointestinal tract [10, 15].

CA IX is a transmembrane zinc metalloenzyme that catalyzes the reversible hydration of  $\text{CO}_2$  to give  $\text{HCO}_3^-$  and  $\text{H}^+$ , enabling the tumor to regulate pH, allowing its spread and survival [12, 13, 16-20]. Expression of CA IX is commonly used as a histologic marker of tissue hypoxia, with detection using M75 [18] or G250 [21], two different monoclonal antibodies specific for CA IX. There are several antibody- and antibody-fragment-based imaging agents with in vivo data that indirectly target hypoxic tumors by binding to CA IX [22, 23].

Our groups have shown that small-molecule sulfonamides are able to discriminate oxygen levels in tissues and bind preferentially to CA IX only in hypoxic cells, while CA IX-targeting antibodies also bind upon reoxygenation [24]. Therefore, our attention has turned to small molecules to develop radiopharmaceuticals to detect CA IX positive tumors with PET. To date, very few small molecules that incorporate a primary sulfonamide functional group, which is required for tight binding to the active site zinc in CA IX (see examples in Figure 1), have been developed and tested for CA IX imaging with PET in vivo [25-29]. Compound [ $^{18}\text{F}$ ]U-104 proved to be ineffective because of poor PK [28]. [ $^{18}\text{F}$ ]VM4-037 was found to be safe for use in healthy volunteers [25], but no CA IX-dependent uptake was found in vivo [30, 31]. In a recent phase-II pilot study of two patients with clear cell renal cell carcinoma (RCC) primary tumors with this agent, uptake was observed in both healthy and cancerous kidney as well as metastases, and CA IX selectivity was not confirmed [32], limiting the use of this imaging agent in RCC. The trivalent sulfonamide compounds [ $^{18}\text{F}$ ]AmBF<sub>3</sub>-(ABS)<sub>3</sub> and [ $^{18}\text{F}$ ]AmBF<sub>3</sub>-(ABS)<sub>3</sub> have demonstrated imaging efficacy in vivo [26] enabling tumor visualization with a respective tumor-to-blood ratio (TBR) of  $3.93 \pm 1.26$  or  $2.88 \pm 1.81$  in CA IX-expressing HT-29 tumors 1 h after injection. Interestingly, the mono-valent variants showed a TBR close to unity and hence were less effective as imaging agents [26]. No discrimination between CA IX-expressing or nonexpressing tumors was shown, but preinjection of acetazolamide effectively blocked uptake of [ $^{18}\text{F}$ ]AmBF<sub>3</sub>-(ABS)<sub>3</sub> in the tumor. Recently another series of mono-, di-, and trivalent sulfonamides based on  $^{68}\text{Ga}$ -DOTA/NOTGA as the PET reporter group were tested in a CA IX-expressing HT-29 tumor xenograft, and again only the trivalent sulfonamide ( $^{68}\text{Ga}$ -NOTGA-AEBSA<sub>3</sub>) had a TBR that significantly differed from that of the controls (where test animals were first treated

with acetazolamide as a CA IX-blocking sulfonamide) [27].

$^{68}\text{Ga}$  ( $t_{1/2} = 68$  min) has been used to label small molecules, biological macromolecules, and nano- and microparticles [33]. It is a favorable positron emitter because its  $\gamma$  emission is negligible and it can be produced in a  $^{68}\text{Ge}/^{68}\text{Ga}$  generator, so an on-site cyclotron is not required [34]. As the parent radionuclide  $^{68}\text{Ge}$  has a long half-life ( $t_{1/2} = 270.8$  days), it can be stored for relatively long periods [34]. To make PET imaging with sulfonamides suitable for eventual use in cancer patients, the purpose of the present work is to design and synthesize novel small-molecule  $^{68}\text{Ga}$ -labeled imaging agents that can selectively target CA IX-positive tumor cells *in vivo*. Specifically, agents with improved PK properties, CA IX targeting, TBR, and image contrast compared with those previously described are sought.

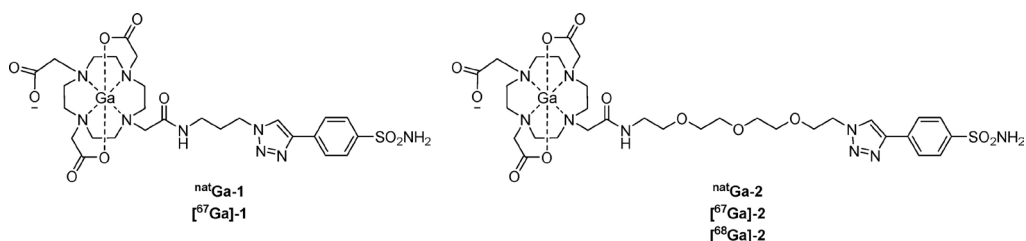


**Figure 1.** (A) Nitroimidazole hypoxia-targeted cytotoxic drug TH-302 and small-molecule nitroimidazole PET imaging agents for hypoxia:  $^{18}\text{F}$ -MISO,  $^{18}\text{F}$ -FAZA, and  $^{18}\text{F}$ -HX4. (B) Small-molecule primary sulfonamides investigated in animal models for CA IX imaging with PET [25-28].

## Results and Discussion

### Compound Design and Synthesis.

Most small-molecule CA inhibitors incorporate a primary sulfonamide functional group, which imparts molecular recognition specificity for the zinc in the active site of CAs but not the metals of other metalloenzymes [29]. The active site of CA IX is, however, structurally similar to those of CA I and CA II, the major CA isozymes within red blood cells, (CA I:  $1.6 \pm 2.3$  mg/g of hemoglobin (Hb); CA II:  $1.8 \pm 0.3$  mg/g of Hb) [35]. As a consequence of the binding of sulfonamide-based imaging agents to CA I and CA II in red blood cells, increased background signal and reduced image contrast have hampered the efforts of others in this field [2, 36, 37]. Our group has contributed substantially to the development of CA inhibitors with enhanced selectivity for CA IX over CA I and CA II in vitro and, via extrapolation, in vivo [4]. We have shown that the different CA active sites have variable tolerance to the nature of moieties appended to the aromatic sulfonamide CA targeting group [38-42]. This attribute allows fine-tuning of the bioactive, physicochemical, and toxicological properties of the compound to better target a particular CA isozyme [43]. The CA IX targeting agents of this study, compounds **1** ( $^{nat}\text{Ga}$  and  $^{67}\text{Ga}$ ) and **2** ( $^{nat}\text{Ga}$ ,  $^{67}\text{Ga}$ , and  $^{68}\text{Ga}$ ), extend our established design principles. These compounds are primary sulfonamides tethered to a metal chelator, 1,4,7,10-tetraazacyclododecane-1,4,7,10-tetraacetic acid (DOTA), via either an intervening aliphatic triazole linker (**1**) or a hydrophilic triazole poly(ethylene glycol) (PEG) linker (**2**) (Figure 2). The DOTA macrocycle is the workhorse metal ion chelator for molecular imaging agents, forming stable complexes with the PET imaging isotope  $^{68}\text{Ga}$  [44].  $^{68}\text{Ga}$  is becoming a relevant isotope for routine clinical examinations, with  $^{68}\text{Ga}$  PET imaging agents such as  $^{68}\text{Ga}$ -DOTATATE and  $^{68}\text{Ga}$ -HBED-PSMA in clinical use [45, 46].  $^{67}\text{Ga}$  is a common radionuclide for use with single photon emission computed tomography (SPECT). The most widely used application is of  $^{67}\text{Ga}$ -citrate for inflammation and infection imaging. The relatively long half-life ( $t_{1/2} = 3.26$  days) makes  $^{67}\text{Ga}$  a useful tool for the assessment of key parameters of gallium-based radiopharmaceuticals, including radiochemical stability, metabolic stability, and plasma protein binding, and this in turn informs subsequent decisions on in vivo protocols. The preparation of  $^{67}\text{Ga}$  complexes also permits the optimization of radiolabeling conditions, purification methodology, and reformulation procedures prior to using the shorter-half-life PET radionuclide  $^{68}\text{Ga}$ . We first synthesized the “cold” compounds,  $^{nat}\text{Ga}$ -**1** and  $^{nat}\text{Ga}$ -**2**, followed by the corresponding radiolabeled compounds [ $^{67}\text{Ga}$ ]-**1** and [ $^{67}\text{Ga}$ ]-**2** to establish optimized radiolabeling conditions. [ $^{68}\text{Ga}$ ]-**2** was selected as the target compound for in vivo PET imaging studies.

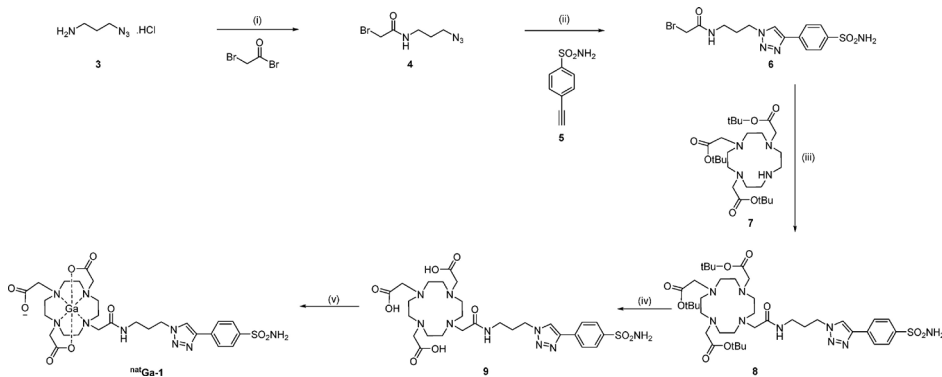


**Figure 2.** Target [sulfonamide]–[triazole linker]–[DOTA] compounds for use as CA IX imaging agents.

The compound design as [sulfonamide]–[variable linker]–[DOTA] is deliberately modular. This enables a straightforward synthesis using copper-catalyzed azide–alkyne cycloaddition (CuAAC), or “click chemistry”, to combine the components. CuAAC is one of the most accomplished reactions for combining groups to pool their individual properties into a single molecule [47]. The biopharmaceutical stability of the resulting triazole is favorable, as it is resistant to acidic, basic, reductive, and oxidative conditions in addition to enzymatic degradation [48]. Scaffold **2** employs a tetraethylene glycol linker, which is a shortened PEG chain with good biopharmaceutical properties, polarity, and water solubility, aiding the eventual formulation [49]. The PEG-based linker was additionally selected to enhance the likelihood that the agents would have improved specificity for CA IX. The increased polarity reduces plasma protein binding and membrane permeability and thus may lessen the off-target binding to CA I and CA II in red blood cells [50]. A previous generation of DOTA-based scaffolds were designed by Rami and co-workers, but to the best of our knowledge, these were not radiolabeled or evaluated as CA IX imaging agents *in vivo* [51, 52].

The target compounds **1** and **2** are synthesized from three modular components, [sulfonamide], [linker], and [DOTA], with incorporation of the gallium cation as the final step (Schemes 1 and 2). The synthesis of the [sulfonamide] component, 4-ethynylbenzenesulfonamide (**5**), has been described previously [53]. The [linker] components, **4** and **11**, were designed with orthogonal end groups. An azide facilitates the reaction with **5** via CuAAC, while the bromide provides an orthogonal leaving group facilitating the  $S_N2$  substitution reaction with the [DOTA] component **7**. Linkers **4** and **11** were prepared by reaction of bromoacetyl bromide (3.3 equiv) with amino azides **3** [54] and **10**, respectively [55]. The [sulfonamide] component **5** and [linker] components **4** and **11** were subjected to  $CuSO_4$  (0.01–0.05 equiv), sodium ascorbate (0.1 equiv), and TBTA (0.01–0.05 equiv) to generate **6** and **12**, respectively. The removal of excess copper ions from **6** and **12** was achieved by a solid EDTA chase or by washing the organic phases with EDTA (1.0 M) in ammonium

hydroxide (28.0–30.0%,  $\text{NH}_3$  basis) solution. The [DOTA] component **7** was prepared from commercially available cyclen as described by Prashun et al [56].  $\text{S}_{\text{N}}2$  substitution of **6** and **12** with **7** using anhydrous conditions gave the *t*Bu-protected compounds **8** and **13** in reasonable yields. Treatment of compounds **8** and **13** with either neat formic acid or 1:1 TFA/DCM removed the *t*Bu protecting groups to provide the nonmetalated precursor compounds **9** and **14** in high yield. Next, the target  $^{\text{nat}}\text{Ga}$  complexes,  $^{\text{nat}}\text{Ga-1}$  and  $^{\text{nat}}\text{Ga-2}$ , were prepared in quantitative yield from **9** and **14** using  $\text{Ga}(\text{NO}_3)_3 \cdot x\text{H}_2\text{O}$  in  $\text{H}_2\text{O}$  with the pH adjusted to pH 4.5 with 1.0 M HCl or 1.0 M KOH. Compounds **9** and **14** were purified by reversed-phase HPLC (RP-HPLC) prior to biological evaluation and radiolabeling with  $^{67}\text{Ga}$  and/or  $^{68}\text{Ga}$ .

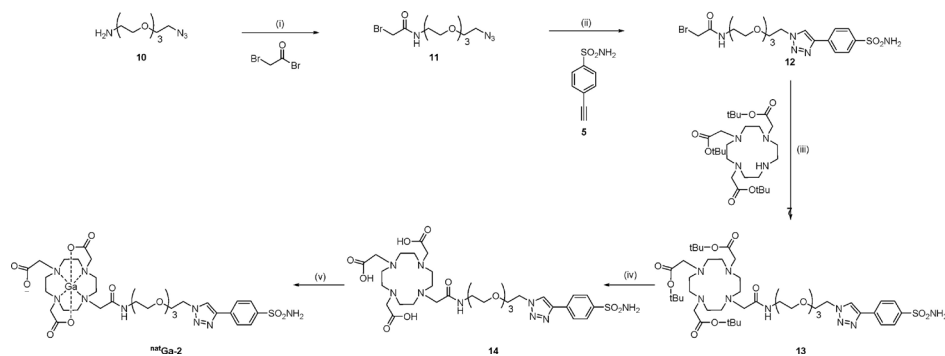


**Scheme 1.** Synthesis of  $^{\text{nat}}\text{Ga-1}$ <sup>a</sup>

<sup>a</sup>Reagents and conditions: (i) bromoacetyl bromide (3.3 equiv), 1.0 M aqueous NaOH (3 equiv), DCM, rt, 18 h; (ii) **5** (1.0 equiv),  $\text{CuSO}_4$  (0.05 equiv), sodium ascorbate (0.1 equiv), TBTA (0.05 equiv), 2:1 DMSO/ $\text{H}_2\text{O}$ , 45 °C, 3 h; (iii) **7** (1.2 equiv),  $\text{K}_2\text{CO}_3$  (1.2 equiv), anhydrous MeCN, rt, 18 h; (iv) 1:1 TFA/DCM, rt, 18 h; (v)  $\text{Ga}(\text{NO}_3)_3 \cdot x\text{H}_2\text{O}$  (1.1 equiv),  $\text{H}_2\text{O}$ , 80 °C, 2–4 h.

### Carbonic Anhydrase Binding

The CA binding data for  $^{\text{nat}}\text{Ga-1}$ ,  $^{\text{nat}}\text{Ga-2}$ , and the reference CA inhibitor acetazolamide were measured for the cancer-associated CA isozymes CA IX and XII and the off-target CA isozymes CA I and CA II. Compounds  $^{\text{nat}}\text{Ga-1}$  and  $^{\text{nat}}\text{Ga-2}$  have low affinity for CA I but bind equally well to CA II, CA IX, and CA XII ( $K_i$  range 59.6–84.7 nM) (Table 1). Binding to CA II supports the significance and importance of designing probes to have reduced cell-membrane permeability, as this limits access of the probes to the intracellular CA II.

**Scheme 2.** Synthesis of <sup>nat</sup>Ga-2<sup>a</sup>

<sup>a</sup>Reagents and conditions: (i) bromoacetyl bromide (3.3 equiv), NaOH (1.0 M, 2 equiv), DCM, rt, 18 h; (ii) **5** (1.0 equiv), CuSO<sub>4</sub> (0.01 equiv), sodium ascorbate (0.1 equiv), TBTA (0.01 equiv), 2:1 DMSO/H<sub>2</sub>O, 30 °C, 18 h; (iii) **7** (1.2 equiv), K<sub>2</sub>CO<sub>3</sub> (1.3 equiv), anhydrous MeCN, 60 °C, 3 h; (iv) 1:1 TFA/DCM, rt, 18 h; (v) Ga(NO<sub>3</sub>)<sub>3</sub>·xH<sub>2</sub>O (1.1 equiv), H<sub>2</sub>O, 80 °C, 2–4 h.

**Table 1.** Inhibition Data for Human CA Isozymes I, II, IX, and XII with Compounds <sup>nat</sup>Ga-1 and <sup>nat</sup>Ga-2 and the Reference Compound Acetazolamide

compd	<i>K<sub>i</sub></i> (nM) <sup>a,b</sup>				selectivity <sup>c</sup>		
	hCA I	hCA II	hCA IX	hCA XII	CA I/CA IX	CA II/CA IX	CA XII/CA IX
acetazolamide <sup>d</sup>	250	12	25	n/a	10	0.48	n/a
<sup>nat</sup> Ga-1	387	72.5	84.7	59.6	4.57	0.85	0.70
<sup>nat</sup> Ga-2	169	78.3	63.1	56.8	2.67	1.24	0.90

<sup>a</sup>Errors were in the range of ±5% of the reported value, from three determinations. <sup>b</sup>Measured using a stopped-flow assay that monitors the physiological reaction (CA-catalyzed hydration of CO<sub>2</sub>) [57, 58]. <sup>c</sup>Selectivity is determined by the ratio of *K<sub>i</sub>* values for CA isozymes I, II, and XII relative to CA IX. <sup>d</sup>Literature acetazolamide values [59].

## Radiochemistry

Compounds **9** and **14** were successfully radiolabeled with <sup>67</sup>Ga under standard conditions (0.1 M sodium acetate, pH 4.5, 10 min, 95 °C). To test the robustness of the radiolabeling method developed, the compound amount was progressively reduced from 10 to 1 nmol and the radiochemical yield quantified by RP-HPLC (Table 2). It was shown that **9** was successfully radiolabeled (to give [<sup>67</sup>Ga]-**1**) down to 2 nmol of compound (98%) but at 1 nmol, only 61% radiolabeling was achieved. However, **14** was radiolabeled efficiently (to give [<sup>67</sup>Ga]-**2**) down to 1 nmol of compound (>99%). Purification of the radiolabeled products

was carried out using either RP-HPLC or rapid reversed phase C-18 solid-phase extraction (SPE). Both [<sup>67</sup>Ga]-**1** and [<sup>67</sup>Ga]-**2** were reformulated into phosphate-buffered saline (PBS).

**Table 2.** Radiochemical Yields of [<sup>67</sup>Ga]-**1** and [<sup>67</sup>Ga]-**2** at Varying Compound Concentrations<sup>a</sup>

amount of compd (nmol)	radiochemical yield (%) <sup>b</sup>	
	9 → [ <sup>67</sup> Ga]- <b>1</b>	14 → [ <sup>67</sup> Ga]- <b>2</b>
25	100	100
10	>99	>98
5	n/a	>99
2	98	100
1	61	>99

<sup>a</sup>Reaction conditions: Compound 9 or 14 (1 mM in water), sodium acetate (0.1 M, to pH 4.5), <sup>67</sup>GaCl<sub>3</sub> (18–21 MBq in 0.1 M HCl), 95 °C, 10 min. <sup>b</sup>As determined by RP-HPLC (conditions available in the Supporting Information). <sup>c</sup>Labeling in HEPES buffer proceeded with >99% radiochemical yield. <sup>d</sup>±standard deviation based on two radiolabeling experiments.

Compound **14** was radiolabeled with <sup>68</sup>Ga (200–800 MBq, eluted from a <sup>68</sup>Ge/<sup>68</sup>Ga generator (IDB Holland, Baarle-Nassau, The Netherlands) in about 1 mL of 0.6 M HCl), in 400 µL of 3.0 M sodium acetate or ammonium acetate (pH 4.3, 10 min, 99 °C) in high radiochemical purity (>95%) as determined by radio-RP-HPLC (Inertsil ODS C18, 5 µM, 4.6 mm × 250 mm, 100:0 → 0:100 H<sub>2</sub>O + 0.1% TFA/MeCN + 0.1% TFA, 1.0 mL/min).

### Biopharmaceutical Properties

The stability of the <sup>67</sup>Ga radiolabeled compounds [<sup>67</sup>Ga]-**1** and [<sup>67</sup>Ga]-**2** was examined in PBS (pH 7.4). The compounds were found to be stable, with ≥95% of the parent compounds remaining after 18 h of incubation at 37.5 °C and ≥90% after 96 h of incubation. The protein binding of [<sup>67</sup>Ga]-**1** and [<sup>67</sup>Ga]-**2** to human serum was minimal (< 7%, n = 3) after 48 h. [<sup>67</sup>Ga]-**2** exhibited favorable radiochemical purity (data not shown), good stability, and good preliminary physicochemical properties. Hence, additional biopharmaceutical properties of cold <sup>nat</sup>Ga-**2** were assessed (Table 3); by extrapolation, these properties should reflect those expected for the radiolabeled analogue [<sup>68</sup>Ga]-**2**. The in vitro metabolic stability of compound <sup>nat</sup>Ga-**2** in mouse liver microsomes was measured in the presence and absence of NADPH, the cofactor required for oxidative metabolism by cytochrome P450s. Compound <sup>nat</sup>Ga-**2** exhibited minimal microsomal degradation (t<sub>1/2</sub> > 247 min), and it is expected that compound <sup>nat</sup>Ga-**2** is subject to low hepatic clearance in vivo. The in

vitro intrinsic clearance of <sup>nat</sup>Ga-2 was low (<7 μL min<sup>-1</sup> (mg protein)<sup>-1</sup>). The in vitro membrane permeability ( $P_{app}$ ) of <sup>nat</sup>Ga-2 in the Caco-2 cell model (pH 7.4) was measured. <sup>nat</sup>Ga-2 was not detected in the Caco-2 assay acceptor chamber, while good mass balance (92% ± 6%) confirmed minimal retention of the compound within the cell monolayer and minimal nonspecific adsorption. The experimental value measured,  $P_{app} < 0.7$  cm/s, indicates that <sup>nat</sup>Ga-2 has very low cell membrane permeability. The stability and extent of plasma protein binding of <sup>nat</sup>Ga-2 in mouse plasma was analyzed. The measured concentration of <sup>nat</sup>Ga-2 in mouse plasma samples (37 °C) quenched at 2 min was unchanged. However, at 10 min the concentration of <sup>nat</sup>Ga-2 had dropped but then remained steady over the remainder of the 4 h incubation. Plasma protein binding of <sup>nat</sup>Ga-2 was low (39%) following 4 h of incubation. The cytotoxicity and cell viability of <sup>nat</sup>Ga-2 were tested via a standard methyl thiazolyl tetrazolium assay, with no toxicity observed up to 1 mM <sup>nat</sup>Ga-2 in normoxia (data not shown). Collectively, these additional properties of <sup>nat</sup>Ga-2 are indicative of a safe, well-tolerated compound with physicochemical properties suited to preferential targeting of CA IX over intracellular CAs and hence a favorable TBR of the corresponding <sup>68</sup>Ga compound.

**Table 3.** Biopharmaceutical Properties of Compound <sup>nat</sup>Ga-2

degradation $t_{1/2}$ (min) <sup>a</sup>	in vitro $CL_{int}$ (μL min <sup>-1</sup> )mg of protein <sup>-1</sup> ) <sup>a</sup>	microsome-predicted $E_H$ <sup>b</sup>	$P_{app}$ (cm/s) <sup>c</sup>	plasma protein binding (4 h) <sup>d</sup>
>247	<7	<0.13	<0.7	39%

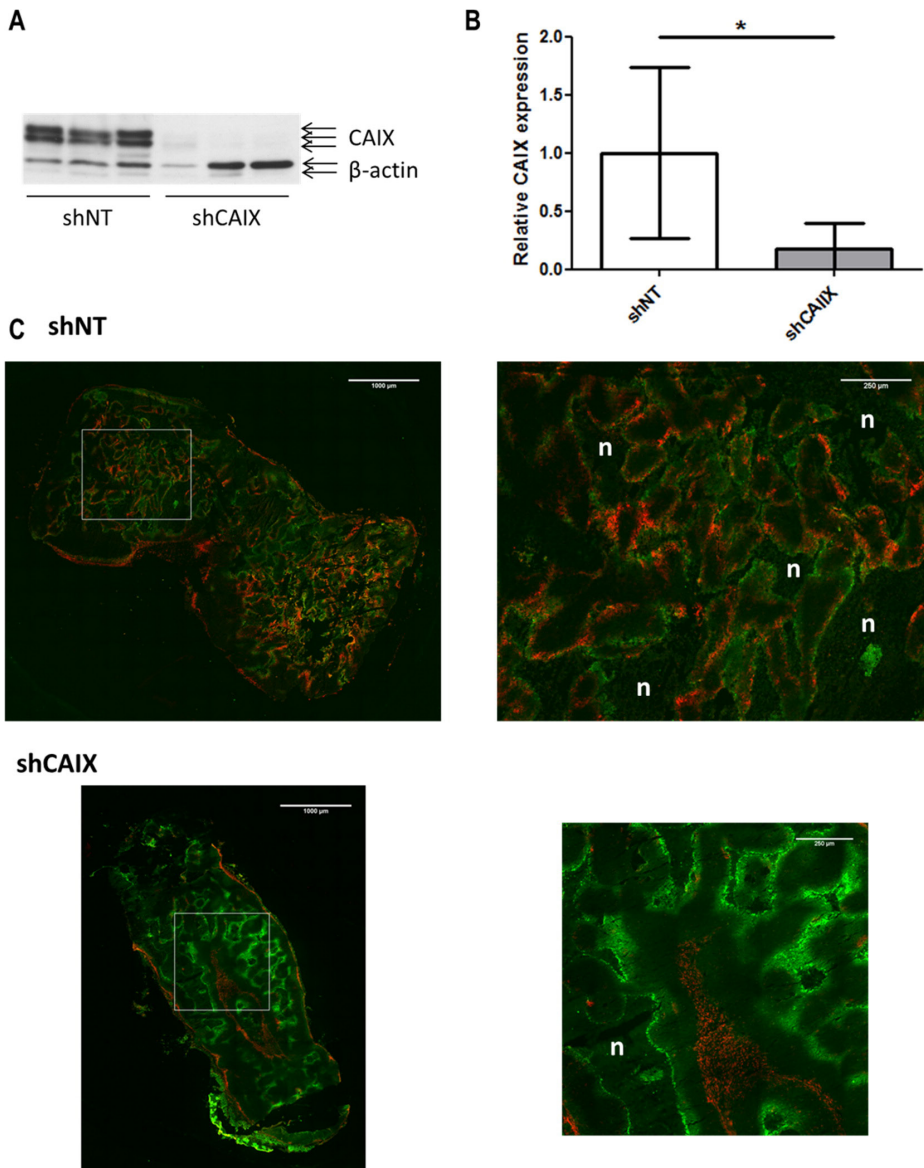
<sup>a</sup>The metabolic stability parameters for compound <sup>nat</sup>Ga-2 are based on NADPH-dependent degradation profiles in mouse liver microsomes. In vitro  $CL_{int}$  is the intrinsic clearance value. <sup>b</sup>Predicted in vivo hepatic extraction ratio ( $E_H$ ).

<sup>c</sup> $P_{app}$  = apparent permeability across Caco-2 monolayers. <sup>d</sup>Average of duplicate determinations.

### Small Animal PET and PET/CT Imaging Studies

Our lead compound, [<sup>68</sup>Ga]-2, was chosen for follow-up in vivo PET studies and was injected intravenously into mice bearing HCT116 tumors with high or low CA IX expression to assess the selectivity of uptake using PET. The efficiency of CA IX genetic silencing was determined by Western blot analysis and immunofluorescence. In agreement with previous studies [60, 61], CA IX levels were significantly lower in CA IX-knockdown tumors than in CA IX-expressing tumors (Figure 3A, B). Additionally, as determined by immunofluorescence staining, membranous CA IX expression was colocalized with the exogenous hypoxia marker pimonidazole in CA IX-expressing tumors, whereas in CA IX-knockdown

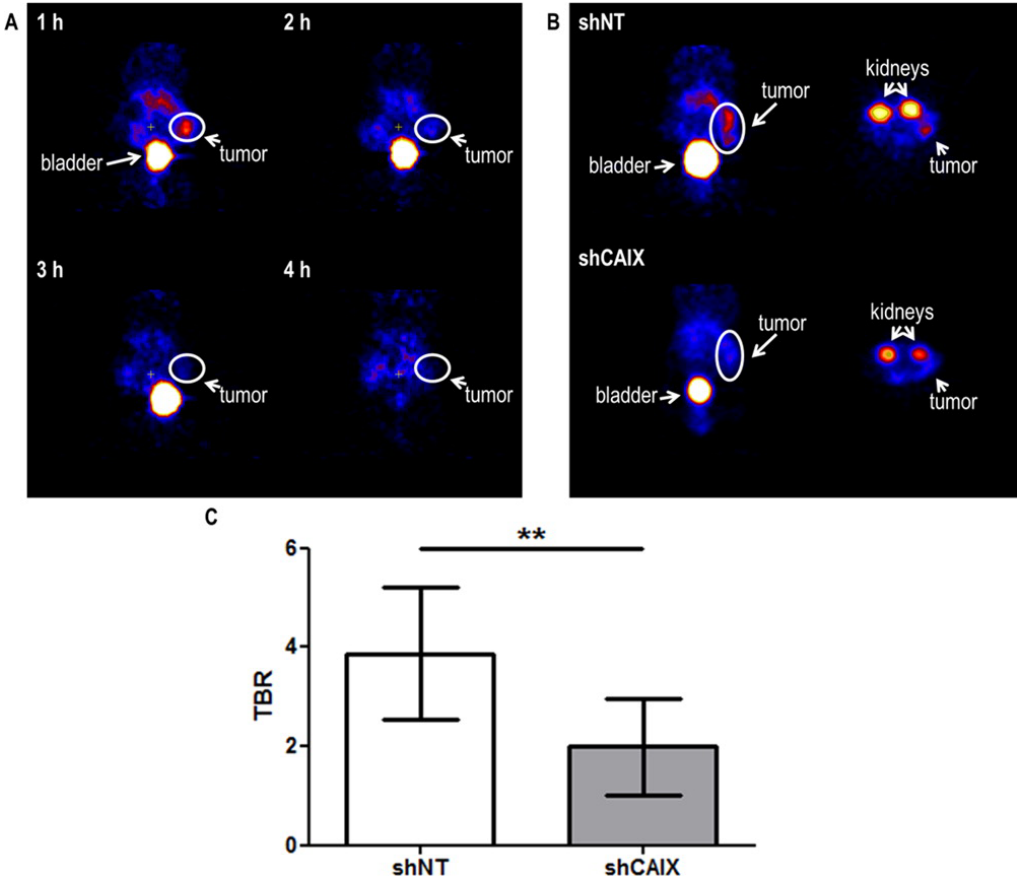
tumors very low or no CA IX expression was present (Figure 3C). This confirms efficient CA IX knockdown and thus CA IX-dependent uptake of [ $^{68}\text{Ga}$ ]-2.



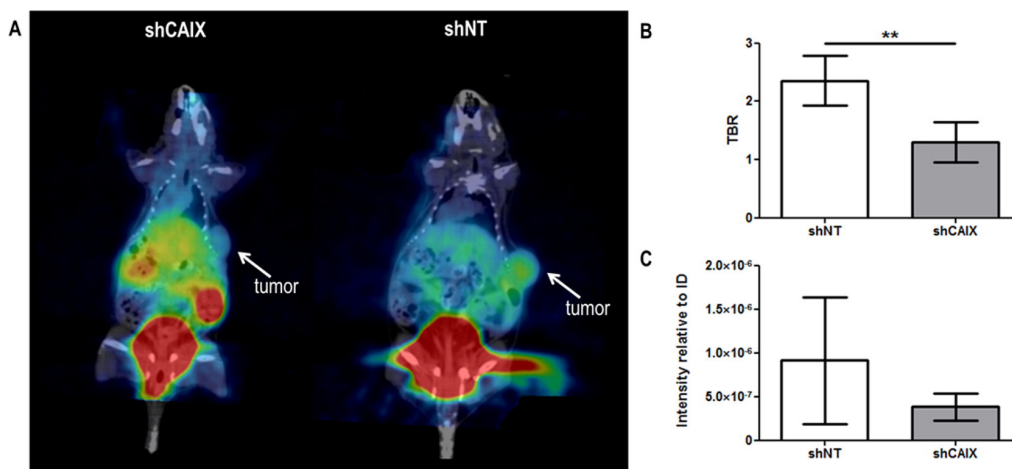
**Figure 3.** CA IX expression in mice bearing CA IX-expressing (shNT) or CA IX-knockdown (shCA IX) tumors. (A) Western blot showing CA IX protein levels in representative samples. (B) Quantification of CA IX protein levels as determined by Western blot for all shNT and shCA IX tumors. (C) Immunofluorescence staining of CA IX (red) and the hypoxia marker pimonidazole (green). Right-side images are magnifications of areas within the white rectangles in the left-side images. “n” indicates necrotic areas.

In order to determine the optimal imaging time point,  $\mu$ PET scans were acquired hourly from 1 to 4 h post injection (h p.i.) of [<sup>68</sup>Ga]-**2**. Tumor uptake in the CA IX-expressing model was clearly observed and found to be highest at 1 h p.i. (Figure 4A). This time point was selected for all of the subsequent experiments. Additionally, it was found that the agent was rapidly excreted renally, as observed by the high presence of the agent in the kidneys and bladder. Mass spectrometry analysis of the urine confirmed that the compound was cleared without metabolism.

To assess the compound selectivity, uptake was compared between mice with either CA IX-expressing or CA IX-knockdown tumors. Although CA IX-knockdown tumors tend to grow slower than their CA IX-expressing counterparts [61], the tumor volumes at the time of scans were not statistically different ( $P = 0.422$ ) between the two groups ( $315 \pm 104$  and  $277 \pm 63$  mm<sup>3</sup> for CA IX-expressing and CA IX-knockdown tumors, respectively). The TBR was significantly higher ( $P < 0.01$ ) in mice bearing CA IX-expressing tumors ( $3.87 \pm 1.34$ ) compared with mice bearing CA IX-knockdown tumors ( $1.99 \pm 0.99$ ) (Figure 4B, C). Uptake of [<sup>68</sup>Ga]-**2** was therefore found to be CA IX-dependent. However, the lack of anatomical information in the acquired PET images prompted us to verify colocalization with computed tomography (CT). Therefore, the experiments were repeated to include CT scans, enabling better tumor delineation in the fused PET/CT images and more clearly confirming the localization of the agent in the tumor. Again the tumor volumes at the time of scans were not statistically different ( $P = 0.071$ ) between the two groups ( $492 \pm 390$  and  $125 \pm 44$  mm<sup>3</sup> for CA IX-expressing and CA IX-knockdown tumors respectively). Similar to the first experiment, the TBR was significantly higher ( $P < 0.01$ ) in mice bearing CA IX-expressing tumors ( $2.36 \pm 0.424$ ) than in mice bearing CA IX-knockdown tumors ( $1.30 \pm 0.350$ ) (Figure 5A, B). Autoradiography analysis of tumor sections supported the  $\mu$ PET results, showing a higher signal intensity relative to injected dose (ID) in CA IX-expressing tumors ( $9.12 \cdot 10^{-7} \pm 7.25 \cdot 10^{-7}$ ) compared with CA IX-knockdown tumors ( $3.84 \cdot 10^{-7} \pm 1.53 \cdot 10^{-7}$ ) (Figure 5C). Low uptake of [<sup>68</sup>Ga]-**2** was also observed in the CA IX-knockdown model, which can be explained by residual CA IX expression in these tumors. Nevertheless, the significantly higher uptake of [<sup>68</sup>Ga]-**2** in tumors with high CA IX expression confirms the selectivity of this imaging compound.



**Figure 4.** [ $^{68}\text{Ga}$ ]-2 uptake in mice bearing CA IX-expressing (shNT) or CA IX-knockdown (shCA IX) tumors. (A) Representative  $\mu\text{PET}$  scans at 1–4 h p.i. in a shNT-tumor bearing mouse. (B) Representative  $\mu\text{PET}$  scans at 1 h p.i. (C) TBRs of [ $^{68}\text{Ga}$ ]-2 uptake determined from PET scans of shNT-tumor bearing mice ( $n = 11$ ) and shCA IX-tumor bearing mice ( $n = 6$ ). \*\*,  $P < 0.01$ .



**Figure 5.**  $^{68}\text{Ga}$ -2 uptake in mice bearing CA IX-expressing (shNT) or CA IX-knockdown (shCA IX) tumors. (A) Representative  $\mu\text{PET}/\text{CT}$  fusion images at 1 h p.i. (B) TBRs of  $^{68}\text{Ga}$ -2 uptake determined from PET scans of shNT-tumor bearing mice ( $n = 4$ ) and shCA IX-tumor bearing mice ( $n = 5$ ). \*\*,  $P < 0.01$ . (C) Signal intensity relative to injected dose (ID) as determined by autoradiography analysis of tumor sections from shNT-tumor bearing mice ( $n = 6$ ) and shCA IX-tumor bearing mice ( $n = 6$ ).

## Conclusion

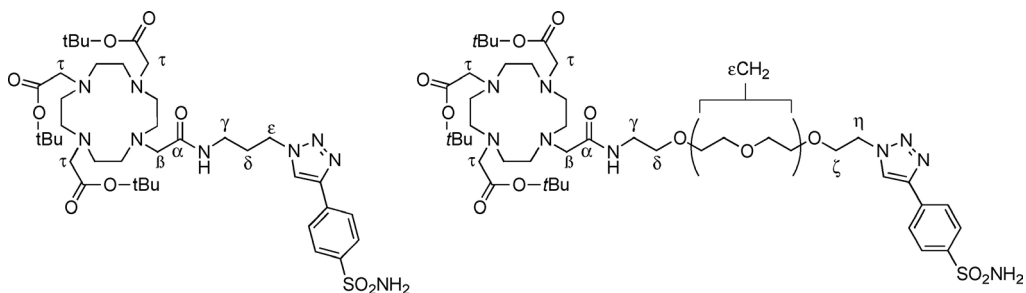
This study provides the first evidence of noninvasive, specific detection of CA IX *in vivo* using a CA IX-targeting small-molecule PET radiotracer,  $^{68}\text{Ga}$ -2. The synthesis of the unlabeled precursor of  $^{68}\text{Ga}$ -2 (compound **14**) and the radiochemistry to introduce  $^{68}\text{Ga}$  were straightforward, proceeded in good yields, and were reproducible, and the biopharmaceutical properties were favorable. This study is a promising step toward a new predictive tool that will enable testing of the potential of CA IX expression as a biomarker for selection of patients eligible for CA IX-targeting anticancer therapies.

## Experimental Section

### Chemistry - General Methods

All of the starting materials and reagents were purchased from commercial suppliers. Where specified, solvents were available commercially dried or were dried prior to use. Reactions took place open to the atmosphere unless otherwise specified. Reaction prog-

ress was monitored by thin-layer chromatography (TLC) using silica gel 60 F254 plates with detection by short-wave UV fluorescence ( $\lambda = 254$  nm) and staining with ninhydrin (1 g of ninhydrin, 200 mL of EtOH, 8 mL of acetic acid),  $\text{KMnO}_4$  (0.75 g of  $\text{KMnO}_4$ , 5 g of  $\text{K}_2\text{CO}_3$ , 75 mg of NaOH, 100 mL of  $\text{H}_2\text{O}$ ), or vanillin stain (5 g of vanillin in an 87:10.2:2.8 EtOH/ $\text{H}_2\text{O}/\text{H}_2\text{SO}_4$  mixture with subsequent heating); by TLC using RP-18 silica gel 60 F254 plates with detection by short-wave UV fluorescence; or by high-performance liquid chromatography (HPLC) on an Agilent 1100 system using a Thermo Betasil C18 column (150 mm  $\times$  4.6 mm, 5  $\mu\text{m}$ ) and a gradient method of 95:5  $\rightarrow$  5:95  $\text{H}_2\text{O}$  (+0.1% TFA)/acetonitrile (+0.1% TFA) over 10 min at a flow rate of 1 mL/min. Silica gel flash chromatography was performed using silica gel 60 Å (230–400 mesh). NMR ( $^1\text{H}$ ,  $^{13}\text{C}\{^1\text{H}\}$ ,  $^1\text{H}-^1\text{H}$  gCOSY, and HSQC) spectra were recorded on either a 400 or 500 MHz spectrometer at 30 °C.  $^1\text{H}$  NMR spectra were referenced to the residual solvent peak ( $\text{CDCl}_3$ , 7.26 ppm;  $\text{DMSO}-d_6$ , 2.50 ppm).  $^{13}\text{C}$  NMR spectra were referenced to the internal solvent ( $\text{CDCl}_3$ , 77.0 ppm;  $\text{DMSO}-d_6$ , 39.5 ppm). Multiplicity is indicated as follows: s (singlet), d (doublet), t (triplet), q (quartet), quint (quintuplet), m (multiplet), dd (doublet of doublets), ddd (doublet of doublets of doublets), b (broad). Coupling constants ( $J$ ) are reported in hertz. Mestrenova 6.1 software was used for NMR analysis. Melting points are uncorrected. Mass spectra (low- and high-resolution) were recorded using electrospray as the ionization technique in positive-ion and/or negative-ion mode as stated. The purities of all final compounds (**8**, **9**,  $^{\text{nat}}\text{Ga-1}$ , and  $^{\text{nat}}\text{Ga-2}$ ) were  $\geq 95\%$  as determined by HPLC with UV detection. Compounds **3**, **4**, **5**, **7**, and **10** were synthesized as described elsewhere, with characterization in agreement with the literature [53, 54, 56, 62-65]. The atom labeling of DOTA compounds used for NMR assignments is shown in Scheme 3.



**Scheme 3.** Atom Labeling of DOTA Compounds

## Chemistry – Synthesis Methods

### General Procedure 1: Synthesis of Brominated [linker] Components

The amino azide precursor (1 equiv) was suspended in a biphasic DCM/NaOH(aq) solution (2:1, 2–3 equiv of NaOH) and cooled to 0 °C. Bromoacetyl bromide (3 equiv) was added dropwise to the DCM layer. The solution was then stirred vigorously overnight at rt. The reaction mixture was diluted with DCM and H<sub>2</sub>O, and the aqueous fraction was extracted with DCM (2 × 50 mL). The organic fractions were combined and washed with 50 mM Na<sub>2</sub>CO<sub>3</sub> (3 × 50 mL), dried with MgSO<sub>4</sub>, filtered, and concentrated. The crude compound was sufficiently pure and used crude in the next step.

### General Procedure 2: Addition of “Cold” Ga

The parent compound (**9** or **14**, 1 equiv) was suspended in H<sub>2</sub>O, and excess Ga(NO<sub>3</sub>)<sub>3</sub>·*x*-H<sub>2</sub>O(aq) was added. The pH of the reaction mixture was adjusted to ~4.5 using KOH (1.0 M) or HCl (1.0 M). The reaction mixture was heated at 80 °C, and the pH was monitored and adjusted accordingly to maintain pH 4.5. The reaction mixture stabilized after ~2 h. Reaction progress was monitored by LC–MS. Products were purified by RP-18 flash column chromatography (H<sub>2</sub>O/MeOH 100:0 → 5:95), and the solvent was removed in vacuo, leaving a hygroscopic solid.

### *N*-(3-Azidopropyl)-2-bromoacetamide (**4**)

The title compound was synthesized from 3-azido-1-propanamine HCl salt (**3**) (1.5 g, 11 mmol) and NaOH (2 equiv) using general procedure 1 and isolated as a yellow oil (1.9 g, 78%). *R*<sub>f</sub> 0.13 (90:10 DCM/MeOH). <sup>1</sup>H NMR (500 MHz, CDCl<sub>3</sub>): δ<sub>H</sub> 6.72 (br s, 1H, NH), 3.88 (s, 2H, βCH<sub>2</sub>), 3.40–3.36 (m, 4H, γCH<sub>2</sub>, εCH<sub>2</sub>), 1.82 (quint, 2H, *J* = 6.60 Hz, δCH<sub>2</sub>). <sup>13</sup>C NMR (125 MHz, CDCl<sub>3</sub>): δ<sub>C</sub> 165.8 (αC=O), 49.5 (εCH<sub>2</sub> or γCH<sub>2</sub>), 38.1 (εCH<sub>2</sub> or γCH<sub>2</sub>), 29.3 (βCH<sub>2</sub>), 28.6 (δCH<sub>2</sub>). LRMS (ESI<sup>-</sup>): *m/z* = 221, 219 [M – H; <sup>81</sup>Br, <sup>79</sup>Br]<sup>-</sup>. HRMS (ESI)<sup>+</sup>: calcd for C<sub>5</sub>H<sub>9</sub><sup>79</sup>BrN<sub>4</sub>NaO<sup>+</sup>, 242.9852; found, 242.9852. The <sup>1</sup>H NMR data were in agreement with the data reported in the literature [62].

### 2-Bromo-*N*-(3-[4-(4-sulfamoylphenyl)-1*H*-1,2,3-triazol-1-yl]propyl)acetamide (**6**)

CuSO<sub>4</sub> (7 mg, 0.027 mmol) and sodium ascorbate (10.8 mg, 0.055 mmol) were combined in 1 mL of H<sub>2</sub>O and added to a solution of alkyne **11** (100 mg, 0.55 mmol), azide **5** (145 mg, 0.66 mmol), and TBTA (14.5 mg, 0.027 mmol) in DMSO (2 mL). The mixture was left to stir at 45 °C, and the reaction was monitored by TLC. Once the reaction was complete (1.5 h), the reaction mixture was filtered through Celite and washed with H<sub>2</sub>O, and the

filtrate was redissolved in DMF. The DMF was concentrated to a minimum amount before EtOAc (30 mL) was added and the organic phase was rapidly washed with EDTA in ammonium hydroxide (1.0 M, 50 mL). The organic fraction was dried ( $\text{MgSO}_4$ ) and filtered, and the remaining residue was purified by flash column chromatography (90:10 EtOAc/MeOH). The product was isolated as a white powder (0.04 g, 18%).  $R_f$  0.36 (80:20 DCM/MeOH), mp 182–185 °C.  $^1\text{H}$  NMR (500 MHz,  $\text{DMSO-}d_6$ ):  $\delta_{\text{H}}$  8.70 (s, 1H, triazole CH), 8.39 (t, 1H, NH), 8.02 (m, 2H, 2  $\times$  ArCH), 7.89 (m, 2H, 2  $\times$  ArCH), 7.37 (s, 2H,  $\text{SO}_2\text{NH}_2$ ), 4.45 (t,  $J$  = 7.0 Hz, 2H,  $\epsilon\text{CH}_2$ ), 3.85 (s, 2H,  $\beta\text{CH}_2$ ), 3.15 (q,  $J$  = 6.7 Hz, 2H,  $\gamma\text{CH}_2$ ), 2.08–2.02 (quint,  $J$  = 6.9 Hz, 2H,  $\delta\text{CH}_2$ ).  $^{13}\text{C}$  NMR (500 MHz,  $\text{DMSO-}d_6$ ):  $\delta_{\text{C}}$  166.2 ( $\alpha\text{C}=\text{O}$ ), 145.0 (Cq), 143.1 (triazole Cq), 133.9 (Cq), 126.4 (2  $\times$  CHAr), 125.3 (2  $\times$  CHAr), 122.6 (triazole CH), 47.4 ( $\epsilon\text{CH}_2$ ), 36.3 ( $\gamma\text{CH}_2$ ), 29.5 ( $\beta\text{CH}_2$  and  $\delta\text{CH}_2$ ), 29.4 ( $\beta\text{CH}_2$  and  $\delta\text{CH}_2$ ). LRMS (ESI<sup>-</sup>):  $m/z$  = 402, 400 [M - H;  $^{81}\text{Br}$ ,  $^{79}\text{Br}$ ]<sup>-</sup>. HRMS (ESI): calcd for  $\text{C}_{13}\text{H}_{16}\text{BrN}_5\text{O}_3\text{S}^+$ , 402.0228; found, 402.0208.

**Tri-*tert*-butyl 2,2',2''-(10-(2-Oxo-2-((3-(4-(4-sulfamoylphenyl)-1*H*-1,2,3-triazol-1-yl)propyl)amino)ethyl)-1,4,7,10-tetraazacyclododecane-1,4,7-triyl)triacetate (8)**

Compound **7** (109 mg, 0.21 mmol), **6** (85 mg, 0.21 mmol), and  $\text{K}_2\text{CO}_3$  (58 mg, 0.42 mmol) were dissolved in anhydrous MeCN (5 mL), and the reaction mixture was stirred overnight at room temperature. The mixture was filtered through Celite and washed with MeOH. The residue was purified by flash column chromatography (gradient 100% DCM  $\rightarrow$  85:15 DCM/MeOH). Appropriate fractions were combined, and the product was isolated as a hygroscopic solid (59.3 mg, 33%).  $R_f$  0.04 (95:5 DCM/MeOH).  $^1\text{H}$  NMR (400 MHz,  $\text{DMSO-}d_6$ , 85 °C):  $\delta_{\text{H}}$  8.63 (s, 1H, CH triazole), 8.17 (t,  $J$  = 5.38 Hz, 1H, NH), 7.98 (m, 2H, 2  $\times$  ArCH), 7.91 (m, 2H, 2  $\times$  ArCH), 7.20 (s, 2H,  $\text{SO}_2\text{NH}_2$ ), 4.45 (t,  $J$  = 7.1 Hz, 2H,  $\epsilon\text{CH}_2$ ), 3.53 (MeOH), 3.19 (m, 2H,  $\gamma\text{CH}_2$ ), 3.08 (s, 6H,  $\tau\text{CH}_2$ ), 2.94 (dt,  $J$  = 42.0, 5.2 Hz, 2H,  $\text{CH}_2$  Aza), 2.61 (br, 7H,  $\text{CH}_2$  Aza), 2.30 (br, 7H,  $\text{CH}_2$  Aza), 2.10 (quint,  $J$  = 6.9 Hz, 2H,  $\delta\text{CH}_2$ ), 1.44 (s, 9H, *t*Bu), 1.40 (s, 18H, 2  $\times$  *t*Bu).  $^{13}\text{C}$  NMR (75.5 MHz,  $\text{DMSO-}d_6$ ):  $\delta_{\text{C}}$  172.5 (C=O), 172.2 (2  $\times$  C=O), 171.6 (C=O), 145.0 (Cq triazole), 143.1 (Cq Ar), 133.9 (Cq Ar), 126.4 (2  $\times$  ArCH), 125.3 (2  $\times$  ArCH), 122.5 (CH triazole), 81.1 (Cq *t*Bu), 80.9 (2  $\times$  Cq *t*Bu), 69.8 (MeOH), 60.18 ( $\tau\text{CH}_2$ ), 55.7 ( $\tau\text{CH}_2$ ), 55.3 ( $\tau\text{CH}_2$ ), 54–49 ( $\text{CH}_2$  Aza in baseline), 47.6 ( $\epsilon\text{CH}_2$ ), 36.0 ( $\gamma\text{CH}_2$ ), 29.6 ( $\delta\text{CH}_2$ ), 27.9 ( $\beta\text{CH}_3$ ), 27.5 ( $\text{CH}_3$  *t*Bu). LRMS (ESI<sup>+</sup>):  $m/z$  = 836 [M + H]<sup>+</sup>. HRMS (ESI): calcd for  $\text{C}_{39}\text{H}_{65}\text{N}_9\text{NaO}_9\text{S}^+$ , 858.4518; found, 858.4513.

**2,2',2''-(10-(2-Oxo-2-((3-(4-(4-sulfamoylphenyl)-1*H*-1,2,3-triazol-1-yl)propyl)amino)ethyl)-1,4,7,10-tetraazacyclododecane-1,4,7-triyl)triacetic Acid (9)**

Compound **8** (87.7 mg, 0.1 mmol) was dissolved in 1:1 DCM/TFA (8 mL), and the solution

was stirred at 40 °C for 3 h. The reaction progress was monitored by LC-MS and RP-18 TLC. When conversion was complete, the solvent was removed in vacuo and then coevaporated with water (×3) followed by lyophilization.  $R_f$  0.76 (50:50 MeOH/H<sub>2</sub>O RP-18 TLC). Samples for radiolabeling were purified using HPLC (isocratic 7:93 MeCN/H<sub>2</sub>O + 0.1% formic acid on a Waters Atlantis T3 C18 column (19 mm × 150 mm, 10 μM) at a flow rate of 12 mL/min). Product fractions were collected, and the solvent was removed in vacuo (8.5 mg, 52% HPLC recovery). <sup>1</sup>H NMR (500 MHz, DMSO-*d*<sub>6</sub>): δ<sub>H</sub> 8.69 (s, 1H, CH triazole), 8.57 (t,  $J$  = 5.2 Hz, 1H, NH), 8.01 (m, 2H, 2 × ArCH), 7.90 (s, 2H, 2 × ArCH), 7.38 (s, 2H, SO<sub>2</sub>NH<sub>2</sub>), 4.48 (t,  $J$  = 6.8 Hz, 2H, εCH<sub>2</sub>), 4.1–3.0 (m, signals masked by broad H<sub>2</sub>O peak), 3.18 (q,  $J$  = 5.1 Hz, 2H, γCH<sub>2</sub>), 2.08 (quint, 2H, δCH<sub>2</sub>). Correlations under the H<sub>2</sub>O peak were observed in the <sup>1</sup>H–<sup>1</sup>H gCOSY and HSQC spectra. LRMS (ESI<sup>+</sup>):  $m/z$  = 668 [M + H]<sup>+</sup>. HRMS (ESI): calcd for C<sub>27</sub>H<sub>42</sub>N<sub>9</sub>O<sub>9</sub>S<sup>+</sup>, 668.2821; found, 668.2819.

#### ***N*-[2-[2-[2-(2-Azidoethoxy)ethoxy]ethoxy]ethyl]-2-bromoacetamide (11)**

The title compound was synthesized from 11-azido-3,6,9-trioxaundecanamine (**10**) (450 mg, 2.08 mmol) using general procedure 1 and isolated as a yellow oil (0.54 g, 76%).  $R_f$  0.35 (95:5 DCM/MeOH). <sup>1</sup>H NMR (500 MHz, CDCl<sub>3</sub>): δ<sub>H</sub> 6.92 (s, 1H, NH), 3.87 (s, 2H, βCH<sub>2</sub>), 3.71–3.63 (m, 10H, εCH<sub>2</sub>, ζCH<sub>2</sub>), 3.59 (t,  $J$  = 5.1 Hz, 2H, δCH<sub>2</sub>), 3.49 (m, 2H, γCH<sub>2</sub>), 3.39 (t,  $J$  = 5.0 Hz, 2H, ηCH<sub>2</sub>N<sub>3</sub>). <sup>13</sup>C NMR (125 MHz, CDCl<sub>3</sub>): δ<sub>C</sub> 165.8 (αC=O), (70.9, 70.8, 70.7, 70.5, 70.2, εCH, ζCH<sub>2</sub>), 69.5 (δCH<sub>2</sub>), 50.8 (ηCH<sub>2</sub>), 40.1 (γCH<sub>2</sub>), 29.2 (βCH<sub>2</sub>). LRMS (ESI<sup>-</sup>):  $m/z$  339, 337 [M – H, <sup>81</sup>Br, <sup>79</sup>Br]<sup>-</sup>. HRMS (ESI<sup>+</sup>): calcd for C<sub>10</sub>H<sub>19</sub><sup>79</sup>BrN<sub>4</sub>O<sub>4</sub><sup>+</sup>, 339.0662; found, 339.0684. The <sup>1</sup>H NMR data were in agreement with the data reported in the literature [66].

#### **2-Bromo-*N*-[[2-(2-[2-[4-(4-sulfamoylphenyl)-1H-1,2,3-triazol-1-yl]ethoxy]ethoxy)ethoxy]methyl]acetamide (12)**

CuSO<sub>4</sub> (2 mg, 0.007 mmol) and sodium ascorbate (14 mg, 0.071 mmol) were combined in 1 mL of H<sub>2</sub>O and added to a solution of azide **11** (264 mg, 0.78 mmol), alkyne **5** (128 mg, 0.71 mmol), and TBTA (4 mg, 0.007 mmol) in DMSO (2 mL). The mixture was left to stir at 45 °C, and the reaction was monitored by TLC. Once the reaction was complete, the reaction mixture was diluted with H<sub>2</sub>O and EtOAc, and the aqueous phase was extracted with EtOAc (4 × 30 mL). The organic fractions were combined and washed with EDTA (1.0 M) in ammonium hydroxide (28.0–30.0%, NH<sub>3</sub> basis) solution, dried (Na<sub>2</sub>SO<sub>4</sub>), filtered, and purified by flash column chromatography (95:5 EtOAc/MeOH or DCM/MeOH). The product was isolated as a yellow gum (0.148 g, 40%).  $R_f$  0.2 (95:5 DCM/MeOH), mp 85–90 °C. <sup>1</sup>H NMR (500 MHz, DMSO-*d*<sub>6</sub>): δ<sub>H</sub> 8.66 (s, 1H, triazole CH), 8.28 (br t,  $J$  = 5.90 Hz, 1H, NH),

8.02 (m, 2H, 2 × ArCH), 7.90 (m, 2H, 2 × ArCH), 7.36 (s, 2H, SO<sub>2</sub>NH<sub>2</sub>), 4.60 (t, *J* = 5.2 Hz, 2H, ηCH<sub>2</sub>), 3.88 (t, *J* = 5.2 Hz, 2H, ζCH<sub>2</sub>), 3.84 (s, 2H, βCH<sub>2</sub>), 3.58–3.45 (m, 8H, εCH<sub>2</sub>), 3.39 (t, *J* = 5.7 Hz, 2H, δCH<sub>2</sub>NH), 3.20 (q, *J* = 5.67 Hz, 2H, γCH<sub>2</sub>). <sup>13</sup>C NMR (500 MHz, DMSO-*d*<sub>6</sub>): δ<sub>c</sub> 166.0 (αC=O), 144.9 (C<sub>q</sub> Ar-triazole), 143.0 (C<sub>q</sub> Ar-SO<sub>2</sub>NH<sub>2</sub>), 133.9 (C<sub>q</sub> triazole), 126.3 (2 × ArCH), 125.25 (2 × ArCH), 122.84 (CH triazole), 69.7–69.5 (εCH<sub>2</sub>, 4C), 68.7 (δCH<sub>2</sub> or ζCH<sub>2</sub>), 68.6 (δCH<sub>2</sub> or ζCH<sub>2</sub>), 54.8 (DCM), 49.7 (ηCH<sub>2</sub>), 48.6 (γCH<sub>2</sub>), 29.4 (βCH<sub>2</sub>). LRMS (ESI<sup>+</sup>): *m/z* = 544, 542 [M + Na, <sup>81</sup>Br, <sup>79</sup>Br]<sup>+</sup>; 522, 520 [M + H, <sup>81</sup>Br, <sup>79</sup>Br]<sup>+</sup>. HRMS (ESI): calcd for C<sub>18</sub>H<sub>26</sub><sup>79</sup>Br-N<sub>5</sub>NaO<sub>6</sub>S<sup>+</sup>, 542.0679; found, 542.0681.

**Tri-*tert*-butyl 2,2',2''-(10-(2-Oxo-14-(4-(4-sulfamoylphenyl)-1*H*-1,2,3-triazol-1-yl)-6,9,12-trioxa-3-azatetradecyl)-1,4,7,10-tetraazacyclododecane-1,4,7-triyl)triacetate (13)**

Compound **12** (0.196 g, 0.37 mmol), **7** (253 mg, 0.49 mmol), and K<sub>2</sub>CO<sub>3</sub> (68 mg, 0.49 mmol) were dissolved in anhydrous MeCN (8 mL), and the reaction mixture was stirred at 60 °C for 3h. The mixture was filtered through Celite, washed (MeCN), and concentrated, and the remaining residue was purified by column chromatography (90:10 DCM/MeOH). The fractions were monitored by HPLC, and positive fractions were combined to give the title compound as a hygroscopic off-white solid (0.268 g, 76%). *R*<sub>f</sub> 0.28 (90:10 DCM/MeOH). <sup>1</sup>H NMR (500 MHz, DMSO-*d*<sub>6</sub>): δ<sub>H</sub> 8.67 (s, 1H, CH triazole), 8.18 (t, *J* = 5.9 Hz, 1H, NH), 8.02 (m, 2H, 2 × ArCH), 7.90 (m, 2H, 2 × ArCH), 7.37 (s, 2H, SO<sub>2</sub>NH<sub>2</sub>), 4.59 (t, *J* = 5.1 Hz, 2H, ηCH<sub>2</sub>), 3.88 (t, *J* = 5.1 Hz, 2H, ζCH<sub>2</sub>), 3.50 (m, 8H, εCH<sub>2</sub>), 3.41 (t, *J* = 5.94 Hz, 2H, δCH<sub>2</sub>), 3.21 (m, 2H, γCH<sub>2</sub>), 3.1–2.0 (br, m, 24H, Aza CH<sub>2</sub>, βCH<sub>2</sub>, 3 × τCH<sub>2</sub>), 1.43 (s, 9H, *t*Bu), 1.41 (s, 18H, 2 × *t*Bu). <sup>13</sup>C NMR (125 MHz, DMSO-*d*<sub>6</sub>): δ<sub>c</sub> 172.5 (C=O), 172.1 (2 × C=O), 171.6 (C=O), 144.9 (C<sub>q</sub> triazole), 143.1 (C<sub>q</sub> Ar), 134.0 (C<sub>q</sub> Ar), 126.3 (2 × ArCH), 125.2 (2 × ArCH), 122.8 (CH triazole), 81.1 (C<sub>q</sub> *t*Bu), 80.9 (2 × C<sub>q</sub> *t*Bu), 69.6–69.5 (εCH<sub>2</sub>, βCH<sub>2</sub>), 68.8 (ζCH<sub>2</sub>), 68.5 (δCH<sub>2</sub>), 59.7 (τCH<sub>2</sub>), 55.7 (τCH<sub>2</sub>), 55.3 (τCH<sub>2</sub>), 49.7 (ηCH<sub>2</sub>), 38.5 (γCH<sub>2</sub>), 27.5 (CH<sub>3</sub> *t*Bu), CH<sub>2</sub> Aza peaks masked in baseline. LRMS (ESI<sup>+</sup>): *m/z* = 954 [M + H]<sup>+</sup>. HRMS (ESI): calcd for C<sub>44</sub>H<sub>75</sub>N<sub>9</sub>NaO<sub>12</sub>S<sup>+</sup>, 976.5148; found, 976.5155.

**2-[4,10-Bis(carboxymethyl)-7-[[[2-[2-(2-[2-[4-(4-sulfamoylphenyl)-1*H*-1,2,3-triazol-1-yl]ethoxy]ethoxy]ethoxy]ethyl]carbamoyl]methyl]-1,4,7,10-tetraazacyclododecan-1-yl]acetic Acid (14)**

Compound **13** (0.219 mg, 0.23 mmol) was dissolved in formic acid or 1:1 TFA/DCM (10 mL), and the solution was stirred at 60 °C. The reaction was monitored by HPLC. Upon completion, water (10 mL) was added, and the solvent was removed in vacuo and then

coevaporated with water (×3) followed by lyophilization. The sample was purified by reversed-phase column chromatography using a gradient of 100% H<sub>2</sub>O → 95:5 MeOH/H<sub>2</sub>O, and the product was isolated as a hygroscopic white gum (144 mg, 80%). *R<sub>f</sub>* 0.53 (50:50 MeOH/H<sub>2</sub>O RP-18 TLC). Samples were further purified via HPLC prior to radiolabeling (isocratic 10:90 MeCN/H<sub>2</sub>O + 0.1% formic acid on a Waters Atlantis T3 C18 column (19 mm × 150 mm, 10 μm) at a flow rate of 12 mL/min). The product fractions were collected, and the solvent was removed in vacuo (19%). <sup>1</sup>H NMR (500 MHz, DMSO-*d*<sub>6</sub>): δ<sub>H</sub> 8.67 (s, 1H, CH triazole), 8.17 (br, 1H, NH), 8.02 (m, 2H, 2 × ArCH), 7.90 (m, 2H, 2 × ArCH), 7.38 (s, 2H, SO<sub>2</sub>NH<sub>2</sub>), 4.60 (t, *J* = 5.0 Hz, 2H, ηCH<sub>2</sub>), 3.88 (t, *J* = 5.3 Hz, 2H, ζCH<sub>2</sub>), the remaining signals were masked by the broad H<sub>2</sub>O peak. Correlations were observed in the <sup>1</sup>H-<sup>1</sup>H gCOSY and HSQC spectra. LRMS (ESI<sup>+</sup>): *m/z* 786 [M + H]<sup>+</sup>. HRMS (ESI): calcd for C<sub>32</sub>H<sub>51</sub>N<sub>9</sub>NaO<sub>12</sub>S<sup>+</sup>, 808.3281; found, 808.3278.

**2,2',2''-(10-(2-Oxo-2-((3-(4-(4-sulfamoylphenyl)-1H-1,2,3-triazol-1-yl)propyl)amino)ethyl)-1,4,7,10-tetraazacyclododecane-1,4,7-triyl)triacetic Acid Gallium Complex (<sup>nat</sup>Ga-1)**

Compound **9** (48 mg, 0.071 mmol) was treated as per general procedure 2 to give the title compound as a hygroscopic white solid. LRMS (ESI<sup>-</sup>): *m/z* = 734 [M - H]<sup>-</sup>. HRMS (ESI): calcd for C<sub>27</sub>H<sub>38</sub>GaN<sub>9</sub>NaO<sub>9</sub>S<sup>+</sup>, 756.1661; found, 756.1660.

**2-[4,10-Bis(carboxymethyl)-7-[[[2-[2-(2-[2-[4-(4-sulfamoylphenyl)-1H-1,2,3-triazol-1-yl]ethoxy]ethoxy]ethoxy]ethyl]carbamoyl)methyl]-1,4,7,10-tetraazacyclododecan-1-yl]acetic Acid Gallium Complex (<sup>nat</sup>Ga-2)**

Compound **14** (50 mg, 0.064 mmol) was treated as per general procedure 2 to give the title compound as a hygroscopic white solid. *R<sub>f</sub>* 0.65 (RP-18 TLC, 60:40 H<sub>2</sub>O/MeOH). LRMS (ESI<sup>+</sup>): *m/z* 852 [M + H]<sup>+</sup>. HRMS (ESI): calcd for C<sub>32</sub>H<sub>49</sub>GaN<sub>9</sub>O<sub>12</sub>S<sup>+</sup>, 852.2472; found, 852.2460.

### Cell Culture

Human MDA-MB-231 breast cancer cells (ATCC-26) for toxicity studies were cultured in Roswell Park Memorial Institute (RPMI) 1640 medium supplemented with 10% fetal bovine serum (FBS), 100 units/mL penicillin, and 100 μg/mL streptomycin at 37 °C and 5% CO<sub>2</sub>. Cells were seeded at 3 × 10<sup>4</sup> cells/well (200 μL, RPMI-1640) and allowed to grow for 24 h before being exposed to the compound of interest. Untreated cells were used as a control. HCT116 human colorectal carcinoma cells (ATCC CCL-247) stably expressing a

CA IX-targeting shRNA (shCA IX) or nontargeting shRNA (shNT) construct established as described previously [61] were routinely cultured in Dulbecco's modified Eagle's medium (DMEM) supplemented with 10% FBS at 37 °C.

### Cell Proliferation Assay

Compounds were dissolved in RPMI medium to a final concentration of 1 mM, and linear dilutions ranging from 1 mM to 1  $\mu$ M were carried out in culture medium. After 24 h of treatment at 37 °C and 5% CO<sub>2</sub>, MTT (20  $\mu$ L, 5 mg/mL) was added. After 3 h, SDS (50  $\mu$ L, 20% (w/v) SDS in 0.01 M HCl) was added, and the plates were left overnight before being read by a SpectraMax fluorescence plate reader (Molecular Devices) at 570 nm. Experiments were performed in triplicate and, where possible, were repeated three times. Values were determined using the GraphPad Prism software ([www.graphpad.com](http://www.graphpad.com)).

### Radiolabeling

#### Radiolabeling with <sup>67</sup>Ga

[<sup>67</sup>Ga]GaCl<sub>3</sub> in 0.1 M HCl was prepared from commercial [<sup>67</sup>Ga]citrate for injection (Lantheus) via standard conversion methods [67]. In an acid-washed microcentrifuge tube, the DOTA complex (25  $\mu$ L, 1 mM H<sub>2</sub>O) and sodium acetate buffer (100  $\mu$ L, 0.1 M, pH 4.3) were combined, and the solution was agitated. <sup>67</sup>GaCl<sub>3</sub> (18–21 MBq in 0.1 M HCl) was added, and the solution was heated at 95 °C for 10 min using a solid-state heating block. The sample was stirred via convection. Once the reaction was complete, a sample (20  $\mu$ L, ~3 MBq) was analyzed by HPLC, and the radiochemical purity was noted. The solutions were purified by HPLC (Atlantis T3, 10 mm  $\times$  250 mm, 5  $\mu$ m, flow rate 3 mL/min) or rapid reversed-phase C-18 SPE (washed with copious amounts of H<sub>2</sub>O and compounds eluted in 50:50 EtOH/H<sub>2</sub>O).

#### Stability of [<sup>67</sup>Ga]-1 and [<sup>67</sup>Ga]-2 versus Human Serum

Human serum (150  $\mu$ L) was placed in a previously acid-washed 0.5 mL microcentrifuge tube. To this was added 10 $\times$  PBS concentrate (15  $\mu$ L), water (60  $\mu$ L), and the radiocomplex (75  $\mu$ L in water, 0.24–0.28 MBq). The mixture was agitated via a bench vortex mixer and then incubated at 37.5 °C for the course of the study. Aliquots (5–15  $\mu$ L) were injected onto a Phenomenex Biosep SEC-S 3000 column (300 mm  $\times$  7.8 mm i.d., 5  $\mu$ m, pore size 290 Å) with a mobile phase of 50 mM sodium phosphate and 300 mM NaCl (pH 7.0, 0.2  $\mu$ m filtered) at 1 mL/min on an HPLC system. Serum uptake was assessed as a percentage of the total activity in the chromatogram.

### Stability of [<sup>67</sup>Ga]-1 and [<sup>67</sup>Ga]-2 in Phosphate-Buffered Saline

In a previously acid-washed 0.5 mL microcentrifuge tube, 10× PBS concentrate (20 μL), water (160 μL), and the radiocomplex (20 μL in water, 0.2–0.23 MBq) were combined. The solution was agitated and then incubated at 37.5 °C for the course of the study. Aliquots (5–50 μL) were injected onto a Waters Atlantis T3 C18 column (150 mm × 4.6 mm i.d., 3 μm) with a mobile phase of 16:84 MeCN/ammonium formate buffer (120 mM, pH 4.43, 0.2 μm filtered) at 0.6 mL/min on a HPLC system. Stability was assessed as a percentage of the parent radiocomplex.

### Radiolabeling with <sup>68</sup>Ga

The reaction progress was monitored by radio-HPLC equipped with an Inertsil ODS C18 column (5 μm, 4.6 mm × 250 mm) using a gradient method (100% H<sub>2</sub>O → 100% MeCN over 17 min, 1 mL/min). Sodium acetate or ammonium acetate buffer (3 M, 400 μL, pH 4.3–4.5) was combined with ~800 MBq of <sup>68</sup>Ga in aqueous HCl (0.6 M, ~1.2 mL), which was eluted from an iThemba 1480 MBq <sup>68</sup>Ge/<sup>68</sup>Ga generator. Compound **14** in H<sub>2</sub>O (40 μL, 1 mM) was added, and the solution was mixed by Eppendorf pipet (pH ~4.5) and then heated at 99 °C for 10 min. Reaction mixtures were analyzed by radio-HPLC, and the radiochemical purity was consistently >95%. The specific activity of [<sup>68</sup>Ga]-**2** at the time of radiolabeling was ~20 MBq/nmol (800 MBq/40 nmol). Small-animal PET imaging studies with [<sup>68</sup>Ga]-**2** were carried out between 1 and 2.5 h post radiolabeling of **14** → [<sup>68</sup>Ga]-**2**. No further purification was carried out prior to imaging. Samples (~3.7 MBq) were diluted in 0.9% saline solution prior to injection.

### CA Inhibition Assay

An Applied Photophysics stopped-flow instrument was used for assaying the CA-catalyzed CO<sub>2</sub> hydration activity [58]. IC<sub>50</sub> values were obtained from dose–response curves working at seven different concentrations of test compound by nonlinear least-squares fitting using GraphPad Prism; values represent means of at least three different determinations as described previously [39]. The inhibition constants ( $K_i$ ) were then derived using the Cheng–Prusoff equation:  $K_i = IC_{50}/(1 + [S]/K_m)$ , where [S] is the CO<sub>2</sub> concentration at which the measurement was carried out and  $K_m$  is the concentration of substrate at which the enzyme activity is half-maximal. All of the enzymes used were recombinant, produced in *Escherichia coli* as reported earlier [68, 69]. The following concentrations of enzymes were used in the assay: hCA I, 10.4 nM; hCA II, 8.3 nM; hCA IX, 8.0 nM; hCA XII, 12.4 nM.

### Animal Model

Animal experiments were performed using adult NMRI-*nu* mice. Animal facilities and experiments were in accordance with local institutional guidelines for animal welfare and were approved by the Maastricht University Animal Ethical Committee (no. 2014-020). HCT116 cells stably expressing either a CA IX-targeting shRNA (shCA IX) ( $n = 10$ ) or CA IX-nontargeting shRNA (shNT) ( $n = 10$ ) construct established as described previously [61] were resuspended in BD Matrigel Basement Membrane Matrix (BD Biosciences) and injected ( $10^6$ ) subcutaneously into the lateral flank of the animal.

### Image Acquisition

Once tumors reached a volume between 180 and 300 mm<sup>3</sup>, animals were intravenously injected via the lateral tail vein with ~3.7 MBq of the <sup>68</sup>Ga-labeled sulfonamide compound diluted in 0.9% saline solution via an IV line flushed with 10% heparin saline solution. For PET and CT scans, animals receiving only a PET scan were anesthetized with isoflurane (induction 4%, maintenance 1–2%); animals receiving both PET and CT scans were anesthetized with an intraperitoneal injection of a 100 mg/kg ketamine/10 mg/kg xylazine mixture. PET image acquisition was performed using a Focus 120 microPET (Siemens Medical Solutions USA, Inc.). Animals receiving only a PET scan underwent a 9 min emission scan at 1, 2, 3, and 4 h p.i., whereas animals receiving both PET and CT scans underwent a 15 min emission scan 1 h p.i. The OSEM-3D-reconstructed PET images were viewed and analyzed using the PMOD software (PMOD Technologies Ltd.). Activity data (Bq/mL) were obtained by manually delineating volumes of interest (VOIs) in the PET images for mice that received only a PET scan or in the fused PET/CT images for mice that received both PET and CT scans, using the PMOD software. The tumor itself was delineated as tumor VOI (T), whereas the heart outflow area was delineated as blood VOI (B). Standardized uptake values (SUVs) were calculated by correcting the activity data for the <sup>68</sup>Ga injected dose, decay toward injection time, and weight of the animal. Data were quantified by calculating the T/B activity ratios (TBRs). CT image acquisition was performed using the SmART system (X-RAD 225CX; Precision X-ray, North Branford, CT, USA). Tumor volume at time of scanning was determined by delineating the tumor on the CT image using the PMOD software.

### Western Blot

Samples from tumors were minced, and proteins were isolated using RIPA buffer completed with a protease inhibitor cocktail (complete EDTA-free; Roche). Bradford assay (BioRad)

was performed for protein quantification. Proteins were separated on a 10% SDS-PAGE gel and blotted onto a nitrocellulose membrane (GE Healthcare) by electrotransfer. Membranes were blocked in 5% nonfat dry milk and probed overnight with mouse anti-CA IX monoclonal antibody (M75, kindly provided by S. Pastorekova, Institute of Virology, Slovak Academy of Science, Bratislava, Slovak Republic) and mouse anti- $\beta$ -actin monoclonal antibody (Cell Signaling). Subsequently, membranes were probed with horseradish peroxidase-linked horse anti-mouse IgG antibodies (Cell Signaling), which were detected with Western blot detection reagents (Thermo Fisher Scientific).

### **Immunofluorescence**

Mice were injected intravenously with the hypoxia marker pimonidazole 1 h before sacrifice. After sacrifice, tumors were collected and sections were made. The sections were fixed with cold acetone, and nonspecific binding was blocked using 1% normal goat serum at room temperature for 30 min. The sections were incubated overnight at 4 °C with rabbit anti-CA IX polyclonal antibody (1:1000, Novus Biologicals) and fluorescein isothiocyanate-conjugated mouse antipimonidazole monoclonal antibody (1:100, Hypoxyprobe, Bioconnect). Subsequently, the sections were incubated at room temperature for 1 h with Alexa Fluor 594-conjugated goat anti-rabbit secondary antibody (1:500, Invitrogen). Mounting was done using fluorescence mounting medium (Dako).

### **Autoradiography**

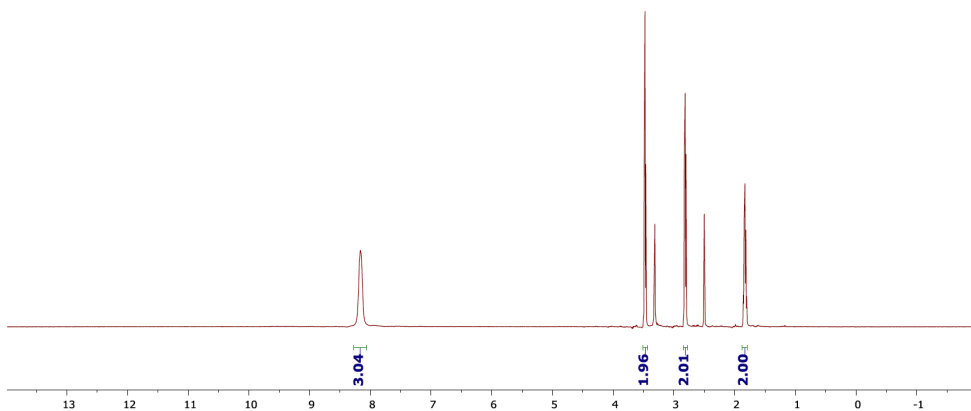
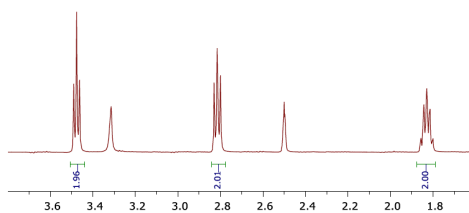
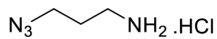
Tumor sections (30  $\mu$ m) were made using a cyrotome (Leica) and placed on high-resolution phosphorimaging plates (Storage Phosphor Screen BAS-IP SR 2040 E Super Resolution, GE Healthcare) overnight. The plates were read using a Typhoon FLA 7000 laser scanner (GE Healthcare). Signal intensities were determined using the ImageQuant TL software (GE Healthcare) and normalized per animal to the respective ID.

### **Statistics**

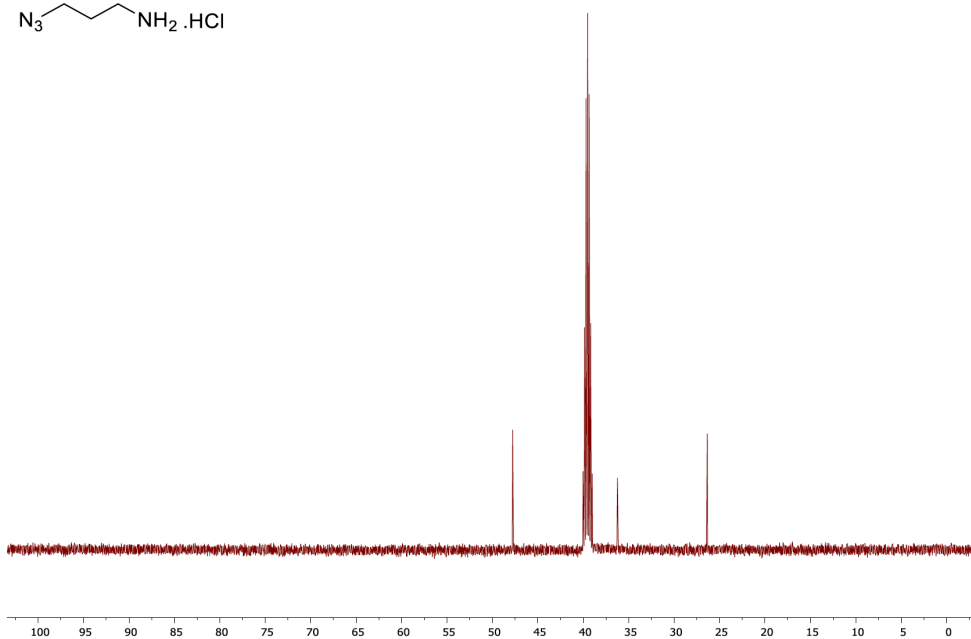
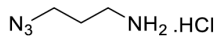
All of the statistical analyses were performed using GraphPad Prism version 5.03. Unpaired Student's *t* test was used to determine the statistical significance of differences between two independent groups of variables.

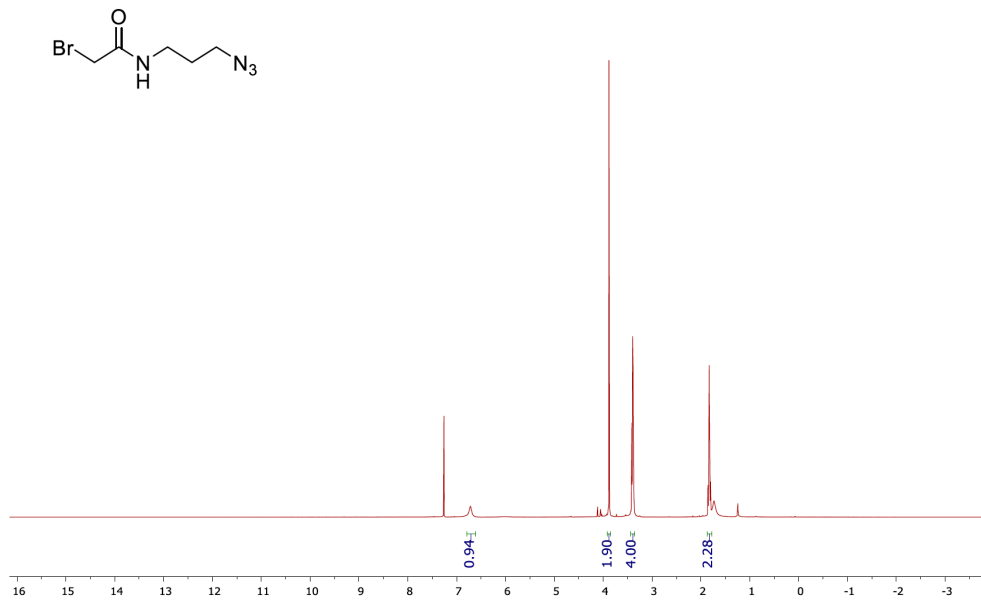
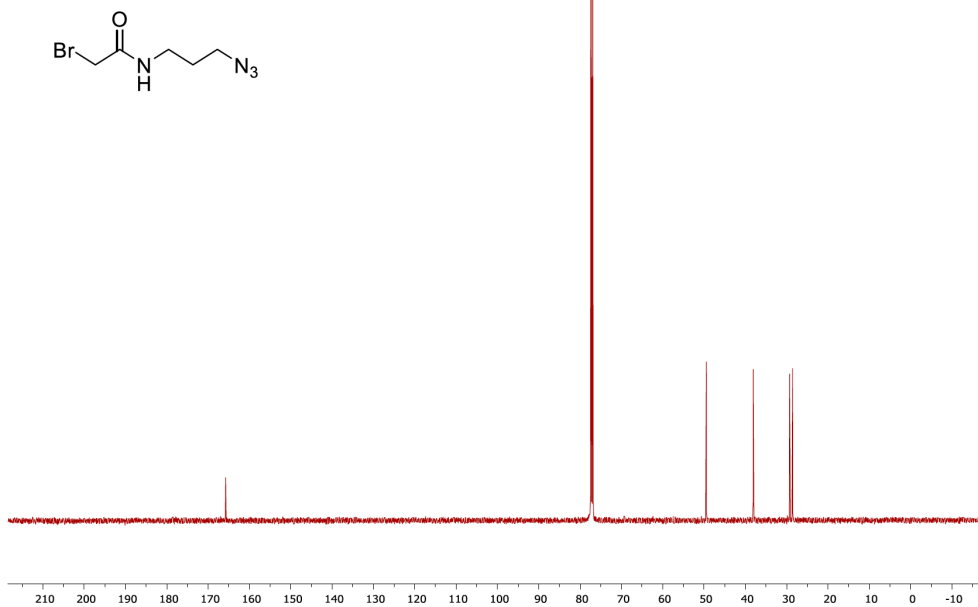
## Supporting information

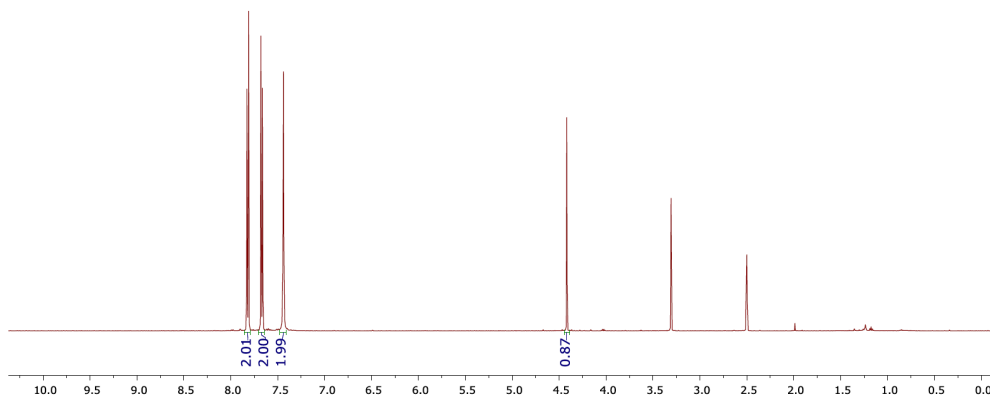
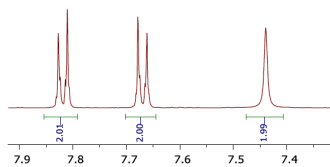
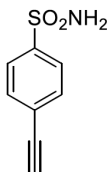
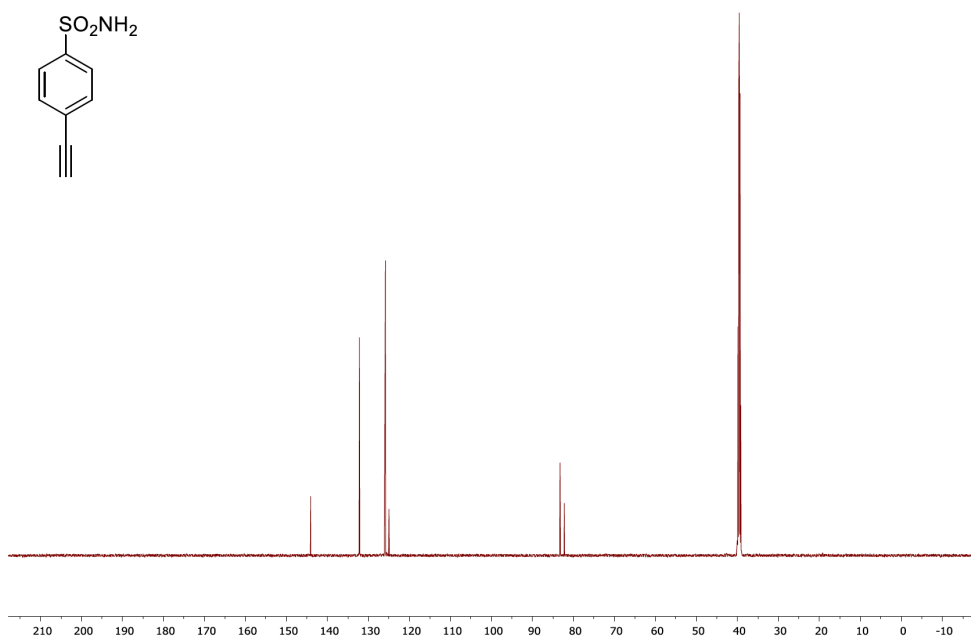
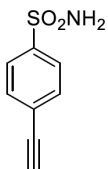
Compound 3 500 MHz  $^1\text{H}$  NMR ( $\text{CD}_3)_2\text{SO}$

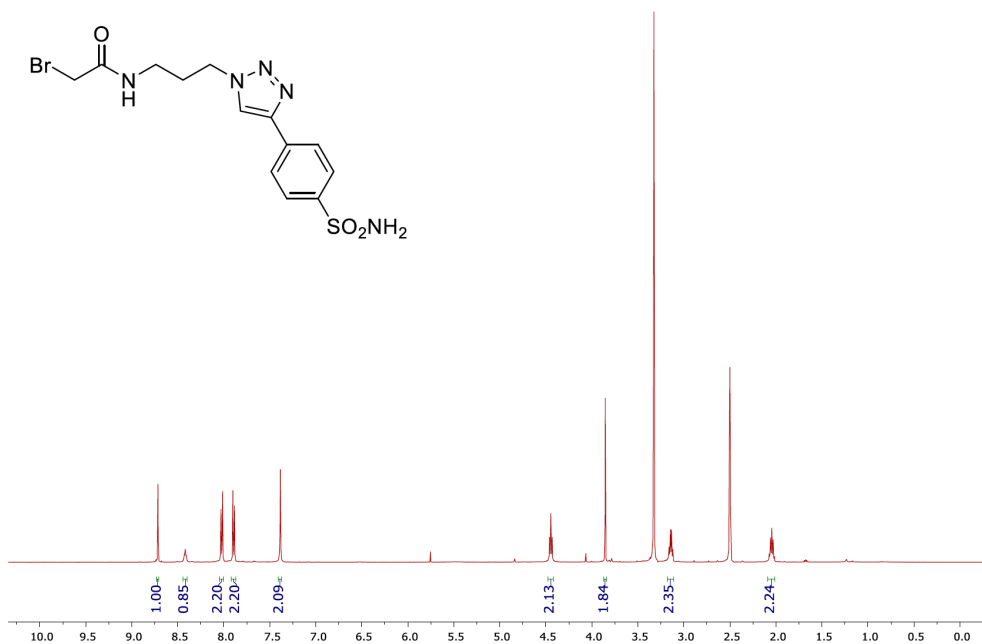
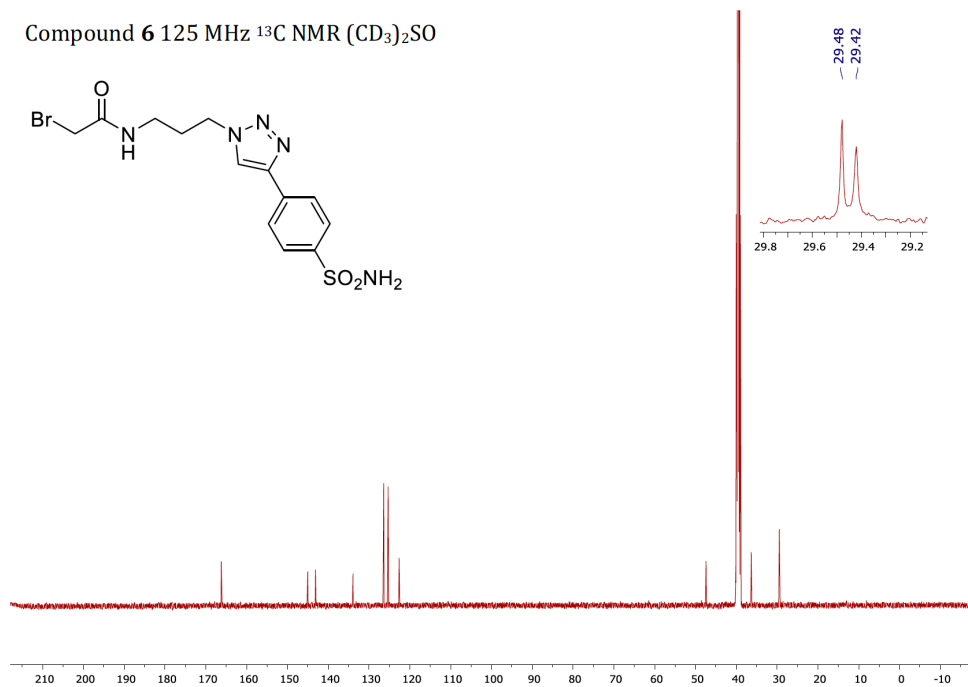


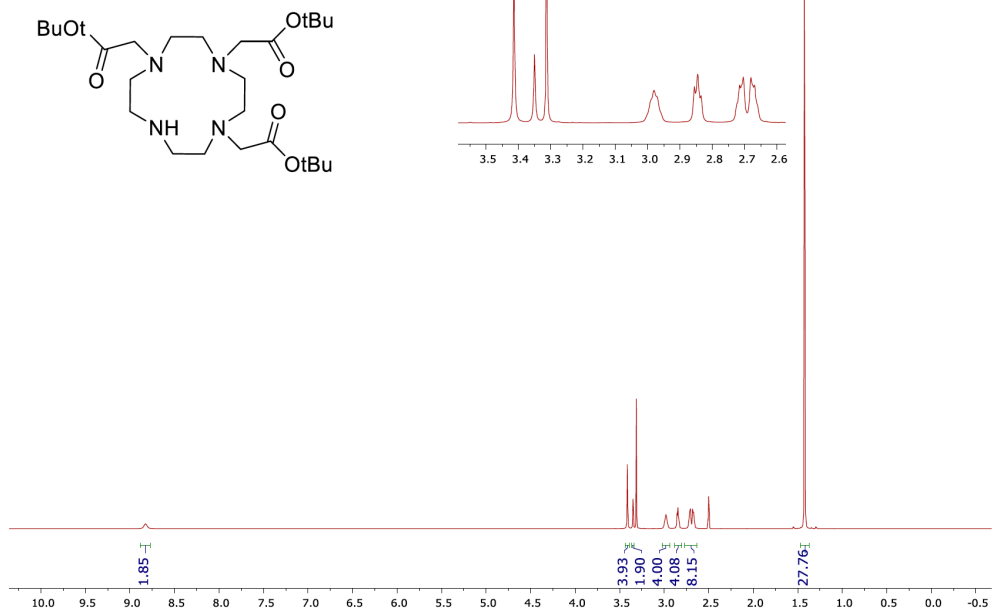
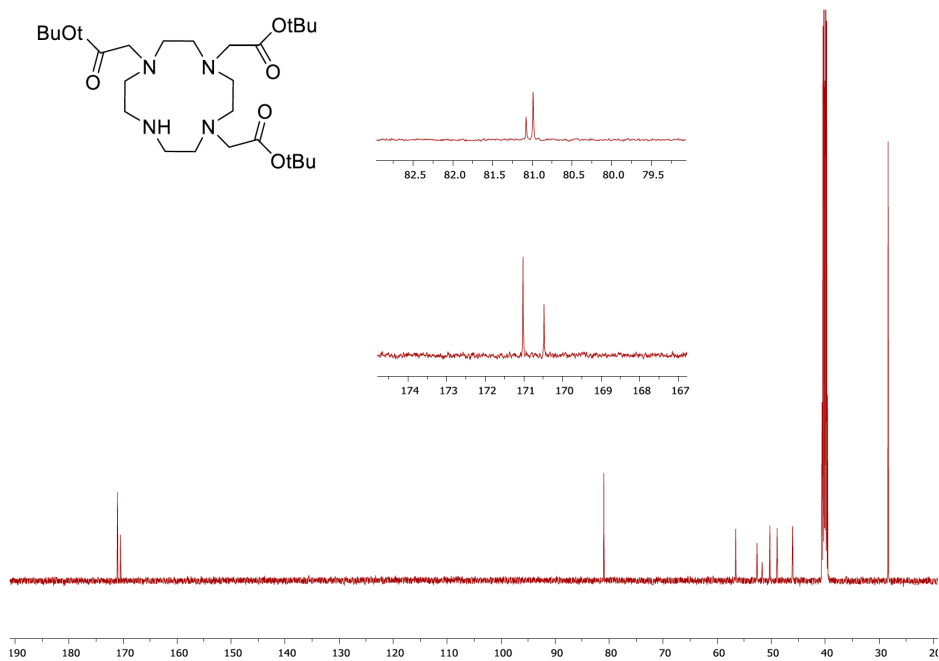
Compound 3 125MHz  $^{13}\text{C}$  NMR ( $\text{CD}_3)_2\text{SO}$



Compound **4** 500 MHz <sup>1</sup>H NMR CDCl<sub>3</sub>Compound **4** 125 MHz <sup>13</sup>C NMR CDCl<sub>3</sub>

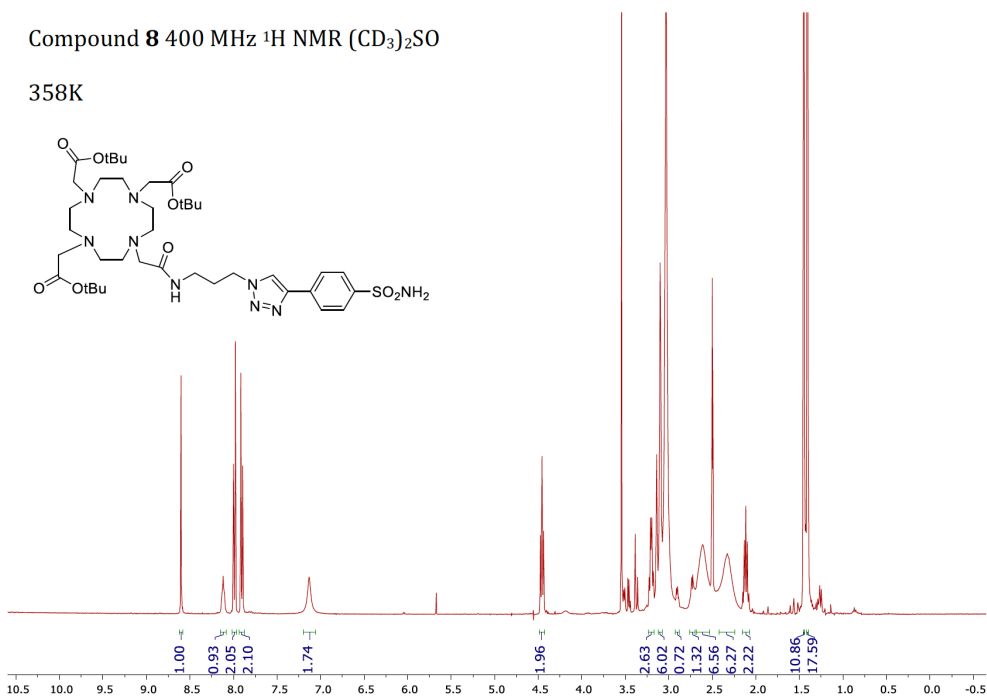
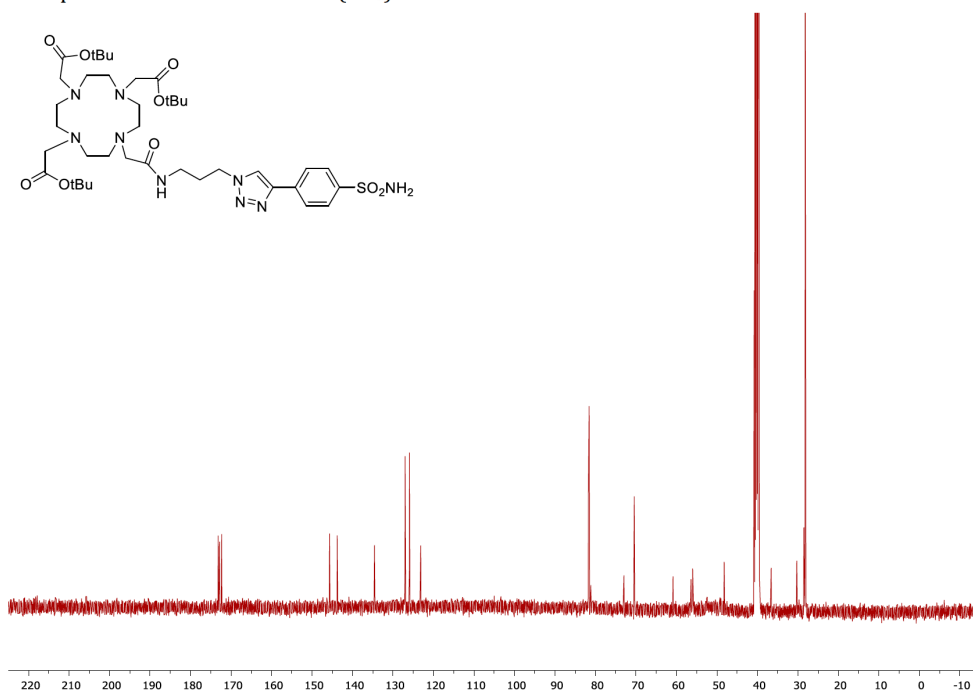
Compound 5 500 MHz  $^1\text{H}$  NMR  $(\text{CD}_3)_2\text{SO}$ Compound 5 125MHz  $^{13}\text{C}$  NMR  $(\text{CD}_3)_2\text{SO}$ 

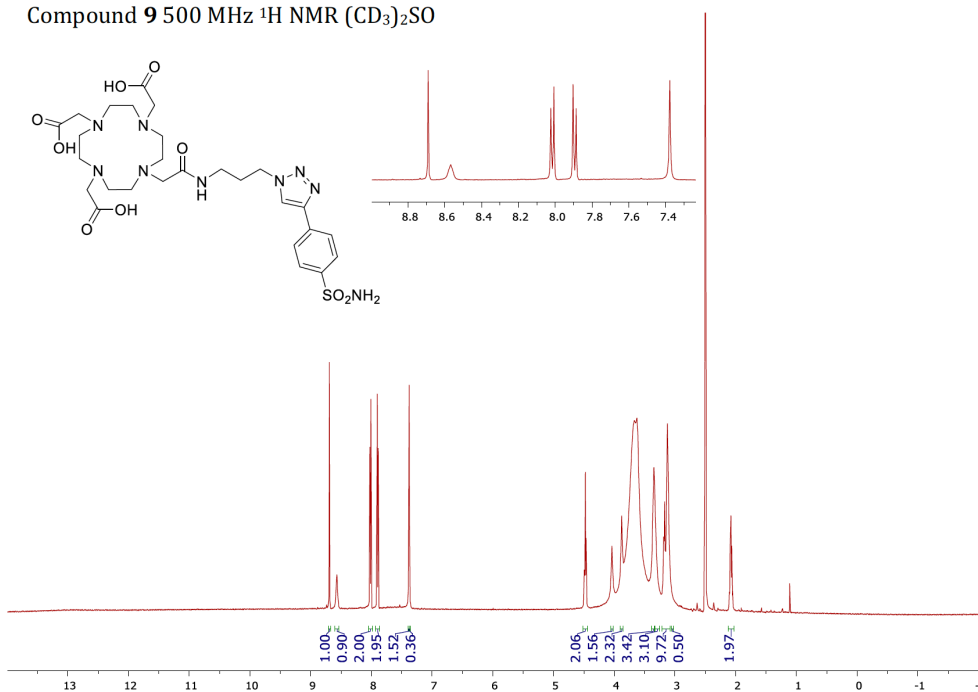
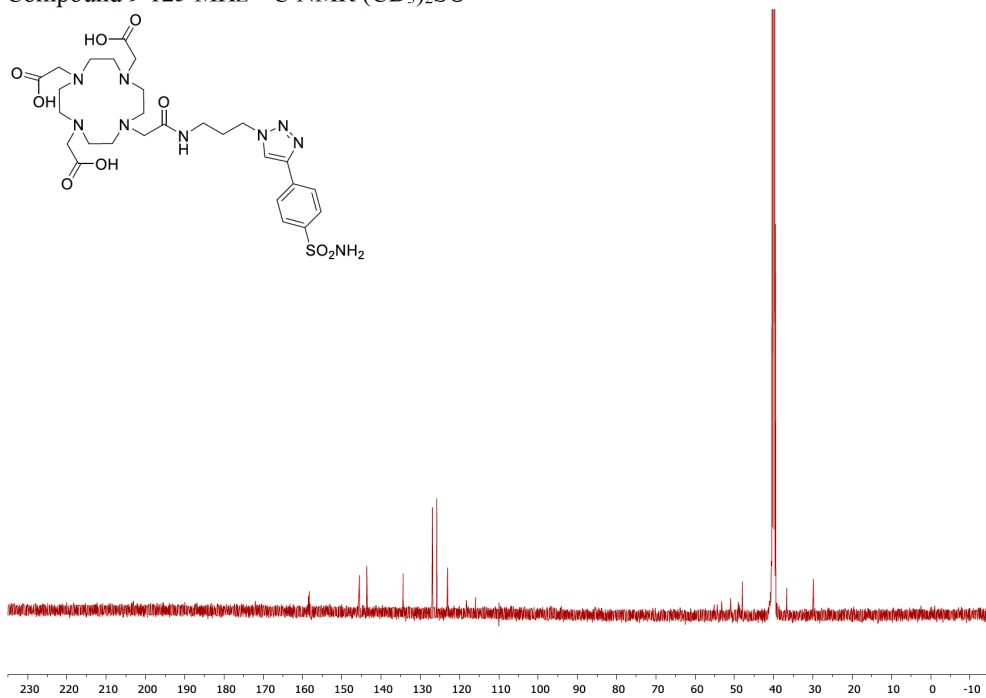
Compound **6** 500 MHz <sup>1</sup>H NMR (CD<sub>3</sub>)<sub>2</sub>SOCompound **6** 125 MHz <sup>13</sup>C NMR (CD<sub>3</sub>)<sub>2</sub>SO

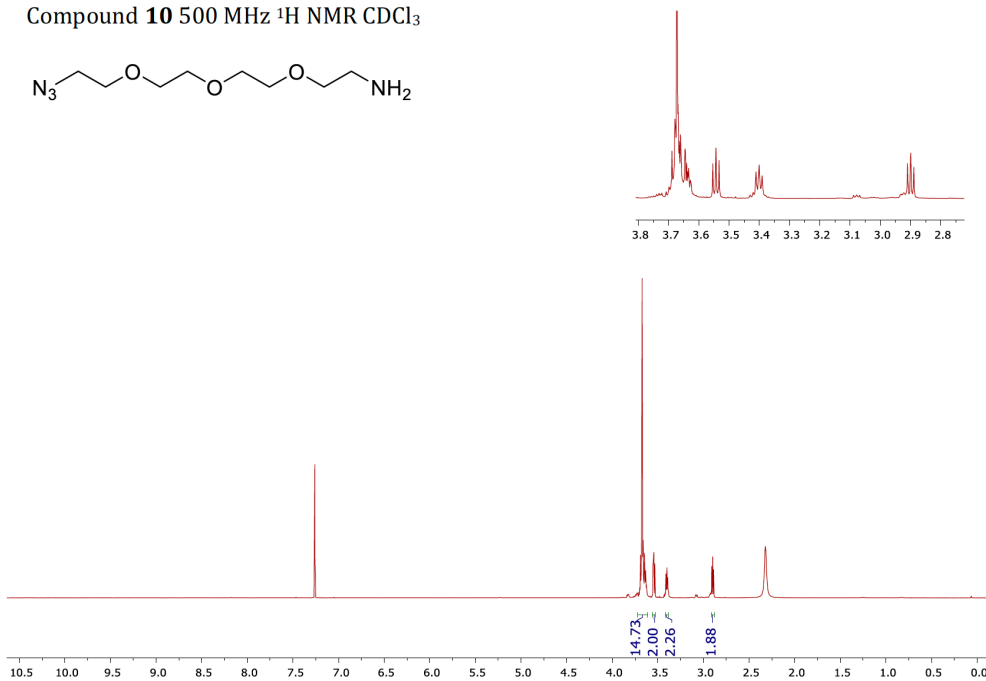
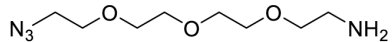
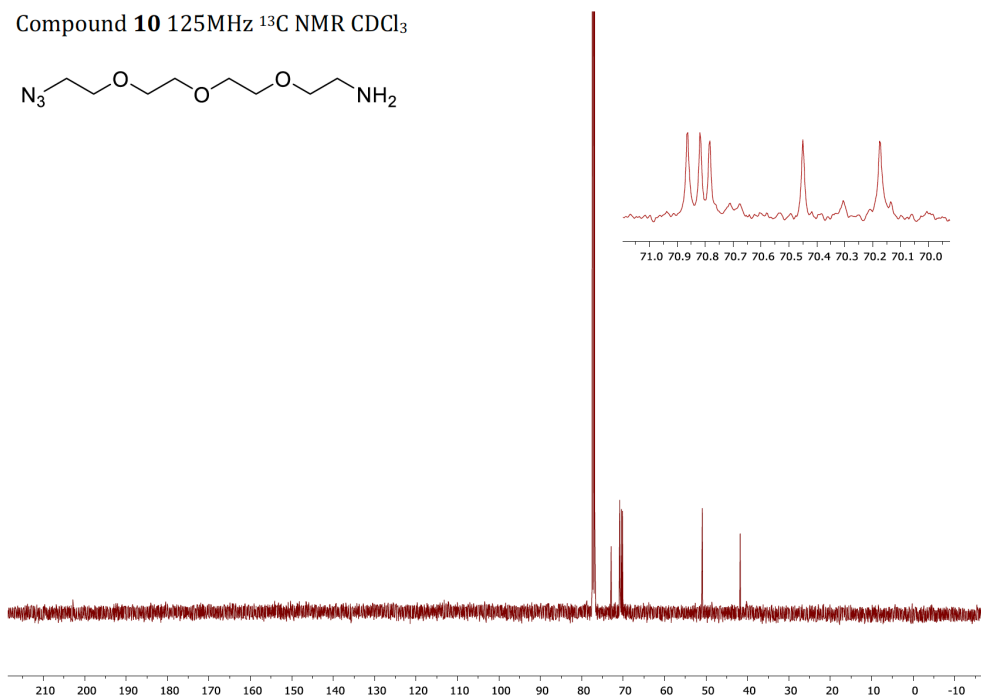
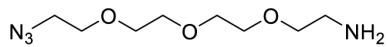
Compound 7 500 MHz  $^1\text{H}$  NMR DMSO  $d_6$ Compound 7 125MHz  $^{13}\text{C}$  NMR  $(\text{CD}_3)_2\text{SO}$ 

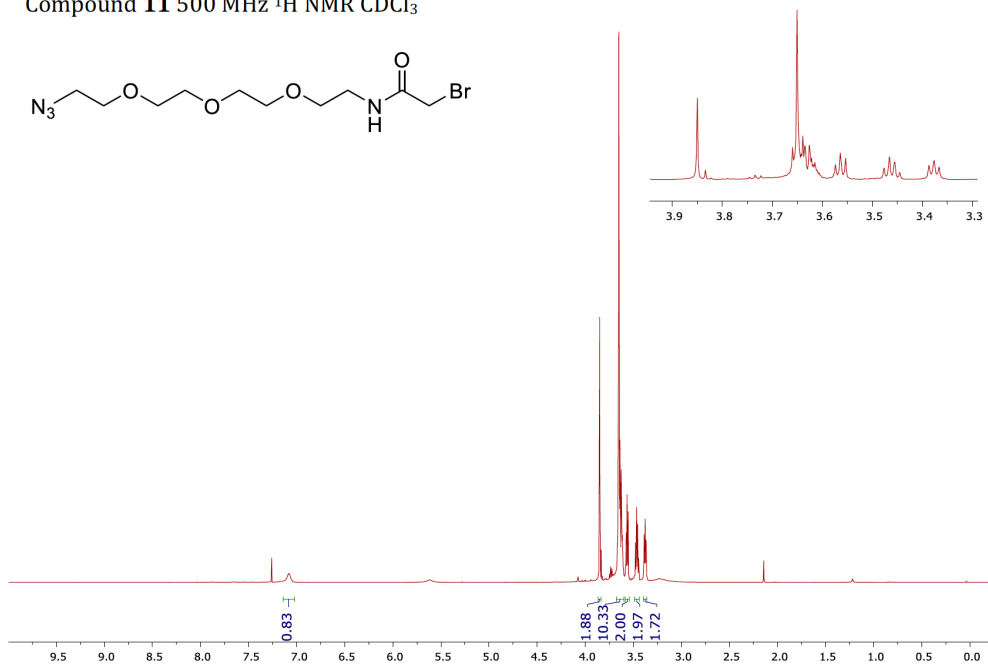
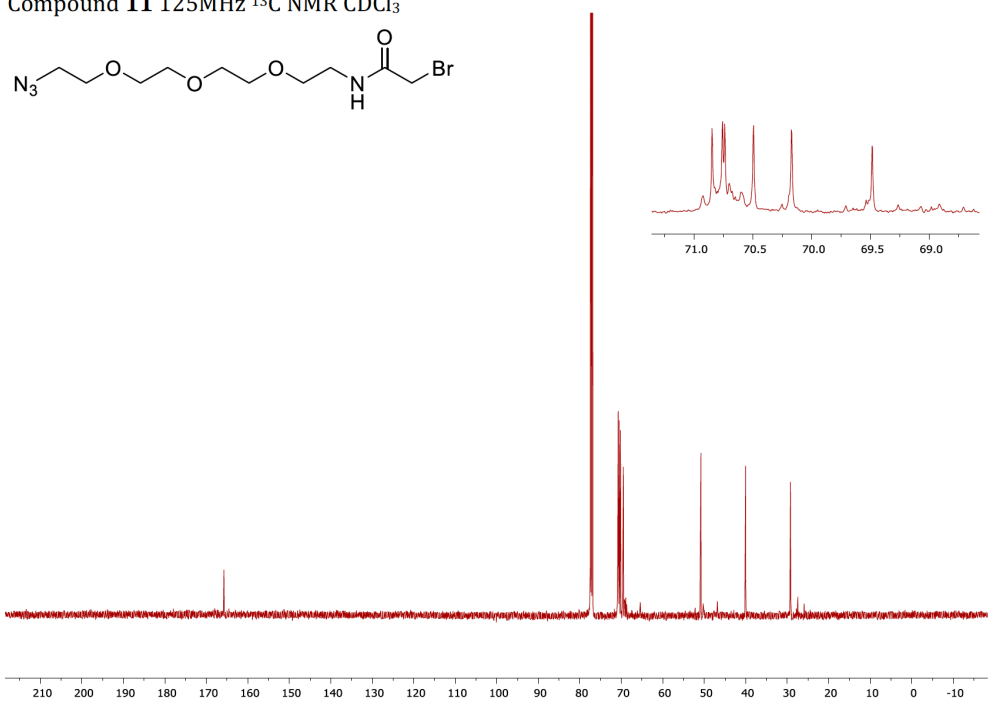
Compound **8** 400 MHz  $^1\text{H}$  NMR ( $\text{CD}_3$ ) $_2\text{SO}$ 

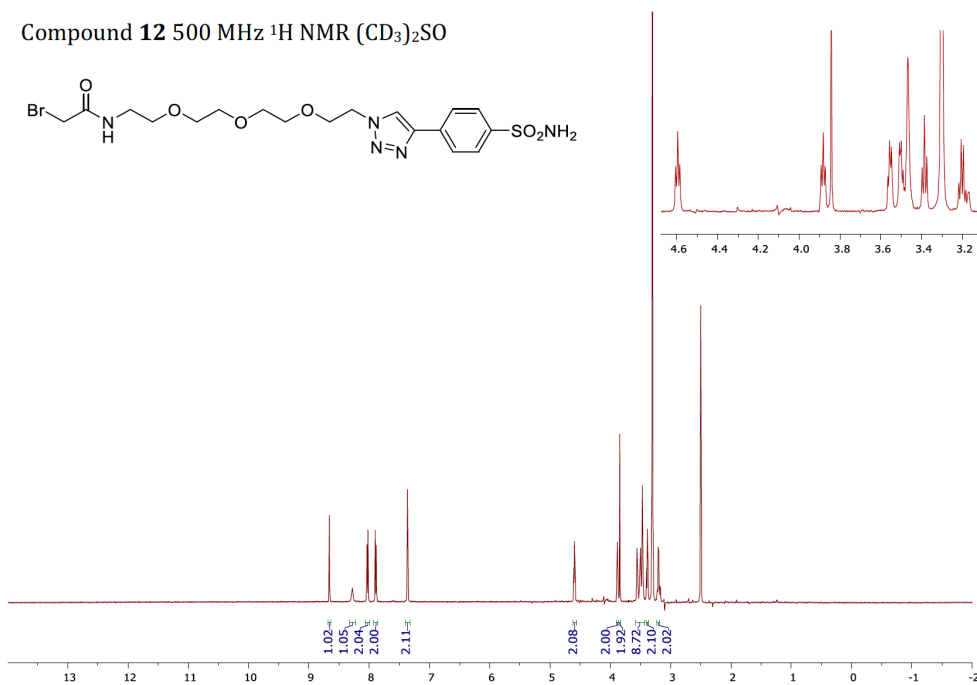
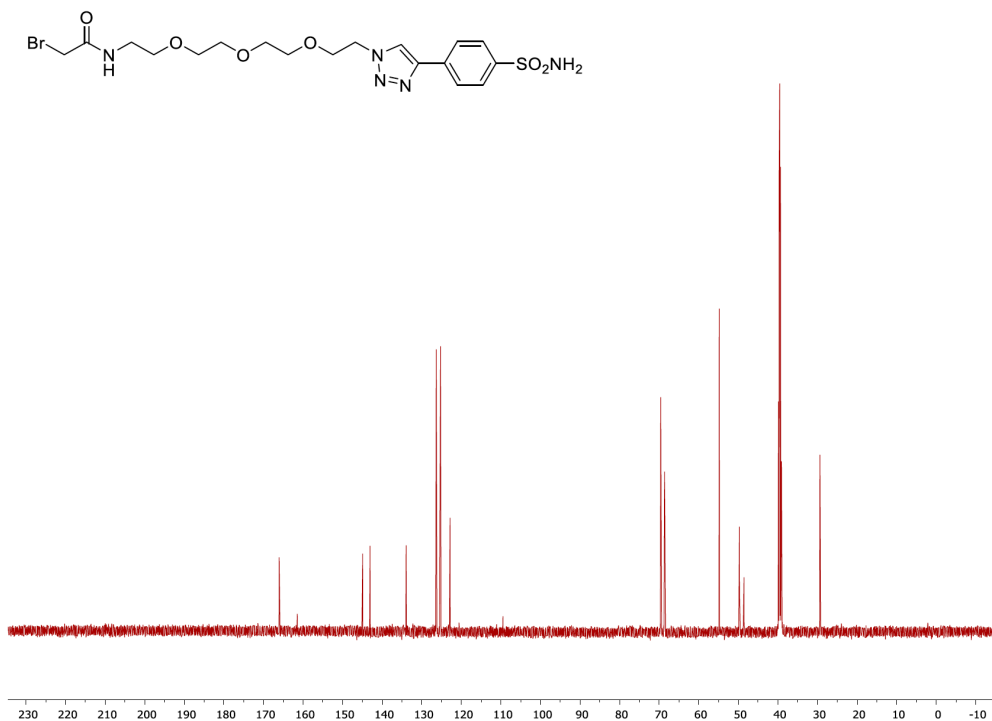
358K

Compound **8** 125 MHz  $^{13}\text{C}$  NMR ( $\text{CD}_3$ ) $_2\text{SO}$  358 K

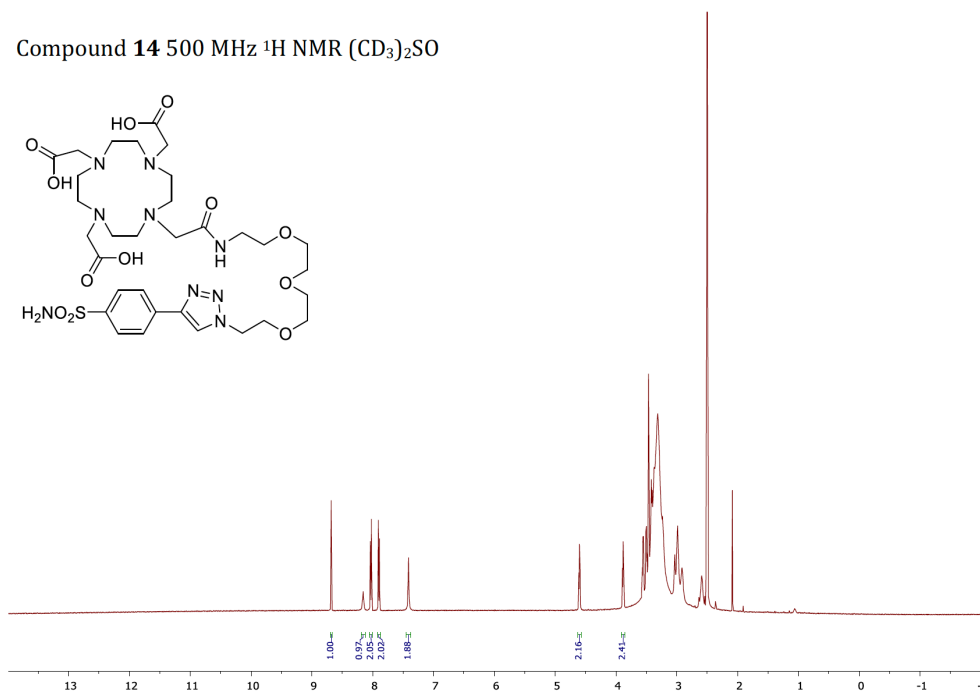
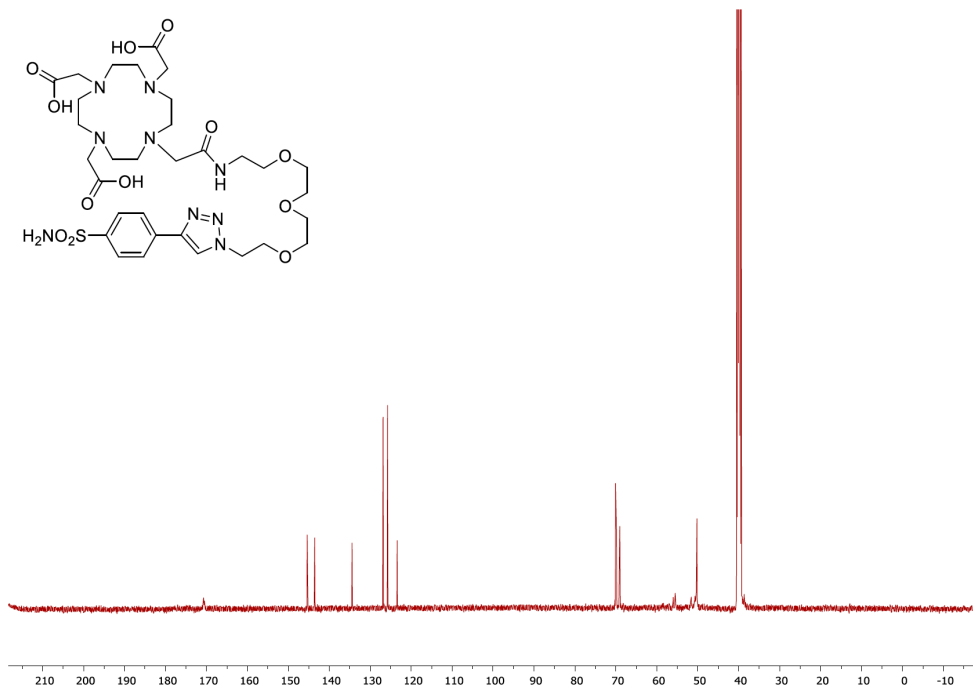
Compound **9** 500 MHz  $^1\text{H}$  NMR ( $\text{CD}_3$ ) $_2\text{SO}$ Compound **9** 125 MHz  $^{13}\text{C}$  NMR ( $\text{CD}_3$ ) $_2\text{SO}$ 

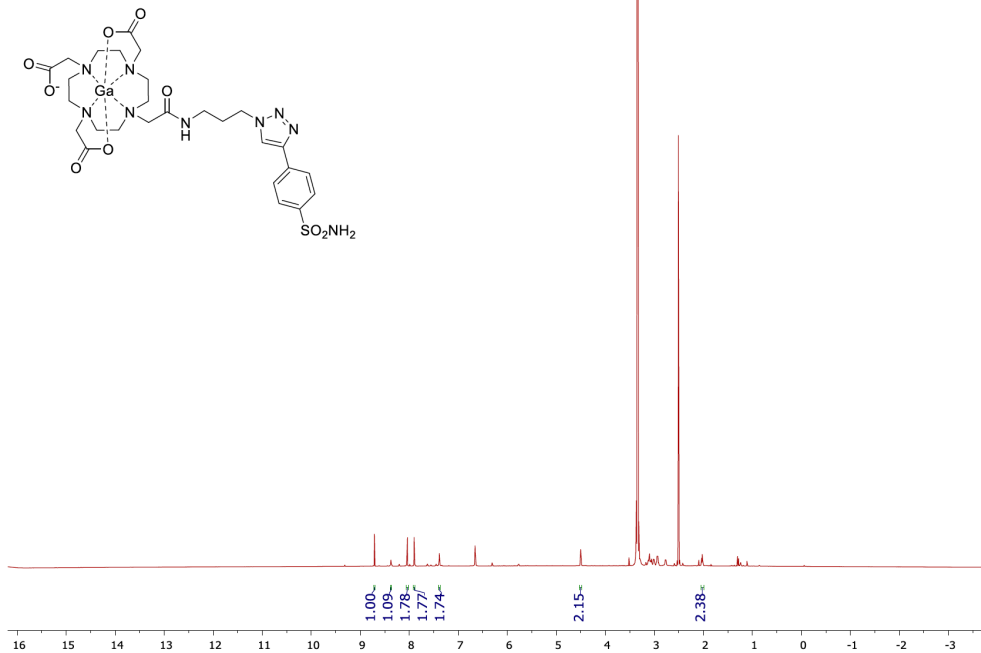
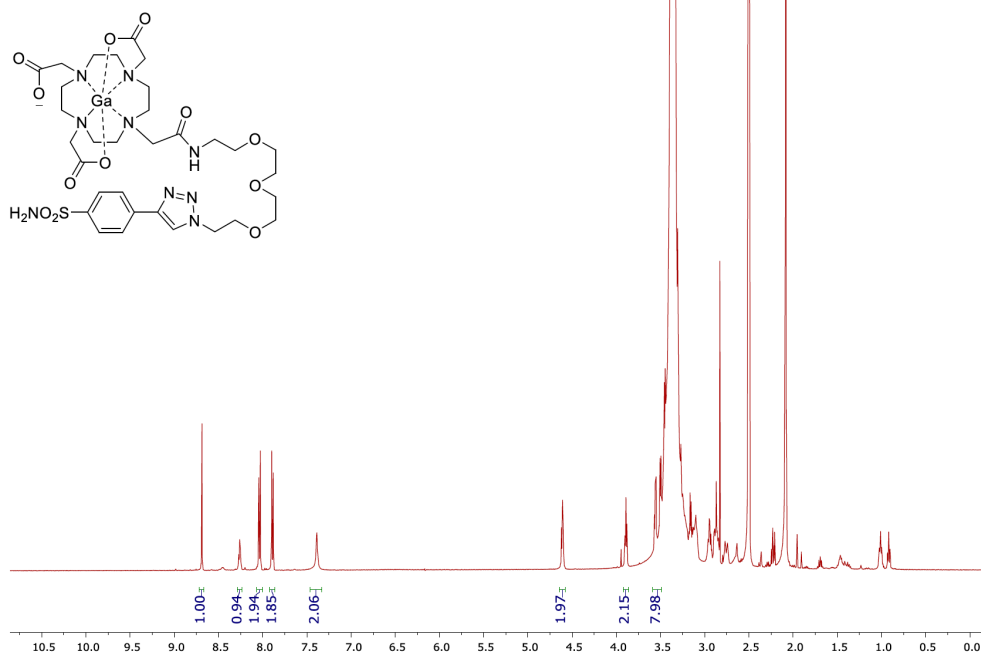
Compound **10** 500 MHz <sup>1</sup>H NMR CDCl<sub>3</sub>Compound **10** 125MHz <sup>13</sup>C NMR CDCl<sub>3</sub>

Compound **11** 500 MHz  $^1\text{H}$  NMR  $\text{CDCl}_3$ Compound **11** 125MHz  $^{13}\text{C}$  NMR  $\text{CDCl}_3$ 

Compound **12** 500 MHz  $^1\text{H}$  NMR ( $\text{CD}_3)_2\text{SO}$ Compound **12** 125 MHz  $^{13}\text{C}$  NMR ( $\text{CD}_3)_2\text{SO}$ 



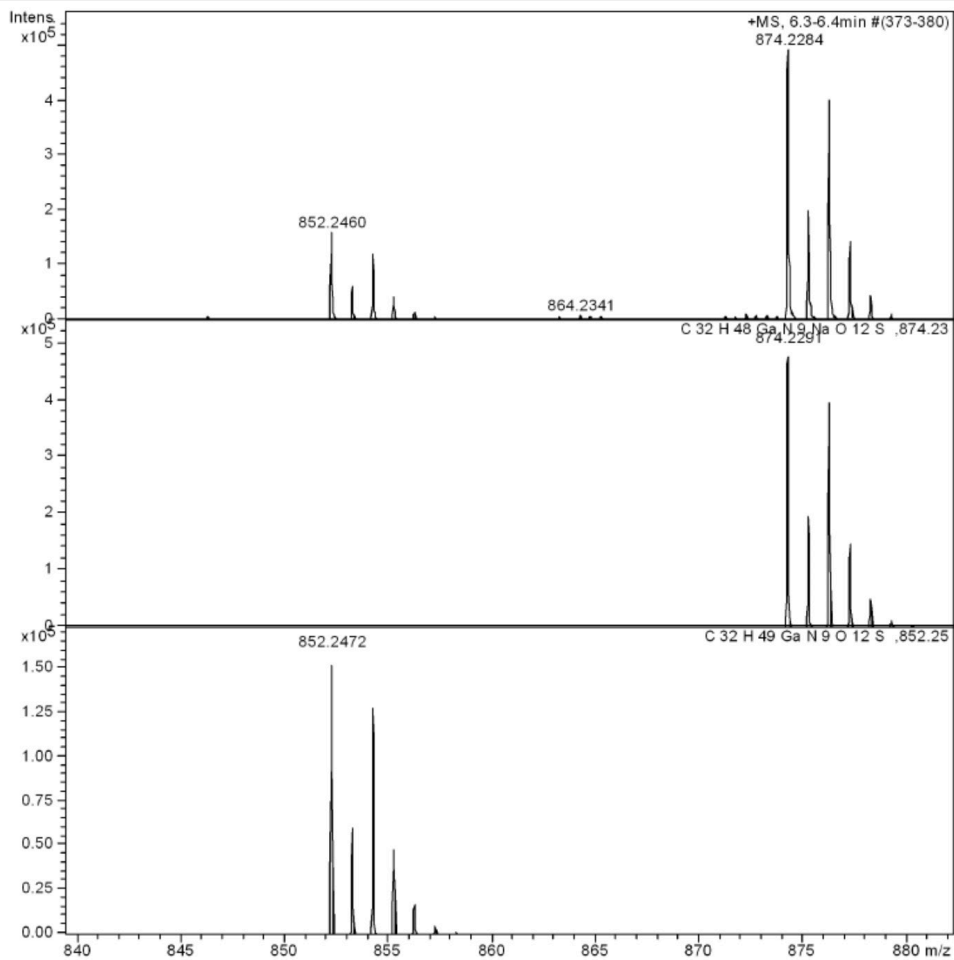
Compound **14** 500 MHz  $^1\text{H}$  NMR ( $\text{CD}_3$ ) $_2\text{SO}$ Compound **14** 125 MHz  $^{13}\text{C}$  NMR ( $\text{CD}_3$ ) $_2\text{SO}$ 

Compound [natGa]-1 500 MHz  $^1\text{H}$  NMR ( $\text{CD}_3$ ) $_2\text{SO}$ Compound [natGa]-2 500 MHz  $^1\text{H}$  NMR ( $\text{CD}_3$ ) $_2\text{SO}$ 

HRMS for compound [<sup>nat</sup>Ga]-2 showing characteristic splitting pattern

**Acquisition Parameter**

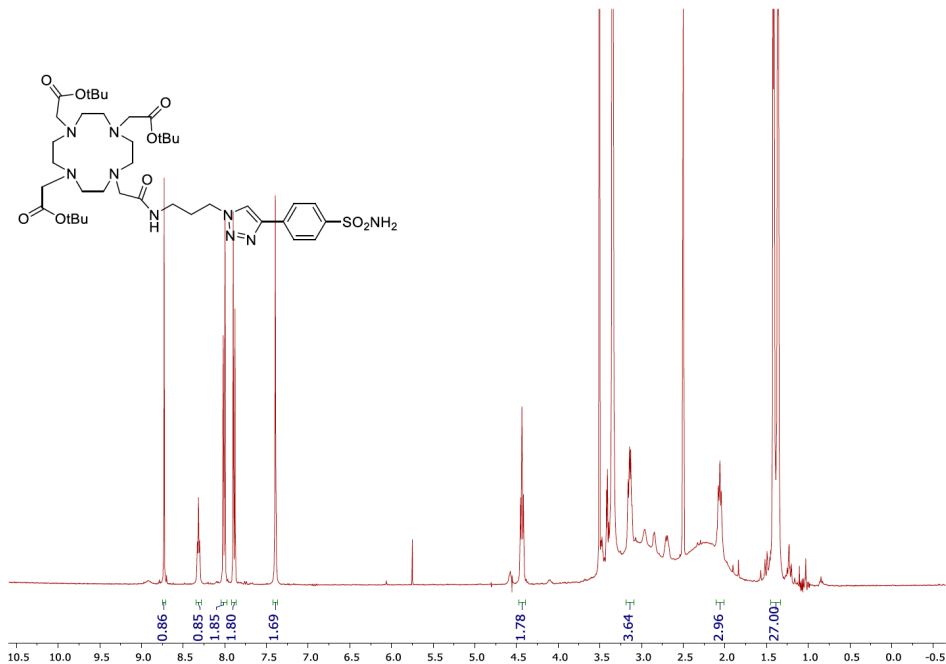
Source Type	ESI	Ion Polarity	Positive	Set Nebulizer	0.4 Bar
Focus	Not active	Set Capillary	4500 V	Set Dry Heater	180 °C
Scan Begin	50 m/z	Set End Plate Offset	-500 V	Set Dry Gas	4.0 l/min
Scan End	3000 m/z	Set Collision Cell RF	550.0 Vpp	Set Divert Valve	Waste



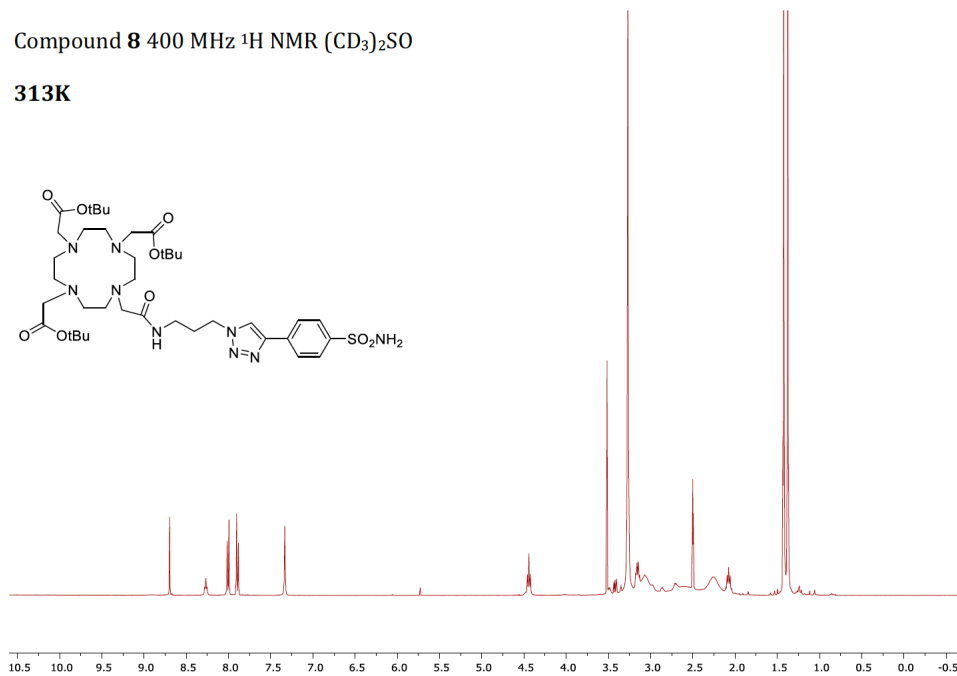
3

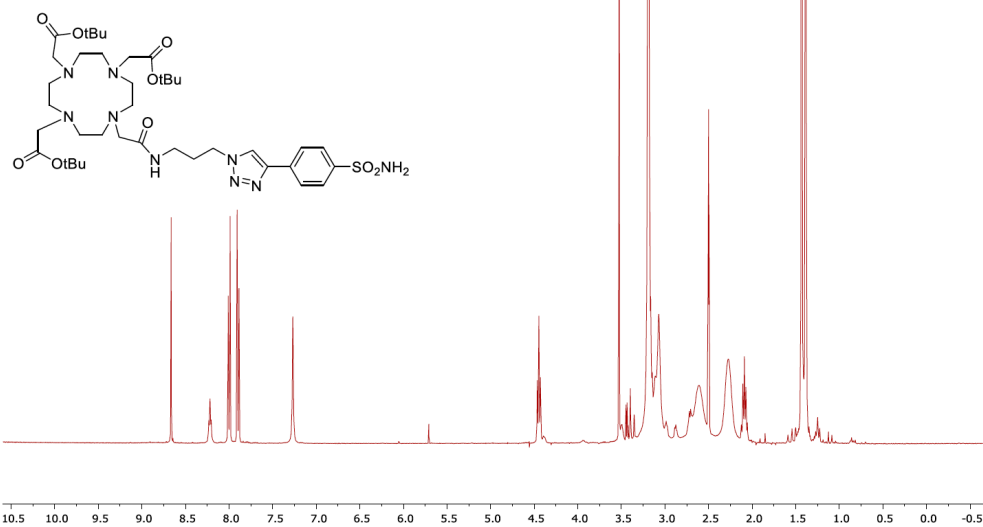
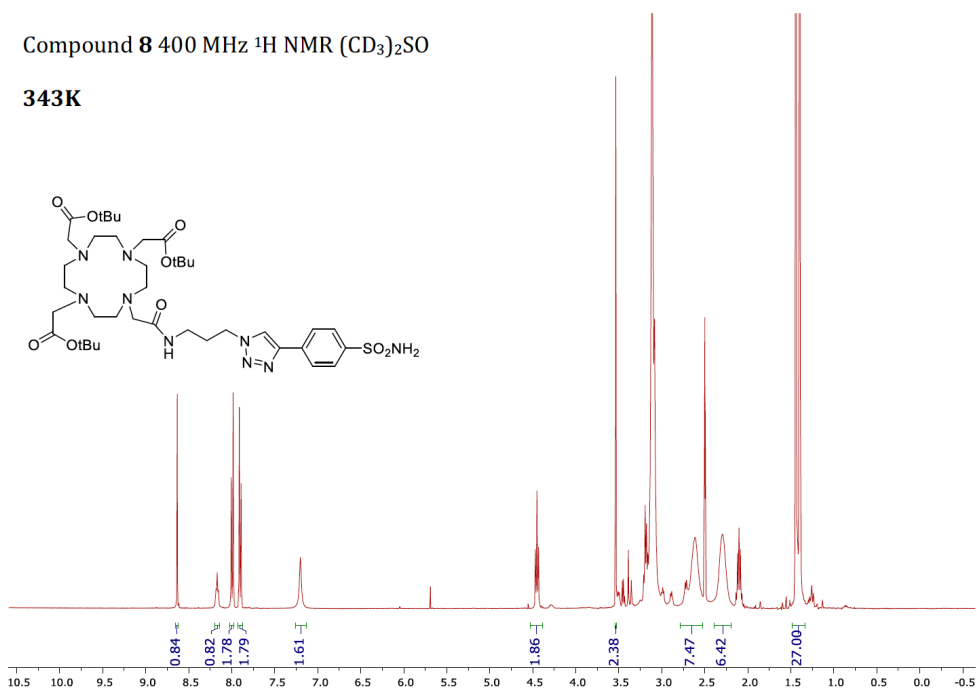
VT experimental data for compound **8**Compound **8** 400 MHz  $^1\text{H}$  NMR ( $\text{CD}_3$ ) $_2\text{SO}$ 

298K

Compound **8** 400 MHz  $^1\text{H}$  NMR ( $\text{CD}_3$ ) $_2\text{SO}$ 

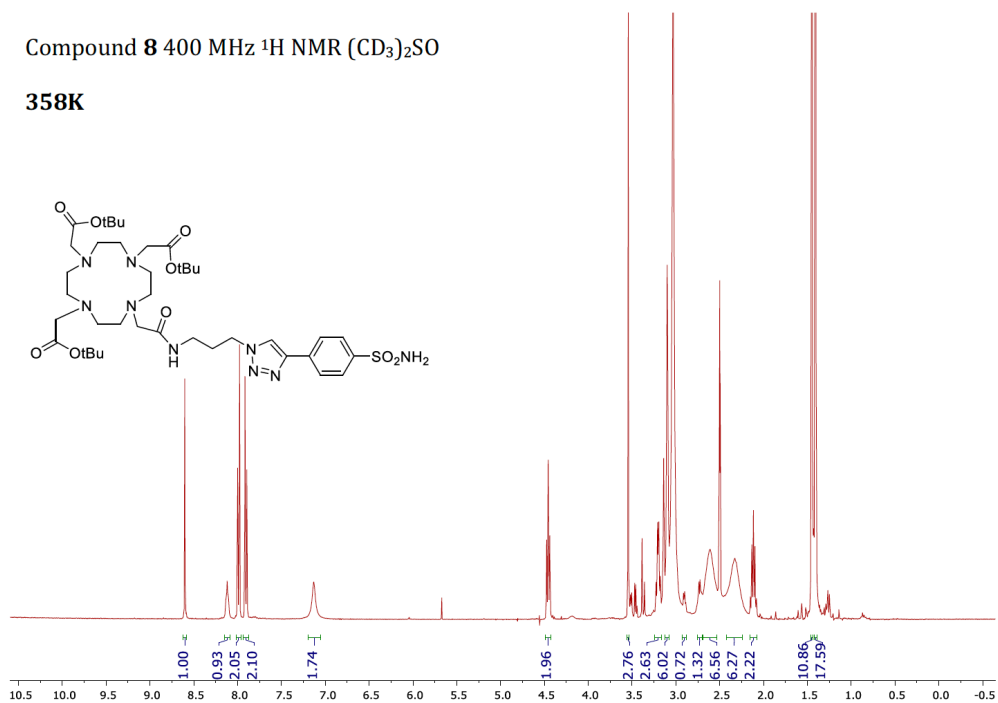
313K



Compound **8** 400 MHz  $^1\text{H}$  NMR ( $\text{CD}_3$ ) $_2\text{SO}$ **328K**Compound **8** 400 MHz  $^1\text{H}$  NMR ( $\text{CD}_3$ ) $_2\text{SO}$ **343K**

Compound **8** 400 MHz  $^1\text{H}$  NMR ( $\text{CD}_3$ ) $_2\text{SO}$ 

358K



### Radiolabeling with $^{67}\text{Ga}$ additional data

**Table 4:** HPLC conditions for purification of  $^{67}\text{Ga}$  DOTA complexes [ $^{67}\text{Ga}$ ]-1 and [ $^{67}\text{Ga}$ ]-2 at 25→1 nmole

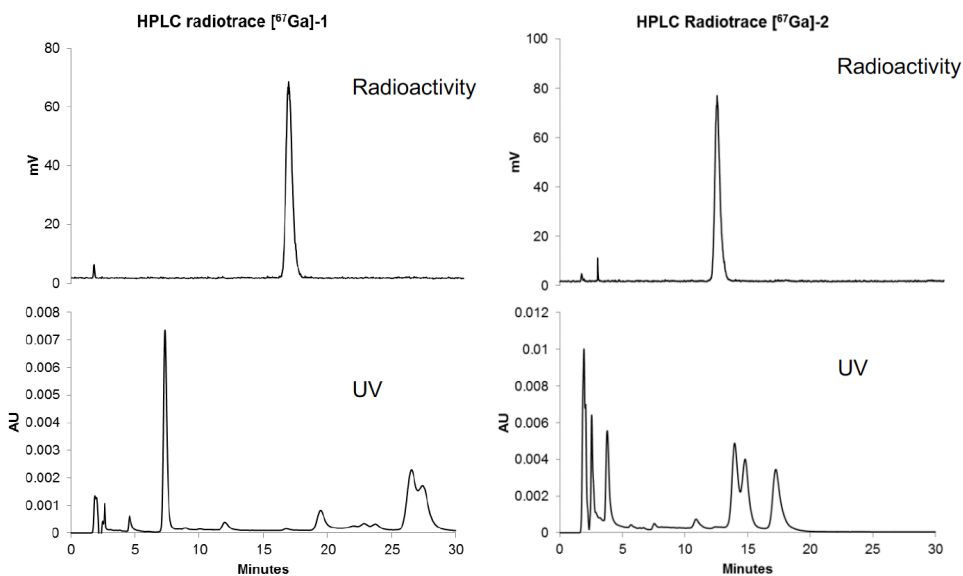
Sample	Compound (nmol)	Column <sup>a</sup>	Flow rate (ml/min)	Mobile Phase <sup>b</sup>	Retention Time (min)
[ $^{67}\text{Ga}$ ]-1	25	Analytical	1.5	8:92	17.7
	10	Analytical	1.5	8:92	16.6
	2	Semi	3	12:88	15.7
	1	Semi	3	12:88	15.9
[ $^{67}\text{Ga}$ ]-2	25	Analytical	1.5	12:88	13.5
	10	Analytical	1.5	12:88	12.3
	5	Semi	3	16:84	13.6
	2	Semi	3	16:84	13.4
	1	Semi	3	16:84	13.2

<sup>a</sup> Where Analytical refers to the Atlantis® T3, 4.6 × 150 mm, 3  $\mu\text{M}$  analytical column and Semi to the Atlantis® T3, 10 × 250 mm, 5  $\mu\text{M}$  semi-preparatory column. Injection sizes adjusted appropriately for each column size.

<sup>b</sup> Mobile phase expressed as a ratio of MeCN: Ammonium formate buffer (120 mM, pH 4.3)

**Analytical radio-trace chromatograms of complexes [<sup>67</sup>Ga]-1 and [<sup>67</sup>Ga]-2 produced in high yield from ~20 MBq of <sup>67</sup>GaCl<sub>3</sub> - 10 nmol**

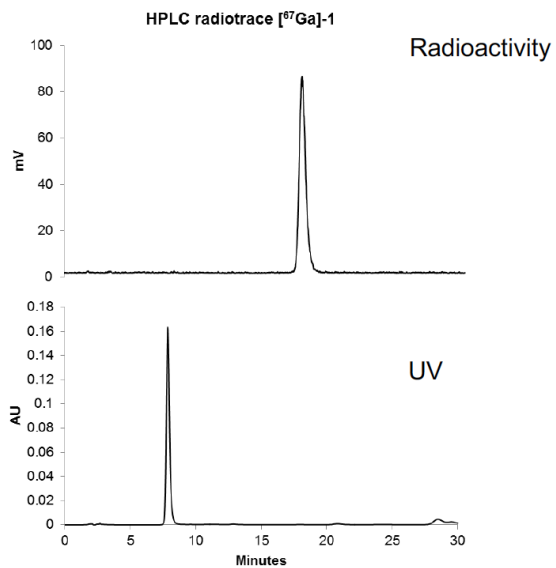
Atlantis® T3 4.6 × 150 mm, 3 μm, 1.5 ml/min flow rate (10 nmol of either compound **9** or compound **14**), ~20 MBq <sup>67</sup>GaCl<sub>3</sub> in sodium acetate buffer (pH 4.3)



**Analytical radio-trace chromatograms of compound [<sup>67</sup>Ga]-1 – 25 nmol**

Atlantis® T3 4.6 × 150 mm, 3 μm, 1.5 ml/min flow rate (25 nmole compound **9**, ~20 MBq <sup>67</sup>GaCl<sub>3</sub> in sodium acetate buffer (pH 4.3))

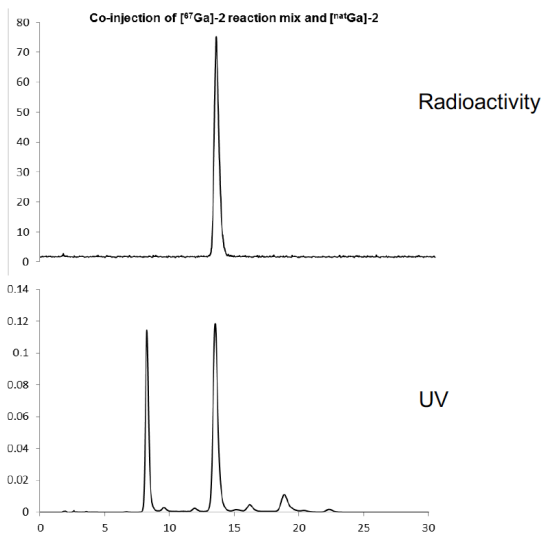
3



**Analytical radio-trace chromatograms of compound [<sup>67</sup>Ga]-2 co-injected with [<sup>nat</sup>-Ga]-2 and compound 14.**

Atlantis® T3 4.6 × 150 mm, 3 μm, 1.5 ml/min flow rate, 12:88 MeCN: NH<sub>4</sub>CO<sub>2</sub>H (120 mM, pH 4.3).

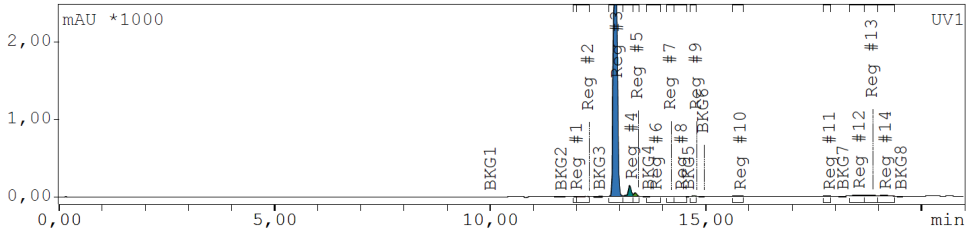
Compound 14 elutes at 8.2 minutes, [<sup>nat/67</sup>Ga]-2 at 13.5 minutes.

**[<sup>68</sup>Ga]-2 example analytical data**

(Inertsil ODS C18, 5 μM, 4.6 × 250 mm, 100:0 → 0:100 H<sub>2</sub>O + 0.1% TFA/ MeCN +0.1% TFA, 1 ml/min)

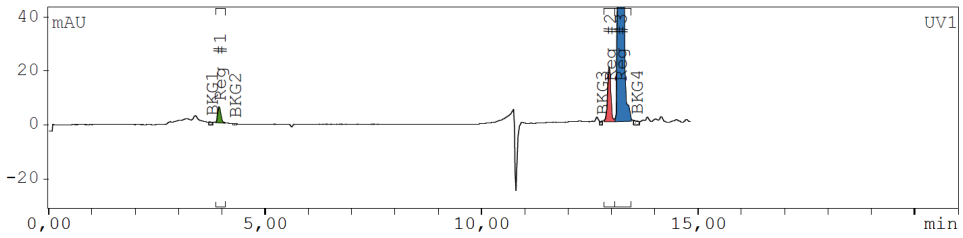
Compound 14

Retention time 12.90 minutes



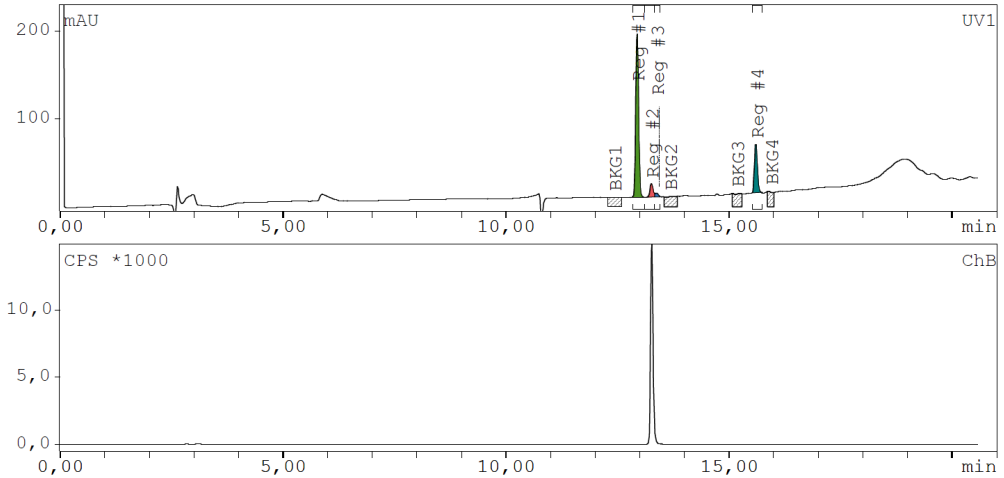
[<sup>nat</sup>Ga]-2

Retention time 13.20 minutes



[<sup>68</sup>Ga]-2

Retention time 13.28 minutes



**Table 5:** SMILES Strings

Cmpnd	SMILES
3	<chem>NCCCN=[N+]=[N-].Cl</chem>
4	<chem>BrCC(NCCCN=[N+]=[N-])=O</chem>
5	<chem>C#CC1=CC=C(S(=O)(N)=O)C=C1</chem>
6	<chem>BrCC(NCCCN1C=C(C2=CC=C(S(=O)(N)=O)C=C2)N=N1)=O</chem>
8	<chem>O=C(OC(C)(C)C)CN1CCN(CC(OC(C)(C)C)=O)CCN(CC(OC(C)(C)C)=O)CCN(CC(NCCCN2C=C(C3=C-C=C(S(=O)(N)=O)C=C3)N=N2)=O)CC1</chem>
9	<chem>OC(CN1CCN(CC(NCCCN2C=C(C3=CC=C(S(=O)(N)=O)C=C3)N=N2)=O)CCN(CC(O)=O)CCN(CC(O)=O)CC1)=O</chem>
10	<chem>NCCOCCOCCOCCN=[N+]=[N-]</chem>
11	<chem>BrCC(NCCOCCOCCOCCN=[N+]=[N-])=O</chem>
12	<chem>BrCC(NCCOCCOCCOCCN1C=C(C2=CC=C(S(=O)(N)=O)C=C2)N=N1)=O</chem>
13	<chem>O=C(OC(C)(C)C)CN1CCN(CC(OC(C)(C)C)=O)CCN(CC(OC(C)(C)C)=O)CCN(CC(NCCOCCOCCOCC-CN2C=C(C3=CC=C(S(=O)(N)=O)C=C3)N=N2)=O)CC1</chem>
14	<chem>OC(CN1CCN(CC(NCCOCCOCCOCCN2C=C(C3=CC=C(S(=O)(N)=O)C=C3)N=N2)=O)CCN(CC(O)=O)CCN(CC(O)=O)CC1)=O</chem>

## Acknowledgements

This work was funded by the Cancer Council Queensland (Project No. APP1058222) and the Australian Institute of Nuclear Science and Engineering (AINSE) (Project nos. ALNGRA15021 and ALNGRA13520). We thank the Australian Research Council (FT10100185 to S-AP). Authors acknowledge financial support from the Dutch Cancer Society (KWF UM 2012-5394 and KWF MAC 2013-6089). HCT116 human colorectal carcinoma cells (ATCC® CCL-247™) stably expressing a CA IX-targeting shRNA (shCA IX) or non-targeting shRNA (shNT) construct was kindly provided by Adrian Harris of the Weatherall Institute of Molecular Medicine, University of Oxford, John Radcliffe Hospital, Oxford, UK.

## References

1. Hanahan, D.; Weinberg, Robert A. Hallmarks of Cancer: The Next Generation. *Cell* **2011**, *144*, 646-674.
2. Horsman, M. R.; Mortensen, L. S.; Petersen, J. B.; Busk, M.; Overgaard, J. Imaging hypoxia to improve radiotherapy outcome. *Nat. Rev. Clin. Oncol.* **2012**, *9*, 674-687.
3. Rockwell, S.; Dobrucki, I. T.; Kim, E. Y.; Marrison, S. T.; Vu, V. T. Hypoxia and radiation therapy: Past history, ongoing research, and future promise. *Curr. Mol. Med.* **2009**, *9*, 442-458.
4. Peeters, S. G. J. A.; Zegers, C. M. L.; Biemans, R.; Lieuwes, N. G.; van Stiphout, R. G. P. M.; Yaromina, A.; Sun, J. D.; Hart, C. P.; Windhorst, A. D.; van Elmpt, W.; Dubois, L. J.; Lambin, P. TH-302 in Combination with Radiotherapy Enhances the Therapeutic Outcome and Is Associated with Pretreatment [18F]HX4 Hypoxia PET Imaging. *Clin. Cancer Res.* **2015**, *21*, 2984-2992.
5. Peeters, S. G. J. A.; Zegers, C. M. L.; Lieuwes, N. G.; van Elmpt, W.; Eriksson, J.; van Dongen, G. A. M. S.; Dubois, L.; Lambin, P. A Comparative Study of the Hypoxia PET Tracers [18F]HX4, [18F]FAZA, and [18F]FMISO in a Preclinical Tumor Model. *Int. J. Radiation Oncol. Biol. Phys.* **2015**, *91*, 351-359.
6. Zegers, C. M. L.; van Elmpt, W.; Reymen, B.; Even, A. J. G.; Troost, E. G. C.; Öllers, M. C.; Hoebbers, F. J. P.; Houben, R. M. A.; Eriksson, J.; Windhorst, A. D.; Mottaghy, F. M.; De Ruyscher, D.; Lambin, P. In Vivo Quantification of Hypoxic and Metabolic Status of NSCLC Tumors Using [18F]HX4 and [18F]FDG-PET/CT Imaging. *Clin. Cancer Res.* **2014**, *20*, 6389-6397.
7. Zegers, C. M. L.; Elmpt, W.; Szardenings, K.; Kolb, H.; Waxman, A.; Subramaniam, R. M.; Moon, D. H.; Brunetti, J. C.; Srinivas, S. M.; Lambin, P.; Chien, D. Repeatability of hypoxia PET imaging using [18F]HX4 in lung and head and neck cancer patients: a prospective multicenter trial. *Eur. J. Nucl. Med. Mol. Imaging*, **2015**, *42*, 1840-1849.
8. Loon, J.; Janssen, M. H. M.; Öllers, M.; Aerts, H. J. W. L.; Dubois, L.; Hochstenbag, M.; Dingemans, A.-M. C.; Lalisang, R.; Brans, B.; Windhorst, B.; Dongen, G. A.; Kolb, H.; Zhang, J.; Ruyscher, D.; Lambin, P. PET imaging of hypoxia using [18F]HX4: a phase I trial. *Eur. J. Nucl. Med. Mol. Imaging*, **2010**, *37*, 1663-1668.
9. Greer, S. N.; Metcalf, J. L.; Wang, Y.; Ohh, M. The updated biology of hypoxia-inducible factor. *EMBO J.* **2012**, *31*, 2448-2460.
10. Potter, C. P. S.; Harris, A. L. Diagnostic, prognostic and therapeutic implications of carbonic anhydrases in cancer. *Brit. J. Cancer* **2003**, *89*, 2-7.
11. Kaluz, S.; Kaluzová, M.; Liao, S.-Y.; Lerman, M.; Stanbridge, E. J. Transcriptional control of the tumor- and hypoxia-marker carbonic anhydrase 9: A one transcription factor (HIF-1) show? *BBA-Rev. Cancer*, **2009**, *1795*, 162-172.
12. Bao, B.; Groves, K.; Zhang, J.; Handy, E.; Kennedy, P.; Cuneo, G.; Supuran, C. T.; Yared, W.; Rajopadhye, M.; Peterson, J. D. *In Vivo* Imaging and Quantification of Carbonic Anhydrase IX Expression as an Endogenous Biomarker of Tumor Hypoxia. *PLoS ONE*, **2012**, *7*, e50860.
13. Potter, C.; Harris, A. L. Hypoxia Inducible Carbonic Anhydrase IX, Marker of Tumour: Hypoxia, Survival Pathway and Therapy Target. *Cell Cycle* **2003**, *3*, 159-162.

14. van Kuijk, S. J. A.; Yaromina, A.; Houben, R.; Niemans, R.; Lambin, P.; Dubois, L. J. Prognostic Significance of Carbonic Anhydrase IX Expression in Cancer Patients: A Meta-Analysis. *Front. Oncol.* **2016**, *6*, 69, 1-16
15. Neri, D.; Supuran, C. T. Interfering with pH regulation in tumours as a therapeutic strategy. *Nat. Rev. Drug Discov.* **2011**, *10*, 767-777.
16. Lawrentschuk, N.; Lee, F. T.; Jones, G.; Rigopoulos, A.; Mountain, A.; O'Keefe, G.; Papenfuss, A. T.; Bolton, D. M.; Davis, I. D.; Scott, A. M. Investigation of hypoxia and carbonic anhydrase IX expression in a renal cell carcinoma xenograft model with oxygen tension measurements and 124I-cG250 PET/CT. *Urol. Oncol-Semin. Ori.* **2011**, *29*, 411-420.
17. Carlin, S.; Khan, N.; Ku, T.; Longo, V. A.; Larson, S. M.; Smith-Jones, P. M. Molecular Targeting of Carbonic Anhydrase IX in Mice with Hypoxic HT29 Colorectal Tumor Xenografts. *PLoS ONE*, **2010**, *5*, 1-9.
18. Pastorek, J.; Pastorekova, S. Hypoxia-induced carbonic anhydrase IX as a target for cancer therapy: From biology to clinical use. *Semin. Cancer Biol.* **2015**, *31*, 52-64.
19. Swietach, P.; Vaughan-Jones, R. D.; Harris, A. L. Regulation of tumor pH and the role of carbonic anhydrase 9. *Cancer Metastasis Rev.* **2007**, *26*, 299-310.
20. Parks, S. K.; Chiche, J.; Pouyssegur, J. pH control mechanisms of tumor survival and growth. *J. Cell. Physiol.* **2011**, *226*, 299-308.
21. Oosterwldk, E.; Ruiter, D. J.; Hoedemaeker, P. J.; Pauwels, E. K. J.; Jonas, U.; Zwartendijk, I.; Warnaar, S. O. Monoclonal antibody G 250 recognizes a determinant present in renal-cell carcinoma and absent from normal kidney. *Int. J. Cancer*, **1986**, *38*, 489-494.
22. Sneddon, D.; Poulsen, S.-A. Agents described in the Molecular Imaging and Contrast Agent Database for imaging carbonic anhydrase IX expression. *J. Enzym. Inhib. Med. Chem.* **2014**, *29*, 753-763.
23. Dubois, L. J.; Niemans, R.; van Kuijk, S. J. A.; Panth, K. M.; Parvathaneni, N.-K.; Peeters, S. G. J. A.; Zegers, C. M. L.; Rekers, N. H.; van Gisbergen, M. W.; Biemans, R.; Lieuwes, N. G.; Spiegelberg, L.; Yaromina, A.; Winum, J.-Y.; Vooijs, M.; Lambin, P. New ways to image and target tumour hypoxia and its molecular responses. *Radiother. Oncol.* **2015**, *116*, 352-357.
24. Dubois, L.; Douma, K.; Supuran, C. T.; Chiu, R. K.; van Zandvoort, M. A. M. J.; Pastoreková, S.; Scozzafava, A.; Wouters, B. G.; Lambin, P. Imaging the hypoxia surrogate marker CA IX requires expression and catalytic activity for binding fluorescent sulfonamide inhibitors. *Radiother. Oncol.* **2007**, *83*, 367-373.
25. Doss, M.; Kolb, H. C.; Walsh, J. C.; Mocharla, V. P.; Zhu, Z.; Haka, M.; Alpaugh, R. K.; Chen, D. Y. T.; Yu, J. Q. Biodistribution and Radiation Dosimetry of the Carbonic Anhydrase IX Imaging Agent [18F]VM4-037 Determined from PET/CT Scans in Healthy Volunteers. *Mol. Imaging Biol.* **2014**, *16*, 739-746.
26. Lau, J.; Liu, Z.; Lin, K.-S.; Pan, J.; Zhang, Z.; Vullo, D.; Supuran, C. T.; Perrin, D. M.; Bénard, F. Trimeric Radiofluorinated Sulfonamide Derivatives to Achieve In Vivo Selectivity for Carbonic Anhydrase IX-Targeted PET Imaging. *J. Nucl. Med.* **2015**, *56*, 1434-1440.
27. Lau, J.; Zhang, Z.; Jenni, S.; Kuo, H.-T.; Liu, Z.; Vullo, D.; Supuran, C. T.; Lin, K.-S.; Bénard, F. PET Imaging of Carbonic Anhydrase IX Expression of HT-29 Tumor Xenograft Mice with 68Ga-Labeled Benzenesulfonamides. *Mol. Pharm.*

- 2016**, *13*, 1137-1146
28. Pan, J.; Lau, J.; Mesak, F.; Hundal, N.; Pourghasian, M.; Liu, Z.; Bénard, F.; Dedhar, S.; Supuran, C. T.; Lin, K.-S. Synthesis and evaluation of <sup>18</sup>F-labeled carbonic anhydrase IX inhibitors for imaging with positron emission tomography. *J. Enzym. Inhib. Med. Chem.* **2014**, *29*, 249-255.
  29. Day, J. A.; Cohen, S. M. Investigating the Selectivity of Metalloenzyme Inhibitors. *J. Med. Chem.* **2013**, *56*, 7997-8007.
  30. Peeters, S. J. A.; Dubois, L.; Lieuwes, N.; Laan, D.; Mooijer, M.; Schuit, R.; Vullo, D.; Supuran, C.; Eriksson, J.; Windhorst, A.; Lambin, P. [<sup>18</sup>F]VM4-037 MicroPET Imaging and Biodistribution of Two In Vivo CAIX-Expressing Tumor Models. *Mol. Imaging Biol.* **2015**, *17*, 615-619.
  31. Metwalli, A. R.; Turkbey, B.; McKinney, Y.; Weaver, J.; Yaqub-Ogun, N.; Merino, M.; Lindenberg, M. L.; Linehan, W. M.; Choyke, P. L. Results of a phase II trial of novel carbonic anhydrase IX radiotracer <sup>18</sup>F-VM4-037 in renal cell carcinoma. In *2014 Genitourinary Cancer Symposium*, San Francisco, USA, 2014.
  32. Turkbey, B.; Lindenberg, M. L.; Adler, S.; Kurdziel, K. A.; McKinney, Y. L.; Weaver, J.; Vocke, C. D.; Anver, M.; Brat-slavsky, G.; Eclarinal, P.; Kwarteng, G.; Lin, F. I.; Yaqub-Ogun, N.; Merino, M. J.; Marston Linehan, W.; Choyke, P. L.; Metwalli, A. R. PET/CT imaging of renal cell carcinoma with <sup>18</sup>F-VM4-037: a phase II pilot study. *Abdom. Radiol.* **2015**, *41*, 109-118.
  33. Velikyan, I. Prospective of (<sup>68</sup>Ga)-Radiopharmaceutical Development. *Theranostics* **2014**, *4*, 47-80.
  34. Ambrosini, V.; Tomassetti, P.; Franci, R.; Fanti, S. Imaging of NETs with PET radiopharmaceuticals. *Q. J. Nucl. Med. Mol. Imaging* **2010**, *54*, 16-23.
  35. Carter, N. D.; Heath, R.; Welty, R. J.; Hewe'lt-Emmett, D.; Jeffery, S.; Shiels, A.; Tashian, R. E. Red Cells Genetically Deficient in Carbonic Anhydrase II Have Elevated Levels of a Carbonic Anhydrase Indistinguishable from Muscle CA IIIa. *Ann. N.Y. Acad. Sci.* **1984**, *429*, 284-286.
  36. Akurathi, V.; Dubois, L.; Celen, S.; Lieuwes, N. G.; Chitneni, S. K.; Cleynhens, B. J.; Innocenti, A.; Supuran, C. T.; Verbruggen, A. M.; Lambin, P.; Bormans, G. M. Development and biological evaluation of <sup>99m</sup>Tc-sulfonamide derivatives for in vivo visualization of CA IX as surrogate tumor hypoxia markers. *Eur. J. Med. Chem.* **2014**, *71*, 374-384.
  37. Akurathi, V.; Dubois, L.; Lieuwes, N. G.; Chitneni, S. K.; Cleynhens, B. J.; Vullo, D.; Supuran, C. T.; Verbruggen, A. M.; Lambin, P.; Bormans, G. M. Synthesis and biological evaluation of a <sup>99m</sup>Tc-labelled sulfonamide conjugate for in vivo visualization of carbonic anhydrase IX expression in tumor hypoxia. *Nuc. Med. Biol.* **2010**, *37*, 557-564.
  38. Lopez, M.; Salmon, A. J.; Supuran, C. T.; Poulsen, S.-A. Carbonic Anhydrase Inhibitors Developed Through "Click Tailing". *Curr. Pharm. Des.* **2010**, *16*, 3277-3287.
  39. Lopez, M.; Drillaud, N.; Bornaghi, L. F.; Poulsen, S.-A. Synthesis of S-Glycosyl Primary Sulfonamides. *J. Org. Chem.* **2009**, *74*, 2811-2816.
  40. Salmon, A. J.; Williams, M. L.; Maresca, A.; Supuran, C. T.; Poulsen, S.-A. Synthesis of glycoconjugate carbonic anhydrase inhibitors by ruthenium-catalysed azide-alkyne 1,3-dipolar cycloaddition. *Bioorg. Med. Chem. Lett.* **2011**, *21*, 6058-6061.

41. Rankin, G. M.; Vullo, D.; Supuran, C. T.; Poulsen, S.-A. Phosphate Chemical Probes Designed for Location Specific Inhibition of Intracellular Carbonic Anhydrases. *J. Med. Chem.* **2015**, *58*, 7580-7590.
42. Moeker, J.; Mahon, B. P.; Bornaghi, L. F.; Vullo, D.; Supuran, C. T.; McKenna, R.; Poulsen, S.-A. Structural Insights into Carbonic Anhydrase IX Isoform Specificity of Carbohydrate-Based Sulfamates. *J. Med. Chem.* **2014**, *57*, 8635-8645.
43. 43. Poulsen, S.-A. Carbonic anhydrase inhibition as a cancer therapy: a review of patent literature, 2007 – 2009. *Expert Opin. Ther. Pat.* **2010**, *20*, 795-806.
44. Price, E. W.; Orvig, C. Matching chelators to radiometals for radiopharmaceuticals. *Chem. Soc. Rev.* **2014**, *43*, 260-290.
45. Mojtahedi, A.; Thamake, S.; Tworowska, I.; Ranganathan, D.; Delpassand, E. S. The value of (68)Ga-DOTATATE PET/CT in diagnosis and management of neuroendocrine tumors compared to current FDA approved imaging modalities: a review of literature. *Am. J. Nucl. Med. Mol. Imaging* **2014**, *4*, 426-434.
46. Eder, M.; Neels, O.; Müller, M.; Bauder-Wüst, U.; Remde, Y.; Schäfer, M.; Hennrich, U.; Eisenhut, M.; Afshar-Oromieh, A.; Haberkorn, U.; Kopka, K. Novel Preclinical and Radiopharmaceutical Aspects of [(68)Ga]Ga-PSMA-HBED-CC: A New PET Tracer for Imaging of Prostate Cancer. *Pharmaceuticals* **2014**, *7*, 779-796.
47. Meldal, M.; Tornøe, C. W. Cu-Catalyzed Azide-Alkyne Cycloaddition. *Chem. Rev.* **2008**, *108*, 2952-3015.
48. Tron, G. C.; Piralì, T.; Billington, R. A.; Canonico, P. L.; Sorba, G.; Genazzani, A. A. Click chemistry reactions in medicinal chemistry: Applications of the 1,3-dipolar cycloaddition between azides and alkynes. *Med. Res. Rev.* **2008**, *28*, 278-308.
49. Kadajji, V. G.; Betageri, G. V. Water Soluble Polymers for Pharmaceutical Applications. *Polymers* **2011**, *3*, 1972-2009.
50. Knop, K.; Hoogenboom, R.; Fischer, D.; Schubert, U. S. Poly(ethylene glycol) in Drug Delivery: Pros and Cons as Well as Potential Alternatives. *Angew. Chem. Int. Ed.* **2010**, *49*, 6288-6308.
51. Rami, M.; Cecchi, A.; Montero, J.-L.; Innocenti, A.; Vullo, D.; Scozzafava, A.; Winum, J.-Y.; Supuran, C. T. Carbonic Anhydrase Inhibitors: Design of Membrane-Impermeant Copper(II) Complexes of DTPA-, DOTA-, and TETA-Tailed Sulfonamides Targeting the Tumor-Associated Transmembrane Isoform IX. *ChemMedChem* **2008**, *3*, 1780-1788.
52. Rami, M.; Montero, J.-L.; Dubois, L.; Lambin, P.; Scozzafava, A.; Winum, J.-Y.; Supuran, C. T. Carbonic anhydrase inhibitors: Gd(III) complexes of DOTA- and TETA-sulfonamide conjugates targeting the tumor associated carbonic anhydrase isozymes IX and XII. *New J. Chem.* **2010**, *34*, 2139-2144.
53. Wilkinson, B. L.; Innocenti, A.; Vullo, D.; Supuran, C. T.; Poulsen, S.-A. Inhibition of Carbonic Anhydrases with Glycosyltriazole Benzene Sulfonamides. *J. Med. Chem.* **2008**, *51*, 1945-1953.
54. Hannant, J.; Hedley, J. H.; Pate, J.; Walli, A.; Farha Al-Said, S. A.; Galindo, M. A.; Connolly, B. A.; Horrocks, B. R.; Houlton, A.; Pike, A. R. Modification of DNA-templated conductive polymer nanowires via click chemistry. *Chem. Commun.* **2010**, *46*, 5870-5872.
55. Barnett, D. J. Radiopharmaceutical compositions. In Google Patents: 2012.
56. Prasuhn, J. D. E.; Yeh, R. M.; Obenaus, A.; Manchester, M.; Finn, M. G. Viral MRI contrast agents: coordination of Gd by native virions and attachment of Gd complexes by azide-alkyne cycloaddition. *Chem. Commun.* **2007**, 1269-1271.

57. Supuran, C. T.; Scozzafava, A. Benzolamide is not a Membrane-impermeant Carbonic Anhydrase Inhibitor. *J. Enzym. Inhib. Med. Chem.* **2004**, *19*, 269-273.
58. Khalifah, R. G. The Carbon Dioxide Hydration Activity of Carbonic Anhydrase: I. Stop-flow Kinetic Studies on the Native Human Isozymes B and C. *J. Biol. Chem.* **1971**, *246*, 2561-2573.
59. Rami, M.; Dubois, L.; Parvathaneni, N.-K.; Alterio, V.; van Kuijk, S. J. A.; Monti, S. M.; Lambin, P.; De Simone, G.; Supuran, C. T.; Winum, J.-Y. Hypoxia-Targeting Carbonic Anhydrase IX Inhibitors by a New Series of Nitroimidazole-Sulfonamides/Sulfamides/Sulfamates. *J. Med. Chem.* **2013**, *56*, 8512-8520.
60. Dubois, L.; Peeters, S. G. J. A.; van Kuijk, S. J. A.; Yaromina, A.; Lieuwes, N. G.; Saraya, R.; Biemans, R.; Rami, M.; Parvathaneni, N. K.; Vullo, D.; Vooijs, M.; Supuran, C. T.; Winum, J.-Y.; Lambin, P. Targeting carbonic anhydrase IX by nitroimidazole based sulfamides enhances the therapeutic effect of tumor irradiation: A new concept of dual targeting drugs. *Radiother. Oncol.* **2013**, *108*, 523-528.
61. Dubois, L.; Peeters, S.; Lieuwes, N. G.; Geusens, N.; Thiry, A.; Wigfield, S.; Carta, F.; McIntyre, A.; Scozzafava, A.; Dogné, J.-M.; Supuran, C. T.; Harris, A. L.; Masereel, B.; Lambin, P. Specific inhibition of carbonic anhydrase IX activity enhances the in vivo therapeutic effect of tumor irradiation. *Radiother. Oncol.* **2011**, *99*, 424-431.
62. Lam, C. F. C.; Giddens, A. C.; Chand, N.; Webb, V. L.; Copp, B. R. Semi-synthesis of bioactive fluorescent analogues of the cytotoxic marine alkaloid discorhabdin C. *Tetrahedron* **2012**, *68*, 3187-3194.
63. Bakleh, M. E.; Sol, V.; Estieu-Gionnet, K.; Granet, R.; Déléris, G.; Krausz, P. An efficient route to VEGF-like peptide porphyrin conjugates via microwave-assisted 'click-chemistry'. *Tetrahedron* **2009**, *65*, 7385-7392.
64. Goswami, L. N.; Houston, Z. H.; Sarma, S. J.; Jalisatgi, S. S.; Hawthorne, M. F. Efficient synthesis of diverse heterobifunctionalized clickable oligo(ethylene glycol) linkers: potential applications in bioconjugation and targeted drug delivery. *Org. Biomol. Chem.* **2013**, *11*, 1116-1126.
65. Raghunand, N.; Guntle, G. P.; Gokhale, V.; Nichol, G. S.; Mash, E. A.; Jagadish, B. Design, Synthesis, and Evaluation of 1,4,7,10-Tetraazacyclododecane-1,4,7-triacetic Acid Derived, Redox-Sensitive Contrast Agents for Magnetic Resonance Imaging. *J. Med. Chem.* **2010**, *53*, 6747-6757.
66. Kale, R. R.; Clancy, C. M.; Vermillion, R. M.; Johnson, E. A.; Iyer, S. S. Synthesis of soluble multivalent glycoconjugates that target the Hc region of botulinum neurotoxin A. *Bioorg. Med. Chem. Lett.* **2007**, *17*, 2459-2464.
67. Ščasár, V.; Lier, J. E. The use of SEP-PAK SI cartridges for the preparation of gallium chloride from the citrate solution. *Eur. J. Nucl. Med.* **20**, 273-273.
68. Winum, J.-Y.; Vullo, D.; Casini, A.; Montero, J.-L.; Scozzafava, A.; Supuran, C. T. Carbonic Anhydrase Inhibitors. Inhibition of Cytosolic Isozymes I and II and Transmembrane, Tumor-Associated Isozyme IX with Sulfamates Including EMATE Also Acting as Steroid Sulfatase Inhibitors. *J. Med. Chem.* **2003**, *46*, 2197-2204.
69. Vullo, D.; Innocenti, A.; Nishimori, I.; Pastorek, J. r.; Scozzafava, A.; Pastoreková, S.; Supuran, C. T. Carbonic anhydrase inhibitors. Inhibition of the transmembrane isozyme XII with sulfonamides—a new target for the design of antitumor and antiglaucoma drugs? *Bioorg. Med. Chem. Lett.* **2005**, *15*, 963-969.



# CHAPTER 4

## New approach of delivering cytotoxic drugs towards CA IX expressing cells: A concept of dual-target drugs

Simon J.A. van Kuijk\*, Nanda Kumar Parvathaneni\*, **Raymon Niemans\***, Marike W. van Gisbergen\*, Fabrizio Carta, Daniela Vullo, Silvia Pastorekova, Ala Yaromina, Claudiu T. Supuran, Ludwig J. Dubois#, Jean-Yves Winum#, Philippe Lambin#

\*These authors contributed equally.

#These authors contributed equally.

### **Previously published:**

*van Kuijk, S.J., et al., New approach of delivering cytotoxic drugs towards CAIX expressing cells: A concept of dual-target drugs. Eur J Med Chem, 2017. 127: p. 691-702.*

## Abstract

Carbonic anhydrase IX (CAIX) is a hypoxia-regulated and tumor-specific protein that maintains the pH balance of cells. Targeting CAIX might be a valuable approach for specific delivery of cytotoxic drugs, thereby reducing normal tissue side-effects. A series of dual-target compounds were designed and synthesized incorporating a sulfonamide, sulfamide, or sulfamate moiety combined with several different anti-cancer drugs, including the chemotherapeutic agents chlorambucil, tirapazamine, and temozolomide, two Ataxia Telangiectasia and Rad3-related protein inhibitors (ATRi), and the anti-diabetic biguanide agent phenformin. An ATRi derivative (12) was the only compound to show a preferred efficacy in CAIX overexpressing cells versus cells without CAIX expression when combined with radiation. Its efficacy might however not solely depend on binding to CAIX, since all described compounds generally display low activity as carbonic anhydrase inhibitors. The hypothesis that dual-target compounds specifically target CAIX expressing tumor cells was therefore not confirmed. Even though dual-target compounds remain an interesting approach, alternative options should also be investigated as novel treatment strategies.

## Introduction

Solid tumors are characterized by a hypoxic microenvironment caused by their immature and inadequate vascular supply of oxygen and nutrients. These hostile hypoxic conditions result in a phenotype that is associated with a worse prognosis [1] and resistance to standard treatment options such as radiotherapy, chemotherapy, and surgery [2-4]. Several different approaches are currently being investigated to target these hypoxic areas to make tumors more sensitive to standard treatment modalities [5-7].

Carbonic anhydrase IX (CAIX) can be a valuable therapeutic target since it plays an important role in maintaining the intracellular pH homeostasis [8, 9]. Furthermore its expression is predominantly tumor specific [5, 8, 10] and directly regulated via the hypoxia-inducible factor (HIF) pathway [11]. Even though alternative pathways are also able to modulate CAIX expression [12-14], its significant prognostic value in many different tumor types [15] has promoted investigations in its use as an imaging agent for diagnostic and prognostic purposes [5, 16-19]. Together these characteristics of CAIX support investigations into the therapeutic targeting of CAIX to improve efficacy of standard treatments. The function of CAIX is evolutionary conserved and catalyzes the hydration of carbon dioxide to bicarbonate at the cell membrane. The bicarbonate is transported back intracellular from the extracellular space, whereas the free proton is extruded in the extracellular space. CAIX thereby maintains the balance between an acidic extracellular and alkaline intracellular pH of tumor cells, the latter of which would otherwise acidify due to the increased acid production resulting from their glycolytic metabolism [8, 9]. Many different inhibitors are currently being developed to specifically target the tumor-associated CAIX isoform and have shown promise in reducing tumor cell survival, migration, invasion, and reduce tumor xenograft growth and metastases formation [20-23]. Furthermore, the combination therapy of CAIX inhibitors (CAIXi) with standard treatment options was previously found to increase the efficacy of radiotherapy [24] and of weakly basic chemotherapeutic agents such as doxorubicin [25].

The predominant expression of CAIX on hypoxic tumor cells can also be exploited to direct cytotoxic agents specifically to those CAIX expressing cancer cells thereby possibly minimizing normal tissue toxicity. This can be achieved by conjugating anti-cancer drugs with CAIX inhibiting molecules that bind to the  $Zn^{2+}$  active site of CAIX and hence inhibit its enzymatic function [8, 26, 27], *i.e.* a so-called dual-targeting approach. Our group showed

previously that such a dual-target approach with a sulfamide CAIXi moiety coupled to the radiosensitizing compound nitroimidazole to be a more effective radiosensitizer than an indanesulfonamide CAIXi [28]. Alternative novel dual-target compounds have been developed to investigate this strategy of dual-targeting further in the context of anti-cancer agents to target CAIX. Here we have designed five different classes of dual-target compounds conjugated to CAIXi (sulfonamide, sulfamide, or sulfamate), which included the chemotherapeutic anti-cancer agents chlorambucil, tirapazamine, and temozolomide, two ataxia telangiectasia and Rad3-related protein inhibitors (ATRi), and the biguanide agent phenformin, previously used in diabetes treatment. We hypothesize that these new dual-target compounds will have the ability to specifically target CAIX expressing cells and modulate their efficacy in a CAIX-dependent manner.

## Results and discussion

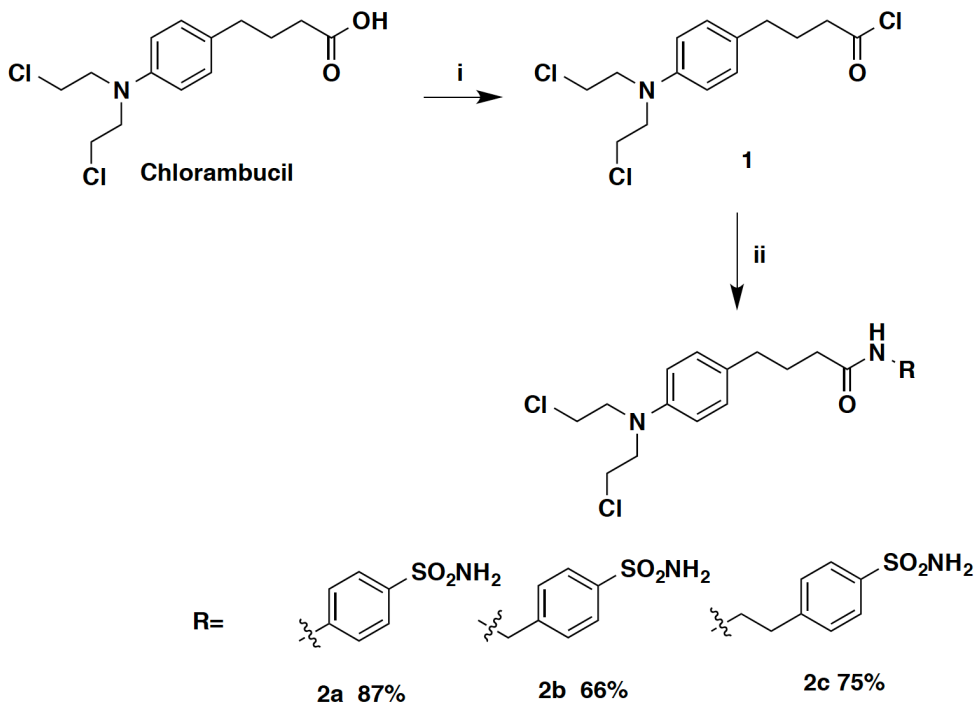
### Chemistry

Chlorambucil was converted to its acid chloride [29] **1** by using oxalyl chloride. This chlorambucil acid chloride reacted with different benzene sulfonamides under basic condition to obtain good yields of chlorambucil derivatives **2a**, **2b** and **2c**. Chlorambucil carbamate derivatives were obtained by converting compound **1** into a methyl ester [30] using methanol. This ester was reduced to alcohol [31], *i.e.* compound **3**, after treating with lithium aluminium hydride. Compound **3** was treated with triphosgene to obtain its respective chloroformate [32], *i.e.* compound **4** (Scheme 2). The reaction of chlorambucil chloroformate (**4**) with different benzene sulfonamides resulted in compounds **5a**, **5b** and **5c** (Scheme 3).

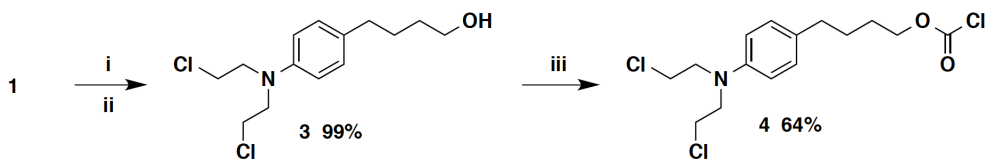
Tirapazamine derivatives **8** and **11** were synthesized from **6** and **9** with the previously described procedure [33]. In short, **6** and **9** reacted with 4-(2-aminoethyl) benzene sulfonamide under reflux conditions and was followed by oxidation of the mono-oxides (Scheme 4).

The ATRi derivatives **12** and **13** were synthesized from commercially available VE-821 and VE-822 (MedChemTronica) using a classical synthetic strategy described previously [25] (Scheme 5).

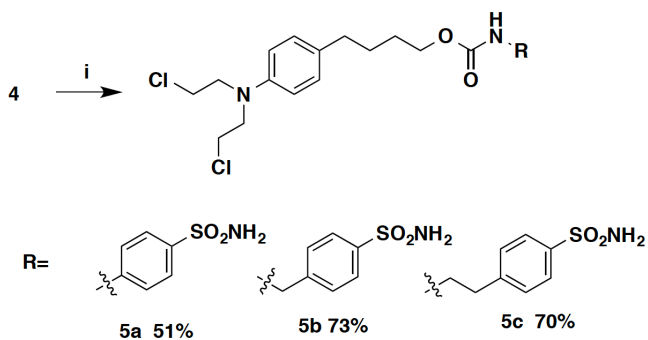
**Scheme 1.** Reagents and conditions: (i)  $(\text{COCl})_2$ , DMF, DCM, 0 °C-rt; (ii) DIPEA, THF, 0 °C-rt.



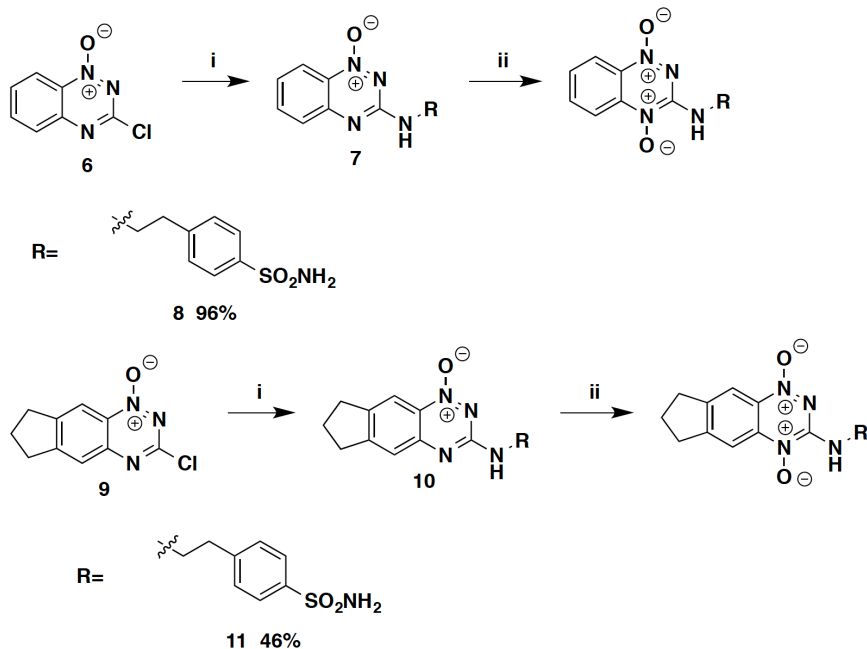
**Scheme 2.** Reagents and conditions: (i) MeOH, DCM; (ii) LAH, THF; (iii) Triphosgene,  $\text{Na}_2\text{CO}_3$ , Toluene, DMF.



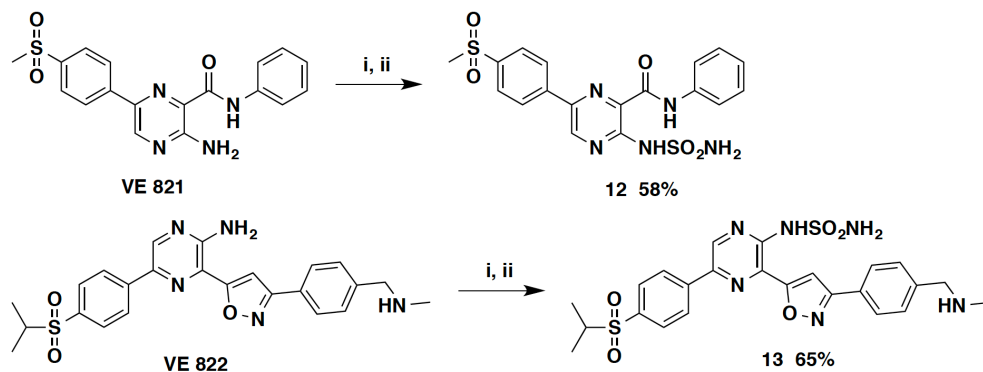
**Scheme 3.** Reagents and conditions: (i) DIPEA, THF, 0 °C-rt.



**Scheme 4.** Reagents and conditions: (i) RNH<sub>2</sub> (3 equiv.), DME, reflux; (ii) TFAA, H<sub>2</sub>O<sub>2</sub>, DCM, rt.



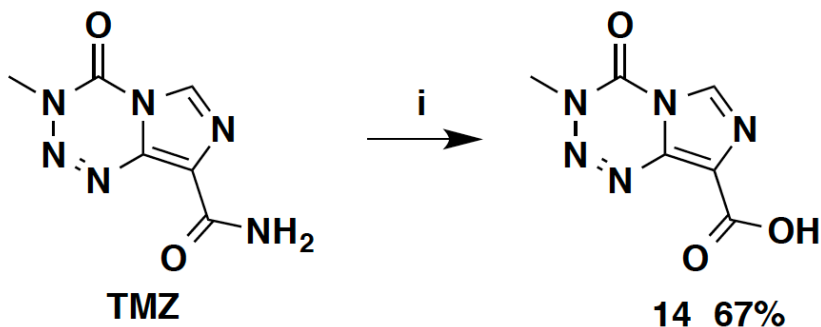
**Scheme 5.** Reagents and conditions: (i) ClSO<sub>2</sub>NCO, tBuOH, NEt<sub>3</sub>, DCM, 0 °C to rt; (ii) 20% TFA-DCM.



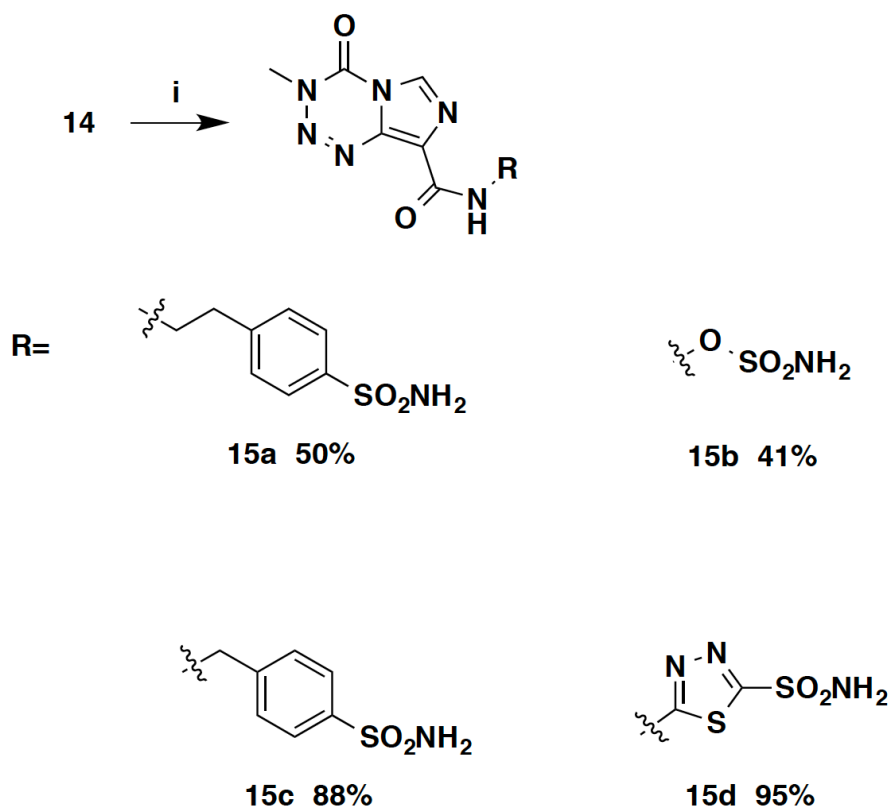
Commercially purchased temozolomide (SelleckChem) was converted into its respective acid by treating with concentrated sulfuric acid and sodium nitrate at 0 °C–15 °C (Scheme 6) [34]. Reacting the temozolomic acid with different benzenesulfonamides, aminoxysulfonamide [35] Reacting the temozolomic acid with different benzenesulfonamides, aminoxysulfonamide [35] and 5-amino-1,3,4-thiadiazole-2-sulfonamide hydrochloride under

known amide bond formation conditions [34] resulted in compounds **15a**, **15b**, **15c** and **15d** (Scheme 7).

**Scheme 6.** Reagents and conditions: (i) Con.  $H_2SO_4$ ,  $NaNO_2$ , 0 °C to 15 °C

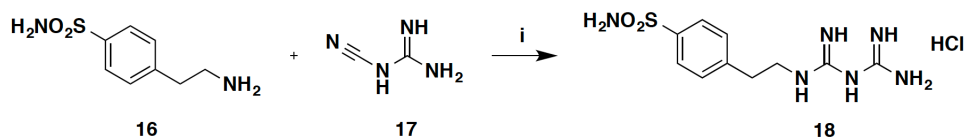


**Scheme 7.** Reagents and conditions: (i) BOP,  $NEt_3$ , DCM, rt.



The compound **18** was obtained by a slight modification based on the method reported by Kelarev et al. [36]. The commercially available compounds 4-(2-aminoethyl) benzenesulfonamide **16** and cyanoguanidine **17** were coupled in n-butanol using a stoichiometric amount of hydrochloric acid (Scheme 8).

**Scheme 8.** Reagents and conditions: (i) 6.0 M HCl aq, nBuOH, reflux.



4

### Binding affinity human CAs

Increased binding affinity to human carbonic anhydrases (CAs) as compared with their respective parental compound are observed (Table 1) for most of the compounds, except for the CAIXi conjugated ATRi (**12** and **13**), which do not bind to any of the four tested human CA isoforms included ( $K_i > 50000$  nM). The  $K_i$  values of the other dual-targeting compounds are higher than of the previously reported CAIXi [20] with **15a** showing relatively good  $K_i$  for the CAII and CAIX isoforms, but not for CAXII. Only the phenformin derivative **18** was found to be selective for the transmembrane CAIX and CAXII isoforms. To investigate whether the biological efficacy of the functionalized compounds is dependent on CAIX expression, canine kidney epithelial (MDCK) cells without CAIX (CAIX<sup>-</sup>), *i.e.* both human and canine [37], or MDCK cells transfected with human CAIX [37], *i.e.* overexpressing CAIX (CAIX<sup>+</sup>), were used. Western blotting confirmed differential expression of CAIX in these cells both under normoxic and hypoxic conditions (Supplementary Fig. S1).

### Chlorambucil derivatives

Chlorambucil (4-[p-[bis(2-chloroethyl)amino]phenyl]butyric acid) is a nitrogen mustard that acts as a bifunctional alkylating agent used for decades to treat cancers originating in the blood and lymphatic system, *e.g.* chronic lymphocytic leukemia and lymphomas [38]. Even though reported data suggest chlorambucil efficacy to increase in an acidic microenvironment [39], the CAIXi moiety (benzenesulfonamides) with different linkers (*i.e.* amide, carbamate) might allow for specific targeting of the compounds to these areas in the tumor. The six CAIXi conjugated chlorambucil derivatives (**2a**, **2b**, **2c**, **5a**, **5b**, and **5c**, Scheme 1 and Scheme 2) lead to reduced cell viability as compared to the parental compound, which was only marginally effective (Table 2, Supplementary Fig. S1).

**Table 1:** Binding affinity ( $K_i$ ) to human CAI, CAII, CAIX, and CAXII of the parental compounds (bold) and their CAIXi conjugated derivatives.

Compound	$K_i$ (nM) <sup>a</sup>				Selectivity Ratios <sup>b</sup>	
	hCA I	hCA II	hCA IX	hCA XII	$K_i$ hCA II / $K_i$ hCA IX	$K_i$ hCA II / $K_i$ hCA XII
Chlorambucil	>50000	>50000	>50000	>50000		
2a	73.0	9.0	172	689	0.05	0.01
2b	5950	747	8970	7340	0.08	0.10
2c	8400	450	4610	10160	0.10	0.04
5a	5580	553	2740	9380	0.20	0.06
5c	6140	265	4130	9570	0.06	0.03
5c	5670	504	3850	13600	0.13	0.04
Tirapazamine	>50000	>50000	>50000	>50000		
8	567	7.1	383	14600	0.02	<0.01
11	428	8.1	307	624	0.03	0.01
Temozolomide	>50000	>50000	>50000	>50000		
15a	91.3	9.2	37.1	9300	0.25	<0.01
15b	>50000	>50000	>50000	>50000		
15c	539	90.5	271	12400	0.33	0.01
15d	743	15.7	176	92.7	0.09	0.17
ATRi VE-821	>50000	>50000	>50000	>50000		
12	>50000	>50000	>50000	>50000		
ATRi VE-822	>50000	>50000	>50000	>50000		
13	>50000	>50000	>50000	>50000		
Phenformin	>50000	>50000	>50000	>50000		
18	4435	501	20.2	1.7	24.8	295
Acetazolamide <sup>c</sup>	250	12.1	25.3	5.7	0.48	2.12

<sup>a</sup>Values reported (in nM) are the average of three different estimations with errors between 5–10% of the reported values. Reported values >50000 indicates no binding of the compound towards the CA isoforms.

<sup>b</sup>Selectivity ratios of the cytosolic hCAII over the tumor-associated hCAIX and hCAXII isoforms.

<sup>c</sup>Non-specific CAI acetazolamide is included as a reference.

The therapeutic efficacy of these compounds however was not increased in the CAIX<sup>+</sup> MDCK cells as compared with the CAIX<sup>-</sup> MDCK cells. Furthermore, none of the six compounds showed an increased efficacy upon hypoxia exposure (0.2% O<sub>2</sub>). In contrast, some of the chlorambucil dual-target derivatives were less cytotoxic (*i.e.* higher IC<sub>50</sub>, Table 2) in CAIX expressing cells independent of oxygen levels, which contradicts the studies demonstrating an increased efficacy of chlorambucil in an acidic micromilieu [39]. All together

from these results it can be concluded that the CAIXi conjugated chlorambucil derivatives do not show an increased efficacy in a CAIX or hypoxia dependent manner.

**Table 2:** Estimated IC<sub>50</sub> of the cytotoxic parental compounds (bold) and their CAIXi conjugated derivatives obtained with cell viability assays for MDCK CAIX<sup>-</sup> and MDCK CAIX<sup>+</sup> cells exposed to normoxic and hypoxic conditions.

Compound	Normoxia (μM) <sup>a</sup>		Hypoxia (μM) <sup>a</sup>	
	CAIX <sup>-</sup>	CAIX <sup>+</sup>	CAIX <sup>-</sup>	CAIX <sup>+</sup>
Chlorambucil <sup>b</sup>	93	>100	~100	>100
2a	~100	87	~100	95
2b	18	98	14	92
2c	18	~100	18	~100
5a	8	56	8	62
5b	86	98	52	100
5c	89	99	81	~100
Tirapazamine <sup>c</sup>	>300	>300	<50	95
8	>300	>300	~300	>300
11	>300	>300	>300	>300
Temozolomide <sup>d</sup>	775	>1000	~1000	>1000
15a	>1000	>1000	>1000	>1000
15b	719	>1000	~1000	>1000
15c	>1000	>1000	>1000	>1000
15d	>1000	>1000	>1000	>1000

<sup>a</sup>No IC<sub>50</sub> reached is indicated with >. Estimated IC<sub>50</sub> value higher than the maximum concentration included is indicated with ~.

<sup>b</sup>Included concentrations for chlorambucil were 1, 10, and 100 μM.

<sup>c</sup>Included concentrations for tirapazamine were 50, 100, 200, and 300 μM.

<sup>d</sup>Included concentrations for temozolomide were 100, 400, 700, and 1000 μM.

### Tirapazamine derivatives

The hypoxia-activated prodrug tirapazamine (3-amino-1,2,4-benzotriazine-1,4-dioxide) has been tested in several clinical trials in combination with chemo- and/or radiotherapy [40]. The cytotoxicity of tirapazamine results from activation by reductive enzymes that add an electron to the parent drug to produce a radical species that causes DNA damage. Nevertheless, no definitive conclusions regarding its clinical efficacy can be drawn since addition of tirapazamine to standard treatment (*i.e.* radio-chemotherapy) did not result in an increased benefit in phase III clinical trials. In addition, tirapazamine treatment was often characterized by toxic side-effects, such as nausea, vomiting, and diarrhea, which

limited its therapeutic gain [40]. Targeting tirapazamine towards the CAIX expressing (hypoxic) areas in tumors by conjugating tirapazamine with the benzenesulfonamide CAIXi might thereby prove a valuable approach to reduce normal tissue toxicity and increase the efficacy of the compounds (**8** and **11**) in CAIX expressing (hypoxic) cells. Cell viability assays (Table 2, Supplementary Fig. S2) confirmed that the parental compound was specifically effective in hypoxic cells, and more effective in CAIX<sup>-</sup> cells ( $IC_{50} < 50$  versus  $95 \mu\text{M}$ ,  $p = 0.037$ ). The CAIXi conjugated tirapazamine derivatives however abrogated the effect observed for the parental compound, both during hypoxia and normoxia, which was independent of CAIX levels (Table 2).

### Temozolomide derivatives

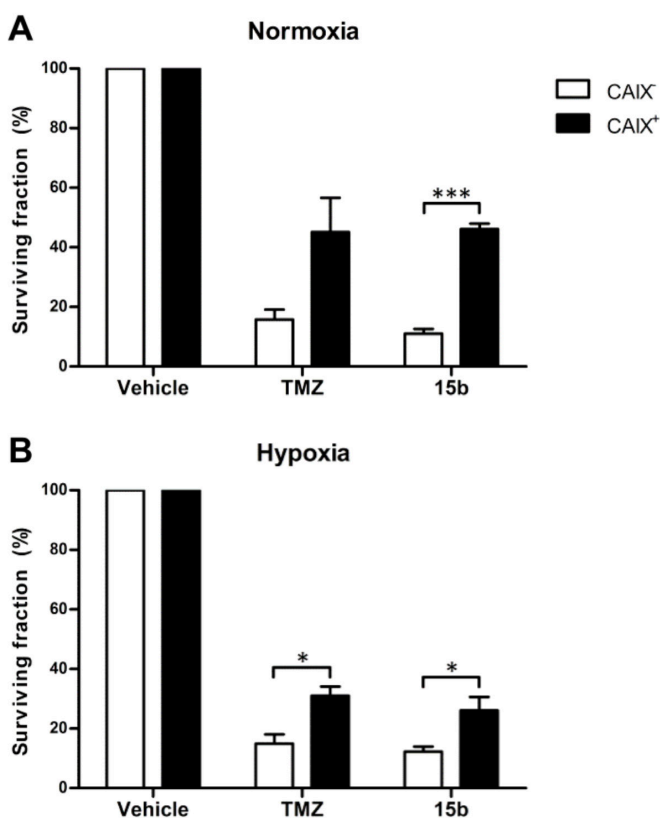
The current treatment of glioblastoma is based on radiotherapy combined with temozolomide, which has been shown to increase survival in phase III clinical trials [41]. Temozolomide is a methylating agent that spontaneously hydrolyzes to its active metabolite 3-methyl-(triazene-1-yl)imidazole-4-carboxamide (MTIC) at physiological pH [42].

The acidic extracellular pH in tumors might therefore reduce spontaneous temozolomide conversion and thereby decrease its efficacy. Inhibiting CAIX function is known to decrease extracellular acidification *in vitro* [24, 25, 28, 43], and we hypothesized that conjugating temozolomide with a sulfonamide or sulfamate moiety (**15a**, **15b**, **15c**, and **15d**) will specifically target hypoxic tumors and increase temozolomide conversion and thereby its efficacy. Nevertheless, while temozolomide resulted in lower cell viability in CAIX<sup>-</sup> cells, consistent with the pH-dependent mechanism of activation, the CAIXi conjugated temozolomide derivatives **15a**, **15c**, and **15d** were ineffective in reducing cell viability in both MDCK cell lines during normoxic and hypoxic conditions within the concentration range tested in the present study (Table 2, Supplementary Fig. S3). In contrast, **15b** was similarly effective as the parental temozolomide compound (Table 2).

This dual-target compound was therefore investigated further in clonogenic survival assays in which the medium of the cells was acidified because of CAIX function during hypoxic conditions (Supplementary Fig. S1)[44]. Temozolomide was again more effective in reducing clonogenic cell survival in the CAIX<sup>-</sup> MDCK cells as compared with the CAIX<sup>+</sup> MDCK cells (Fig. 1), similarly to its efficacy on cell viability. During hypoxia however temozolomide caused no difference in clonogenic survival as compared to normoxia, even though hypoxia is required to activate CAIX and cause extracellular acidification [43, 45] and is therefore hypothesized to reduce temozolomide conversion and efficacy. In contrast, the

CAIXi conjugated derivative **15b** significantly reduced clonogenic cell survival in hypoxic versus normoxic conditions in the CAIX<sup>+</sup> cells (surviving fraction is  $46.1 \pm 3.1$  versus  $26.1\% \pm 7.9$  during normoxia and hypoxia respectively,  $p < 0.05$ ). Nevertheless, the effect of **15b** on survival was not significantly different from the parental temozolomide compound. In addition, the low binding affinity of the compound (Table 1) combined with its relatively low efficacy in the CAIX<sup>+</sup> as compared to the CAIX<sup>-</sup> cells minimizes its potential for further development. These results furthermore suggest that temozolomide efficacy is not affected by CAIX dependent changes in extracellular pH during hypoxia. A reduction of temozolomide conversion and efficacy might require lower pH levels, *i.e.* pH < 6.6, which may have not been achieved in the present experiments [8, 9, 39].

4



**Figure 1.** Clonogenic cell survival of confluent MDCK CAIX<sup>-</sup> and CAIX<sup>+</sup> cells during normoxia (21% O<sub>2</sub>) and hypoxia (0.02% O<sub>2</sub>) when exposed to temozolomide (TMZ) and the CAIXi conjugated derivative **15b**. Surviving fraction (%) was normalized to vehicle control. Average  $\pm$  SEM of three independent biological repeats is shown. Asterisks indicate statistical significance (\* $p < 0.05$ ; \*\*\* $p < 0.001$ ).

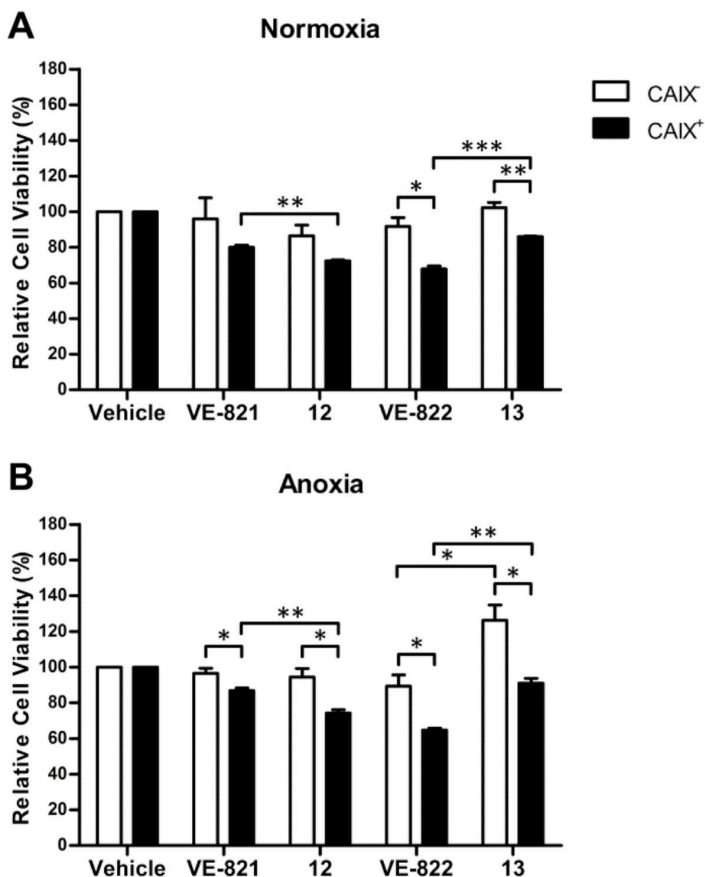
### ATR inhibitor derivatives

Preclinical experiments have shown that Ataxia Telangiectasia and Rad3-related protein inhibitors (ATRi) reduce the DNA repair capacity resulting in enhanced cell death and decreased tumor growth when combined with either chemo- or radiotherapy [46-48]. However, ATRi are not highly tumor specific, thus targeting these compounds towards the CAIX expressing areas of a tumor might increase their therapeutic benefit. The effect on cell viability of the parental ATRi (VE-821 and VE-822) and their CAIXi conjugated derivatives (**12** and **13**) was tested in combination with radiotherapy to induce DNA damage where a higher radiation dose was applied to anoxic cells, since those are more radioresistant [49, 50]. The parental ATRi and the CAIXi conjugated derivatives in combination with radiation decreased cell viability as compared to radiation only in the CAIX<sup>+</sup> cells ( $p < 0.05$ ) under both normoxic and anoxic conditions, but not in the CAIX<sup>-</sup> cells (Fig. 2).

The only exception is the derivative **13**, which had no significant effect on cell viability during anoxic conditions in both cell lines as compared to radiation alone ( $p = 0.09$  and  $p = 0.08$  for CAIX<sup>-</sup> and CAIX<sup>+</sup> cells, respectively). More importantly, the CAIXi conjugated derivative **12** was more effective than its respective parental ATRi (VE-821) in the CAIX<sup>+</sup> ( $p < 0.01$  during normoxia and anoxia), but not the CAIX<sup>-</sup> cells ( $p = 0.52$  and  $p = 0.72$  for normoxia and anoxia, respectively), suggesting a CAIX specific effect. In contrast, the CAIXi conjugated derivative **13** in combination with radiation was less effective in reducing cell viability than the parental compound VE-822 in CAIX<sup>+</sup> cells ( $p < 0.001$  and  $p < 0.01$  during normoxic and anoxic conditions, respectively). Although radiation induced similar effects on cell viability during normoxic and anoxic conditions, the efficacy of derivative **12** did not increase further during anoxic conditions as compared to normoxic conditions, even though CAIX expression is upregulated under hypoxic conditions (Supplementary Fig. S1) and these conditions are essential for CAIXi binding [43, 45].

Although derivative **12** indeed proved to be more effective in CAIX<sup>+</sup> than in CAIX<sup>-</sup> cells in combination with radiation, its efficacy might however not be solely dependent on binding to CAIX, which is consistent with unfavorable  $K_i$  values of the compound (Table 1). Exposing both cell lines to ATRi without irradiation decreased cell viability of both cell lines during normoxic and anoxic conditions, although this effect appeared to be slightly more pronounced in the CAIX<sup>-</sup> cells (Supplementary Fig. S5). Differences in ATRi response between the cell lines when combined with radiation might be explained by a lower number of cells in the resistant S-phase of the cell cycle [51] or by a decreased DNA repair ca-

capacity in cells with lower intracellular pH [52-54], *i.e.* those that do not express CAIX. This may also explain the difference in sensitivity to cytotoxic drugs between both cell lines, although further investigations are required to prove this causal relationship.

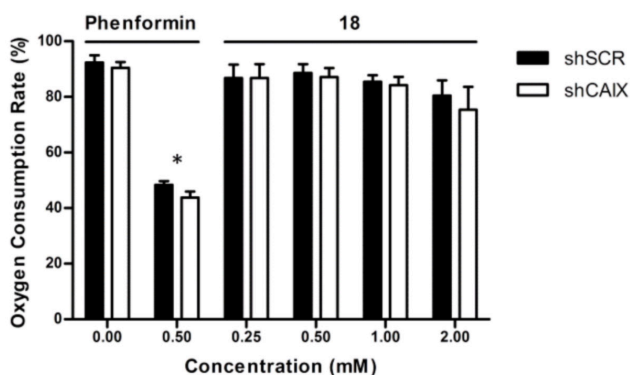


**Figure 2.** Relative cell viability (%) in MDCK CAIX<sup>-</sup> and CAIX<sup>+</sup> cells exposed to ATR inhibitors (VE-821 and VE-822) or the CAIXi conjugated derivatives (12 and 13) in combination with radiation during normoxia (21% O<sub>2</sub>) and anoxia (<0.02% O<sub>2</sub>). Normoxic cells were irradiated with 2 Gy and anoxic cells with 4 Gy to induce similar effects on cell viability. Cells were exposed to 500 nM VE-821 and 12, and to 50 nM VE-822 and 13. Average  $\pm$  SEM of three independent biological repeats is shown. Asterisks indicate statistical significance (\*p<0.05; \*\*p<0.01; \*\*\*p<0.001).

### Phenformin derivatives

Phenformin (1-(diaminomethylidene)-2-(2-phenylethyl)guanidine) is a drug used to treat diabetes, but was withdrawn from the North-American market in the 1970s by the Food

and Drug Administration (FDA) due to a high risk of developing lactic acidosis [55]. Treating patients with a similar but less potent drug metformin was found to be associated with a decrease in cancer incidence and an increased life span of cancer patients [56]. The repurposing of these compounds as anti-cancer agents is therefore being investigated where phenformin is found to be more lipophilic, thereby requiring less active transport than metformin [57]. The proposed mechanism of action of phenformin is its ability to inhibit mitochondrial respiration, which will consequently result in a decreased ATP production, thereby reducing tumor cell growth and improving tumor oxygenation as a result of decreased oxygen consumption [58, 59]. Conjugating phenformin with CAIXi might make the drug more tumor-specific leading to reduced normal tissue toxicity. Since tumor cells are more sensitive to phenformin treatment due to their altered energy metabolism, human colorectal HCT116 cells, with or without CAIX knockdown [24, 28] were used to study the effect of phenformin and its CAIXi conjugated derivative **18** on mitochondrial respiration. Western blotting confirms low expression of CAIX in CAIX KD cells under hypoxic conditions as compared with control cells (Supplementary Fig. S1B). As expected, CAIX levels were low in both cell lines under normoxic conditions. Phenformin significantly reduced Oxygen Consumption Rate (OCR) in both cell lines ( $p < 0.05$ ), independent of CAIX expression levels (Fig. 3). In contrast, the CAIXi conjugated derivative **18** was ineffective in reducing OCR, even when a fourfold higher concentration was used.



**Figure 3.** Oxygen consumption rate (OCR) of HCT116 cells with CAIX (shSCR) or without CAIX expression (shCAIX) exposed to phenformin or the CAIXi conjugated derivative **18**. OCR was normalized to baseline OCR levels before compound injection. Average  $\pm$  SEM of four independent biological repeats is shown. Asterisks indicate statistical significance ( $*p < 0.05$ ).

## Conclusion

Overall our hypothesis that newly designed dual-target drugs are more selective for CAIX expressing cells and are able to modulate their own efficacy by inhibiting CAIX function was not confirmed. Of all derivatives included, only one (*i.e.* the ATRi derivative **12**) proved more effective than its parental compound when combined with irradiation in CAIX<sup>+</sup> cells versus CAIX<sup>-</sup> cells. Nevertheless, the effect of this compound may not only be related to binding of the compound to CAIX due to limited binding affinity and the lack of further increase in its efficacy under hypoxic conditions. The rest of the derivatives included in this study did not show an increased efficacy in CAIX<sup>+</sup> versus CAIX<sup>-</sup> cells, or an efficacy that depended on oxygen levels, *i.e.* hypoxia versus normoxia. Nevertheless, since the parental compounds proved effective in these experiments the conjugation of the CAIXi moiety with the cytotoxic compounds may have caused conformational changes, thereby altering the compounds efficacy. In addition, these conformational changes may have also limited the binding of the CAIXi moiety (sulfonamide, sulfamide or aminoxysulfonamide) into the Zn<sup>2+</sup> containing active pocket of CAIX, which explains the lack of CAIX specificity and binding affinity for human CAs (Table 1) of the compounds. Alternative strategies to target the CAIX expressing cells in a tumor, e.g. antibody targeting or an increased number of CAIXi conjugated molecules [60], might therefore be more promising options to pursue in the future.

## Experimental section

### Chemistry

#### *General*

Unless otherwise specified, reagents and solvents were of commercial quality and were used without further purification. All reactions were carried out under an inert atmosphere of nitrogen. TLC analyses were performed on silica gel 60 F<sub>254</sub> plates (Merck Art.1.05554). Spots were visualized under 254 nm UV illumination, or by ninhydrin solution spraying. Melting points (mp) were determined on a Büchi Melting Point 510 and are uncorrected. <sup>1</sup>H and <sup>13</sup>C NMR spectra were recorded on Bruker DRX-400 spectrometer using DMSO-<sub>d6</sub> as a solvent and tetramethylsilane as an internal standard. For <sup>1</sup>H NMR spectra, chemical shifts are expressed in δ (ppm) downfield from tetramethylsilane, and coupling constants (*J*) are expressed in Hertz. Electron Ionization mass spectra were recorded in positive or

negative mode on a Waters MicroMass ZQ. All compounds that were tested in the biological assays were analyzed by High-resolution ESI mass spectra (HRMS) using a Q-ToF I mass spectrometer fitted with an electrospray ion source in order to confirm the purity of >95%.

#### 4-(4-(Bis(2-chloroethyl)amino)phenyl)butanoyl chloride (1)

Oxalyl chloride (32.8 mmol, 2.0 equiv.) was added slowly over a period of 1.0 h at 5–10 °C to a stirred solution of chlorambucil (16.4 mmol, 1.0 equiv.) in DCM (25.0 mL, 5.0 vol) and a catalytic amount of N, N-dimethylformamide. The reaction mixture was stirred at ambient temperature for 2–3 h, after which excess oxalyl chloride and DCM were removed under reduced pressure. The chlorambucil acid chloride that was obtained was a pale green solid in quantitative yield, which was used as such for the synthesis of Compounds **2a–c**.

#### 4-(4-(Bis(2-chloroethyl)amino)phenyl)butan-1-ol (3)

Compound **1** (15.5 mmol, 1.0 equiv.) was dissolved in DCM (125 mL) and methanol (75 mL, 3 vol) was slowly added over a period of 1 h at 15–20 °C. The reaction mixture was stirred at ambient temperature for 2 h. The reaction mixture was concentrated and the residue was dissolved in ethyl acetate (125 mL, 5 vol) and washed successively with a 5% aq. NaHCO<sub>3</sub>. Evaporation of the solvent under reduced pressure resulted in the chlorambucil methyl ester (16.4 mmol, 1.0 equiv.) in 95% yield as a light brown oil, which was added to a suspension of lithium aluminium hydride (32.8 mmol, 2 equiv.) in anhydrous THF (100 mL, 4 vol) at 0–5 °C for a period of 1 h. The reaction mixture was thereafter allowed to stir at ambient temperature for 2–3 h. Next, the reaction mixture was cooled to 0–5 °C and quenched slowly with ethyl acetate (250 mL, 10 vol) followed by water (100 mL, 4 vol). The reaction mixture was filtered through celite and ethyl acetate (50 mL, 2 vol) was used to wash the celite bed. The organic layer was washed with water (100 mL, 4 vol), dried over anhydrous Na<sub>2</sub>SO<sub>4</sub>, and filtered. Evaporation of the solvent under reduced pressure resulted in 99% yield of the crude alcohol as a pale yellow oil, which was used in the next step.

#### 4-(4-(Bis(2-chloroethyl)amino)phenyl)butyl carbonochloridate (4)

DMF (1.4 g) and sodium carbonate (75.79 mmol, 1.1 equiv.) were added to a solution of triphosgene (37.89 mmol, 0.55 equiv.) in toluene (300 mL, 15 vol) at ambient temperature. The reaction mixture was cooled to 0–5 °C and maintained at the same temperature for 30 min. Next, a solution of **3** (68.9 mmol, 1.0 equiv.) in toluene (100 mL, 5 vol) was added to

the stirred reaction mixture at 0–5 °C during 30 min. This reaction mixture was stirred for 4–5 h at room temperature. The reaction mixture was filtered thereafter and the solid was washed with toluene (100 mL, 5 vol). Evaporation of the solvent under reduced pressure resulted in the chloroformate **4** with a 64% yield as a yellow viscous liquid, which was used for the synthesis of carbamates (compounds **5a–c**).

#### **General procedure for the preparation of compounds (2a–c and 5a–c)**

To a solution of aminoalkylbenzene sulfonamide (1.0 equiv.) in acetonitrile (225 mL, 15 vol) and N,N-diisopropylethylamine (2.5 equiv.) a solution of compound **1** (**2a–c**) or compound **4** (**5a–c**) (1.0 equiv.) in acetonitrile (75 mL, 5 vol) was added over a period of 1 h and stirred overnight at ambient temperature. After completion, the reaction mixture was concentrated and the residue obtained was dissolved in ethyl acetate (150 mL, 10 vol). The organic layer was successively washed with 2 N HCl solution (100 mL × 2) in water, dried over anhydrous Na<sub>2</sub>SO<sub>4</sub>, and filtered. After evaporation of the solvent under reduced pressure a pale yellow solid was obtained as a crude product. This crude product was purified with column chromatography using a silica gel (40% ethyl acetate in hexane) to obtain compound **2a–c** and **5a–c** in a 51–87% yield.

General procedure for amination of 3-Chlorobenzotriazine-1,4-di-N-oxides (7 and 10)

4-(2-Aminoethyl) benzene sulfonamide (8.25 mmol, 3.0 equiv.) was added to a stirring solution of 3 chlorobenzotriazine-1,4-di-N-oxide (2.75 mmol, 1.0 equiv.) in dimethoxyethane (30 mL) and the mixture was stirred overnight at reflux temperature. The next day mixture was cooled to room temperature and concentrated under vacuum, after which the residue was dissolved in ammonium hydroxide solution and extracted with ethyl acetate. The organic layer was dried over Na<sub>2</sub>SO<sub>4</sub>, filtered and concentrated under vacuum. The residue was purified by chromatography using a silica gel with methylene chloride-methanol 98:2 v-v as an eluent to obtain the expected compound as a yellow powder with an 85–94% yield.

#### **General procedure for oxidation (8 and 11)**

Hydrogen peroxide (12.9 mmol, 10 equiv.) was added dropwise to a stirred solution of trifluoroacetic anhydride (12.9 mmol, 10 equiv.) in DCM at 0 °C. This reaction mixture was stirred at 0 °C for 5 min, warmed to room temperature for 10 min, and cooled to 5 °C. Next, the mixture was added to a stirred solution of mono oxide (1.29 mmol, 1.0 equiv.) in DCM at 0 °C and stirred at room temperature for 2–3 days. The reaction mixture was

carefully diluted with water and basified with aqueous  $\text{NH}_4\text{OH}$  and extracted with  $\text{CHCl}_3$ . The organic fraction was dried over anhydrous  $\text{Na}_2\text{SO}_4$ , filtered and evaporated to obtain the residue. This residue was purified by chromatography using a silica gel with methylene chloride-methanol 98:2 v-v as an eluent to obtain the expected compound as an orange red powder with a 46–96% yield.

#### **General procedure for synthesis of ATRi derivatives (12 and 13)**

A solution of VE-821 or VE-822 (0.54 mmol, 1.0 equiv.) and triethylamine (1.62 mmol, 3.0 equiv.) in 10 mL of methylene chloride was added to a mixture of chlorosulfonyl isocyanate (0.68 mmol, 1.2 equiv.) and tert-butanol (0.648 mmol, 1.2 equiv.) in 2 mL of methylene chloride. The mixture was stirred at room temperature for 1.0 h, diluted with ethyl acetate, and washed with water. The organic layer was then dried over anhydrous  $\text{Na}_2\text{SO}_4$ , filtered and concentrated under vacuum. The residue was purified by chromatography with a silica gel and methylene chloride-methanol 98:2 as an eluent. This intermediate was thereafter diluted in a solution of trifluoro acetic acid in methylene chloride (20% vol.) and stirred at room temperature for 6 h. Next, the mixture was concentrated under vacuum and co-evaporated with diethyl ether multiple times to obtain the expected compound with a 58–65% yield.

#### **General procedure for synthesis of temozolomide derivatives**

To a slurry of 3-methyl-4-oxo-3,4-dihydroimidazo[5,1-d][1,2,3,5] tetrazine-8-carboxylic acid (1.0 mmol, 1.0 equiv.) in DCM, BOP (1.0 mmol, 1.0 equiv.), amine (1.1 mmol, 1.1 equiv.) and triethylamine (2.5 mmol, 2.5 equiv.) were added. This reaction mixture was stirred overnight at room temperature and filtered to obtain the expected compounds with a 41–95% yield.

#### **4-(4-(Bis(2-chloroethyl)amino)phenyl)-N-(4-sulfamoylphenyl)butanamide (2a)**

mp: 155–157 °C;  $^1\text{H}$  NMR (400 MHz,  $\text{DMSO-d}_6$ ),  $\delta$  10.22 (s, 1H), 7.73 (d,  $J = 4.4$ , 4H), 7.23 (s, 2H), 7.05 (d,  $J = 8.7$ , 2H), 6.67 (d,  $J = 8.7$ , 2H), 3.70 (d,  $J = 8.6$ , 8H), 2.54–2.50 (m, 2H), 2.34 (t,  $J = 8.6$ , 2H), 1.90–1.78 (m, 2H);  $^{13}\text{C}$  NMR (101 MHz,  $\text{DMSO-d}_6$ ),  $\delta$  171.68, 144.46, 142.23, 138.03, 129.53, 126.65, 118.51, 111.90, 52.22, 41.17, 35.84, 33.54, 26.87; MS (ESI<sup>+</sup>)  $m/z$  458.11 [M+H]<sup>+</sup>, 460.10 [M+2]<sup>+</sup>. HRMS (ESI<sup>+</sup>) [M+H]<sup>+</sup> calculated for  $[\text{C}_{20}\text{H}_{26}\text{N}_3\text{O}_3\text{SCl}_2]^+$ : 458.1072, found: 458.1075.

## 4-(4-(bis(2-chloroethyl)amino)phenyl)-N-(4-sulfamoylbenzyl)butanamide (2b)

mp: 130–132 °C;  $^1\text{H NMR}$  (400 MHz, DMSO- $d_6$ ),  $\delta$  8.41 (t,  $J = 5.9$ , 1H), 7.76 (d,  $J = 8.3$ , 2H), 7.41 (d,  $J = 8.3$ , 2H), 7.31 (s, 2H), 7.02 (d,  $J = 8.6$ , 2H), 6.66 (d,  $J = 8.6$ , 2H), 4.31 (d,  $J = 5.9$ , 2H), 3.69 (s, 8H), 2.45 (t,  $J = 7.5$ , 2H), 2.15 (t,  $J = 7.5$ , 2H), 1.82–0.72 (m, 2H);  $^{13}\text{C NMR}$  (101 MHz, DMSO- $d_6$ ),  $\delta$  172.15, 144.42, 143.92, 142.54, 129.86, 129.33, 127.46, 125.68, 111.89, 52.22, 41.67, 41.17, 34.84, 33.66, 27.39; MS (ESI+)  $m/z$  472.12 [M+H] $^+$ , 474.12 [M+2] $^+$ . HRMS (ESI+) [M+H] $^+$  calculated for  $[\text{C}_{21}\text{H}_{28}\text{N}_3\text{O}_3\text{SCl}_2]^+$ : 472.1228, found: 472.1236.

## 4-(4-(Bis(2-chloroethyl)amino)phenyl)-N-(4-sulfamoylphenethyl)butanamide (2c)

mp: 108–110 °C;  $^1\text{H NMR}$  (400 MHz, DMSO- $d_6$ ),  $\delta$  7.89 (t,  $J = 5.6$ , 1H), 7.74 (d,  $J = 8.3$ , 2H), 7.38 (d,  $J = 8.3$ , 2H), 7.30 (s, 2H), 7.00 (d,  $J = 8.6$ , 2H), 6.66 (d,  $J = 8.6$ , 2H), 3.70 (d,  $J = 8.9$ , 8H), 3.29 (dd,  $J = 13.0, 5.6$ , 2H), 2.78 (t,  $J = 7.5$ , 2H), 2.41 (t,  $J = 7.5$ , 2H), 2.08–1.98 (m, 2H), 1.76–1.65 (m, 2H);  $^{13}\text{C NMR}$  (101 MHz, DMSO- $d_6$ ),  $\delta$  171.95, 144.39, 143.80, 142.01, 129.89, 129.21, 125.67, 111.87, 52.23, 41.17, 34.87, 33.61, 27.32; MS (ESI+)  $m/z$  486.14 [M+H] $^+$ , 488.14 [M+2] $^+$ . HRMS (ESI+) [M+H] $^+$  calculated for  $[\text{C}_{22}\text{H}_{30}\text{N}_3\text{O}_3\text{SCl}_2]^+$ : 486.1385, found 486.1387.

## 4-(4-(Bis(2-chloroethyl)amino)phenyl)butyl (4-sulfamoylphenyl)carbamate(5a)

mp: 156–158 °C;  $^1\text{H NMR}$  (400 MHz, DMSO- $d_6$ ),  $\delta$  10.01 (s, 1H), 7.76–7.69 (m, 2H), 7.64–7.56 (m, 2H), 7.22 (s, 2H), 7.04 (d,  $J = 8.7$ , 2H), 6.66 (d,  $J = 8.7$ , 2H), 4.12 (t,  $J = 6.0$ , 2H), 3.77–3.63 (m, 8H), 1.70–1.54 (m, 4H);  $^{13}\text{C NMR}$  (101 MHz, DMSO- $d_6$ ),  $\delta$  153.50, 144.40, 142.34, 137.48, 130.06, 129.30, 126.77, 117.50, 111.89, 64.43, 52.22, 41.17, 33.68, 28.09, 27.62; MS (ESI+)  $m/z$  488.12 [M+H] $^+$ , 490.12 [M+2] $^+$ . HRMS (ESI+) [M+H] $^+$  calculated for  $[\text{C}_{21}\text{H}_{28}\text{N}_3\text{O}_4\text{SCl}_2]^+$ : 488.1178, found: 488.1184.

## 4-(4-(Bis(2-chloroethyl)amino)phenyl)butyl (4-sulfamoylbenzyl)carbamate(5b)

mp: 98–100 °C;  $^1\text{H NMR}$  (400 MHz, DMSO- $d_6$ ),  $\delta$  7.76 (t,  $J = 8.5$ , 3H), 7.41 (d,  $J = 8.5$ , 2H), 7.31 (s, 2H), 7.02 (d,  $J = 8.6$ , 2H), 6.66 (d,  $J = 8.6$ , 2H), 4.23 (d,  $J = 6.1$ , 2H), 3.98 (s, 2H), 3.75–3.63 (m, 8H), 2.47 (s, 2H), 1.55 (m, 4H);  $^{13}\text{C NMR}$  (101 MHz, DMSO- $d_6$ ),  $\delta$  156.63, 144.37, 143.97, 142.61, 130.13, 129.26, 127.27, 125.70, 111.88, 63.84, 52.23, 43.37, 41.18, 33.68, 28.31, 27.64; MS (ESI+)  $m/z$  502.13 [M+H] $^+$ , 504.13 [M+2] $^+$ . HRMS (ESI+) [M+H] $^+$  calculated for  $[\text{C}_{22}\text{H}_{30}\text{N}_3\text{O}_4\text{SCl}_2]^+$ : 502.1334, found: 502.1338.

## 4-(4-(Bis(2-chloroethyl)amino)phenyl)butyl (4-sulfamoylphenethyl)carbamate(5c)

mp: 100–102 °C;  $^1\text{H NMR}$  (400 MHz, DMSO- $d_6$ ),  $\delta$  7.77–7.70 (m, 2H), 7.37 (d,  $J = 8.2$ , 2H),

7.30 (s, 2H), 7.19 (t,  $J = 5.5$ , 1H), 7.02 (d,  $J = 8.6$ , 2H), 6.66 (d,  $J = 8.6$ , 2H), 3.94 (d,  $J = 5.5$ , 2H), 3.69 (s, 8H), 3.21 (dd,  $J = 13.3, 6.6$ , 2H), 2.76 (dd,  $J = 16.9, 9.8$ , 2H), 2.46 (s, 2H), 1.52 (s, 4H);  $^{13}\text{C}$  NMR (101 MHz, DMSO- $d_6$ ),  $\delta$  156.30, 144.37, 143.58, 142.03, 130.15, 129.19, 125.67, 111.88, 63.51, 52.23, 41.28, 35.09, 33.67, 28.32, 27.63; MS (ESI $^+$ )  $m/z$  516.15 [M+H] $^+$ , 518.15 [M+2] $^+$ . HRMS (ESI $^+$ ) [M+H] $^+$  calculated for  $[\text{C}_{23}\text{H}_{32}\text{N}_3\text{O}_4\text{SCl}_2]^+$ : 516.1491, found: 516.1490.

### 3-(4-Sulfamoylphenethylamino) benzo [e][1,2,4] triazine 1-oxide (7)

Compound **7** was synthesized from **6** by a general amination method and resulted in a yellow solid with a yield of 94%. mp: 250–252 °C;  $^1\text{H}$  NMR (400 MHz, DMSO- $d_6$ ),  $\delta$  8.15 (s, 1H), 8.13 (s, 1H), 8.03 (s, 1H), 7.82–7.71 (m, 3H), 7.60 (d,  $J = 8.0$ , 1H), 7.47 (d,  $J = 8.0$ , 2H), 7.38–7.30 (m, 1H), 7.28 (s, 2H), 3.60 (d,  $J = 6.2$ , 2H), 3.01 (dd,  $J = 6.2$ , 2H);  $^{13}\text{C}$  NMR (101 MHz, DMSO- $d_6$ )  $\delta$  158.80, 143.70, 142.07, 135.76, 129.25, 125.92, 124.66, 119.93, 41.92, 34.09; MS (ESI $^+$ )  $m/z$  346.10 [M+H] $^+$ . HRMS (ESI $^+$ ) [M+H] $^+$  calculated for  $[\text{C}_{15}\text{H}_{16}\text{N}_5\text{O}_3\text{S}]^+$ : 346.0974, found: 346.0973.

### 3-((4-Sulfamoylphenethyl)amino)benzo[e][1,2,4]triazine 1,4-dioxide (8)

Compound **8** was synthesized from **7** by a general oxidation method, resulting in an orange red solid with a yield of 96%. mp: 210–212 °C;  $^1\text{H}$  NMR (400 MHz, DMSO- $d_6$ ),  $\delta$  8.31 (t,  $J = 6.1$ , 1H), 8.22 (d,  $J = 8.1$ , 1H), 8.13 (d,  $J = 8.1$ , 1H), 7.97–7.89 (m, 1H), 7.75 (d,  $J = 8.3$ , 2H), 7.61–7.53 (m, 1H), 7.47 (d,  $J = 8.3$ , 2H), 7.29 (s, 2H), 3.67 (dd,  $J = 7.2, 6.1$ , 2H), 3.03 (t,  $J = 7.2$ , 2H);  $^{13}\text{C}$  NMR (101 MHz, DMSO- $d_6$ ),  $\delta$  149.67, 143.19, 142.16, 138.19, 135.48, 130.07, 129.26, 127.04, 125.71, 121.13, 116.89, 41.76, 34.18; MS (ESI $^+$ )  $m/z$  362.09 [M+H] $^+$ . HRMS (ESI $^+$ ) [M+H] $^+$  calculated for  $[\text{C}_{15}\text{H}_{16}\text{N}_5\text{O}_4\text{S}]^+$ : 362.0923, found: 362.0928.

### 3-(4-Sulfamoylphenethylamino)-7,8-dihydro-6H-indeno [5,6-e][1,2,4] triazine 1-oxide (10)

Compound **10** was synthesized from **9** by using a general amination method, which resulted in a yellow solid with a 85% yield. mp: 238–240 °C;  $^1\text{H}$  NMR (400 MHz, DMSO- $d_6$ ),  $\delta$  7.95 (s, 1H), 7.82 (s, 1H), 7.74 (t,  $J = 10.0$ , 2H), 7.49–7.39 (m, 3H), 7.28 (s, 2H), 3.57 (dd,  $J = 13.0, 6.8$ , 2H), 3.02–2.90 (m, 6H), 2.11–1.99 (m, 2H);  $^{13}\text{C}$  NMR (101 MHz, DMSO- $d_6$ ),  $\delta$  157.56, 153.64, 142.79, 141.97, 130.10–127.99, 125.35, 112.78, 41.77, 32.35, 31.60, 25.25; MS (ESI $^+$ )  $m/z$  386.13 [M+H] $^+$ . HRMS (ESI $^+$ ) [M+H] $^+$  calculated for  $[\text{C}_{18}\text{H}_{20}\text{N}_5\text{O}_3\text{S}]^+$ : 386.1287, found: 386.1291.

3-((4-Sulfamoylphenethyl) amino)-7,8-dihydro-6H-indeno [5,6-e][1,2,4] triazine  
1,4-dioxide (11)

Compound **11** was synthesized from **10** by using a general oxidation method resulting in an orange red solid with a yield of 46%. mp: 218–220 °C; <sup>1</sup>H NMR (400 MHz, DMSO-d<sub>6</sub>), δ 8.19 (s, 1H), 7.98 (d, *J* = 24.2, 2H), 7.75 (d, *J* = 7.8, 2H), 7.46 (d, *J* = 7.7, 2H), 7.29 (s, 2H), 3.65 (d, *J* = 6.2, 2H), 3.12–2.92 (m, 6H), 2.17–1.99 (m, 2H); <sup>13</sup>C NMR (101 MHz, DMSO-d<sub>6</sub>), δ 154.56, 149.25, 145.07, 143.22, 142.15, 129.23, 125.71, 41.76, 32.74, 31.80, 25.24; MS (ESI<sup>+</sup>) *m/z* 402.12 [M+H]<sup>+</sup>. HRMS (ESI<sup>+</sup>) [M+H]<sup>+</sup> calculated for [C<sub>18</sub>H<sub>20</sub>N<sub>5</sub>O<sub>4</sub>S]<sup>+</sup>: 402.1236, found: 402.1234.

6-(4-(Methylsulfonyl)phenyl)-N-phenyl-3-(sulfamoylamino)pyrazine-2-carboxamide  
(12)

Compound **12** was synthesized from commercially purchased VE-821 by using the general procedure described above, which resulted in a yellow solid with an overall yield of 58%. mp: 233–235 °C; <sup>1</sup>H NMR (400 MHz, DMSO-d<sub>6</sub>), δ 11.27 (s, 1H), 10.82 (s, 1H), 9.28 (s, 1H), 8.64 (d, *J* = 8.6, 2H), 8.08 (d, *J* = 8.6, 2H), 7.83–7.76 (m, 2H), 7.68 (s, 2H), 7.48–7.39 (m, 2H), 7.23 (dd, *J* = 14.0, 6.6, 1H), 3.30 (s, 3H); <sup>13</sup>C NMR (101 MHz, DMSO-d<sub>6</sub>), δ 164.59–163.27, 149.32–147.73, 144.46–143.38, 141.16, 139.57, 137.17–136.45, 128.69, 127.46, 125.15, 122.08, 43.46; MS (ESI<sup>+</sup>) *m/z* 448.07 [M+H]<sup>+</sup>. HRMS (ESI<sup>+</sup>) [M+H]<sup>+</sup> calculated for [C<sub>18</sub>H<sub>18</sub>N<sub>5</sub>O<sub>2</sub>S<sub>2</sub>]<sup>+</sup>: 448.0749, found: 448.0748.

5-(4-(Isopropylsulfonyl) phenyl)-3-(3-(4-((methylamino) methyl) phenyl) isoxazol-5-yl)  
pyrazin-2-carboxamide (13)

Compound **13** was synthesized from commercially purchased VE-822 by using the general procedure described above, which resulted in a yellow solid with an overall yield of 65%. mp: 242–244 °C; <sup>1</sup>H NMR (400 MHz, DMSO-d<sub>6</sub>), δ 8.94 (s, 1H), 8.38 (d, *J* = 8.5, 2H), 8.02 (d, *J* = 8.2, 2H), 7.93 (d, *J* = 8.5, 2H), 7.79 (s, 1H), 7.54 (d, *J* = 8.2, 2H), 7.20 (s, 2H), 6.96 (s, 2H), 4.17 (s, 2H), 3.54–3.38 (m, 1H), 2.58 (s, 3H), 1.17 (t, *J* = 14.1, 6H); <sup>13</sup>C NMR (101 MHz, DMSO-d<sub>6</sub>), δ 167.67, 162.00, 151.75, 142.47, 141.04, 139.53, 137.62, 135.78, 129.00, 127.17, 125.69, 124.47, 102.16, 54.22, 53.49, 34.94, 15.19; MS (ESI<sup>+</sup>) *m/z* 543.15 [M+H]<sup>+</sup>. HRMS (ESI<sup>+</sup>) [M+H]<sup>+</sup> calculated for [C<sub>24</sub>H<sub>27</sub>N<sub>6</sub>O<sub>5</sub>S<sub>2</sub>]<sup>+</sup>: 543.1484, found: 543.1484.

3-Methyl-4-oxo-N-(4-sulfamoylphenethyl)-3,4-dihydroimidazo[5,1-d][1,2,3,5]tetrazine-  
8-carboxamide (15a)

Compound **15a** was synthesized from **14** by reacting it with 4-(2-aminoethyl) benzene

sulfonamide using the general procedure for synthesizing temozolomide derivatives described above. This reaction resulted in a white solid with a yield of 50%. mp: 195–197 °C;  $^1\text{H}$  NMR (400 MHz, DMSO- $d_6$ ),  $\delta$  8.83 (s, 1H), 8.58 (t,  $J$  = 5.9, 1H), 7.74 (d,  $J$  = 8.3, 2H), 7.44 (d,  $J$  = 8.3, 2H), 7.30 (s, 2H), 3.86 (s, 3H), 3.58 (dd,  $J$  = 13.4, 6.8, 2H), 2.96 (t,  $J$  = 7.1, 2H);  $^{13}\text{C}$  NMR (101 MHz, DMSO- $d_6$ ),  $\delta$  159.67, 143.64, 142.05, 139.20, 134.45, 130.30, 129.14, 128.46, 125.73, 36.16, 34.78; MS (ESI $^+$ )  $m/z$  378.10 [M+H] $^+$ . HRMS (ESI $^+$ ) [M+H] $^+$  calculated for [C $_{14}$ H $_{16}$ N $_7$ O $_4$ S] $^+$ : 378.0984, found: 378.0986.

3-Methyl-4-oxo-N-(sulfamoyloxy)-3,4-dihydroimidazo[5,1-d][1,2,3,5]tetrazine-8-carboxamide (15b)

Compound **15b** was synthesized from **14** by reacting it with aminoxysulfonamide using the general procedure for synthesizing temozolomide derivatives described above. This reaction resulted in a white solid with a yield of 41%. mp: 195–197 °C;  $^1\text{H}$  NMR (400 MHz, DMSO- $d_6$ ),  $\delta$  8.81 (s, 1H), 7.80 (s, 1H), 7.67 (s, 1H), 7.30 (s, 2H), 3.86 (s, 3H);  $^{13}\text{C}$  NMR (101 MHz, DMSO- $d_6$ )  $\delta$  161.51, 139.16, 134.57, 130.51, 128.37, 45.72.

3-Methyl-4-oxo-N-(4-sulfamoylbenzyl)-3,4-dihydroimidazo [5,1-d][1,2,3,5]tetrazine-8-carboxamide (15c)

Compound **15c** was synthesized from **14** by reacting it with 4-(aminomethyl) benzene sulfonamide hydrochloride using the general procedure for synthesizing temozolomide derivatives described above. This reaction resulted in a white solid with a yield of 88%. mp: 185–187 °C;  $^1\text{H}$  NMR (400 MHz, DMSO- $d_6$ )  $\delta$  9.20 (t,  $J$  = 6.2, 1H), 8.87 (s, 1H), 7.77 (d,  $J$  = 8.3, 2H), 7.50 (d,  $J$  = 8.3, 2H), 7.31 (s, 2H), 4.55 (d,  $J$  = 6.3, 2H), 3.87 (s, 3H);  $^{13}\text{C}$  NMR (101 MHz, DMSO- $d_6$ ),  $\delta$  159.96, 143.85, 142.63, 142.63, 138.96, 134.69, 130.11, 129.28, 128.62, 127.68, 125.77, 41.94, 36.23; MS (ESI $^+$ )  $m/z$  364.08 [M+H] $^+$ . HRMS (ESI $^+$ ) [M+H] $^+$  calculated for [C $_{13}$ H $_{14}$ N $_7$ O $_4$ S] $^+$ : 364.0828, found: 364.0826.

3-Methyl-4-oxo-N-(5-sulfamoyl-1,3,4-thiadiazol-2-yl)-3,4-dihydroimidazo[5,1-d][1,2,3,5]tetrazine-8-carboxamide (15d)

Compound **15d** was synthesized from **14** by reacting it with 5-amino-1, 3,4-thiadiazole-2-sulfonamide hydrochloride using the general procedure for synthesizing temozolomide derivatives described above. This reaction resulted in a light yellow solid with a yield of 95%. mp: 128–130 °C;  $^1\text{H}$  NMR (400 MHz, DMSO- $d_6$ ),  $\delta$  8.63 (s, 1H), 8.06 (s, 1H), 7.81 (s, 1H), 7.35 (s, 2H), 3.83 (s, 3H);  $^{13}\text{C}$  NMR (101 MHz, DMSO- $d_6$ ),  $\delta$  171.73, 170.89, 165.39, 161.04, 157.91, 139.53, 134.24, 127.88; MS (ESI $^+$ )  $m/z$  358.01 [M+H] $^+$ . HRMS

(ESI<sup>+</sup>) [M+H]<sup>+</sup> calculated for [C<sub>8</sub>H<sub>8</sub>N<sub>9</sub>O<sub>4</sub>S<sub>2</sub>]<sup>+</sup>: 358.0141, found: 358.0140.

Synthesis of 4-(2-(3-carbamimidoylguanidino)ethyl)benzenesulfonamide hydrochloride salt (**18**)

4-(2-Aminoethyl)benzenesulfonamide **16** (0.5g, 1.0 equiv.) and cyanoguanidine **17** (0.21g, 1.0 equiv.) were suspended in n-butanol (5.0 mL) and treated with a 6.0 M aqueous hydrochloric acid solution (1.0 equiv., 0.4 mL). The mixture was treated at 100 °C overnight and the solvents were removed under vacuum. The residue was thereafter crystallized from isopropyl alcohol (IPA) to obtain compound **18** as a white solid with a 75% yield. mp: 154–159 °C; <sup>1</sup>H NMR (400 MHz, DMSO-d<sub>6</sub>), δ 7.87 (d, 2H, *J* = 8.4, Ar-H), 7.82 (brs, 2H, exchangeable with D<sub>2</sub>O), 7.50 (d, 2H, *J* = 8.4, Ar-H), 7.38 (brs, 1H, exchangeable with D<sub>2</sub>O), 6.62 (brs, 2H, exchangeable with D<sub>2</sub>O), 3.15 (t, 2H, *J* = 6.7), 2.98 (t, 2H, *J* = 6.7); <sup>13</sup>C NMR (101 MHz, DMSO-d<sub>6</sub>), δ 164.0, 143.7, 142.0, 130.3, 127.0, 119.3, 61.4, 34.1; MS (ESI<sup>+</sup>) *m/z* 285.11 [M+H]<sup>+</sup>.

### CA inhibition assays

To measure the CA-catalyzed CO<sub>2</sub> hydration activity an Applied Photophysics stopped-flow instrument was used [61]. To maintain ionic strength Na<sub>2</sub>SO<sub>4</sub> (20 mM) was used with HEPES (20 mM, pH 7.5) as a buffer and Phenol red (0.2 mM) as an indicator working at the maximum absorbance of 557 nm, which was used to follow the initial rates of the CA-catalyzed CO<sub>2</sub> hydration for a duration of 10–100 s. To determine the kinetic parameters and inhibition constants varying CO<sub>2</sub> concentrations were included (1.7–17 mM). Initial velocity was assayed with at least six traces of the initial 5–10% of the reaction for each compound. Compounds were dissolved in distilled-deionized water (0.01 nM). The combined enzyme solutions and compounds were incubated for 15 min at room temperature to allow for the E-I complex formation prior to measurements. The nonlinear least-squares method of PRISM 3 was used to estimate the inhibition constants and the mean of three independent estimations is reported. The CA isoforms included are recombinant proteins obtained in house.

### Biological assays

#### Cells

All cell lines used were cultured in DMEM supplemented with 10% fetal bovine serum. Canine kidney epithelial MDCK cells overexpressing human CAIX (CAIX<sup>+</sup>) or a scrambled control vector (CAIX<sup>-</sup>) have been described before [37, 44]. The HCT116 constitutive CAIX

knockdown cell line and its scrambled control have also been described before and were kindly provided by Professor Adrien Harris (Weatherall Institute of Molecular Medicine, University of Oxford, John Radcliffe hospital, Oxford, UK) [24, 28, 62]. Cells were exposed to hypoxic or anoxic conditions in a hypoxic chamber (MACS VA500 microaerophilic workstation, Don Whitley Scientific, UK) with 0.2 or  $\leq 0.02\%$  O<sub>2</sub>, respectively, and 5% CO<sub>2</sub> and residual N<sub>2</sub> to upregulate and activate CAIX. Normoxic cells were grown in normal incubators with 21% O<sub>2</sub>, 5% CO<sub>2</sub> at 37 °C.

### ***Cell viability assays***

The efficacy of the cytotoxic derivatives was compared to their respective parental compounds in cell viability assays using alamarBlue® (Invitrogen). In short, MDCK cells were seeded in 96-well plates and allowed to attach overnight. The next day plates were exposed to hypoxia and DMEM was replaced with pre-incubated hypoxic DMEM. In contrast, testing the ATRi was performed in anoxic conditions to decrease the radiosensitivity of the cells. In parallel normoxic 96-well plates were incubated in normal incubators with 21% O<sub>2</sub> and 5% CO<sub>2</sub>. Compounds were dissolved in DMSO (0.5%, Sigma-Aldrich) and final concentrations were made with pre-incubated hypoxic or normoxic DMEM and added to the wells after 24 h of exposure. To test the ATR inhibitors cells were exposed to the compounds 1 h prior to irradiation and the 96-well plates were irradiated (225 kV Philips X-ray tube) with 2 Gy (normoxia) or 4 Gy (anoxia). Cells were exposed to compounds for a total of 2 h for chlorambucil and tirapazamine, or 72 h for temozolomide and the ATR inhibitors, after which medium was washed off and replaced with fresh medium. For chlorambucil, tirapazamine, and ATR inhibitor derivatives cells were allowed to grow for an additional 72 h under normoxic conditions prior to measurement, whereas cells exposed to temozolomide derivatives remained in hypoxic conditions prior to measurement. Cells were allowed to convert alamarBlue® for 2 h during normoxic conditions, which corresponds with their metabolic function and is a measure for cell viability.

### ***Clonogenic assays***

Clonogenic survival of MDCK cells was determined with high cell numbers to allow for CAIX-dependent extracellular acidification [44]. These cells were exposed to temozolomide or 15b for 24 h during normoxic or hypoxic conditions after which cells were trypsinized and reseeded in triplicate with known cell numbers. Cells were allowed to grow for 7 days to form colonies that were quantified after staining and fixation with 0.4% methylene blue in 70% ethanol. Surviving fraction was normalized to vehicle (0.5% DMSO).

### ***Basal respiration measurements***

Oxygen Consumption Rates (OCR) were determined using the Seahorse XF96 extracellular Flux analyzer (Agilent Technologies). Cells were seeded in a XF96 cell plate with normal growth medium at an optimized cell density of  $1.5 \times 10^4$  cells/well. Plates were placed in a 5% CO<sub>2</sub> incubator at 37 °C in order to let the cells attach. Subsequently cells were incubated for 18 h under hypoxic conditions (0.2% O<sub>2</sub>). Culture medium was exchanged with DMEM containing 25 mM d-glucose, 4 mM l-glutamine and 1 mM sodiumpyruvate (GIBCO, Thermo Fisher) 60 min prior to the assay and plates were placed in a CO<sub>2</sub>-free incubator at 37 °C. Prior to the first injection, baseline OCR was determined using a mixing period of 5 min and a measurement period of 3 min followed by 3 loops of mixing and measuring for 3 min each. Medium containing vehicle (PBS, Lonza), Phenformin Hydrochloride (Sigma-Aldrich), or the CAIXi conjugated phenformin derivative 18 were injected followed by several mixing and measurements cycles. Subsequently cells were washed with PBS and lysed in a 0.05% SDS (Sigma-Aldrich) solution. Protein quantification for normalization purposes was performed using Pierce™ BCA Protein Assay Kit (Thermo Fisher).

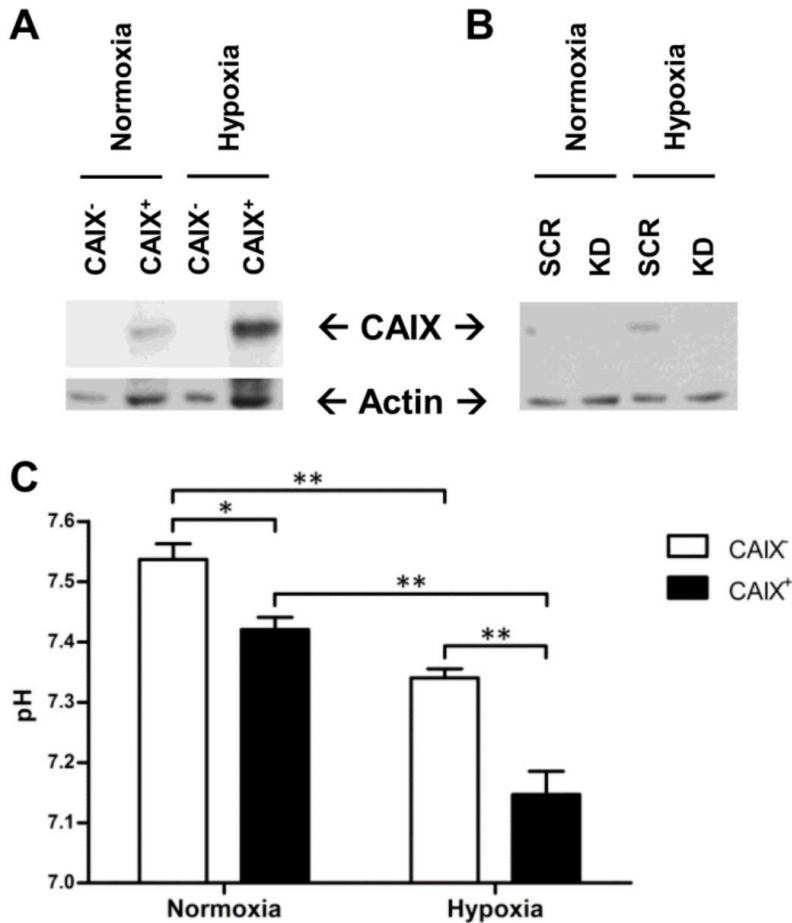
### ***Western blot***

To validate CAIX expression in the genetically modified cell lines protein immunoblotting was performed after 24 h of hypoxia exposure (0.2% O<sub>2</sub>) as described previously [43]. Primary antibodies used included the anti-CAIX M75 antibody (kindly provided by Professor Silvia Pastorekova, Institute of Virology, Slovak Academy of Science, Slovak Republic), and anti-β-actin (MP Biomedicals, #691001) as a reference protein.

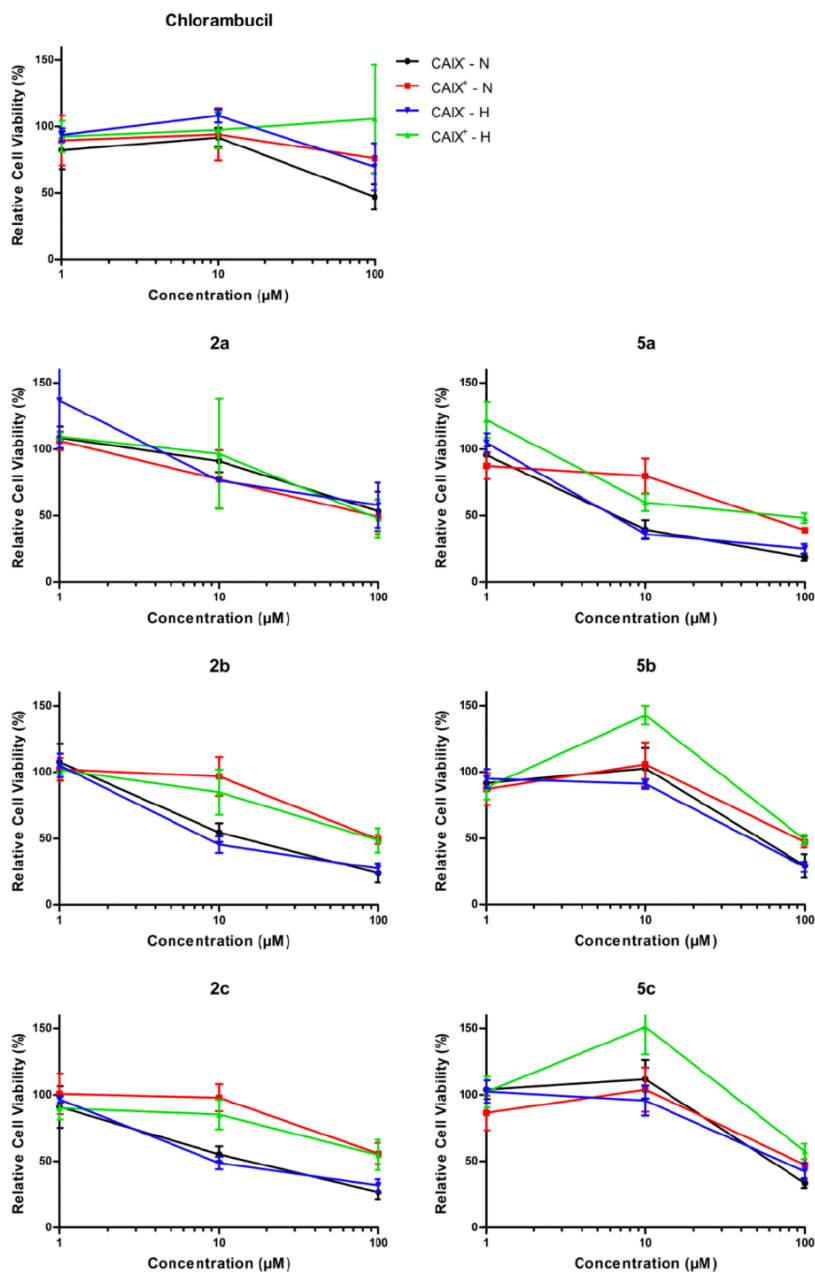
### ***Statistical analyses***

GraphPad Prism (version 5.03) was used for all statistical analyses. For the cytotoxic compounds IC<sub>50</sub> values were estimated with the curve of the log(inhibitor) vs. normalized response (Variable slope). Means between groups were compared using unpaired t-tests, where  $p < 0.05$  indicated statistical significance.

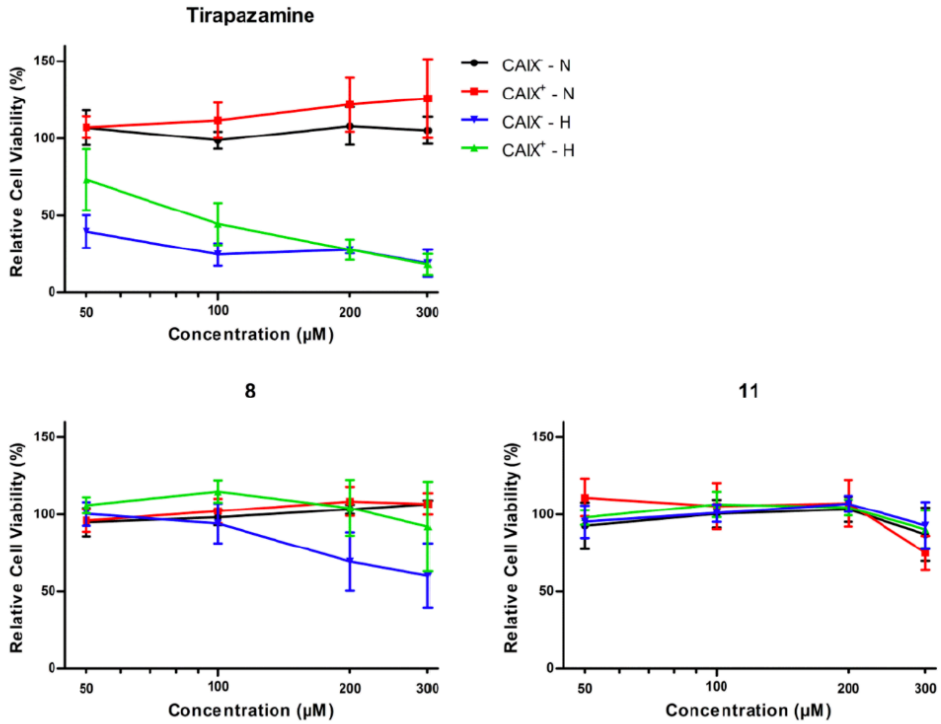
## Supplementary data



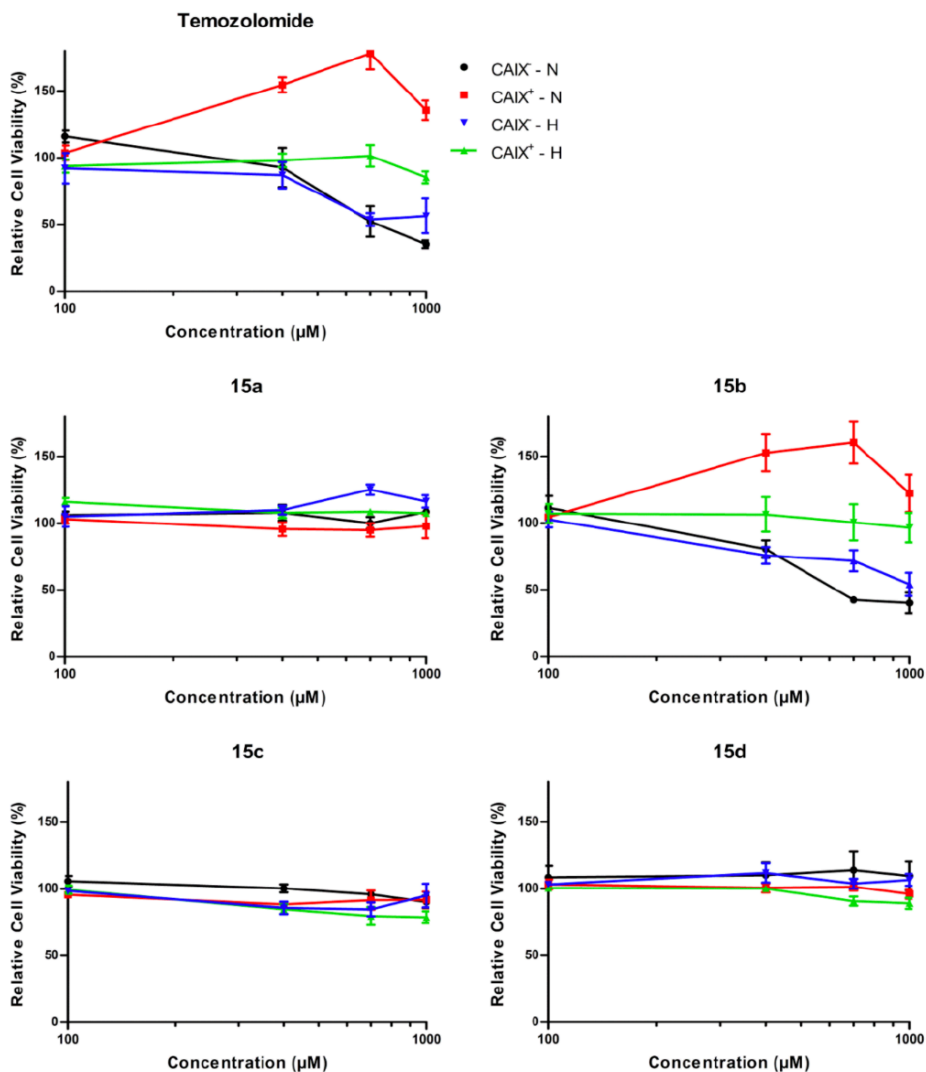
**Supplementary Figure S1.** CAIX protein expression during normoxia and hypoxia of the MDCK (A) and HCT116 (B) cells and pH measurements of MDCK cells (C). Expression of  $\beta$ -actin was included as a reference protein. CAIX<sup>+</sup> MDCK cells are overexpressing CAIX, and CAIX<sup>-</sup> cells are control cells lacking both human and canine CAIX expression. HCT116 scrambled control vector cells (SCR) show hypoxia-dependent CAIX expression, whereas CAIX knockdown (KD) cells do not. During normoxic conditions HCT116 SCR cells have no detectable levels of CAIX, since the dot (B) is an artefact on film. The pH of the culture medium was measured of the MDCK cells after 24 hours of normoxic or hypoxic exposure (C). Mean  $\pm$  SEM of three independent biological repeats are shown.



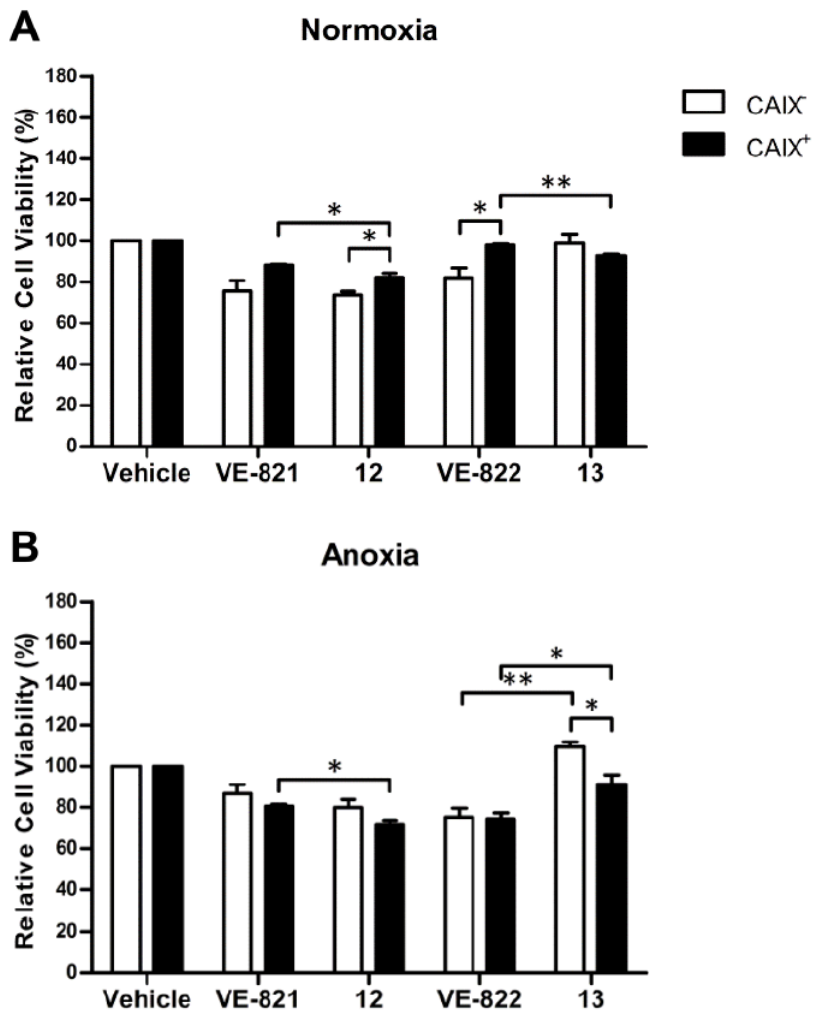
**Supplementary Figure S2.** Relative cell viability of CAIX<sup>+</sup> and CAIX<sup>-</sup> MDCK cells exposed to increasing concentrations of chlorambucil or the CAIXi conjugated derivatives during normoxic (N) and hypoxic (H) conditions. Relative cell viability was normalized to vehicle control (0.5% DMSO). Average  $\pm$  SEM of three independent biological repeats is shown.



**Supplementary Figure S3.** Relative cell viability of CAIX<sup>+</sup> and CAIX<sup>-</sup> MDCK cells exposed to increasing concentrations of tirapazamine or the CAIXi conjugated derivatives during normoxic (N) and hypoxic (H) conditions. Relative cell viability was normalized to vehicle control (0.5% DMSO). Average ± SEM of three independent biological repeats is shown

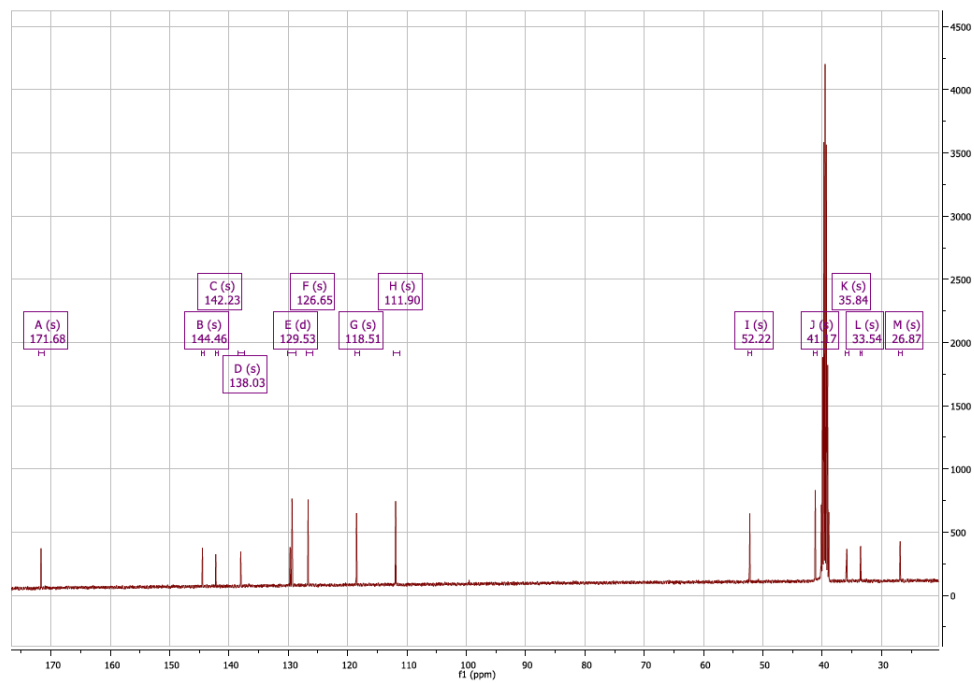
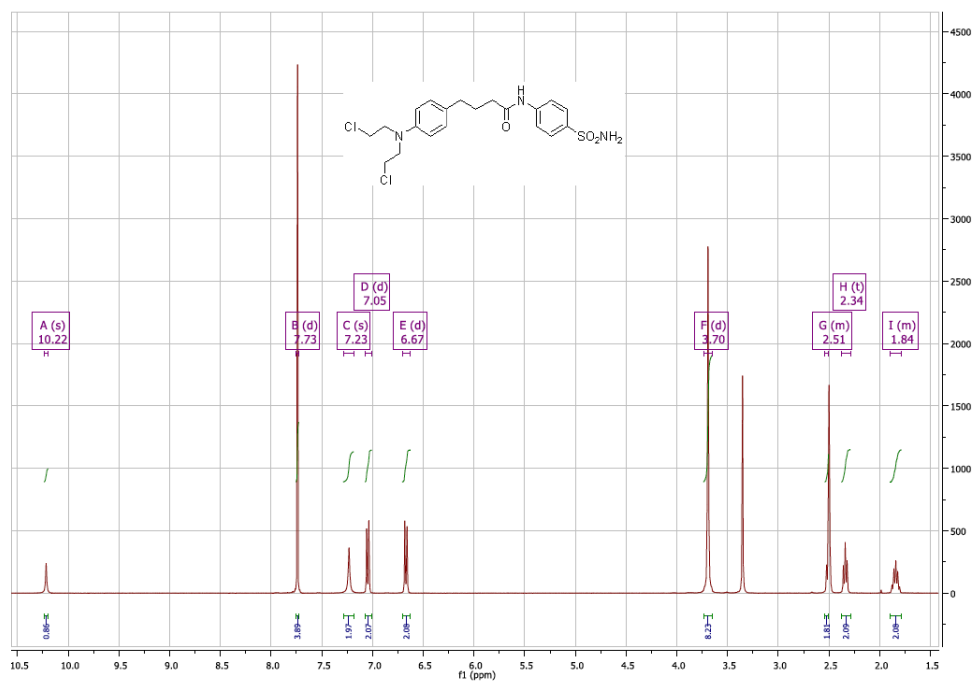


**Supplementary Figure S4.** Relative cell viability of CAIX<sup>+</sup> and CAIX<sup>-</sup> MDCK cells exposed to increasing concentrations of temozolomide or the CAIXi conjugated derivatives during normoxic (N) and hypoxic (H) conditions. Relative cell viability was normalized to vehicle control (0.5% DMSO). Average  $\pm$  SEM of three independent biological repeats is shown.

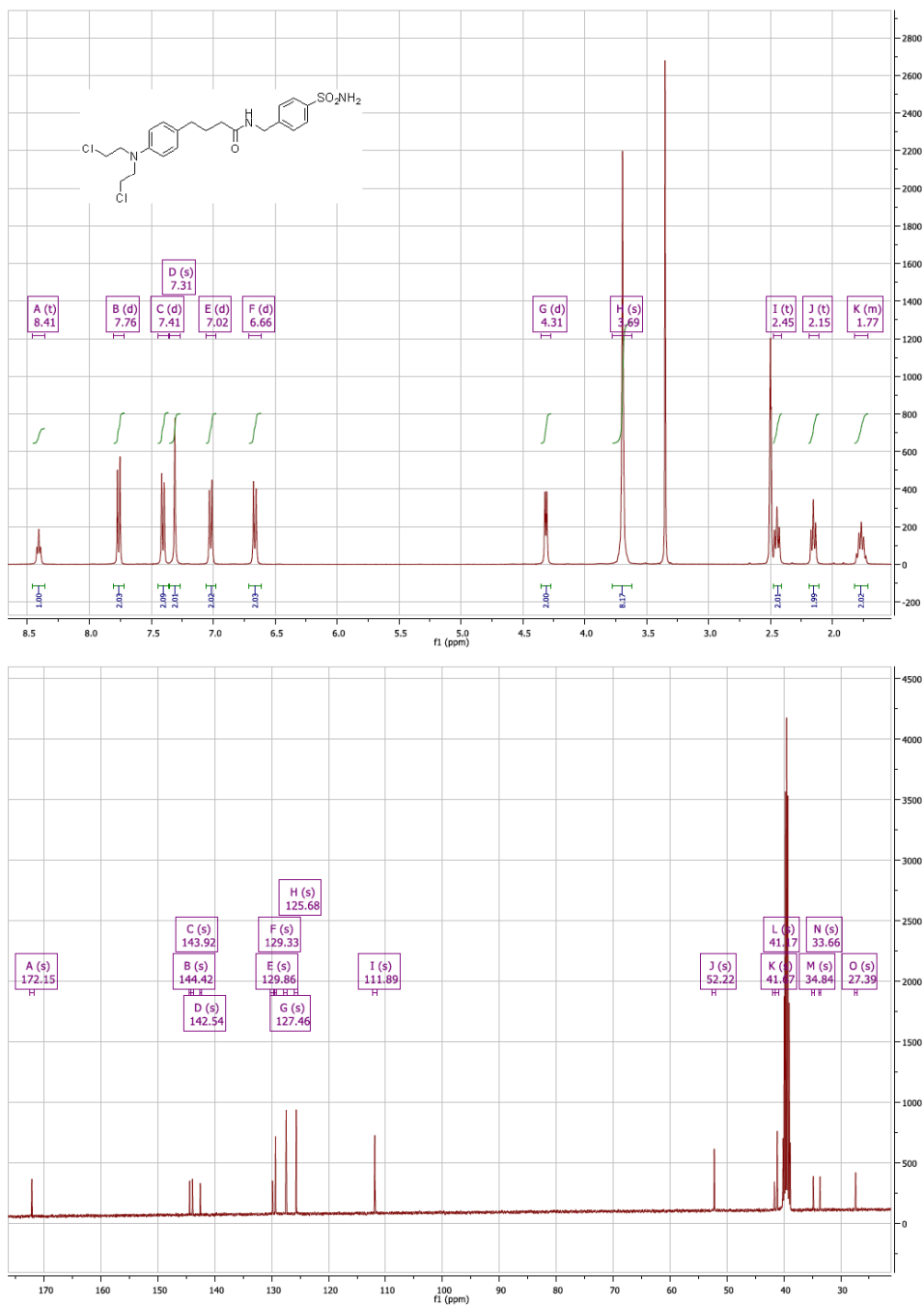


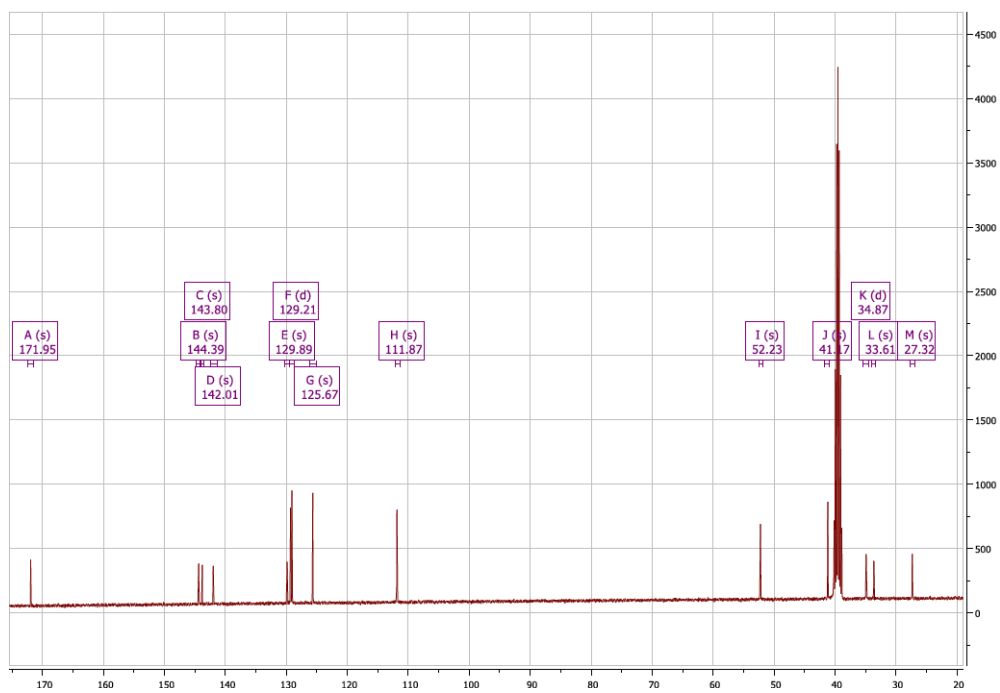
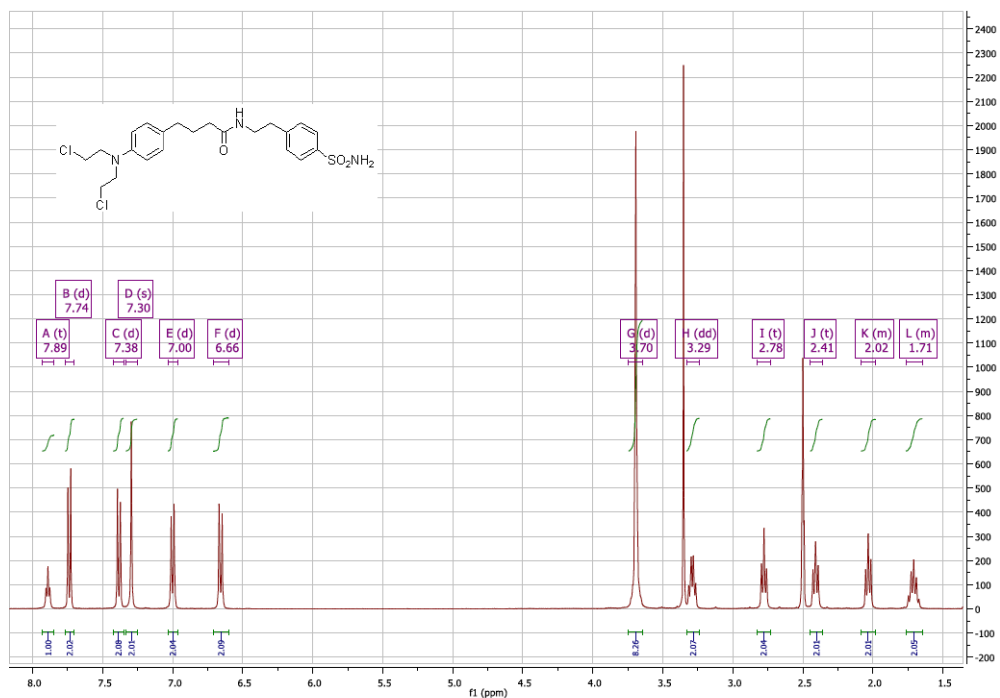
**Supplementary Figure S5.** Relative cell viability (%) in MDCK CAIX<sup>-</sup> and CAIX<sup>+</sup> cells exposed to ATR inhibitors (VE-821 and VE-822) or the CAIXi conjugated derivatives (**12** and **13**) without radiation during normoxia (21% O<sub>2</sub>) and anoxia (<0.02% O<sub>2</sub>). Cells were exposed to 500 nM VE-821 and **12**, and to 50 nM VE-822 and **13**. Average ± SEM of three independent biological repeats is shown. Asterisks indicate statistical significance (\*p < 0.05; \*\*p < 0.01; \*\*\*p < 0.001).

## NMR spectra 1: 4-(4-(bis(2-chloroethyl)amino)phenyl)-N-(4-sulfamoylphenyl)butanamide (2a).

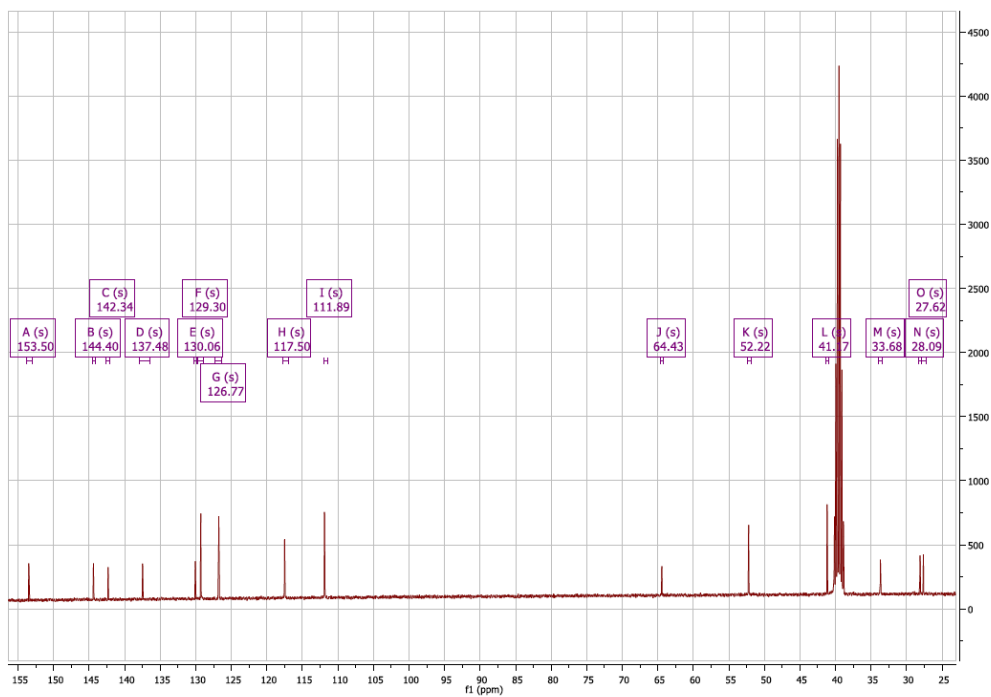
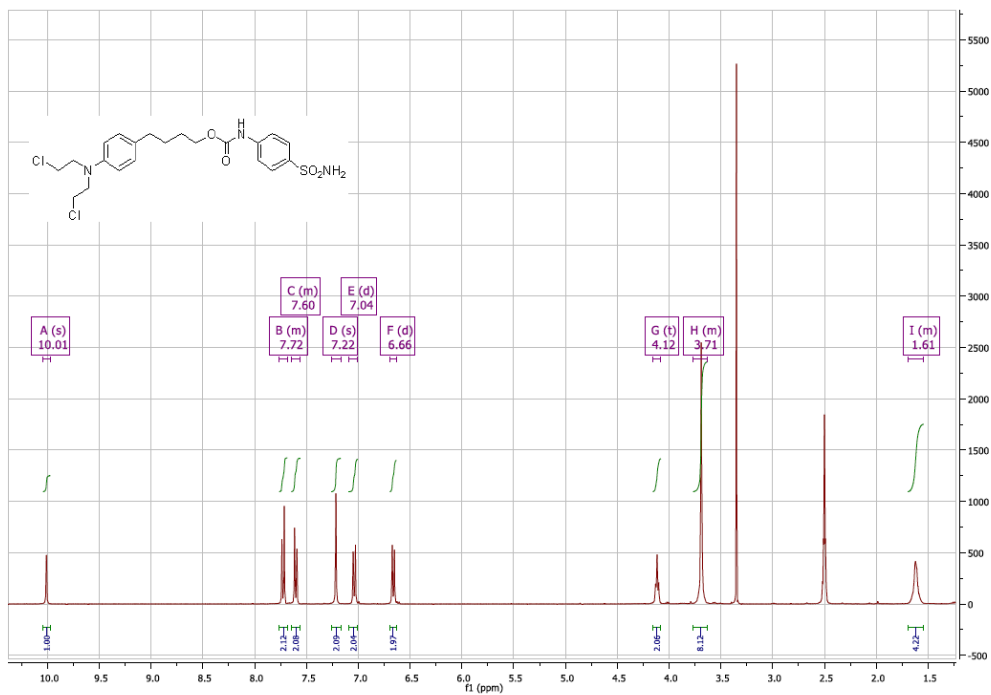


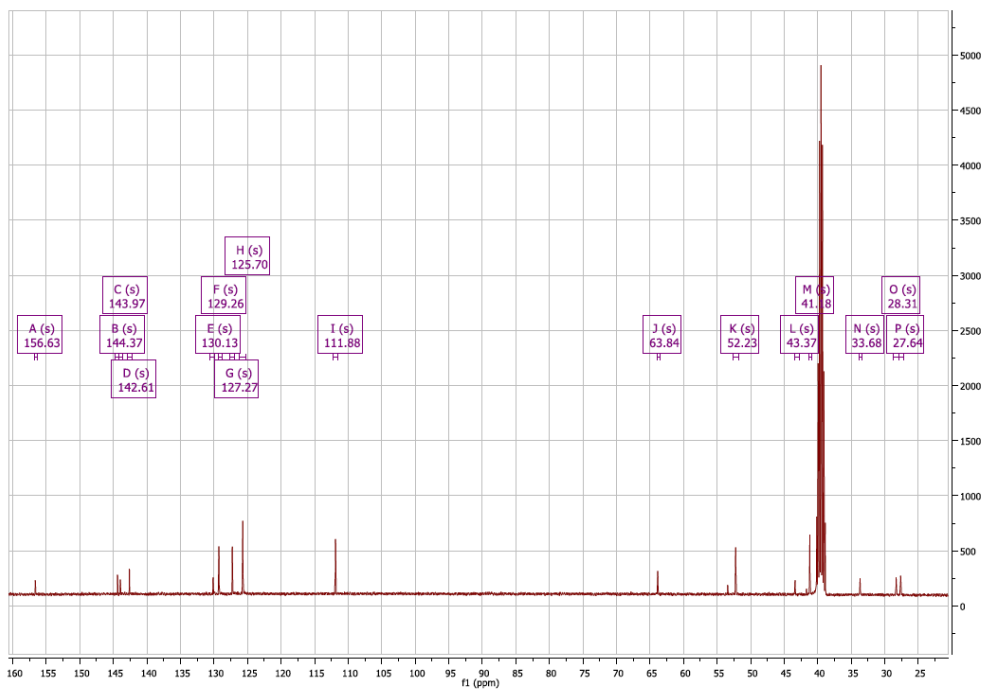
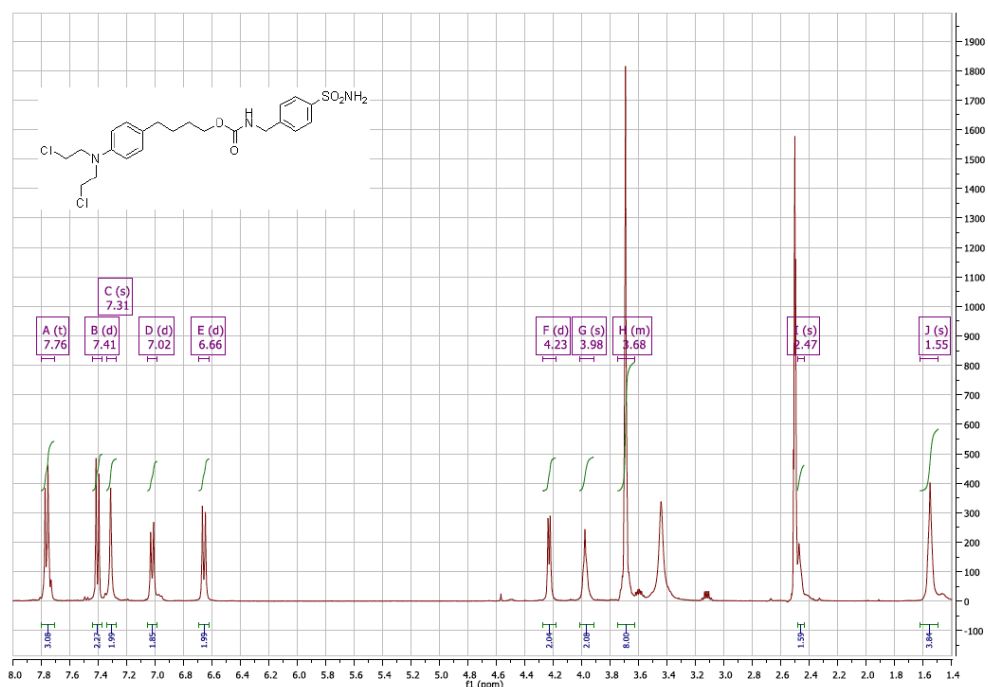
**NMR spectra 2: 4-(4-(bis(2-chloroethyl)amino)phenyl)-N-(4-sulfamoylbenzyl)butanamide (2b).**



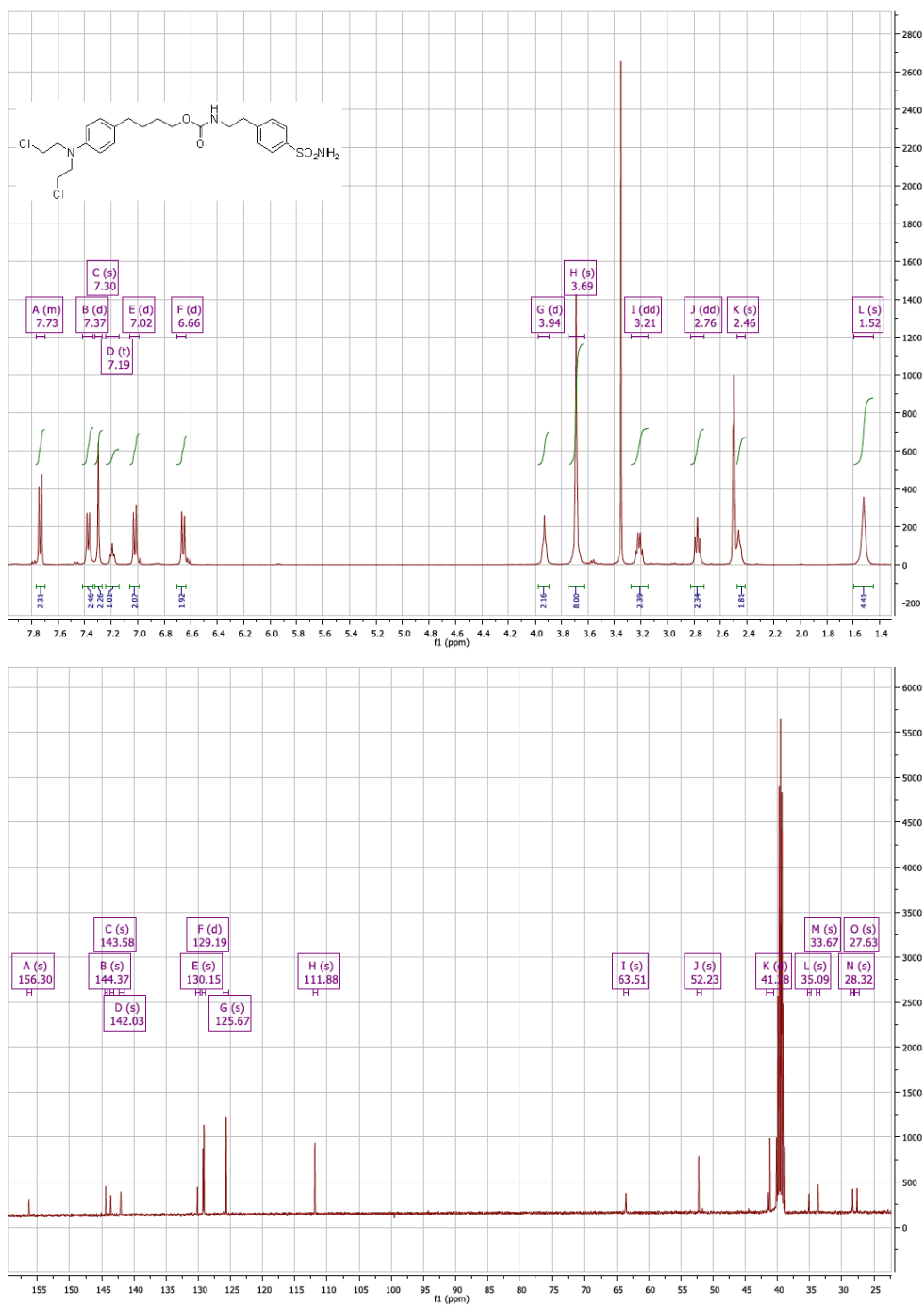
**NMR spectra 3: 4-(4-(bis(2-chloroethyl)amino)phenyl)-N-(4-sulfamoylphenethyl)butanamide(2c).**


**NMR spectra 4:** 4-(4-(bis(2-chloroethyl)amino)phenyl)butyl (4-sulfamoylphenyl)carbamate(5a).

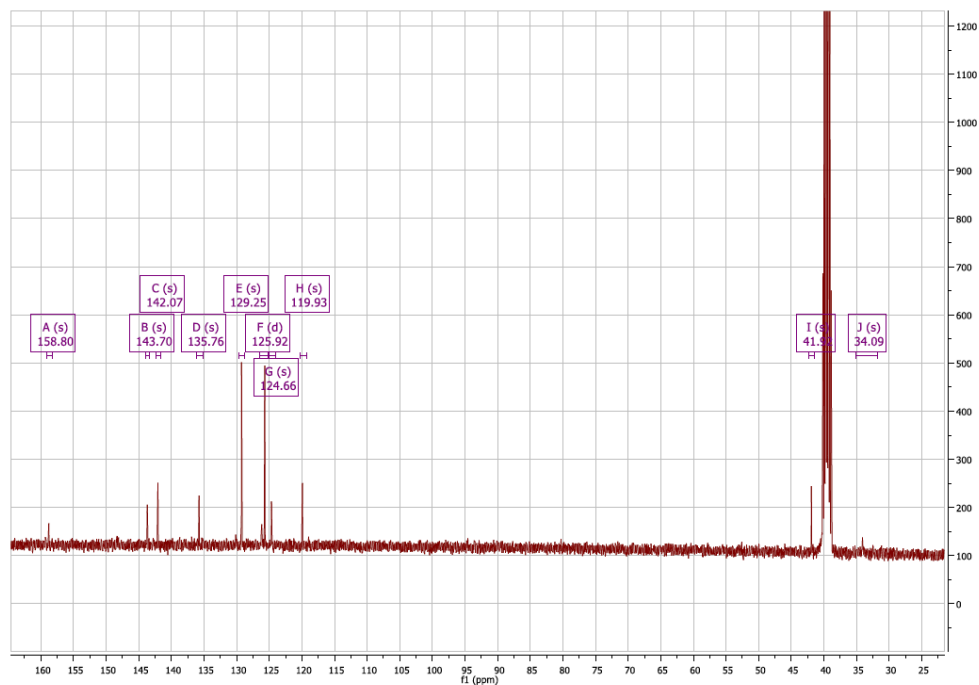
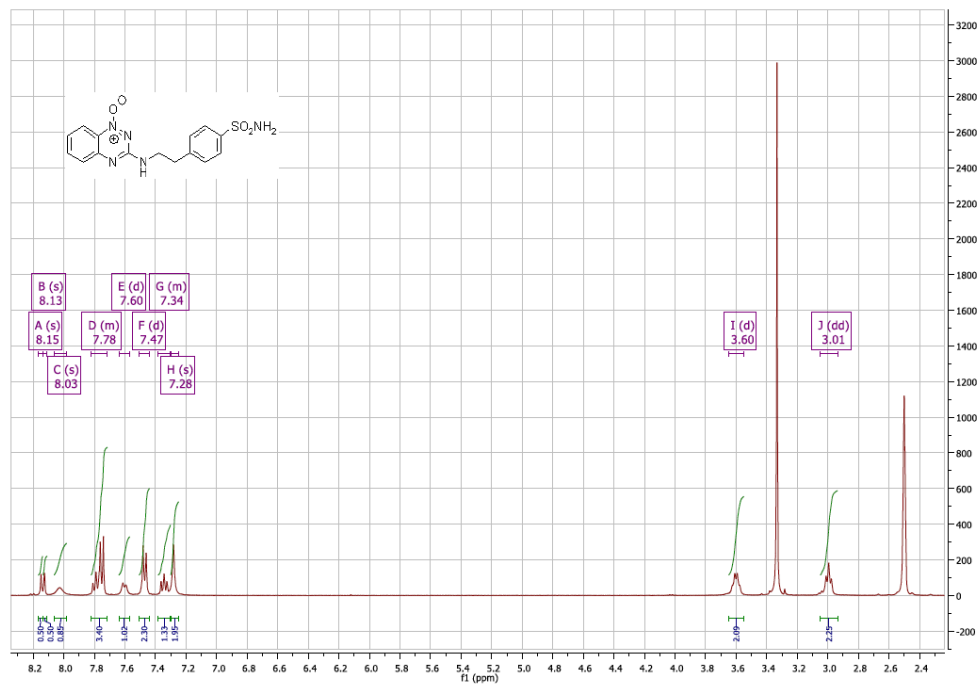


**NMR spectra 5: 4-(4-(bis(2-chloroethyl)amino)phenyl)butyl (4-sulfamoylbenzyl)carbamate(5b).**


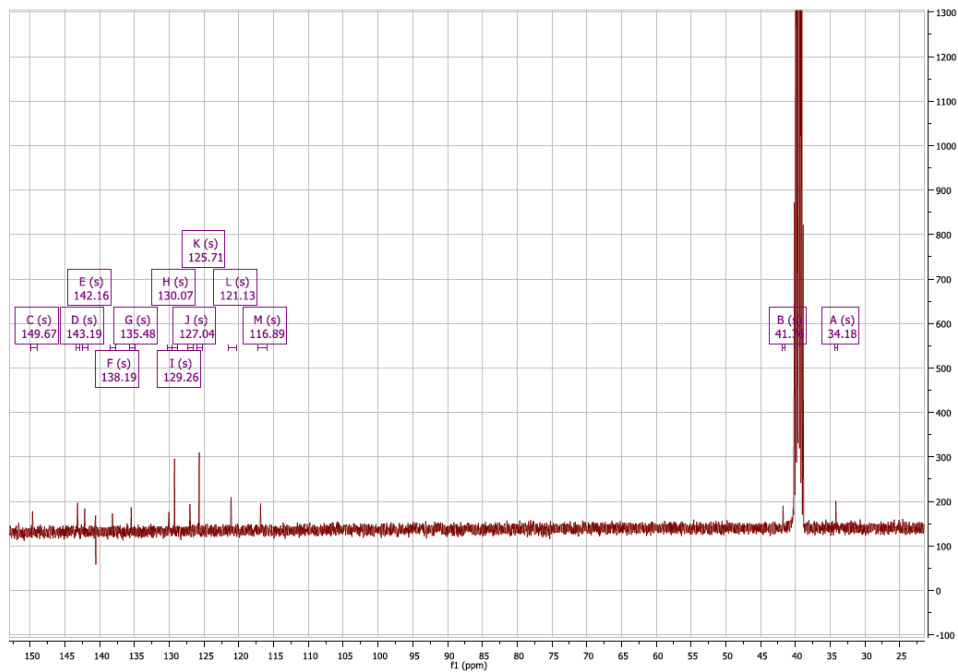
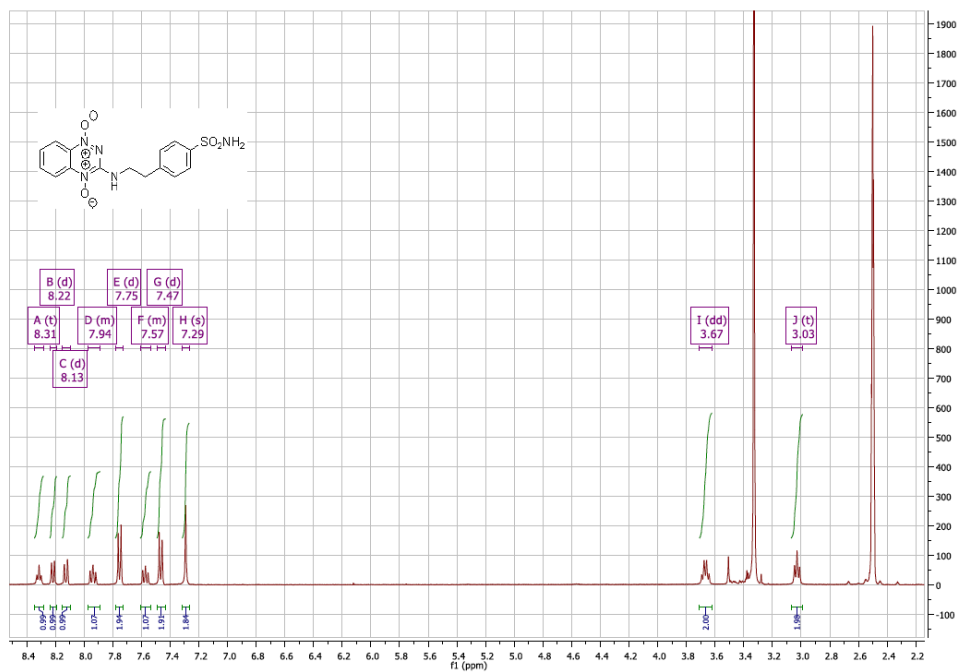
**NMR spectra 6:** 4-(4-(bis(2-chloroethyl)amino)phenyl)butyl (4-sulfamoylphenethyl)carbamate(5c).



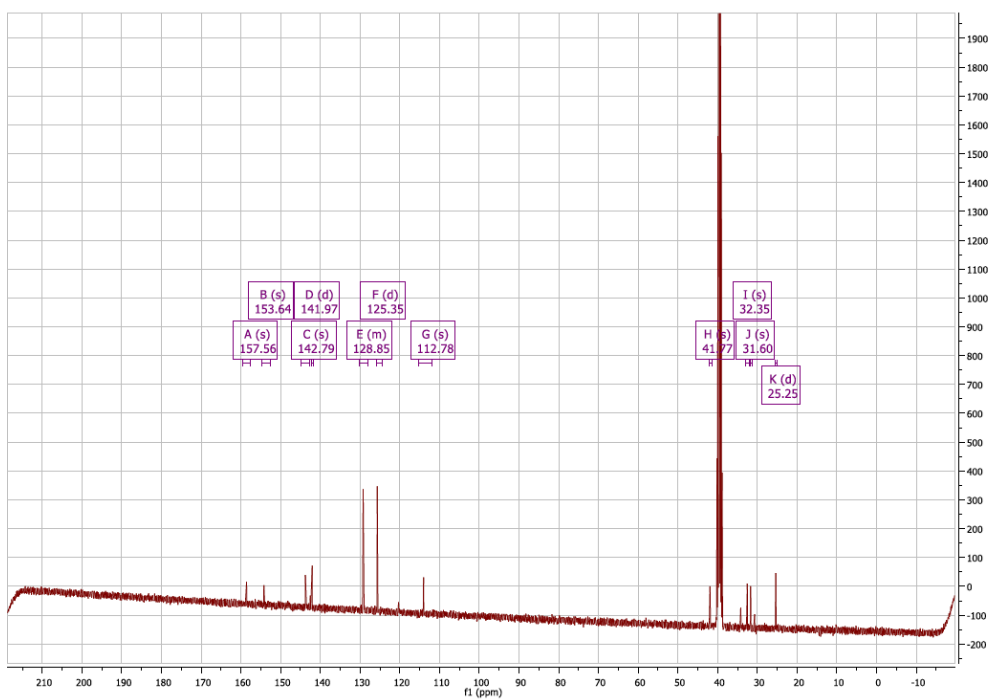
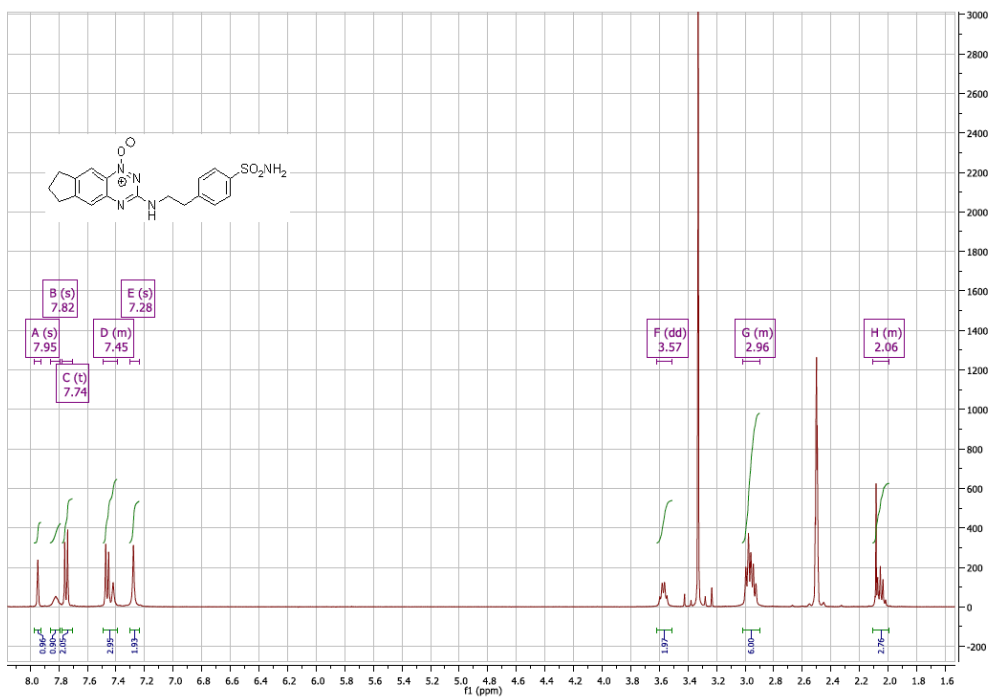
## NMR spectra 7: 3-(4-sulfamoylphenethylamino) benzo [e][1,2,4] triazine 1-oxide (7).



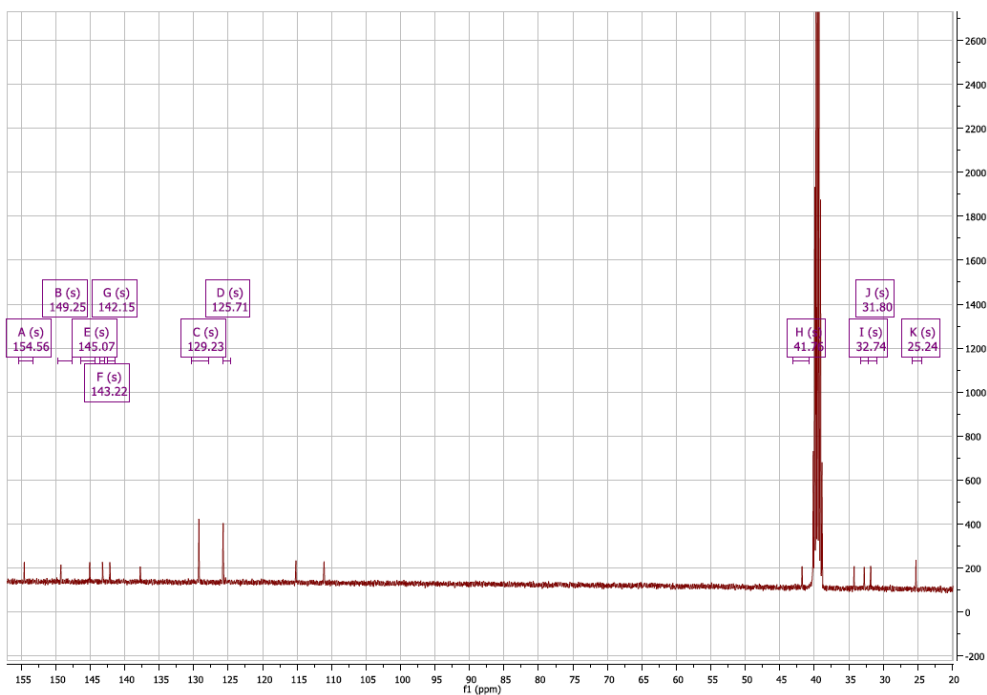
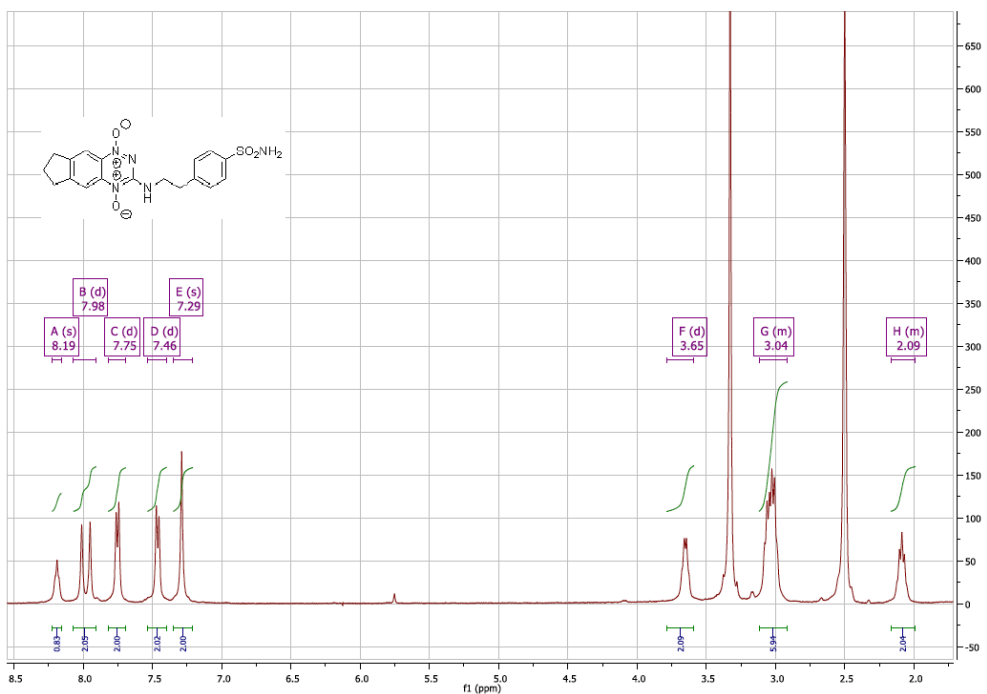
**NMR spectra 8:** 3-((4-sulfamoylphenethyl)amino)benzo[e][1,2,4]triazine 1,4-dioxide (**8**).

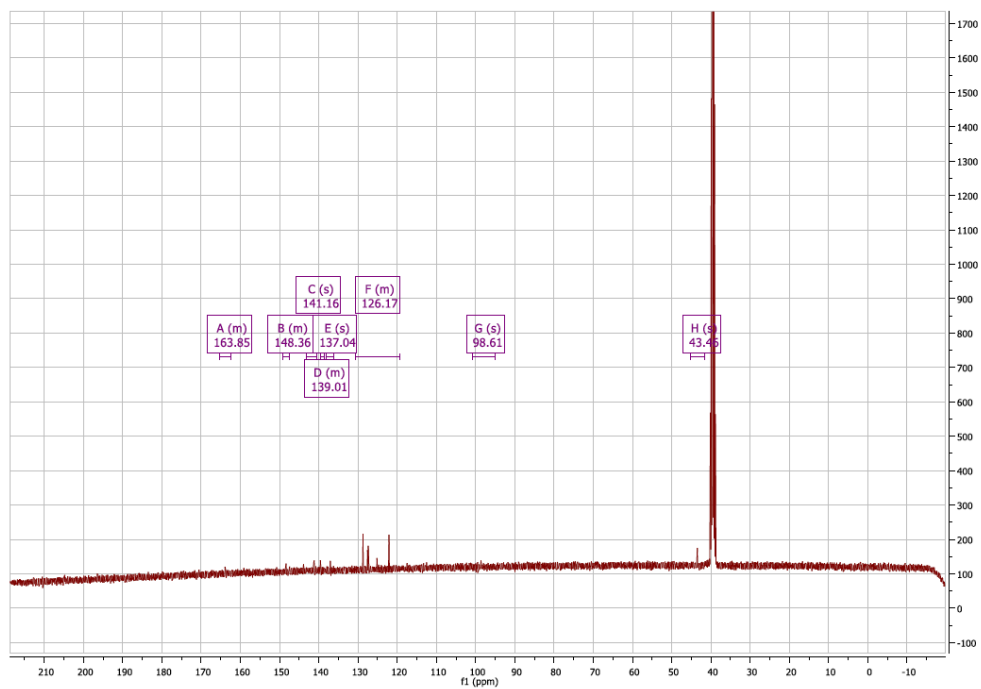
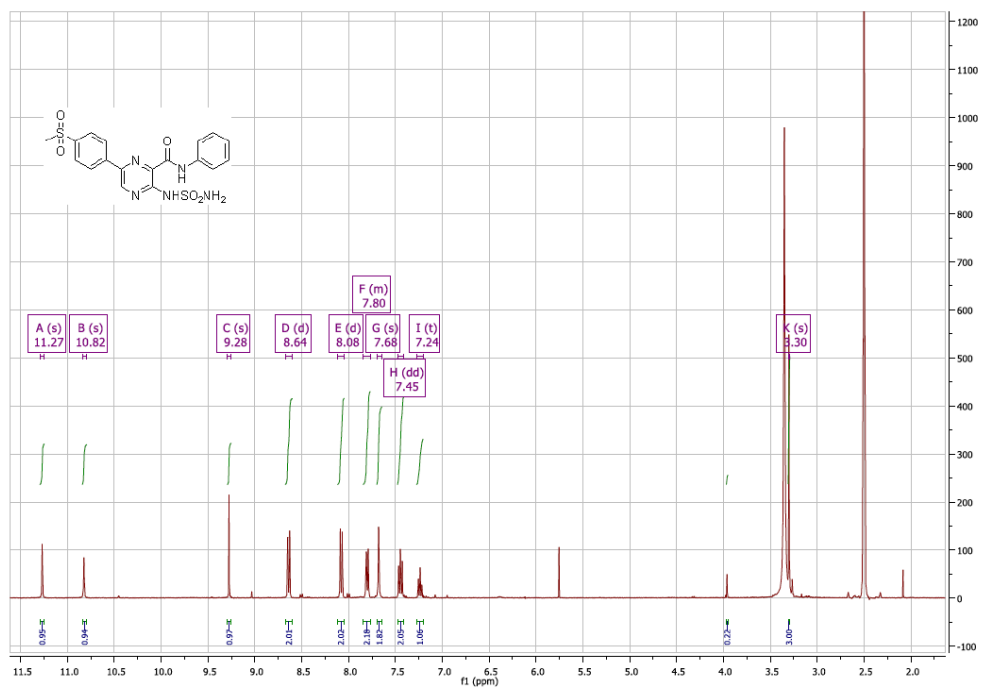


4

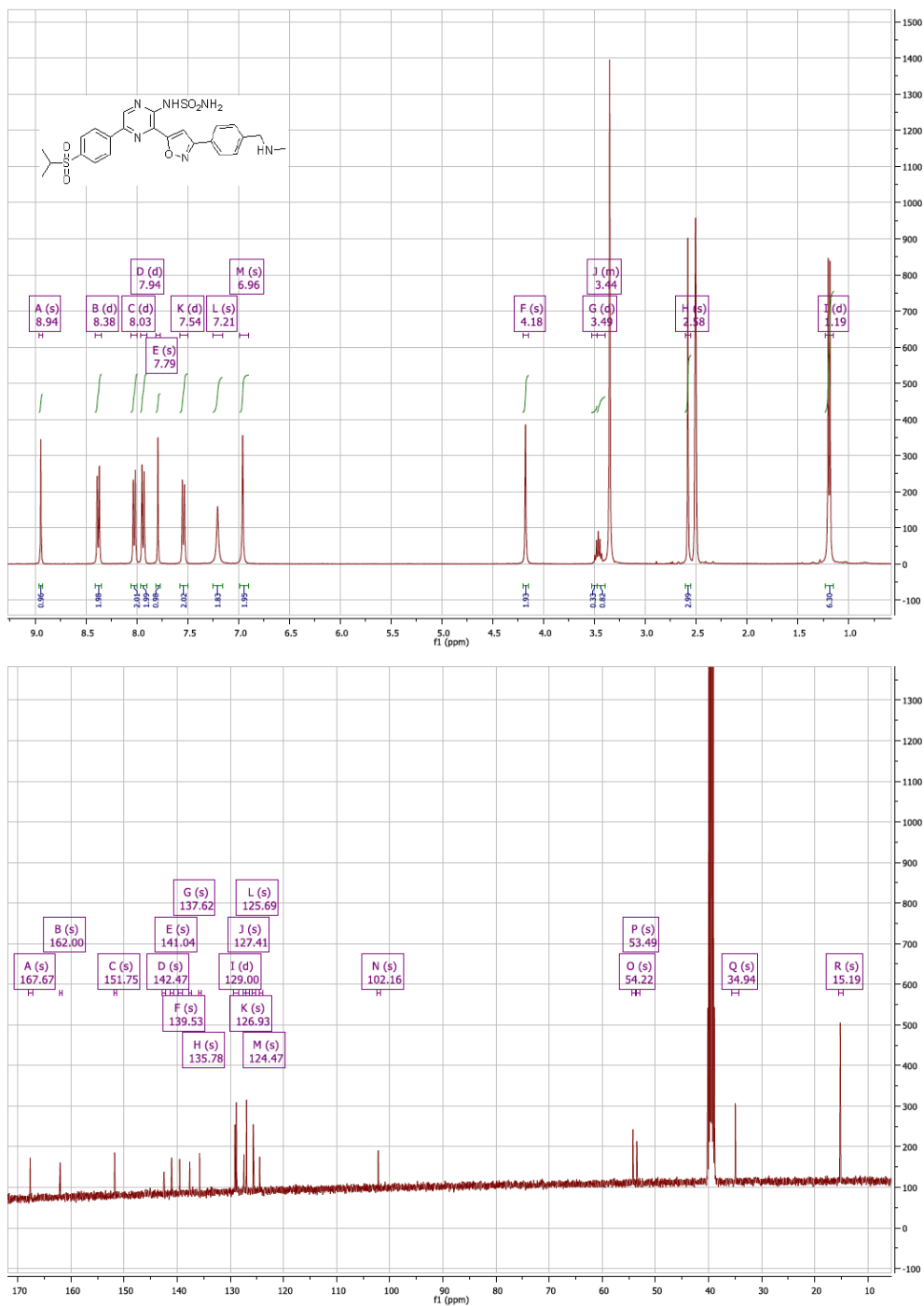
**NMR spectra 9: 3-(4-sulfamoylphenethylamino)-7,8-dihydro-6H-indeno [5,6-e][1,2,4] triazine 1-oxide (10).**


**NMR spectra 10: 3-((4-sulfamoylphenethyl) amino)-7,8-dihydro-6H-indeno [5,6-e][1,2,4] triazine 1,4-dioxide (11).**

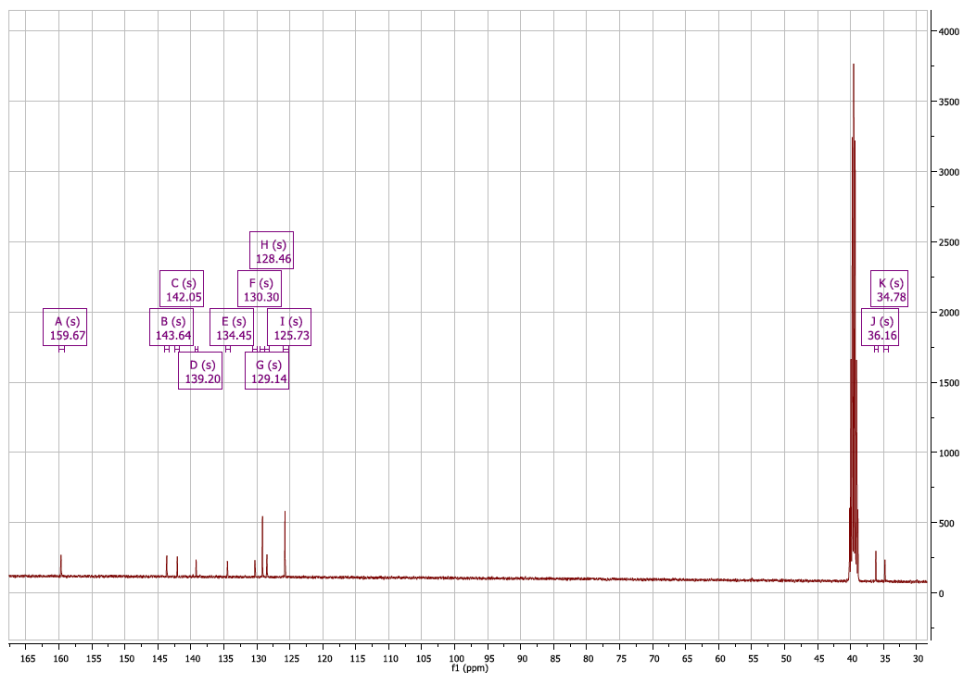
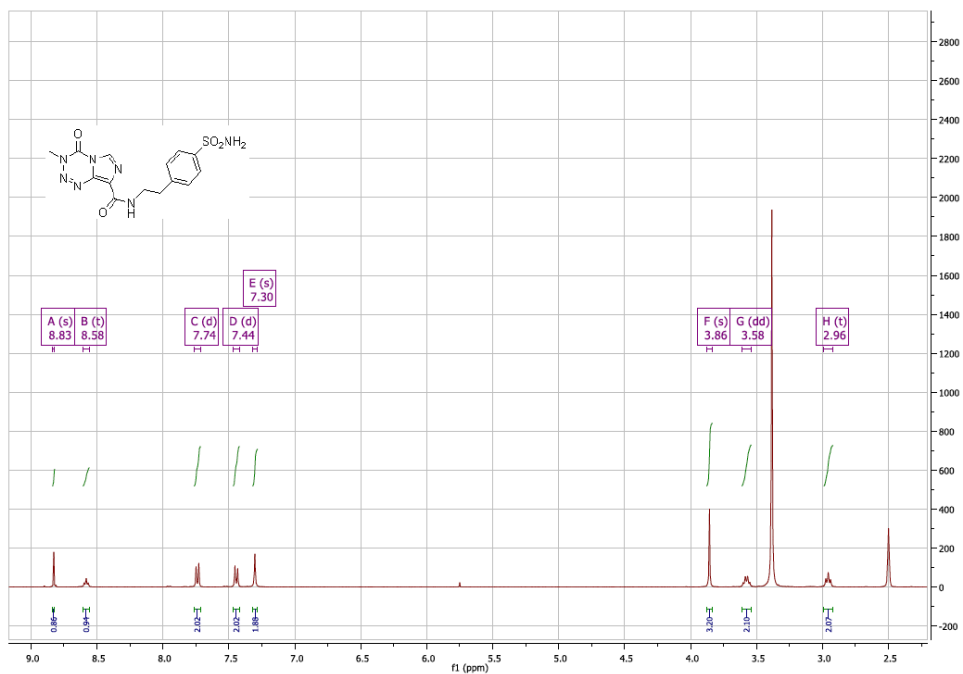


**NMR spectra 11: 6-(4-(methylsulfonyl)phenyl)-N-phenyl-3-(sulfamoylamino)pyrazine-2-carboxamide (12).**


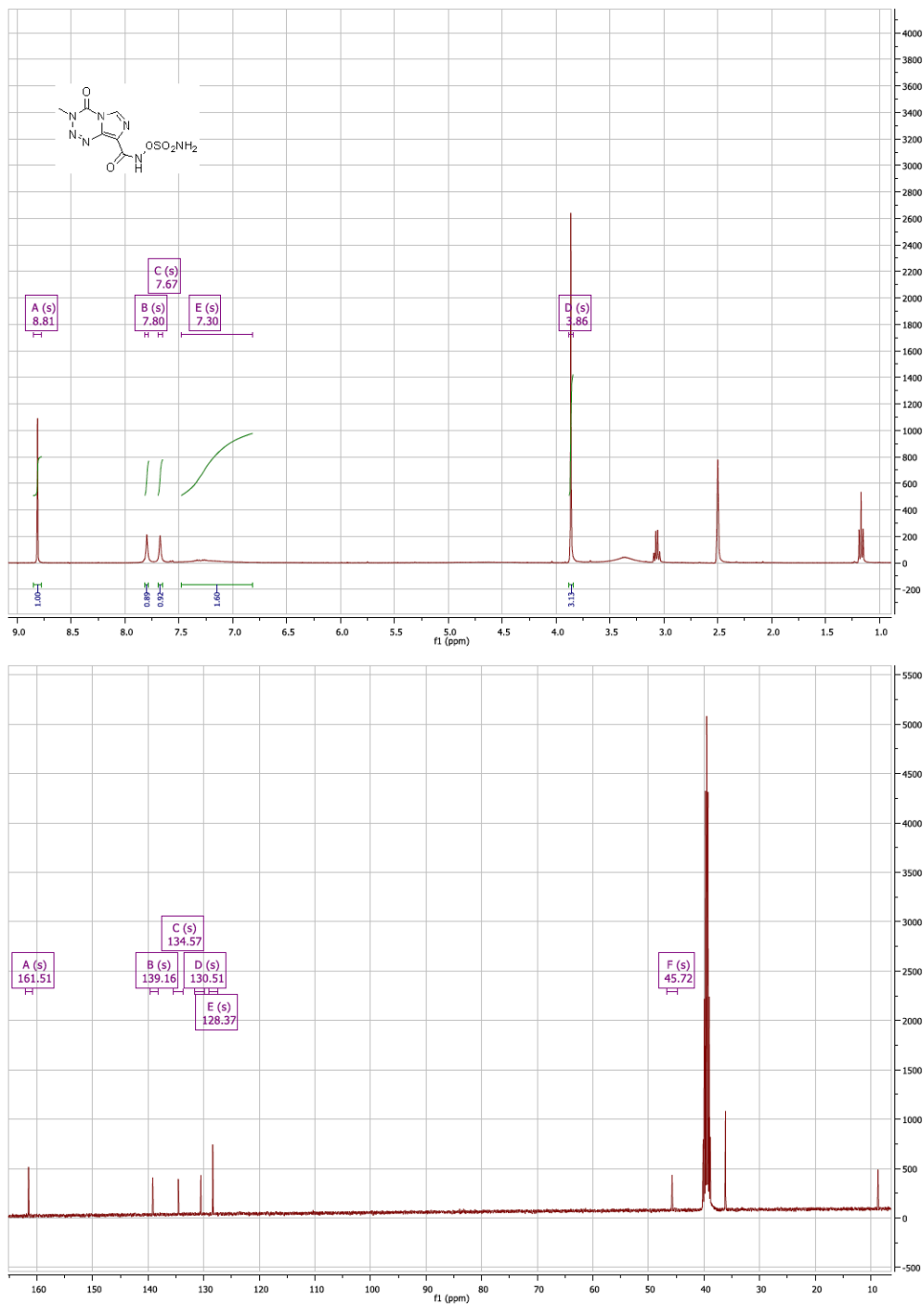
**NMR spectra 12:** 5-(4-(isopropylsulfonyl) phenyl)-3-(3-(4-((methylamino) methyl) phenyl) isoxazol-5-yl) pyrazin-2-carboxamide (**13**).



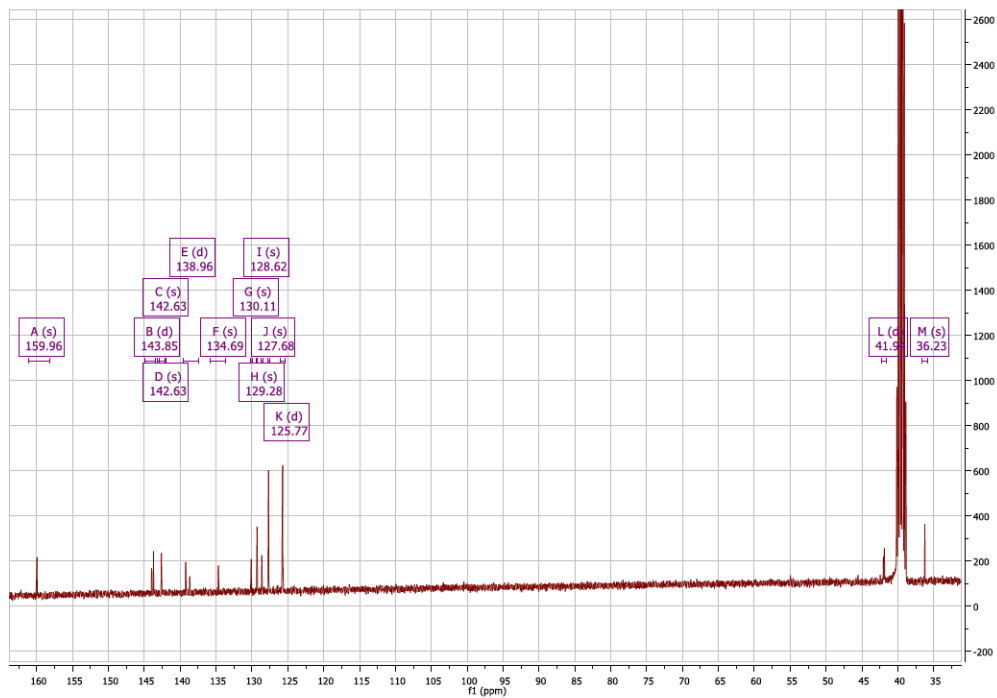
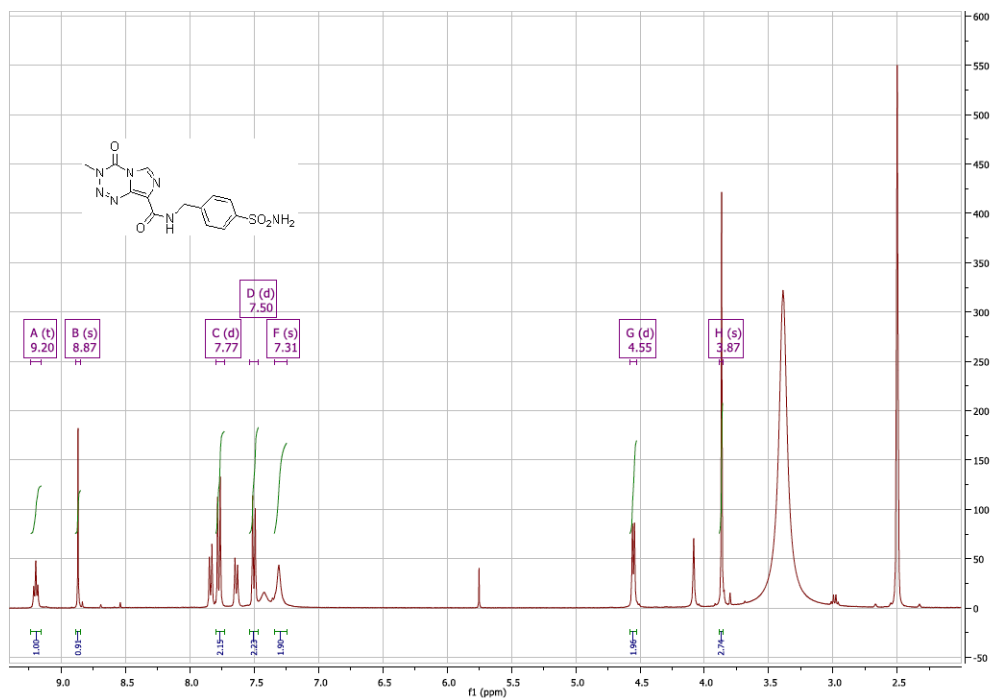
**NMR spectra 13:** 3-methyl-4-oxo-N-(4-sulfamoylphenethyl)-3,4-dihydroimidazo[5,1-d][1,2,3,5]tetrazine-8-carboxamide (**15a**).



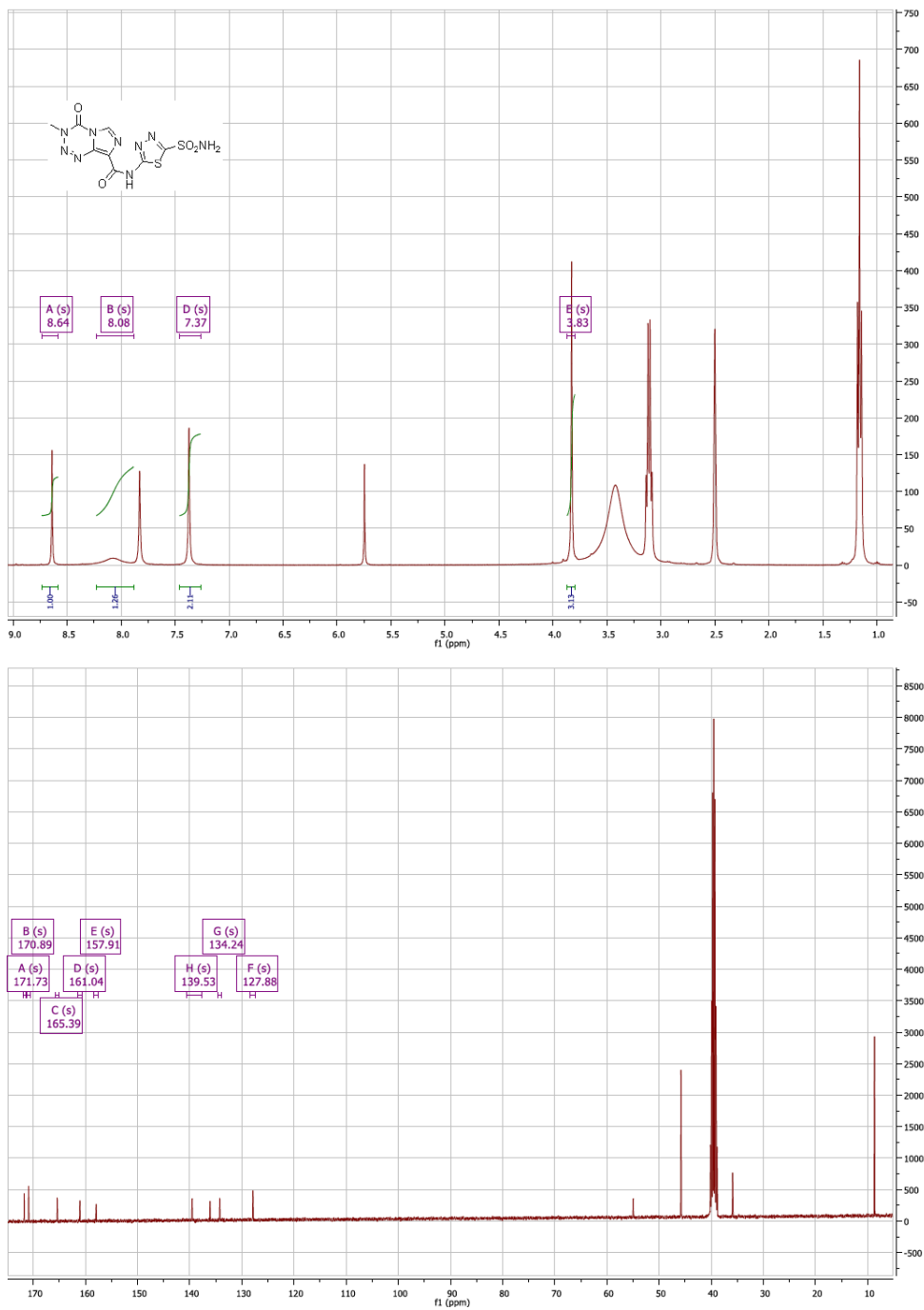
**NMR spectra 14:** 3-methyl-4-oxo-N-(sulfamoyloxy)-3,4-dihydroimidazo[5,1-d][1,2,3,5]tetrazine-8-carboxamide (15b).



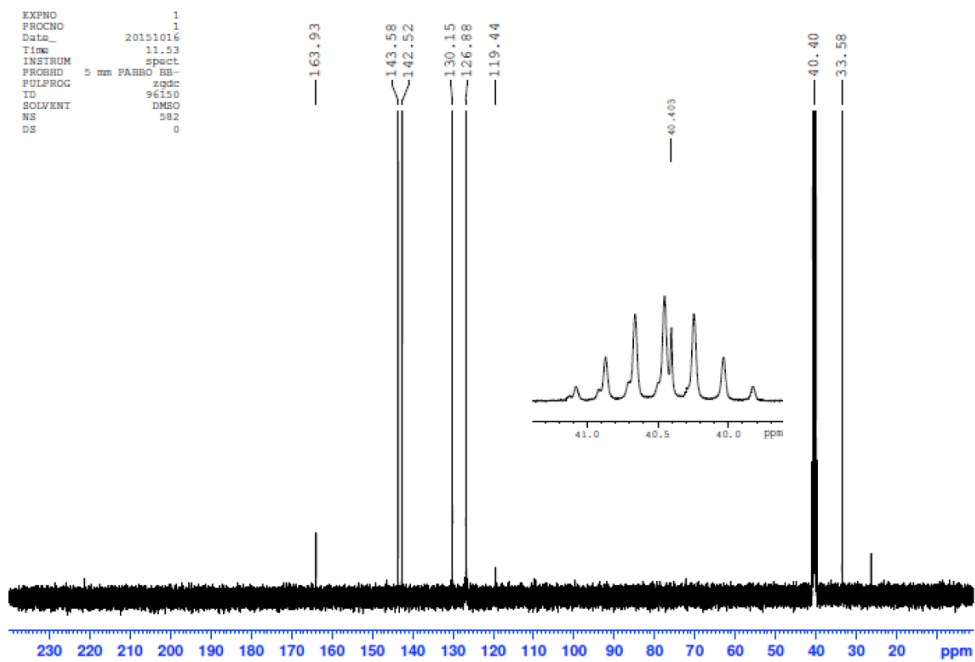
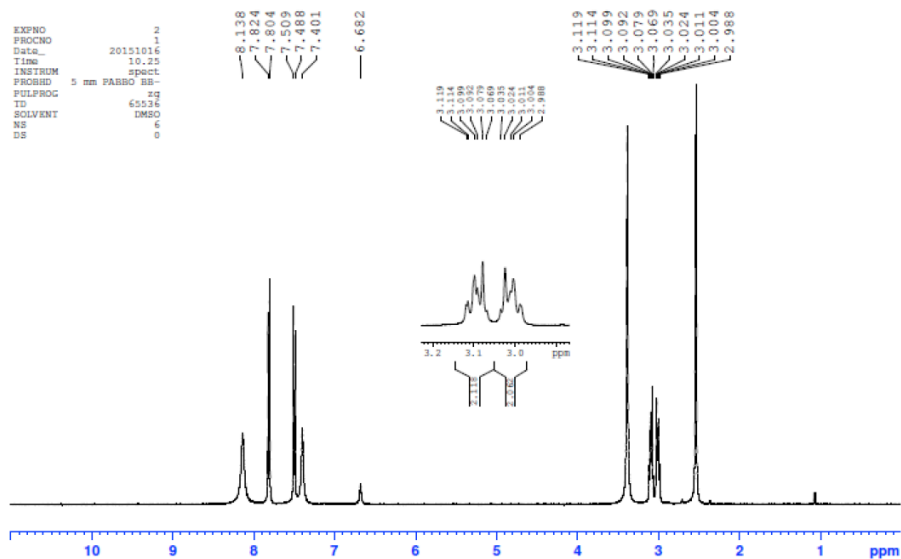
**NMR spectra 15:** 3-methyl-4-oxo-N-(4-sulfamoylbenzyl)-3,4-dihydroimidazo[5,1-d][1,2,3,5]tetrazine-8-carboxamide (**15c**).



**NMR spectra 16:** 3-methyl-4-oxo-N-(5-sulfamoyl-1,3,4-thiadiazol-2-yl)-3,4-dihydroimidazo[5,1-d][1,2,3,5]tetrazine-8-carboxamide (**15d**).



NMR spectra 17: 4-(2-(3-carbamimidoylguanidino)ethyl)benzenesulfonamide hydrochloride salt (**18**)



## Acknowledgements

Authors acknowledge the aid of Advinus Therapeutics Ltd. for synthesis of compounds 1, 2a, 2b, 2c, 3, 4, 5a, 5b and 5c. This work was supported by METOXIA (Metastatic Tumors Facilitated by Hypoxic Micro-Environment; EU 7th Research Framework Programme - Theme HEALTH; Grant no.: 222741) NGI Pre-Seed grant (n° 93612005), Kankeronderzoekfonds Limburg from the Health Foundation Limburg and the Dutch Cancer Society (KWF UM 2011-5020, KWF UM 2009-4454, KWF MAC 2013-6425, KWF MAC 2013-6089, KWF 2015-7635).

## References

1. Nordmark, M., et al., *Prognostic value of tumor oxygenation in 397 head and neck tumors after primary radiation therapy. An international multi-center study.* Radiotherapy and oncology : journal of the European Society for Therapeutic Radiology and Oncology, 2005. **77**(1): p. 18-24.
2. Hockel, M., et al., *Association between tumor hypoxia and malignant progression in advanced cancer of the uterine cervix.* Cancer research, 1996. **56**(19): p. 4509-15.
3. Wojtkowiak, J.W., et al., *Drug resistance and cellular adaptation to tumor acidic pH microenvironment.* Molecular pharmaceutics, 2011. **8**(6): p. 2032-8.
4. Good, J.S. and K.J. Harrington, *The hallmarks of cancer and the radiation oncologist: updating the 5Rs of radiobiology.* Clinical oncology, 2013. **25**(10): p. 569-77.
5. Dubois, L.J., et al., *New ways to image and target tumour hypoxia and its molecular responses.* Radiotherapy and oncology : journal of the European Society for Therapeutic Radiology and Oncology, 2015. **116**(3): p. 352-7.
6. Pettersen, E.O., et al., *Targeting tumour hypoxia to prevent cancer metastasis. From biology, biosensing and technology to drug development: the METOXIA consortium.* Journal of enzyme inhibition and medicinal chemistry, 2015. **30**(5): p. 689-721.
7. Ebbesen, P., et al., *Taking advantage of tumor cell adaptations to hypoxia for developing new tumor markers and treatment strategies.* Journal of enzyme inhibition and medicinal chemistry, 2009. **24 Suppl 1**: p. 1-39.
8. Neri, D. and C.T. Supuran, *Interfering with pH regulation in tumours as a therapeutic strategy.* Nature reviews. Drug discovery, 2011. **10**(10): p. 767-77.
9. Pastorek, J. and S. Pastorekova, *Hypoxia-induced carbonic anhydrase IX as a target for cancer therapy: from biology to clinical use.* Seminars in cancer biology, 2015. **31**: p. 52-64.
10. Pastorek, J., et al., *Cloning and characterization of MN, a human tumor-associated protein with a domain homologous to carbonic anhydrase and a putative helix-loop-helix DNA binding segment.* Oncogene, 1994. **9**(10): p. 2877-88.
11. Wykoff, C.C., et al., *Hypoxia-inducible expression of tumor-associated carbonic anhydrases.* Cancer research, 2000. **60**(24): p. 7075-83.
12. Kaluz, S., et al., *Lowered oxygen tension induces expression of the hypoxia marker MN/carbonic anhydrase IX in the absence of hypoxia-inducible factor 1 alpha stabilization: a role for phosphatidylinositol 3'-kinase.* Cancer research, 2002. **62**(15): p. 4469-77.
13. van den Beucken, T., et al., *Hypoxia-induced expression of carbonic anhydrase 9 is dependent on the unfolded protein response.* The Journal of biological chemistry, 2009. **284**(36): p. 24204-12.
14. Kopacek, J., et al., *MAPK pathway contributes to density- and hypoxia-induced expression of the tumor-associated carbonic anhydrase IX.* Biochimica et biophysica acta, 2005. **1729**(1): p. 41-9.
15. van Kuijk, S.J., et al., *Prognostic Significance of Carbonic Anhydrase IX Expression in Cancer Patients: A Meta-Analysis.* Frontiers in oncology, 2016. **6**: p. 69.

16. Peeters, S.G., et al., *[(18)F]VM4-037 MicroPET Imaging and Biodistribution of Two In Vivo CAIX-Expressing Tumor Models*. Molecular imaging and biology : MIB : the official publication of the Academy of Molecular Imaging, 2015. **17**(5): p. 615-9.
17. Akurathi, V., et al., *Development and biological evaluation of (9)(9)mTc-sulfonamide derivatives for in vivo visualization of CA IX as surrogate tumor hypoxia markers*. European journal of medicinal chemistry, 2014. **71**: p. 374-84.
18. Akurathi, V., et al., *Synthesis and biological evaluation of a 99mTc-labelled sulfonamide conjugate for in vivo visualization of carbonic anhydrase IX expression in tumor hypoxia*. Nuclear medicine and biology, 2010. **37**(5): p. 557-64.
19. Sneddon, D., et al., *Synthesis and in Vivo Biological Evaluation of 68Ga-Labeled Carbonic Anhydrase IX Targeting Small Molecules for Positron Emission Tomography*. Journal of medicinal chemistry, 2016.
20. Monti, S.M., C.T. Supuran, and G. De Simone, *Anticancer carbonic anhydrase inhibitors: a patent review (2008 - 2013)*. Expert opinion on therapeutic patents, 2013. **23**(6): p. 737-49.
21. Gieling, R.G., et al., *Antimetastatic effect of sulfamate carbonic anhydrase IX inhibitors in breast carcinoma xenografts*. Journal of medicinal chemistry, 2012. **55**(11): p. 5591-600.
22. Ward, C., et al., *Evaluation of carbonic anhydrase IX as a therapeutic target for inhibition of breast cancer invasion and metastasis using a series of in vitro breast cancer models*. Oncotarget, 2015. **6**(28): p. 24856-70.
23. Lock, F.E., et al., *Targeting carbonic anhydrase IX depletes breast cancer stem cells within the hypoxic niche*. Oncogene, 2013. **32**(44): p. 5210-9.
24. Dubois, L., et al., *Specific inhibition of carbonic anhydrase IX activity enhances the in vivo therapeutic effect of tumor irradiation*. Radiotherapy and oncology : journal of the European Society for Therapeutic Radiology and Oncology, 2011. **99**(3): p. 424-31.
25. Rami, M., et al., *Hypoxia-targeting carbonic anhydrase IX inhibitors by a new series of nitroimidazole-sulfonamides/sulfamides/sulfamates*. Journal of medicinal chemistry, 2013. **56**(21): p. 8512-20.
26. McDonald, P.C., et al., *Recent developments in targeting carbonic anhydrase IX for cancer therapeutics*. Oncotarget, 2012. **3**(1): p. 84-97.
27. Supuran, C.T., *Carbonic anhydrases: novel therapeutic applications for inhibitors and activators*. Nature reviews. Drug discovery, 2008. **7**(2): p. 168-81.
28. Dubois, L., et al., *Targeting carbonic anhydrase IX by nitroimidazole based sulfamides enhances the therapeutic effect of tumor irradiation: a new concept of dual targeting drugs*. Radiotherapy and oncology : journal of the European Society for Therapeutic Radiology and Oncology, 2013. **108**(3): p. 523-8.
29. Barman, S., et al., *Coumarin-benzothiazole-chlorambucil (Cou-Benz-Cbl) conjugate: an ESIPT based pH sensitive photoresponsive drug delivery system*. Journal of Materials Chemistry B, 2015. **3**(17): p. 3490-97.
30. Bekele, T., et al., *Catalytic, enantioselective [4 + 2]-cycloadditions of ketene enolates and o-quinones: efficient entry to chiral, alpha-oxygenated carboxylic acid derivatives*. Journal of the American Chemical Society, 2006. **128**(6): p. 1810-1.
31. Gill, M. and A.F. Smrdel, *Pigments of fungi, part 16. Synthesis of methyl (R)-(+)-tetrahydro-2-methyl-5-oxo-2-fura-*

- acetate and its (S)-(-)-antipode, chiroptical references for determination of the absolute stereochemistry of fungal pre-anthraquinones.* Tetrahedron Asymmetry, 1990. **1**(7): p. 453-64.
32. Deshmukh, A.R. and V. Gumaste, *Process for preparing alkyl/aryl chloroformates*, 2005, Google Patents.
  33. Hay, M.P., et al., *Tricyclic [1,2,4]triazine 1,4-dioxides as hypoxia selective cytotoxins.* Journal of medicinal chemistry, 2008. **51**(21): p. 6853-65.
  34. Arrowsmith, J., et al., *Antitumor imidazotetrazines. 41. Conjugation of the antitumor agents mitozolomide and temozolomide to peptides and lexitropsins bearing DNA major and minor groove-binding structural motifs.* Journal of medicinal chemistry, 2002. **45**(25): p. 5458-70.
  35. Ombouma, J., et al., *Carbonic Anhydrase Glycoinhibitors belonging to the Aminoxyulfonamide Series.* ACS medicinal chemistry letters, 2015. **6**(7): p. 819-21.
  36. Kelarev, V.I., et al., *Synthesis of N-substituted 6-alkyl-2,4-diamino-1,3,5-triazines containing long alkyl radicals.* Zhurnal Organicheskoi Khimii, 1988. **24**: p. 1100-1105.
  37. Svastova, E., et al., *Carbonic anhydrase IX reduces E-cadherin-mediated adhesion of MDCK cells via interaction with beta-catenin.* Experimental cell research, 2003. **290**(2): p. 332-45.
  38. Goede, V., et al., *Past, present and future role of chlorambucil in the treatment of chronic lymphocytic leukemia.* Leukemia & lymphoma, 2015. **56**(6): p. 1585-92.
  39. Horsman, M.R. and P. Vaupel, *Pathophysiological Basis for the Formation of the Tumor Microenvironment.* Frontiers in oncology, 2016. **6**: p. 66.
  40. Reddy, S.B. and S.K. Williamson, *Tirapazamine: a novel agent targeting hypoxic tumor cells.* Expert opinion on investigational drugs, 2009. **18**(1): p. 77-87.
  41. Omuro, A. and L.M. DeAngelis, *Glioblastoma and other malignant gliomas: a clinical review.* JAMA, 2013. **310**(17): p. 1842-50.
  42. Fukushima, T., H. Takeshima, and H. Kataoka, *Anti-glioma therapy with temozolomide and status of the DNA-repair gene MGMT.* Anticancer research, 2009. **29**(11): p. 4845-54.
  43. Dubois, L., et al., *Imaging the hypoxia surrogate marker CA IX requires expression and catalytic activity for binding fluorescent sulfonamide inhibitors.* Radiotherapy and oncology : journal of the European Society for Therapeutic Radiology and Oncology, 2007. **83**(3): p. 367-73.
  44. Ditte, P., et al., *Phosphorylation of carbonic anhydrase IX controls its ability to mediate extracellular acidification in hypoxic tumors.* Cancer research, 2011. **71**(24): p. 7558-67.
  45. Dubois, L., et al., *Imaging of CA IX with fluorescent labelled sulfonamides distinguishes hypoxic and (re)-oxygenated cells in a xenograft tumour model.* Radiotherapy and oncology : journal of the European Society for Therapeutic Radiology and Oncology, 2009. **92**(3): p. 423-8.
  46. Fokas, E., et al., *Targeting ATR in vivo using the novel inhibitor VE-822 results in selective sensitization of pancreatic tumors to radiation.* Cell death & disease, 2012. **3**: p. e441.
  47. Josse, R., et al., *ATR inhibitors VE-821 and VX-970 sensitize cancer cells to topoisomerase I inhibitors by disabling DNA*

- replication initiation and fork elongation responses*. Cancer research, 2014. **74**(23): p. 6968-79.
48. Hall, A.B., et al., *Potentialiation of tumor responses to DNA damaging therapy by the selective ATR inhibitor VX-970*. Oncotarget, 2014. **5**(14): p. 5674-85.
  49. Gray, L.H., et al., *The concentration of oxygen dissolved in tissues at the time of irradiation as a factor in radiotherapy*. The British journal of radiology, 1953. **26**(312): p. 638-48.
  50. Wright, E.A. and P. Howard-Flanders, *The influence of oxygen on the radiosensitivity of mammalian tissues*. Acta radiologica, 1957. **48**(1): p. 26-32.
  51. Doyen, J., et al., *Knock-down of hypoxia-induced carbonic anhydrases IX and XII radiosensitizes tumor cells by increasing intracellular acidosis*. Frontiers in oncology, 2012. **2**: p. 199.
  52. Kulshrestha, A., et al., *Selective inhibition of tumor cell associated Vacuolar-ATPase 'a2' isoform overcomes cisplatin resistance in ovarian cancer cells*. Molecular oncology, 2016.
  53. De Milito, A. and S. Fais, *Tumor acidity, chemoresistance and proton pump inhibitors*. Future oncology, 2005. **1**(6): p. 779-86.
  54. Liao, C., et al., *Genomic screening in vivo reveals the role played by vacuolar H+ ATPase and cytosolic acidification in sensitivity to DNA-damaging agents such as cisplatin*. Molecular pharmacology, 2007. **71**(2): p. 416-25.
  55. van Gisbergen, M.W., et al., *How do changes in the mtDNA and mitochondrial dysfunction influence cancer and cancer therapy? Challenges, opportunities and models*. Mutation research. Reviews in mutation research, 2015. **764**: p. 16-30.
  56. Pollak, M., *Potential applications for biguanides in oncology*. The Journal of clinical investigation, 2013. **123**(9): p. 3693-700.
  57. Pernicova, I. and M. Korbonits, *Metformin--mode of action and clinical implications for diabetes and cancer*. Nature reviews. Endocrinology, 2014. **10**(3): p. 143-56.
  58. Liu, Z., et al., *Phenformin Induces Cell Cycle Change, Apoptosis, and Mesenchymal-Epithelial Transition and Regulates the AMPK/mTOR/p70s6k and MAPK/ERK Pathways in Breast Cancer Cells*. PloS one, 2015. **10**(6): p. e0131207.
  59. Shackelford, D.B., et al., *LKB1 inactivation dictates therapeutic response of non-small cell lung cancer to the metabolism drug phenformin*. Cancer cell, 2013. **23**(2): p. 143-58.
  60. Krall, N., et al., *A small-molecule drug conjugate for the treatment of carbonic anhydrase IX expressing tumors*. Angewandte Chemie, 2014. **53**(16): p. 4231-5.
  61. Khalifah, R.G., *The carbon dioxide hydration activity of carbonic anhydrase. I. Stop-flow kinetic studies on the native human isoenzymes B and C*. The Journal of biological chemistry, 1971. **246**(8): p. 2561-73.
  62. McIntyre, A., et al., *Carbonic anhydrase IX promotes tumor growth and necrosis in vivo and inhibition enhances anti-VEGF therapy*. Clinical cancer research : an official journal of the American Association for Cancer Research, 2012. **18**(11): p. 3100-11.



# CHAPTER 5

Novel fluorinated carbonic anhydrase IX inhibitors reduce hypoxia-induced acidification and clonogenic survival of cancer cells

Justina Kazokaitė, **Raymon Niemans**, Virginija Dudutienė, Holger M. Becker, t Leitāns, Asta Zubrienė, Lina Baranauskienė, Gabor Gondi, Reinhard Zeidler, Jurgita Matulienė, Kaspars Tārs, Ala Yaromina, Philippe Lambin, Ludwig J. Dubois, Daumantas Matulis

*Accepted and to be published by Oncotarget.*

## Abstract

Human carbonic anhydrase (CA) IX has emerged as a promising anticancer target and a diagnostic biomarker for solid hypoxic tumors. Novel fluorinated CA IX inhibitors exhibited up to 50 picomolar affinity towards the recombinant human CA IX, selectivity over other CAs, and direct binding to Zn(II) in the active site of CA IX inducing novel conformational changes as determined by X-ray crystallography. Mass spectrometric gas-analysis confirmed the CA IX-based mechanism of the inhibitors in a CRISPR/Cas9-mediated CA IX knockout in HeLa cells. Hypoxia-induced extracellular acidification was significantly reduced in HeLa, H460, MDA-MB-231, and A549 cells exposed to the compounds, with the  $IC_{50}$  values up to 1.29 nM. A decreased clonogenic survival was observed when hypoxic H460 3D spheroids were incubated with our lead compound. These novel compounds are therefore promising agents for CA IX-specific therapy.

## Introduction

Tumor hypoxia promotes invasiveness and is associated with resistance to chemotherapeutics and radiation and thus poor prognosis [1-5]. Human carbonic anhydrase IX (CA IX) shows limited expression in normal tissues [6] and is significantly up-regulated by hypoxia-inducible factor 1 $\alpha$  (HIF-1 $\alpha$ ) [7] or other alternative microenvironmental factors [8-12] in a variety of tumors. CA IX is crucial for cancer cell survival because bicarbonate and protons, produced upon CA IX-catalyzed reversible hydration of CO<sub>2</sub>, are necessary to maintain the cellular pH balance: bicarbonate is transported into the cell to neutralize intracellular acid, while protons increase extracellular acidification [13-16]. CA IX also stimulates cell spreading and epithelial-mesenchymal transition [17, 18]. Therefore, CA IX has been proposed to be a promising tumor hypoxia biomarker for diagnostic and targeted drug delivery applications [19].

Sulfonamides are classical CA inhibitors, where the deprotonated sulfonamide group is required for displacement of the catalytic Zn<sup>2+</sup>-bound water molecule to bind directly with Zn<sup>2+</sup> in the active site to inhibit CA [20, 21]. Therefore, the binding affinity can be enhanced using inhibitors with the lowered pK<sub>a</sub> of the sulfonamide group [21, 22]. Introduction of fluorine atoms that lower the pK<sub>a</sub> due to their electron-withdrawing capabilities is one of the choices due to unique features, such as high electronegativity, small size, low atomic weight, and contribution to increased lipophilicity. Fluorine is found in ~20% of current pharmaceuticals and this trend is increasing [23]. Krishnamurthy and colleagues investigated fluorinated benzenesulfonamides and concluded that fluorine is the best choice for electron-withdrawing substituents [21]. We expanded this strategy and created new routes for functionalization of pentafluorobenzenesulfonamides [24, 25] including *para*-, *ortho*-, and *meta*-substituted fluorinated benzenesulfonamides. The bulky hydrophobic groups at *ortho* or *meta* positions are necessary for the favorable hydrophobic contacts with the amino acids of CA IX binding pocket [26]. Here we present novel the *ortho*-substituted fluorinated benzenesulfonamides VR16-09 and VR16-10 (Table 1, Scheme 1) in combination with the previously chemically and biophysically characterized *meta* and *ortho*-substituted fluorinated inhibitors VD11-4-2 and VD12-09 [26]. We hypothesized that these benzenesulfonamides will exhibit high affinity and strong selectivity towards recombinant CA IX and will possess significant functional effects in cancer cell lines on reducing hypoxia-induced acidosis as well as hypoxia-dependent clonogenic survival, providing efficacious opportunity to target CA IX-expressing cells.

## Results and discussion

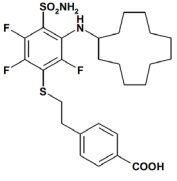
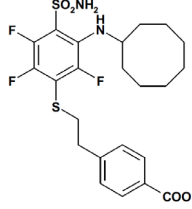
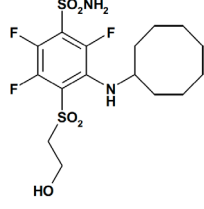
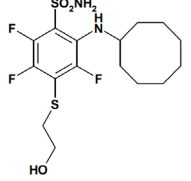
### Binding and inhibition of recombinant CA isoforms

The affinities of VR16-09 and VR16-10 to 12 catalytically active recombinant CA isoforms were determined by the fluorescent thermal-shift assay (FTSA) and compared with previously published [26] inhibitors VD11-4-2 and VD12-09 (Table 1). The  $K_i$  values against CA IX and CA XII were also measured by the stopped-flow inhibition assay (SFA) of the  $\text{CO}_2$  hydration CA enzymatic activity (Table 1). FTSA revealed that VR16-09 bound CA IX significantly ( $K_d = 0.16$  nM) stronger than other CA isoforms ( $K_d > 200$   $\mu\text{M}$ ) (Table 1, Figure 1A-C). VR16-09 with the bulky aminocyclododecyl group exhibited greater selectivity towards CA IX as compared with VR16-10, VD12-09, and VD11-4-2 bearing aminocyclooctyl groups. SFA did not allow the determination of  $K_i < \sim 2$  nM against CA IX, because the concentration of CA IX was 10 nM, thus limiting the determination of  $IC_{50}$  at 5 nM. Therefore, the  $K_d$ s determined by the FTSA should be used rather than SFA. Nevertheless, SFA confirmed that VR16-09 and VR16-10 efficiently inhibited the CA IX activity (Figure 1D-F). These compounds are advantageous compared to SLC-0111 that has entered the clinical trials ( $K_{i(\text{CA IX})} = 45$  nM,  $K_{i(\text{CA XII})} = 4.5$  nM and only 20-fold selectivity over CA II, thus would possibly exhibit larger adverse effects [27, 28]). In contrast, selectivity of VR16-09 for CA IX over CA I and CA II is more than one million-fold.

**Table 1:** The dissociation constants ( $K_d$ s) of VR16-09, VR16-10, VD11-4-2, and VD12-09 for 12 recombinant catalytic domains of human active CA isoforms as determined by FTSA at pH 7.0 (37 °C). The  $K_i$  values determined by SFA (pH 7.5, 25 °C) are shown in the parentheses. Uncertainties of FTSA and SFA measurements do not exceed 2-fold.

CA isoform	$K_d$ ( $K_i$ ), nM			
	VR16-09	VR16-10	VD11-4-2*	VD12-09*
CA I	$^3200\ 000$	5000	710	50 000
CA II	$^3200\ 000$	1000	60	1 300
CA III	$^3200\ 000$	$^3200\ 000$	40 000	$^3200\ 000$
CA IV	$^3200\ 000$	1820	25	1 700
CA VA	$^3200\ 000$	5000	2 500	3 300
CA VB	45000	100	5.6	210
CA VI	$^3200\ 000$	26300	95	4 300

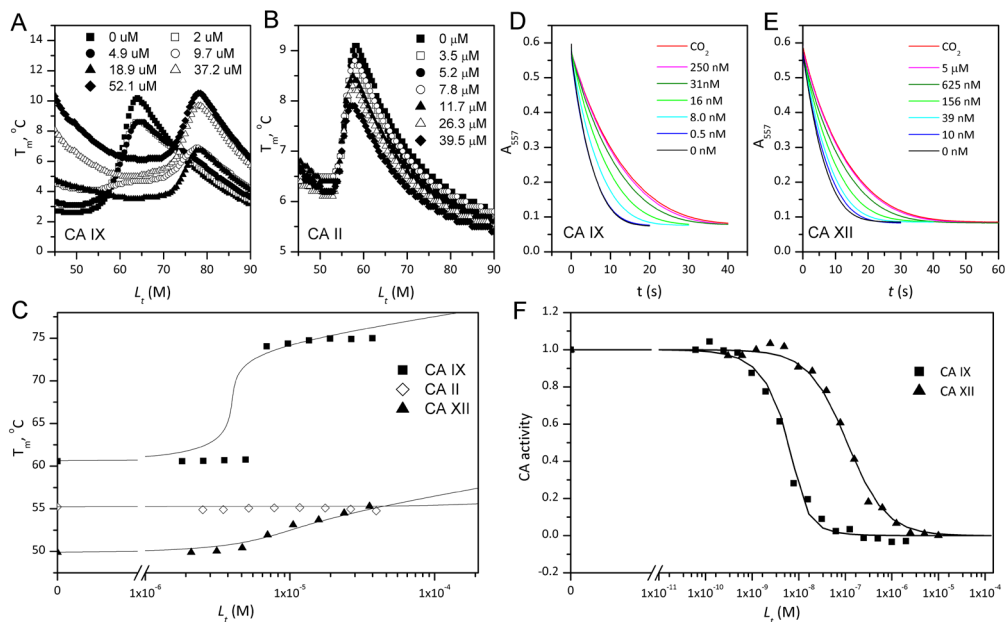
**Table 1 continued:** The dissociation constants ( $K_d$ 's) of VR16-09, VR16-10, VD11-4-2, and VD12-09 for 12 recombinant catalytic domains of human active CA isoforms as determined by FTSA at pH 7.0 (37 °C). The  $K_i$  values determined by SFA (pH 7.5, 25 °C) are shown in the parentheses. Uncertainties of FTSA and SFA measurements do not exceed 2-fold.

CA isoform	$K_d$ ( $K_i$ ), nM			
	VR16-09	VR16-10	VD11-4-2*	VD12-09*
				
CA VII	37 000	100	9.8	330
CA IX	<b>0.16</b> (<1)	<b>0.20</b> (<1)	<b>0.05</b>	<b>1.1</b>
CA XII	710 (100)	370	3.3	330
CA XIII	20	40	3.6	140
CA XIV	170	170	1.6	170

\* $K_d$  values of VD11-4-2 and VD12-09 towards CA isoforms have been already published [26].

### Crystal structures of inhibitors bound to recombinant CA IX

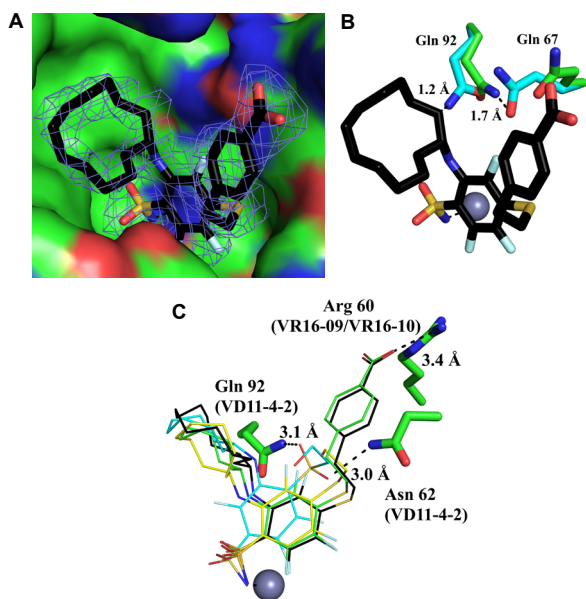
The structures of the CA IX catalytic domain in complex with VR16-09 (PDB ID: 6G98), VR16-10 (PDB ID: 6G9U), VD12-09 (PDB ID: 6FE0) and VD11-4-2 (PDB ID: 6FE1) were determined by X-ray crystallography at resolutions ranging from 1.75 Å to 2.47 Å (Figure 2, Table S1). The sulfonamide moiety and trifluorobenzene cycle of all observed ligands fit in the conserved region of the CA IX active site, the cycloalkane tail moieties were guided towards the hydrophobic part of the active site and moieties with terminal hydroxyl group were located in the hydrophilic part of the active site. The sulfonamide amino group formed a coordination bond with Zn(II), as observed in many other CA-sulfonamide complexes. All ligands were positioned very similarly within the active site of CA IX, except with some differences occurring in the case of VD11-4-2 (Figure 2). VD11-4-2 also formed two additional hydrogen bonds with Asn62 and Gln92, which might explain its stronger affinity for CA IX as compared to other analyzed compounds. All four crystal structures showed that some conformational changes have occurred in the CA IX active site pocket as compared to other known CA IX structures [29, 30]. In order to fully understand conformational changes occurring in those cases, we determined also apo (ligand free) CA IX structure at 1.87 Å resolution (PDB ID: 6FE2). In case of VR16-09, the cyclododecyl moiety altered rotamer of Gln92, which in turn changed the conformation of Gln67 (Figure 2).



**Figure 1:** The binding affinity by FTSA (panels A-C) and inhibition by SFA (panels D-F) of VR16-09 towards human recombinant CAs. Thermal melting curves of 8  $\mu\text{M}$  CA IX (A) and 5  $\mu\text{M}$  CA II (B) determined by ANS fluorescence in the presence of various VR16-09 concentrations. C – Melting temperatures ( $T_m$ ) of CA IX (■), CA II (◇) and CA XII (▲) as a function of added compound concentration. The lines were regressed according to [60]. Absorbance decrease due to enzymatic acidification of the medium by CA IX (D) or CA XII (E) for various VR16-09 concentrations. F – Fraction inhibition of CA IX (■) or CA XII (▲) as a function of the total VR16-09 concentration. The lines are fit according to the Morrison equation [50].

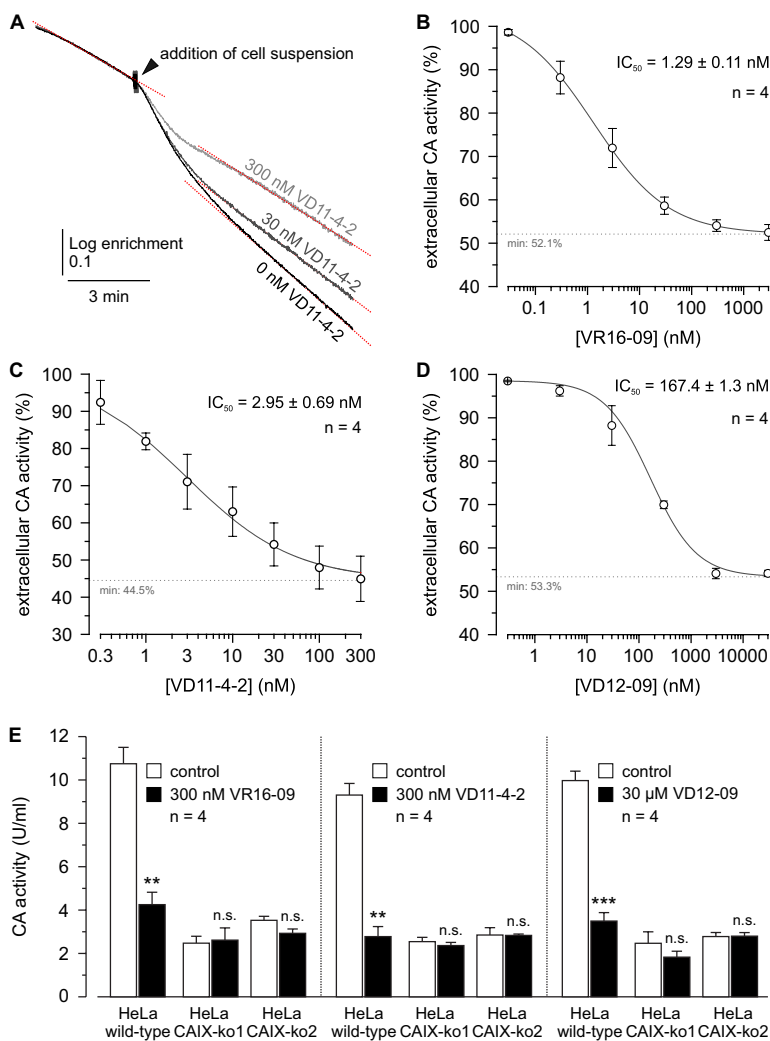
### CA IX-dependent functional activities of inhibitors in cancer cells

Compounds were evaluated for their biological functional activities in a panel of human cancer cell lines. CA IX expression was increased in hypoxic (0.2%  $\text{O}_2$ ) A549 (lung), AsPC-1 (pancreatic), MDA-MB-231 (breast), H460 (lung), and HeLa (cervical) cancer cells, whereas CA XII expression was similar under normoxia and hypoxia (Figures S1, S2). We evaluated the potency of the compounds to inhibit the CA catalytic activity in hypoxic MDA-MB-231 cells by determining the rate of the  $\text{CO}_2/\text{HCO}_3^-$  hydration/dehydration reaction via  $^{18}\text{O}$  depletion from  $^{13}\text{C}^{18}\text{O}_2$ , measured by mass-spectrometric (MS) gas analysis. Addition of cell suspension resulted in an acceleration of the reaction, indicating CA catalytic activity in MDA-MB-231 cells (Figure 3A). Pre-incubation of the cell suspension with VR16-09, VD11-4-2, or VD12-09 resulted in a dose-dependent decrease in CA activity (Figure 3B-D). To verify the CA IX specificity, hypoxic HeLa cells, in which CA IX was knocked out (KO) (Figure S3),



**Figure 2:** Crystal structure of VR16-09 (panel A, PDB ID: 6G98) bound in the active site of human recombinant CA IX. The  $F_o - F_c$  omit map is contoured at  $3\sigma$ . Panel B shows that VR16-09 fitted in apo-CA IX structure (PDB ID: 6FE2), demonstrating collision points with residues indicating too short inter-atomic distances if conformational changes had not occurred. Protein and ligand carbons are shown in green and black, respectively, and apo-CA IX residues are shown in light blue. Atom colors are: oxygen (red), nitrogen (blue), fluorine (light blue), and sulfur (yellow). Panel C shows comparison of binding modes for compounds VR16-09 (black carbons), VR16-10 (green carbons), VD12-09 (yellow carbons), and VD11-4-2 (light blue carbons). The zinc ion is shown as a gray sphere and residues participating in hydrogen bonds or charged interactions are also specified for the respective inhibitors. The figure was prepared using Pymol [61].

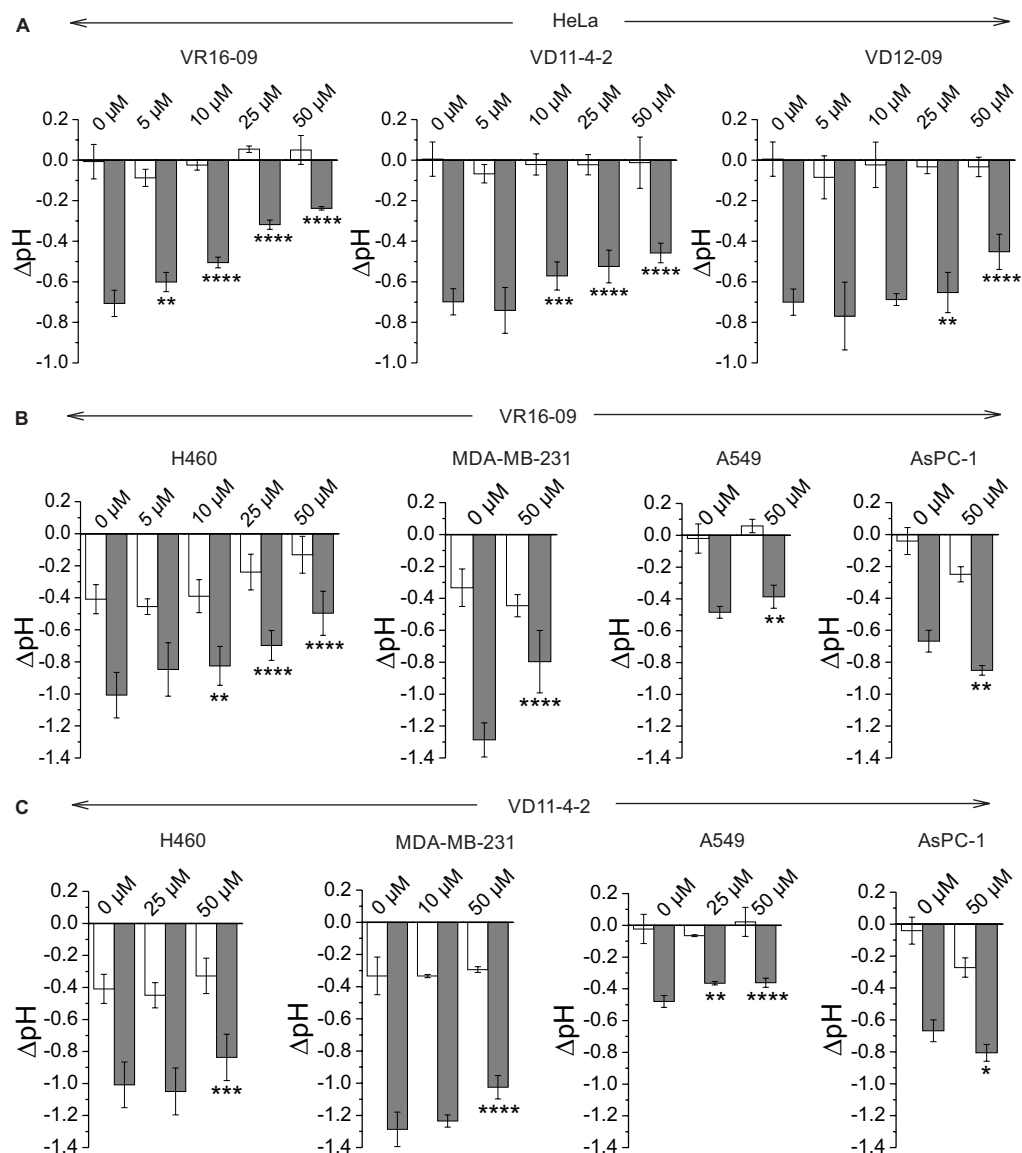
were exposed to VR16-09, VD11-4-2 and VD12-09 at concentrations of near maximum inhibition of extracellular CA activity in hypoxic MDA-MB-231 cells. In both HeLa CA IX KO lines, VR16-09 (300 nM), VD11-4-2 (300 nM), or VD12-09 (30  $\mu$ M) did not alter CA activity (Figure 3E), although considerable CA activity remained, indicating activity of other CA isoforms. In HeLa wild-type (WT) cells, CA activity decreased ( $P < 0.01$ ) to 30-40%, values that did not significantly differ from the two HeLa CA IX KO cell lines. Thus, VR16-09, VD11-4-2, and VD12-09 specifically target CA IX, while other CAs remain unaffected. Previously Frost and colleagues reported a  $K_i$  value of 85.3 nM against extracellular CA for the fluorescent sulfonamide Cpd 5c in intact hypoxic MDA-MB-231 cells using the same  $^{18}O$  exchange assay [31]. Extracellular CA activity of MDA-MB-231 cells was also significantly reduced by 1  $\mu$ M acetazolamide [32]. The inhibitors VR16-09 and VD11-4-2 exhibited higher effect towards CA IX expressed in cellular models than previously reported compounds likely due to higher affinity.



**Figure 3:**  $\text{IC}_{50}$  determination of VR16-09, VD11-4-2, and VD12-09 in hypoxic MDA-MB-231 cells and CA IX-dependent mode of action for inhibitors in hypoxic HeLa CA IX KO cells. A – Original recordings of the log enrichment of MDA-MB-231 cells pre-incubated with VD11-4-2 for up to 3 h. The beginning of each trace shows the rate of degradation of the  $^{18}\text{O}$ -labeled substrate in the non-catalyzed reaction. B-D – Relative CA activity in MDA-MB-231 cells, incubated under hypoxia (1%  $\text{O}_2$ ) for 3 days. Cells were pre-incubated with VR16-09 (B), VD11-4-2 (C), or VD12-09 (D) for up to 3 h. CA activity was determined by MS gas-analysis from the increase in the rate of log enrichment after addition of cell suspension. CA activity in the presence of inhibitor was normalized to the activity in the absence of inhibitor. E – CA activity in HeLa-WT and HeLa-CA IX-KO cells, before (white bars) and after addition of VR16-09, VD11-4-2 or VD12-09 (black bars). Average + SD of 4 independent experiments per cell line are shown. Asterisks indicate significant difference between CA activity before and after addition of inhibitor (\*\*p < 0.01, \*\*\*p < 0.001, n.s.: not significant).

The functional activity of inhibitors was further confirmed by measuring the rise in extracellular pH directly inside a hypoxic chamber [33]. VR16-09, VD11-4-2, and VD12-09 significantly ( $p < 0.05$ ) reduced hypoxia-induced acidification of HeLa cells in a dose-dependent manner, while the effect on cells exposed to normoxia was negligible (Figure 4A). This functional activity was the most pronounced for VR16-09 at 50  $\mu\text{M}$ , which significantly reduced hypoxia-induced acidosis of 4 investigated cell lines (Figure 4A, 4B). VD11-4-2 also significantly reduced ( $p < 0.05$ ) hypoxic acidification of HeLa, H460, MDA-MB-231, and A549 cells (Figure 4A, 4C). A 4-fold lower concentration of sodium bicarbonate in the medium was used for A549 to determine the functional effects of the compounds due to relatively low levels of hypoxia-induced CA IX (Figure S1). VD12-09 exhibited functional activity in HeLa cells (Figure 4A). The smallest, albeit significant ( $p < 0.05$ ), impact on extracellular acidification was found for VR16-10 (Figure S4). Interestingly, inhibitors VR16-09 and VR16-10 differ structurally by the size of the hydrophobic ring at *ortho* position. Thus, a 12-carbon ring of VR16-09 was found to be more favorable than an 8-carbon ring of VR16-10 because  $\sim 3$ -fold higher functional effects of VR16-09 on the reduction of hypoxia-induced acidification of H460 cells were observed, even though their affinities towards recombinant CA IX were similar ( $K_d$ s of 0.16 and 0.20 nM, respectively). Functional activities of several CA IX-targeting agents, such as fluorescent sulfonamide [33] and nitroimidazole-based inhibitors [34, 35] have been previously reported using the same method in HeLa cells, where a dose-dependent reduction in hypoxia-induced extracellular acidification was observed. Results of the current study indicate that the inhibitors investigated here are more efficacious in decreasing extracellular acidification than previously described compounds because of their significant functionality at lower concentrations (5-50  $\mu\text{M}$ ), highlighting the potential for CA IX-targeting therapy.

Interestingly, hypoxia-induced acidosis of AsPC-1 cells increased after exposure to VR16-09 or VD11-4-2 (Figure 4B, 4C), related to the unique expression of monocarboxylate transporter 1 (MCT1) under both normoxic and hypoxic conditions in these cells (Figure S5A). Recently, CA IX was proposed to be a 'H<sup>+</sup>-distributing antenna' for MCT1 to facilitate rapid extrusion of lactate and H<sup>+</sup> from the cell [36]. Even though the catalytic activity of CA IX was inhibited in AsPC-1 by compounds, the rise of acidification might be caused by MCT1 which is further non-catalytically stimulated by CA IX. In contrast, MCT4 was expressed in all tested cell lines and was up-regulated in response to hypoxia (Figure S5B), in line with previously confirmed HIF-1 $\alpha$ -dependent mechanism of MCT4 expression in cancer cells [37].



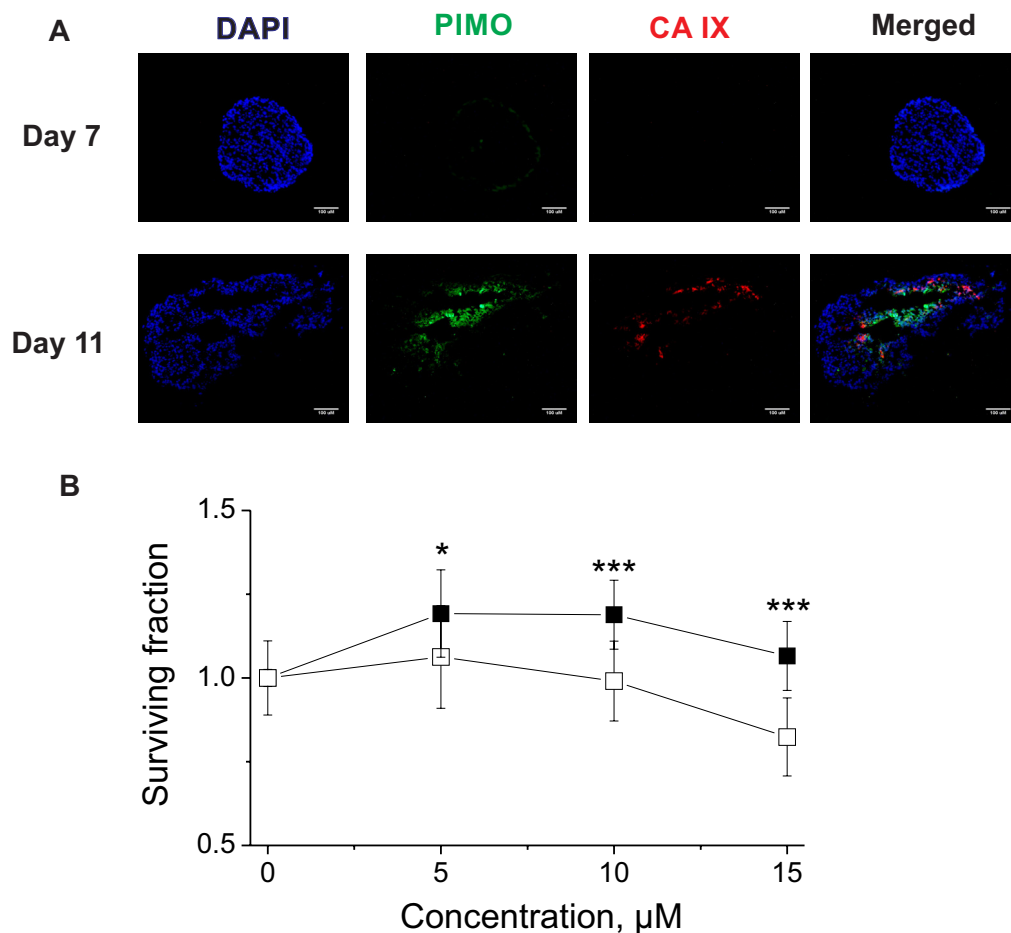
**Figure 4:** A – Changes in extracellular acidification of HeLa cells after the treatment with VR16-09, VD11-4-2 or VD12-09 for 72 h under normoxia (21% O<sub>2</sub>; white bars) or hypoxia (0.2% O<sub>2</sub>; grey bars). B-C – Effect of VR16-09 (B) and VD11-4-2 (C) on the hypoxia-induced extracellular acidification of H460, MDA-MB-231, A549, and AsPC-1 after the exposure for 72 h. Average  $\pm$  SD of at least 3 independent experiments is shown. Asterisks indicate significant difference between medium pH of cells exposed to DMSO and cells treated with various doses of inhibitor under hypoxic conditions (\* $p$ <0.05; \*\* $p$ <0.01, \*\*\* $p$ <0.001, \*\*\*\* $p$ <0.0001).

### **Inhibitor-induced cytotoxicity**

Cytotoxicity of tested compounds was higher in normoxic than hypoxic cell monolayers, as determined by cell viability assay using alamarBlue® after treatment for 48 h or 72 h (Figure S6A, S6B, Table S2). Inhibitors were less effective in reducing viability of hypoxic CA IX-expressing cells than normoxic cells without or with significantly lower CA IX expression. Sensitivity of HeLa and H460 cells to VR16-10 was the lowest and is in line with the lowest VR16-10 functional activity measured by extracellular pH assay. Therefore, VR16-10 was not investigated further. Similarly, compounds were more effective in reducing clonogenic survival in normoxic compared to hypoxic monolayer HeLa cells (Figure S6C). Our results correlate with previously published cytotoxicity profiles of benzenesulfonamides, including SLC-0111 [38], sulfamate S4 [39], and dual-target compounds bearing various CA IX-targeting moieties combined with different anti-cancer drugs [40], which showed more effective cell kill in normoxia than hypoxia. We hypothesize that higher cytotoxicity of inhibitors in normoxic cells as compared with hypoxic cells could be due to the affinity of investigated compounds towards CA XII, expressed in all cell lines investigated here and shown to be up-regulated to compensate the CA IX knockdown [41]. Thus, new cellular models with both CA IX and CA XII KO would be crucial to determine the link between functional activity of compounds and CA IX or CA XII-dependent cellular mechanisms.

### **Hypoxia-dependent effect on spheroid clonogenic survival**

To confirm the CA IX-dependent efficacy of the compounds, H460 spheroids were employed. Immunofluorescence analysis confirmed overlap between CA IX expression and pimonidazole (PIMO)-positive hypoxia in sections of H460 spheroids grown for 11 days, whereas neither CA IX nor hypoxia were found in spheroids grown for 7 days (Figure 5A). Therefore, non-hypoxic (4 days) and hypoxic (11 days) H460 spheroids were exposed to VR16-09 using an effective dose based on extracellular pH assays (Figure 4A, 4B) for 24 h and afterwards plated for clonogenic survival. In contrast to 2D cell viability and clonogenic survival assays, a hypoxia-dependent effect on clonogenic survival of VR16-09 was found in H460 spheroids (Figure 5B). The 3D cell models reflect important properties of *in vivo* tumors such as interactions between cells, oxygen gradients, penetration of drugs, response and resistance, and production/deposition of extracellular matrix, which are absent in rapidly and uncontrollably growing 2D cells [42-44]. Our study confirms the importance of using *in vitro* 3D cellular models for screening of CA IX-targeting inhibitors.



**Figure 5:** A – Immunofluorescence images of H460 spheroids stained for DAPI (blue), PIMO (green) and CA IX (red). The scale bar indicates 100 μM. B – Survival of clonogenic cells derived from non-hypoxic (■) and hypoxic (□) H460 spheroids exposed to VR16-09 for 24 h on day 4 or day 11, respectively. Asterisks indicate statistically significant differences between the surviving fractions of clonogenic cells derived from normoxic or hypoxic spheroids after exposure to the same dose (\* $p < 0.05$ , \*\*\* $p < 0.001$ ).

## Conclusions

In conclusion, the integrative set of synthesis, inhibitory activities, biophysical binding profiles, crystallographic analysis, and effects in 2D and 3D cancer cell culture models is described in the present study. X-ray analysis demonstrated novel, previously unseen conformational changes in CA IX active site due to ligand binding. Our compounds exhibited high affinity and selectivity towards recom-

binant CA IX, reached nanomolar CA IX-dependent functional effects as well reduced hypoxia-induced acidification in a variety of cancer cell lines. Interestingly, hypoxia-dependent reduction of clonogenic survival was only observed in spheroids, highlighting the importance of investigating CA IX-targeting compounds in 3D cell models resembling the naturally occurring hypoxic microenvironment with clonogenic survival as endpoint. The newly designed compounds are therefore promising agents for CA IX-specific therapy.

## Materials and Methods

### Chemistry

**VR16-09** and **VR16-10** were synthesized following a similar route as described in our previous research [24]. Pentafluorobenzenesulfonyl chloride (**1**, Acros Organics) was converted to pentafluorobenzenesulfonamide (**2**) via amination with aqueous ammonia (scheme 1) by our improved method [25]. On the basis of our previous investigations, sulfonamide **2** undergoes aromatic nucleophilic substitution reactions with sulfur-centered nucleophiles readily and forms exclusively the *para*-substituted products. High reactivity of polyfluorinated compounds leads to the formation of monosubstituted or even further substituted compounds. The subsequent *ortho*-substitution occurs in the case of 4-substituted-2,3,5,6-tetrafluorobenzenesulfonamides, bearing non-oxidized sulfur-centered substitutes at *para* position. Similarly, sulfonamide **2** was treated with 4-(2-mercaptoethyl) benzoic acid (**7**) to furnish *para*-substituted compound **3** and subsequent aromatic nucleophilic substitution reactions with cyclododecylamine and cyclooctylamine in DMSO in the presence of Et<sub>3</sub>N yielded desirable compounds **VR16-09** and **VR16-10**. Since suitable sulfur-centered nucleophile **7** was not commercially available, it was synthesized using literature methods. Starting from commercially available (2-bromoethyl)benzene (**4**, Acros Organics), Friedel-Crafts acylation with acetyl chloride proceeded in high yield. Acylation was accomplished as described in literature [45], except for changing highly toxic solvent carbon disulfide to more acceptable dichloromethane. Conversion of methyl ketone **5** into benzoic acid **6** was carried out via haloform reaction by the method of Foreman and McElvain [46]. Finally, benzoic acid **6** was treated with thiourea in refluxing water to generate intermediate salt, which was partitioned by adding sodium hydroxide solution as described by Takano [47].

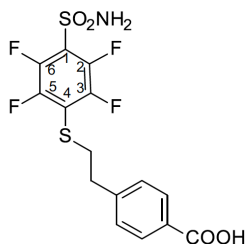
### Compound characterization

All starting materials and reagents were commercial products. They were used without further purification. Melting points of the compounds were determined in open capillaries on a Thermo Scientif-



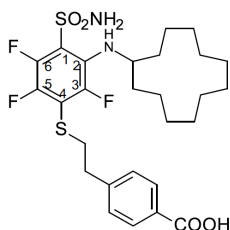
**Pentafluorobenzenesulfonamide (2)**

The solution of pentafluorobenzenesulfonyl chloride (**1**) (1.00 g, 3.75 mmol) and THF (60 mL) was cooled to  $\sim -10^{\circ}\text{C}$  and aqueous ammonia ( $\sim 1.20$  mL, 25 %) was added dropwise while stirring until the solution was at pH  $\sim 7$ . After stirring for an additional 1 h, the solvent was removed under reduced pressure and the white solid was washed with cold  $\text{H}_2\text{O}$ . Recrystallization was accomplished from  $\text{H}_2\text{O}$ . Yield: 0.84 g (90 %), mp  $156\text{--}157^{\circ}\text{C}$  close to the value in the literature, mp  $156^{\circ}\text{C}$  [48].  $^1\text{H}$  NMR (400 MHz,  $\text{DMSO-}d_6$ ): 8.48 (2H, s,  $\text{SO}_2\text{NH}_2$ ).  $^{19}\text{F}$  NMR (376 MHz,  $\text{DMSO-}d_6$ ):  $-139.5$  (2F, dd,  $^1J = 19$  Hz,  $^2J = 6$  Hz),  $-149.39$  (1F, t,  $J = 22$  Hz),  $-161.03$  (2F, t,  $J = 20$  Hz).

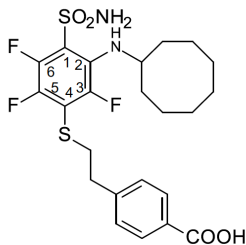
**4-(2-([4-(Aminosulfonyl)-2,3,5,6-tetrafluorophenyl]thio)ethyl)benzoic acid (3)**

The mixture of pentafluorobenzenesulfonamide (**2**) (2.00 g, 8.09 mmol), 4-(2-mercaptoethyl)benzoic acid (**7**) (1.77 g, 9.71 mmol),  $\text{Et}_3\text{N}$  (2.50 mL, 17.9 mmol), and MeOH (20 mL) was stirred at ambient temperature for 24 h. The solution was acidified to pH = 5 with conc. HCl and MeOH was removed under reduced pressure. The white solid was washed with water and dried. Recrystallization was accomplished from EtOH. Yield: 2.42 g (73 %), mp  $235\text{--}236^{\circ}\text{C}$ .  $^1\text{H}$  NMR ( $\text{DMSO-}d_6$ , 400 MHz)  $\delta$  12.87 (1H, br s, COOH), 8.40 (2H, s,  $\text{SO}_2\text{NH}_2$ ), 7.85 (2H, d,  $J = 8.1$  Hz, ArH), 7.36 (2H, d,  $J = 8.1$  Hz, ArH), 3.36 (2H, t,  $J = 7.3$  Hz,  $\text{SCH}_2\text{CH}_2$ ), 2.95 (2H, t,  $J = 7.3$  Hz,  $\text{SCH}_2\text{CH}_2$ ).  $^{13}\text{C}$  NMR ( $\text{DMSO-}d_6$ , 100 MHz)  $\delta$  167.57 (CO), 146.85 (C3, C5, dd,  $^1J$  ( $^{19}\text{F-}^{13}\text{C}$ ) = 244.2 Hz,  $^2J$  ( $^{19}\text{F-}^{13}\text{C}$ ) = 17.1 Hz), 142.99 (C2, C6, dd,  $^1J$  ( $^{19}\text{F-}^{13}\text{C}$ ) = 254.0 Hz,  $^2J$  ( $^{19}\text{F-}^{13}\text{C}$ ) = 17.1 Hz), 144.79 (Ar), 129.78 (Ar), 129.53 (Ar), 129.28 (Ar), 122.92 (C4, t,  $J$  ( $^{19}\text{F-}^{13}\text{C}$ ) = 15.3 Hz), 118.64 (C1, t,  $J$  ( $^{19}\text{F-}^{13}\text{C}$ ) = 20.4 Hz), 35.91 ( $\text{SCH}_2\text{CH}_2$ ), 34.79 ( $\text{SCH}_2\text{CH}_2$ ).  $^{19}\text{F}$  NMR ( $\text{DMSO-}d_6$ , 376 MHz)  $\delta$ :  $-133.0$  (2F, dd,  $^1J = 24.3$  Hz,  $^2J = 9.9$  Hz),  $-139.1$  (2F, dd,  $^1J = 24.2$  Hz,  $^2J = 9.9$  Hz). HRMS for  $\text{C}_{15}\text{H}_{11}\text{F}_4\text{NO}_4\text{S}_2$  [(M-H) $^-$ ]: calcd. 407.9993, found 407.9986.

**4-(2-([4-(Aminosulfonyl)-3-(cyclododecylamino)-2,5,6-tetrafluorophenyl]thio)ethyl)benzoic acid (VR16-09)**



The mixture of 4-(2-([4-(aminosulfonyl)-2,3,5,6-tetrafluorophenyl]thio)ethyl)benzoic acid (**3**) (0.40 g, 0.98 mmol), cyclododecylamine (0.286 g, 1.56 mmol), Et<sub>3</sub>N (0.34 mL, 2.44 mmol), and DMSO (6 mL) was stirred at 70°C for 36 h. The solution was cooled to room temperature, diluted with water (20 mL) and acidified to pH = 5 with 2M HCl. The white solid was filtered, washed with water and dried. Recrystallization was accomplished from EtOH:H<sub>2</sub>O (2:1). Yield: 0.36 g (64 %), mp 169-170°C. <sup>1</sup>H NMR (DMSO-*d*<sub>6</sub>, 400 MHz) δ 12.86 (1H, br s, COOH), 8.13 (2H, s, SO<sub>2</sub>NH<sub>2</sub>), 7.85 (2H, d, *J* = 8.1 Hz, ArH), 7.33 (2H, d, *J* = 8.1 Hz, ArH), 6.19 (1H, d, *J* = 9.2 Hz, NH), 3.69 (1H, br s (unresolved m), CH of cyclododecane), 3.28 (2H, t, *J* = 7.3 Hz, SCH<sub>2</sub>CH<sub>2</sub>), 2.91 (2H, t, *J* = 7.3 Hz, SCH<sub>2</sub>CH<sub>2</sub>), 1.8-1.1 (22H, m, cyclododecane). <sup>13</sup>C NMR (DMSO-*d*<sub>6</sub>, 100 MHz) δ 167.63 (CO), 148.18 (C3, d, *J* (<sup>19</sup>F-<sup>13</sup>C) = 244 Hz), 144.84 (C6, ddd, <sup>1</sup>*J* (<sup>19</sup>F-<sup>13</sup>C) = 249.6 Hz, <sup>2</sup>*J* (<sup>19</sup>F-<sup>13</sup>C) = 15.6 Hz), <sup>3</sup>*J* (<sup>19</sup>F-<sup>13</sup>C) = 3.6 Hz), 144.86 (Ar), 141.62 (C5, ddd, <sup>1</sup>*J* (<sup>19</sup>F-<sup>13</sup>C) = 236.5 Hz, <sup>2</sup>*J* (<sup>19</sup>F-<sup>13</sup>C) = 15.3 Hz, <sup>3</sup>*J* (<sup>19</sup>F-<sup>13</sup>C) = 4.6 Hz), 132.81 (C2, d, *J* (<sup>19</sup>F-<sup>13</sup>C) = 15.1 Hz), 129.78 (Ar), 129.57 (Ar), 129.14 (Ar), 119.53 (C1, dd, <sup>1</sup>*J* (<sup>19</sup>F-<sup>13</sup>C) = 11.9 Hz, <sup>2</sup>*J* (<sup>19</sup>F-<sup>13</sup>C) = 4.5 Hz), 117.52 (C4, dd, <sup>1</sup>*J* (<sup>19</sup>F-<sup>13</sup>C) = 23.8 Hz, <sup>2</sup>*J* (<sup>19</sup>F-<sup>13</sup>C) = 19.1 Hz), 52.68 (CH of cyclododecane, d, *J* = 10.6 Hz), 35.85 (SCH<sub>2</sub>CH<sub>2</sub>), 34.73 (SCH<sub>2</sub>CH<sub>2</sub>), 30.95 (cyclododecane), 24.10 (cyclododecane), 23.75 (cyclododecane), 23.40 (cyclododecane), 23.23 (cyclododecane), 21.28 (cyclododecane). <sup>19</sup>F (DMSO-*d*<sub>6</sub>, 376 MHz) δ -120.6 (C3-F, d, *J* = 11.3 Hz), -137.0 (C5-F, dd, <sup>1</sup>*J* = 27 Hz, <sup>2</sup>*J* = 11.5 Hz), -145.1 (C6-F, dd, <sup>1</sup>*J* = 27 Hz, <sup>2</sup>*J* = 2.5 Hz). HRMS for C<sub>27</sub>H<sub>35</sub>F<sub>3</sub>N<sub>2</sub>O<sub>4</sub>S<sub>2</sub> [(M-H)<sup>-</sup>]: calcd. 571.1918, found 571.1924.

**4-(2-([4-(Aminosulfonyl)-3-(cyclooctylamino)-2,5,6-tetrafluorophenyl]thio)ethyl)benzoic**

The mixture of 4-(2-([4-(aminosulfonyl)-2,3,5,6-tetrafluorophenyl]thio)ethyl)benzoic acid (**3**) (0.40 g, 0.98 mmol), cyclooctylamine (0.214 mL, 1.56 mmol), Et<sub>3</sub>N (0.34 mL, 2.44 mmol), and DMSO (6 mL) was stirred at 70°C for 24 h. The solution was cooled to room temperature, diluted with water (20 mL) and acidified to pH = 5 with 2M HCl. The white solid was filtered, washed with water and dried. Recrystallization was accomplished from EtOH:H<sub>2</sub>O (2:1). Yield: 0.32 g (64 %), mp 166-168°C. <sup>1</sup>H NMR (DMSO-*d*<sub>6</sub>, 400 MHz) δ 12.87 (1H, br s, COOH), 8.11 (2H, s, SO<sub>2</sub>NH<sub>2</sub>), 7.85 (2H, d, *J* = 8.1 Hz, ArH), 7.33 (2H, d, *J* = 8.1 Hz, ArH), 6.33 (1H, d, *J* = 8.7 Hz, NH), 3.71 (1H, br s (unresolved m), CH of cyclooctane), 3.30 (2H, t, *J* = 7.3 Hz, SCH<sub>2</sub>CH<sub>2</sub>), 2.91 (2H, t, *J* = 7.3 Hz, SCH<sub>2</sub>CH<sub>2</sub>), 1.9-1.4 (14H, m, cyclooctane). <sup>13</sup>C NMR (DMSO-*d*<sub>6</sub>, 100 MHz) δ 167.64 (CO), 148.16 (C3, d, *J* (<sup>19</sup>F-<sup>13</sup>C) = 242.7 Hz), 144.84 (C6, ddd, *J* (<sup>19</sup>F-<sup>13</sup>C) = 249.7 Hz, <sup>2</sup>*J* (<sup>19</sup>F-<sup>13</sup>C) = 15.7 Hz, <sup>3</sup>*J* (<sup>19</sup>F-<sup>13</sup>C) = 3.8 Hz), 144.9 (Ar), 141.62 (C5, ddd, *J* (<sup>19</sup>F-<sup>13</sup>C) = 236.0 Hz, <sup>2</sup>*J* (<sup>19</sup>F-<sup>13</sup>C) = 15.1 Hz, <sup>3</sup>*J* (<sup>19</sup>F-<sup>13</sup>C) = 4.4 Hz), 132.21 (C2, d, *J* (<sup>19</sup>F-<sup>13</sup>C) = 14.1 Hz), 129.81 (Ar), 129.53 (Ar), 129.21 (Ar), 119.41 (C1, dd, *J* (<sup>19</sup>F-<sup>13</sup>C) = 11.5 Hz, <sup>2</sup>*J* (<sup>19</sup>F-<sup>13</sup>C) = 4.9 Hz), 117.51 (C4, dd, *J* (<sup>19</sup>F-<sup>13</sup>C) = 23.7 Hz, <sup>2</sup>*J* (<sup>19</sup>F-<sup>13</sup>C) = 18.5 Hz), 55.66 (CH of cyclooctane, d, *J* = 11.4 Hz), 35.86 (SCH<sub>2</sub>CH<sub>2</sub>), 34.63 (SCH<sub>2</sub>CH<sub>2</sub>), 32.62 (cyclooctane), 27.29 (cyclooctane), 25.94 (cyclooctane), 25.53 (cyclooctane), 23.38 (cyclooctane). <sup>19</sup>F NMR (DMSO-*d*<sub>6</sub>, 376MHz) δ -120.81 (C3-F, dd, *J* = 11.4 Hz, <sup>2</sup>*J* = 3.1 Hz), -137.1 (C5-F, dd, *J* = 27.0 Hz, <sup>2</sup>*J* = 11.5 Hz), -145.2 (C6-F, dd, *J* = 26.9 Hz, <sup>2</sup>*J* = 3.0 Hz). HRMS for C<sub>23</sub>H<sub>27</sub>F<sub>3</sub>N<sub>2</sub>O<sub>4</sub>S<sub>2</sub> [(M-H)<sup>-</sup>]: calcd. 515.1292, found 515.1284.

**1-[4-(2-Bromoethyl)phenyl]ethanone (5)**

A mixture of AlCl<sub>3</sub> (2.91 g, 21.82 mmol), acetyl chloride (1.71 mL, 24.05 mmol) and CH<sub>2</sub>Cl<sub>2</sub> (50 mL) was stirred at 0°C – +5°C until AlCl<sub>3</sub> dissolved. Solution of (2-bromoethyl)benzene (**4**) (2.00 mL, 14.64 mmol) in acetyl chloride (3.4 mL) was then added dropwise at 0°C – +2°C. The resulting mixture was stirred at 0°C – +2°C for 1h and then poured into a mixture of concentrated HCl (20 mL) and ice (200 mL). This mixture was extracted with CH<sub>2</sub>Cl<sub>2</sub> (30 mL × 3). The combined organic extracts were washed with 1N NaOH, water and brine, dried over Na<sub>2</sub>SO<sub>4</sub> and concentrated under reduced pressure. The resultant residue was subjected to flash chromatography (silica gel, hexane/EtOAc, 9:1) to afford compound **5** (2.83 g, 85 %) as an oil. <sup>1</sup>H NMR (400 MHz, DMSO-*d*<sub>6</sub>) δ 7.94 (2H, d, *J* = 8.2

Hz, ArH), 7.33 (2H, d,  $J = 8.2$  Hz, ArH), 3.61 (2H, t,  $J = 7.3$  Hz, CH<sub>2</sub>), 3.24 (2H, t,  $J = 7.3$  Hz, CH<sub>2</sub>), 2.60 (3H, s, COCH<sub>3</sub>).

#### 4-(2-Bromoethyl)benzoic acid (6)

A solution of sodium hydroxide (4.16 g, 104 mmol) in H<sub>2</sub>O/dioxane (50 mL/40 mL) was prepared in three-necked, round bottomed flask fitted with a thermometer and a dropping funnel. The solution was cooled to 0°C in an ice-salt bath, and bromine (2.04 mL, 39.6 mmol) was slowly added with stirring at 0°C – +7°C. 1-[4-(2-Bromoethyl)phenyl]ethanone (**5**) (3.00 g, 13.2 mmol) was then added dropwise to sodium hypobromite solution at 0°C – +2°C. The resulting mixture was stirred at 0°C – +5°C for 1.5 h and then acidified with concentrated HCl. The precipitated acid was filtered, washed with water and dried. Recrystallization was accomplished from toluene. Yield: 2.50 g (83 %), mp 207-208°C, close to the value in the literature mp 205-207°C [46]. <sup>1</sup>H NMR (400 MHz, DMSO-*d*<sub>6</sub>) δ 12.91 (1H, br s, COOH), 7.89 (2H, d,  $J = 8.3$  Hz, ArH), 7.41 (2H, d,  $J = 8.4$  Hz, ArH), 3.78 (2H, t,  $J = 7.1$  Hz, CH<sub>2</sub>), 3.21 (2H, t,  $J = 7.1$  Hz, CH<sub>2</sub>).

#### 4-(2-Mercaptoethyl)benzoic acid (7)

The mixture of 4-(2-bromoethyl)benzoic acid (**6**) (2.00 g, 8.73 mmol), thiourea (0.80 g, 10.43 mmol), H<sub>2</sub>O (20 mL) was refluxed for 3 h. The solution was cooled to room temperature and 10 % (w/v) aqueous NaOH (18 mL) was added and the mixture was refluxed again for 1h. The solution was then cooled to room temperature, acidified to pH = 5 with 2M HCl and filtered. The white solid was washed with water and dried. Recrystallization was accomplished from EtOH. Yield: 1.47 g (92 %), mp 157-159°C, close to the value in the literature mp 156-158°C [47]. <sup>1</sup>H NMR (400 MHz, DMSO-*d*<sub>6</sub>) δ 12.85 (1H, br s, COOH), 7.88 (2H, d,  $J = 8.2$  Hz, ArH), 7.36 (2H, d,  $J = 8.2$  Hz, ArH), 2.92 (2H, t,  $J = 7.4$  Hz, CH<sub>2</sub>), 2.77 (2H, q,  $J = 6.8$  Hz, CH<sub>2</sub>), 2.30 (1H, t,  $J = 7.7$  Hz, SH).

#### CA inhibition assay

The enzymatic activity of carbonic anhydrase isoforms and their inhibition was determined by the stopped-flow CO<sub>2</sub> hydration assay where the formed acid was followed by the absorbance change of a pH indicator. The Applied Photophysics SX.18MV-R stopped-flow spectrometer was used to measure the absorbance change of Phenol-Red pH indicator at 557 nm [49]. Saturated CO<sub>2</sub> solution was prepared by bubbling the CO<sub>2</sub> gas in MilliQ water at 25 °C for 1 h. Experiments were performed at 25 °C using 25 mM Hepes buffer containing 50 mM NaCl (pH 7.5), 0–10 μM compound with the final 0.4% (v/v) DMSO concentration. The final enzyme concentration was 10 nM for CA IX and 20 nM for CA XII. Raw curves of absorbance change were analyzed using Origin 8.1 (OriginLab Corporation) and the slope values were used to evaluate the rates of CO<sub>2</sub> hydration. Spontaneous CO<sub>2</sub> hydration

rate was used as a zero value, while the CA catalyzed reaction rate - as a maximum value. The  $K_d$  values were determined using the Morrison equation [50]:

$$\text{CA act. (\%)} = \left( 1 - \frac{([CA] + [I] + K_d) - \sqrt{([CA] + [I] + K_d)^2 - 4[CA][I]}}{2[CA]} \right) 100\%$$

### Fluorescent thermal shift assay

The binding affinity of synthesized compounds to recombinant human CAs was measured by the fluorescent thermal shift assay (FTSA) where the thermal stabilization of the protein by the compound was determined by following the fluorescence dependence on temperature at various added compound concentrations. The melting temperature ( $T_m$ ) of CA was measured using the Corbett Rotor-Gene 6000 instrument (QIAGEN Rotor-Gene Q, excitation at  $365 \pm 20$  nm, emission detection at  $460 \pm 15$  nm). The protein was heated from 25 to 99 °C at a rate of 1° C/min and the fluorescence change of the solvatochromic dye 8-anilino-1-naphthalene sulfonate (ANS) was followed. The samples consisted of 5-10 μM CA, 0-200 μM ligand, 50 μM ANS, and 50 mM sodium phosphate buffer containing 100 mM NaCl at pH 7.0, with the final DMSO concentration of 2% (v/v). Protein unfolding profiles and the melting temperatures were determined at each ligand concentration while recording extrinsic fluorescence of ANS. Data analysis was performed as previously described [51]. All experiments were repeated at least twice.

### CA IX purification, crystallization and X-ray crystallography data collection

Protein was prepared and crystalized as described previously [30]. Data were collected at beamline BL14.1, Helmholtz-Zentrum Berlin, in Berlin, Germany. Images were processed by MOSFLM [52] and reflections scaled by SCALA [53]. The structure was determined by molecular replacement in MOLREP [54]. The ligand parameter files were generated by LIBCHECK [55]. Ligand modeling and manual refinement of the structure were done in COOT, followed by refinement in REFMAC. Data processing, refinement, and validation statistics are shown in Table S1.

### Cell culture

Human cervical (HeLa), lung (H460, A549), breast (MDA-MB-231), and pancreatic (AsPC-1) cancer cells were cultured in Dulbecco's Modified Eagle's Medium (DMEM, Lonza) supplemented with 10% fetal bovine serum (FBS, Lonza). Cells were exposed to hypoxic conditions in the hypoxic chamber (MACS VA500 microaerophilic workstation, Don Whitley Scientific, UK) with 0.2% O<sub>2</sub>, 5% CO<sub>2</sub> and residual N<sub>2</sub>. Simultaneously, normoxic cells were grown in the humidified incubator with 21% O<sub>2</sub>, 5% CO<sub>2</sub> at 37°C.

### Generating HeLa CA IX knockout cells

HeLa CA IX knockout (KO) clones were established as described elsewhere [56]. HeLa cells were routinely cultured in DMEM (Lonza) supplemented with 10% FBS (Lonza) and transfected with a vector containing a CA IX-CRISPR guide RNA (CACCGGGGAATCCTCCTGCATCCG) using linear polyethylenimine (P-PEI, Polysciences Inc.). 24 h after transfection, selection with puromycin was started and maintained for 48 h, after which monoclones were picked and routinely cultured. After exposure to hypoxia (0.2%, 24 h), an initial screening for CA IX expression was performed by Western blotting (Figure S3), followed by genetic confirmation of CA IX KO in clones that showed no CA IX expression. This was done by single allele sequencing using the TOPO® TA Cloning® Kit (Invitrogen) according to the manufacturer's protocol. KO-causing mutations in the *CA9* gene were confirmed in two alleles per clone.

### Determination of CA catalytic activity in cancer cells via gas-analysis mass spectrometry

Catalytic activity of CA in hypoxic MDA-MB-231 and HeLa cancer cells was determined by monitoring the  $^{18}\text{O}$  depletion of doubly labeled  $^{13}\text{C}^{18}\text{O}_2$  through several hydration and dehydration steps of  $\text{CO}_2$  and  $\text{HCO}_3^-$  at 24 °C [57,58]. The reaction sequence of  $^{18}\text{O}$  loss from  $^{13}\text{C}^{18}\text{O}^{18}\text{O}$  ( $m/z = 49$ ) over the intermediate product  $^{13}\text{C}^{18}\text{O}^{16}\text{O}$  ( $m/z = 47$ ) and the end product  $^{13}\text{C}^{16}\text{O}^{16}\text{O}$  ( $m/z = 45$ ) was monitored with a quadrupole mass spectrometer (OmniStar GSD 320; Pfeiffer Vacuum, Asslar, Germany). The relative  $^{18}\text{O}$  enrichment was calculated from the measured 45, 47, and 49  $m/z$  abundance as a function of time according to:  $\log \text{enrichment} = \log (49 \times 100 / (49 + 47 + 45))$ . For the calculation of CA activity, the rate of  $^{18}\text{O}$  depletion was obtained from the linear slope of the log enrichment over the time, using OriginPro 8.6 (OriginLab Corporation). The rate was compared with the corresponding rate of the non-catalyzed reaction. Enzyme activity in units (U) was calculated from these two values as defined by Badger and Price [59]. From this definition, one unit corresponds to 100% stimulation of the non-catalyzed  $^{18}\text{O}$  depletion of doubly labeled  $^{13}\text{C}^{18}\text{O}_2$ . MDA-MB-231 cells were cultured in Gibco Leibovitz-L15 medium (Life Technologies GmbH, Darmstadt, Germany), supplemented with 10% fetal calf serum, 5 mM glucose and 1% penicillin/streptomycin, pH 7.4. HeLa cells were cultured in RPMI-1640 Medium (Sigma Aldrich, Schnellendorf, Germany), supplemented with 10% fetal calf serum and 1% penicillin / streptomycin. Both cell lines were cultured under hypoxia (1%  $\text{O}_2$ ) for 3 days prior to measurements. Cells were trypsinized, washed and resuspended in HEPES-buffered saline (143 mM NaCl, 5 mM KCl, 2 mM  $\text{CaCl}_2$ , 1 mM  $\text{MgSO}_4$ , 1 mM  $\text{Na}_2\text{HPO}_4$ , 10 mM HEPES, pH 7.2). For determination of  $IC_{50}$  values, 2 cell culture plates (58  $\text{cm}^2$ ), grown to 80% confluency, were used for every single measurement. To ensure an equal amount of cells within one set of measurements, cells from several plates were pooled and then aliquoted according to the number of tested inhibitor concentrations. For the determination of  $IC_{50}$ , the cell suspensions were incubated in the

corresponding concentration of inhibitor for up to 3 h. For every measurement, the non-catalyzed reaction was determined for 6 min in the presence of inhibitor, before cell suspension was added to the measuring cuvette and the catalyzed reaction was determined for 8 min. CA activity in the presence of inhibitor was normalized to the activity in the absence of inhibitor.  $IC_{50}$  values were determined by Hill equation using OriginPro 8.6. To investigate specificity of the inhibitors in HeLa WT and HeLa CA IX KO cells, the non-catalyzed reaction was determined for 6 min in the absence of inhibitor, before a suspension of  $5 \times 10^6$  cells was added to the measuring cuvette. After the catalyzed reaction was determined for 6 min, the inhibitor was added to the cuvette and the reaction was determined for another 6 min.

### **Extracellular acidification (pH) assay**

HeLa, H460, MDA-MB-231, and AsPC-1 cells were cultured in DMEM (Lonza) supplemented with 10% FBS (Lonza), whereas A549 cells were grown in-house made analogous medium differing only by a lower amount of sodium bicarbonate (final concentration 10 mM). Cell densities for each cell line were optimized to get ~100% confluence at the end of experiment under normoxic and hypoxic (0.2% O<sub>2</sub>) conditions upon vehicle (0.05% DMSO) treatment. Such conditions were necessary to obtain the highest possible level of CA IX-dependent extracellular acidification. Cells were plated in 6 cm dishes and allowed to attach overnight in normoxia. The next day cells were exposed to 5-50  $\mu$ M doses of each inhibitor or DMSO for 72 h in parallel under normoxic or hypoxic conditions and pH of the culture medium was measured at the end of each experiment as previously reported [33]. Results are shown as a difference between the pH of medium in the control plate (without seeded cells) and the pH of medium in the targeted plate (cells exposed to the compound or vehicle).

### **Cell viability assay**

Cytotoxicity of inhibitors was determined by the alamarBlue® cell viability assay (Life Technologies). Cell densities for HeLa, H460, MDA-MB-231, A549, and AsPC1 were optimized to get ~80% confluence at the end of experiment under normoxic and hypoxic (0.2% O<sub>2</sub>) conditions upon vehicle (0.25% DMSO) treatment. Briefly, cells were seeded in 96-well plates and allowed to attach overnight in normoxia. On the next day, cells were exposed to normoxia or hypoxia and medium was replaced with pre-incubated normoxic or hypoxic medium with final concentrations of 10-150  $\mu$ M of inhibitor or DMSO. After 72h, cells were incubated with 10% alamarBlue® for 2 h under normoxia at 37°C. The fluorescence signal was measured using the multi-mode microplate reader (FLUOstar® Omega, BMG Labtech) at 580 nm (excitation wavelength 540 nm). Response to treatments was quantified by evaluating  $EC_{50}$  values (concentration of inhibitor that leads to half-maximum viability response determined by Hill fit).

### Clonogenic cell survival assays

Clonogenic survival of HeLa cell monolayers was evaluated using cell densities applied in the extracellular acidification assay to determine the effect of inhibitors on the clonogenic cell survival while having the same acidification conditions. Cells were exposed to 10-50  $\mu\text{M}$  VR16-09, VD11-4-2, VD12-09, or 0.25% DMSO for 72 h upon normoxic or hypoxic conditions (0.2%  $\text{O}_2$ ). Such doses of inhibitors significantly reduced hypoxia-induced acidification. Then cells were trypsinized, reseeded in triplicate with known cell densities and allowed to form colonies for 14 days. To test inhibitors in 3D cell models, non-hypoxic and hypoxic H460 spheroids were exposed to 5-15  $\mu\text{M}$  doses of VR16-09 or 0.25% DMSO for 24 h on day 4 or day 11, respectively. Single cell suspensions were prepared and cells were plated in triplicate with known cell densities and allowed to form colonies for 14 days. Colonies were quantified after staining and fixation with 0.4% methylene blue in 70% ethanol. Surviving fraction was normalized to vehicle (DMSO).

### Spheroid growth

To prepare plates for the growth of attachment-free H460 spheroids, autoclaved 1.5% w/v agarose (Sigma-Aldrich) was dispensed in the inner 60 wells of 96-well plates (50  $\mu\text{L}$ /well) and left for polymerization at room temperature for 30 min. H460 cells were plated in modified 96-well plates to the surface of agarose menisci with a density of 500 cells/well. The DMEM was refreshed every two days. After 7 or 11 days in culture, spheroids were incubated with 20  $\mu\text{g}/\text{mL}$  pimonidazole (PIMO, Hypoxyprobe-1, HP-1000, BioConnect) for 2 h at 37°C, collected and cryoconserved for immunofluorescence analysis (see below). In parallel 4 or 11 days after cell seeding, spheroids of homogeneous volume were treated with 5-15  $\mu\text{M}$  VR16-09 or 0.25% DMSO for 24 h and collected for clonogenic survival assay.

### Western blot

Protein isolates were prepared by incubating scraped cells in RIPA buffer on ice for 30 min, followed by centrifugation to remove cell debris. Protein concentrations were determined using Bradford protein quantification reagent (BioRad). Western blot was performed using primary antibodies, including mouse anti-CA IX (M75, 1:40, kindly provided by Silvia Pastorekova, Institute of Virology, Slovak Academy of Science, Slovak Republic), mouse anti-CA XII (clone 15A4, 1:100, kindly provided by Aurelija Žvirblienė, Institute of Biotechnology, Vilnius University, Lithuania), rabbit anti-MCT1 (1:100), rabbit anti-MCT4 (1:400, kindly provided by Holger M. Becker, University of Veterinary Medicine Hannover, Hannover, Germany), rabbit anti-lamin A (1:10.000, Sigma-Aldrich), and mouse anti-ac-tin (1:2.000.000, MP Biomedicals). Primary antibodies were incubated overnight at 4°C, whereas horseradish peroxidase-linked secondary antibodies (1:2.000, Cell Signaling) were incubated for 1

h at room temperature. Amersham ECL Western Blotting Detection Reagent (GE Healthcare Life Sciences) was applied for the detection of CA XII, MCT1, MCT4, and lamin A, while SuperSignal™ West Pico PLUS Chemiluminescent Substrate (Life Technologies) was used for the visualization of CA IX and actin.

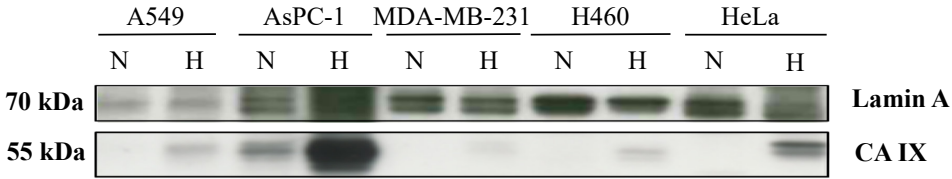
### **Immunofluorescence analysis**

H460 spheroids of day 7 and day 11 were cryoconserved. Frozen sections (7 µm) of spheroids were fixed in acetone (4°C, 10 min), air-dried and rehydrated in phosphate buffered saline (PBS). Non-specific binding was blocked by incubation with 0.5% goat serum in PBS for 30 min at room temperature. Sections were stained (37°C, 1 h) using primary rabbit anti-PIMO (1:250) or mouse anti-CA IX (1:100, M75), followed by incubation (37°C, 1 h) with secondary goat anti-rabbit Alexa488 or goat anti-mouse Alexa594, respectively (both 1:500, from Invitrogen). Nuclei were stained with DAPI (final concentration 5 µg/mL) for 2 min at room temperature. Staining without primary antibody was used as negative control. Sections were viewed at 10X magnification by Nikon Eclipse E800 microscope (Nikon Instruments Inc.).

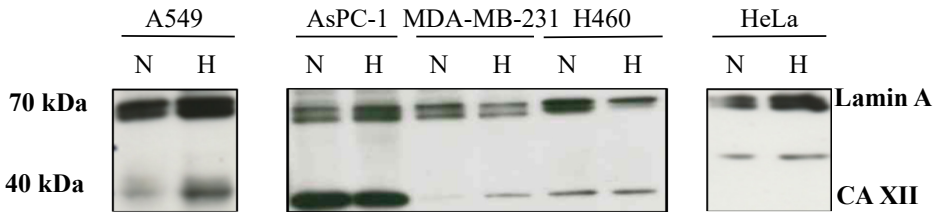
### **Statistics**

Statistical analysis was performed using GraphPad Prism (version 6.01). A non-parametric Mann-Whitney U test for small groups was applied to evaluate the statistical significance of differences between two independent groups of variables and  $p < 0.05$  was assumed to be significant (\* $p < 0.05$ ; \*\* $p < 0.01$ , \*\*\* $p < 0.001$ , \*\*\*\* $p < 0.0001$ ).

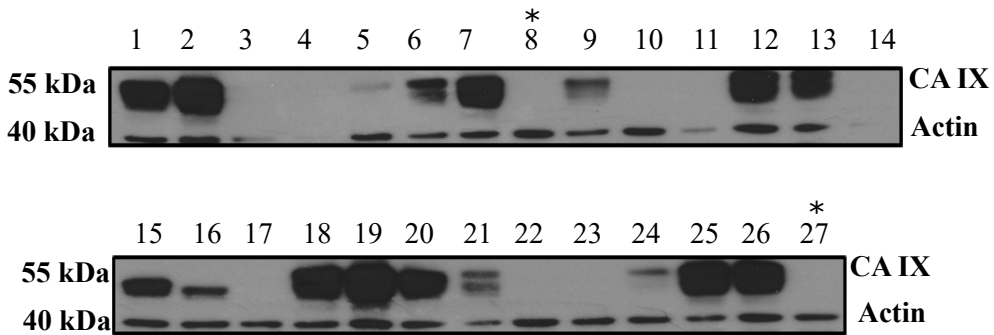
## Supplementary data



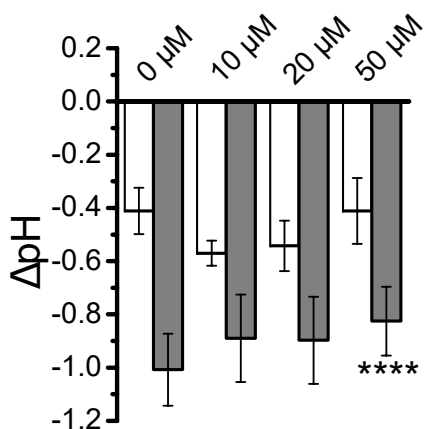
**Figure S1:** Western blot analysis of CA IX expression in A549, AsPC-1, MDA-MB-231, H460, and HeLa cells after exposure to normoxia (N, 21%) or hypoxia (H, 0.2%) for 72 h. Lamin A was used as loading control.



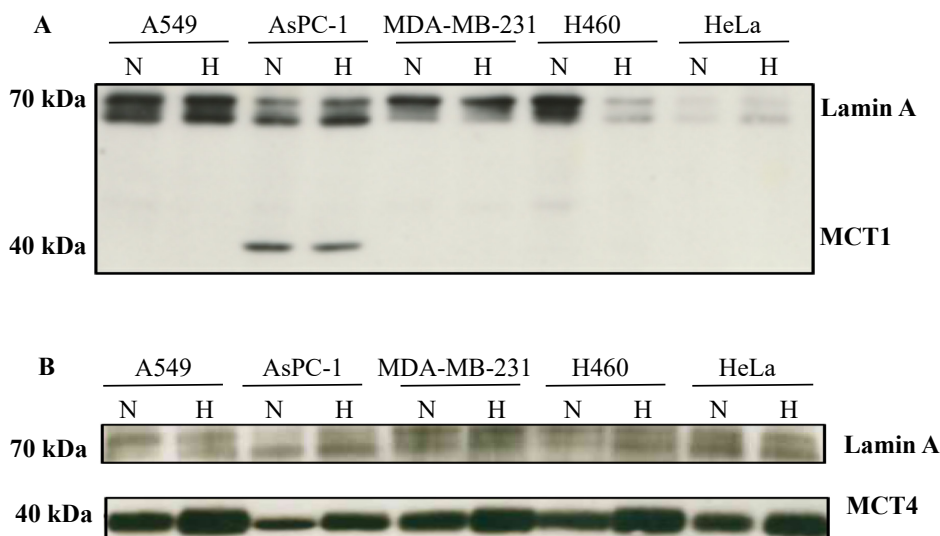
**Figure S2:** Western blot analysis of CA XII expression in A549, AsPC-1, MDA-MB-231, H460, and HeLa cells after exposure to normoxia (N, 21%) or hypoxia (H, 0.2%) for 72h. The MW of CA XII in HeLa was found to be larger than in other tested cell lines, suggesting variability of CA XII isoforms or their post-translational modifications in different cell lines. Lamin A was used as loading control.



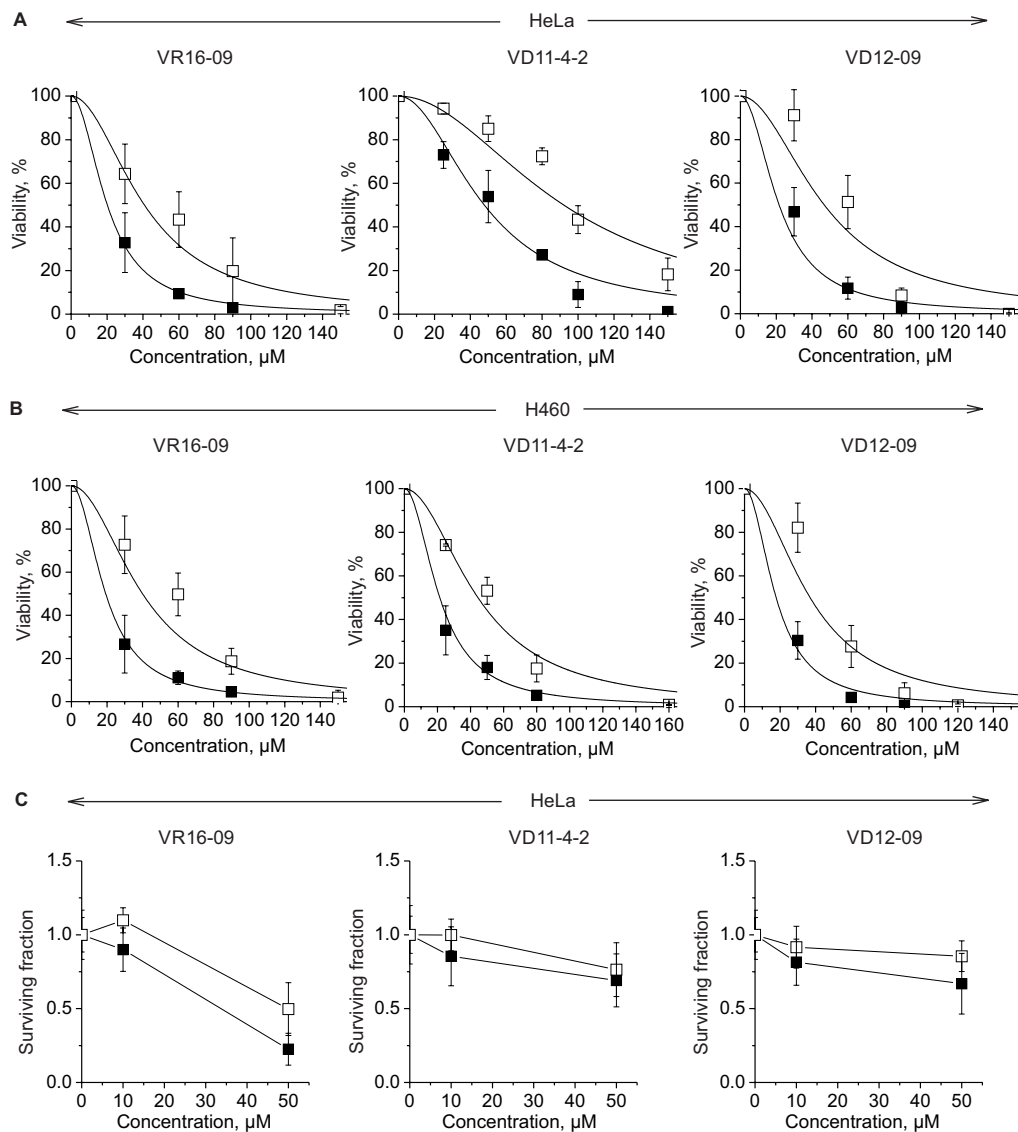
**Figure S3:** Western blot analysis of CA IX expression in a panel of expected HeLa CA IX KO clones after exposure to hypoxia (0.2%) for 24 h. Clones 8 and 27, marked by asterisks, represent selected HeLa CA IX KO clones 1 and 2, respectively, which were used in experiments after genetic confirmation of KO-causing mutations in the *CA9* gene in two alleles per clone. The growth rate of clones 8 and 27 were similar as compared to HeLa WT cells. Actin was used as loading control.



**Figure S4:** Dose-dependent reduction of extracellular acidification of H460 cells after VR16-10 exposure for 72 h under normoxia (21% O<sub>2</sub>; white bars) or hypoxia (0.2% O<sub>2</sub>; grey bars). Results are shown as a difference between the pH of medium in the control plate (DMEM without seeded cells) and the pH of medium in the targeted plate (H460 exposed to the compound or vehicle) after the incubation for 72 h. Asterisks indicate significant difference of medium pH of cells exposed to DMSO and cells treated with various doses of inhibitor under hypoxic conditions (\*\*\*\*p<0.0001).



**Figure S5:** Western blot analysis of MCT1 (A) and MCT4 (B) expression in A549, AsPC-1, MDA-MB-231, H460, and HeLa cell lines after exposure to normoxia (N, 21%) or hypoxia (H, 0.2%) for 72 h. Lamin A was used as loading control.



**Figure S6:** Cytotoxicity profiles of compounds. A – Dose-response curves representing the cytotoxicity of VR16-09, VD11-4-2, and VD12-09 in HeLa cells after 72 h exposure in normoxia (21% O<sub>2</sub>; ■) or hypoxia (0.2% O<sub>2</sub>; □). B – Dose-response curves showing the cytotoxicity of compounds for H460 cells after 72 h exposure in normoxia or hypoxia. C – Clonogenic survival of monolayer HeLa cells after the exposure to compounds for 72 h under normoxia and hypoxia. Surviving fraction was normalized to vehicle control. Average ± SD of 3 independent repeats is shown.

**Table S1:** X-ray crystallographic data processing, refinement, and validation statistics for CA IX in complex with VD11-4-2 (PDB ID: 6FE1) or VD12-09 (PDB ID: 6FE0). \*Values in parenthesis are for the high resolution.

Structure	CA IX- VD11-4-2	CA IX- VD12-09
Space group	H3	H3
Cell dimensions		
a=b (Å)	152.0	152.3
c (Å)	172.2	171.5
Resolution (Å)	25-1.95	26-1.91
Highest resolution shell (Å)	1.95-2.06	1.91-2.01
Number of reflections	107506	112458
Number of reflections in test set	5404	5544
test set		
Completeness (%)	99.4 (98.7)	97.1 (98.3)
R <sub>merge</sub>	0.07 (0.50)	0.08 (0.54)
<I/σI>	8.7 (2.0)	8.2 (2.0)
Average multiplicity	3.0 (2.7)	2.7 (2.7)
R-factor	0.18 (0.34)	0.17 (0.28)
R <sub>free</sub>	0.22 (0.33)	0.20 (0.29)
Average B factor (Å <sup>2</sup> )	38.7	29.6
Average B factor for inhibitor (Å <sup>2</sup> )	47.4	35.9
<B> from Wilson plot (Å <sup>2</sup> )	24.8	23.1
Number of protein atoms	7736	7451
Number of inhibitor atoms	112	104
Number of solvent molecules	736	792
r.m.s. deviations from ideal values		
Bond lengths (Å)	0.01	0.01
Bond angles (°)	1.51	1.48
Outliers in Ramachandran	0.31	0.00
plot (%)		
PDB code	6FE1	6FE0

**Table S2:**  $EC_{50}$  values for VR16-09, VR16-10, VD11-4-2, and VD12-09 evaluated by alamarBlue® cell viability assay. Cytotoxic ratios (CR) of selectivity to hypoxia are indicated. The HeLa, H460, A549, and MDA-MB-231 cells were exposed to the compounds under normoxia (21% O<sub>2</sub>) or hypoxia (0.2% O<sub>2</sub>) for 72 h, while AsPC-1 cells – for 48 h. Results of at least 3 independent repeats are shown (mean ± SD). ND – not determined.

[O <sub>2</sub> ]	$EC_{50}$ $\mu$ M											
	VR16-09			VR16-10			VD11-4-2			VD12-09		
	21%	0.2%	CR	21%	0.2%	CR	21%	0.2%	CR	21%	0.2%	CR
<b>HeLa</b>	20.2±4.3	40.8±9.6	0.46±0.06	93.3±5.8	>150	>0.62	47.8±9.6	92.2±8.3	0.52±0.08	21.6±4.1	46.9±7.0	0.44±0.10
<b>H460</b>	19.3±3.6	40.0±9.6	0.49±0.04	83.3±15.3	>150	>0.55	21.4±3.1	44.6±6.4	0.48±0.05	17.8±2.2	37.0±7.6	0.46±0.09
<b>A549</b>	17.0±1.0	76.7±2.9	0.22±0.02	ND	ND	ND	43.8±2.5	105±6	0.42±0.04	33.8±2.5	98.8±8.5	0.34±0.04
<b>MDA-MB-231</b>	74.2±3.8	84.2±4.9	0.88±0.03	ND	ND	ND	52.8±7.1	64.3±11.5	0.83±0.08	55.4±6.6	67.6±7.1	0.82±0.09
<b>AsPC-1</b>	153±23	160±17	0.96±0.12	ND	ND	ND	165±6	145±6	1.14±0.09	100±20	83.3±5.8	1.19±0.17

## Acknowledgements

We thank Rianne Biemans and Natasja Lieuwes for their skillful assistance with viability, clonogenic survival, and extracellular pH measuring experiments. The work was supported by grants from the Research Council of Lithuania (Jurgita Matulienė, SEN-04/2015), by the Deutsche Forschungsgemeinschaft (Holger M. Becker, BE 4310/6-1), by the European Research Council (Philippe Lambin, Hypoximmuno, ERC-ADG-2015, n° 694812), and the Dutch Cancer Society (Philippe Lambin, Ludwig J. Dubois, UM 2012-5394 and MAC 2013-6089).

### Conflict of interest

DM declares that he has patents and patent applications pending on CA inhibitors.

### PDB ID codes

Atomic coordinates along with experimental data of CA IX in complex with following compounds were deposited in Protein Data Bank: VR16-09 (PDB ID: 6G98), VR16-10 (PDB ID: 6G9U), VD12-09 (PDB ID: 6FE0) and VD11-4-2 (PDB ID: 6FE1) Coordinates of unliganded CA IX X-ray structure were also deposited (PDB ID: 6FE2).

## References

1. Harris AL. Hypoxia—a Key Regulatory Factor in Tumour Growth. *Nature Reviews. Cancer.* 2002; 2:38–47.
2. Pettersen EO, Ebbesen P, Gieling RG, Williams KJ, Dubois L, Lambin P, Ward C, Meehan J, Kunkler IH, Langdon SP, Ree AH, Flatmark K, Lyng H *et al.* Targeting Tumour Hypoxia to Prevent Cancer Metastasis. From Biology, Biosensing and Technology to Drug Development: The METOXIA Consortium. *J Enzyme Inhib Med Chem.* 2015; 30:689–672.
3. Höckel M, Vaupel P. Tumor Hypoxia: Definitions and Current Clinical, Biologic, and Molecular Aspects. *J Natl Cancer Inst.* 2001; 93:266–276.
4. Wilson WR, Hay MP. Targeting Hypoxia in Cancer Therapy. *Nature Reviews. Cancer.* 2011; 11:393–410.
5. Wojtkowiak JW, Verduzco D, Schramm KJ, Gillies RJ. Drug Resistance and Cellular Adaptation to Tumor Acidic pH Microenvironment. *Mol Pharm.* 2011; 8:2032–2038.
6. Pastoreková S, Parkkila S, Parkkila AK, Opavský R, Zelník V, Saarnio J, Pastorek J. Carbonic Anhydrase IX, MN/CA IX: Analysis of Stomach Complementary DNA Sequence and Expression in Human and Rat Alimentary Tracts. *Gastroenterology.* 1997; 112:398–408.
7. Wykoff CC, Beasley NJ, Watson PH, Turner KJ, Pastorek J, Sibtain A, Wilson GD, Turley H, Talks KL, Maxwell PH, Pugh CW, Ratcliffe PJ, Harris AL. Hypoxia-Inducible Expression of Tumor-Associated Carbonic Anhydrases. *Cancer Res.* 2000; 60:7075–7083.
8. Simko V, Takacova M, Debreova M, Laposova K, Ondriskova-Panisova E, Pastorekova S, Csaderova L, Pastorek J. Dexamethasone Downregulates Expression of Carbonic Anhydrase IX via HIF-1 $\alpha$  and NF- $\kappa$ B-Dependent Mechanisms. *Int J Oncol.* 2016; 49:1277–1288.
9. Andreucci E, Peppicelli S, Carta F, Brisotto G, Biscontin E, Ruzzolini J, Bianchini F, Biagioni A, Supuran CT, Calorini L. Carbonic Anhydrase IX Inhibition Affects Viability of Cancer Cells Adapted to Extracellular Acidosis. *J Mol Med (Berlin, Germany).* 2017; 95:1341–1353.
10. Ilnatko R, Kubes M, Takacova M, Sedlakova O, Sedlak J, Pastorek J, Kopacek J, Pastorekova S. Extracellular Acidosis Elevates Carbonic Anhydrase IX in Human Glioblastoma Cells via Transcriptional Modulation That Does Not Depend on Hypoxia. *Int J Oncol.* 2006; 29:1025–1033.
11. Zatovicova M, Sedlakova O, Svastova E, Ohradanova A, Ciampor F, Arribas J, Pastorek J, Pastorekova S. Ectodomain Shedding of the Hypoxia-Induced Carbonic Anhydrase IX Is a Metalloprotease-Dependent Process Regulated by TACE/ADAM17. *Br J Cancer.* 2005; 93:1267–1276.
12. Závada J, Závadová Z, Zaťovicová M, Hyršl L, Kawaciuk I. Soluble Form of Carbonic Anhydrase IX (CA IX) in the Serum and Urine of Renal Carcinoma Patients. *Br J Cancer.* 2003; 89:1067–1071.
13. Pastorek J, Pastoreková S, Callebaut I, Mornon JP, Zelník V, Opavský R, Zaťovicová M, Liao S, Portetelle D, Stanbridge EJ. Cloning and Characterization of MN, a Human Tumor-Associated Protein with a Domain Homologous to Carbonic Anhydrase and a Putative Helix-Loop-Helix DNA Binding Segment. *Oncogene.* 1994; 9:2877–2888.
14. Svastová E, Hulíková A, Rafajová M, Zaťovicová M, Gibadulinová A, Casini A, Cecchi A, Scozzafava A, Supuran CT,

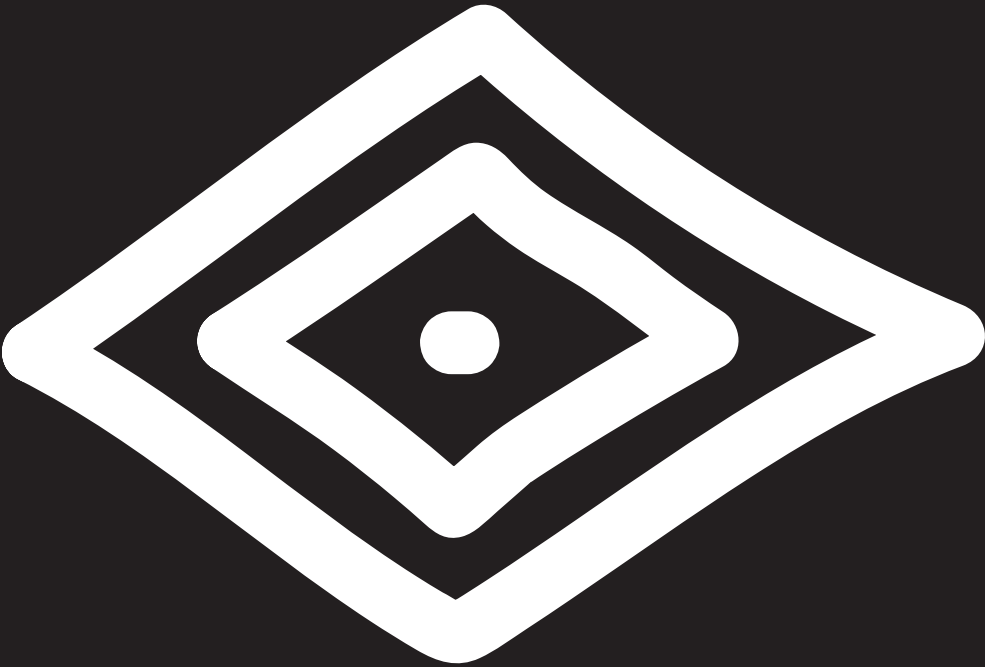
- Pastorek J, Pastoreková S. Hypoxia Activates the Capacity of Tumor-Associated Carbonic Anhydrase IX to Acidify Extracellular pH. *FEBS Lett.* 2004; 577: 439–445.
15. Ditte P, Dequiedt F, Svastova E, Hulikova A, Ohradanova-Repic A, Zatovicova M, Csaderova L, Kopacek J, Supuran CT, Pastorekova S, Pastorek J. Phosphorylation of Carbonic Anhydrase IX Controls Its Ability to Mediate Extracellular Acidification in Hypoxic Tumors. *Cancer Research.* 2011; 71:7558–7567.
  16. Swietach P, Vaughan-Jones RD, Harris AL. Regulation of Tumor pH and the Role of Carbonic Anhydrase 9. *Cancer Metastasis Rev.* 2007; 26:299–310.
  17. Csaderova L, Debreova M, Radvak P, Stano M, Vrestiakova M, Kopacek J, Pastorekova S, Svastova E. The Effect of Carbonic Anhydrase IX on Focal Contacts during Cell Spreading and Migration. *Front Physiol.* 2013; 4(271):1–12.
  18. Svastova E, Witariski W, Csaderova L, Kosik I, Skvarkova L, Hulikova A, Zatovicova M, Barathova M, Kopacek J, Pastorek J, Pastorekova S. Carbonic Anhydrase IX Interacts with Bicarbonate Transporters in Lamellipodia and Increases Cell Migration via Its Catalytic Domain. *J Biol Chem.* 2012; 287:3392–3402.
  19. Pastorek J, Pastorekova S. Hypoxia-Induced Carbonic Anhydrase IX as a Target for Cancer Therapy: From Biology to Clinical Use. *Semin Cancer Biol.* 2015; 31:52–64.
  20. Gaspari R, Rechlin C, Heine A, Bottegoni G, Rocchia W, Schwarz D, Bomke J, Gerber HD, Klebe G, Cavalli A. Kinetic and Structural Insights into the Mechanism of Binding of Sulfonamides to Human Carbonic Anhydrase by Computational and Experimental Studies. *J Med Chem.* 2016; 59:4245–4256.
  21. Krishnamurthy VM, Bohall BR, Kim CY, Moustakas DT, Christianson DW, Whitesides GM. Thermodynamic Parameters for the Association of Fluorinated Benzenesulfonamides with Bovine Carbonic Anhydrase II. *Chemistry, an Asian Journal.* 2007; 2:94–105.
  22. Krishnamurthy VM, Kaufman GK, Urbach AR, Gitlin I, Gudiksen KL, Weibel DB, Whitesides GM. Carbonic Anhydrase as a Model for Biophysical and Physical-Organic Studies of Proteins and Protein-Ligand Binding. *Chem Rev.* 2008; 108:946–1051.
  23. Zhou Y, Wang J, Gu Z, Wang S, Zhu W, Aceña JL, Soloshonok VA, Izawa K, Liu H. Next Generation of Fluorine-Containing Pharmaceuticals, Compounds Currently in Phase II–III Clinical Trials of Major Pharmaceutical Companies: New Structural Trends and Therapeutic Areas. *Chem Rev.* 2016; 116:422–518.
  24. Dudutienė V, Zubrienė A, Smirnov A, Timm DD, Smirnovienė J, Kazokaitė J, Michailovienė V, Zakšauskas A, Manakova E, Gražulis S, Matulis D. Functionalization of Fluorinated Benzenesulfonamides and Their Inhibitory Properties toward Carbonic Anhydrases. *ChemMedChem.* 2015; 10:662–687.
  25. Dudutienė V, Zubrienė A, Smirnov A, Gyltė J, Timm D, Manakova E, Gražulis S, Matulis D. 4-Substituted-2,3,5,6-Tetrafluorobenzenesulfonamides as Inhibitors of Carbonic Anhydrases I, II, VII, XII, and XIII. *Bioorganic Med Chem.* 2013; 21:2093–2106.
  26. Dudutienė V, Matulienė J, Smirnov A, Timm DD, Zubrienė A, Baranauskienė L, Morkūnaitė V, Smirnovienė J, Michailovienė V, Juozapaitienė V, Mickevičiūtė A, Kazokaitė J, Bakšytė S *et al.* Discovery and Characterization of Novel Selective Inhibitors of Carbonic Anhydrase IX. *J Med Chem.* 2014; 57:9435–9446.

27. Lou Y, McDonald PC, Oloumi A, Chia S, Ostlund C, Ahmadi A, Kyle A, Auf dem Keller U, Leung S, Huntsman D, Clarke B, Sutherland BW, Waterhouse D *et al.* Targeting Tumor Hypoxia: Suppression of Breast Tumor Growth and Metastasis by Novel Carbonic Anhydrase IX Inhibitors. *Cancer Research*. 2011; 71:3364–3376.
28. Pacchiano F, Carta F, McDonald PC, Lou Y, Vullo D, Scozzafava A, Dedhar S, Supuran CT. Ureido-Substituted Benzenesulfonamides Potently Inhibit Carbonic Anhydrase IX and Show Antimetastatic Activity in a Model of Breast Cancer Metastasis. *J Med Chem*. 2011; 54:1896–1902.
29. Alterio V, Hilvo M, Di Fiore A, Supuran CT, Pan P, Parkkila S, Scaloni A, Pastorek J, Pastorekova S, Pedone C, Scozzafava A, Monti SM, De Simone G. Crystal Structure of the Catalytic Domain of the Tumor-Associated Human Carbonic Anhydrase IX. *Proc Natl Acad Sci USA*. 2009; 106:16233–16238.
30. Leitans J, Kazaks A, Balode A, Ivanova J, Zalubovskis R, Supuran CT, Tars K. Efficient Expression and Crystallization System of Cancer-Associated Carbonic Anhydrase Isoform IX. *J Med Chem*. 2015; 58:9004–9009.
31. Li Y, Tu C, Wang H, Silverman DN, Frost SC. Catalysis and pH Control by Membrane-Associated Carbonic Anhydrase IX in MDA-MB-231 Breast Cancer Cells. *J Biol Chem*. 2011; 286:15789–15796.
32. Tu C, Foster L, Alvarado A, McKenna R, Silverman DN, Frost SC. Role of Zinc in Catalytic Activity of Carbonic Anhydrase IX. *Arch Biochem Biophys*. 2012; 521:90–94.
33. Dubois L, Douma K, Supuran CT, Chiu RK, van Zandvoort MA, Pastoreková S, Scozzafava A, Wouters BG, Lambin P. Imaging the Hypoxia Surrogate Marker CA IX Requires Expression and Catalytic Activity for Binding Fluorescent Sulfonamide Inhibitors. *Radiother Oncol*. 2007; 83:367–373.
34. Rami M, Dubois L, Parvathaneni NK, Alterio V, van Kuijk SJ, Monti SM, Lambin P, De Simone G, Supuran CT, Winum JY. Hypoxia-Targeting Carbonic Anhydrase IX Inhibitors by a New Series of Nitroimidazole-Sulfonamides/Sulfamides/Sulfamates. *J Med Chem*. 2013; 56:8512–8520.
35. Dubois L, Peeters SG, van Kuijk SJ, Yaromina A, Lieuwes NG, Saraya R, Biemans R, Rami M, Parvathaneni NK, Vullo D, Vooijs M, Supuran CT, Winum JY, Lambin P. Targeting Carbonic Anhydrase IX by Nitroimidazole Based Sulfamides Enhances the Therapeutic Effect of Tumor Irradiation: A New Concept of Dual Targeting Drugs. *Radiother Oncol*. 2013; 108:523–528.
36. Jamali S, Klier M, Ames S, Barros LF, McKenna R, Deitmer JW, Becker HM. Hypoxia-Induced Carbonic Anhydrase IX Facilitates Lactate Flux in Human Breast Cancer Cells by Non-Catalytic Function. *Sci Rep*. 2015; 5:13605.
37. Ullah MS, Davies AJ, Halestrap AP. The Plasma Membrane Lactate Transporter MCT4, but Not MCT1, Is up-Regulated by Hypoxia through a HIF-1 $\alpha$ -Dependent Mechanism. *J Biol Chem*. 2006; 281:9030–9037.
38. Angeli A, Tanini D, Peat TS, Di Cesare Mannelli L, Bartolucci G, Capperucci A, Ghelardini C, Supuran CT, Carta F. Discovery of New Selenoureido Analogues of 4-(4-Fluorophenylureido)Benzenesulfonamide as Carbonic Anhydrase Inhibitors. *ACS Med Chem Lett*. 2017; 8:963–968.
39. Meehan J, Ward C, Turnbull A, Bukowski-Wills J, Finch AJ, Jarman EJ, Xintaropoulou C, Martinez-Perez C, Gray M, Pearson M, Mullen P, Supuran CT, Carta F *et al.* Inhibition of pH Regulation as a Therapeutic Strategy in Hypoxic Human Breast Cancer Cells. *Oncotarget*. 2017; 8:42857–42875.

40. van Kuijk SJA, Parvathaneni NK, Niemans R, van Gisbergen MW, Carta F, Vullo D, Pastorekova S, Yaromina A, Supuran CT, Dubois LJ, Winum JY, Lambin P. New Approach of Delivering Cytotoxic Drugs towards CA IX Expressing Cells: A Concept of Dual-Target Drugs. *Eur J Med Chem.* 2017; 127:691–702.
41. Chiche J, Ilc K, Laferrière J, Trottier E, Dayan F, Mazure NM, Brahimi-Horn MC, Pouysségur J. Hypoxia-Inducible Carbonic Anhydrase IX and XII Promote Tumor Cell Growth by Counteracting Acidosis through the Regulation of the Intracellular pH. *Cancer Research.* 2009; 69:358–368.
42. Zanoni M, Piccinini F, Arienti C, Zamagni A, Santi S, Polico R, Bevilacqua A, Tesei A. 3D Tumor Spheroid Models for in Vitro Therapeutic Screening: A Systematic Approach to Enhance the Biological Relevance of Data Obtained. *Sci Rep.* 2016; 6:1–11.
43. Baker BM, Chen CS. Deconstructing the Third Dimension: How 3D Culture Microenvironments Alter Cellular Cues. *J Cell Sci.* 2012; 125:3015–3024.
44. Kimlin LC, Casagrande G, Virador VM. In Vitro Three-Dimensional (3D) Models in Cancer Research: An Update. *Mol Carcinogen.* 2013; 52:167–182.
45. Wang Z, Tang J, Salomon CE, Dreis CD, Vince R. Pharmacophore and Structure-Activity Relationships of Integrase Inhibition within a Dual Inhibitor Scaffold of HIV Reverse Transcriptase and Integrase. *Bioorganic Med Chem.* 2010; 18:4202–4211.
46. Foreman EL, McElvain SM. The Reaction of Organic Halides with Piperidine. V. Negatively Substituted Ethyl Bromides. *J Am Chem Soc.* 1940; 62:1435–1438.
47. Takano S, Yamazoe S, Koyasu K, Tsukuda T. Slow-Reduction Synthesis of a Thiolate-Protected One-Dimensional Gold Cluster Showing an Intense Near-Infrared Absorption. *J Am Chem Soc.* 2015; 137:7027–7030.
48. Robson P, Smith TA, Stephens R, Tatlow JC. Aromatic Polyfluoro-Compounds. Part XIII. Derivatives of Penta- and 2,3,5,6-Tetra-Fluorothiophenol. *J Chem Soc.* 1963; 0:3692–3703.
49. Khalifah RG. The Carbon Dioxide Hydration Activity of Carbonic Anhydrase. I. Stop-Flow Kinetic Studies on the Native Human Isoenzymes B and C. *J Biol Chem.* 1971; 246:2561–2573.
50. Smirnovienė J, Smirnovas V, Matulis D. Picomolar Inhibitors of Carbonic Anhydrase: Importance of Inhibition and Binding Assays. *Anal Biochem.* 2017; 522:61–72.
51. Baranauskienė L, Hilvo M, Matulienė J, Golovenko D, Manakova E, Dudutienė V, Michailovienė V, Torresan J, Jachno J, Parkkila S, Maresca A, Supuran CT, Gražulis S, Matulis D. Inhibition and Binding Studies of Carbonic Anhydrase Isozymes I, II and IX with Benzimidazo[1,2-c][1,2,3]Thiadiazole-7-Sulphonamides. *J Enzyme Inhib Med Chem.* 2010; 25:863–870.
52. Leslie AGW. Recent changes to the MOSFLM package for processing film and image plate data. *Newsletter on Protein Crystallography.* 1992; 26.
53. Evans PR. SCALA. *Newsletter on Protein Crystallography.* 1997; 33:22–24.
54. Vagin A, Teplyakov A. MOLREP: An Automated Program for Molecular Replacement. *J Appl Crystallogr.* 1997; 30:1022–1025.

55. Vagin AA, Murshudov GN, Strokopytov BV. BLANC: The Program Suite for Protein Crystallography. *J Appl Crystallog.* 1998; 31:98–102.
56. Ran FA, Hsu PD, Wright J, Agarwala V, Scott DA, Zhang F. Genome Engineering Using the CRISPR-Cas9 System. *Nat Protoc.* 2013; 8:2281–2308.
57. Becker HM, Hirnet D, Fecher-Trost C, Sültemeyer D, Deitmer JW. Transport Activity of MCT1 Expressed in *Xenopus* Oocytes Is Increased by Interaction with Carbonic Anhydrase. *J Biol Chem.* 2005; 280:39882–39889.
58. Tu CK, Silverman DN. Solvent Deuterium Isotope Effects in the Catalysis of Oxygen-18 Exchange by Human Carbonic Anhydrase II. *Biochemistry.* 1982; 21:6353–6360.
59. Price GD, Badger MR. Isolation and Characterization of High CO<sub>2</sub>-Requiring-Mutants of the Cyanobacterium *Synechococcus* PCC7942 : Two Phenotypes That Accumulate Inorganic Carbon but Are Apparently Unable to Generate CO<sub>2</sub> within the Carboxysome. *Plant Physiol.* 1989; 91:514–525.
60. Cimperman P, Baranauskienė L, Jachimovičiūtė S, Jachno J, Torresan J, Michailovienė V, Matulienė J, Sereikaitė J, Bumelis V, Matulis D. A Quantitative Model of Thermal Stabilization and Destabilization of Proteins by Ligands. *Biophys J.* 2008; 95:3222–3231.
61. The PyMOL Molecular Graphics System, version 1.5.0.1.; Schrödinger, LLC.: New York, 2012.





# CHAPTER 6

Hypoxia-activated prodrugs and  
(lack of) clinical progression:  
the need for hypoxia-based  
biomarker patient selection in  
phase III clinical trials

Linda Spiegelberg, Ruud Houben, **Raymon Niemans**, Dirk de Ruyscher, Ala Yaromina,  
Jan Theys, Christopher Guise, Jeff B. Smaill, Adam V. Patterson, Philippe Lambin, Ludwig  
Dubois

*In preparation.*

## Abstract

Hypoxia-activated prodrugs are designed to specifically address the hypoxic cells of tumors, which are an important cause of treatment resistance to conventional therapies. Despite promising pre-clinical and clinical phase I and II results, the most important of which are listed in this review, the implementation of hypoxia-activated prodrugs in the clinic has, so far, not been successful. The lack of stratification of patients based on tumoral hypoxia status, which can vary widely, is sufficient to account for the failure of phase III trials. To increase the beneficial effect of hypoxia-activated prodrugs, hypoxia stratification of patients is needed. Here, we propose a biomarker-stratified enriched phase III study design in which only biomarker-positive (i.e. hypoxia-positive) patients are randomized between standard treatment and the combination of standard treatment with hypoxia-activated prodrugs. This implies the necessity of a phase II study in which the threshold for the hypoxia biomarker of choice will be evaluated. The total number of patients needed for both clinical studies is far lower than in currently used randomize-all designs. Furthermore, we elaborate on the improvements in HAP design that are feasible to increase the treatment success rates.

## Introduction

Tumor hypoxia is a well-known tumor microenvironmental parameter present in most solid tumors which hampers the efficacy of conventional anti-cancer treatments. Blood vessels within rapidly expanding tumor tissue often fail to develop properly, being primitive (dilated and leaky), chaotic (irregular and tortuous) and dysfunctional (blind ends and arteriovenous shunts). Two forms of tumor hypoxia can be distinguished, namely diffusion-limited (chronic), and perfusion-limited (acute) [1]. Both radiotherapy (RT) and chemotherapy are dependent on the blood supply to exert their effects. In case of radiotherapy, oxygen reacts rapidly to modify the fundamental biological lesion that is caused by ionizing radiation [2]. This produces permanent DNA damage, while in the absence of oxygen much of the damage can be restored by the cells itself, rendering a hypoxic cell to be three times more resistant to RT [3]. Chemotherapeutic resistance is caused by several hypoxia-related factors. First of all, the hypoxic cells of the tumors are difficult to reach, existing in a pharmacological sanctuary due to the aberrant blood supply. Additionally, decreased cellular proliferation, lost sensitivity to p53-mediated apoptosis and upregulation of genes involved in drug resistance also contribute to hypoxia-related chemoresistance [4, 5]. Furthermore tumor hypoxia leads, through hypoxia inducible factor (HIF)-related gene expression and the unfolded protein response (UPR), to an increased metastatic potential and thus poorer outcome [6]. Hypoxia is an attractive target for anti-cancer therapies, since it is uniquely present in tumors and is a key factor that leads to rapid disease progression and poor prognosis [7].

Tumor hypoxia can be addressed in different ways and approaches are primarily based on oxygen modification strategies, oxygen mimetics and cytotoxic agents. Oxygen modification strategies aim to either increase tumor oxygenation or decrease oxygen consumption of cells. Hyperbaric oxygen therapy, hyperthermia and carbogen breathing combined with nicotinamide have been used in clinical trials as adjuvant therapies to increase tumor oxygenation. In hyperbaric oxygen therapy, 100% oxygen is breathed under elevated pressure, leading to systemically increased oxygen tension [8]. Hyperthermia, the mild local elevation of temperature, leads to dilatation of blood vessels thereby stimulating blood flow [9]. Carbogen (95% oxygen, 5% carbon dioxide) breathing in combination with the vasodilator nicotinamide also increases blood flow, thereby decreasing hypoxia. The latter has been clinically investigated in combination with accelerated radiotherapy (ARCON trial) [10, 11]. However, the beneficial effect on survival and outcome of these therapies is still debated and the high costs, difficulty of practical planning and toxicities prevent them from wide clinical use [12-15]. Decreasing hypoxia by reducing the cellular oxygen consumption using e.g. metformin, an inhibitor of mitochondrial complex 1 activity [16], has been shown to increase tumor radiosensitivity in a

mouse xenograft model [17] and is currently under investigation in a phase II trial in cervix cancer (NTC02394652).

Oxygen mimetics are used to sensitize hypoxic cells to radiation by replacing oxygen in the millisecond chemical reactions needed to fix DNA damage. Although in vitro and in vivo studies were promising, clinical use was hampered by the high doses that were needed to achieve radiosensitizing effects, giving rise to significant toxicities [18].

Lastly, hypoxic cells can be directly sterilized by hypoxia-activated prodrugs (HAPs). Different classes of HAPs exist, all of which are activated by reduction facilitated by cellular oxidoreductases [19]. Typically, the initial reduction event is reversible in the presence of oxygen. Under hypoxia DNA-reactive cytotoxins are formed that kill the hypoxic cells [20]. Several HAPs have been developed and are under extensive preclinical- and clinical evaluation. This review summarizes the (pre)clinical development of two clinically advanced HAPs (PR-104 and TH-302), addresses different hypoxia-related biomarkers and finally proposes a clinical trial design with biomarker assessment for phase III studies that may result in positive studies and thus clinical implementation of this promising anti-cancer therapy.

## The road to clinical failure

6

### Tirapazamine

TPZ is the first HAP that was evaluated and after extensive preclinical testing, demonstrated clinical safety in 1994 [21]. Despite early promise results of phase III clinical trials were disappointing; no therapeutic benefit could be established compared to standard chemoradiotherapy or chemotherapy alone [22]. It was hypothesized that the lack of effect was due to poor extravascular transport due to excessive drug consumption, coupled with the observation that TPZ is activated under relatively mild hypoxia also present in liver, GI tract and bone marrow, which may have contributed to toxicities. Notably, the aromatic *N*-oxide class is prone to rapid redox cycling [23] which may account for other dose limiting side effects such as muscle cramping and severe fatigue. Several analogues of tirapazamine with improved diffusion properties have been developed but none have progressed to clinical trials [24].

### PR-104

Novel HAPs, activated under lower levels of hypoxia compared to TPZ, have been developed [25]. Examples include PR-104, which upon activation gives rise to a relatively stable cytotoxic metabolite

that can diffuse from the hypoxic cell to neighboring, normoxic cells, creating a localized bystander effect [26].

This HAP is a dinitrobenzamide mustard and has undergone broad preclinical and clinical investigation. The HAP contains a latent nitrogen mustard moiety that becomes activated under severe hypoxia and causes cell kill by inducing DNA cross-links [27]. Several preclinical studies have investigated the effect of PR-104 in different xenograft tumor models, either as monotherapy or in combination with standard anti-tumor therapies. In tumor growth delay and tumor excision assays PR-104 was proven to be effective, in terms of increased cell kill or inhibition of tumor growth. Furthermore, combination of PR-104 with radiotherapy or chemotherapy enhanced these effects [25, 27-30]. Direct comparison with TPZ indicated superiority of PR-104 presumably caused by its bystander effect [25, 27]. This bystander effect is hard to prove *in vivo*, but *in vitro* models have been established. Wilson et al used a multicellular layered cell culture system and showed lack of bystander effect in TPZ, whereas three dinitrobenzamide agents provided efficient bystander effects [26]. Clinical safety and tolerability of PR-104 was evaluated in patients with solid tumors refractory to standard treatment [31]. In this study, with an every 3-week schedule, PR-104 was well tolerated with neutropenia as the primary toxicity. McKeage and colleagues investigated a weekly administration schedule and found that thrombocytopenia (decrease of thrombocytes leading to excessive bleeding) and neutropenia were the dose limiting toxicities (DLTs). Therefore, a short course of treatment combined with radiotherapy was proposed [32]. A recent phase I study in patients with myeloid leukemia suggested the safe use of lower doses PR-104 in combination therapies [33]. However, the phase I study of Abou-Alfa and colleagues, in which PR-104 was combined with the tyrosine kinase inhibitor Sorafenib in advanced hepatocellular carcinoma, was stopped because the therapy was poorly tolerated by patients [34]. Combination with the chemotherapeutics gemcitabine or docetaxel in advanced solid tumors was also halted due to dose-limiting thrombocytopenia [35]. Another study using PR-104 and docetaxel in non-small cell lung cancer was terminated early because interim analysis showed a low probability of significant results (NCT00862134).

Apart from the hypoxic activation of PR-104, Guise and colleagues showed that aldo-keto reductase 1C3 (AKR1C3) is able to reduce PR-104 into its active form independent of oxygen [36]. AKR1C3 is highly expressed in different tumor cell lines and could therefore provide a more individualized target for PR-104 treatment of patients. However, AKR1C3 metabolism negates hypoxia targeting and expression was also shown in normal human tissues, including bone marrow cells which likely suppressed the therapeutic index of PR-104. Two of the above mentioned clinical studies that were terminated ([34] and NCT00862134) were based on the high AKR1C3 expression in the tumor (hepatocellular carcinoma and non-small cell lung cancer respectively). The possibility to use tumor

AKR1C3 expression as an individualized target for PR-104 treatment has not proven successful, and the activation of the prodrug in normal tissues opposes its further use in anti-cancer treatment.

### **TH-302 (Evofosfamide)**

Another HAP that has undergone clinical testing is TH-302, a 2-nitroimidazole-based nitrogen mustard prodrug. Under hypoxia its reduction leads to the release of isophosphoramidate mustard (IPM) which alkylates DNA. However the IPM active metabolite is charged at physiological pH [37] suggesting it will not readily diffuse through membranes to surrounding cells to exert its cytotoxic effect. Preclinical research regarding the effect of TH-302 in *in vivo* tumor models is more widespread. As for PR-104, TH-302 has been tested as monotherapy as well as in different combinations with existing anticancer therapies. TH-302 monotherapy inhibited tumor growth and combination with chemo- or radiotherapy significantly enhanced the effect in most studies and models [38, 39]. In an extensive monotherapy study using 11 xenograft models, Sun et al found a good correlation between the hypoxic fraction in the tumor measured at baseline by pimonidazole immunohistochemical staining and TH-302 efficacy [40]. In the three non-responding tumor models, hypoxic fractions were below 5%. Additionally, a causal relationship was found between the tumor oxygenation levels and the therapeutic efficacy. This effect was confirmed in a study of Peeters et al [41] and provides a proof-of-principle for TH-302 activity in hypoxic tumor cells. Furthermore, several studies have shown that the response to TH-302 could be predicted using different imaging methods [41, 42].

Besides the combination of TH-302 with chemo- or radiotherapy, other approaches have been used to augment the effect of TH-302. The exacerbation of transient hypoxia by either hydralazine or pyruvate has been tested and in both cases tumor growth delay was increased [43-45]. Hypoxia modification seems therefore feasible and triple combination with chemo- or radiotherapy could further enhance treatment outcome. However, optimal treatment schedules should be carefully considered since the increased hypoxia may oppose the effect of chemo- or radiotherapy. Other recent studies aimed to enhance the cytotoxicity of TH-302 by sensitizing tumor cells to DNA-damage induced apoptosis using Chk1 or mTOR-inhibitors, and showed enhanced anti-tumor activity [46, 47].

Clinical safety and therapeutic efficacy testing in several phase I and II studies with TH-302 led to promising results. TH-302 was well tolerated with dose limiting skin and mucosal toxicities. The combination of TH-302 with doxorubicin resulted in increased hematologic toxicity of doxorubicin, but this was manageable with prophylactic growth factor support. Evidence of anti-tumor activity was established, as well as a favorable progression free survival, overall survival and tumor response [48-51]. This paved the way for phase III clinical trials, the results of which were eagerly awaited. Two extensive trials, with more than 600 patients each, were carried out in advanced pancreatic

cancer (MAESTRO; NCT01746979) and soft tissue sarcoma (TH CR-406/SARC021) and evaluated the effect on overall survival of the addition of TH-302 to conventional therapies (gemcitabine and doxorubicin, respectively) [52]. Both trials failed to meet their primary endpoints of improving overall survival. However, for the MAESTRO trial, the hazard ratio of 0.84 nearly reached significance ( $p=0.0588$ ). The researchers pointed out three potential factors explaining these disappointing findings. Firstly, the placebo-group performed better than the initial assumptions and secondly, slightly more patients in the control-arm received second-line therapy following disease progression than in the experimental arm [53]. Finally, intent to treat rules led to 2 patients out of 693 being randomly assigned to receive TH-302 + gemcitabine but, due to delays, eventually led to receiving gemcitabine + placebo following re-randomization. Statistical analysis of overall survival by treatment-received, rather than intent-to-treat, did achieve significance ( $p=0.0485$ ).

Because of these negative trials, TH-302 appears to follow in the footsteps of TPZ, whereby neither have achieved positive phase III results after promising phase I and II studies. Remarkably, all trial designs lacked one critical feature, namely the assessment of the levels of tumoral hypoxia. It has been shown in a broad range of tumors that hypoxia levels can vary widely [54, 55]. For pancreatic cancer, values ranging from 0-26% are reported [56]. Patients with a low hypoxic fraction are not expected to benefit from combination treatment. In the MAESTRO trial, where results were approaching significance, it would have been of great importance to have information regarding the hypoxic status of the tumors of each individual patient.

## Hypoxia selection by biomarkers

In different studies, tumor hypoxia was shown to be a prognostic biomarker, indicative for treatment outcome independent of the applied therapy [57, 58]. On the other hand, it could also be applied as a predictive biomarker, potentially forecasting the efficacy of treatment. The need to measure hypoxia is therefore evident and, to date, multiple approaches exist to detect hypoxia either directly or indirectly.

Direct  $pO_2$  measurements using oxygen electrodes inserted into the tumor have been used extensively to determine the oxygenation status of solid tumors. The procedure is safe, although highly invasive and thus repeated measurements are not feasible. Furthermore, since no discrimination between necrotic and hypoxic areas can be made, the amount of hypoxic tissue can be overrated and the fact that it requires skillful personnel to operate the system makes the inter-operator variability

high [59]. Direct imaging of oxygen using  $^{19}\text{F}$  MRI or blood oxygen level dependent MRI (BOLD MRI) is also possible, however these have their own limitations. In the case of  $^{19}\text{F}$  MRI, local injections into the tumor are necessary while in BOLD MRI the signal can be influenced by factors other than hypoxia, resulting in low specificity [60]. A promising MRI technique proposed by O'Connor and colleagues is oxygen enhanced MRI (OE-MRI), which is less invasive and potentially more specific [61, 62].

Indirect methods can be based on exogenous or endogenous markers for hypoxia. Exogenous injectable markers include different 2-nitroimidazole compounds such as pimonidazole and EF5 [57]. They form stable adducts with macromolecules only at low oxygen tension, which can be detected by antibodies and quantified immunohistochemically. However, additional tumor biopsies and expertise in staining quantification are needed for this purpose. Therefore, clinical usage remains limited and validation is still needed. When labeled with  $^{18}\text{F}$ , these 2-nitroimidazole compounds can also be used to image hypoxia using noninvasive positron emission tomography (PET). Well-known PET tracers for hypoxia include FMISO, FAZA and HX4 (extensively summarized in [63]). FMISO, the first tracer that was developed and the one that has been studied most extensively, could identify hypoxia in different human tumors [55], although limited clearance of the unbound tracer due to its high lipophilicity leads to low tumor specificity. FAZA and HX4 partly overcome that problem because they are more hydrophilic. FMISO and FAZA were clinically shown to have prognostic potential [64, 65]. In a simulation study, HX4 showed the highest clearance and image contrast, but also the largest patient-to-patient variability [66]. A preclinical study that compared HX4, FAZA and FMISO in a rat rhabdomyosarcoma model showed different characteristics for the tracers regarding tumor-to-background ratio, spatial reproducibility and sensitivity to oxygen modification, perhaps making it a challenge to identify the optimal hypoxia tracer [67].

Endogenous markers of hypoxia are based on the biological consequences of hypoxia. Hypoxia stabilizes hypoxia inducible factor 1 (HIF-1) which in turn regulates the expression of certain proteins and genes. In this respect the expression of HIF-1 itself, and its downstream targets such as carbonic anhydrase IX (CAIX) and glucose transporter 1 (Glut-1) have been investigated immunohistochemically and it was shown that elevated expression is in general associated with poorer outcome in patients with certain solid tumors [68, 69]. However, correlation with direct  $\text{pO}_2$  measurements is minimal and these proteins can be influenced by factors other than hypoxia.

To improve specificity, various hypoxia gene expression signatures have been developed by different groups [70]. For example, Toustrup and colleagues identified 15 hypoxia responsive genes in head and neck squamous cell carcinomas that could characterize the hypoxic state of a tumor, and showed that they were associated with a poorer clinical outcome. Also, this outcome could be improved by

hypoxic modification using nimorazole [71].

The measurement of secreted markers in the blood would be a faster and easier method to establish tumor hypoxia, without the need for biopsy material. In this respect, plasma osteopontin (OPN) has been shown to be associated with tumor  $pO_2$  in a few studies [68]. Furthermore, OPN levels were shown to be an independent prognostic marker for head and neck squamous cell carcinoma (HNSCC) [72]. Although this method is non-invasive and offers the opportunity to do serial measurements, this indirect method could suffer from systemic influences.

Altogether, it is not obvious which biomarker will be the most useful for patient selection in clinical trials. All available methods and biomarkers to assess tumor hypoxia have their advantages and disadvantages. Since tumor hypoxia is heterogeneous and dynamic, probably a combination of biomarkers is necessary to identify patients with hypoxic tumors.

## Improved hypoxia-activated prodrugs

Each HAP candidate is a bespoke invention [38, 39, 73]. The diversity of pharmacophores and their mechanism of action indicate every HAP candidate will have tailored requirements as design criteria for optimal activity are stringent [74]. It is notable that several HAPs were identified through in vitro screening campaigns that selected for the pharmacodynamic (PD) endpoint of maximal individual cell kill under low cell density conditions [75, 76]. This process of employing anti-proliferative assays generally favors selection of HAP candidates with high rates of reductive metabolism coupled with poor or zero diffusion of cytotoxic metabolites, since both features act to maximize the measured endpoint of individual cell sterilization in low-cell density monolayers.

It has been demonstrated that selecting an optimal HAP benefits from sophisticated multi-parameter modelling to carefully balance drug diffusion/consumption for adequate tissue penetration and thus maximize distal hypoxic cell kill [25, 77, 78]. For example, the clinical failure of TPZ is likely due, in part, to poor tissue penetration [77, 78] and inadequate oxygen inhibition [25], with toxicity preventing schedule/dose intensification [79]. HAPs such as PR-104 [27] possess several optimal properties, including good extravascular transport (tissue penetration) [20, 74], strict oxygen inhibition ( $K_{O_2} \sim 0.1 \mu M$ ) [80] and adequate cytotoxic metabolite redistribution ('bystander effect') [26, 81]. Disappointingly, several unforeseen problems led to the subsequent clinical failure of PR-104, most notably the aerobic activation of PR-104A by human aldo-keto reductase 1C3 (AKR1C3)

[82] and high levels of circulating cytotoxic metabolites [83]. Both features likely contributed to the dose-limiting myelotoxicity in clinical trials [32].

Optimizing HAP design for maximal bystander effect is also challenging. It typically encourages selection of candidates with more lipophilic metabolites, ignoring the rules of lipophilic efficiency which can have negative consequences, such as high protein binding, excessive microsomal metabolism and poor formulation properties [84-86]. Further, given bystander effects operate at the micron scale (< 0.1 mm) and intratumor heterogeneity of hypoxia is generally a macro scale (> 100 mm) phenomenon, the proposed solution does not strictly address the problem. Thus, while controlled metabolite redistribution may exert certain benefits such as overcoming localized cell-to-cell heterogeneity of oxidoreductases or oxygen concentration, it is not the panacea of successful HAP design. There is a need for predictive biomarkers to guide clinical development of HAPs, including identification of the oxidoreductase enzymes necessary to catalyze their activation via electron donation. The human flavoproteome, comprising 79 unique flavoenzymes [87], likely plays a major role in the bioreductive transformation of HAPs, which is in agreement with the known involvement of individual oxidoreductases [88-102]. Approaches aimed at identifying these key catalytic proteins, their relative contributions and tissue distributions will ultimately guide the clinical application of HAPs.

## Clinical trial design optimization

The phase III studies for TPZ and TH-302 had roughly the same trial design, in which all patients were randomized to receive either standard of care, or the combination of standard treatment with the HAP. Biomarker assessment was not incorporated in the design of these studies, although in some cases retrospective information about hypoxia status was available. For example, a retrospective study on the Danish Head And Neck Cancer 5 trial using the aforementioned 15 hypoxia gene signature showed that the radiosensitizer nimorazole only benefitted the hypoxic group [71]. Recently, this signature has been technically validated [103] and was found suitable for use in prospective studies. An EORTC phase III trial in which non-responders (patients with less hypoxic tumors) are randomized for treatment with or without nimorazole is currently recruiting patients (NCT02661152) to verify whether the routinely used nimorazole can be omitted for less hypoxic HNSCC patients. Plasma OPN levels were retrospectively detected in a subset of patients from a phase III trial of carboplatin/paclitaxel with or without TPZ [104]. It was shown that pretreatment plasma levels of OPN were significantly associated with patient response and that it thus may have utility as a prognostic biomarker. Rischin and colleagues applied FMISO-PET hypoxia scans pre- and

mid-treatment in a subset of patients from a larger multi-centered phase II tirapazamine trial [105]. The risk of loco-regional failure in the patients with hypoxic tumors was significantly higher when patients were treated by standard therapy, compared with combination therapy.

These retrospective results strongly indicate that assessing the hypoxia status of tumors is of utmost importance to guide the success of HAPs. However, in the aforementioned studies, lack of hypoxia evaluation in patients hampers robust clinical development. For future prospective clinical trials, hypoxia status assessment should be incorporated. Not only will this increase the chance of demonstrating the beneficial effect of HAPs, but fewer patients will be needed to do so.

First of all, regardless of the biomarker that will be used, a clear threshold must be established in order to categorize patients into biomarker-positive and biomarker-negative. This should be done in a phase II setting since these studies are designed to determine whether new treatments show promising effects for further testing in phase III trials. As such, a single arm study design is usually sufficient for phase II studies. However, this becomes less straightforward in treatment regimens that are expected to have an effect in a selected (e.g. biomarker-positive) patient population only. This is also important for an adequate assessment of the expected treatment effect for a phase III study and subsequently an adequate power and sample size determination. Biomarker-adaptive designs or biomarker-stratified phase II studies have been developed to address the issue of identifying a possible biomarker-positive threshold and have been recently reviewed [106]. Some examples worth mentioning are the Multi-arm multi-stage, the Adaptive parallel Simon two-stage and the Tandem two-stage design.

In Multi-arm multi-stage designs [107], multiple treatment arms are tested simultaneously, but some are dropped early for futility. The different arms can be made up of different treatment regimens, but also of different patient groups with respect to biomarker classification. In the first stage of the Adaptive parallel Simon two-stage design [108], two parallel phase II studies are performed. In case of efficacy in both arms, biomarker selection will be stopped in the second stage. In case of efficacy in the biomarker-positive group only, the second stage will be completed with inclusion of biomarker-positive patients only. In the Tandem two stage design [109], a phase II study is started with an unselected patient population. If the treatment appears effective after the first stage, the study is completed by including patients from the unselected population. If the first stage is unsuccessful, a second trial is started in a selected population.

The practical implications of these designs can be shown by an example. As a reference, a standard

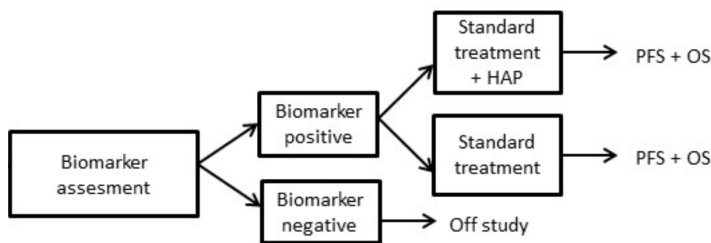
optimal two-stage phase II design is used [110]. Alpha and beta for all calculations are set at 0.05 and 0.20 respectively. Median survival of a poor (reference) treatment is determined at 12 months and the hazard ratio (HR) of a more active treatment is assumed to be 0.60. This corresponds to survival probabilities at 12 months of 0.50 for the reference treatment and 0.66 for a more active treatment. The sample size for the first stage of the study is 21 patients. If 11 or fewer patients respond to the treatment, the study is terminated. If the trial goes on to the second stage, a total of 72 patients will be studied. If the total number responding is less than or equal to 42, the new treatment is rejected. When applying this example on a Multi-arm multi-stage design, the sample size will depend on the number of arms. Each arm will have at most 72 patients, but it is likely that some arms will be terminated after 21 patients. In the adaptive parallel Simon two-stage design, two phase II studies are started. After 21 patients per study for the first stage, one of the trials is stopped. The other is continued until 72 patients have been included. This brings the total number to 93 patients. In the Tandem two stage design, the number of patients depends on the number of times that the first stage is unsuccessful. So, at the very least 72 patients will be included, and an additional 21 for each first stage that is terminated.

In conclusion, establishing a threshold for biomarker positive patient selection can increase the number of patients needed in a phase II study. However, adequate patient selection based on the predictive or prognostic evidence of a biomarker can increase power and/or decrease the required sample size for a subsequent phase III trial.

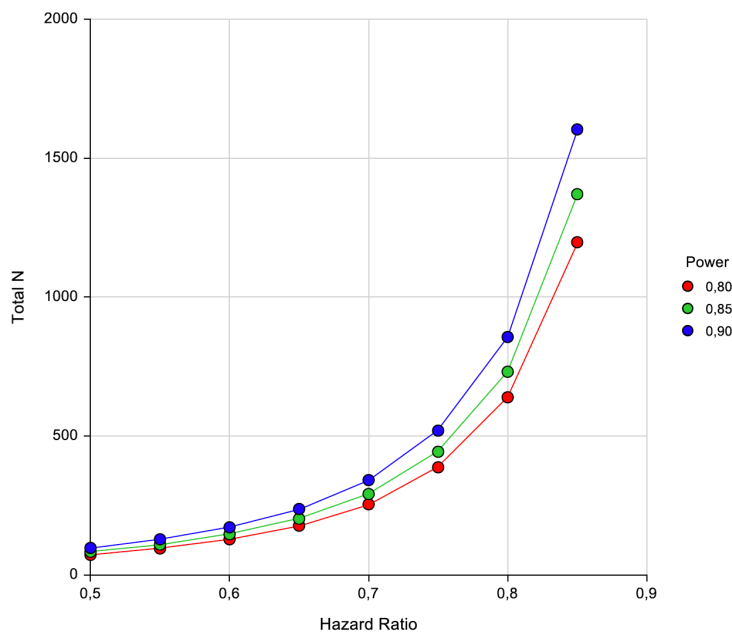
6

Multiple reviews have addressed the numerous phase III trial designs in which biomarkers can be incorporated [111-113]. For hypoxia-activated prodrugs we propose the targeted or enriched design, in which only the biomarker-positive patients are randomized between standard treatment and standard treatment in combination with the HAP (Figure 1). This design is commonly used, and is appropriate when there is preliminary evidence to suggest that treatment benefit is only expected in biomarker-positive patients. When an appropriate cut-off point has been established (in the aforementioned phase II study), the study is very efficient, increases the power and, above all, requires a small sample size. By using biomarker-stratification, the HR is expected to be much lower than in a randomize-all design, which affects the number of patients needed for the study in order to demonstrate a significant difference of the treatment regimen. Figure 2 shows numbers of patients needed for different HRs and different power levels assuming a median survival control of 12 months. Based on retrospective information about hypoxia status in previous studies [11, 114], we presume that a decline of HR of 0.3 is feasible when HAP treatment is only given to hypoxia-positive patients instead of to the whole group of patients. When assuming a HR of 0.8 for the whole group

of patients, this means that 109 patients would be needed for this phase III study compared to 951 when all patients are randomized (with a power of 0.9). This huge difference in total number of patients needed in phase III more than compensates for the extra patients needed in the phase II biomarker optimization phase. Even with lower differences in HR, a large difference in patients needed to show a significant effect of the therapy exists. This will mean a shorter time period to complete the study and assist patients to avoid potentially futile treatment regimens, an ethically responsible approach that will lead to reduced costs.



**Figure 1:** Enriched/targeted study design



**Figure 2:** number of patients needed per hazard ratio for different levels of power.

## Conclusion

The high incidence of tumor hypoxia in cancer and its associated poor prognosis justifies expansion of ongoing efforts to address this unmet need. Hypoxia is arguably the best validated target in oncology yet to be addressed by a successful therapy. Surprisingly, 50 years of HAP design has failed to yield a clinically approved agent. The reasons for this failure are multifaceted, some of which are addressed in this review. Current phase III studies have omitted to stratify patients based on the hypoxia-status of the tumor. A biomarker-stratified enriched study design, with upfront assessment of the hypoxia biomarker threshold, will increase the chance to proof the beneficial effect of HAPs with fewer patients needed and subsequent implementation in clinical practice. The oncology community has the requisite tools to achieve success and they should be utilised constructively.

## References

1. Harris, A.L., *Hypoxia--a key regulatory factor in tumour growth*. Nature reviews. Cancer, 2002. **2**(1): p. 38-47.
2. Lomax, M.E., L.K. Folkes, and P. O'Neill, *Biological consequences of radiation-induced DNA damage: relevance to radiotherapy*. Clin Oncol (R Coll Radiol), 2013. **25**(10): p. 578-85.
3. Brown, J.M., *The hypoxic cell: a target for selective cancer therapy--eighteenth Bruce F. Cain Memorial Award lecture*. Cancer Research, 1999. **59**(23): p. 5863-5870.
4. Brown, J.M. and W.R. Wilson, *Exploiting tumour hypoxia in cancer treatment*. Nature reviews. Cancer, 2004. **4**(6): p. 437-447.
5. Cosse, J.-P.P. and C. Michiels, *Tumour hypoxia affects the responsiveness of cancer cells to chemotherapy and promotes cancer progression*. Anti-cancer agents in medicinal chemistry, 2008. **8**(7): p. 790-797.
6. Lu, X. and Y. Kang, *Hypoxia and hypoxia-inducible factors: master regulators of metastasis*. Clinical cancer research : an official journal of the American Association for Cancer Research, 2010. **16**(24): p. 5928-5935.
7. Vaupel, P., *Hypoxia and aggressive tumor phenotype: implications for therapy and prognosis*. Oncologist, 2008. **13** Suppl 3: p. 21-6.
8. Daruwalla, J. and C. Christophi, *Hyperbaric oxygen therapy for malignancy: a review*. World journal of surgery, 2006. **30**(12): p. 2112-2131.
9. Song, C.W., H. Park, and R.J. Griffin, *Improvement of tumor oxygenation by mild hyperthermia*. Radiation research, 2001. **155**(4): p. 515-528.
10. Janssens, G.O., et al., *Quality-of-life after radiotherapy for advanced laryngeal cancer: Results of a phase III trial of the Dutch Head and Neck Society*. Radiotherapy and oncology : journal of the European Society for Therapeutic Radiology and Oncology, 2016. **119**(2): p. 213-220.
11. Janssens, G.O., et al., *Accelerated radiotherapy with carbogen and nicotinamide for laryngeal cancer: results of a phase III randomized trial*. Journal of clinical oncology : official journal of the American Society of Clinical Oncology, 2012. **30**(15): p. 1777-1783.
12. Kelleher, D.K. and P. Vaupel, *No sustained improvement in tumor oxygenation after localized mild hyperthermia*. Advances in experimental medicine and biology, 2010. **662**: p. 393-398.
13. Mallory, M., et al., *Therapeutic hyperthermia: The old, the new, and the upcoming*. Critical reviews in oncology/hematology, 2015.
14. Wenwu, L., et al., *Hyperbaric oxygen and cancer: more complex than we expected*. Targeted oncology, 2013. **8**(2): p. 79-81.
15. Overgaard, J., *Hypoxic radiosensitization: adored and ignored*. Journal of Clinical Oncology, 2007. **25**(26): p. 4066-4074.
16. Gisbergen, V.M.W., A.M. Voets, and M.H.W. Starmans, *How do changes in the mtDNA and mitochondrial dysfunction influence cancer and cancer therapy? Challenges, opportunities and models. ... Research/Reviews in ...*, 2015.

17. Zannella, V.E., et al., *Reprogramming metabolism with metformin improves tumor oxygenation and radiotherapy response*. *Clinical Cancer ...*, 2013.
18. Rockwell, S., et al., *Hypoxia and radiation therapy: past history, ongoing research, and future promise*. *Current molecular medicine*, 2009. **9**(4): p. 442-458.
19. Wilson, W.R. and M.P. Hay, *Targeting hypoxia in cancer therapy*. *Nature reviews. Cancer*, 2011. **11**(6): p. 393-410.
20. Foehrenbacher, A., et al., *Design of optimized hypoxia-activated prodrugs using pharmacokinetic/pharmacodynamic modeling*. *Frontiers in oncology*, 2013. **3**: p. 314.
21. Doherty, N., et al., *Muscle cramping in phase I clinical trials of tirapazamine (SR 4233) with and without radiation*. *International Journal of ...*, 1994.
22. Reddy, S.B. and S.K. Williamson, *Tirapazamine: a novel agent targeting hypoxic tumor cells*. *Expert opinion on investigational drugs*, 2009. **18**(1): p. 77-87.
23. Wardman, P., et al., *Radicals from one-electron reduction of nitro compounds, aromatic N-oxides and quinones: the kinetic basis for hypoxia-selective, bioreductive drugs*. *Biochem Soc Symp*, 1995. **61**: p. 171-94.
24. Hicks, K.O., et al., *Pharmacokinetic/pharmacodynamic modeling identifies SN30000 and SN29751 as tirapazamine analogues with improved tissue penetration and hypoxic cell killing in tumors*. *Clinical cancer research : an official journal of the American Association for Cancer Research*, 2010. **16**(20): p. 4946-4957.
25. Hicks, K.O., et al., *Oxygen dependence and extravascular transport of hypoxia-activated prodrugs: comparison of the dinitrobenzamide mustard PR-104A and tirapazamine*. *International journal of radiation oncology, biology, physics*, 2007. **69**(2): p. 560-571.
26. Wilson, W.R., et al., *Bystander effects of bioreductive drugs: potential for exploiting pathological tumor hypoxia with dinitrobenzamide mustards*. *Radiation research*, 2007. **167**(6): p. 625-636.
27. Patterson, A.V., et al., *Mechanism of action and preclinical antitumor activity of the novel hypoxia-activated DNA cross-linking agent PR-104*. *Clinical cancer research : an official journal of the American Association for Cancer Research*, 2007. **13**(13): p. 3922-3932.
28. Abbattista, M.R., et al., *Pre-clinical activity of PR-104 as monotherapy and in combination with sorafenib in hepatocellular carcinoma*. *Cancer biology & therapy*, 2015. **16**(4): p. 610-622.
29. Benito, J., et al., *Pronounced hypoxia in models of murine and human leukemia: high efficacy of hypoxia-activated prodrug PR-104*. *PloS one*, 2011. **6**(8).
30. Hunter, F.W., et al., *Dual targeting of hypoxia and homologous recombination repair dysfunction in triple-negative breast cancer*. *Molecular cancer therapeutics*, 2014. **13**(11): p. 2501-2514.
31. Jameson, M.B., et al., *A phase I trial of PR-104, a nitrogen mustard prodrug activated by both hypoxia and aldo-keto reductase 1C3, in patients with solid tumors*. *Cancer chemotherapy and pharmacology*, 2010. **65**(4): p. 791-801.
32. McKeage, M.J., et al., *A phase I trial of PR-104, a pre-prodrug of the bioreductive prodrug PR-104A, given weekly to solid tumour patients*. *BMC cancer*, 2011. **11**: p. 432.
33. Konopleva, M., et al., *Phase I/II study of the hypoxia-activated prodrug PR104 in refractory/relapsed acute myeloid*

- leukemia and acute lymphoblastic leukemia*. Haematologica, 2015.
34. Abou-Alfa, G.K., et al., *PR-104 plus sorafenib in patients with advanced hepatocellular carcinoma*. Cancer chemotherapy and pharmacology, 2011. **68**(2): p. 539-545.
  35. McKeage, M.J., et al., *PR-104 a bioreductive pre-prodrug combined with gemcitabine or docetaxel in a phase Ib study of patients with advanced solid tumours*. BMC cancer, 2012. **12**: p. 496.
  36. Guise, C.P., et al., *The bioreductive prodrug PR-104A is activated under aerobic conditions by human aldo-keto reductase 1C3*. Cancer research, 2010. **70**(4): p. 1573-1584.
  37. Millis, K.K., et al., *Comparison of the protonation of isophosphoramidate mustard and phosphoramidate mustard*. J Med Chem, 1995. **38**(12): p. 2166-75.
  38. Guise, C.P., et al., *Bioreductive prodrugs as cancer therapeutics: targeting tumor hypoxia*. Chinese journal of cancer, 2014. **33**(2): p. 80-86.
  39. Phillips, R.M., *Targeting the hypoxic fraction of tumours using hypoxia-activated prodrugs*. Cancer chemotherapy and pharmacology, 2016. **77**(3): p. 441-457.
  40. Sun, J.D., et al., *Selective tumor hypoxia targeting by hypoxia-activated prodrug TH-302 inhibits tumor growth in preclinical models of cancer*. Clinical cancer research : an official journal of the American Association for Cancer Research, 2012. **18**(3): p. 758-770.
  41. Peeters, S.G., et al., *TH-302 in combination with radiotherapy enhances the therapeutic outcome and is associated with pretreatment [18F]HX4 hypoxia PET imaging*. Clinical cancer research : an official journal of the American Association for Cancer Research, 2015.
  42. Stokes, A.M., C.P. Hart, and C.C. Quarles, *Hypoxia Imaging With PET Correlates With Antitumor Activity of the Hypoxia-Activated Prodrug Evofosfamide (TH-302) in Rodent Glioma Models*. Tomography : a journal for imaging research, 2016. **2**(3): p. 229-237.
  43. Bailey, K.M., et al., *Evaluation of the "steal" phenomenon on the efficacy of hypoxia activated prodrug TH-302 in pancreatic cancer*. PloS one, 2014. **9**(12).
  44. Takakusagi, Y., et al., *Pyruvate induces transient tumor hypoxia by enhancing mitochondrial oxygen consumption and potentiates the anti-tumor effect of a hypoxia-activated prodrug TH-302*. PloS one, 2014. **9**(9).
  45. Wojtkowiak, J.W., et al., *Pyruvate sensitizes pancreatic tumors to hypoxia-activated prodrug TH-302*. Cancer & metabolism, 2015. **3**(1): p. 2.
  46. Meng, F., et al., *Enhancement of hypoxia-activated prodrug TH-302 anti-tumor activity by Chk1 inhibition*. BMC cancer, 2015. **15**(1): p. 422.
  47. Sun, J.D., et al., *Combination treatment with hypoxia-activated prodrug evofosfamide (TH-302) and mTOR inhibitors results in enhanced antitumor efficacy in preclinical renal cell carcinoma models*. American journal of cancer research, 2015. **5**(7): p. 2139-2155.
  48. Borad, M.J., et al., *Randomized Phase II Trial of Gemcitabine Plus TH-302 Versus Gemcitabine in Patients With Advanced Pancreatic Cancer*. Journal of clinical oncology : official journal of the American Society of Clinical Oncology,

2015. **33**(13): p. 1475-1481.
49. Chawla, S.P., et al., *Phase II study of the safety and antitumor activity of the hypoxia-activated prodrug TH-302 in combination with doxorubicin in patients with advanced soft tissue sarcoma*. Journal of clinical oncology : official journal of the American Society of Clinical Oncology, 2014. **32**(29): p. 3299-3306.
  50. Ganjoo, K.N., et al., *A phase I study of the safety and pharmacokinetics of the hypoxia-activated prodrug TH-302 in combination with doxorubicin in patients with advanced soft tissue sarcoma*. Oncology, 2011. **80**(1-2): p. 50-56.
  51. Weiss, G.J., et al., *Phase I study of the safety, tolerability, and pharmacokinetics of TH-302, a hypoxia-activated pro-drug, in patients with advanced solid malignancies*. Clinical cancer research : an official journal of the American Association for Cancer Research, 2011. **17**(9): p. 2997-3004.
  52. Tap, W.D., et al., *Doxorubicin plus evofosfamide versus doxorubicin alone in locally advanced, unresectable or meta-static soft-tissue sarcoma (TH CR-406/SARC021): an international, multicentre, open-label, randomised phase 3 trial*. The Lancet. Oncology, 2017. **18**(8): p. 1089-1103.
  53. Available from: <https://gicasy.org/maestro-trial-evofosfamidegemcitabine-pdac-fails-improve-os>.
  54. Mortensen, L., et al., *Identifying hypoxia in human tumors: a correlation study between 18F-FMISO PET and the Eppendorf oxygen-sensitive electrode*. Acta oncologica, 2010. **49**(7): p. 934-940.
  55. Rasey, J.S., et al., *Quantifying regional hypoxia in human tumors with positron emission tomography of [18F]fluoromisonidazole: a pretherapy study of 37 patients*. International journal of radiation oncology, biology, physics, 1996. **36**(2): p. 417-428.
  56. Dhani, N.C., et al., *Analysis of the intra- and intertumoral heterogeneity of hypoxia in pancreatic cancer patients receiving the nitroimidazole tracer pimonidazole*. British journal of cancer, 2015. **113**(6): p. 864-871.
  57. Walsh, J.C., et al., *The clinical importance of assessing tumor hypoxia: relationship of tumor hypoxia to prognosis and therapeutic opportunities*. Antioxidants & redox signaling, 2014. **21**(10): p. 1516-1554.
  58. Hoogsteen, I.J., et al., *Tumor microenvironment in head and neck squamous cell carcinomas: predictive value and clinical relevance of hypoxic markers. A review*. Head & neck, 2007. **29**(6): p. 591-604.
  59. Milosevic, M., et al., *The human tumor microenvironment: invasive (needle) measurement of oxygen and interstitial fluid pressure*. Seminars in radiation oncology, 2004. **14**(3): p. 249-258.
  60. Peerlings, J., et al., *Hypoxia and hypoxia response-associated molecular markers in esophageal cancer: A systematic review*. Methods (San Diego, Calif.), 2017.
  61. Dewhirst, M.W. and S.R. Brier, *Oxygen-Enhanced MRI Is a Major Advance in Tumor Hypoxia Imaging*. Cancer Research, 2016. **76**(4): p. 769-772.
  62. O'Connor, J.P., et al., *Oxygen-Enhanced MRI Accurately Identifies, Quantifies, and Maps Tumor Hypoxia in Preclinical Cancer Models*. Cancer Research, 2016. **76**(4): p. 787-795.
  63. Peeters, S.G., et al., *Current pre-clinical and clinical applications of hypoxia PET imaging using 2-nitroimidazoles*. The quarterly journal of nuclear medicine and molecular imaging : official publication of the Italian Association of Nuclear Medicine (AIMN) [and] the International Association of Radiopharmacology (IAR), [and] Section of the

- Society of... 2014.
64. Eschmann, S.M., F. Paulsen, and M. Reimold, *Prognostic impact of hypoxia imaging with 18F-misonidazole PET in non-small cell lung cancer and head and neck cancer before radiotherapy*. Journal of nuclear ..., 2005.
  65. Mortensen, L.S., J. Johansen, and J. Kallehauge, *FAZA PET/CT hypoxia imaging in patients with squamous cell carcinoma of the head and neck treated with radiotherapy: results from the DAHANCA 24 trial*. Radiotherapy and ..., 2012.
  66. Wack, L.J., et al., *Comparison of [18F]-FMISO, [18F]-FAZA and [18F]-HX4 for PET imaging of hypoxia--a simulation study*. Acta Oncol, 2015. **54**(9): p. 1370-7.
  67. Peeters, S.G., et al., *A comparative study of the hypoxia PET tracers [<sup>18</sup>F]HX4, [<sup>18</sup>F]FAZA, and [<sup>18</sup>F]FMISO in a preclinical tumor model*. International journal of radiation oncology, biology, physics, 2015. **91**(2): p. 351-359.
  68. Le, Q.-T.T. and D. Courter, *Clinical biomarkers for hypoxia targeting*. Cancer metastasis reviews, 2008. **27**(3): p. 351-362.
  69. van Kuijk, S.J., et al., *Prognostic Significance of Carbonic Anhydrase IX Expression in Cancer Patients: A Meta-Analysis*. Frontiers in oncology, 2016. **6**: p. 69.
  70. Harris, B.H., et al., *Gene Expression Signatures as Biomarkers of Tumour Hypoxia*. Clin Oncol (R Coll Radiol), 2015. **27**(10): p. 547-60.
  71. Toustrup, K., et al., *Gene expression classifier predicts for hypoxic modification of radiotherapy with nimorazole in squamous cell carcinomas of the head and neck*. Radiotherapy and oncology : journal of the European Society for Therapeutic Radiology and Oncology, 2012. **102**(1): p. 122-129.
  72. Petrik, D., et al., *Plasma osteopontin is an independent prognostic marker for head and neck cancers*. Journal of clinical oncology : official journal of the American Society of Clinical Oncology, 2006. **24**(33): p. 5291-5297.
  73. Hay, M.P., K.O. Hicks, and J. Wang, *Hypoxia-directed drug strategies to target the tumor microenvironment*. Advances in experimental medicine and biology, 2014. **772**: p. 111-145.
  74. Wilson, W.R., et al., *Targeting tumor hypoxia with prodrugs: Challenges and opportunities*, in *AACR Education Book*. 2008. p. 293-310.
  75. Duan, J.X., et al., *Potent and highly selective hypoxia-activated achiral phosphoramidate mustards as anticancer drugs*. J Med Chem, 2008. **51**(8): p. 2412-20.
  76. Zeman, E.M., et al., *SR-4233: a new bioreductive agent with high selective toxicity for hypoxic mammalian cells*. Int J Radiat Oncol Biol Phys, 1986. **12**(7): p. 1239-42.
  77. Hicks, K.O., et al., *Use of three-dimensional tissue cultures to model extravascular transport and predict in vivo activity of hypoxia-targeted anticancer drugs*. Journal of the National Cancer Institute, 2006. **98**(16): p. 1118-1128.
  78. Hicks, K.O., et al., *Multicellular resistance to tirapazamine is due to restricted extravascular transport: a pharmacokinetic/pharmacodynamic study in HT29 multicellular layer cultures*. Cancer Res, 2003. **63**(18): p. 5970-7.
  79. Hancock, S.L., et al., *Clinical evaluation of the hypoxic cytotoxin tirapazamine (SR-4233): phase I experience with repeated dose administration during fractionated irradiation*. Int J Radiat Oncol Biol Phys, 1996. **36**(1).
  80. Hicks, K.O., et al., *Oxygen dependence and extravascular transport of hypoxia-activated prodrugs: comparison*

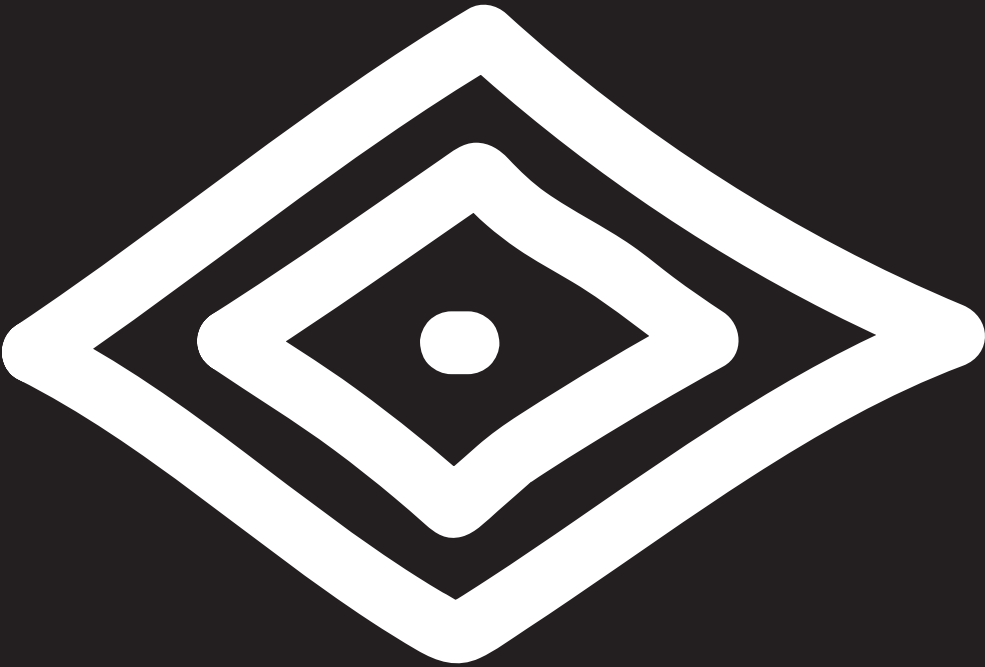
- of the dinitrobenzamide mustard PR-104A and tirapazamine. *Int J Radiat Oncol Biol Phys*, 2007. **69**(2): p. 560-71.
81. Foehrenbacher, A., et al., *The Role of Bystander Effects in the Antitumor Activity of the Hypoxia-Activated Prodrug PR-104*. *Frontiers in oncology*, 2013. **3**: p. 263.
  82. Guise, C.P., et al., *The bioreductive prodrug PR-104A is activated under aerobic conditions by human aldo-keto reductase 1C3*. *Cancer Res*, 2010. **70**(4): p. 1573-84.
  83. Gu, Y., G.J. Atwell, and W.R. Wilson, *Metabolism and excretion of the novel bioreductive prodrug PR-104 in mice, rats, dogs, and humans*. *Drug Metab Dispos*, 2010. **38**(3): p. 498-508.
  84. Arnott, J.A. and S.L. Planey, *The influence of lipophilicity in drug discovery and design*. *Expert Opin Drug Discov*, 2012. **7**(10): p. 863-75.
  85. Leeson, P.D. and B. Springthorpe, *The influence of drug-like concepts on decision-making in medicinal chemistry*. *Nat Rev Drug Discov*, 2007. **6**(11): p. 881-90.
  86. van de Waterbeemd, H., D.A. Smith, and B.C. Jones, *Lipophilicity in PK design: methyl, ethyl, futile*. *J Comput Aided Mol Des*, 2001. **15**(3): p. 273-86.
  87. Lienhart, W.D., V. Gudipati, and P. Macheroux, *The human flavoproteome*. *Arch Biochem Biophys*, 2013. **535**(2): p. 150-62.
  88. Guise, C.P., et al., *Diflavin oxidoreductases activate the bioreductive prodrug PR-104A under hypoxia*. *Mol Pharmacol*, 2012. **81**(1): p. 31-40.
  89. Guise, C.P., et al., *Identification of human reductases that activate the dinitrobenzamide mustard prodrug PR-104A: a role for NADPH:cytochrome P450 oxidoreductase under hypoxia*. *Biochem Pharmacol*, 2007. **74**(6): p. 810-20.
  90. Hunter, F.W., et al., *The flavoprotein FOXRED2 reductively activates nitro-chloromethylbenzindolines and other hypoxia-targeting prodrugs*. *Biochem Pharmacol*, 2014. **89**(2): p. 224-35.
  91. Wang, J., et al., *The 2-nitroimidazole EF5 is a biomarker for oxidoreductases that activate the bioreductive prodrug CEN-209 under hypoxia*. *Clin Cancer Res*, 2012. **18**(6): p. 1684-95.
  92. Baumann, R.P., et al., *Reversal of mitomycin C resistance by overexpression of bioreductive enzymes in Chinese hamster ovary cells*. *Cancer Res*, 2001. **61**(21): p. 7770-6.
  93. Hunter, F.W., et al., *Homologous recombination repair-dependent cytotoxicity of the benzotriazine di-N-oxide CEN-209: comparison with other hypoxia-activated prodrugs*. *Biochemical pharmacology*, 2012. **83**(5): p. 574-585.
  94. Meng, F., et al., *Molecular and cellular pharmacology of the hypoxia-activated prodrug TH-302*. *Molecular cancer therapeutics*, 2012. **11**(3): p. 740-751.
  95. Su, J., C.P. Guise, and W.R. Wilson, *FSL-61 is a 6-nitroquinolone fluorogenic probe for one-electron reductases in hypoxic cells*. *Biochem J*, 2013. **452**(1): p. 79-86.
  96. Bailey, S.M., et al., *Involvement of NADPH: cytochrome P450 reductase in the activation of indoloquinone EO9 to free radical and DNA damaging species*. *Biochem Pharmacol*, 2001. **62**(4): p. 461-8.
  97. Belcourt, M.F., et al., *Differential toxicity of mitomycin C and porfiromycin to aerobic and hypoxic Chinese hamster ovary cells overexpressing human NADPH:cytochrome c (P-450) reductase*. *Proc Natl Acad Sci U S A*, 1996. **93**(1): p.

- 456-60.
98. Saunders, M.P., et al., *The relative importance of NADPH: cytochrome c (P450) reductase for determining the sensitivity of human tumour cells to the indolequinone EO9 and related analogues lacking functionality at the C-2 and C-3 positions*. *Biochem Pharmacol*, 2000. **59**(8): p. 993-6.
  99. Saunders, M.P., et al., *NADPH:cytochrome c (P450) reductase activates tirapazamine (SR4233) to restore hypoxic and oxid cytotoxicity in an aerobic resistant derivative of the A549 lung cancer cell line*. *Br J Cancer*, 2000. **82**(3): p. 651-6.
  100. Patterson, A.V., et al., *Importance of P450 reductase activity in determining sensitivity of breast tumour cells to the bio-reductive drug, tirapazamine (SR 4233)*. *Br J Cancer*, 1995. **72**(5): p. 1144-50.
  101. Patterson, A.V., et al., *Overexpression of human NADPH:cytochrome c (P450) reductase confers enhanced sensitivity to both tirapazamine (SR 4233) and RSU 1069*. *Br J Cancer*, 1997. **76**(10): p. 1338-47.
  102. Tercel, M., et al., *Hypoxia-activated prodrugs: substituent effects on the properties of nitro seco-1,2,9,9a-tetrahydro-cyclopropa[c]benz[e]indol-4-one (nitroCBI) prodrugs of DNA minor groove alkylating agents*. *Journal of medicinal chemistry*, 2009. **52**(22): p. 7258-7272.
  103. Toustrup, K., et al., *Validation of a 15-gene hypoxia classifier in head and neck cancer for prospective use in clinical trials*. *Acta oncologica (Stockholm, Sweden)*, 2016. **55**(9-10): p. 1091-1098.
  104. Mack, P.C., et al., *Lower osteopontin plasma levels are associated with superior outcomes in advanced non-small-cell lung cancer patients receiving platinum-based chemotherapy: SWOG Study S0003*. *Journal of clinical oncology : official journal of the American Society of Clinical Oncology*, 2008. **26**(29): p. 4771-4776.
  105. Rischin, D., et al., *Prognostic significance of [18F]-misonidazole positron emission tomography-detected tumor hypoxia in patients with advanced head and neck cancer randomly assigned to chemoradiation with or without tirapazamine: a substudy of Trans-Tasman Radiation Oncology Group Study 98.02*. *Journal of clinical oncology : official journal of the American Society of Clinical Oncology*, 2006. **24**(13): p. 2098-2104.
  106. Antoniou, M., A.L. Jorgensen, and R. Kolamunnage-Dona, *Biomarker-Guided Adaptive Trial Designs in Phase II and Phase III: A Methodological Review*. *PLoS One*, 2016. **11**(2): p. e0149803.
  107. Parmar, M.K., et al., *Speeding up the evaluation of new agents in cancer*. *J Natl Cancer Inst*, 2008. **100**(17): p. 1204-14.
  108. Jones, C.L. and E. Holmgren, *An adaptive Simon Two-Stage Design for Phase 2 studies of targeted therapies*. *Contemp Clin Trials*, 2007. **28**(5): p. 654-61.
  109. Pusztai, L., K. Anderson, and K.R. Hess, *Pharmacogenomic predictor discovery in phase II clinical trials for breast cancer*. *Clin Cancer Res*, 2007. **13**(20): p. 6080-6.
  110. Simon, R., *Optimal two-stage designs for phase II clinical trials*. *Control Clin Trials*, 1989. **10**(1): p. 1-10.
  111. Wilhelm-Benartzi, C.S., et al., *Challenges and methodology in the incorporation of biomarkers in cancer clinical trials*. *Critical reviews in oncology/hematology*, 2017. **110**: p. 49-61.
  112. Freidlin, B., L.M. McShane, and E.L. Korn, *Randomized clinical trials with biomarkers: design issues*. *Journal of the National Cancer Institute*, 2010. **102**(3): p. 152-160.
  113. Buyse, M., et al., *Integrating biomarkers in clinical trials*. *Expert review of molecular diagnostics*, 2011. **11**(2):

p. 171-182.

114. Toustrup, K, et al, *Hypoxia gene expression signatures as prognostic and predictive markers in head and neck radiotherapy*. *Seminars in radiation oncology*, 2012. **22**(2): p. 119-127.





# CHAPTER 7

Hypoxic cell killing by  
CP-506, a novel  
hypoxia-activated prodrug

**Raymon Niemans**, Ala Yaromina, Jan Theys, Maria Abbattista, Rianne Biemans, Natasja Lieuwes, Alexandra Mowday, Amir Ashoorzadeh, Sofie Deschoemaeker, Arne Heyerick, Christopher Guise, Jeff B Smaill, Adam V Patterson, Ludwig Dubois, Philippe Lambin

*In preparation.*

## Abstract

Tumor hypoxia, present in the majority of solid tumors, has been associated with poor prognosis and is generally seen as a therapeutic problem. The use of hypoxia-activated prodrugs (HAPs) to eradicate hypoxic cells is a promising approach in cancer treatment. The clinical use of the HAP PR-104 in treatment of solid tumors is limited due to its off-target, aerobic activation by the reductase AKR1C3 and potentially by the undesired *in vivo* glucuronidation of the compound. To tackle these limitations, PR-104 was chemically modified, resulting in the novel HAP CP-506. In the present study we show for the first time promising therapeutic efficacy of CP-506 in 2D and 3D *in vitro* cell culture models and *in vivo* in a series of tumor-bearing animal models. Additionally, in line with an oxygen-dependent cytotoxic effect *in vitro* we demonstrate that CP-506 effectively decreases the hypoxic fraction in some tumor models, with the optimal time point to detect this decrease depending on dosing and tumor model. The hypoxia-specific activation of CP-506 is an important feature, opening opportunities for combination treatment with e.g. radiotherapy and immunotherapy.

## Introduction

The majority of solid tumors contain hypoxic areas, in which cells receive an insufficient oxygen supply due to the tumor outgrowing its already abnormal and chaotic vasculature [1, 2]. Tumor hypoxia has been associated with poor prognosis and is generally seen as a therapeutic problem [2, 3]. The use of hypoxia-activated prodrugs (HAPs) to eradicate these hypoxic cells is a promising approach in cancer treatment. HAPs are prodrugs that release or are activated to an effector, generally a cytotoxin, specifically in a hypoxic micro-environment. For maximal therapeutic potential, HAPs should preferentially be activated at oxygen levels low enough to prevent activation under physiological oxygen conditions. The active metabolite(s) should be able to kill non-proliferating cells present in hypoxic tumor areas. A sufficient bystander effect, i.e. the ability to diffuse from the hypoxic activator cells to the more-oxygenated surrounding cells and kill these too, is another important characteristic of the active metabolite(s), since it increases the efficacy of the HAP [4].

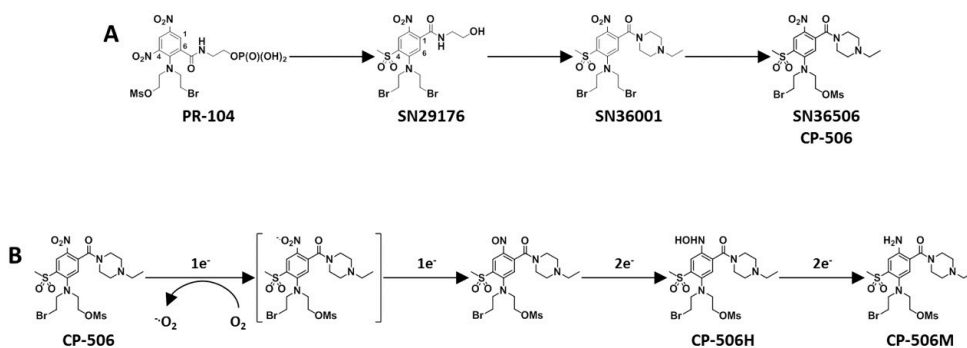
The HAP has to be enzymatically reduced in order to release or activate the effector [5]. The general activation mechanism is provided by one-electron reductases. These reduce the HAP to an inactive intermediate, which, when sufficient oxygen is present, is back-oxidized to the parental HAP and reactive oxygen species (ROS). Superoxide dismutases scavenge these ROS, ensuring that the HAP is not toxic in well-oxygenated tissues. In hypoxic tumor regions, however, this inactive intermediate is further reduced, or fragments, to an active, cytotoxic metabolite [6]. Depending on the HAP, an off-target activation mechanism can be present, in which two-electron reductases bypass the oxygen-sensing intermediate by reducing the HAP immediately to its active metabolite [7].

Several HAPs are being investigated in different stages of clinical development [4, 8]. PR-104 is a pre-prodrug, which in plasma is rapidly hydrolyzed by phosphatases to the prodrug PR-104A. This prodrug is reduced by one-electron reductases (e.g. cytochrome P450 oxidoreductase (POR) and methionine synthase reductase (MTRR) [9, 10]) to an inactive intermediate. When oxygen is present, this intermediate is immediately back-oxidized, whereas in hypoxic conditions it is further reduced to the DNA-crosslinking PR-104H (hydroxylamine) and PR-104M (amine) metabolites [11]. The DNA inter-strand crosslinks caused by these active metabolites disrupt replication forks during mitosis, representing the main mechanism underlying PR-104 cytotoxicity [12, 13]. *In vitro* and *in vivo*, PR-104 was found to be selectively active in hypoxia in a range of cancer cell lines and human

tumor xenografts [14]. Based on these promising results, clinical trials were initiated, however, phase 1 trials testing PR-104 in patients with solid tumors showed dose-limiting myelosuppression, predominantly neutropenia and thrombocytopenia [15, 16]. Severe dose-limiting myelotoxicity was also observed in a phase 2 clinical trial combining PR-104 with gemcitabine or docetaxel [17]. In depth *in vitro* research elucidated that PR-104 can be activated in aerobic conditions and thus in an oxygen-independent manner, by the two-electron reductase aldo-keto reductase 1C3 (AKR1C3) [9, 18]. This reductase is highly expressed in CD4<sup>+</sup> myeloid progenitor cells [19], likely explaining the observed dose-limiting toxic effects in the clinical trials. In advanced hepatocellular carcinoma, the combination of PR-104 and sorafenib was also poorly tolerated due to significant thrombocytopenia and neutropenia [20]. In these patients glucuronidation, which normally greatly contributes to PR-104A clearance in humans [21], is compromised, thus exacerbating the toxicity of PR-104A due to impaired clearance [20-22]. Glucuronidation of PR-104A can also limit its effectiveness by suppressing its nitroreduction [21]. The toxicities of PR-104 prevent plasma concentrations to be high enough for antitumor effects to be observed [15, 16, 23], limiting its clinical applicability in solid tumors. In a phase 1/2 trial in acute myeloid leukemia (AML) and acute lymphoblastic leukemia (ALL), which are AKR1C3 positive, some patients did show a positive response to PR-104 treatment, although no correlation was found between functional AKR1C3 and drug efficacy [24]. PR-104 could thus potentially be used for the treatment of these acute leukemias.

To tackle the limitations of aerobic activation and glucuronidation, PR-104 was chemically modified (Unpublished data; Figure 1A). The intermediate SN29176 was synthesized by changing several functional groups of PR-104. First, the 4-nitro group was replaced by a methylsulfone group, which is not reduced by one-electron reductases but is strongly electron withdrawing. It thereby tunes the 2-nitro group into the correct E1 range to ensure strong oxygen inhibition of nitro-radical formation. This 2-nitro group is thereby the only remaining nitro-group, forcing it to be the site of bioreduction. Second, the functional group at the carbon-6 position was removed and replaced by an amide group at the carbon-1 position, which should prevent AKR1C3 metabolism and thus aerobic activation of the compound. Third, the mesylate group of PR-104 was changed to bromide, since dibromo mustards are preferred for ease of synthesis. Additionally, dibromo mustards have an increased lipophilicity and can therefore more easily diffuse through the cell membrane, expected to increase the bystander effect of the compound. Next, SN36001 was synthesized from SN29176 by replacing the only left alcohol group with a 1-ethyl-piperazine

group. This converts the molecule from a pre-prodrug to a prodrug, i.e. it does not have to be hydrolyzed anymore before it can be reduced (activated). Additionally, since the molecule has no residual alcohol groups, the compound will not be glucuronidated and will thus potentially be cleared slower, increasing plasma exposure. Finally, since compounds with a dibromo mustard group degrade more rapidly, one bromide was replaced back with a mesylate group leading to the final compound SN36506, re-named to CP-506, a novel HAP. In summary, CP-506 is a HAP with favorable properties compared to its predecessor PR-104: it is designed to be resistant to AKR1C3 metabolism and to glucuronidation, to be water soluble, and to have a high bystander effect. Its proposed mechanism of action is similar but not identical to PR-104, lacking aerobic two-electron reduction (Figure 1B), i.e. CP-506 is reduced solely by one-electron reductases to an oxygen sensing intermediate, which is back-oxidized in the presence of sufficient oxygen. In the absence of oxygen, it is further reduced to its active CP-506H (hydroxylamine) and CP-506M (amine) metabolites. These metabolites can kill cells by crosslinking DNA.



**Figure 1:** A) Development route of CP-506 from PR-104. B) Activation mechanism of CP-506. For a detailed description, see text.

In the present study we assessed the hypoxia-selective cytotoxic effects of CP-506 in a series of 2D and 3D *in vitro* models and in *in vivo* human tumor xenograft models.

## Materials & methods

### Cell culture

Cells were routinely cultured at 37 °C in a 5% CO<sub>2</sub> incubator in Dulbecco's Modified Eagle Medium (DMEM; Lonza) (UT-SCC-5, MDA-MB-231, MDA-MB-468, HCT116, H460, H1299, DLD-1, A2780, FaDu, C51, CT26, LLC), Roswell Park Memorial Institute 1640 Medium (RPMI; Lonza) (H1650, LNCaP, PC3, R1), or McCoy's 5A (Modified) Medium (Gibco) (DU145) supplemented with MEM Non-essential Amino Acids (Sigma-Aldrich) (FaDu only) and 10% fetal bovine serum (FBS; Lonza). Tissue of origin of all cancer cell lines are summarized in Table 1. AKR1C3-overexpressing HCT116 cells (HCT116<sup>AKR1C3</sup>) have been generated and validated previously [18].

### Cell viability assays

Cell viability assays were performed in plastic 96-well plates. Alternatively, when cells were not able to survive a 24 h anoxic incubation, the assay was performed in 35 mm glass dishes since glass holds less oxygen and thus does not need a 24 h anoxic incubation before compound exposure to guarantee that cells are fully anoxic. Cells were seeded in either plastic 96-well plates or 35 mm glass dishes and allowed to attach and grow in normoxia (21% O<sub>2</sub>, 5% CO<sub>2</sub>). Culture medium was pre-incubated in normoxia in a normal incubator or in anoxia ( $\leq$  0.02% O<sub>2</sub>, 5% CO<sub>2</sub>, residual N<sub>2</sub>) in an anoxic chamber (MACS VA-500 microaerophilic workstation, Don Whitley Scientific). Dishes and plates were transferred to anoxia and medium was changed with pre-incubated medium for a 24 h anoxic incubation (control plates remained in normoxia). CP-506 was dissolved in pre-incubated medium in the corresponding oxygen condition using dimethyl sulfoxide (DMSO; final concentration 0.1%; Sigma-Aldrich). Culture medium on cells was replaced with CP-506-containing medium, and after a 4 h exposure all plates or dishes were transferred to normoxia, washed with phosphate-buffered saline (PBS) and fresh culture medium was added. After 72 h cell viability was assessed using the alamarBlue® cell viability reagent (Thermo Fisher Scientific) according to the manufacturer's protocol. Treatment response was quantified as IC<sub>50</sub>, i.e. the CP-506 concentration that reduced cell viability by 50%. The hypoxia cytotoxicity ratio (HCR) was calculated by dividing the normoxic IC<sub>50</sub> by the corresponding anoxic IC<sub>50</sub>.

### Multicellular layer clonogenic assays

Multicellular layer (MCL) clonogenic assays were performed as described previously [25]. Briefly, MCLs cells were grown submerged in stirred medium with 10% FBS, penicillin and

streptomycin for 3 days and were exposed to the HAP in 10 mL of the same medium with magnetic stirring for 5 h. With H460 MCLs this was done under either anoxic (95% N<sub>2</sub>, 5% CO<sub>2</sub>) or hyperoxic (95% O<sub>2</sub>, 5% CO<sub>2</sub>) conditions, the latter to extinguish central hypoxia in the MCL. With HCT116 and HCT116<sup>AKR1C3</sup> MCLs this was done in hyperoxic conditions only. MCLs were then trypsinized and single cells were plated for clonogenic survival. Colonies (>50 cells) were grown for 10 days and counted after fixation and staining with 0.2% methylene blue in 50% aqueous ethanol. Treatment response was quantified as IC<sub>10</sub>, i.e. the CP-506 concentration that induced 90% clonogenic cell kill.

### **Spheroid culture**

Spheroids were grown by culturing cells in agarose-coated 96-well plates as previously described [26] or in Corning® Costar® 96-well ultra-low attachment plates (Sigma-Aldrich). After 7 days of culture, half of the culture medium was renewed every 2-3 days. Spheroid growth was monitored with an IX81 inverted microscope (Olympus) equipped with an EXi Aqua camera (QImaging), using the µManager open-source microscopy software [27, 28]. Spheroid sizes were determined using the MATLAB-based and open-source SpheroidSizer software [29].

### **Hypoxia staining in spheroids**

Spheroids were incubated with 20 µg/mL of the hypoxia marker pimonidazole (NPI, Inc.) for 2 h at 37 °C, after which they were collected and snap-frozen. Spheroids were cut into 7 µm sections, which were fixed with ice-cold acetone. Sections were washed with PBS, and non-specific binding was blocked with 0.5% normal goat serum (NGS) in PBS for 30 min at room temperature (RT). Sections were incubated overnight with rabbit anti-pimonidazole antibody (1:250; HP3 kit, NPI, Inc.) at 4 °C. Sections were then washed with PBS and incubated with Alexa Fluor® 488-conjugated goat anti-rabbit IgG antibody (1:500; Thermo Fisher Scientific) for 1 h at RT. Sections were washed with PBS, nuclei were stained with DAPI (300 nM, Thermo Fisher Scientific) for 10 min at RT, sections were washed again, and slides were mounted with cover slips using DakoCytomation fluorescent medium (Dako).

### **Spheroid clonogenic assays**

Spheroids were incubated with CP-506 for 4 h, after which spheroids were collected and trypsinized with 0.5% trypsin-EDTA for 30 min at 37 °C. Single cells were plated for clonogenic survival. Colonies were grown for 10 days and counted after fixation and staining with 0.4% methylene blue in 70% aqueous ethanol.

### Animal models

Animal experiments were performed using adult NMRI-*nu*, NIH-III, CD-1 or CB17 SCID mice. Animal facilities and experiments were in accordance with institutional guidelines for animal welfare and were approved by the responsible animal ethical committees. Cells were resuspended in BD Matrigel™ Basement Membrane Matrix (BD Biosciences) or  $\alpha$ MEM and injected subcutaneously (s.c.) into the lateral flank of the animal. Tumors were measured in two or three dimensions using a caliper. Tumor volume was calculated using the formula  $(a^2 \times b)/2$  or  $(a-0.5) \times (b-0.5) \times (c-0.5) \times \pi/6$  (0.5 mm being a correction for thickness of the skin), respectively. Once tumors reached  $\sim 200 \text{ mm}^3$  (treatment starting volume), mice were randomized into different treatment groups. Group sizes and tumor start volumes are summarized in Supplementary table 1. Mice received one intraperitoneal (i.p.) injection per day of either vehicle (saline or 2% DMSO in water for injection) or CP-506 at the indicated dose for 5 consecutive days (QD5) ( $n = 3-10$  per group). Tumor growth was monitored 3 times per week or daily after treatment, depending on the tumor model. Tumor response was quantified as the time to reach 4 times the starting tumor volume ( $T4 \times SV$ ). Tumor volumes and  $T4 \times SV$  are presented as mean  $\pm$  standard deviation. To estimate the magnitude of treatment effect, enhancement ratio (ER) was determined as the ratio between mean  $T4 \times SV$  of CP-506 and vehicle treated groups.

### Hypoxia staining in tumors

Mice bearing H460, HCT116, or MDA-MB-231 tumors were treated with vehicle/CP-506 (QD5, 800 mg/kg), while mice with MDA-MB-468 were treated with several schedules (QD1: 800 mg/kg, QD3 and QD5: 400 mg/kg). Group sizes are indicated in Supplementary table 1. All animals were injected i.p. with the hypoxia marker pimonidazole (60 mg/kg in saline; NPI, Inc.) 1 h (H460, HCT116, MDA-MB-231), 24 h (MDA-MB-468), 2 d (MDA-MB-231) or 7 d (MDA-MB-231) after the last CP-506 injection and 1 h prior to tumor harvesting. In MDA-MB-231- and MDA-MB-468-tumor-bearing mice another hypoxia marker, CCI-103F (100 mg/kg in 10% DMSO in peanut oil; NPI, Inc.), was injected i.p. 2 h prior to treatment start or 2 h before the last vehicle/CP-506, respectively. Tumors were collected and snap-frozen, and 7  $\mu\text{m}$  sections were cut from the central part of the tumor. Two sections per tumor with inter-section distance of  $\sim 50-64 \mu\text{m}$  were used for analysis. Sections were fixed with ice-cold acetone and nonspecific binding was blocked with 5% NGS in 0.2% PBS-Tween-20 at RT for 30 min. Sections were incubated overnight at 4  $^\circ\text{C}$  with either rabbit anti-pimonidazole antibody (1:250; NPI, Inc) or with a mixture of FITC-labeled mouse anti-pimonidazole antibody (1:100; NPI, Inc.) and rabbit anti-CCI-103F (F6) anti-

body (1:250; NPI, Inc.). Then sections were washed with 0.2% PBS-Tween-20 and incubated for 1 h at RT with either Alexa Fluor® 488-conjugated goat anti rabbit IgG antibody (1:500; Thermo Fisher Scientific) or with Alexa Fluor® 594-conjugated goat anti-rabbit IgG antibody (1:500; Thermo Fisher Scientific). Sections were washed again with 0.2% PBS-Tween-20 and slides were mounted with coverslips using DakoCytomation fluorescent medium (Dako).

Images were acquired as described previously [30]. Three sections were excluded from the analysis due to pronounced cutting or staining artefacts. Hypoxic fractions (HFs) were assessed using the ImageJ software (National Institutes of Health) in a semi-automated way as described previously [30, 31]. The thresholds to define positive areas were defined by one investigator (A.Y.) for each tumor section according to the signal intensity and background staining. The procedure of threshold setting is arbitrary but, on the basis of evaluation of the CCI-103F positive tumor area in 17 tumors independently by A.Y. and J.T., showed to possess good inter-observer reproducibility ( $R^2 = 0.97$ ,  $p < 0.0001$ , Supplementary figure 1). Similar analysis was previously performed for pimonidazole-labeled area and demonstrated low inter-observer variability [31]. HF was calculated as percentage of pixels positive for pimonidazole- or CCI-103F divided by the viable tumor area ( $HF_{pimo}$  and  $HF_{CCI}$ , respectively).

### Statistical analyses

Differences in survival, defined as the fraction of tumors not reaching  $4\times$  start volume ( $4\times SV$ ), between groups were analyzed using a log-rank test. Differences in mean time to reach  $4\times$  start volume ( $T_{4\times SV}$ ) and HFs were analyzed using an unpaired two-tailed t-test.  $p \leq 0.05$  was considered statistically significant. All analyses and statistics were performed using the GraphPad Prism 5.04 software (GraphPad Software, Inc.).

## Results

### Hypoxia selective cytotoxicity of CP-506 in several *in vitro* 2D cultures

To determine the hypoxia selective cytotoxicity of CP-506 in *in vitro* 2D monolayer cultures,  $IC_{50}$  values were determined in a panel of 18 tumor cell lines in normoxic (21%  $O_2$ ) and anoxic ( $\leq 0.02\%$   $O_2$ ) conditions after a 4 h incubation with CP-506 (Table 1). In normoxic conditions,  $IC_{50}$  was reached only in the A2780 and CT26 cell lines; for all other cell lines  $IC_{50}$

was higher than 500  $\mu\text{M}$ , the highest dose of CP-506 tested in these assays, confirming lack of activation in normoxic conditions. In anoxic conditions,  $\text{IC}_{50}$  ranged from 13  $\mu\text{M}$  (R1) to 220  $\mu\text{M}$  (UT-SCC-5). HCRs ranged from >2.3 (UT-SCC-5) to >12.8 (MDA-MB-468) in the human cell lines; the highest HCR (>38.5) was found in the rat cell line R1. Taken together, these data indicate hypoxia selective cytotoxicity of CP-506 in *in vitro* monolayer cultures.

**Table 1:**  $\text{IC}_{50}$  values in normoxic (21%  $\text{O}_2$ ) and anoxic ( $\leq 0.02\% \text{O}_2$ ) conditions after 4 h CP-506 exposure and hypoxia cytotoxicity ratio (HCR, normoxic  $\text{IC}_{50}$  divided by anoxic  $\text{IC}_{50}$ ) of CP-506 in *in vitro* monolayer cultures. All tumor cell lines are of human origin unless otherwise specified.

Cell line	Cancer type	$\text{IC}_{50}$ in normoxia ( $\mu\text{M}$ )	$\text{IC}_{50}$ in anoxia ( $\mu\text{M}$ )	HCR
H460	Non-small cell lung carcinoma	>500	81	>6.2
H1299	Non-small cell lung carcinoma	>500	187	>2.7
H1650	Non-small cell lung carcinoma	>500	102	>4.9
LNCaP	Prostate carcinoma	>500	76	>6.6
PC3	Prostate adenocarcinoma	>500	194	>2.6
DU145	Prostate carcinoma	>500	146	>3.4
HCT116	Colorectal carcinoma	>500	64	>7.8
DLD-1	Colorectal adenocarcinoma	>500	137	>3.7
MDA-MB-231	Mammary gland/breast adenocarcinoma	>500	202	>2.5
MDA-MB-468	Mammary gland/breast adenocarcinoma	>500	39	>12.8
UT-SCC-5	Head and neck squamous cell carcinoma	>500	220	>2.3
FaDu	Head and neck squamous cell carcinoma	>500	196	>2.6
A2780	Ovarian carcinoma	244	49	5.0
C51	Colon carcinoma (mouse)	>500	78	>6.4
CT26	Colon carcinoma (mouse)	408	81	5.0
LLC	Lung carcinoma (mouse)	>500	92	>5.4
R1	Rhabdomyosarcoma (rat)	>500	13	>38.5

### Hypoxia selective cytotoxicity of CP-506 in several *in vitro* 3D cultures

To further determine the hypoxia selective cytotoxicity of CP-506, 3D *in vitro* cell culture systems were used. In line with the data obtained in 2D cultures, CP-506 had no cytotoxic effects in the concentration range tested (0-100  $\mu\text{M}$ ) in hyperoxic H460 multicellular layers (MCLs). In anoxic MCLs, however, a concentration-dependent effect was observed. Anoxic  $\text{IC}_{10}$  was found to be 32  $\mu\text{M}$ . Treatment of anoxic MCLs with 100  $\mu\text{M}$  CP-506 resulted in 99% of clonogenic cell kill relative to the hyperoxic control (Figure 2A).

Additionally, H460 and HCT116 spheroid cultures were set up. As these spheroids grow, they naturally form a hypoxic core due to limited O<sub>2</sub> diffusion. Evaluation of hypoxia marker pimonidazole labeling indicated that H460 spheroids are not yet hypoxic at day 7 (mean spheroid size 0.04 ± 0.007 mm<sup>3</sup>), but become pimonidazole positive, i.e. hypoxic, at day 11 (mean spheroid size 0.13 ± 0.028 mm<sup>3</sup>) after cell seeding (Figure 2B). CP-506 had no cytotoxic effects in the concentration range tested (0-250 μM) in H460 spheroids at day 4 after seeding, whereas a concentration-dependent effect was observed, with an IC<sub>50</sub> of 233 μM, in pimonidazole-positive (hypoxic) H460 spheroids at day 11 after seeding (Figure 2C). HCT116 cells only grow into spheroids when seeding high cell densities. Additionally, it takes 5 days for these cells to form spheroids. At this time, these spheroids are already large (mean spheroid size 0.20 ± 0.019 mm<sup>3</sup>) and are hypoxic (pimonidazole positive) (Figure 2B). It was not possible to obtain smaller, non-hypoxic HCT116 spheroids. In hypoxic (pimonidazole-positive) HCT116 spheroids at day 5 after seeding a concentration-dependent effect of CP-506 was observed, with an IC<sub>50</sub> of 137 μM (Figure 2C). Taken together, these data indicate hypoxia selective cytotoxicity of CP-506 in *in vitro* multilayer and spheroid cultures.

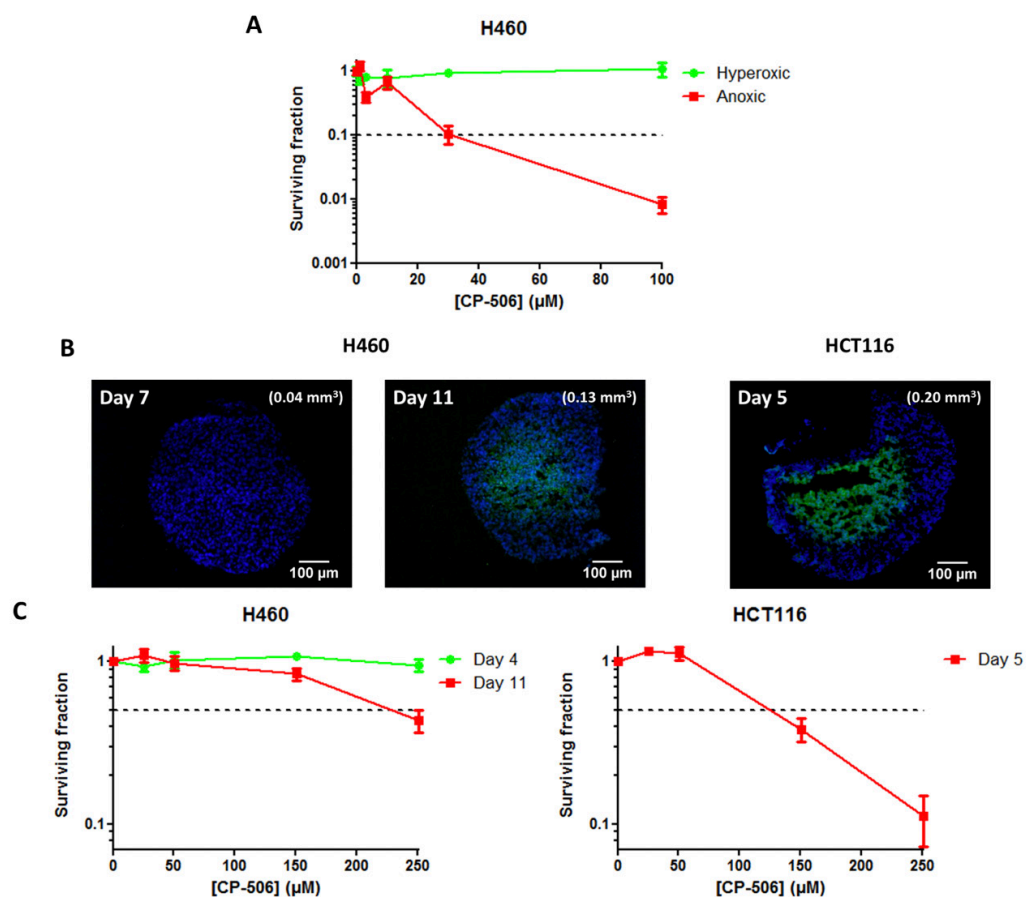
### **CP-506 is not activated by AKR1C3**

One major advantage of CP-506 over its predecessor PR-104 is that it is designed to not be activated by AKR1C3 in aerobic conditions. To confirm this, MCL cultures consisting of HCT116 wild-type cells or HCT116 cells overexpressing AKR1C3 (HCT116<sup>AKR1C3</sup>) were exposed to 10 μM PR-104A or CP-506 in hyperoxic conditions to ensure HAP activation would be due to oxygen-independent activation by AKR1C3 only. PR-104 drastically (> 99.99%) decreased survival of hyperoxic clonogenic HCT116<sup>AKR1C3</sup> cells but not HCT116 cells, whereas CP-506 had no effect in both MCLs, confirming resistance to AKR1C3 activation (Figure 3).

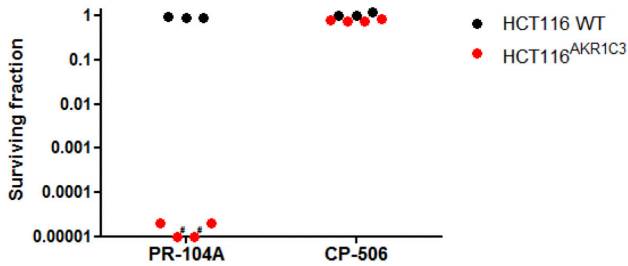
### **CP-506 inhibits tumor growth in several *in vivo* human tumor xenograft models**

Mice bearing tumor xenografts were treated with CP-506 800 mg/kg QD5. CP-506 significantly improved tumor response in H460 (p = 0.0453), HCT116 (p = 0.0101) and MDA-MB-231 (p = 0.0007) tumors, with enhancement ratios of 1.54, 1.65 and 2.35, respectively (Figure 4A). Mean T4×SV of CP-506 treated tumors was significantly longer compared to vehicle treated tumors for H460 (20.0 ± 6.3 vs 13.1 ± 6.5 d; p = 0.0444), HCT116 (33.5 ± 9.0 vs 20.4 ± 6.8 d; p = 0.0095) and MDA-MB-231 (59.4 ± 12.3 vs 25.3 ± 7.5 d; p = 0.0004) (Figure 4A). Results with the H460 tumor model were independently validated in a second

laboratory, where CP-506 significantly ( $p = 0.0011$ ) improved tumor response (Supplementary figure 2). In studies with limited number of tumors and no histology treatment arms, tumor response to CP-506 varied (Supplementary figure 2). In UT-SCC-5 tumors CP-506 only marginally improved tumor response ( $p = 0.0931$ ). In FaDu tumors, a positive trend was observed but was not significant ( $p = 0.0565$ ), possibly due to the limited number of animals. In A2780 and SiHa tumors, CP-506 did significantly ( $p = 0.0246$  and  $0.0353$ , respectively) improve tumor response.



**Figure 2:** CP-506 decreases clonogenic survival selectively in an oxygen-dependent manner. A) Effects of CP-506 on clonogenic survival in hyperoxic and anoxic H460 multicellular layer (MCL) cultures. B) Hypoxia staining in H460 and HCT116 spheroids at different time points after cell seeding. Mean spheroid sizes are indicated between parentheses. Blue: DAPI (nuclei); green: pimonidazole (hypoxia). C) Effects of CP-506 on clonogenic survival in H460 and HCT116 spheroids at different spheroid sizes with differential hypoxic status.



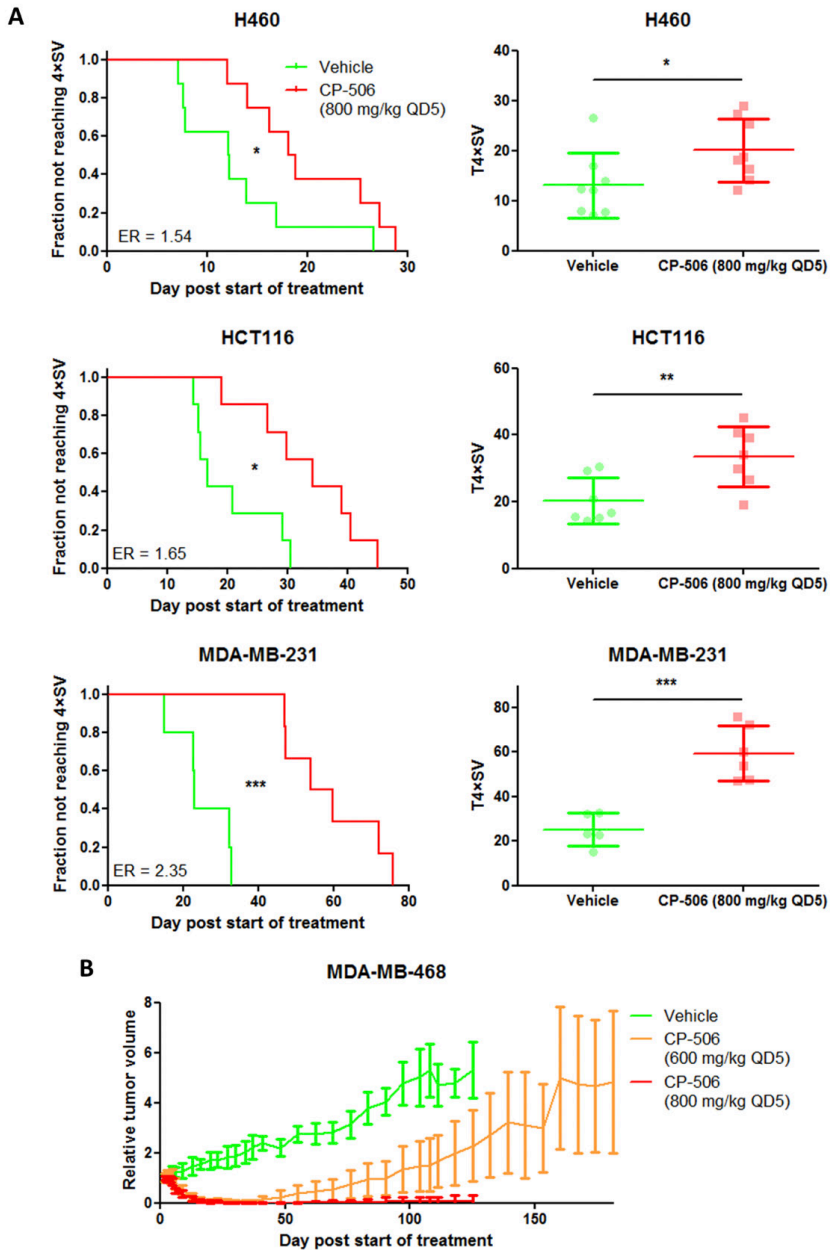
**Figure 3:** CP-506 is not metabolized by AKR1Cs. Effects of PR-104A and CP-506 (10  $\mu$ M) on clonogenic survival in hyperoxic HCT116 and HCT116<sup>AKR1C3</sup> multicellular layer cultures. # indicates an actual value of 0.

In a study with MDA-MB-468 tumors CP-506 caused complete tumor regression (Supplementary figure 3). Since this was the best-responding *in vivo* tumor model, we wanted to independently confirm these data by repeating this study in an external laboratory. An additional, lower dose of CP-506 was also included. In line with the results of the first experiment, CP-506 (800 mg/kg QD5) caused complete tumor regression, with no regrowth of tumors during the follow-up time of 125 days after start of treatment. The lower dose of CP-506 (600 mg/kg QD5) inhibited tumor growth, albeit to a lesser extent than the higher dose (Figure 4B).

In all tumor models, CP-506 caused body weight loss, which was however not severe (> 20%; with the exception of one FaDu tumor-bearing animal) and recoverable within a couple of days after end of treatment (Supplementary figure 4).

### Impact of CP-506 on hypoxic fraction in *in vivo* tumor xenografts

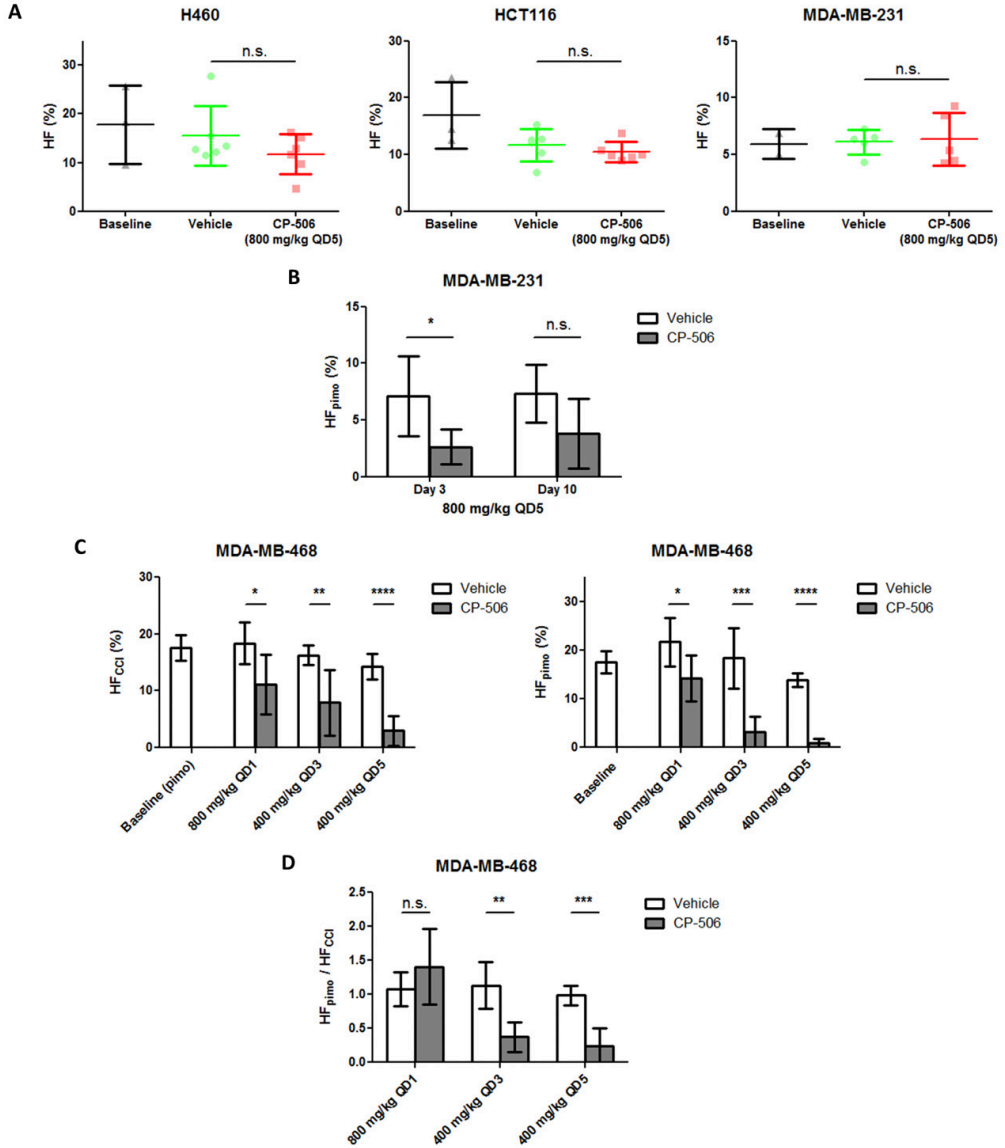
The effect of CP-506 on the hypoxic fraction (HF) of tumor xenografts was assessed by pimonidazole staining of tumors from mice treated with CP-506 (800 mg/kg, QD5) in comparison to vehicle-treated tumors. Analysis confirmed that tumors were hypoxic at treatment starting volume, with HF of  $17.8 \pm 8.1\%$  in H460,  $16.9 \pm 5.8\%$  in HCT116,  $5.9 \pm 1.3\%$  in MDA-MB-231 and  $17.6 \pm 2.2\%$  in MDA-MB-468 (Figure 5A & Supplementary figure 5A). In H460, HCT116 and MDA-MB-231 tumors, there were no significant differences in tumor volume between vehicle-treated and CP-506-treated tumors (Supplementary figure 5B). CP-506 administered for 5 consecutive days did not significantly reduce HF at end of treatment:  $15.5 \pm 6.2\%$  (vehicle) vs  $11.8 \pm 4.2\%$  (CP-506),  $11.6 \pm 2.8\%$  vs  $10.5 \pm 1.7\%$  and  $6.1 \pm 1.1\%$  vs  $6.4 \pm 2.3\%$ , respectively (Figure 5A).



**Figure 4:** CP-506 inhibits tumor growth of several human tumor xenografts. A) Effect of CP-506 on H460, HCT116 and MDA-MB-231 tumor xenograft growth. Left: Kaplan-Meier curves of the fraction of tumors not reaching 4× starting volume (SV). Right: time to reach 4× starting volume (T4×SV) of individual tumors, with mean ± standard deviation. \*:  $p \leq 0.05$ ; \*\*:  $p \leq 0.01$ ; \*\*\*:  $p \leq 0.001$ . B) Effect of CP-506 on MDA-MB-468 tumor xenograft growth, mean ± standard deviation.

To further investigate the effect of CP-506 on HF, the latter was assessed at additional, later time points in MDA-MB-231 xenografts. An additional hypoxia marker, CCI-103F, was injected prior to treatment, to investigate whether pimonidazole-positive cells were already present at start of treatment (and thus CCI-103F-positive), or if they were formed after start of treatment (and thus CCI-103F-negative). This indicates the effectiveness of CP-506 in eradicating these hypoxic tumor cells. 3 days after end of treatment (7 days after start of treatment), CP-506 significantly ( $p = 0.0172$ ) decreased  $HF_{pimo}$  from  $7.1 \pm 3.5\%$  to  $2.6 \pm 1.5\%$ . 10 days after end of treatment (14 days after start of treatment), CP-506 decreased  $HF_{pimo}$  from  $7.3 \pm 2.6\%$  to  $3.8 \pm 3.1\%$  (Figure 5B & Supplementary figure 6A) but was not significant ( $p = 0.2149$ ) likely because of the low ( $n = 2$ ) number of animals in the vehicle-treated group due to low tumor take (60%) in this experiment.  $HF_{CCI}$  was very low in both vehicle- and CP-506-treated tumors 7 days (1.1% vs 2.0%) and 14 days (0.6% vs 0.8%) after CCI-103F injection, reflecting turnover of the hypoxic cells within these periods of time. Tumor volumes were not significantly different between treatment groups at both time points (Supplementary figure 6B).

Changes in HF in MDA-MB-468 xenografts were evaluated using the double hypoxia marker approach. Since CP-506 800 mg/kg QD5 previously resulted in total tumor regression, different dosing regimens of CP-506 were tested. Both  $HF_{CCI}$  and  $HF_{pimo}$  decreased in a dose-dependent manner in CP-506 treated tumors and were significantly different from  $HF_{CCI}$  and  $HF_{pimo}$  in vehicle-treated tumors. A single injection of CP-506 (800 mg/kg) decreased  $HF_{CCI}$  from  $18.4 \pm 3.7\%$  to  $11.1 \pm 5.3\%$  ( $p = 0.0197$ ) and  $HF_{pimo}$  from  $21.7 \pm 5.0\%$  to  $14.2 \pm 4.7\%$  ( $p = 0.0238$ ). Three injections of CP-506 (400 mg/kg) reduced  $HF_{CCI}$  from  $16.3 \pm 1.8\%$  to  $7.9 \pm 5.8\%$  ( $p = 0.0067$ ) and  $HF_{pimo}$  from  $18.4 \pm 6.2\%$  to  $3.2 \pm 3.1\%$  ( $p = 0.0003$ ). Five injections of CP-506 (400 mg/kg) almost abolished  $HF_{CCI}$  from  $14.3 \pm 2.2\%$  to  $3.0 \pm 2.6\%$  ( $p < 0.0001$ ) and  $HF_{pimo}$  from  $13.9 \pm 1.4\%$  to  $0.9 \pm 0.9\%$  ( $p < 0.0001$ ) (Figure 5C & Supplementary figure 6A). Tumor volumes did not differ between treatment groups (Supplementary figure 7B). Furthermore, the  $HF_{pimo}/HF_{CCI}$  ratio decreased in a dose-dependent manner, suggesting effective eradication of hypoxic tumor cells, with no significant difference between vehicle (1.07) and CP-506 QD1 (1.40) treated tumors, a significant difference ( $p = 0.0011$ ) between vehicle (1.13) and CP-506 QD3 (0.37) treated tumors and a significant difference ( $p = 0.0002$ ) between vehicle (0.98) and CP-506 QD5 (0.24) treated tumors (Figure 5D).



**Figure 5:** A) Hypoxic fraction (HF) in H460, HCT116 and MDA-MB-231 tumor xenografts as assessed by pimonidazole staining. B) HF in MDA-MB-468 tumor xenografts as assessed by CCI-103F staining (left) or pimonidazole staining (right). C) Ratio of HF assessed by pimonidazole staining and HF assessed by CCI-103F staining in MDA-MB-468 tumor xenografts.

## Discussion

In the present study we show the first promising therapeutic efficacy of the novel HAP CP-506 in 2D and 3D *in vitro* cell culture models and *in vivo* in a series of tumor-bearing animal models. In line with an oxygen-dependent cytotoxic effect *in vitro* we demonstrated that CP-506 effectively decreased hypoxic fraction in several tumor models, with the optimal time point to detect this decrease being dependent on dosing and tumor model. The hypoxia-specific activation of CP-506 is an important feature, opening opportunities for combination treatment with e.g. radiotherapy and immunotherapy.

In *in vitro* 2D monolayer cell cultures, we demonstrated that CP-506 is selectively cytotoxic in anoxic conditions in all tested cell lines, resulting in hypoxia cytotoxicity ratios ranging between >2.3 and >38.5. This is in line with reported HCRs for PR-104 (~10 to ~100) [14] but is lower than HCRs for the HAP evofosfamide (TH-302), for which HCRs up to 600 have been reported [32], differences in absolute numbers that can at least partially be explained by differential experimental set-up. Also, in our experiments  $IC_{50}$  under normoxic conditions was not reached in the majority of cell lines, and thus the exact HCRs in these cell lines are potentially largely underestimated.

The results demonstrating selective activation of CP-506 under anoxic conditions in 2D cell cultures were confirmed in 3D *in vitro* cellular models, where the cytotoxic effect of CP-506 on clonogenic survival in MCLs was found to be greater compared to 2D monolayers. It should be noted that in monolayer culture assays cell metabolism (as surrogate for cell viability) was used as an endpoint to determine CP-506 cytotoxicity, whereas in 3D culture assays clonogenicity was used, which is considered to be the golden standard for this purpose [33]. As the used endpoints differ between these assays, their results are not fully comparable with each other. However, we speculate that the increased cytotoxicity found in the MCL assays might indicate a bystander effect of CP-506. It is suggested that in monolayer cultures CP-506 metabolites diffuse out of the activating cells into the cell culture medium, resulting in an underestimation of the total cytotoxic effect CP-506. In 3D MCL cultures, however, CP-506 metabolites potentially diffuse into the surrounding cells, resulting in a greater total effect of CP-506. Next to the MCL models, hypoxia-selective cytotoxicity of CP-506 was further confirmed in 3D *in vitro* spheroid models, which naturally form a hypoxic core as they grow, due to limited O<sub>2</sub> diffusion. In these spheroid assays the observed cytotoxic effect of CP-506 was smaller compared to their respective monolayer

cell cultures, which seems counter-intuitive as in tumor cell spheroids, just like in MCL cultures, the bystander effect should play a larger role than in monolayer cell cultures. However, it should be noted that although spheroids were found to be hypoxic by means of pimonidazole staining, the severity, i.e. the exact  $O_2$  concentration in the hypoxic core, remains unknown. Pimonidazole already forms covalent bonds with cellular macromolecules at oxygen levels of 1.3% (10 mmHg) [34], whereas preliminary data suggests that CP-506 needs a much lower oxygen concentration, i.e. anoxic conditions, to be activated (data not shown). It is thus possible that although the used tumor cell spheroids had a hypoxic pimonidazole-positive core, oxygen levels in a large part of this core were still relatively too high for sufficient activation of CP-506. Also, the differences in used endpoint between these assays can also be an influencing factor.

*In vivo* CP-506 was found to inhibit tumor growth in several human tumor xenograft models without severe toxicity. This is in line with other HAPs such as PR-104 [14] and evofosfamide [35], which all showed potent antitumor effects at tolerable doses in several *in vivo* human tumor xenograft models. Although a clear therapeutic benefit was observed, i.e. significant growth inhibition, CP-506 did not reduce HF in H460, HCT116 and MDA-MB-231 xenografts harvested within an hour after the end of treatment. This indicates that the selected time point for histological evaluation might have been too early to detect the consequences of CP-506 activation *in vivo* and that eradication of hypoxic cells occurs at a later time point. Alternatively, it can be speculated that the formation of new hypoxic cells as a consequence of cell proliferation might compensate for the cell kill caused by CP-506 during treatment. Afterwards, the cumulative cytotoxic effects of CP-506 might exceed cell proliferation, resulting in a net decrease of HF and tumor growth inhibition. Indeed, this is supported by CP-506 causing a decrease in HF in the MDA-MB-231 xenograft model 3 days after the end of treatment (7 days after start of treatment). A similar trend is seen at 10 days after the end of treatment (14 days after start of treatment), however data interpretation should be done carefully because of the low number of animals in the vehicle-treated group. In the MDA-MB-468 tumor model, CP-506 caused a decrease in tumor volume already after one injection and, correspondingly, HF was significantly reduced as assessed using CCI-103F and pimonidazole hypoxia markers. Using an alternative treatment regimen with multiple lower CP-506 doses, HF was reduced even more with increasing number of injections, with an almost total eradication of hypoxic tumor cells after 5 injections. CCI-103F and pimonidazole have been shown to mark the same hypoxic cells [36]. In our experiment CCI-103F was injected 2 h before the last injection and

pimonidazole 24 h after the last injection in the MDA-MB-468 tumor model. While the  $\text{HF}_{\text{pimo}}/\text{HF}_{\text{CCI}}$  ratio decreased with increasing number of injections, this ratio remained largely unchanged in vehicle-treated tumors, suggesting that within these 24 h significantly more hypoxic cells (marked by CCI-103F) are being killed by CP-506 than new ones (marked by pimonidazole) are being formed [36, 37]. Alternatively, we speculate that oxygen consumption might be reduced in the better-oxygenated tumor areas because of cell kill due to the bystander effect of CP-506. This potentially allows more oxygen into the previously hypoxic areas, and thus reduces HF. This effect likely varies highly from tumor model to tumor model, depending on how tissue damage caused by CP-506 is resolved in the model. Hypoxic cell turnover might be of influence in response to CP-506 by tumors [38]. If the turnover is fast, the effect of CP-506 might be limited: the hypoxic cells can die naturally before they die of the cytotoxic effects of CP-506. The effect of CP-506 will in that case be limited to the bystander effect in the surrounding well-oxygenated cancer cells. If the hypoxic cell turnover is slow, however, meaning the hypoxic cells live longer, the DNA-cross-links caused by CP-506 will have time to accumulate in these cells and ultimately cause hypoxic cell death, as well as death of adjacent cells due to the bystander effect. The total effect will thus potentially be larger. Whether or not the effect of CP-506 depends on hypoxic cell turnover requires further investigation.

In the previous study on the HAP evofosfamide, we reported tumor xenograft growth inhibition that was associated with baseline HF [30]. HF was assessed by means of  $^{18}\text{F}$ -HX4 hypoxia positron emission tomography (PET) imaging, in the same animals that underwent evofosfamide treatment. In the present study, pimonidazole was used as a hypoxia marker, stained *ex vivo* in different animals than the ones receiving CP-506 treatment. As mentioned before, pimonidazole positivity of tissue does not necessarily indicate sufficiently low oxygen concentrations for CP-506 activation. Also, *ex vivo* pimonidazole staining only provides a 2D image of what actually is a 3D structure, and might therefore not be representative for the actual HF in the whole tumor. A better alternative would be to assess hypoxia *in vivo* right before start of treatment in the same animal that will actually undergo the treatment, using a non-invasive 3D imaging technique, such as aforementioned  $^{18}\text{F}$ -HX4 hypoxia PET imaging [30]. This also enables determination of HF at multiple timepoints, e.g. before and after treatment.

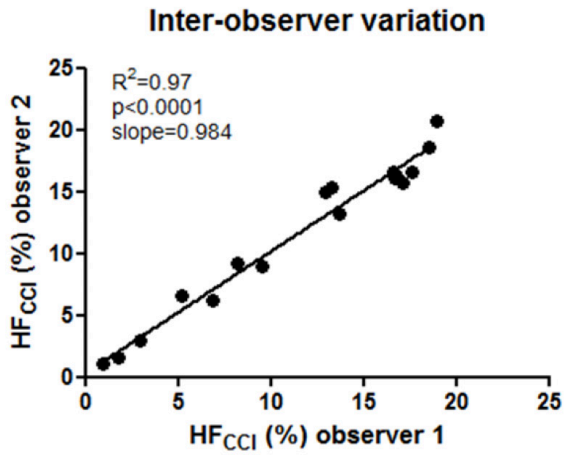
In the present study, no correlation was found between tumor growth inhibition across different tumor models and the respective cytotoxic effects found *in vitro* or the baseline

HF as determined with pimonidazole. Taken together, the data indicate that hypoxia is required to activate CP-506, but is not the only factor that determines response to CP-506 treatment. Expression levels of nitroreductases that can activate CP-506 found within the tumor are a known key determinant for cellular sensitivity to HAPs [9, 39]. Additionally, intrinsic sensitivity of the tumor to the cytotoxic CP-506 metabolites likely plays a role as well. Intrinsic sensitivity might for instance be dependent on the functioning of DNA repair pathways in the tumor cells. For example, tirapazamine, evofosfamide and PR-104 are more effective in tumor cells in which homologous recombination (HR) genes are knocked down or knocked out [12, 32, 40]. HR deficiency in several cancer cell types and a human tumor xenograft model increases cytotoxicity of evofosfamide and PR-104 [41, 42]. Experiments to unravel exactly which factors and mechanisms determine sensitivity to CP-506, and to what extent, are currently ongoing.

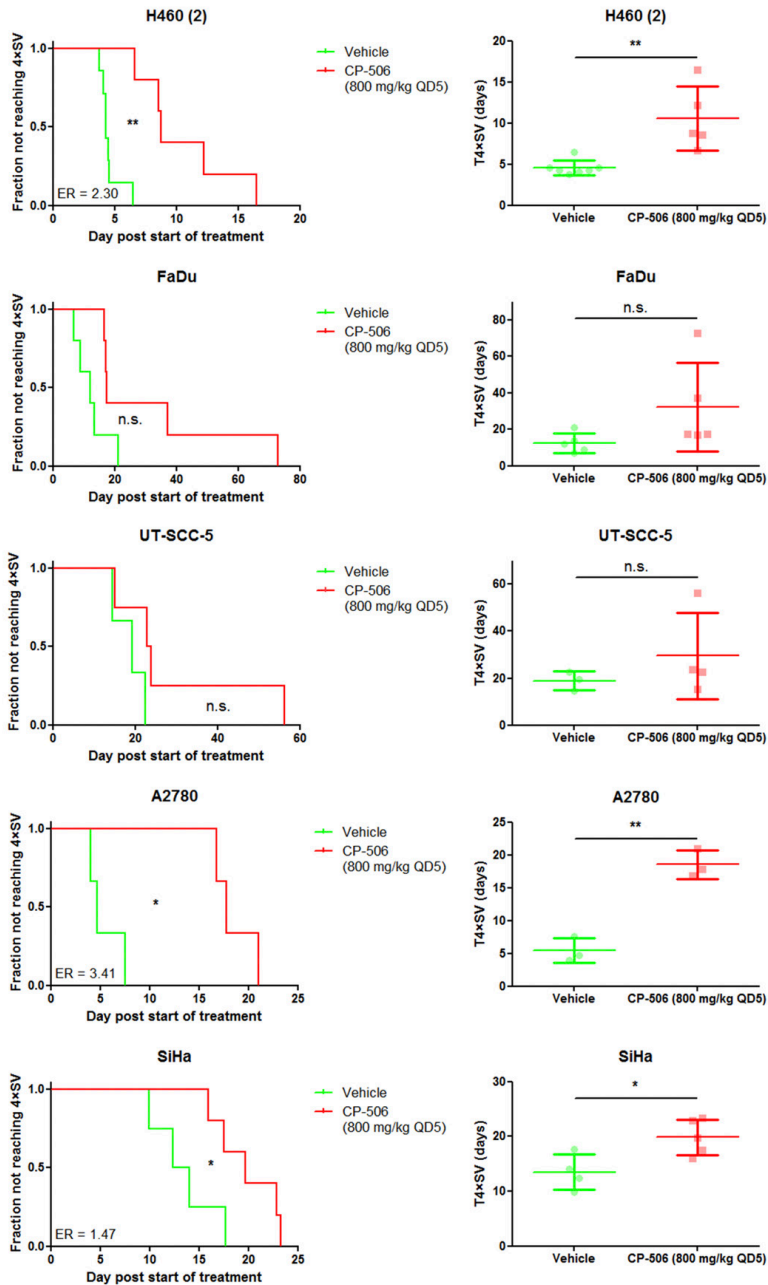
As CP-506 only targets hypoxic tumor cells, it is to be expected that in a clinical setting CP-506 monotherapy is insufficient to completely eradicate a tumor. In general, HAPs are to be combined with another treatment modality which kills aerobic tumor cells. This way, complimentary cell kill can be achieved, increasing therapeutic potential of the treatment. Experiments to assess the effects of CP-506 in combination therapies with radiotherapy and/or immunotherapy are currently ongoing.

In conclusion, CP-506 was developed as an improved successor of PR-104 and we have shown its hypoxia selective cell killing effects. CP-506 has important advantage over PR-104, since CP-506 cannot be activated in aerobic conditions by the two-electron reductase AKR1C3. Additionally, CP-506 cannot be glucuronidated and is water soluble. As such, CP-506 is a promising novel HAP with potential favorable properties for future clinical use. Experiments to determine its exact mechanism of action, its effects when used in a combination therapy together with radiotherapy and/or immunotherapy, and factors influencing tumor sensitivity to CP-506 are currently ongoing.

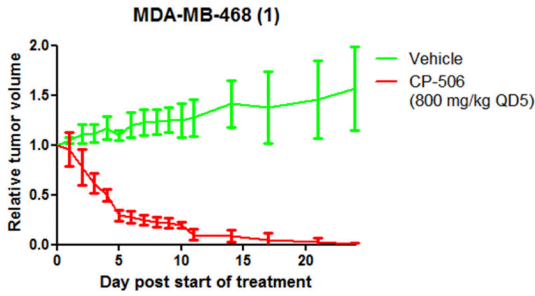
## Supplementary figures



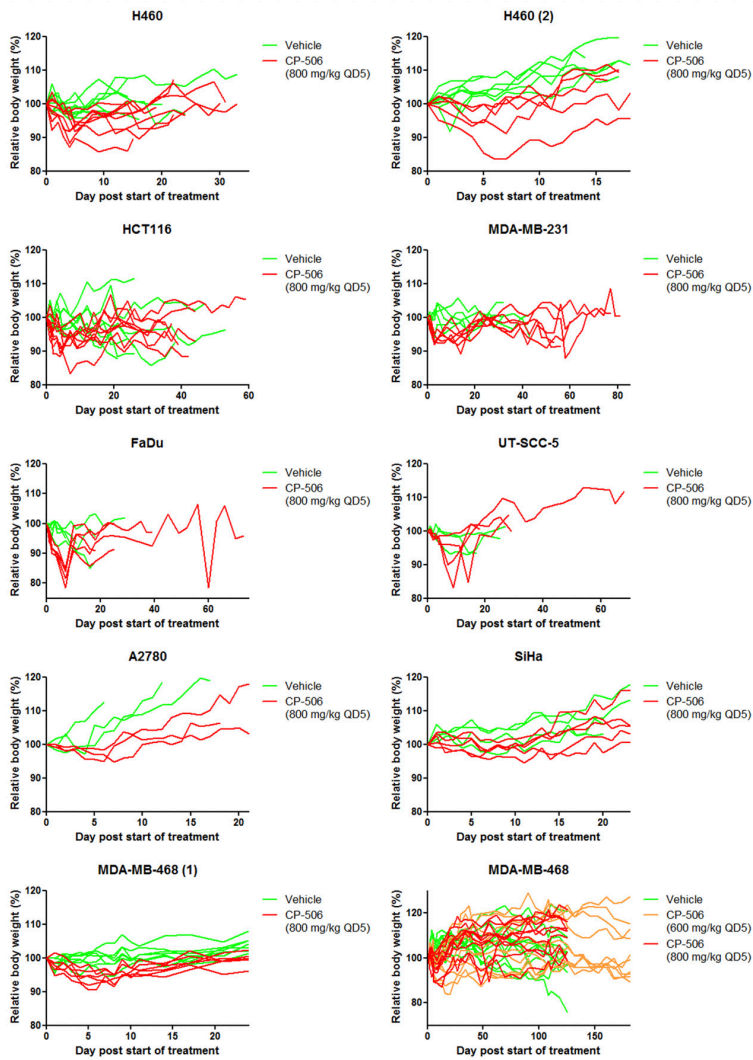
Supplementary figure 1: Inter-observer variation in HF<sub>CCl</sub> assessed by two independent researchers.



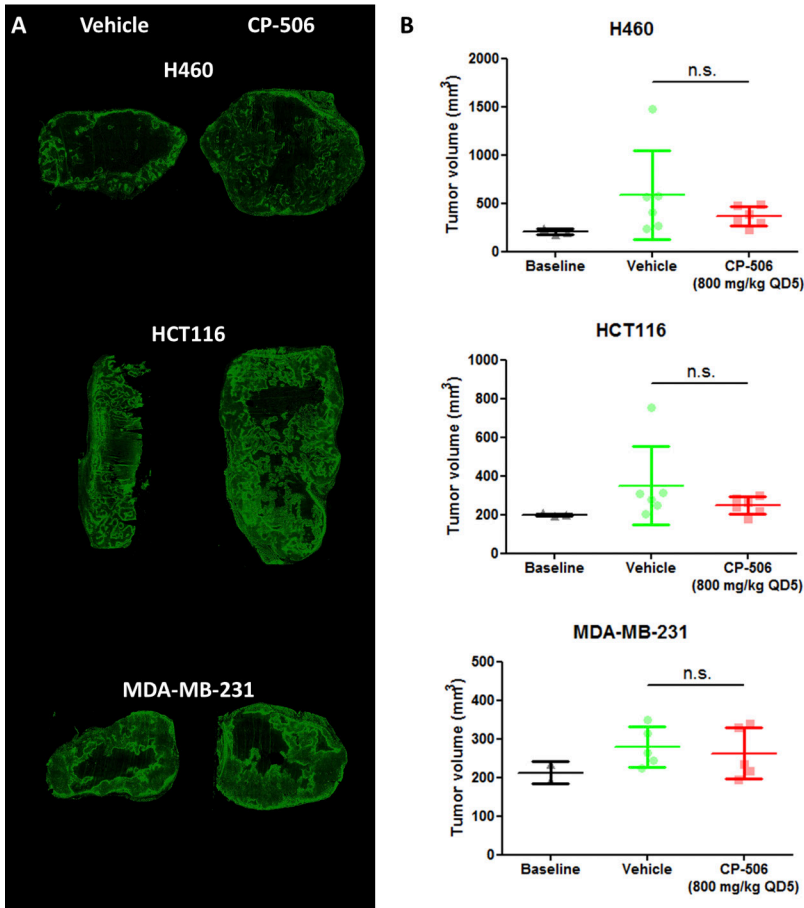
**Supplementary figure 2:** Effects of CP-506 on H460, FaDu, UT-SCC-5, A2780 and SiHa tumor xenograft growth. Left: Kaplan-Meier curves of the fraction of tumors not reaching 4× starting volume (SV). Right: time to reach 4× starting volume (T4×SV) of individual tumors, with mean ± standard deviation. \*:  $p \leq 0.05$ ; \*\*:  $p \leq 0.01$ .



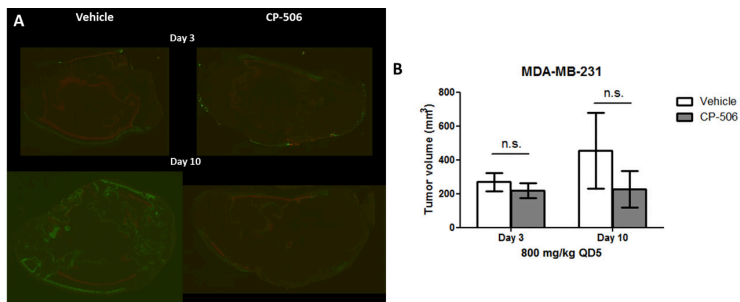
Supplementary figure 3: Effects of CP-506 on MDA-MB-468 tumor xenografts growth.



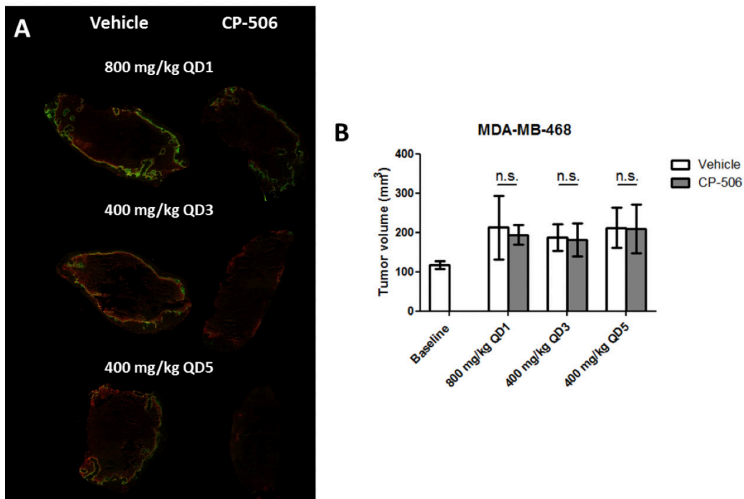
Supplementary figure 4: Body weight of mice bearing different human tumor xenografts, treated with CP-506.



**Supplementary figure 5:** A) Representative images of pimonidazole (hypoxia) staining of whole tumor cross-sections derived from vehicle and CP-506 treated human tumor xenografts. B) Volumes of vehicle and CP-506 treated human tumor xenografts at time of tumor excision.



**Supplementary figure 6:** A) Representative images of pimonidazole (green) and CCI-103F (red) hypoxia staining of vehicle and CP-506 treated MDA-MB-231 xenografts. B) Tumor volumes of vehicle and CP-506 treated MDA-MB-231 xenografts at time of tumor extraction.



**Supplementary figure 7:** A) Representative images of pimonidazole (green) and CCI-103F (red) hypoxia staining of vehicle and CP-506 treated MDA-MB-468 xenografts. B) Tumor volumes of vehicle and CP-506 treated MDA-MB-468 xenografts at time of tumor extraction.

**Supplementary table 1:** Group size and tumor starting volumes of all *in vivo* experiments reported in this study.

Experiment	H460 growth delay + HF assessment						FaDu growth delay	
<b>Group</b>	Vehicle	CP-506 800 mg/kg QD5	Baseline HF	Vehicle HF	CP-506 800 mg/kg QD5 HF	Vehicle	CP-506 800 mg/kg QD5	
Number of mice	8	8	3	6	6	5	5	
<b>Starting volume</b> (mm <sup>3</sup> , mean ± SD)	227 ± 61	226 ± 18	204 ± 28	276 ± 100	241 ± 38	238 ± 67	220 ± 48	
Experiment	HCT116 growth delay + HF assessment						UT-SCC-5 growth delay	
<b>Group</b>	Vehicle	CP-506 800 mg/kg QD5	Baseline HF	Vehicle HF	CP-506 800 mg/kg QD5 HF	Vehicle	CP-506 800 mg/kg QD5	
Number of mice	7	7	3	6	6	3	4	
<b>Starting volume</b> (mm <sup>3</sup> , mean ± SD)	211 ± 31	211 ± 11	198 ± 7	234 ± 74	243 ± 90	213 ± 20	219 ± 15	
Experiment	MDA-MB-231 growth delay + HF assessment						MDA-MB-468 growth delay (1)	
<b>Group</b>	Vehicle	CP-506 800 mg/kg QD5	Baseline HF	Vehicle HF	CP-506 800 mg/kg QD5 HF	Vehicle	CP-506 800 mg/kg QD5	
Number of mice	5	6	2	5	5	7	6	
<b>Starting volume</b> (mm <sup>3</sup> , mean ± SD)	208 ± 24	198 ± 11	212 ± 29	206 ± 18	209 ± 24	205 ± 25	205 ± 19	
Experiment	A2780 growth delay			SiHa growth delay		H460 growth delay (2)		
<b>Group</b>	Vehicle	CP-506 800 mg/kg QD5	Vehicle	CP-506 800 mg/kg QD5	Vehicle	CP-506 800 mg/kg QD5	CP-506 800 mg/kg QD5	
Number of mice	3	3	4	5	7	5	5	
<b>Starting volume</b> (mm <sup>3</sup> , mean ± SD)	362 ± 191	308 ± 116	260 ± 45	234 ± 26	201 ± 43	217 ± 72		

Supplementary table 1 continued.

Experiment Group	MDA-MB-468 growth delay (2)		MDA-MB-231 HF assessment	
	Vehicle	CP-506 600 mg/kg QD5	CP-506 800 mg/kg QD5 HF day 3	Vehicle HF day 10
Number of mice	10	10	6	5
Starting volume (mm <sup>3</sup> , mean ± SD)	143 ± 33	146 ± 45	209 ± 15	211 ± 22
		147 ± 34	215 ± 33	

Experiment Group	MDA-MB-468 HF assessment			
	Baseline HF	Vehicle QD1 HF	CP-506 800 mg/kg QD1 HF	CP-506 400 mg/kg QD3 HF
Number of mice	6	6	6	6
Starting volume (mm <sup>3</sup> , mean ± SD)	117 ± 10	183 ± 66	178 ± 46	183 ± 29
		174 ± 25	178 ± 32	181 ± 47

## Acknowledgements

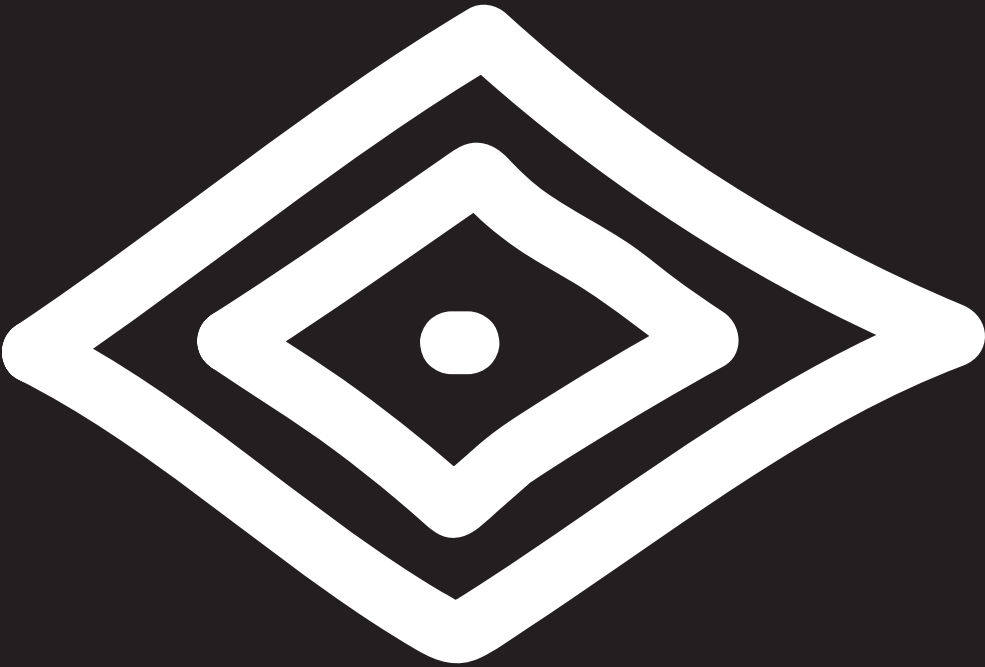
The authors acknowledge financial support from ERC advanced grant (ERC ADG-2015, n° 694812), The Dutch Cancer Society (KWF UM 2012-5394, KWF MAC 2013-6089), Kankeronderzoekfonds Limburg from the Health Foundation Limburg, and from the Worldwide Cancer Research, formerly known as AICR (n° 15-0345).

## References

- Forster, J.C., et al., *A review of the development of tumor vasculature and its effects on the tumor microenvironment*. Hypoxia (Auckl), 2017. **5**: p. 21-32.
- Hockel, M. and P. Vaupel, *Tumor hypoxia: definitions and current clinical, biologic, and molecular aspects*. J Natl Cancer Inst, 2001. **93**(4): p. 266-76.
- Nordsmark, M., et al., *Prognostic value of tumor oxygenation in 397 head and neck tumors after primary radiation therapy. An international multi-center study*. Radiother Oncol, 2005. **77**(1): p. 18-24.
- Phillips, R.M., *Targeting the hypoxic fraction of tumours using hypoxia-activated prodrugs*. Cancer Chemother Pharmacol, 2016. **77**(3): p. 441-57.
- Denny, W.A., W.R. Wilson, and M.P. Hay, *Recent developments in the design of bioreductive drugs*. Br J Cancer Suppl, 1996. **27**: p. S32-8.
- Wilson, W.R. and M.P. Hay, *Targeting hypoxia in cancer therapy*. Nat Rev Cancer, 2011. **11**(6): p. 393-410.
- Workman, P., *Enzyme-directed bioreductive drug development revisited: a commentary on recent progress and future prospects with emphasis on quinone anticancer agents and quinone metabolizing enzymes, particularly DT-diaphorase*. Oncol Res, 1994. **6**(10-11): p. 461-75.
- Mistry, I.N., et al., *Clinical Advances of Hypoxia-Activated Prodrugs in Combination With Radiation Therapy*. Int J Radiat Oncol Biol Phys, 2017. **98**(5): p. 1183-1196.
- Guise, C.P., et al., *Identification of human reductases that activate the dinitrobenzamide mustard prodrug PR-104A: a role for NADPH:cytochrome P450 oxidoreductase under hypoxia*. Biochem Pharmacol, 2007. **74**(6): p. 810-20.
- Guise, C.P., et al., *Diflavin oxidoreductases activate the bioreductive prodrug PR-104A under hypoxia*. Mol Pharmacol, 2012. **81**(1): p. 31-40.
- Guise, C.P., et al., *Bioreductive prodrugs as cancer therapeutics: targeting tumor hypoxia*. Chin J Cancer, 2014. **33**(2): p. 80-6.
- Gu, Y., et al., *Roles of DNA repair and reductase activity in the cytotoxicity of the hypoxia-activated dinitrobenzamide mustard PR-104A*. Mol Cancer Ther, 2009. **8**(6): p. 1714-23.
- Singleton, R.S., et al., *DNA cross-links in human tumor cells exposed to the prodrug PR-104A: relationships to hypoxia, bioreductive metabolism, and cytotoxicity*. Cancer Res, 2009. **69**(9): p. 3884-91.
- Patterson, A.V., et al., *Mechanism of action and preclinical antitumor activity of the novel hypoxia-activated DNA cross-linking agent PR-104*. Clin Cancer Res, 2007. **13**(13): p. 3922-32.
- Jameson, M.B., et al., *A phase I trial of PR-104, a nitrogen mustard prodrug activated by both hypoxia and aldo-keto reductase 1C3, in patients with solid tumors*. Cancer Chemother Pharmacol, 2010. **65**(4): p. 791-801.
- McKeage, M.J., et al., *A phase I trial of PR-104, a pre-prodrug of the bioreductive prodrug PR-104A, given weekly to solid tumour patients*. BMC Cancer, 2011. **11**: p. 432.
- McKeage, M.J., et al., *PR-104 a bioreductive pre-prodrug combined with gemcitabine or docetaxel in a phase Ib study*

- of patients with advanced solid tumours*. BMC Cancer, 2012. **12**: p. 496.
18. Guise, C.P., et al., *The bioreductive prodrug PR-104A is activated under aerobic conditions by human aldo-keto reductase 1C3*. Cancer Res, 2010. **70**(4): p. 1573-84.
  19. Birtwistle, J., et al., *The aldo-keto reductase AKR1C3 contributes to 7,12-dimethylbenz(a)anthracene-3,4-dihydrodiol mediated oxidative DNA damage in myeloid cells: implications for leukemogenesis*. Mutat Res, 2009. **662**(1-2): p. 67-74.
  20. Abou-Alfa, G.K., et al., *PR-104 plus sorafenib in patients with advanced hepatocellular carcinoma*. Cancer Chemother Pharmacol, 2011. **68**(2): p. 539-45.
  21. Gu, Y., M.D. Tingle, and W.R. Wilson, *Glucuronidation of anticancer prodrug PR-104A: species differences, identification of human UDP-glucuronosyltransferases, and implications for therapy*. J Pharmacol Exp Ther, 2011. **337**(3): p. 692-702.
  22. Abbattista, M.R., et al., *Pre-clinical activity of PR-104 as monotherapy and in combination with sorafenib in hepatocellular carcinoma*. Cancer Biol Ther, 2015. **16**(4): p. 610-22.
  23. Patel, K., et al., *A combined pharmacokinetic model for the hypoxia-targeted prodrug PR-104A in humans, dogs, rats and mice predicts species differences in clearance and toxicity*. Cancer Chemother Pharmacol, 2011. **67**(5): p. 1145-55.
  24. Konopleva, M., et al., *Phase I/II study of the hypoxia-activated prodrug PR104 in refractory/relapsed acute myeloid leukemia and acute lymphoblastic leukemia*. Haematologica, 2015. **100**(7): p. 927-34.
  25. Wilson, W.R., et al., *Bystander effects of bioreductive drugs: potential for exploiting pathological tumor hypoxia with dinitrobenzamide mustards*. Radiat Res, 2007. **167**(6): p. 625-36.
  26. Yahyanejad, S., et al., *An image guided small animal radiation therapy platform (SmART) to monitor glioblastoma progression and therapy response*. Radiother Oncol, 2015. **116**(3): p. 467-72.
  27. Edelstein, A.D., et al., *Advanced methods of microscope control using muManager software*. J Biol Methods, 2014. **1**(2).
  28. Edelstein, A., et al., *Computer control of microscopes using microManager*. Curr Protoc Mol Biol, 2010. **Chapter 14**: p. Unit14 20.
  29. Chen, W., et al., *High-throughput image analysis of tumor spheroids: a user-friendly software application to measure the size of spheroids automatically and accurately*. J Vis Exp, 2014(89).
  30. Peeters, S.G., et al., *TH-302 in Combination with Radiotherapy Enhances the Therapeutic Outcome and Is Associated with Pretreatment [18F]HX4 Hypoxia PET Imaging*. Clin Cancer Res, 2015. **21**(13): p. 2984-92.
  31. Yaromina, A., et al., *Pimonidazole labelling and response to fractionated irradiation of five human squamous cell carcinoma (hSCC) lines in nude mice: the need for a multivariate approach in biomarker studies*. Radiother Oncol, 2006. **81**(2): p. 122-9.
  32. Meng, F., et al., *Molecular and cellular pharmacology of the hypoxia-activated prodrug TH-302*. Mol Cancer Ther, 2012. **11**(3): p. 740-51.

33. Franken, N.A., et al., *Clonogenic assay of cells in vitro*. Nat Protoc, 2006. **1**(5): p. 2315-9.
34. Gross, M.W., et al., *Calibration of misonidazole labeling by simultaneous measurement of oxygen tension and labeling density in multicellular spheroids*. Int J Cancer, 1995. **61**(4): p. 567-73.
35. Sun, J.D., et al., *Comparison of hypoxia-activated prodrug evofosfamide (TH-302) and ifosfamide in preclinical non-small cell lung cancer models*. Cancer Biol Ther, 2016. **17**(4): p. 371-80.
36. Ljungkvist, A.S., et al., *Changes in tumor hypoxia measured with a double hypoxic marker technique*. Int J Radiat Oncol Biol Phys, 2000. **48**(5): p. 1529-38.
37. Bennewith, K.L. and R.E. Durand, *Quantifying transient hypoxia in human tumor xenografts by flow cytometry*. Cancer Res, 2004. **64**(17): p. 6183-9.
38. Ljungkvist, A.S., et al., *Hypoxic cell turnover in different solid tumor lines*. Int J Radiat Oncol Biol Phys, 2005. **62**(4): p. 1157-68.
39. Hunter, F.W., et al., *Identification of P450 Oxidoreductase as a Major Determinant of Sensitivity to Hypoxia-Activated Prodrugs*. Cancer Res, 2015. **75**(19): p. 4211-23.
40. Evans, J.W., et al., *Homologous recombination is the principal pathway for the repair of DNA damage induced by tirapazamine in mammalian cells*. Cancer Res, 2008. **68**(1): p. 257-65.
41. Hunter, F.W., et al., *Homologous recombination repair-dependent cytotoxicity of the benzotriazine di-N-oxide CEN-209: comparison with other hypoxia-activated prodrugs*. Biochem Pharmacol, 2012. **83**(5): p. 574-85.
42. Hunter, F.W., et al., *Dual targeting of hypoxia and homologous recombination repair dysfunction in triple-negative breast cancer*. Mol Cancer Ther, 2014. **13**(11): p. 2501-14.



# CHAPTER 8

Antitumor effects of the novel hypoxia-activated prodrug CP-506 combined with radiotherapy or immunotherapy

**Raymon Niemans**, Damiënne Marcus, Rianne Biemans, Natasja Lieuwes, Jan Theys, Ala Yaromina, Ludwig Dubois, Philippe Lambin

*In preparation.*

## Abstract

Hypoxia, a common feature of solid tumors, is associated with poor prognosis. It aggravates the malignant tumor cell phenotype, increases resistance to radiotherapy, and it is suggested to negatively influence immunotherapy treatment outcome. As these strategies are effective against the well oxygenated tumor cells, combination with a specific hypoxia targeting strategy is a potentially promising approach. One treatment approach of specifically targeting hypoxic tumor cells is using hypoxia-activated prodrugs (HAPs). Here we tested the combination treatments of single dose radiotherapy and/or immunotherapy (the immunocytokine L19-IL2) with the novel HAP CP-506. CP-506 increased time to reach 4 times start volume ( $T4 \times SV$ ) when combined with radiotherapy (from  $7.5 \pm 2.1$  to  $13.3 \pm 2.9$  d,  $p < 0.001$ ) or immunotherapy (from  $6.8 \pm 2.0$  to  $11.6 \pm 4.2$  d,  $p = 0.028$ ) in a preclinical *in vivo* CT26 tumor model. This increase in therapeutic efficacy is dependent on the model and treatment schedule used. CP-506 is thus a promising candidate for further preclinical evaluation and clinical efficacy validation of combination approaches.

## Introduction

Hypoxic areas are present in the majority of solid tumors, due to the tumor outgrowing its already abnormal and chaotic vasculature, resulting in cells receiving insufficient oxygen [1, 2]. Tumor hypoxia is associated with poor prognosis, and it aggravates the malignant tumor cell phenotype [2, 3]. Additionally, hypoxic tumor cells are more resistant to ionizing radiation. In these cells the so-called oxygen-enhancement effect is missing or reduced, since there is no oxygen present to “fix” the DNA radicals formed by ionizing radiation [4-6]. Also, intrinsic resistance to ionizing radiation is higher in hypoxic cells, e.g. through increased levels of heat-shock proteins, increased numbers of cells with diminished apoptotic potential or increased proliferation potential [7-11]. Thus, the combination treatment of radiotherapy with a hypoxia targeting strategy is promising, in that the two can yield at least complementary cell kill: radiotherapy targets the aerobic tumor cells, and the other targets the hypoxic, radioresistant tumor cells.

Lately, immunotherapies, in which the patient’s own immune system is induced and/or stimulated to eradicate cancer cells, have emerged as promising new cancer treatments [12]. One such novel therapy is the combination of the immunocytokine L19-IL2 and radiotherapy. L19-IL2 is a fusion protein of L19, a small-immuno-protein targeting the extra domain B (ED-B) of fibronectin (a marker for tumor neoangiogenesis), and IL2, a cytokine that acts as an important immune response activator [13]. This fusion protein can thus selectively deliver IL2 to ED-B expressing tumor cells and enhance an anticancer immune response. Indeed, it was recently shown that the combination of L19-IL2 and radiotherapy induces long-lasting antitumor effects, depending on ED-B expression and T cell infiltration, or a natural killer cell immune response [14, 15]. Additionally, it has been observed that this combination treatment results in an abscopal effect, i.e. tumor response outside the irradiation field, and a memory effect [16]. However, it is suggested that hypoxia can negatively influence immunotherapy treatment outcome because it can interfere with T lymphocyte effector function, regulate natural killer and natural killer T cell activity, induce resistance to cell-mediated cytotoxicity, induce immune suppression, contribute to immune tolerance, impair T cell infiltration, etc. [17, 18]. Adding a hypoxia targeting treatment to the combination of L19-IL2 and radiotherapy can therefore improve its effectiveness.

One strategy of specifically targeting hypoxic tumor cells is using hypoxia-activated pro-

drugs (HAPs). HAPs are inactive prodrugs that are specifically activated in hypoxic areas only, where they are reduced by nitroreductases to their active metabolite(s). These metabolites are generally cytotoxins that kill the activating tumor cell. The active metabolites can also diffuse into surrounding cells, killing these too; this is called the bystander effect [19]. Previously, we reported promising therapeutic efficacy results on the novel HAP CP-506 [Chapter 7]. We showed that CP-506 exhibits hypoxia-selective cytotoxicity in a number of *in vitro* monolayer cultures as well as in several *in vitro* multilayer and spheroid cultures. Additionally, CP-506 inhibited tumor growth in several *in vivo* human tumor xenograft models, accompanied by a significant decrease in hypoxic fraction during or early after treatment in some of the tumor models. Taken together, the combination of CP-506 with radiotherapy or with radiotherapy and L19-IL2 might be a promising approach. In this study, we investigated the combination of CP-506 with radiotherapy and/or L19-IL2 in several *in vivo* tumor models, hypothesizing that CP-506 will increase therapeutic outcome of these treatments.

## Materials & methods

### Animal models

Animal experiments were performed using adult NMRI-*nu* nude mice (for the human H460 non-small cell lung carcinoma) or BALB/c mice (for the murine CT26 colorectal carcinoma). Animal facilities and experiments were in accordance with institutional guidelines for animal welfare and were approved by the responsible animal ethical committees. Per xenograft,  $1.5 \times 10^6$  cells were resuspended in BD Matrigel™ Basement Membrane Matrix (BD Biosciences) and injected subcutaneously into the lateral flank of the animal. Tumors were measured in three dimensions using a caliper, and a 0.5 mm correction in each dimension was applied for thickness of the skin. Tumor volume was thus calculated using the formula  $(a-0.5) \times (b-0.5) \times (c-0.5) \times \pi / 6$ . Upon reaching a tumor volume of approximately 200 mm<sup>3</sup>, mice were randomly assigned to a treatment group. Tumor starting volumes and group sizes (n = 6-8) were similar across treatment arms within one experiment (Supplementary table 1). CP-506 or vehicle (saline) control was administered via intraperitoneal (i.p.) injection. L19-IL2 or vehicle (PBS) control was administered via intravenous (i.v.) injection. Radiotherapy (Varian Truebeam linear accelerator; 15 MeV electrons) was applied as a single dose. Treatment schedules and doses are described in Figures 1-4. Tumor growth was monitored 3 times per week or daily after treatment until 4× tumor starting

volume ( $4 \times SV$ ) or a maximum tumor volume of  $2000 \text{ mm}^3$  was reached. Survival was defined as the fraction of tumors not reaching  $4 \times SV$ . Tumor response was quantified as the time required to reach  $4 \times SV$  ( $T4 \times SV$ ).

### **Hypoxia staining in tumors**

Mice bearing CT26 tumors were injected i.p. with the hypoxia marker pimonidazole (60 mg/kg in saline; NPI, Inc.) upon the tumor reaching SV ( $n = 4$ , tumor volume  $190 \pm 47 \text{ mm}^3$ ). 1 h later, mice were injected i.v. with Hoechst 33342 (15 mg/kg in saline; Sigma-Aldrich). 1 min later mice were sacrificed, tumors were collected and snap-frozen. Whole tumor cross-sections ( $7 \mu\text{m}$ ) from the central part of the tumor were fixed with ice-cold acetone and nonspecific binding was blocked with 5% normal goat serum in 0.2% PBS-Tween-20 at room temperature for 30 min. Sections were incubated overnight at  $4^\circ\text{C}$  with a mixture of rabbit anti-pimonidazole antibody (1:250; NPI, Inc.) and rat anti-mouse CD31 antibody (1:500; BD Biosciences). Then sections were washed with 0.2% PBS-Tween-20 and incubated for 1 h at room temperature with Alexa Fluor® 488-conjugated goat anti-rabbit IgG (1:500; Thermo Fisher Scientific) and Alexa Fluor® 594-conjugated goat anti-rat IgG (1:500; Thermo Fisher Scientific). Sections were washed again with 0.2% PBS-Tween-20 and slides were mounted with cover slips using DakoCytomation fluorescent medium (Dako). Images were acquired as described previously [20]. Hypoxic fractions were assessed using the ImageJ software (National Institutes of Health) in a semi-automated way as described previously [20, 21]. The thresholds to define positive areas were defined for each tumor section according to the signal intensity and background staining and has previously been demonstrated to have low inter-observer variability [21]. Hypoxic fraction (HF) was calculated as percentage of pixels positive for pimonidazole divided by the viable tumor area.

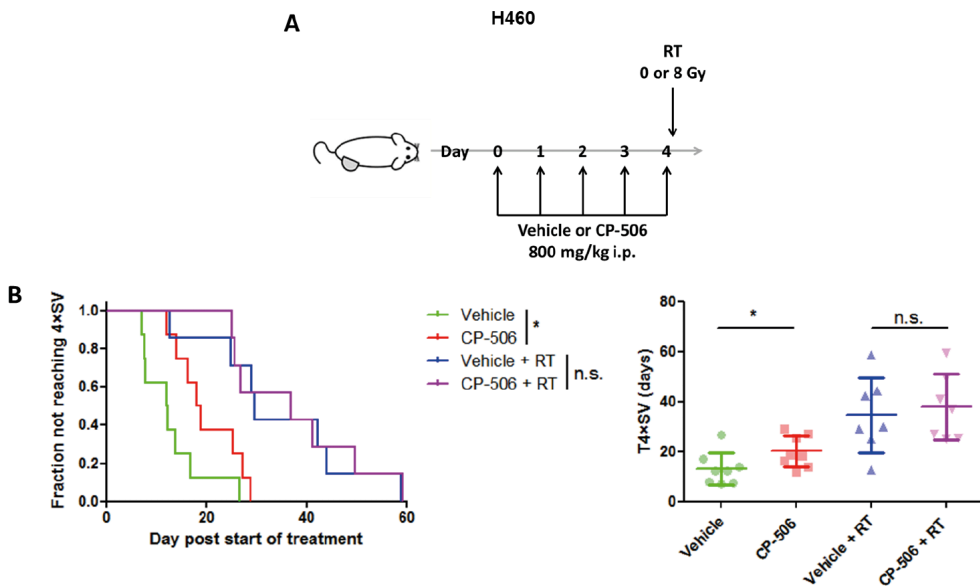
### **Statistical analyses**

Differences in survival between treatment groups were analyzed using a log-rank test. Differences in mean times to reach  $T4 \times SV$  were analyzed using an unpaired two-tailed t-test. Synergism between two treatments was assessed using a two-way ANOVA. When  $p \leq 0.05$ , results were considered statistically significant. All analyses were performed using the GraphPad Prism 5.04 software (GraphPad Software, Inc.).

## Results

To determine the effect of the combination of CP-506 followed by radiotherapy, mice bearing H460 tumor xenografts were treated with CP-506 (800 mg/kg) or vehicle once a day for 5 consecutive days (QD5), followed by radiotherapy (sham or single dose 8 Gy) 2 h after the last injection (Figure 1A). As reported previously [Chapter 7], CP-506 significantly ( $p = 0.044$ ) increased T4×SV compared to vehicle treated tumors (from  $13.1 \pm 6.5$  to  $20.1 \pm 6.3$  d). The combination of CP-506 followed by radiotherapy did not increase T4×SV compared to animals treated with vehicle followed by RT (Figure 1B).

CP-506 caused slight body weight loss within a couple of days in most animals. This body weight loss was however not severe ( $< 20\%$ ) and all mice recovered within days after the last injection. Radiotherapy did not cause additional body weight loss (Supplementary figure 1).



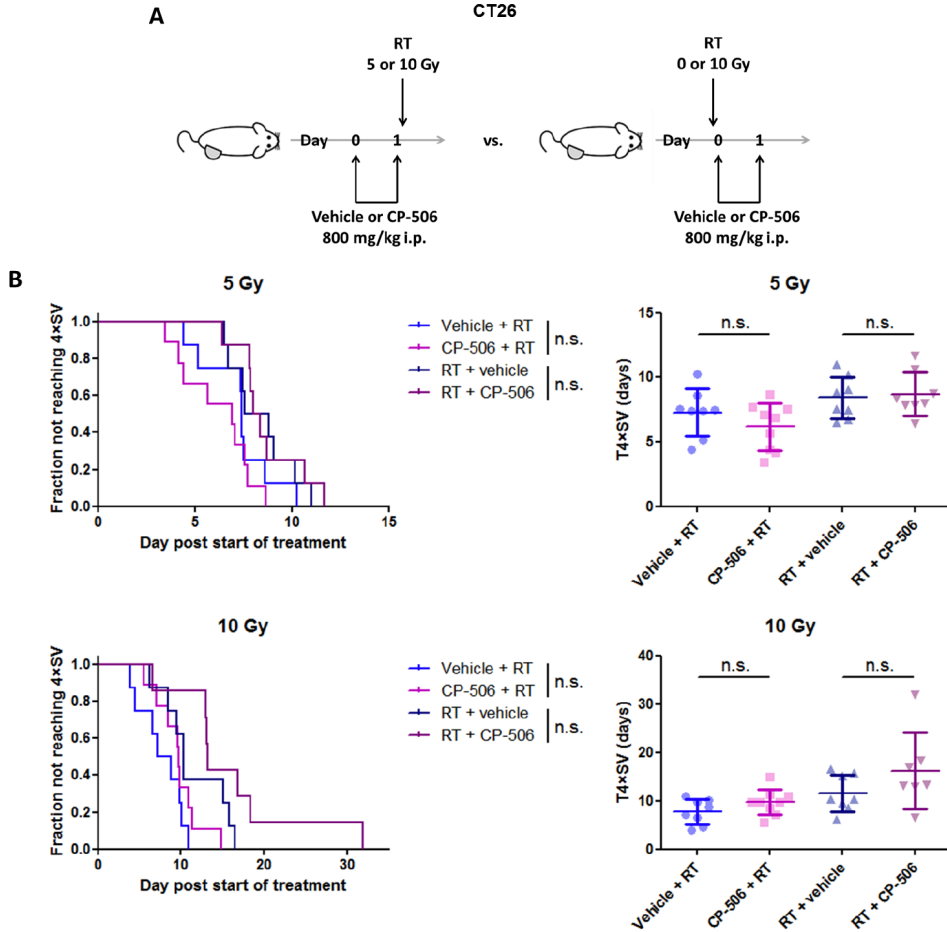
**Figure 1:** **A)** treatment scheme: mice bearing H460 tumor xenografts were treated with CP-506 or vehicle followed by radiotherapy. **B)** Effect of CP-506 monotherapy and CP-506 in combination with RT on tumor response. **Left:** Kaplan–Meier representation of the data. **Right:** T4×SV for each individual tumor (symbols). Horizontal bars indicate mean values  $\pm$  standard deviation. Relevant statistical comparisons are indicated: n.s.: not significant; \*:  $p \leq 0.05$ .

To further investigate the effects of radiotherapy and CP-506, the CT26 syngeneic tumor model was used. The choice of a murine tumor model is dictated by the necessity of immune competent mice to evaluate CP-506 in combination with immunotherapy in further experiments. Histological investigations using the hypoxia marker pimonidazole confirmed the presence of hypoxic cells in CT26 tumors prior to treatment, although hypoxic fraction was found to be highly variable between the tumors, ranging from 0.8% to 10.3% with no correlation between HF and tumor size (Supplementary figure 1). We investigated if treatment outcome differs depending on whether CP-506 is administered before or after single dose irradiation. Since CT26 tumors grow fast (volume doubling time  $3.0 \pm 0.8$  d), it is not recommendable to administer CP-506 QD5 when comparing CP-506 before and after radiotherapy because tumor volumes at time of radiotherapy would differ ~3-fold between treatment groups, biasing the results. Also, this would shorten follow-up time after treatment and endpoint ( $4 \times SV$ ) would possibly be reached before the effect of the treatment would be visible. Therefore, instead of 5 injections (QD5), two injections of CP-506 were administered within 24 hours (QD2). Mice bearing a CT26 syngeneic tumor were treated first with CP-506 (800 mg/kg, QD2) followed by radiotherapy (5 or 10 Gy) 30 min after the last injection ("CP-506 + RT") or with the respective vehicle control ("Vehicle + RT"). Alternatively, mice were treated first with radiotherapy (5 or 10 Gy) immediately followed by CP-506 (800 mg/kg, QD2) ("RT + CP-506") or with the respective vehicle control ("RT + vehicle") (Figure 2A). A trend towards increased response was apparent for CP-506 administered after 10 Gy radiation, however, none of the treatment combinations of CP-506 and radiotherapy significantly increased  $T4 \times SV$  compared to the respective vehicle controls (Figure 2B).

CP-506 caused a slight body weight loss within a couple of days in some animals. This body weight loss was not severe ( $< 20\%$ ) and all mice recovered within days after the last injection (Supplementary figure 2).

Next, we further explored the trend towards increased response when CP-506 was administered after radiotherapy, and assessed if radiotherapy followed by five CP-506 injections would enhance treatment outcome in the CT26 syngeneic tumor model. Mice were first treated with radiotherapy (5 Gy), immediately followed by five injections of CP-506 (800 mg/kg, QD5) (Figure 3A). Corresponding controls were also included. Whereas CP-506 alone did not significantly increase  $T4 \times SV$  compared to vehicle controls, the combination of radiotherapy followed by CP-506 significantly ( $p < 0.001$ ) prolonged  $T4 \times SV$  (from  $7.5 \pm$

2.1 to  $13.3 \pm 2.9$  d) compared to radiotherapy controls (Figure 3B). Radiation and CP-506 were found to inhibit tumor growth synergistically ( $p = 0.0146$ ).

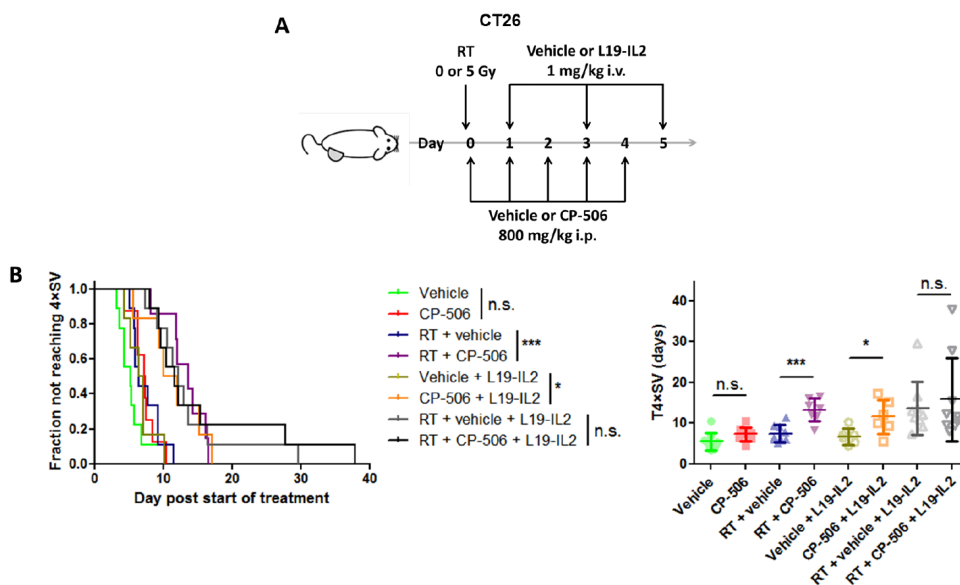


**Figure 2:** **A)** treatment scheme: mice bearing CT26 syngeneic tumors were treated with CP-506 or vehicle followed by radiotherapy. Alternatively, mice were treated first with radiotherapy followed by CP-506 or vehicle. **B)** Effect of CP-506 monotherapy and CP-506 in combination with RT on tumor response. **Left:** Kaplan–Meier representation of the data. **Right:** T4xSV for each individual tumor (symbols). Horizontal bars indicate mean values  $\pm$  standard deviation. Relevant statistical comparisons are indicated: n.s.: not significant

In parallel to this experiment, we tested whether CP-506 can increase therapeutic efficacy of L19-IL2 immunotherapy or radiotherapy and L19-IL2. To test this hypothesis, mice received radiotherapy (5 Gy), followed by CP-506 (800 mg/kg, QD5) and L19-IL2 (1 mg/

kg on days 1, 3 and 5 after start of treatment). Corresponding vehicle controls were also included (Figure 3A). The combination treatment of CP-506 and L19-IL2 significantly ( $p = 0.028$ ) increased  $T4 \times SV$  ( from  $6.8 \pm 2.0$  to  $11.6 \pm 4.2$  d) compared to the respective vehicle controls (Figure 3B). The triple combination treatment of radiotherapy followed by CP-506 and L19-IL2 did not further improve therapeutic effect compared to the respective vehicle controls (Figure 3B).

CP-506 caused slight body weight loss within a couple of days in some animals. This body weight loss was severe ( $< 20\%$ ) in only one mouse, and all mice recovered within days after the last injection. Body weight loss was highest in the triple combination group (Supplementary figure 3).

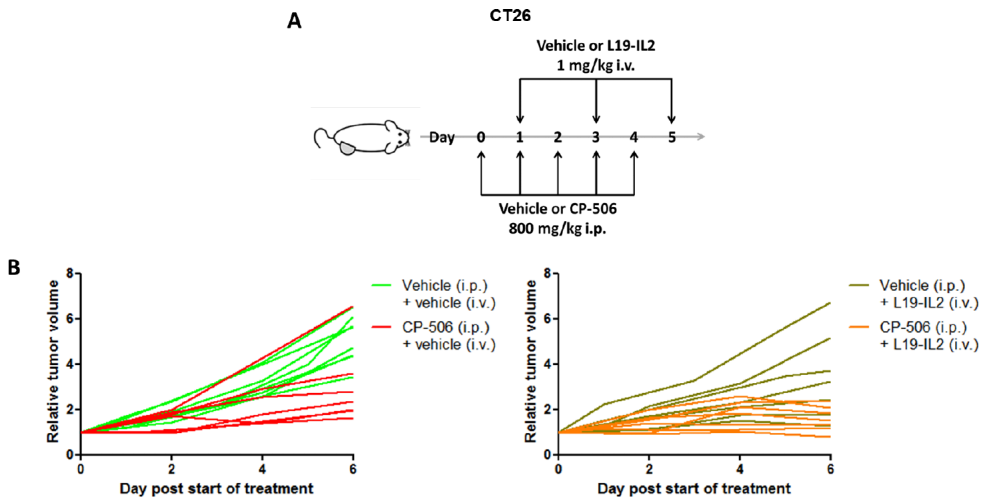


**Figure 3:** **A)** treatment scheme: mice bearing CT26 syngeneic tumors were treated with CP-506, radiotherapy and/or L19-IL2. Corresponding vehicle controls were also included. **B)** Effect of CP-506 monotherapy and CP-506 in combination with RT on tumor response. **Left:** Kaplan–Meier representation of the data. **Right:**  $T4 \times SV$  for each individual tumor (symbols). Horizontal bars indicate mean values  $\pm$  standard deviation. Relevant statistical comparisons are indicated: n.s.: not significant; \*:  $p \leq 0.05$ ; \*\*\*:  $p \leq 0.001$ .

To further investigate the effects of the combination treatment of CP-506 and L19-IL2, the previous experiment was repeated: mice bearing a CT26 syngeneic tumor were treated with vehicle/CP-506 (800 mg/kg, QD5) and vehicle/L19-IL2 (1 mg/kg on days 1, 3 and 5

after start of treatment) (Figure 4A). This time, however, main purpose of the experiment was to investigate immunological and histological parameters directly after treatment, which is currently ongoing. Animals were sacrificed 24 h after the last L19-IL2 injection. The effects of treatment with CP-506 and L19-IL2 were found to be similar in the two independent experiments, confirming that CP-506 enhances therapeutic effect of L19-IL2 (Figure 4B).

CP-506 as a monotherapy caused slight body weight loss within a couple of days in some animals. This body weight loss was, however, not severe (< 20%). Body weight loss was more pronounced in CP-506 + L19-IL2 treated animals, with some animals approaching or losing more than 20% (Supplementary figure 3). Additionally, these mice showed clinical signs of distress (less active, cowering in the corner of the cage, and reduced grooming) which were not observed in the previous experiment. Since mice were sacrificed 6 days after start of treatment, it is unknown if this body weight loss and these clinical symptoms were recoverable. It is unknown why these effects were seen in this but not in the previous experiment.



**Figure 4:** **A)** treatment scheme: mice bearing CT26 syngeneic tumors were treated with CP-506 and L19-IL2). Corresponding vehicle controls were also included. **B)** Changes in tumor volumes relative to pre-treatment tumor volume.

## Discussion

Combining radiotherapy and/or immunotherapy with a hypoxia-activated prodrug (HAP) is a promising approach, as tumor hypoxia increases resistance to radiotherapy and it is suggested to negatively influence immunotherapy treatment outcome. Targeting of the hypoxic tumor cells by the HAP might thus be beneficial, in that it targets those cells which are radioresistant, and potentially promotes effectiveness of an immune response. In this study, we show that the combination of the HAP CP-506 with radiotherapy can induce synergistic anticancer effects. This effect, however, depends on treatment scheme and tumor model. Additionally, we show that combining immunotherapy with CP-506 significantly enhances tumor response.

As previously reported [Chapter 7], CP-506 resulted in monotherapeutic efficacy in H460 human tumor xenografts in line with the results in other human tumor xenografts. In this study we show that there is no monotherapeutic efficacy of CP-506 in the CT26 syngeneic tumor model. This could be caused by the tumor not being hypoxic enough, the tumor cells not expressing (sufficient levels of) the oxidoreductases needed to activate the HAP, or a low intrinsic sensitivity of the tumor cells to the HAP, e.g. due to well-functioning DNA damage repair mechanisms [22-24]. Baseline hypoxic fraction (HF) in H460 xenografts ranges from 9.5% to 25.6% [Chapter 7], whereas in CT26 syngeneic tumors it ranges from 0.8% to 10.3%. This high variability and low HF in some CT26 tumors might partially explain the lack of CP-506 efficacy in this tumor model. Furthermore, preliminary data suggests that the levels of oxidoreductases in murine models are much lower compared with human tumor cell lines [Adam V Patterson *et al.*, unpublished data]. Experiments to determine which reductases are mainly responsible for CP-506 activation are ongoing. DNA repair capacity likely plays a role in sensitivity to CP-506 as well, as the HAPs tirapazamine, evofosfamide (TH-302) and PR-104 are more effective in tumor cells with homologous recombination (HR) deficiencies [25-27]. Also, HR deficiency in several cancer cell types and a human tumor xenograft model increases cytotoxicity of DNA-alkylating HAPs, to which CP-506 belongs [28, 29]. Exactly how and to what extent these and other factors determine CP-506 efficacy remains to be elucidated.

The effect of adding CP-506 to radiotherapy depends on the used treatment scheme and tumor model. For H460 xenografts, for which CP-506 (QD5) was administered before irradiation, no beneficial effect was found. The observed effect of radiotherapy alone was,

however, not in line with our expectations, and was far greater than in our previous studies (e.g. as in [20]: T4×SV of ~16 d vs ~35 d in the present study). Additionally, the fact that CP-506 did not reduce HF directly after treatment in the H460 xenograft model [Chapter 7] might explain the lack of increased efficacy in this model when radiotherapy was applied at this time point. In contrast, CP-506 (QD5) did synergistically improve treatment outcome when administered after radiotherapy in the CT26 syngeneic tumor model. It is possible that CP-506 alone does kill hypoxic tumor cells, however, not to such a degree to result in a measurable inhibition of tumor growth. The proliferation and repopulation of tumor cells may be too fast even during treatment, especially in murine tumors. This repopulation might originate from the surrounding well-oxygenated cells. Inactivating these cells with radiotherapy may slow down the repopulation and as a result decrease tumor growth rate. Additionally, we speculate that irradiated cells with sub-lethal damage might be more sensitive to CP-506. Further research is needed to fully elucidate the underlying mechanisms of the observed synergistic effect. This effect also demonstrates that tumors not responding to CP-506 monotherapy may respond when CP-506 is combined with radiotherapy.

To further study differences in treatment outcome between CP-506 administration before or after radiotherapy, an additional experiment was performed using CT26 tumor-bearing mice using two radiation dose levels. Instead of five, only two injections of CP-506 were administered, as tumor volumes at time of radiotherapy would otherwise differ ~3-fold between treatment groups and endpoint would likely be reached before the effect of the treatment would be visible. CP-506, however, did not improve treatment outcome regardless of whether given before or after irradiation and of radiation dose. Two injections of CP-506 in this experiment are thus probably not sufficient to cause beneficial effects.

As proof of principle, we used single dose radiotherapy in our experiments, as a large single dose as used here would sterilize normoxic cells and ensure tumor regrowth to solely depend on surviving hypoxic tumor cells [30]. In clinical practice, however, fractionated radiotherapy schedules are generally used with 2 Gy per fraction. It has been demonstrated that tumors reoxygenate, i.e. HF decreases, during fractionated radiotherapy, which can potentially diminish the effect from HAPs [31, 32]. Beneficial effects of adding evofosfamide to radiotherapy have been reported, for both evofosfamide administered before [20] and after [33] radiotherapy, but also when adding it to a fractionated radiotherapy schedule [34]. It would thus be interesting to test the combination of CP-506 with fractionated

radiotherapy. As CP-506 can reduce HF in *in vivo* human tumor xenografts at later time points [Chapter 7], we speculate that it can also increase efficacy of fractionated radiotherapy, or, alternatively, of single dose radiotherapy applied at a later time point.

In line with our hypothesis, CP-506 improved treatment outcome when combined with L19-IL2. This might be due to the decreased HF after CP-506 treatment, as hypoxia can negatively influence immunotherapy treatment outcome [17, 18]. HF after treatment is, however, yet to be determined. This would be in line with the results showing that evofosfamide sensitizes murine models of prostate cancer to an immunotherapy (antibody blockade of CTLA-4 and PD-1) by disrupting the HF [35]. Another possibility is that CP-506 causes immunogenic cell death (ICD): the process in which dying, stressed or injured cells start expressing, secreting or releasing damage-associated molecular patterns (DAMPs). These DAMPs can act as signals for the immune system and elicit an antitumor immune response [36]. CP-506 would thus kill (hypoxic) tumor cells, which undergo ICD thereby initiating an antitumor immune response, which in itself, however, is insufficient to result in tumor growth inhibition in the CT26 tumor model. In the combination treatment of CP-506 and L19-IL2, however, this immune response is further enhanced by the IL2 cytokine, resulting in tumor growth inhibition. Similar results have been observed previously for the combination of radiotherapy and L19-IL2, although in different murine models [14]. Further research is needed to elucidate how and to what extent CP-506 can cause ICD, and how this influences treatment outcome in the combination treatment with L19-IL2.

Adding radiotherapy to the combination of CP-506 and L19-IL2 did not further enhance treatment outcome. As radiotherapy can also induce ICD [36], it cannot be excluded that the immune responses caused by CP-506 and radiotherapy are highly similar and overlapping, and might not be additive, i.e., the anti-tumor immune response is already maximally enhanced by one of the treatments. This is supported, at least in part, by similar therapeutic efficacy of CP-506 monotherapy and radiotherapy. In one of the experiments, this combination caused severe body weight loss and discomfort in some animals. Due to a very short follow-up time in this experiment, it remains unknown whether these effects are reversible. More research is needed to elucidate the exact interactions of these treatments, and how they influence treatment outcome and toxicity. Experiments to study immunological and histological parameters after treatment are ongoing.

In conclusion, in the present study we have shown that CP-506 can improve radiotherapy

and immunotherapy outcome in preclinical *in vivo* animal tumor models, depending on the model and treatment schedule. CP-506 is a promising candidate for clinical efficacy validation, however, first more preclinical research is needed to determine the underlying mechanisms of the interplay between the treatments. Additionally, it is of importance to determine which factors, such as expression levels of nitroreductases that can activate it, affect CP-506 efficacy, and to what extent.

## Supplementary table and figures

**Supplementary table 1:** Group size and tumor starting volumes of all in vivo experiments reported in this study.

Experiment H460: CP-506 + RT				
Group	Vehicle	CP-506	Vehicle + RT	CP-506 + RT
Number of mice	8	8	7	7
Starting volume (mm <sup>3</sup> , mean ± SD)	227 ± 61	226 ± 18	213 ± 30	234 ± 58

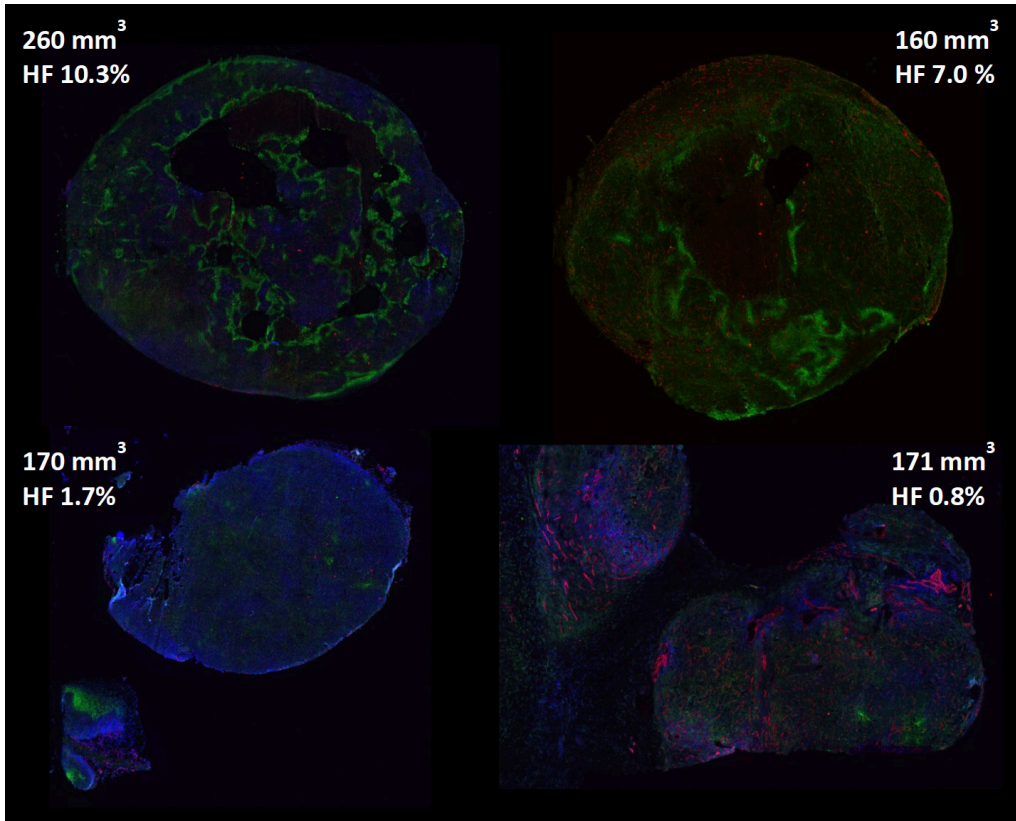
Experiment CT26: CP-506 + RT vs RT + CP-506								
Group	Vehicle + 5 Gy	CP-506 + 5 Gy	5 Gy + vehicle	5 Gy + CP-506	Vehicle + 10 Gy	CP-506 + 10 Gy	10 Gy + vehicle	10 Gy + CP-506
Number of mice	8	9	8	8	8	9	8	8
Starting volume (mm <sup>3</sup> , mean ± SD)	209 ± 30	189 ± 23	219 ± 38	222 ± 39	211 ± 34	206 ± 33	255 ± 62	242 ± 64

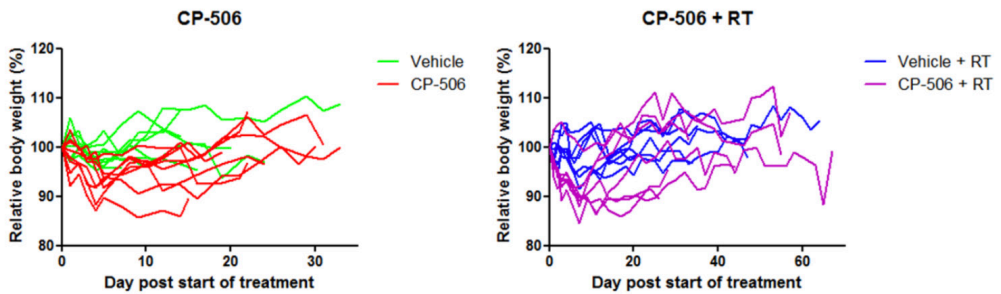
Experiment CT26: RT + CP-506 + L19-IL2								
Group	Vehicle	CP-506	RT + vehicle	RT + CP-506	Vehicle + L19-IL2	CP-506 + L19-IL2	RT + vehicle + L19-IL2	RT + CP-506 + L19-IL2
Number of mice	9	8	9	7	6	6	9	9
Starting volume (mm <sup>3</sup> , mean ± SD)	241 ± 36	225 ± 29	239 ± 36	245 ± 40	235 ± 42	220 ± 33	239 ± 30	226 ± 27

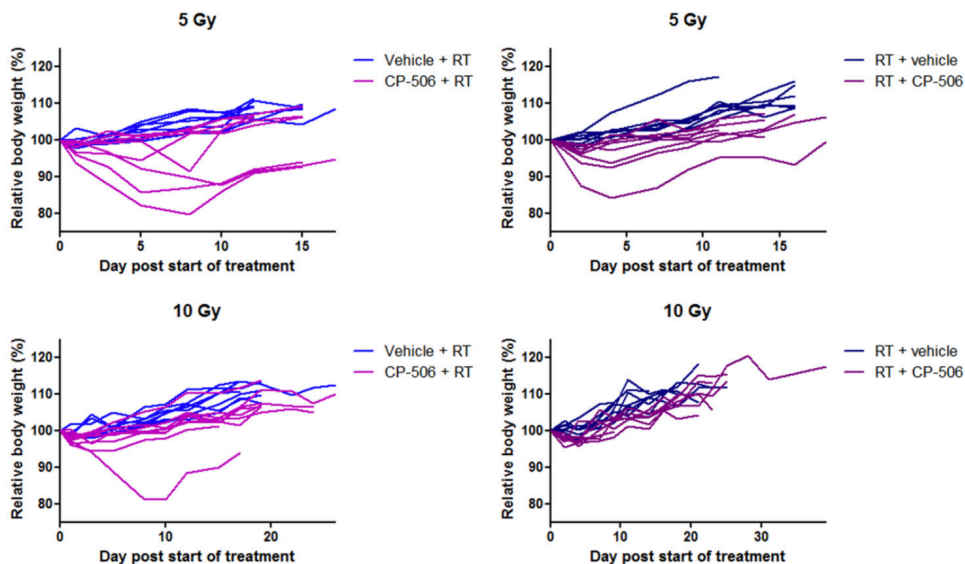
Experiment CT26: CP-506 + L19-IL2 (2)				
Group	Vehicle + vehicle	CP-506 + vehicle	Vehicle + L19-IL2	CP-506 + L19-IL2
Number of mice	8	7	7	7
Starting volume (mm <sup>3</sup> , mean ± SD)	203 ± 40	245 ± 74	221 ± 48	214 ± 48



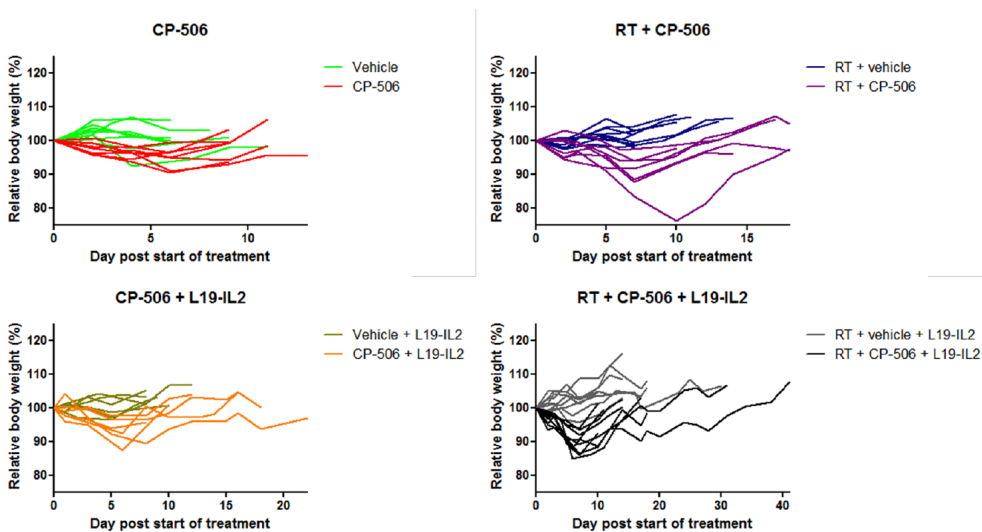
**Supplementary figure 1:** Baseline hypoxic fraction (HF) of CT26 tumors. Blue: Hoechst (nuclei); red: CD31 (blood vessels); green: pimonidazole (hypoxia).



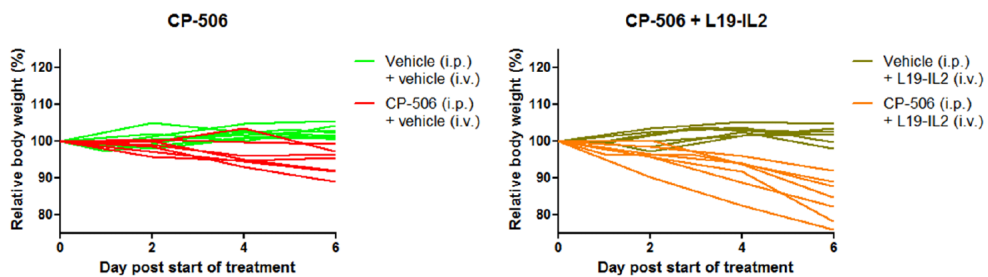
**Supplementary figure 2:** Body weight relative to body weight at start of treatment of animals treated with CP-506 compared to vehicle with (right) or without (left) radiation (RT).



**Supplementary figure 3:** Body weight relative to body weight at start of treatment of animals treated with CP-506 compared to vehicle with (right) or without (left) radiation (RT).



**Supplementary figure 4:** Body weight relative to body weight at start of treatment of animals treated with a combination of vehicle or CP-506 and radiation (RT).



**Supplementary figure 5:** Body weight relative to body weight at start of treatment of animals treated with a combination of vehicle, CP-506, L19-IL2 and/or radiation (RT).

## Acknowledgements

The authors acknowledge financial support from ERC advanced grant (ERC ADG-2015, n° 694812), The Dutch Cancer Society (KWF UM 2012-5394, KWF MAC 2013-6089) and from the Worldwide Cancer Research, formerly known as AICR (n° 15-0345).

## References

1. Forster, J.C., et al., *A review of the development of tumor vasculature and its effects on the tumor microenvironment*. Hypoxia (Auckl), 2017. **5**: p. 21-32.
2. Hockel, M. and P. Vaupel, *Tumor hypoxia: definitions and current clinical, biologic, and molecular aspects*. J Natl Cancer Inst, 2001. **93**(4): p. 266-76.
3. Nordsmark, M., et al., *Prognostic value of tumor oxygenation in 397 head and neck tumors after primary radiation therapy. An international multi-center study*. Radiother Oncol, 2005. **77**(1): p. 18-24.
4. Gray, L.H., et al., *The concentration of oxygen dissolved in tissues at the time of irradiation as a factor in radiotherapy*. Br J Radiol, 1953. **26**(312): p. 638-48.
5. Hall, E.J. and A.J. Giaccia, *Radiobiology for the radiologist*. 6th ed. 2006, Philadelphia: Lippincott Williams & Wilkins. ix, 546 p.
6. Tannock, I., *The basic science of oncology*. 5th ed. 2013, New York: McGraw-Hill. xi, 575 p.
7. Hockel, M., et al., *Hypoxic cervical cancers with low apoptotic index are highly aggressive*. Cancer Res, 1999. **59**(18): p. 4525-8.
8. Graeber, T.G., et al., *Hypoxia-mediated selection of cells with diminished apoptotic potential in solid tumours*. Nature, 1996. **379**(6560): p. 88-91.
9. Kim, C.Y., et al., *Selection of human cervical epithelial cells that possess reduced apoptotic potential to low-oxygen conditions*. Cancer Res, 1997. **57**(19): p. 4200-4.
10. Samali, A. and T.G. Cotter, *Heat shock proteins increase resistance to apoptosis*. Exp Cell Res, 1996. **223**(1): p. 163-70.
11. Zhivotovsky, B., B. Joseph, and S. Orrenius, *Tumor radiosensitivity and apoptosis*. Exp Cell Res, 1999. **248**(1): p. 10-7.
12. Khalil, D.N., et al., *The future of cancer treatment: immunomodulation, CARs and combination immunotherapy*. Nat Rev Clin Oncol, 2016. **13**(5): p. 273-90.
13. Carnemolla, B., et al., *Enhancement of the antitumor properties of interleukin-2 by its targeted delivery to the tumor blood vessel extracellular matrix*. Blood, 2002. **99**(5): p. 1659-65.
14. Zegers, C.M., et al., *Radiotherapy combined with the immunocytokine L19-IL2 provides long-lasting antitumor effects*. Clin Cancer Res, 2015. **21**(5): p. 1151-60.
15. Rekers, N.H., et al., *Combination of radiotherapy with the immunocytokine L19-IL2: Additive effect in a NK cell dependent tumour model*. Radiother Oncol, 2015. **116**(3): p. 438-42.
16. Rekers, N.H., et al., *The immunocytokine L19-IL2: An interplay between radiotherapy and long-lasting systemic anti-tumour immune responses*. 2017. 00-00.
17. Chaplin, D., et al., *Therapeutic significance of microenvironmental factors*. Blood Perfusion and Microenvironment of Human Tumors, 1998: p. 131-143.
18. Chouaib, S., et al., *Hypoxic stress: obstacles and opportunities for innovative immunotherapy of cancer*. Oncogene, 2017. **36**(4): p. 439-445.
19. Phillips, R.M., *Targeting the hypoxic fraction of tumours using hypoxia-activated prodrugs*. Cancer Chemother Phar-

- macol, 2016. **77**(3): p. 441-57.
20. Peeters, S.G., et al., *TH-302 in Combination with Radiotherapy Enhances the Therapeutic Outcome and Is Associated with Pretreatment [18F]HX4 Hypoxia PET Imaging*. Clin Cancer Res, 2015. **21**(13): p. 2984-92.
  21. Yaromina, A., et al., *Pimonidazole labelling and response to fractionated irradiation of five human squamous cell carcinoma (hSCC) lines in nude mice: the need for a multivariate approach in biomarker studies*. Radiother Oncol, 2006. **81**(2): p. 122-9.
  22. Guise, C.P., et al., *Identification of human reductases that activate the dinitrobenzamide mustard prodrug PR-104A: a role for NADPH:cytochrome P450 oxidoreductase under hypoxia*. Biochem Pharmacol, 2007. **74**(6): p. 810-20.
  23. Hunter, F.W., et al., *Identification of P450 Oxidoreductase as a Major Determinant of Sensitivity to Hypoxia-Activated Prodrugs*. Cancer Res, 2015. **75**(19): p. 4211-23.
  24. Hunter, F.W., B.G. Wouters, and W.R. Wilson, *Hypoxia-activated prodrugs: paths forward in the era of personalised medicine*. Br J Cancer, 2016. **114**(10): p. 1071-7.
  25. Evans, J.W., et al., *Homologous recombination is the principal pathway for the repair of DNA damage induced by tirapazamine in mammalian cells*. Cancer Res, 2008. **68**(1): p. 257-65.
  26. Meng, F., et al., *Molecular and cellular pharmacology of the hypoxia-activated prodrug TH-302*. Mol Cancer Ther, 2012. **11**(3): p. 740-51.
  27. Gu, Y., et al., *Roles of DNA repair and reductase activity in the cytotoxicity of the hypoxia-activated dinitrobenzamide mustard PR-104A*. Mol Cancer Ther, 2009. **8**(6): p. 1714-23.
  28. Hunter, F.W., et al., *Homologous recombination repair-dependent cytotoxicity of the benzotriazine di-N-oxide CEN-209: comparison with other hypoxia-activated prodrugs*. Biochem Pharmacol, 2012. **83**(5): p. 574-85.
  29. Hunter, F.W., et al., *Dual targeting of hypoxia and homologous recombination repair dysfunction in triple-negative breast cancer*. Mol Cancer Ther, 2014. **13**(11): p. 2501-14.
  30. Hill, R.P., R.S. Bush, and P. Yeung, *The effect of anaemia on the fraction of hypoxic cells in an experimental tumour*. Br J Radiol, 1971. **44**(520): p. 299-304.
  31. Stanley, J.A., W.U. Shipley, and G.G. Steel, *Influence of tumour size on hypoxic fraction and therapeutic sensitivity of Lewis lung tumour*. Br J Cancer, 1977. **36**(1): p. 105-13.
  32. Wouters, B.G. and J.M. Brown, *Cells at intermediate oxygen levels can be more important than the "hypoxic fraction" in determining tumor response to fractionated radiotherapy*. Radiat Res, 1997. **147**(5): p. 541-50.
  33. Takakusagi, Y., et al., *Radiotherapy Synergizes with the Hypoxia-Activated Prodrug Evofosfamide: In Vitro and In Vivo Studies*. Antioxid Redox Signal, 2018. **28**(2): p. 131-140.
  34. Lohse, I., et al., *Targeting hypoxic microenvironment of pancreatic xenografts with the hypoxia-activated prodrug TH-302*. Oncotarget, 2016. **7**(23): p. 33571-80.
  35. Ai, M., et al., *Tumor hypoxia drives immune suppression and immunotherapy resistance*. Journal for Immunotherapy of Cancer, 2015. **3**(Suppl 2): p. P392-P392. Krysko, D.V., et al., *Immunogenic cell death and DAMPs in cancer therapy*. Nat Rev Cancer, 2012. **12**(12): p. 860-75.
  36. Krysko, D.V., et al., *Immunogenic cell death and DAMPs in cancer therapy*. Nat Rev Cancer, 2012. **12**(12): p. 860-75.



# CHAPTER 9

Discussion and  
future perspectives

## Indirect targeting of tumor hypoxia by targeting carbonic anhydrase IX

### Novel carbonic anhydrase IX inhibitors in cancer treatment

Tumor hypoxia is a promising therapeutic target to exploit in cancer treatment, however, so far almost none of these treatments have been implemented in clinical practice. One way of targeting tumor hypoxia is to target its molecular response, e.g. targeting a hypoxia-inducible factor (HIF)-regulated protein which is implicated in cancer progression. One such protein is carbonic anhydrase IX (CA IX), which is mainly HIF regulated [1] and highly tumor specific [2]. CA IX expression is a negative prognostic factor in cancer patients regardless of the tumor type or site [3]. Also, CA IX has been found to select for and to maintain an aggressive cancer cell phenotype and to promote metastasis formation. This makes CA IX an attractive target for anticancer treatment [4-8].

Over the years, a large variety of CA IX inhibitors has been developed and tested [9-11], among which the novel fluorinated high-affinity CA IX inhibitors whose design, synthesis and biological evaluation are described in Chapter 5. All of these inhibitors bind into the active pocket of CA IX, and thus inhibit the conversion of carbon dioxide and water to bicarbonate and a proton [9, 10, 12]. This leads to decreased extracellular acidification, increased intracellular acidification and subsequent cell death [13, 14]. We have observed the same effects with the CA IX inhibitors described in Chapter 5. These inhibitors are thus potential agents for CA IX specific anticancer therapy. As CA IX is involved in tumor cell invasion and migration, CA IX inhibitors have the potential to inhibit these tumor cell properties, thereby also inhibiting metastasis formation. Indeed, the CA IX inhibitor S4 has demonstrated anti-metastatic potential [15, 16], although it remains unclear if this effect is not just due to decreased cell viability [15-17]. It would be interesting and important to study the effects of the novel CA IX inhibitors described in Chapter 5 on tumor cell invasion and migration.

Therapeutic success of cytotoxic compounds frequently used as anticancer agents is often limited due to systemic toxicity. Therefore, novel dual target drugs were designed, synthesized and biologically evaluated, as described in Chapter 4. These compounds are a new approach of delivering cytotoxic drugs specifically to CA IX expressing cells, which consist of different anticancer drugs conjugated to a CA IX targeting moiety. This should increase tumor specificity of the parental drugs and potentially decrease normal tissue toxicity. However, of all tested compounds, only an ATR inhibitor derivative was more effective in combination with radiotherapy in CA IX overexpressing cells compared to CA IX non-ex-

pressing cells. Furthermore, this compound showed poor binding affinity to recombinant CA IX, and showed no increased efficacy in hypoxic conditions. Therefore, the cytotoxic effect of this compound is probably not CA IX dependent; thus, none of the dual target compounds evaluated in Chapter 4 reduced tumor cell viability in a CA IX specific manner. The problem with conjugating two molecules is that there is a chance of conformational changes occurring to one, or maybe even both the molecules. In the case of the dual target compounds described in Chapter 4, this might have led to alteration of the efficacy of the cytotoxic moiety, and/or decreased binding affinity and/or specificity of the CA IX inhibiting moiety. Indeed,  $K_i$  values were observed to be higher for the tested compounds. Because of this observation, and the observed lack of efficacy, further development of these compounds has not been continued. Another dual target compound, consisting of the cytotoxic agent mertansine (DM1, a tubulin inhibitor) conjugated to a acetazolamide derivative (general CA inhibitor), was recently shown to exhibit a potent antitumor effect *in vivo* [18]. The dual targeting compound strategy thus remains of interest for further exploration.

*In vitro* monolayer cell cultures lack several important characteristics which are present in the tumor microenvironment, including pH, oxygen and nutrient gradients, and the presence of different cell types [19]. Some of these characteristics can be simulated using 3D *in vitro* cell culture methods: for example, in Chapter 7 we have shown the presence of an oxygen gradient in tumor cell spheroids. Others have also reported  $O_2$  and pH gradients in tumor cell spheroids [20]. In Chapter 5, hypoxia-dependent reduction of clonogenic survival by the lead CA IX inhibitor was only observed in spheroids, not in *in vitro* 2D cultures, highlighting the importance of these 3D cell culture models. However, even these cultures lack certain properties of tumors *in vivo*, like the presence of different cell types (e.g. tumor stroma). It is therefore essential that the efficacy of the CA IX inhibitors which proved most potent in 3D cell culture models is also validated in *in vivo* human tumor xenograft models. So far, this has been done with only a few inhibitors [11]. S4 therapy was found to have no effect on hypoxic fraction, proliferation and apoptosis in human tumor xenografts [21], and was ineffective in decreasing tumor xenograft growth [15]. It did, however, inhibit metastasis formation in human breast cancer xenografts [15]. Other CA IX inhibitors were able to inhibit osteosarcoma growth *in vivo* [22]. SLC-0111, another CA IX inhibitor, suppressed primary tumor growth and metastasis formation in *in vivo* human breast cancer xenografts [23]. The efficacy of the lead CA IX inhibitor described in Chapter 5 also needs to be tested in *in vivo* human tumor xenografts models, before proceeding into clinical trials.

Interestingly, there are preclinical indications that CA IX inhibition might radiosensitize cells. CA IX inhibitors have been shown to increase radiotherapy efficacy in human tumor xenografts [24]. Furthermore, it has been shown that CA IX knockdown in tumor cells leads to a lower number of cells in the S-phase of the cell cycle and increases radiosensitivity [25]. The exact mechanism underlying radiosensitization remains to be elucidated, however it would be interesting to test if the CA IX inhibitors described in Chapter 5 would also radiosensitize human tumor cells.

### **Future directions regarding CA IX targeting anticancer therapies**

Several CA IX inhibitors thus hold promise as anticancer therapies, however, so far, only SLC-0111 has been translated into clinical trials [11]. Results of a phase 1 clinical trial have not been published yet [26], but a second trial combining SLC-0111 with gemcitabine has recently been posted [27]. CA IX inhibitors have thus not proven their worth as anticancer therapies in clinical practice yet. It is expected that, should the SLC-0111 trials present positive results, more CA IX inhibitors might proceed into clinical trials. However, before implementing any of these compounds into clinical practice, their efficacy in combination with conventional therapies should be assessed, as these combinations have been largely ignored and the underlying mechanisms are poorly understood. Furthermore, because of the wide variety of CA IX inhibitors that are being investigated, there is a need to identify the most promising ones for continuation of clinical development. This identification should be based on the inhibitors' binding affinity, pharmacokinetic characteristics, and *in vitro* and *in vivo* preclinical therapeutic results. These preclinical studies should focus on characterizing the efficacy of the inhibitor in not one but several oncogenic processes, including proliferation, survival, invasion and migration, with the inhibitor as monotherapy as well as in combination with other treatment modalities.

Only patients having tumors expressing CA IX are expected to benefit from a CA IX targeting therapy. In Chapter 3, we demonstrate a novel  $^{68}\text{Ga}$ -labeled CA IX targeting positron emission tomography (PET) tracer to *in vivo* accumulate specifically in CA IX-expressing tumor xenografts, with low uptake in blood and intact clearance to the urine. Incorporating CA IX imaging, e.g. by PET imaging using the lead compound described in Chapter 3, or one of the many other CA IX targeting PET tracers that are being developed [28-32], into future clinical trials is advisable. This would ensure proper patient stratification and a reliable outcome on the efficacy of the CA IX inhibitor.

# Exploiting tumor hypoxia using hypoxia-activated prodrugs

## The novel hypoxia-activated prodrug CP-506

Tumor hypoxia can be directly targeted using hypoxia-activated prodrugs (HAPs). PR-104 is a HAP that has been extensively studied. *In vitro* and *in vivo*, PR-104 was found to be selectively active in hypoxia in a range of cancer cell lines and human tumor xenografts [33]. Clinical trials were initiated, however, clinical development of PR-104 stopped because it was found that it can be activated under normoxia, and thus in an oxygen-insensitive manner, by the two-electron reductase aldo-keto reductase 1C3 (AKR1C3) [34, 35], giving rise to severe dose-limiting myelotoxicity in several clinical trials [36, 37]. To tackle this limitation, the PR-104 molecule was chemically modified to prevent activation by AKR1C3, resulting in the novel HAP CP-506. In this thesis we present the first results of this new HAP: in Chapter 7 we show that CP-506 is indeed resistant to activation by AKR1C3, and that it has hypoxia-selective cytotoxicity in a range of *in vitro* 2D tumor cell monolayer cultures, as well as in several *in vitro* 3D tumor cell multilayer and spheroid cultures. Additionally, we show that it inhibits growth of several human tumor xenograft models *in vivo*, and that it reduces the hypoxic fraction in human breast cancer xenografts. However, treatment with a HAP alone is not sufficient, since well-oxygenated cells will be targeted only to a certain degree (by the HAP's bystander effect). Combining HAPs with other cancer treatments which target these well-oxygenated cells, such as radiotherapy, thus is essential. In Chapter 8, we show promising (preliminary) data demonstrating anticancer effects of CP-506 when combined with radiotherapy or immunotherapy in an *in vivo* syngeneic model. CP-506 has thus shown to be a promising novel HAP with potential favorable properties for future clinical use, although more studies are required to validate our findings and to determine factors determining the therapeutic effect of CP-506 alone or in combination with other treatment modalities.

## Alternative approach: molecularly targeted hypoxia-activated prodrugs

Traditional HAPs, to which CP-506 belongs, generally release a DNA-damaging cytotoxin in hypoxic conditions. This cell killing mechanism is comparable to the one of traditional chemotherapeutics, which may create a toxicity overlap that might limit the future utility of these traditional HAPs in combination with conventional cancer treatments [38]. Therefore, more and more research on HAPs focuses on a new class of HAPs that do not release a potent DNA-damaging cytotoxin, but instead release a molecularly targeted protein ligand.

This way, these HAPs can specifically target anticancer agents to hypoxic tumor cells [38]. The nuclear poly(ADP-ribose) polymerase 1 (PARP1) protein promotes DNA repair by binding to sites of DNA damage [39]. A PARP inhibitor could thus enhance the effect of DNA-damaging treatments. A hypoxia-activated PARP inhibitor, CEP-9722, is currently in phase 2 clinical trials being tested in patients with advanced solid tumors or mantle cell lymphoma either as monotherapy or in combination with gemcitabine, cisplatin or temozolomide [40-43].

Alkyl groups at the O<sup>6</sup> position of guanine can be removed by O<sup>6</sup>-alkylguanine-DNA alkyltransferase (AGT), causing resistance to DNA-alkylators [44]. A HAP of O<sup>6</sup>-benzylguanine, an AGT inhibitor, sensitizes cancer cells to larmustine, an O<sup>6</sup>-alkylator, *in vitro* [45]. It would be interesting to study the anticancer effects of a combination of CP-506, a DNA-alkylator, with a HAP of this subgroup.

Checkpoint kinase 1 (Chk1) and Aurora A kinase fulfill important roles in cell-cycle progression and regulation. Several Chk1 inhibitors have been developed and investigated clinically, but many of these clinical trials were terminated due to cardiotoxicity [46, 47], probably as a result of systemic inhibition of Chk1. CH-01 is a HAP of a Chk1 and Aurora A kinase inhibitor and can thus specifically inhibit these kinases in hypoxic areas only, potentially limiting toxicity in normal, healthy tissues [48]. In several cancer cell lines *in vitro*, CH-01 significantly reduced cell viability in hypoxic conditions [48]. Since Chk1 inhibition leads to radiosensitization of cancer cells *in vivo* [49], it would be interesting to investigate the combination treatment of CH-01 with radiotherapy.

DNA-dependent protein kinase, catalytic subunit (DNA-PKcs) is a DNA-repair protein required for non-homologous end-joining [50]. Inhibition of DNA-PKcs leads to radiosensitization of cancer cells *in vitro* [51], which was also observed with BCCA621C, a HAP of a DNA-PKcs inhibitor [51].

HER signaling pathways are involved in a range of cellular processes, including but not limited to the regulation of cell growth and survival, adhesion, migration and differentiation [52]. In cancer, HER kinases, belonging to the epidermal growth factor receptor (EGFR) tyrosine kinases, are often hyperactivated, potentially causing tumor progression, angiogenesis and metastasis [52]. Interfering with HER signaling pathways is therefore an interesting approach for anticancer therapy. Indeed, tyrosine kinase inhibitors (TKIs) such as erlotinib are used as treatment for non-small cell lung cancer (NSCLC) and other types of cancer in which EGFR mutations are frequently found [53]. However, because of their roles in normal cellular functioning, it is desirable to avoid systemic inhibition of HER kinases. Also, cancer cells often become resistant to existing EGFR TKI treatments [54, 55].

TH-4000 (tarloxotinib) is a HAP of a pan-HER inhibitor. More specifically, it releases an irreversible EGFR TKI specifically in hypoxic conditions, thereby potentially overcoming the limitations of conventional EGFR TKIs [56]. In a range of NSCLC cell lines *in vitro*, TH-4000 was found to specifically kill hypoxic cells. Additionally, in *in vivo* human NSCLC xenograft models it inhibited tumor growth to the same or even to a higher extent than erlotinib [57, 58]. Clinical trials with TH-4000 were started, however, two recent phase 2 trials in patients with NSCLC, head and neck squamous cell carcinoma (HNSCC) and squamous cell carcinoma of the skin were terminated because patients with NSCLC and HNSCC did not achieve the primary interim response rate endpoint [59-61]. It should be noted that these trials did include baseline hypoxia PET imaging using  $^{18}\text{F}$ -HX4, which is an encouraging development that should be incorporated in more future trials, as discussed later.

In summary, several molecularly targeted HAPs have been designed and are in different stages of clinical development up to phase 3 clinical trials, but none have made it into clinical practice yet. Additionally, combining these HAPs with conventional cancer treatments is an interesting approach, which requires further investigations. An important reason for the development of this new class of HAPs is the potential toxicity overlap of traditional HAPs with conventional anticancer treatments, which would limit their use. However, it is expected that this toxicity overlap is minimal for the HAP CP-506, investigated in this thesis. Since CP-506 is activated only in severe hypoxic conditions only found in tumors, and cannot be activated by aerobic two-electron reductases, it is expected that the toxicity of CP-506 is minimal, and that it can thus safely be combined with other anticancer treatments. However, more research is needed to determine the exact mechanism of action of CP-506, factors influencing tumor sensitivity to it, and its mechanisms of action in combination with other treatment modalities, before it can proceed to go into clinical trials. This holds true not only for CP-506, but for every HAP that is intended to go into clinical practice, as discussed below.

### **Future directions regarding hypoxia-activated prodrugs**

Several HAPs so far have shown promising potential in preclinical experiments but could not live up to expectations in clinical trials. What is probably the most important shortcoming of most clinical HAP trials is the failure to stratify patients who would actually benefit from HAP therapy from patients who would not. The difficulties of dividing patients into these subgroups are substantial, because there are several criteria that are involved in determining a HAP's effectiveness, including but not limited to the extent of tumor hypoxia, the tumor reductase expression profile, and the intrinsic sensitivity of tumor cells

to the HAP's active metabolite(s).

Direct measurement of tumor oxygenation is possible using needle electrodes, however the applicability of this technique is limited to accessible tumors, and only very few centers have this equipment [62]. A more applicable option is the noninvasive use of hypoxia tracers such as the PET tracers  $^{18}\text{F}$ -FMISO,  $^{18}\text{F}$ -FAZA and  $^{18}\text{F}$ -HX4 [62], reviewed in Chapter 2. High expression levels of hypoxia- (HIF-)regulated proteins such as CA IX can serve as surrogate hypoxia markers, enabling the use of tracers targeting these proteins, such as the  $^{68}\text{Ga}$ -labeled CA IX targeting small molecule PET tracer we synthesized and investigated in Chapter 3. However, no individual gene can be considered a definitive hypoxia marker [63]. Therefore, a number of hypoxia gene expression signatures, encompassing expression levels of multiple hypoxia-regulated genes, have been developed [64].

Even among homogenous patient populations the incidence and severity of tumor hypoxia can vary extensively; for example, in a study of HNSCC, hypoxic fraction varied 20-fold across 103 patients [65]. In preclinical tumor xenograft models, however, tumor hypoxia is often more extensive and homogeneous. This might overestimate the HAP's actual effectiveness, and is something that should be kept in mind when investigating HAPs [38]. For successful patient stratification in future clinical trials, a form of tumor hypoxia assessment must thus be incorporated to determine the presence, extent and severity of tumor hypoxia in each patient. This was demonstrated in a retrospective sub-study of 45 HNSCC patients within a phase 2 clinical trial in which patients were randomly assigned to chemoradiotherapy with or without tirapazamine (TPZ).  $^{18}\text{F}$ -FMISO PET imaging identified patients with substantial pre-treatment tumor hypoxia. Importantly, adding TPZ to conventional treatments (chemoradiotherapy) in patients having a hypoxic tumor significantly reduced locoregional failure (1 out of 19) compared to standard treatment only (8 out of 13) [66]. The aforementioned hypoxia gene expression signatures also hold promise in this respect. In a retrospective study, patients were classified into 'more hypoxic' and 'less hypoxic' subsets using a 15-gene hypoxia signature. This showed the signature to be a prognostic as well as a predictive factor for the effect of nimorazole in combination with radiotherapy. In patients with hypoxic tumors five-year locoregional control improved from 18 to 49%, whereas it did not improve in patients with less hypoxic tumors [67, 68]. These findings clearly demonstrate the need for tools to assess pre-treatment tumor hypoxia status. Most recent clinical HAP trials, such as the two large-scale phase 3 trials in which no improved overall survival was found when combining evofosfamide with gemcitabine

or doxorubicin [69, 70], did however still not incorporate hypoxia imaging. This might be because many centers do not have the necessary capacity and/or equipment to carry this out, limiting their participation in such trials. Also, the costs associated with hypoxia assessment and subsequent patient stratification would likely be high [38]. The absence of patient stratification could however very well explain the failure of these clinical trials, and thus it is vital that patient stratification based on tumor hypoxia is implemented in future clinical HAP trials. In Chapter 6, we propose a biomarker-stratified enriched study design for these trials, in which only biomarker-positive patients are randomized between standard treatment and the combination of standard treatment with HAPs. The number of patients needed for this phase 3 design is far lower than in current randomize-all designs, even when a phase 2 trial in which the threshold for the hypoxia biomarker of choice is evaluated is done first.

Because of the heterogeneity of tumor hypoxia, the HAP's bystander effect is important for its efficacy. Indeed, the antitumor efficacy of PR-104 is thought to be partially due to its bystander effect [71]. As CP-506 is based on PR-104, it is expected to have a similar bystander effect, and thus that this effect is an important contributor to the total effect of CP-506. However, CP-506 requires severe hypoxic, or anoxic, conditions for its activation. Thus, cells that are hypoxic enough to be radio- or chemoresistant ( $< 0.13\% \text{ O}_2$  [72]), but not enough to activate CP-506, need to be adjacent to an anoxic area to be targeted by CP-506. Because of the large variation in both perfusion and hypoxia in tumors [73], it could be beneficial to incorporate one of the emerging techniques for *in situ* functional imaging of intratumoral heterogeneity [74] into future clinical trials [38].

Tumor hypoxia should not only be present, but should also be treatment-limiting for HAPs to be beneficial. Apparently, this is not always the case, as is evidenced in HNSCC. In this type of cancer, hypoxia is associated with locoregional failure of patients treated with radiotherapy [75]. HNSCC can be divided into subtypes, among which those caused by human papillomavirus (HPV) infection. Positive tumor HPV status is associated with significantly improved overall survival, and the genomic character of these subtypes is different from the HPV-negative subtypes [76, 77]. Using the afore-mentioned 15-gene hypoxia signature, the range and levels of hypoxia were found to be similar in HPV-positive and HPV-negative subtypes [68, 78]. A retrospective study showed, however, that nimorazole did improve radiotherapy treatment outcome in patients with a negative hypoxic tumor HPV status, but not in patients with positive hypoxic tumor HPV status [79]. Another

retrospective study showed that TPZ improved chemoradiotherapy treatment outcome only in patients with a negative hypoxic tumor HPV status [80]. Similar observations were done in prostate cancer: hypoxia was found to be associated with early biochemical relapse after radiotherapy and also with local recurrence in the prostate gland [81]. The same patient cohort was divided into genetic subtypes in a follow-up study, with a high or low percentage of genome alteration. Hypoxia was associated with poor prognosis in the subtype with high genomic instability only, which was validated in another, independent patient cohort [82]. These studies show that in HNSCC and in prostate cancer hypoxia is not always a treatment-limiting factor. Therefore, it could be beneficial in future clinical trials to not only include hypoxia imaging, but also evaluate the genetic subtypes of the disease. More research is needed to elucidate the role of tumor hypoxia in patient prognosis in different cancer types.

Another factor that determines the response of a tumor to HAP treatment is the expression of reductases that can activate the HAP. *In vitro*, the activating enzymes have been identified for several HAPs and include POR, MTRR, NDOR1, NOS, FOXRED2 and CYB5R3 [35, 83-89]. Although these studies identify enzymes capable of activating HAPs, they do not show which are important at endogenous expression levels, as these studies were all performed using gain-of-function models. Gene knockout models and genetic loss-of-functions screens are more suitable to determine the latter. For example, this way POR was identified as the most important determinant of hypoxic cell sensitivity to the HAP SN30000, an optimized analogue of TPZ [90]. It has yet to be determined if POR is equally important in the activation of other HAPs, including CP-506. It would thus be optimal if future clinical trials not only incorporate hypoxia assessment, but also a screening for reductase expression levels, more specifically the reductase(s) that is/are known important mediator(s) of sensitivity to the HAP being investigated. Of interest is that the specific binding of aforementioned nitroimidazole hypoxia markers such as pimonidazole,  $^{18}\text{F}$ -FMISO,  $^{18}\text{F}$ -FAZA and  $^{18}\text{F}$ -HX4 is dependent on hypoxia as well as on one-electron reductase activity [88, 91]. Thus, these PET agents could serve as both hypoxia- and one-electron reductase-markers, assuming that the same reductase(s) are responsible for the activation of an imaging probe and therapeutic agent [73].

Most HAPs, including CP-506, release cytotoxins that react with the DNA. Therefore, DNA damage response pathways are likely a determinant of intrinsic sensitivity of tumor cells to these cytotoxins. Indeed, *in vitro* it was shown that TPZ, evofosfamide and PR-104 are

more effective in tumor cells in which homologous recombination (HR) genes are knocked down or knocked out [84, 92, 93]. It has been found that HR deficiency in several cancer cell types and a human tumor xenograft model increases cytotoxicity of DNA crosslinking HAPs (evofosfamide, PR-104) more than other HAP classes [94, 95]. This suggests that patients with HR defective tumors would benefit most from DNA crosslinking HAPs, to which CP-506 belongs. Thus, it would be beneficial if future clinical trials also incorporate a screening for biomarkers that predict sensitivity of tumor cells to the HAP. However, first more research is needed to identify and validate these biomarkers, as so far only one predictive biomarker (mutation or expression of ERCC1, a DNA repair gene) for a crosslinking agent (cisplatin) has been reported [96], but none are in clinical use [97].

Similarly to hypoxia heterogeneity in tumors, the expression profile of biomarkers for intrinsic sensitivity might also be variable. For example, hypoxia can downregulate DNA repair pathways, including HR [98]. This might increase intrinsic sensitivity of these hypoxic cells to HAPs, as in the case of conventional DNA crosslinking agents [99]. However, the surrounding more oxygenated cells, which are targeted by the HAP's metabolites via its bystander effect, would not have this increased intrinsic sensitivity, limiting this cytotoxicity due to the bystander effect. Therefore, the afore-mentioned emerging techniques for *in situ* functional imaging of intratumoral heterogeneity [74] could be included into future clinical trials not only to determine the variation in perfusion and hypoxia in tumors, but also the variation in expression of biomarker(s) reflecting intrinsic sensitivity to HAPs.

## **Concluding: future directions for exploiting tumor hypoxia for cancer treatment**

Tumor hypoxia is interesting to exploit for cancer treatment. However, the complexity of it and all its involved processes is a likely explanation for the failure of many hypoxia-targeting anticancer therapies that have been developed. However, the success of nimorazole (it being standard of care for the treatment of HNSCC in Denmark [100, 101]) proves that it is possible to exploit tumor hypoxia in cancer treatment. Novel hypoxia-targeting agents need proper preclinical characterization, required for selection of the most optimal drug for clinical testing. These clinical trials require a proper setup, incorporating techniques that allow accurate patient stratification, as it is likely that not all patients will benefit from these agents. This stratification ensures a reliable outcome on the efficacy of the treatment

and improves the chance that in the future more patients will benefit from hypoxia targeting anticancer therapies.

## References

1. Wykoff, C.C., et al., *Hypoxia-inducible expression of tumor-associated carbonic anhydrases*. *Cancer Res*, 2000. **60**(24): p. 7075-83.
2. Pastorekova, S., et al., *Carbonic anhydrase IX, MN/CA IX: analysis of stomach complementary DNA sequence and expression in human and rat alimentary tracts*. *Gastroenterology*, 1997. **112**(2): p. 398-408.
3. van Kuijk, S.J., et al., *Prognostic Significance of Carbonic Anhydrase IX Expression in Cancer Patients: A Meta-Analysis*. *Front Oncol*, 2016. **6**: p. 69.
4. Wykoff, C.C., et al., *Expression of the hypoxia-inducible and tumor-associated carbonic anhydrases in ductal carcinoma in situ of the breast*. *Am J Pathol*, 2001. **158**(3): p. 1011-9.
5. Smeland, E., et al., *Prognostic impacts of hypoxic markers in soft tissue sarcoma*. *Sarcoma*, 2012. **2012**: p. 541650.
6. Stewart, D.J., et al., *Membrane carbonic anhydrase IX expression and relapse risk in resected stage I-II non-small-cell lung cancer*. *J Thorac Oncol*, 2014. **9**(5): p. 675-84.
7. Kim, S.J., et al., *Prognostic value of carbonic anhydrase IX and Ki-67 expression in squamous cell carcinoma of the tongue*. *Jpn J Clin Oncol*, 2007. **37**(11): p. 812-9.
8. Douglas, C.M., et al., *Lack of prognostic effect of carbonic anhydrase-9, hypoxia inducible factor-1alpha and bcl-2 in 286 patients with early squamous cell carcinoma of the glottic larynx treated with radiotherapy*. *Clin Oncol (R Coll Radiol)*, 2013. **25**(1): p. 59-65.
9. Monti, S.M., C.T. Supuran, and G. De Simone, *Anticancer carbonic anhydrase inhibitors: a patent review (2008 - 2013)*. *Expert Opin Ther Pat*, 2013. **23**(6): p. 737-49.
10. Lomelino, C. and R. McKenna, *Carbonic anhydrase inhibitors: a review on the progress of patent literature (2011-2016)*. *Expert Opin Ther Pat*, 2016. **26**(8): p. 947-56.
11. Supuran, C.T., *Carbonic Anhydrase Inhibition and the Management of Hypoxic Tumors*. *Metabolites*, 2017. **7**(3).
12. Supuran, C.T., *Carbonic anhydrases: novel therapeutic applications for inhibitors and activators*. *Nat Rev Drug Discov*, 2008. **7**(2): p. 168-81.
13. Swietach, P., et al., *The role of carbonic anhydrase 9 in regulating extracellular and intracellular pH in three-dimensional tumor cell growths*. *J Biol Chem*, 2009. **284**(30): p. 20299-310.
14. Swietach, P., et al., *Tumor-associated carbonic anhydrase 9 spatially coordinates intracellular pH in three-dimensional multicellular growths*. *J Biol Chem*, 2008. **283**(29): p. 20473-83.
15. Gieling, R.G., et al., *Antimetastatic effect of sulfamate carbonic anhydrase IX inhibitors in breast carcinoma xenografts*. *J Med Chem*, 2012. **55**(11): p. 5591-600.
16. Ward, C., et al., *Evaluation of carbonic anhydrase IX as a therapeutic target for inhibition of breast cancer invasion and metastasis using a series of in vitro breast cancer models*. *Oncotarget*, 2015. **6**(28): p. 24856-70.
17. Winum, J.Y., et al., *Ureido-substituted sulfamates show potent carbonic anhydrase IX inhibitory and antiproliferative activities against breast cancer cell lines*. *Bioorg Med Chem Lett*, 2012. **22**(14): p. 4681-5.

18. Krall, N., et al., *A small-molecule drug conjugate for the treatment of carbonic anhydrase IX expressing tumors*. *Angew Chem Int Ed Engl*, 2014. **53**(16): p. 4231-5.
19. Horsman, M.R. and P. Vaupel, *Pathophysiological Basis for the Formation of the Tumor Microenvironment*. *Front Oncol*, 2016. **6**: p. 66.
20. Gorlach, A. and H. Acker, *pO<sub>2</sub>- and pH-gradients in multicellular spheroids and their relationship to cellular metabolism and radiation sensitivity of malignant human tumor cells*. *Biochim Biophys Acta*, 1994. **1227**(3): p. 105-12.
21. Meijer, T.W., et al., *Tumor microenvironmental changes induced by the sulfamate carbonic anhydrase IX inhibitor S4 in a laryngeal tumor model*. *PLoS One*, 2014. **9**(9): p. e108068.
22. Perut, F., et al., *Carbonic anhydrase IX inhibition is an effective strategy for osteosarcoma treatment*. *Expert Opin Ther Targets*, 2015. **19**(12): p. 1593-605.
23. Lou, Y., et al., *Targeting tumor hypoxia: suppression of breast tumor growth and metastasis by novel carbonic anhydrase IX inhibitors*. *Cancer Res*, 2011. **71**(9): p. 3364-76.
24. Dubois, L., et al., *Specific inhibition of carbonic anhydrase IX activity enhances the in vivo therapeutic effect of tumor irradiation*. *Radiother Oncol*, 2011. **99**(3): p. 424-31.
25. Doyen, J., et al., *Knock-down of hypoxia-induced carbonic anhydrases IX and XII radiosensitizes tumor cells by increasing intracellular acidosis*. *Front Oncol*, 2012. **2**: p. 199.
26. *Safety Study of SLC-0111 in Subjects With Advanced Solid Tumours*. Available A Study of SLC-0111 and Gemcitabine for Metastatic Pancreatic Ductal Cancer in Subjects Positive for CAIX.
27. Akurathi, V., et al., *Development and biological evaluation of (9)(9)mTc-sulfonamide derivatives for in vivo visualization of CA IX as surrogate tumor hypoxia markers*. *Eur J Med Chem*, 2014. **71**: p. 374-84.
28. Akurathi, V., et al., *Synthesis and biological evaluation of a 99mTc-labelled sulfonamide conjugate for in vivo visualization of carbonic anhydrase IX expression in tumor hypoxia*. *Nucl Med Biol*, 2010. **37**(5): p. 557-64.
29. Peeters, S.G., et al., *[(18)F]VM4-037 MicroPET Imaging and Biodistribution of Two In Vivo CAIX-Expressing Tumor Models*. *Mol Imaging Biol*, 2015. **17**(5): p. 615-9.
30. Minn, I., et al., *[64Cu]XYIMSR-06: A dual-motif CAIX ligand for PET imaging of clear cell renal cell carcinoma*. *Oncotarget*, 2016. **7**(35): p. 56471-56479.
31. Cheal, S.M., et al., *Pairwise comparison of 89Zr- and 124I-labeled cG250 based on positron emission tomography imaging and nonlinear immunokinetic modeling: in vivo carbonic anhydrase IX receptor binding and internalization in mouse xenografts of clear-cell renal cell carcinoma*. *Eur J Nucl Med Mol Imaging*, 2014. **41**(5): p. 985-94.
32. Patterson, A.V., et al., *Mechanism of action and preclinical antitumor activity of the novel hypoxia-activated DNA cross-linking agent PR-104*. *Clin Cancer Res*, 2007. **13**(13): p. 3922-32.
33. Guise, C.P., et al., *The bioreductive prodrug PR-104A is activated under aerobic conditions by human aldo-keto reductase 1C3*. *Cancer Res*, 2010. **70**(4): p. 1573-84.

34. Guise, C.P., et al., *Identification of human reductases that activate the dinitrobenzamide mustard prodrug PR-104A: a role for NADPH:cytochrome P450 oxidoreductase under hypoxia*. *Biochem Pharmacol*, 2007. **74**(6): p. 810-20.
35. McKeage, M.J., et al., *PR-104 a bioreductive pre-prodrug combined with gemcitabine or docetaxel in a phase Ib study of patients with advanced solid tumours*. *BMC Cancer*, 2012. **12**: p. 496.
36. Abou-Alfa, G.K., et al., *PR-104 plus sorafenib in patients with advanced hepatocellular carcinoma*. *Cancer Chemother Pharmacol*, 2011. **68**(2): p. 539-45.
37. Mistry, I.N., et al., *Clinical Advances of Hypoxia-Activated Prodrugs in Combination With Radiation Therapy*. *Int J Radiat Oncol Biol Phys*, 2017. **98**(5): p. 1183-1196.
38. Gibson, B.A. and W.L. Kraus, *New insights into the molecular and cellular functions of poly(ADP-ribose) and PARPs*. *Nat Rev Mol Cell Biol*, 2012. **13**(7): p. 411-24.
39. Plummer, R., et al., *Phase 1 dose-escalation study of the PARP inhibitor CEP-9722 as monotherapy or in combination with temozolomide in patients with solid tumors*. *Cancer Chemother Pharmacol*, 2014. **74**(2): p. 257-65.
40. *Study of CEP-9722 in Combination With Gemcitabine and Cisplatin in Patients With Advanced Solid Tumors or Mantle Cell Lymphoma*.
41. *Study of CEP-9722 as Single-Agent Therapy and as Combination Therapy With Temozolomide in Patients With Advanced Solid Tumors*.
42. *Study to Determine the Maximum Tolerated Dose of the PARP Inhibitor CEP-9722 in Patients With Solid Tumors*. Available.
43. Penketh, P.G., et al., *1,2-Bis(methylsulfonyl)-1-(2-chloroethyl)-2-[(methylamino)carbonyl]hydrazine (VNP40101M): I. Direct inhibition of O6-alkylguanine-DNA alkyltransferase (AGT) by electrophilic species generated by decomposition*. *Cancer Chemother Pharmacol*, 2004. **53**(4): p. 279-87.
44. Zhu, R., et al., *Hypoxia-selective O6-alkylguanine-DNA alkyltransferase inhibitors: design, synthesis, and evaluation of 6-(benzyloxy)-2-(aryldiazenyl)-9H-purines as prodrugs of O6-benzylguanine*. *J Med Chem*, 2013. **56**(3): p. 1355-9.
45. Sakurikar, N. and A. Eastman, *Will targeting Chk1 have a role in the future of cancer therapy?* *J Clin Oncol*, 2015. **33**(9): p. 1075-7.
46. Sausville, E., et al., *Phase I dose-escalation study of AZD7762, a checkpoint kinase inhibitor, in combination with gemcitabine in US patients with advanced solid tumors*. *Cancer Chemother Pharmacol*, 2014. **73**(3): p. 539-49.
47. Cazares-Korner, C., et al., *CH-01 is a hypoxia-activated prodrug that sensitizes cells to hypoxia/reoxygenation through inhibition of Chk1 and Aurora A*. *ACS Chem Biol*, 2013. **8**(7): p. 1451-9.
48. Morgan, M.A., et al., *Mechanism of radiosensitization by the Chk1/2 inhibitor AZD7762 involves abrogation of the G2 checkpoint and inhibition of homologous recombinational DNA repair*. *Cancer Res*, 2010. **70**(12): p. 4972-81.
49. Neal, J.A. and K. Meek, *Choosing the right path: does DNA-PK help make the decision?* *Mutat Res*, 2011. **711**(1-2): p. 73-86.
50. Lindquist Kirstin, E., et al., *Selective radiosensitization of hypoxic cells using BCCA621C: a novel hypoxia activated prodrug targeting DNA-dependent protein kinase*, in *Tumor Microenvironment and Therapy*. 2013. p. 46.
51. Luo, M. and L.W. Fu, *Redundant kinase activation and resistance of EGFR-tyrosine kinase inhibitors*. *Am J Cancer Res*,

2014. **4**(6): p. 608-28.
52. Rosell, R., et al., *Screening for epidermal growth factor receptor mutations in lung cancer*. N Engl J Med, 2009. **361**(10): p. 958-67.
  53. Wu, S.G. and J.Y. Shih, *Management of acquired resistance to EGFR TKI-targeted therapy in advanced non-small cell lung cancer*. Mol Cancer, 2018. **17**(1): p. 38.
  54. Kazaz, S.N. and I. Oztop, *Treatment After First-Generation Epidermal Growth Factor Receptor Tyrosine Kinase Inhibitor Resistance in Non-Small-Cell Lung Cancer*. Turk Thorac J, 2017. **18**(3): p. 66-71.
  55. Smail, J.B., et al., *Abstract C46: Design and identification of the novel hypoxia-activated irreversible panHER inhibitor SN29966*. Molecular Cancer Therapeutics, 2009. **8**(12 Supplement): p. C46-C46.
  56. Patterson, A.V., et al., *TH-4000, a hypoxia-activated EGFR/Her2 inhibitor to treat EGFR-TKI resistant T790M-negative NSCLC*. Journal of Clinical Oncology, 2015. **33**(15\_suppl): p. e13548-e13548.
  57. Patterson, A.V., et al., *Abstract 5358: The hypoxia-activated EGFR-TKI TH-4000 overcomes erlotinib-resistance in pre-clinical NSCLC models at plasma levels achieved in a Phase 1 clinical trial*. Cancer Research, 2015. **75**(15 Supplement): p. 5358-5358.
  58. *Threshold Pharmaceuticals Announces Interim Results from Tarloxotinib Program and its Plans to Focus on Evofosfamide and Earlier-Stage Opportunities*. Available from: <http://investor.thresholdpharm.com/releasedetail.cfm?ReleaseID=991559>.
  59. *Study for Treatment of Patients With EGFR Mutant, T790M-negative NSCLC*. Available from: <https://ClinicalTrials.gov/show/NCT02454842>.
  60. *Study for Treatment of Patients With Recurrent or Metastatic SCCHN or SCCS*. Available from: <https://ClinicalTrials.gov/show/NCT02449681>.
  61. Xu, Z., et al., *(18)F-Fluoromisonidazole in tumor hypoxia imaging*. Oncotarget, 2017. **8**(55): p. 94969-94979.
  62. Moon, E.J., et al., *The potential role of intrinsic hypoxia markers as prognostic variables in cancer*. Antioxid Redox Signal, 2007. **9**(8): p. 1237-94.
  63. Harris, B.H., et al., *Gene Expression Signatures as Biomarkers of Tumour Hypoxia*. Clin Oncol (R Coll Radiol), 2015. **27**(10): p. 547-60.
  64. Hoogsteen, I.J., et al., *Hypoxia in larynx carcinomas assessed by pimonidazole binding and the value of CA-IX and vascularity as surrogate markers of hypoxia*. Eur J Cancer, 2009. **45**(16): p. 2906-14.
  65. Rischin, D., et al., *Prognostic significance of [18F]-misonidazole positron emission tomography-detected tumor hypoxia in patients with advanced head and neck cancer randomly assigned to chemoradiation with or without tirapazamine: a substudy of Trans-Tasman Radiation Oncology Group Study 98.02*. J Clin Oncol, 2006. **24**(13): p. 2098-104.
  66. Toustrup, K., et al., *Development of a hypoxia gene expression classifier with predictive impact for hypoxic modification of radiotherapy in head and neck cancer*. Cancer Res, 2011. **71**(17): p. 5923-31.
  67. Toustrup, K., et al., *Gene expression classifier predicts for hypoxic modification of radiotherapy with nimorazole in squamous cell carcinomas of the head and neck*. Radiother Oncol, 2012. **102**(1): p. 122-9.

68. Tap, W.D., et al., *Doxorubicin plus evofosfamide versus doxorubicin alone in locally advanced, unresectable or metastatic soft-tissue sarcoma (TH CR-406/SARC021): an international, multicentre, open-label, randomised phase 3 trial*. *Lancet Oncol*, 2017. **18**(8): p. 1089-1103.
69. *Clinical Trial Testing TH-302 in Combination With Gemcitabine in Previously Untreated Subjects With Metastatic or Locally Advanced Unresectable Pancreatic Adenocarcinoma*. Available from: <https://ClinicalTrials.gov/show/NCT01746979>.
70. Foehrenbacher, A., et al., *The Role of Bystander Effects in the Antitumor Activity of the Hypoxia-Activated Prodrug PR-104*. *Front Oncol*, 2013. **3**: p. 263.
71. Hammond, E.M., et al., *The meaning, measurement and modification of hypoxia in the laboratory and the clinic*. *Clin Oncol (R Coll Radiol)*, 2014. **26**(5): p. 277-88.
72. Hunter, F.W., B.G. Wouters, and W.R. Wilson, *Hypoxia-activated prodrugs: paths forward in the era of personalised medicine*. *Br J Cancer*, 2016. **114**(10): p. 1071-7.
73. O'Connor, J.P., et al., *Imaging intratumor heterogeneity: role in therapy response, resistance, and clinical outcome*. *Clin Cancer Res*, 2015. **21**(2): p. 249-57.
74. Nordsmark, M., et al., *Prognostic value of tumor oxygenation in 397 head and neck tumors after primary radiation therapy. An international multi-center study*. *Radiother Oncol*, 2005. **77**(1): p. 18-24.
75. Ang, K.K., et al., *Human papillomavirus and survival of patients with oropharyngeal cancer*. *N Engl J Med*, 2010. **363**(1): p. 24-35.
76. Cancer Genome Atlas, N., *Comprehensive genomic characterization of head and neck squamous cell carcinomas*. *Nature*, 2015. **517**(7536): p. 576-82.
77. Toustrup, K., et al., *Hypoxia gene expression signatures as prognostic and predictive markers in head and neck radiotherapy*. *Semin Radiat Oncol*, 2012. **22**(2): p. 119-27.
78. Lassen, P., et al., *HPV-associated p16-expression and response to hypoxic modification of radiotherapy in head and neck cancer*. *Radiother Oncol*, 2010. **94**(1): p. 30-5.
79. Trinkaus, M.E., et al., *Correlation of p16 status, hypoxic imaging using [18F]-misonidazole positron emission tomography and outcome in patients with loco-regionally advanced head and neck cancer*. *J Med Imaging Radiat Oncol*, 2014. **58**(1): p. 89-97.
80. Milosevic, M., et al., *Tumor hypoxia predicts biochemical failure following radiotherapy for clinically localized prostate cancer*. *Clin Cancer Res*, 2012. **18**(7): p. 2108-14.
81. Lalonde, E., et al., *Tumour genomic and microenvironmental heterogeneity for integrated prediction of 5-year biochemical recurrence of prostate cancer: a retrospective cohort study*. *Lancet Oncol*, 2014. **15**(13): p. 1521-32.
82. Guise, C.P., et al., *Diflavin oxidoreductases activate the bioreductive prodrug PR-104A under hypoxia*. *Mol Pharmacol*, 2012. **81**(1): p. 31-40.
83. Meng, F., et al., *Molecular and cellular pharmacology of the hypoxia-activated prodrug TH-302*. *Mol Cancer Ther*,

2012. **11**(3): p. 740-51.
84. Patterson, A.V., et al., *Overexpression of human NADPH:cytochrome c (P450) reductase confers enhanced sensitivity to both tirapazamine (SR 4233) and RSU 1069*. Br J Cancer, 1997. **76**(10): p. 1338-47.
85. Papadopoulou, M.V., et al., *Reductive metabolism of the nitroimidazole-based hypoxia-selective cytotoxin NLCQ-1 (NSC 709257)*. Oncol Res, 2003. **14**(1): p. 21-9.
86. Chandor, A., et al., *Metabolic activation of the antitumor drug 5-(Aziridin-1-yl)-2,4-dinitrobenzamide (CB1954) by NO synthases*. Chem Res Toxicol, 2008. **21**(4): p. 836-43.
87. Wang, J., et al., *Identification of one-electron reductases that activate both the hypoxia prodrug SN30000 and diagnostic probe EF5*. Biochem Pharmacol, 2014. **91**(4): p. 436-46.
88. Hunter, F.W., et al., *The flavoprotein FOXRED2 reductively activates nitro-chloromethylbenzindolines and other hypoxia-targeting prodrugs*. Biochem Pharmacol, 2014. **89**(2): p. 224-35.
89. Hunter, F.W., et al., *Identification of P450 Oxidoreductase as a Major Determinant of Sensitivity to Hypoxia-Activated Prodrugs*. Cancer Res, 2015. **75**(19): p. 4211-23.
90. Wang, J., et al., *The 2-nitroimidazole EF5 is a biomarker for oxidoreductases that activate the bioreductive prodrug CEN-209 under hypoxia*. Clin Cancer Res, 2012. **18**(6): p. 1684-95.
91. Evans, J.W., et al., *Homologous recombination is the principal pathway for the repair of DNA damage induced by tirapazamine in mammalian cells*. Cancer Res, 2008. **68**(1): p. 257-65.
92. Gu, Y., et al., *Roles of DNA repair and reductase activity in the cytotoxicity of the hypoxia-activated dinitrobenzamide mustard PR-104A*. Mol Cancer Ther, 2009. **8**(6): p. 1714-23.
93. Hunter, F.W., et al., *Homologous recombination repair-dependent cytotoxicity of the benzotriazine di-N-oxide CEN-209: comparison with other hypoxia-activated prodrugs*. Biochem Pharmacol, 2012. **83**(5): p. 574-85.
94. Hunter, F.W., et al., *Dual targeting of hypoxia and homologous recombination repair dysfunction in triple-negative breast cancer*. Mol Cancer Ther, 2014. **13**(11): p. 2501-14.
95. Gao, Y. and D. Liu, *The roles of excision repair cross-complementation group1 in objective response after cisplatin-based concurrent chemoradiotherapy and survival in head and neck cancers: a systematic review and meta-analysis*. Oral Oncol, 2015. **51**(6): p. 570-7.
96. Bowden, N.A., *Nucleotide excision repair: why is it not used to predict response to platinum-based chemotherapy?* Cancer Lett, 2014. **346**(2): p. 163-71.
97. Scanlon, S.E. and P.M. Glazer, *Multifaceted control of DNA repair pathways by the hypoxic tumor microenvironment*. DNA Repair (Amst), 2015. **32**: p. 180-9.
98. Chan, N., et al., *Chronic hypoxia decreases synthesis of homologous recombination proteins to offset chemoresistance and radioresistance*. Cancer Res, 2008. **68**(2): p. 605-14.
99. Overgaard, J., et al., *A randomized double-blind phase III study of nimorazole as a hypoxic radiosensitizer of primary radiotherapy in supraglottic larynx and pharynx carcinoma. Results of the Danish Head and Neck Cancer Study (DAHANCA) Protocol 5-85*. Radiother Oncol, 1998. **46**(2): p. 135-46.

100. Overgaard, J., et al., *Plasma osteopontin, hypoxia, and response to the hypoxia sensitiser nimorazole in radiotherapy of head and neck cancer: results from the DAHANCA 5 randomised double-blind placebo-controlled trial*. *Lancet Oncol*, 2005. 6(10): p. 757-64.
101. Overgaard, J., et al., *Plasma osteopontin, hypoxia, and response to the hypoxia sensitiser nimorazole in radiotherapy of head and neck cancer: results from the DAHANCA 5 randomised double-blind placebo-controlled trial*. *Lancet Oncol*, 2005. 6(10): p. 757-64.



# ADDENDA

- Summary
- Nederlandstalige samenvatting
- Valorization addendum
- Acknowledgements/Dankwoord
- Curriculum vitae
- List of publications

## Summary

Cancer is a major cause of morbidity and mortality worldwide. Over the years, incidence rates have been, and still are, increasing. Cancer arises due to mutations in the DNA of a normal cell, caused by external mutagens or genetically inherited. These mutations accumulate and slowly transform the normal cell into a malignant cell with increased proliferation and lifespan. Conventional cancer therapies include surgery, radiotherapy and different kinds of chemotherapies. Research on new treatment options more and more focuses on targeted treatments, immunotherapies, and combinations of all of these treatments.

Hypoxia is a common feature of solid tumors, and is caused by an abnormal, chaotic, fragile and hyperpermeable tumor vasculature. Where normal physiological oxygen levels range between 1 and 11%, hypoxic tumor areas can potentially contain no oxygen at all (anoxia). Tumor hypoxia aggravates the malignant tumor cell phenotype and has been associated with poor prognosis. Additionally, tumor hypoxia poses therapeutic problems since it is known to induce resistance to several anticancer therapies, including radiotherapy, chemotherapy, and likely immunotherapy. However, this also makes tumor hypoxia a promising therapeutic target to be exploited in cancer treatment. By combining conventional treatments, which target well-oxygenated cells, with hypoxia-targeting strategies, a greater anticancer effect can be achieved. In this thesis, two strategies to exploit tumor hypoxia in cancer treatment have been explored.

One way of exploiting tumor hypoxia in cancer treatment is by targeting a member of the hypoxia response pathway. HIF-1 $\alpha$  plays a key role in this response of cells to hypoxic stress. Upon stabilization of HIF-1 $\alpha$  in hypoxia, genes having a hypoxia-responsive element (HRE) are transcribed, which aid the cell in its survival in the hypoxic environment. Among these genes is the carbonic anhydrase 9 (*CA9*) gene. CA IX is a transmembrane protein that catalyzes the hydration of carbon dioxide to bicarbonate and a proton. CA IX is predominantly expressed in tumors, has been found to select for and to maintain an aggressive cancer cell phenotype and to promote metastasis formation, and is a negative prognostic factor in cancer patients regardless of the tumor type, site, or treatment. This makes CA IX an attractive target for anticancer treatment.

Only patients with CA IX expressing tumors are expected to benefit from CA IX-targeting anticancer treatments. Therefore, non-invasive detection of CA IX expression can aid in the

successful development of CA IX targeting cancer treatments. In Chapter 3, we describe the design and synthesis of novel gallium-radiolabeled small-molecule sulfonamides targeting CA IX. We demonstrate *in vivo* that the lead  $^{68}\text{Ga}$ -labeled CA IX targeting positron emission tomography (PET) tracer accumulates specifically in CA IX-expressing tumor xenografts in two separate experiments. Additionally, we show that uptake in the blood is low, and that the compound is cleared intact into the urine. Incorporating CA IX imaging, e.g. by using this tracer, into future clinical trials is advisable, ensuring proper patient stratification and a reliable measure of the efficacy of the CA IX inhibitor.

In Chapter 4 we describe the design, synthesis and biological evaluation of novel dual target drugs. These compounds are a new approach of delivering cytotoxic drugs specifically to CA IX expressing cells, which consist of different anticancer agents (chlorambucil, tirapazamine, temozolomide, two different ataxia telangiectasia and Rad3 related (ATR) inhibitors, and the anti-diabetic drug phenformin) conjugated to a CA IX targeting moiety. This should increase tumor specificity of the parental drugs and potentially decrease normal tissue toxicity. However, of all tested compounds, only one of the ATR inhibitor derivatives was more effective in combination with radiotherapy in CA IX overexpressing cells compared to CA IX non-expressing cells. Furthermore, this compound showed poor binding affinity to recombinant CA IX, and showed no increased efficacy in hypoxic conditions. Therefore, the cytotoxic effect of this compound is probably not solely CA IX dependent. Further (pre)clinical development of these compounds has not been continued, however, the general dual targeting compound strategy remains of interest for further exploration. In Chapter 5 we describe the design, synthesis and biological evaluation of novel fluorinated high-affinity CA IX inhibitors. We show that these inhibitors exhibit picomolar affinity to recombinant CA IX and selectivity over other CAs, and that they directly bind to the active site of CA IX. Additionally, they significantly reduced hypoxia-induced extracellular acidification in a range of cancer cell lines. In hypoxic H460 tumor spheroids, the lead inhibitor decreased clonogenic survival. Therefore, these novel compounds are promising agents for CA IX-targeting anticancer therapy. As CA IX is involved in tumor cell invasion and migration, it would be interesting and important to study the effects of these inhibitors on these processes. It is essential that the efficacy of the lead CA IX inhibitor is tested in *in vivo* human tumor xenografts models before proceeding into clinical trials.

Another way of exploiting tumor hypoxia in cancer treatment is by using hypoxia-activated prodrugs (HAPs). HAPs are activated specifically in hypoxic conditions, where they,

in general, act as either radiosensitizers or as DNA-damaging cytotoxins. Several early HAPs yielding good results in *in vitro* tumor cell lines and *in vivo* preclinical animal models stranded in development during clinical trials due to disappointing results. Several other HAPs are in different stages of clinical development. So far, only the hypoxic cell radiosensitizer nimorazole has made it into clinical practice: it significantly improved the effect of radiotherapy in head and neck tumors without major side effects, and is now standard of care for the treatment of head and neck squamous cell carcinoma in Denmark. The absence of patient stratification could very well explain the failure of the other clinical HAP trials, and thus it is vital that patient stratification based on tumor hypoxia is implemented in future clinical HAP trials. In Chapter 6, we propose a biomarker-stratified enriched study design for these trials, in which only biomarker-positive patients are randomized between standard treatment and the combination of standard treatment with HAPs. The number of patients needed for this phase 3 design is far lower than in current randomize-all designs, even when a phase 2 trial, in which the threshold for the hypoxia biomarker of choice is evaluated, is done first.

PR-104 is another HAP that has been extensively studied. *In vitro* and *in vivo*, PR-104 was found to be selectively active in hypoxia in a range of cancer cell lines and human tumor xenografts. However, clinical development of PR-104 as treatment for solid tumors stopped because it was found that it can be activated under normoxia, and thus in an oxygen-insensitive manner, by the two-electron reductase aldo-keto reductase 1C3 (AKR1C3), giving rise to severe dose-limiting myelotoxicity in several clinical trials. To tackle this limitation, the PR-104 molecule was chemically modified to prevent activation by AKR1C3, resulting in the novel HAP CP-506. In Chapter 7 we show that CP-506 is indeed resistant to activation by AKR1C3, and that it reduces cell viability in a range of *in vitro* 2D tumor cell monolayer cultures in a hypoxia-selective manner. Also, in several *in vitro* 3D tumor cell multilayer and spheroid cultures, CP-506 reduces clonogenic survival in a hypoxia-selective manner. Additionally, we show that it inhibits growth of several human tumor xenograft models *in vivo*, and that it reduces the hypoxic fraction in human breast cancer xenografts. CP-506 is thus a promising novel HAP. However, in most cases treatment with a HAP alone will not be sufficient to eradicate a tumor completely, since well-oxygenated cells will be targeted only to a certain degree (by the HAP's bystander effect). Combining HAPs with other cancer treatments which target these well-oxygenated cells, such as radiotherapy, thus is essential. In Chapter 8, we show promising (preliminary) data demonstrating anticancer effects of CP-506 when combined with radiotherapy or immunotherapy in an *in*

*vivo* syngeneic model. We show that it can synergistically inhibit tumor growth when combined with radiotherapy, and that it can improve immunotherapy outcome. CP-506 has thus shown to be a promising novel HAP with potential favorable properties for future clinical use, although more studies are required to validate our findings and to determine factors determining the therapeutic effect of CP-506 alone or in combination with other treatment modalities.

Our results confirm that tumor hypoxia is interesting and promising to exploit for cancer treatment. However, novel hypoxia-targeting agents need proper preclinical characterization, required for selection of the most optimal drug for clinical testing. These clinical trials require a proper design, incorporating techniques that allow accurate patient stratification, as it is likely that not all patients will benefit from these agents. This stratification ensures a reliable measure of treatment efficacy and increases the chance that in the future more patients will benefit from hypoxia targeting anticancer therapies.

## Nederlandstalige samenvatting

Kanker is een van de belangrijkste doodsoorzaken wereldwijd. Het aantal kankerpatiënten is over de jaren heen gestegen, en stijgt nog steeds. Kanker ontstaat door mutaties in het DNA van een normale cel, welke veroorzaakt worden door externe toxische stoffen of welke genetisch geërfd zijn. Deze mutaties stapelen zich op en veranderen de normale cel langzaam in een kwaadaardige cel met verhoogde proliferatie en levensduur. Conventionele kankerbehandelingen zijn onder andere operatie, radiotherapie, en verschillende soorten chemotherapieën. Nieuwe kankerbehandelingen focussen zich steeds meer op therapieën specifiek gericht op bepaalde eigenschappen van de tumor, op immunotherapieën, en op combinaties van al deze behandelingen.

Hypoxie (lage zuurstofconcentratie) is een veel voorkomend kenmerk van solide tumoren, en wordt veroorzaakt door een abnormaal, chaotisch, fragiel en zeer doordringbaar vaatstelsel in de tumor. Normale fysiologische zuurstofniveaus liggen tussen de 1 en 11%; hypoxische tumor regio's bevatten nog lagere zuurstofniveaus tot zelfs helemaal geen zuurstof (anoxie). Tumor hypoxie maakt de tumorcel nog kwaadaardiger, en is geassocieerd met een slechte prognose. Ook veroorzaakt tumor hypoxie problemen bij de behandeling van kanker. Het is bekend dat het resistentie tegen verschillende kankerbehandelingen opwekt, waaronder radiotherapie, chemotherapie, en waarschijnlijk ook immunotherapie. Anderzijds maakt dit tumor hypoxie ook een veelbelovend therapeutisch doelwit om uit te buiten in de behandeling van kanker. Door therapieën die zuurstofrijke cellen aanpakken te combineren met op hypoxie gerichte behandelingen kan een groter effect bereikt worden. In dit proefschrift zijn twee potentiële kankerbehandelingen verkend die zich op tumor hypoxie richten.

Een manier om tumor hypoxie uit te buiten in de behandeling van kanker is door zich te richten op de reactie van een tumorcel op hypoxie. HIF-1 $\alpha$  speelt een sleutelrol in deze reactie. HIF-1 $\alpha$  wordt onder hypoxie gestabiliseerd, waarna genen met een "hypoxie-responsief element" (HRE) eiwitten tot expressie brengen welke de cel helpen om te overleven in de hypoxische omgeving. "Carbonic anhydrase IX" (Koolzuuranhydrase IX; CA IX) is een van deze eiwitten. CA IX is een transmembraan eiwit dat koolstofdioxide omzet naar bicarbonaat en een proton. CA IX komt voornamelijk tot expressie in tumoren, selecteert voor en onderhoudt een agressief fenotype van de kankercel, en bevordert de formatie van metastasen (uitzaaiingen). CA IX expressie is geassocieerd met een slechtere prognose in

kankerpatiënten, ongeacht het type of de plaats van de tumor, of de behandeling. Dit maakt CA IX een aantrekkelijk doelwit voor de behandeling van kanker.

Het ligt in de lijn der verwachting dat enkel patiënten met tumoren die CA IX tot expressie brengen zullen profiteren van een behandeling gericht tegen CA IX. Niet-invasieve detectie van CA IX expressie kan daarom helpen bij het succesvol ontwikkelen van nieuwe kankerbehandelingen gericht tegen CA IX. In Hoofdstuk 3 beschrijven we het ontwerp en de synthese van nieuwe met radioactief gallium gemerkte kleine moleculen, meer specifiek sulfonamides, gericht tegen CA IX. In twee verschillende proefdierexperimenten tonen we aan dat de beste <sup>68</sup>Ga-gemerkte “positron emission tomography” (PET) tracer gericht tegen CA IX specifiek accumuleert in tumoren die CA IX tot expressie brengen. Verder tonen we aan dat de opname in het bloed laag is, en dat de tracer intact in de urine geklaard wordt. We kunnen daarom aanbevelen om in toekomstige klinische studies CA IX expressie in tumoren in beeld te brengen, bijvoorbeeld met behulp van de hier beschreven PET-tracer. Zo kan de werkzaamheid van de behandeling worden geëvalueerd, zoals we beschrijven in Hoofdstuk 2.

In Hoofdstuk 4 beschrijven we het ontwerp, de synthese en de biologische evaluatie van nieuwe zogenaamde “dual-target” stoffen. Dit is een nieuwe manier om toxische stoffen specifiek af te leveren in tumorcellen die CA IX tot expressie brengen. Deze dual-target stoffen bestaan uit verschillende kanker medicijnen (chlorambucil, tirapazamine, temozolomide, twee verschillende “ataxia telangiectasia and Rad3 related” (ATR) remmers, en het anti-diabetisch medicijn fenformine), geconjugeerd met een groep die zich op CA IX richt. Dit zou de tumor specificiteit van het kankermedicijn moeten verhogen, en potentieel de toxiciteit in normale weefsels verlagen. Echter, van alle stoffen die getest zijn was alleen één van ATR-remmer derivaten effectiever in combinatie met radiotherapie in cellen die CA IX tot overexpressie brengen vergeleken met cellen die geen CA IX tot expressie brengen. Deze stof had echter een slechte bindingsaffiniteit met recombinant CA IX, en vertoonde geen verhoogde werkzaamheid in hypoxische condities. Hierom is het toxische effect van deze stof waarschijnlijk niet alleen maar afhankelijk van CA IX. We zijn daarom niet verder gegaan met de (pre)klinische ontwikkeling van al deze stoffen. Echter, het algemene principe van dual-target stoffen blijft interessant voor verder onderzoek.

In Hoofdstuk 5 beschrijven we het ontwerp, de synthese en biologische evaluatie van nieuwe gefluoreerde hoge-affiniteit CA IX remmers. We tonen aan dat deze remmers picomolaire affiniteit voor recombinant CA IX hebben, verhoogde selectiviteit voor CA IX over

andere CAs, en dat deze remmers direct binden in de actieve plek van het CA IX molecuul. Ook verminderen deze remmers significant de door hypoxie geïnduceerde extracellulaire verzuring in verschillende kankercellijnen. De beste remmer vermindert tevens overleving in hypoxische 3D tumor sferoïde structuren. Deze nieuwe stoffen zijn daarom veelbelovend als kankerbehandeling gericht tegen CA IX. Omdat CA IX ook een rol speelt in de invasie en migratie van tumorcellen is het interessant en belangrijk om de effecten van deze remmers op deze processen te onderzoeken. Verder is het essentieel dat de werkzaamheid van de beste CA IX remmer wordt getest in tumordragende proefdieren, voordat er met klinische studies gestart wordt.

Een andere manier om tumor hypoxie te gebruiken in de behandeling van kanker is het gebruiken van “hypoxia-activated prodrugs” (HAPs). HAPs worden specifiek geactiveerd in hypoxische condities, waar ze werken als een stof die cellen gevoeliger maakt voor radiotherapie, of als een DNA-beschadigend toxische stof. Met verschillende HAPs werden in het verleden goede resultaten behaald zowel in kankercellijnen als in proefdieren. In klinische studies waren de resultaten echter teleurstellend, waarna de verdere ontwikkeling van deze stoffen gestopt werd. Verscheidene andere HAPs zijn op dit moment in verschillende fases van klinische ontwikkeling. Momenteel is nimorazole de enige HAP die in de kliniek gebruikt wordt. Nimorazole is een HAP die hypoxische cellen gevoeliger maakt voor radiotherapie; het verhoogt het effect van radiotherapie in hoofd-hals plaveiselcelcarcinoom significant, zonder ernstige bijwerkingen. Nimorazole is nu de standaardbehandeling voor hoofd-hals plaveiselcelcarcinoom in Denemarken. Het ontbreken van stratificatie van patiënten is een aannemelijke verklaring voor het falen van andere klinische studies met HAPs; daarom is het uiterst belangrijk dat stratificatie van patiënten, gebaseerd op de aan- of afwezigheid van tumor hypoxie, geïmplementeerd wordt in toekomstige klinische studies met HAPs. In Hoofdstuk 6 stellen we een door middel van een biomarker gestratificeerd verrijkt studieontwerp voor, waarin alleen biomarker-positieve patiënten gerandomiseerd worden tussen standaardbehandeling en de combinatie van deze standaardbehandeling met HAPs. Het aantal patiënten dat nodig is voor dit fase 3 ontwerp is vele malen lager dan het aantal dat momenteel in klinische studies gebruikt wordt waarbij alle patiënten gerandomiseerd worden, zelfs als er eerst een fase 2 studie gedaan wordt waarin de drempelwaarde van de gekozen biomarker bepaald wordt. PR-104 is een andere HAP welke uitgebreid onderzocht is. Zowel in verschillende kankercellijnen als in proefdieren met verschillende tumortypes van humane oorsprong was het selectief actief in hypoxie. De klinische ontwikkeling van PR-104 als behandeling voor

solide tumoren werd echter stopgezet toen bekend werd dat PR-104 ook onder normale zuurstofspanning geactiveerd kan worden door het twee-elektron reductase “aldo-keto reductase 1C3” (AKR1C3), wat leidde tot ernstige myelotoxiciteit in verschillende klinische studies. Om deze beperking aan te pakken werd het PR-104 molecuul scheikundig veranderd zodat het niet meer door AKR1C3 geactiveerd kan worden, wat resulteerde in de nieuwe HAP CP-506. In Hoofdstuk 7 tonen we aan dat CP-506 inderdaad resistent is tegen activatie door AKR1C3, en dat het de levensvatbaarheid van verschillende kankercellijnen op een hypoxie-selectieve manier vermindert. Verder tonen we aan dat CP-506 de overleving op een hypoxie-selectieve manier vermindert in verschillende 3D kankermodellen, en dat het de groei van verschillende tumor types van humane oorsprong in proefdieren vermindert. Verder vermindert het de hypoxische fractie in borstkanker tumoren. CP-506 is dus een veelbelovende nieuwe HAP. In de meeste gevallen zal behandeling met alleen een HAP echter niet genoeg zijn om een tumor compleet uit te roeien, omdat zuurstofrijke cellen slechts gedeeltelijk worden aangevallen (door het zogenaamde toeschouwerseffect van de HAP). Het is dus essentieel om HAPs te combineren met andere kankerbehandelingen, zoals radiotherapie, die deze zuurstofrijke cellen aanvallen. In Hoofdstuk 8 presenteren we de veelbelovende eerste data welke de effecten van CP-506 tegen kanker aantonen wanneer dit gecombineerd wordt met radiotherapie of immunotherapie. We tonen aan dat CP-506 tumorgroei synergistisch kan remmen wanneer het gecombineerd wordt met radiotherapie, en dat het de uitkomst van immunotherapie kan verbeteren. We tonen dus aan dat CP-506 een veelbelovende nieuwe HAP is met gunstige eigenschappen voor toekomstig gebruik in de kliniek. Wel is er meer onderzoek nodig om onze bevindingen te valideren en om te bepalen welke factoren van invloed zijn op het therapeutisch effect van CP-506 alleen of in combinatie met andere behandelingen.

Onze resultaten bevestigen dat het interessant en veelbelovend is om zich op tumor hypoxie te richten in de behandeling van kanker. Nieuwe op hypoxie-gerichte behandelingen vereisen echter een goede preklinische karakterisatie, welke nodig is om de meest optimale stof voor klinische studies te kiezen. Deze klinische studies moeten een geschikt ontwerp hebben, waarbij technieken worden geïncorporeerd die accurate stratificatie van patiënten mogelijk maken, omdat het in de lijn der verwachting ligt dat niet alle patiënten baat hebben van deze nieuwe behandelingen. Deze stratificatie zorgt ervoor dat een betrouwbare meting van het effect van de behandeling verkregen wordt, en vergroot de kans dat in de toekomst meer patiënten baat zullen hebben van nieuwe kankerbehandelingen gericht tegen tumor hypoxie.

## Valorization addendum

Maastricht University views knowledge valorization as a “process of creating value from knowledge, by making knowledge suitable and/or available for social (and/or economic) use and by making knowledge suitable for translation into competitive products, services, processes and new commercial activities” (adapted definition based on the National Valorization Committee 2011:8). This valorization addendum will reflect on the novelty, (potential) value and relevance for society of the work described in this thesis.

### Cancer

This thesis focuses on new treatment modalities against cancer. Millions of people suffer from cancer, and cancer incidence keeps, unfortunately, rising. Cancer has a huge impact on a patient’s life since treatment is often very demanding for a patient with many hospital visits and (severe) side-effects caused by the treatment(s). Not only the patient him-/herself is affected by the disease as close relatives and friends share the emotional suffering with the patient, and often devote their time to care for the patient. Thus, cancer has a huge overall impact on society with many people suffering from its consequences. Additionally, an economic impact is apparent, in that not only treatments costs are very high, but people (patients as well as their caregivers) also retreat from the workforce because of cancer. This evidences a need for more effective and better tolerable treatment options in the battle against this heinous disease.

### Anticancer treatments in general

Research on new anticancer treatments is nowadays mainly focused on targeted treatments that, compared to the conventional treatments, have the potential to cause fewer side effects, exhibit more localized treatment delivery, achieve higher tumoral concentration of anticancer therapeutics and decrease resistance of the cancer cells towards the treatment. Additionally, combination therapies are extensively being explored. In these therapies different pathways are simultaneously targeted, which can enhance efficacy in an additive or even synergistic manner compared to a monotherapy approach.

Tumor hypoxia is associated with poor prognosis, and is a known therapeutic problem, in that hypoxic tumor cells are more resistant to the conventional anticancer treatments. In this thesis, two strategies have been explored to exploit tumor hypoxia for cancer treatment, by targeting the hypoxia responsive enzyme carbonic anhydrase IX (CA IX), or by

using the hypoxia-activated prodrug (HAP) CP-506, which is to be combined with other anticancer therapies. Should these (combination) treatment strategies ultimately prove successful and applicable in humans, they can, together with any other effective anticancer treatment, aid in reducing the afore-mentioned negative impact of cancer on society.

### **Patient stratification**

Not all cancer patients will benefit from the treatment options explored in this thesis. CA IX inhibitors only work in CA IX expressing tumors. Likewise, HAPs only work in tumors that have sufficiently low oxygen levels for activation of the HAP. However, since the majority of solid tumors does contain hypoxic areas and does express CA IX (in these areas), the potential impact of these treatments is substantial. Proper patient stratification remains, however, needed. This stratification ensures that patients do not receive unnecessary treatment, but will receive the treatment best suited for them. This reduces treatment costs, unnecessary suffering of cancer patients, and increases their chance of cure.

The CA IX positron emission tomography (PET) imaging tracer described in Chapter 3 of this thesis could aid in the stratification of cancer patients since it can be used to detect CA IX expressing tumors, and can thus identify patients who would likely benefit from a CA IX targeting treatment. This technique has many clinical benefits over e.g. tumor biopsies as it is noninvasive, repeatable, and gives an image of CA IX distribution representing the whole tumor. The idea of CA IX PET imaging is not novel, with a number of CA IX-specific imaging tracers being used for preclinical CA IX imaging. However, none of these imaging tracers is currently being used in clinical practice. Before the tracer investigated in this thesis can be used in clinical practice, it will first have to be validated in clinical trials. In a similar manner, hypoxia imaging tracers such as the hypoxia PET tracer  $^{18}\text{F}$ -HX4 can be used for the detection and stratification of patients likely to benefit from CP-506, or any other HAP, treatment. As CA IX is considered to be a surrogate hypoxia marker, the CA IX PET imaging tracer described in this thesis could also be used for this purpose. First, however, this tracer would need to be validated in this context. Compared to e.g.  $^{18}\text{F}$ -HX4, the radioactive particle of this tracer has a shorter half-life, reducing radiation burden to relatives as it has completely decayed within a few hours after imaging. It is also relatively cheaper, and thus reduces treatment costs, as it is easier to synthesize and no cyclotron is needed.

These imaging techniques can not only be used to stratify patients, they can also possibly be used during and after treatment, to assess the effect of the treatment. In this manner

a patient can timely receive additional and/or alternative treatment when the previous treatment proves ineffective. This further increases their chance of cure with fewer side effects.

### **Dual-target drugs**

Dual-target drugs are conjugates of two individual therapeutic agents, each with its own mechanism of action. These agents can also specifically target cancer-associated pathways or proteins, e.g. CA IX. This way, dual-target drugs have the potential to increase tumor specificity of anticancer drugs, increase drug concentrations in the tumor only, and potentially decrease normal tissue toxicity. The dual-target CA IX inhibitors described in Chapter 4 of thesis, however, did not demonstrate effectiveness against cancer cells. Further (pre)clinical development of these compounds has not been continued. However, the relevance of these results should not be underestimated, as they can provide more insights into the underlying principles of dual-target drugs. Our results show that conjugating two molecules does not necessarily result in a compound with the desired characteristics of the parental compounds, and that this conjugation might actually decrease efficacy and/or affinity of the parental compounds. This shows that the underlying mechanisms are complex and require further investigation. Future dual-target compounds thus require extensive characterization: it should be studied whether the conjugation does not interfere with the effects of the compounds. Also, it is needed to investigate whether the active compounds reach their intended target(s). Others have shown that the dual-target approach targeting CA IX can be successful, at least in preclinical *in vivo* studies. CA IX thus remains a good target, and the dual-target drug approach remains viable and promising for further exploration. Further studies will need to prove the clinical relevance of this type of compounds as anticancer treatment.

### **CA IX inhibitors**

The concept of inhibiting CA IX as anticancer treatment is not novel: many CA IX inhibitors have been and are still being investigated preclinically. Only a single small-molecule CA IX inhibitor, SLC-0111, has so far made it into clinical trials. Results of a phase 1 study are eagerly awaited. Should this trial prove that SLC-0111 is safe to use, further trials are needed to assess safety and efficacy of this compound. Should SLC-0111 prove safe to use as well as effective, more CA IX inhibitors may proceed into clinical trials. However, should these trials present negative results, we might have to re-think the use of CA IX inhibitors as anticancer treatments. Many potential compensatory mechanisms can be triggered in

the case of CA IX inhibition, thus it is possible that this inhibition alone is insufficient for a clinically relevant therapeutic outcome. Instead, combining CA IX inhibitors with other treatment modalities might be more effective. A second trial with SLC-0111 has recently been announced online, to determine MTD and collect preliminary data on the therapeutic efficacy of the compound in combination with the chemotherapeutic agent gemcitabine. Results of this trial will provide more insight into the clinical relevance of such combination therapies. Should such combination therapies prove successful, then the CA IX inhibitors described in Chapter 5 of this thesis could possibly be useful in such therapies, as they had very high affinity for CA IX. Promising results with these inhibitors were obtained in *in vitro* assays, however, they will first need to be tested in *in vivo* animal models, before proceeding into clinical trials. Should they prove successful, however, they can contribute to an effective anticancer treatment.

### CP-506

The concept of using HAPs as anticancer treatment is not novel, with many HAPs continuously being developed and (pre)clinically investigated. One HAP, nimorazole, has made its way into clinical practice in Denmark, proving the potential of clinical relevance for this type of compounds. As such, one could argue the novelty of and need for another HAP. Nimorazole is a hypoxic cell radiosensitizer and is thus intended to be used in combination with radiotherapy. CP-506, the HAP described in Chapters 7 and 8 of this thesis, is a hypoxia-specific cytotoxin with a bystander effect. It thus has the potential to not only synergize with or increase the efficacy of radiotherapy, but also other treatment modalities including chemotherapy and immunotherapy. Its predecessor, PR-104, was a successful HAP in preclinical studies, and rapidly proceeded into clinical trials. Toxicity issues, however, hampered the use of PR-104 in solid tumors. The components of the molecule likely to be responsible for this toxicity were altered, resulting in the HAP CP-506. This HAP is thus specifically designed to be an improvement over its predecessor. As other HAPs, CP-506 is mainly intended to be used in combination therapies. The results in Chapters 7 and 8 of this thesis show CP-506 to be a promising candidate for further preclinical evaluation and clinical efficacy validation of combination approaches with radiotherapy and/or immunotherapy. A phase 1 clinical trial is being planned and expected to start in early 2019. This trial will assess the safety of CP-506 treatment in humans for the first time. Afterwards, phase 2 and 3 trials are needed to further validate CP-506 as an effective and safe anticancer treatment, as a monotherapy and in combination therapies. These trials should be set up as we propose in Chapter 6 of this thesis, i.e with proper patient stratification.

This is of importance for the potential success of these promising drugs, as the failure of HAPs in clinical trials so far can (at least partly) be attributed to an improper design of these trials. Proper experimental set-up ensures a reliable outcome on the efficacy of the HAP and improves the chance that in the future more patients will benefit from this promising treatment option. Successful results could lead to CP-506 being on the market in a couple of years. This would provide clinicians and patients with a powerful tool in the battle against cancer.

## Acknowledgements/Dankwoord

I would like to start with thanking everyone who has contributed in some way to this dissertation. Even though I might not name you personally here, do know I am grateful for your contributions, for which I hereby extend a sincere “Thank you very much” :-).

Vervolgens wil een aantal mensen persoonlijk bedanken, beginnend met mijn promotieteam. Philippe, bedankt dat je me 4.5 jaar geleden de kans hebt gegeven om een PhD te beginnen in jouw groep. Ik heb in die tijd mede dankzij jou veel geleerd en me goed kunnen ontwikkelen op academisch gebied.

Ludwig and Ala, I would like to thank the two of you together, as that is how I always see you; as a (very good) team. Thank you for supervising me all these years; for helping me out when needed, for motivating me when needed, for all the excellent, interesting and informative discussions, for your critical and helpful feedback on my work, for your doors always being open, etc. etc., and of course also for all the fun times we had, during experiments, discussions, conferences, or non-work-related matters. The two of you complement each other and form an excellent team that by working together and with others can accomplish a lot. I’ve learned a lot from you and really appreciate all you’ve done for me. Thank you! All other PhD students in our group can rest assured they’re in excellent hands.

I would like to thank the members of the assessment committee, prof. Frans Ramaekers, prof. Kaye Williams, prof. Jan Bussink, prof. Guido Haenen, and Roger Godschalk for reading and assessing my thesis.

Roger en Guido, bij deze wil ik jullie ook nog bedanken voor de begeleiding tijdens de stages die ik bij jullie heb gelopen voordat ik aan mijn PhD begon. Ik heb een erg leuke en leerzame tijd bij jullie gehad, wat me uitstekend heeft voorbereid voor mijn PhD.

I would also like to thank all co-authors of the papers included here for their contributions.

Ilse, bedankt voor het maken van de lay-out en kaft van mijn proefschrift. Het is echt top geworden! Bij deze verwijs ik graag alle PhD-studenten die de lay-out van hun proefschrift willen uitbesteden naar [www.ilsemooder.nl](http://www.ilsemooder.nl).

De mensen van Gildeprint wil ik ook graag bedanken voor hun snelle, concrete antwoorden op vragen, en de snelle en zorgvuldige afhandeling van het printen van dit proefschrift.

En dan de groep waar ik de afgelopen 4.5 jaar mijn tijd heb doorgebracht; mCAT, mGroup, mLab, wat is het nu?

Rianne en Natasja, bedankt voor alle hulp de afgelopen jaren bij al die experimenten. Zonder jullie zat ik nu waarschijnlijk nog coupes te snijden of tumoren te meten... Bedankt voor het uit handen nemen van een deel van die praktische handelingen (die ik ook niet zo leuk vond maar jullie gelukkig wel!) en bij alle verdere ondersteuning. Ook bedankt voor het mij leren van al die nieuwe technieken. Ik vond het altijd erg gezellig om met jullie samen te werken. Veel succes nog met al die databases! En Rianne, succes nog met jullie huis!

Marike, bedankt voor al je hulp bij met name de Seahorse experimenten die ik zo nu en dan moest doen. En voor de hulp bij die dingen die na de goedkeuring van mijn proefschrift nog moesten gebeuren! Maar ook bedankt voor alle gezelligheid in die 4.5 jaar. Ik vond het erg leuk om een tijd een kantoor met je te hebben gedeeld, en onze Coca-Cola uitjes waren natuurlijk ook altijd erg gezellig. Daar moeten we er nog maar eens een van doen! Ik wens jou en Teun alle goeds met jullie nieuwe aanwinst thuis ;-).

Sarah, ook met jou was het erg gezellig toen we nog een kantoor deelden. Bedankt voor al je input en dingen die je me geleerd hebt voornamelijk m.b.t. mijn imaging experimenten.

Linda, met jou was het ook altijd leuk samenwerken. Omdat onze projecten zo dicht bij elkaar lagen was het altijd fijn om daar met elkaar over te kunnen discussiëren (of even de problemen op tafel te kunnen gooien). Ook bedankt voor de gezelligheid op kantoor!

Simon, je was een goede, leuke collega waarmee ik erg goed kon samenwerken en waarvan ik veel geleerd heb. Daarbij was het ook altijd erg gezellig tijdens al die experimenten die we samen gedaan hebben. Dat maakte al die alamarBlue assays toch een stuk draaglijker! Bedankt voor de zeer prettige en leerzame samenwerking in het CA IX project, en voor alles wat je me geleerd hebt. Gelukkig zien we elkaar nog regelmatig en houden we die gezamenlijke uitjes er goed in. We spreken snel weer eens af!

Damiënne, met jou heb ik tijdens onze gedeelde dierstudies uitstekend samen kunnen werken. We waren een erg goed team! Daarbij vond ik het ook erg gezellig en werd het daarmee een stuk leuker in de DM II. Bedankt hiervoor, en nog veel succes met je verdere PhD traject, al voorzie ik daar geen problemen in :-).

Alex, hoewel je nog vrij "vers" bent binnen onze groep heb ik ook met jou kort maar prettig samen kunnen werken. Veel succes met het CP-506 project, je maakt er vast wat moois van. (En vergeet niet om af en toe een pepernootje te pakken... ;-)).

Nanda, I enjoyed working with you. Although I'm still no expert in chemistry, you did teach me some basics and were always willing to explain, thanks for that!

Veronica, although we did not really work together that much, I appreciate the occasional

immunological background information you provided to me.

Deb, I've had a lot of fun "potjes wegen" with you! I really liked working together with you, as well as the things we did outside of work. I hope we can meet up again soon, let us know when you're in the Netherlands!

Justina, thank you for all the wonderful Lithuanian and Russian words you taught me. Very useful! ;-). I've had a lot of fun working together with you, and I think we made a great team. I'm really happy for you and Arvidas that you've got your own apartment in The Netherlands now. Good luck with finishing your PhD!

Natuurlijk zijn er ook heel wat mensen binnen onze afdeling die een significante bijdrage hebben geleverd aan dit boekje. Marc, bedankt voor je nuttige input tijdens meetings en discussies. Kasper, jouw input heb ik ook altijd erg gewaardeerd. Jan, ik vond het fijn dat jij bij mijn HAP-project betrokken was. Je input was altijd zeer waardevol en dankzij je uitstekende kritieke blik en manieren om dingen uit te leggen heb ik er veel van op kunnen steken. Arjan, bedankt voor je hulp met al dat virus- en klonergedoe. Dankzij jou heb ik daar veel van geleerd en is het uiteindelijk nog gelukt ook! En natuurlijk ook bedankt voor al je sterke verhalen, het was toch weer altijd spannend waar je nu weer mee aan zou komen zetten. Lydie, I'd like to thank you too for all the help with cloning etc. You always took the time to answer the hundreds of questions I had :-). Don't forget to pick up GoT again soon! Kim, met jou was het ook altijd een feestje. Soms letterlijk, met die carnavalsmuziek... Mocht je nog eens een boek/film/serie aanbeveling nodig hebben, dan laat het me weten! Carla, bedankt voor alle ondersteuning in de bureaucratische zaken die er (helaas) ook bij horen.

Judith, bedankt voor al je verbouwings- en kattenverhalen. Die vervelen nooit! Veel succes nog met beide ;-). Marijke, bedankt voor de positieve energie die je in ons lab brengt! Tom, bedankt voor de sjaele wazel in de afgelopen jaren ;-). Eloy, I had a lot of fun organizing teambuilding with you! To all of these and other (past and present) lab members: thank you for the awesome time I've had, and thank you for all the help!

I would also like to thank some people in Auckland, where I've stayed for six weeks at the end of my PhD. Adam, thank you very much for inviting me to your lab. I've had an awesome time, both in and outside the lab, and it was a great and educational experience. Alex, first of all thanks for doing all those experiments with me, but also thanks for taking me on all the trips. You showed me some very nice parts of New Zealand, making me definitely want to come back for more :-). I hope you have a similar great time in Maastricht, we'd be

happy to show you some nice things to do too! Maria, thank you for all the help with the excision assays. I'm glad those are over but it was nice working with you! All other people that contributed to me having a great time over there: thank you very much!

Mijn vrienden ben ik natuurlijk ook dank verschuldigd. Sommigen van jullie heb ik de afgelopen jaren vaker gezien dan anderen, vanwege het vaak van twee kanten drukke leven en/of het feit dat velen ook naar "verre oorden" zijn verhuisd. Helaas gebeuren zo'n dingen nou eenmaal, maar ik hoop dat ik jullie toch nog geregeld zal blijven zien en dat we nog veel leuke dingen samen gaan doen. Dat zijn juist altijd goede afleidingen van de serieuze zaken geweest tijdens de afgelopen jaren, bedankt daarvoor!

Stans, altijd gezellig met jou. Gelukkig zien we elkaar weer wat vaker nu je weer in Maastricht woont. Die momenten waardeer ik zeer!

Roel, met jou heb ik altijd de grootste lol (zeker als daar vuurwerk bij komt kijken ;-)). Ik ken je al heel lang, en gelukkig zijn we nog steeds goede vrienden. "Vroeger" tijdens de vele feesten en festivals heb ik me altijd kostelijk geamuseerd. Daar moeten we er op korte termijn snel nog eens een van doen! Decibel 2018? Ook onze bordspelavonden met z'n vieren zijn altijd erg geslaagd. En misschien moeten we het judoën toch nog eens op proberen te pakken?

Willem, ik ben altijd erg blij als er na een werkdag weer een filmavond met jou voor de deur staat. Die moeten we er zeker in houden! Net zoals die Coca-Cola chicken ;-). Ik hoop dat je snel een leuke baan vindt, maar toch stiekem ook wel dat je nog een tijdje in Maastricht blijft wonen (zul je dan zien dat wij gaan verhuizen xD).

Lauren, helaas hebben we elkaar juist tijdens mijn PhD minder vaak gezien als wat ik zou willen, vanwege de "verre" afstand Eijsden-Nieuwegein en omdat we het beide erg druk hadden met ons werk. Maar als we elkaar weer zien is het altijd weer ouderwets gezellig. Ook kunnen we altijd goede gesprekken voeren, zo ook over ons werk en wat we daarin wel en niet willen. Bedankt dat je mijn paranimf wilt zijn! En leuk dat je nu misschien alsnog een PhD wilt gaan doen. Ik hoop van harte dat je snel iets (PhD of niet) vindt (dichter bij ons in de buurt natuurlijk ;-))! Ik wens je er alvast veel succes mee, al weet ik ook dat je dat gegarandeerd niet nodig zult hebben. Dat doe jij wel even!

Kosta, jou ken ik al vanaf de middelbare school, waar we meteen goede vrienden zijn geworden. Toch apart dat we daarna beide dezelfde studie zijn gaan doen, en ook nog eens een PhD. Maar wel erg fijn omdat we op die manier zowel de leuke als de minder leuke

kanten van dit alles beide begrepen en elkaar hierin konden helpen wanneer dat nodig was. Onze lunch-dates waren altijd weer iets waar ik erg naar uit keek! Niet alleen vanwege dat, maar ook omdat we het dan eens even over andere (belangrijkere? ;-)) zaken konden hebben. Verder zou ik volgens mij wel 5 pagina's kunnen vullen met alle dingen die we samen meegemaakt hebben. Ik heb altijd erg veel lol met je en weet zeker dat we dat nog veel meer gaan beleven. Bedankt ook dat je mijn paranimf wilt zijn! Ik wens jou en Joyce alle goeds met kleine Evy en jullie nieuwe huis :-).

Tineke, Marien, Peter, Fenna; bedankt voor het warme onthaal in jullie familie(s), en voor de interesse in mijn werk die jullie altijd tonen. Het is altijd erg gezellig met jullie.

Pap, mam, Melvin en Moniek, uiteraard verdienen jullie hier ook een prominente plaats. Jullie hebben me altijd vrij gelaten om mijn eigen keuzes te maken, maar me hier wel altijd vol in gesteund en ondersteund. Jullie staan altijd voor me klaar en bieden altijd een warm huis om weer naar terug te komen. Het is moeilijk om te verwoorden (zeker omdat ik niet zo'n prater ben zoals jullie weten ;-)) wat jullie allemaal voor me gedaan hebben (te veel) en hoeveel dat voor me betekent (heel veel). Reuze bedankt voor alle praktische/financiële/mentale/ennogveelmeer hulp de afgelopen jaren (en daarvóór natuurlijk ook), voor de interesse in wat ik doe, en natuurlijk ook voor alle leuke dingen die we samen doen. Zonder jullie was de hele weg naar hier een heel stuk moeilijker geweest.

En dan was er nog iemand die mij meermaals verzocht heeft om een paar pagina's over diegene vol te schrijven, maar wie was dat ook alweer... ;-). Maaïke, helaas ga ik dat aantal niet redden, maar kwaliteit over kwantiteit, toch? We zijn nu al 6 jaar samen, en ik weet zeker dat er daar nog vele bij komen. Wat we ook samen doen, het is altijd gezellig. Hoewel ik thuis niet zoveel vertel over mijn werk ben je altijd een luisterend oor als ik dat eens wel doe, ben je altijd geïnteresseerd in wat ik doe, en sta je altijd klaar om te helpen als dat nodig is. Het is altijd fijn om na een werkdag 's avonds weer gezellig met jou samen te zijn. Bedankt voor alle steun de afgelopen jaren, voor alle gezelligheid, voor al je verhaaltjes, natuurlijk ook voor het koken/afwassen e.d. als ik weer eens een hele avond moest bestralen ofzo ;-)... en ook voor de psychologische trucjes die je vast op me hebt toegepast? :-P. Bedankt voor alles wat jou jou maakt! Ik schrijf dit nu in mijn laatste week in Nieuw-Zeeland, en ik kan niet wachten om volgende week weer samen met jou te zijn. Je hebt me uitdrukkelijk verzocht om je geheime identiteit hier niet prijs te geven,

helaas, anders was dit proefschrift meteen een bestseller geworden... Maar ik mis die gekke onzin die we samen altijd verzinnen/doen enorm en kijk daar weer erg naar uit. Ik houd van je!

## Curriculum vitae

Raymon Servatius Theodorus Niemans was born on the 5<sup>th</sup> of October 1989, in the village of Reuver, The Netherlands. He completed his pre-university education (*Voorbereidend Wetenschappelijk Onderwijs*) in 2008 at the Bisschoppelijk College Broekhin in Roermond, The Netherlands, after which he enrolled in the Biomedical Sciences Bachelor's program, with a specialization in Molecular Life Sciences, at Maastricht University, Maastricht, The Netherlands. Here he obtained his first scientific research experience, during an internship at the Department of Toxicology of Maastricht University, in which he worked on implementing a new method to study glucose uptake in vitro. He completed his Bachelor's studies and received the corresponding BSc. degree in 2011, after which he enrolled in the Biomedical Sciences Master's program, with a specialization in Clinical Molecular Sciences, at the same university. Here he further developed his research skills during two internships. The first one was again at the Department of Toxicology of Maastricht University, in which he studied the reactivation of detoxified benzo[a]pyrene metabolites by neutrophil-derived  $\beta$ -glucuronidase. The second internship was at the Karolinska Institutet in Stockholm, Sweden. Here, at the Helleday Laboratory of the Department of Medical Biochemistry and Biophysics, Division of Translational Medicine and Chemical Biology, he worked on characterizing the biological functions of NUDT5, a sanitizer of the DNA precursor pool. He completed his Master's studies and received the corresponding MSc. degree in 2013. His interest in both research and education led him to pursue an academic career. Therefore, he enrolled in a PhD program at the Department of Radiotherapy of Maastricht University in 2014, where his research focused on exploiting tumor hypoxia for cancer treatment. He completed his PhD track in 2018, the results of which are presented in this thesis.

## List of publications

**Niemans R**, Marcus D, Biemans R, Lieuwes N, Theys J, Yaromina A, Dubois LJ, Lambin P. Antitumor effects of the novel hypoxia activated prodrug CP-506 combined with radiotherapy or immunotherapy.

*In preparation.*

**Niemans R**, Yaromina A, Theys J, Abbattista M, Biemans B, Lieuwes N, Mowday A, Ashoorzadeh A, Deschoemaeker S, Heyerick A, Guise C, Smaill JB, Patterson AV, Dubois LJ, Lambin P. Hypoxic cell killing by CP-506, a novel hypoxia-activated prodrug.

*In preparation.*

Spiegelberg L, Houben R, **Niemans R**, de Ruyscher D, Yaromina A, Theys J, Guise C, Smaill JB, Patterson AV, Lambin P, Dubois LJ.

Hypoxia-activated prodrugs and (lack of) clinical progression: the need for hypoxia-based biomarker patient selection in phase III clinical trials.

*In preparation.*

Spiegelberg L, van Hoof S, Biemans R, Lieuwes N, Marcus D, **Niemans R**, Theys J, Yaromina A, Lambin P, Verhaegen F, Dubois LJ.

Evofofamide sensitizes esophageal carcinomas to radiation without increasing normal tissue toxicity.

*Submitted to Clinical Cancer Research.*

Kazokaitė J, **Niemans R**, Dudutienė V, Becker HM, Leitāns J, Zubrienė A, Baranauskienė L, Gondi G, Zeidler R, Matulienė J, Tārs K, Yaromina A, Lambin P, Dubois LJ, Matulis D.

Novel fluorinated carbonic anhydrase IX inhibitors reduce hypoxia-induced acidification and clonogenic survival of cancer cells

*Accepted and to be published by Oncotarget.*

van Kuijk SJ\*, Parvathaneni NK\*, **Niemans R**\*, van Gisbergen MW\*, Carta F, Vullo D, Pastorekova S, Yaromina A, Supuran CT, Dubois LJ#, Winum JY#, Lambin P#.

New approach of delivering cytotoxic drugs towards CAIX expressing cells: A concept of dual-target drugs.

*Eur J Med Chem. 2017 Feb 15;127:691-702.*

van Kuijk SJ\*, Gieling RG\*, **Niemans R**, Lieuwes NG, Biemans R, Telfer BA, Haenen GR, Yaromina A, Lambin P, Dubois LJ#, Williams KJ#.

The Sulfamate Small Molecule CAIX Inhibitor S4 Modulates Doxorubicin Efficacy.

*PLoS One*. 2016 Aug 11;11(8):e0161040.

Sneddon D\*, **Niemans R\***, Bauwens M, Yaromina A, van Kuijk SJ, Lieuwes NG, Biemans R, Pooters I, Pellegrini PA, Lengkeek NA, Greguric I, Tonissen KF, Supuran CT, Lambin P, Dubois L, Poulsen SA.

Synthesis and in Vivo Biological Evaluation of (68)Ga-Labeled Carbonic Anhydrase IX Targeting Small Molecules for Positron Emission Tomography.

*J Med Chem*. 2016 Jul 14;59(13):6431-43.

van Kuijk SJ\*, Yaromina A\*, Houben R, **Niemans R**, Lambin P#, Dubois LJ#.

Prognostic Significance of Carbonic Anhydrase IX Expression in Cancer Patients: A Meta-Analysis.

*Front Oncol*. 2016 Mar 29;6:69.

Dubois LJ, **Niemans R**, van Kuijk SJ, Panth KM, Parvathaneni NK, Peeters SG, Zegers CM, Rekers NH, van Gisbergen MW, Biemans R, Lieuwes NG, Spiegelberg L, Yaromina A, Winum JY, Vooijs M, Lambin P.

New ways to image and target tumour hypoxia and its molecular responses.

*Radiother Oncol*. 2015 Sep;116(3):352-7.

